
6
EPS
European Conference
on Controlled Fusion
and Plasma Physics
Moscow 1973
July 30-August 4
Vol. II

SIXTH EUROPEAN CONFERENCE ON CONTROLLED FUSION AND PLASMA PHYSICS

Moscow USSR
July 30 - August 4. 1973

Vol. II
INVITED PAPERS and SUPPLEMENTARY PAPERS

The Conference Proceedings are distributed free of charge to all registered participants

ORGANIZING COMMITTEE

B.B.Kadomtsev	- president, Kurchatov Institute of Atomic Energy
M.S.Rabinovich	- vice-president, Lebedev Physical Institute
E.P.Velikhov	- vice president, Kurchatov Institute of Atomic Energy
E.I.Kusnetsov	- scientific secretary, USSR State Atomic Energy Committee
D.K.Akulina	- Lebedev Physical Institute
N.V.Belousov	- Academy of Sciences of the USSR
A.B.Beresin	- Ioffe Physico-Technical Institute
N.S.Cheverev	- USSR State Atomic Energy Committee
L.V.Dubovoi	- Efremov Sci.Res.Institute of Electrophysical Apparatus
D.P.Filippov	- USSR State Atomic Energy Committee
V.S.Fursov	- Moscow State University
V.E.Golant	- Ioffe Physico-Technical Institute
I.N.Golovin	- Kurchatov Institute of Atomic Energy
S.G.Gusev	- USSR State Atomic Energy Committee
A.A.Kusovnikov	- Moscow State University
N.I.Leontjev	- Sukhumi Physico-Technical Institute
V.V.Makarov-Zemljansky	- USSR State Atomic Energy Committee
A.T.Matvejev	- Moscow State University
S.V.Mirnov	- Kurchatov Institute of Atomic Energy
M.I.Pergament	- Kuchatov Institute of Atomic Energy
V.D.Pismenny	- Moscow State University
M.K.Romanovsky	- Kurchatov Institute of Atomic Energy
D.D.Ryutov	- Siberian Institute of Nuclear Physics
R.Z.Sagdeev	- High Temperature Institute, Moscow
V.D.Shafranov	- Kurchatov Institute of Atomic Energy
I.S.Shpiegel	- Lebedev Physical Institute
V.T.Tolok	- Physical-Technical Institute, Ukr. SSR

P r e f a c e

This volume contains the Invited Papers and the Supplementary Papers, which have been selected by Paper Selection and Programme Committee /PSPC/ of the "YI European Conference on Controlled Fusion and Plasma Physics".

The Proceedings have been printed by both typing and photo-offset lithograry methods. Only minor editorial work was carried out. It means that the authors must bear responsibility for their texts.

We sincerely thank the authors for carrying out the "Instruction for Preparing Papers". We wish to thank the members of the PSPC and the Scientific Institutions they represent for their co-operation.

The Organizing Committee

PAPER SELECTION AND PROGRAMME COMMITTEE

T. Consoli /France/
V. Copecky /CSSR/
B. Kadomtsev /USSR/
E. Kusnetsov /USSR/
D. Grieger /BRD/
M. Rabinovich /USSR/
P. Reynolds /UK/
V. Shafranov /USSR/

The Conference is under the auspices of the
European Physical Society
/Plasma Physics Division/

Organized
by LEBEDEV PHYSICAL INSTITUTE
KURCHATOV ATOMIC ENERGY INSTITUTE
LOMONOSOV MOSCOW STATE UNIVERSITY

Sponsored
by ACADEMY OF SCIENCES OF THE USSR
USSR STATE ATOMIC ENERGY COMMITTEE
USSR MINISTRY OF HIGHER AND SPECIAL SECONDARY EDUCATION

ПРИВЕТСТВИЕ ЗАМЕСТИТЕЛЯ ПРЕДСЕДАТЕЛЯ ГОСКОМИТЕТА ПО ИСПОЛЬЗОВАНИЮ АТОМНОЙ ЭНЕРГИИ

проф. И.Д.МОРОХОВА

Уважаемые дамы и господа, наши гости, коллеги и товарищи !

Более 20 лет ученые многих лабораторий мира ведут упорную борьбу за овладение энергией управляемого термоядерного синтеза, сулящего человечеству безграничные энергетические перспективы. Я не ошибусь, если скажу, что над этой проблемой работает цвет физической науки, самые талантливые и энергичные ученые. Исследования по проблеме термоядерного синтеза стимулировали громадное расширение наших знаний о плазме, одном из самых распространенных состояний материи, и породили к жизни целый ряд прикладных направлений в науке и технике. Это история взлетов и падений, пессимизма и оптимизма.

В настоящее время наблюдается резкое возрастание интереса к проблеме управляемого синтеза, обусловленное обнадеживающими результатами исследований последних лет.

Решение проблемы управляемых термоядерных реакций - это не просто увлечение физиков, удовлетворяющих свое любопытство за счет государства. Отыскание новых способов получения энергии становится самым актуальным вопросом XX века, острота которого со временем будет только возрастать.

Развитие энергетики за последние 100 лет говорит о непрерывном изменении структуры мирового энергетического баланса в сторону топлива с более высокой теплотворной способностью.

На смену углю пришло жидкое и газообразное горючее, а в настоящее время начинается эпоха ядерного топлива, концентрирующего огромные величины энергии в ничтожной массе вещества.

Долгосрочные потребности в энергии могут быть удовлетворены за счет двух ядерных процессов : деления ядер тяжелых элементов и синтеза ядер изотопов водорода. Атомная энергетика, основывающаяся на первом процессе, уже в полной мере вступила на путь практической утилизации ядерной энергии. Управляемый термоядерный синтез, в случае его реализации, сулит человечеству неисчерпаемый источник дешевой энергии, более чистый и безопасный, позволяющий в принципе лучше решить экологические проблемы Земли.

В последние годы перспектива осуществления управляемого термоядерного синтеза значительно прояснилась благодаря интенсивным исследованиям по ставшим уже классическими направлениям открытых магнитных ловушек, импульсных процессов типа "тэта - пинг" и, главным образом, замкнутых магнитных ловушек типа "токамак". Удалось существенно повысить температуру, плотность и время жизни энергии плазмы. Одним из существенных результатов следует считать сближение результатов экспериментов с теорией. Все это укрепляет уверенность в возможности получения в ближайшем будущем параметров плазмы, необходимых для начала самоподдерживающейся термоядерной реакции.

За последние несколько лет открылась возможность колоссальной концентрации энергии во времени и пространстве в луче лазера и пучке релятивистских электронов, выдвинувшая новые идеи по инициированию управляемых термоядерных реакций синтеза. Это является еще одним фактором, укрепляющим нашу уверенность в успешное решение проблемы.

Достигнутые результаты это только первые,хотя и трудные, шаги на пути решения проблемы. Предстоит еще выяснение громадного количества физических вопросов поведения плазмы, установления законов подобия, разработки новых способов нагрева и диагностики плазмы, достижения параметров плазмы, необходимых для начала самоподдерживающейся термоядерной реакции прежде, чем можно будет приступить к строительству термоядерного реактора.

Проблема получения энергии с помощью управляемого термоядерного синтеза вышла за рамки интересов отдельно взятой страны. Задача, стоящая перед нами, настолько грандиозна, что она требует коллективного усилия всех стран.

В современном мире,полном надежд на положительные результаты начавшейся разрядки международной напряженности, созданы исключительно благоприятные условия для международного сотрудничества в этой области. Что касается Советского Союза, то я могу заверить вас в нашем неизменном и активном содействии такому сотрудничеству во всем многообразии его форм.

Сегодняшняя конференция, несмотря на то, что она называется Европейской, это подведение итогов коллективного труда ученых и инженеров всех лабораторий мира. Она поможет проверить и обсудить достигнутые результаты и наметить оптимальные планы на будущее.

Энергия термоядерного синтеза уже проявила себя в неуправляемом виде. Соединив свои усилия в борьбе за управляемый синтез, человечество лишний раз повышает свои возможности поставить его на службу благосостояния и прогресса народов мира.

Уважаемые дамы и господа, товарищи !

Разрешите мне от имени Государственного комитета по использованию атомной энергии СССР приветствовать Вас в связи с началом УI Европейской конференции по физике плазмы и управляемому термоядерному синтезу и пожелать Вам плодотворных дискуссий, полезного обмена мнениями и приятного пребывания в нашей стране.

Благодарю Вас за внимание !

THE SPEACH OF THE VICE-PRESIDENT OF THE USSR ATOMIC ENERGY COMMITTEE

Prof. I.D.MOROKHOV

Ladies and gentlemen, our guests, colleagues and friends.

More than 20 years scientists of many laboratories of the world carry on a persistent struggle for mastering the energy of controlled thermonuclear fussion, one of the most alluring properties of matter, which opens unlimited energy perspectives for mankind. I shall not make a mistake if I shall say that this problem is being studied by the pick of physical science, by the most talented and energetic scientists. Investigations in the field of thermonuclear fusion have stimulated vast widening of our knowledge of plasma, one of the most widespread states of matter, and have given rise to a wide variety of applied trends in science and technology. This is the history of success and failure, pessimism and optimism.

At present,we observe the wide growth of the interest to thermonuclear fusion the problem, being due to the reassuring results of recent studies.

The solution of the problem of controlled thermonuclear reactions is far from being just an enthusiasm of physicists, satisfying their curiosity at the expence of the state. Finding of new methods of obtaining the energy is becoming the most urgent problem of the XX century, which acuity will only grow in due course.

The development of energetics for the last 100 years shows continuous changes in the structure of the world energetic ba-

lance in the direction of fuel with higher calorific power. Coal was changed by gas- and liquid fuel , and now the nuclear fuel age begins, concentrating a vast amount of energy in an extremely small mass of substance.

Long-term power requirements can be satisfied at the expence of two nuclear processes: fission of heavy element nuclei and fusion of hydrogen isotope nuclei. Nuclear energetics, based on the first process, has taken the path of the practical utilisation of atomic energy. The controlled thermonuclear fusion, in case of its realization, promises for mankind the inexhaustible source of cheap energy, more pure and safe, enabling, in principle to solve better oecological problems of the earth.

In the last few years the perspective of feasibility of the controlled thermonuclear fusion has become more clear, due to intensive investigations in classical directions of open magnetic traps, puls processes "theta-pinch", and mainly, closed magnetic traps "tokamaks". It has been possible to increase considerably the temperature, density and life time of plasma energy. The proximity of experimental results and theory should be considered as one of the most significant results. All this strengthens our confidence, that in the nearest future plasma parameters can be obtained, necessary for the initiation of helf-sustaining thermonuclear reaction.

Over the past few years the possibility was offered of the colossal concentration of energy with space and time in the laser beam and relativistic electron beams which has put forward new ideas on initiating controlled thermonuclear fusion reactions. This is one more factor, which strengthens our confidence in the successful solution of the problem.

The results obtained are only the first, although difficult steps in the solution of the problem. We are still to solve a considerable body of physical problems of plasma behavior, finding similarity laws, working out new methods of plasma heating and diagnostics, obtaining plasma parameters, necessary to initiate the self-sustaining thermonuclear reaction, before we shall be able to begin the construction of thermonuclear reactor.

The problem of energy production by means of controlled thermonuclear fusion has overcome the interests of one single country. The task is so grandiose that it requires collective efforts of all countries.

In the present-day world, full of hopes on positive results in relaxation of international tension, the most favourable conditions have been created for the international cooperation in this field. As for the Soviet Union, I can assure you in our invariable and active assistance in such cooperation in all its variety.

This conference, in spite of the fact that it is called European, is summing up the collective efforts of scientists and engineers all over the world. It will help to check and discuss the obtained results and draw up optimal plans for the future.

The energy of thermonuclear fusion has already shown itself as uncontrolled. Joining our forces in the struggle for controlled thermonuclear fusion, mankind once more increases its possibilities to place it in the service of the prosperity and progress of all nations.

Ladies and gentlemen, comrades

Let me on behalf of the USSR Atomic Energy Committee greet you on the occasion of the beginning of the VI European Conference on Controlled Fusion and Plasma Physics and wish you fruitful discussions, helpful exchange of views and pleasant stay in our country.

Thank you for your attention.

CONTENTS

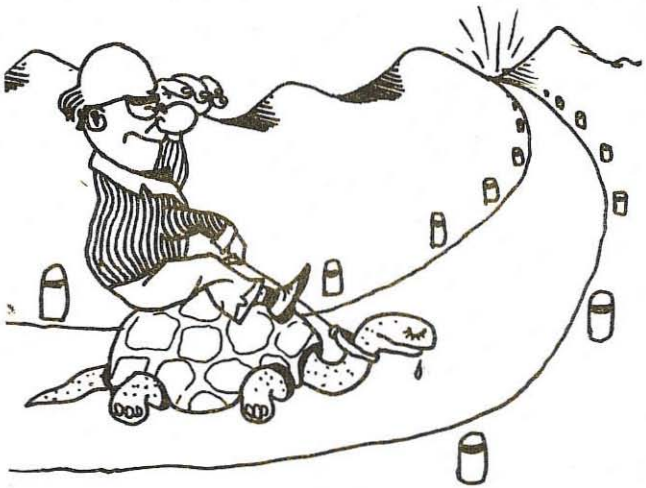

INVITED PAPERS

SUPPLEMENTARY PAPERS[x/]

x/ Number in brackets refers to the number of the paper in the first volume.

INVITED PAPERS

PROGRESS IN THE TOKAMAK RESEARCH

B.B.Kadomtsev

I.V.Kurchatov Institute of Atomic Energy, Moscow, USSR

This paper presents a brief survey of the recent research studies carried out at the Kurchatov Institute of Atomic Energy.

Headed by L.A.Artsimovich they led to impressive results. If to consider the optimal plasma parameters obtained so far they are as follows. The electron temperature is about 3 kev, ion temperature - 0.7ke energy containment time - 0.02 sec, density up to $7.10^{13}cm^{-3}$. The highest value of $n\tau_E$ (the product of density by containment time) is approximately 10^{12}. All these parameters can be obtained with simple and quiescent heating of an initially cold gas by current flowing through the plasma.

At first glance the tokamak devices are very simple. In practice, however, the physical phenomena of the tokamak plasma are very complicated. Just these phenomena were the subject of persistent experimental and sophisticated theoretical investigations for many years.

1. Containment of plasma energy.

The main object of the experimental studies on the TM-3, T-4, T- installations is to investigate the efficiency of tokamak as a magnetic trap. It has been shown earlier that the principal mechanism responsible for energy losses in tokamaks is high electron heat conductivity. Its value is many times greater than the neoclassical one /up to two orders of magnitude/. The mechanism of the anomalous thermal conductivity is not yet clear. To reveal the cause of energy leakage is the primary problem in tokamak investigations.

variables which have an influence on β_J . Nevertheless, the map of points β_J , ν_{ei}/ν_0 is of interest since it shows how the loss rate varies when we diminish ν_{ei} and enter strongly collisionless region. We see when diminishing ν_{ei}/ν_0 the value β_J decreases at first, and then at very small ν_{ei}/ν_0 the plasma confinement improves, and β_J grows again.

Fig. 2 indicates the energy losses in TM-3 as compared to those predicted by the neoclassical theory. One can see that the deviation is of an order of magnitude for the banana region.

Fig. 3 illustrates the same TM-3 experimental data in somewhat different aspect, namely, the relation between the Bohm confinement time and the observed one is shown for different values of the collision parameters ν_{ei}/ν_0 . Excluding three low temperature points at J=12 kA, the rest points are seen to concentrate near the curve which corresponds to $\tau_E = \tau_B \cdot \nu_0/\nu_{ei}$ in a rarefied plasma, and approximately to $\tau_E = 3\tau_B$ in the plateau region.

The relationship $\tau_E = \tau_B \frac{\nu_0}{\nu_{ei}}$ is similar to that found by Yoshikawa for a spherator. It corresponds to qualitative assumption that there should exist perturbations of the drift wave type in a plasma, accompanied by particle transfer proportional to the collision frequency. In other words, we can say that the phase shift between the density and potential fluctuations is determined by dissipation, hense, it should be proportional to the frequency.

Note, that the relationship between the loss rate and Joule heat for $\tau_E = \tau_B \cdot \nu_0/\nu_{ei}$ leads to relation $T_e \cdot n_e^{1.3} = \text{const} \cdot J^2$, where const $\sim a^{-8/3}$. The relationship of such a kind is well fulfiled for TM-3 in the region of rare collisions.

Proceeding from the spherator results Dr.Yoshikawa suggested that the second Bohm limit could be achieved when the collision fre-

quency becomes very small so that the values greater than (100 + 300)τ_B are hardly to be attainable. One can see in Fig.3 that a tendency for changing the relationship $\tau_E = \tau_B \nu_0 / \nu_{ei}$ is not observed in TM-3 at small ν_0 / ν_{ei}, however, only one hundred Bohm values have been achieved so far.

The diffusion time τ_D in the tokamaks is usually greater than the energy containment times τ_E. For example, the relationship between τ_D and τ_E is shown in Fig.4 as a function of density for T-3 and ST.

2. Ion confinement

It has been shown that the ion temperature is in good agreement with that predicted by the neoclassical theory of thermal conductivity for the plateau region. Namely, the experimental data points are in good agreement with the formula $T_i = 6 \cdot 10^{-7} \xi$, where $\xi = A^{-1/2} (J B_z n_e R^2)^{1/3}$, A is the atomic weight of the ions, J is the total current, B_z - the longitudinal magnetic field, n_e - the electron density, R - the major radius of the torus.

An attempt to step in banana region by increasing the total plasma current has been made recently on T-4. It could be expected that the ion temperature would increase more rapidly with the current in this region.

The experimental results shown in Fig.5 indicate that this attempt failed, i.e. no departure from $T_i \sim \xi$ is observed. This is associated with large amount of impurities appearing during current rise. Appearance of the impurities is illustrated in Fig.6 in which the relation between the deuterium ion density and electron concentration is shown as a function of the plasma current.

Note, that the charge exchange process plays a negligible role in the ion energy balance, it is about an order of magnitude less than the effect of thermal conductivity. /Fig.7/.

3. Impurties

The impurties play an essential role now, and as the plasma temperature increases they will cause more and more trouble. For this reason, as well as taking into account a possibility to use the impurities as one of plasma diagnostic tools much attention is being given to investigate their behavior.

It has been shown earlier that the impurities concentrate at the centre of a plasma column under stable discharge conditions. This phenomenon was predicted by the classical theory of the transfer processes. The impurity concentration near the column axis is shown in Fig.8. The distribution of the impurity concentration in T-4 was measured with x-ray emission. Fig. 9 shows that under stable discharge conditions the impurities enter the plasma column monotonically and steadily, and this fact constitutes a serious danger. To decrease the rate of impurity influx into the discharge a divertor should be used.

Another possibility to control the impurity level has been suggested by the experimental evidence that hydromagnetic instabilities have an influence on process of shrinking of impurities. Fig. 10 and 11 show that the impurity concentration at the axis decreases appreciably as the kink instability excites. The impurities are spread transverse the plasma column. This effect is more pronounced in the presence of the disruptive instability.

4. Disruptive instability

The disruptive instability is one of most mysterious phenomena in the tokamak plasma. This instability was first observed on TM-2, and now it is observed in all existing tokamaks. As is well known its appearance is characterized by negative voltage spikes implying that a part of the poloidal field flux is pushed away. Simultaneously, the plasma column is compressed in the direction of the major ra-

dius /Fig.12/. This may be associated with a decrease in the plasma inductance, i.e. with a sharp expansion towards the minor radius. The duration of expansion is small - about 100 μsec or even less. The energy content of the plasma measured from diamagnetic signal data shows that despite a contact between the plasma and limiter during an abrupt expansion the total plasma energy varies very slightly after a spike. Therefore, one may conclude that in the presence of the disruptive instability the poloidal field transfers a certain portion of its energy to the plasma. All these facts seem to be rather mysterious, that is why the disruptive instability has been the subject of detailed experimental investigations for the last few years. Moreover, a theoretical model of the disruptive instability has been recently suggested which permits us to a certain degree to make the first step towards understanding this phenomenon.

The experiments have shown that the disruptive instability is excited only at sufficiantly large currents and pressures. Fig. 13 shows qualitatively the stability domain in variables J - the plasma current, and n_e - the plasma density. In addition to the basic large domain there are two stability islands with large currents, one - with the q-values more than unity, another - with q more than 2. These domains are separated from one another and from the main stability domain by instability slits in which the hydromagnetic modes m=2 and m=3 are unstable. The disruptive instability is excited near these boundaries, thus at high currents it appears to be associated with hydromagnetic kink instabilities. Moreover, the disruptive instability can be excited on the right hand side boundary of the stability domain /Fig.13/, i.e. at large n_e. The lower and left hand boundaries of the stability domain are related to the formation of runaway electrons, they will be considered below.

As we see the disruptive instability occurs in the most interesting region of high currents and densities. It is evident that future generations of installations operating with high plasma currents and densities will face the disruptive instability.

The results of T-6 have been analysed in detail to get the interrelation between the disruptive instability and the kink mode. It has been shown that as a rule the kink mode preceeds the disruptive instability. A typical picture of the oscillations excited before a spike is shown in Fig. 14. Oscillations in the phase shift ϕ of the microwaves probing the plasma are clearly seen. Fig.15 illustrates a region close to the spike. It is seen that as the instability develops the modulation depth of the phase shift at the distance x=2 cm from the centre reaches 25% in 1-2 cycles, then it decreases. The spike leads to a decrease in β_J by 15% and the density in the axial region falls to 30% while the total quantity of particles in the plasma column cross section is only 6% lower. Inspection of the magnetic probe data indicates that the perturbation is of a kink mode type with m=4, or with m=3 under more poor vacuum conditions. Fig. 16 is streak record of the plasma light emission. Developing of the kink mode just before the spike, and sharp expansion of the plasma column at spike are both clearly seen.

Fig. 17 is a picture of CV and OV ion light emission as the kink instability develops /curves 2,3/ and at an instant of a spike /curve 1/. A drop in the light emission of CV indicates a decrease in the plasma temperature while an increased light emission of OV in the central zone of the plasma column can be explained by an assumption that at a spike a portion of cold plasma penetrates the plasma column from the periphery.

The above experimental results indicate that a deep nonlinear phase of hydromagnetic perturbations developed on the plasma column surface are accompanied by the disruptive instability in T-6. These results are in good agreement with a theoretical model proposed recently which assumes that nonlinear excitation of the kink modes should lead to the formation of helical vacuum bubbles penetrating under the plasma surface. /Fig.18/. Such a model explains the sharp expansion of the plasma column boundary, and the conversion of a portion of the poloidal field energy into the plasma energy. This model is able to offer a likely explanation of the negative voltage spikes as well.

The fact that there is a close relation between the disruptive instability and kink modes is additionally supported by the data on HF stabilization of the kink modes of a toroidal plasma column obtained at the Suchumi Institute. Using such a stabilization method the negative voltage spikes disappear completely.

In spite of the above quite convincing arguments the "bubble" model appears to be excessively idealized. There are a number of experimental evidence indicating that the disruptive instability could be a more complicated phenomenon in practice. Thus, as we enter a region of higher densities, i.e. move towards the right hand side boundary /Fig.13/ the coupling between the kink modes and disruptive instability weakens. The kink amplitude drops /Fig.19/ while the disruptive instability grows rapidly. It is most likely that the disruptive instability itself corresponds to a complicated turbulent process. Indeed in this case the probe field oscillations become being uncorrelated /Fig.20/. It is probable that during this turbulent phase there should exist additional possibilities for the energy transfer from the poloidal field to plasma. As the current decreases, i.e. q is increased, the disruptive instability overlaps

with the beam-plasma instabilities caused by runaway electrons, thus the picture becomes more complicated.

5. Runaway electrons

The lower and upper boundaries of the stability domain in Fig.13 are associated with runaway electrons. These boundaries are also shown in Fig. 21 for TM-3. The stability domain is between curves II/ or III for another assembly of the installation/and I. Both the voltage oscillations and plasma column displacements similar to those observed in the presence of the disruptive instability, but with the smaller amplitude were observed. It is quite natural to associate these oscillations with beam-plasma instabilities caused by runaway electrons. The appearance of runaway electrons at low densities looks quite natural because, roughly speaking, there is a deficit of plasma for a proper current to be passed. In the stability domain, the runaway electrons can enter into interactions with the plasma without being accumulated to high densities. When the plasma density increases, and the portion of the runaway electrons decreases their interactions with the plasma become more weak. Correspondingly, the electrons can be accelerated to very high energies and give rise to violation of the plasma equilibrium resulting in a contact between the plasma column and limiter. This occurs on the right hand side boundary II in Fig.21. Such regimes were referred to as uncontrollable.

The beam instabilities along with the kink and disruptive perturbations give rise to a certain kind of plasma activity in tokamaks. They need further study in detail and complete understanding.

6. Plasma resistivity

The tokamak plasma resistivity is usually larger than that determined by the Spitzer formula for a pure hydrogen plasma. As the plasma density decreases this deviation from the classical value increases reaching factor 30 for low densities. This value seems to be very large to be explained by impurities. It is quite likely that in addition to the impurities another collective process of interactions between the current and plasma oscillations is also responsible for this effect.

7. HF heating and feedback control

Development of additional methods of plasma heating and feedback control allowed a departure from the traditional technique of Joule heating and copper shell for equillibrium, being not very efficient at high temperatures and large confinement times. It has been shown that HF heating at the frequencies of the order of electron cyclotron frequency is an efficient and quite convenient method in practice. However, the powers of UHF generators are lower than those of lower frequency generators that is why it is worth - while to investigate HF heating at frequencies close to lower hybride resonance or ion cyclotron harmonics. Such experiments are being carried out on TM-3 and TO-1. HF power up to 100 kw was applied to TM-3. It was shown that HF energy was absorbed by the plasma, the most portion being transferred to the electrons. When a HF pulse is applied the plasma resistivity becomes anomalously large at the periphery. This results in a 35% decrease in the plasma column radius. This effect indicates the presence of some nonlinear collective phenomena during the heating process.

The installation TO-1 has demonstrated the efficiency of plasma heating at the ion cyclotron harmonics. The same installation showed

efficient confinement of a plasma ring in equilibrium using the feedback control. The equilibrium was maintained for 0.3 sec.

8. Finger-ring tokamaks

A new tokamak model of T-9 has been recently put into operation. Another version of the tokamak installations - T-8 with a noncircular elliptical cross section of a plasma column will be constructed soon. The cross section of such a shape has been predicted to reach more high current densities for the same margin of stability. This will permit improvement in Joule heating efficiency. Furthermore, the elliptical shape should improve plasma confinement, and provide additional information on the instability and transfer mechanisms in plasma. Experience gained in controlling the shape of a plasma column may help in designing a divertor.

Only initial experiments have been carried out on T-9. The plasma is still cold and containing a lot of impurities. However, discharges of non-circular plasma column cross section have been already observed, and what is most interesting, we again face the disruptive instability in this case.

9. Conclusion

The tokamak plasma lives a complex life: various instabilities and collective processes develop arbitrarily and interact one with another. Their detailed study is one of the principal objects in the program of physical research. Alongside with the progress in our understanding we observe that the plasma parameters also grow steadily, first of all due to improvements in plasma confinement and increase in temperature. At the present time the tokamaks are facing a new stage connected with achange to large installations, more perfect geometrical configurations, and new heating techniques. We may expect that this stage should advance us still nearer to controlled thermonuclear reactions.

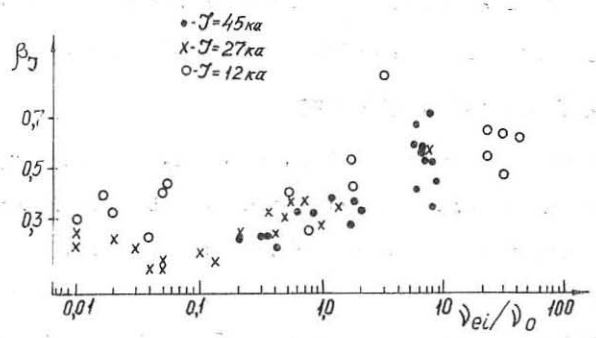

Fig. 1. - β_J as a function of the collision parameter ν_{ei}/ν_0.

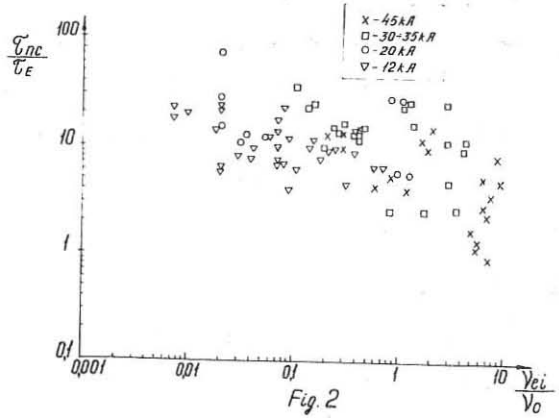

Fig. 2.

Fig. 2. - Relationship between the neoclassical energy containment time τ_{nc} and τ_E measured at different current magnitudes in TM-3 vs the collision parameter ν_{ei}/ν_0.

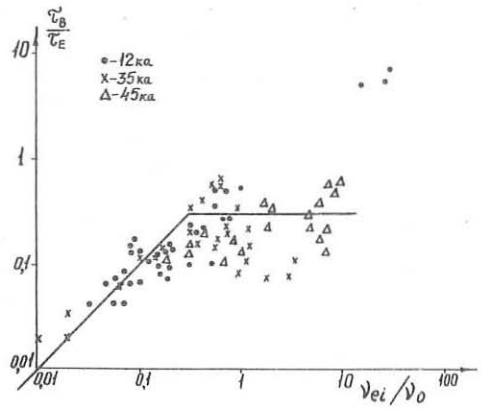

Fig. 3. - The relationship between Bohm containment time τ_B and τ_E measured as a function of ν_{ei}/ν_0.

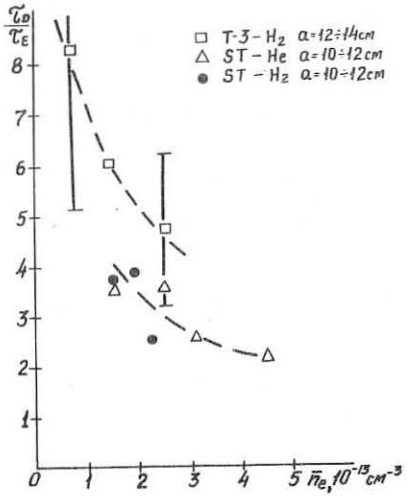

Fig. 4. - τ_D/τ_E as a function of the electron concentration.

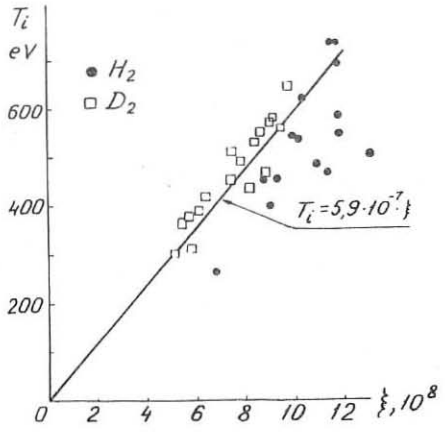

Fig. 5. - Ion temperature vs $\xi = \frac{1}{\sqrt{A}} \sqrt[3]{J B_z n_e R^2}$

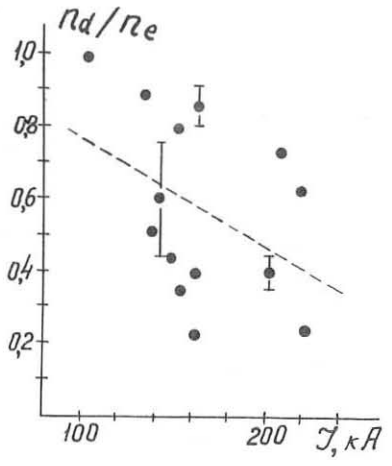

Fig. 6. - The ratio between the electron and deuteron density vs the discharge current on T-4.

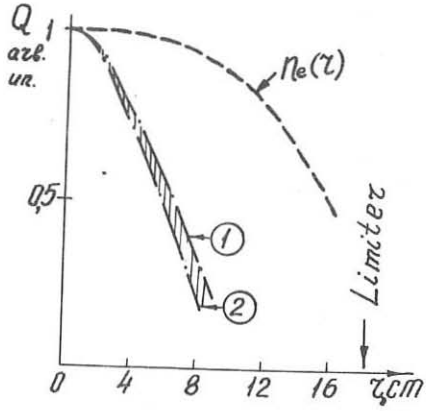

Fig. 8. - Radial distributions of the x-ray target density and the electron density 1.-for bremsstrahlung, 2.-recombination emission.

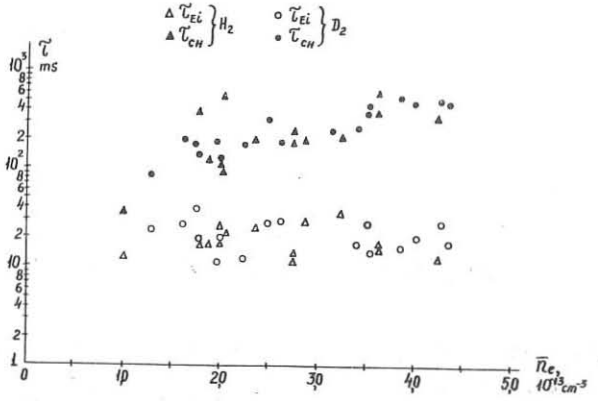

Fig. 7. - Comparison of the total ion lifetime with the charge exchange lifetime on T-4.

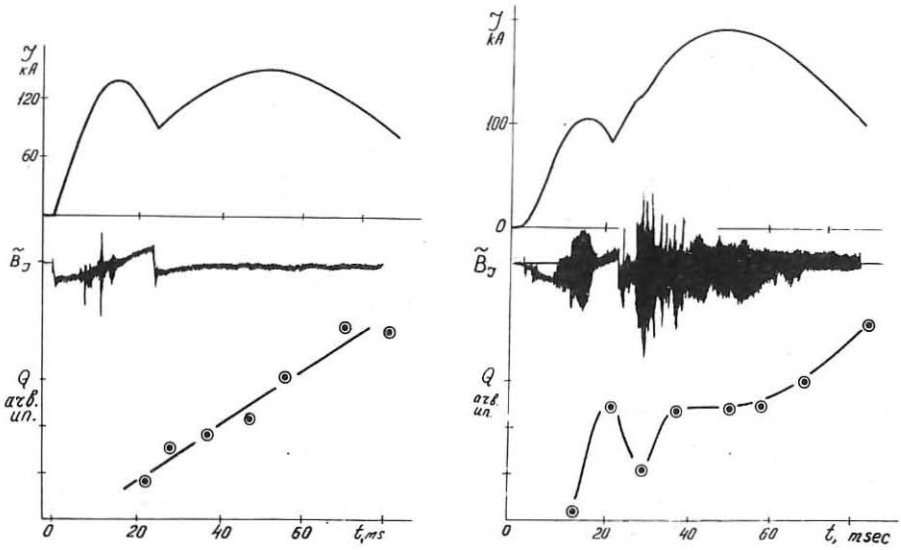

Fig. 9. - Current, poloidal field fluctuations and the x-ray target for stable discharge in T-4.

Fig. 10. Current, poloidal field fluctuations and the x-ray target for the kink mode excited in T-4.

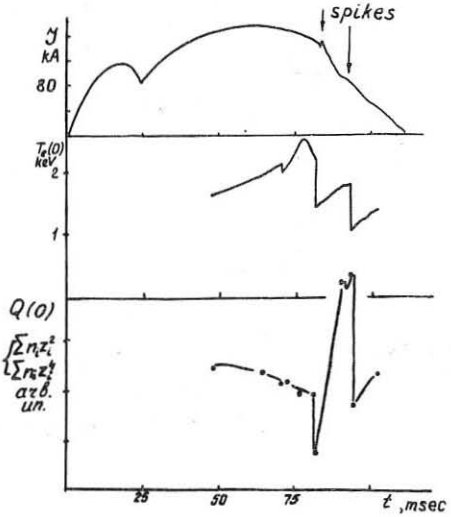

Fig. 11. Current, electron temperature and x-ray target density on the axis of the plasma column for discharge with disruptive instability.

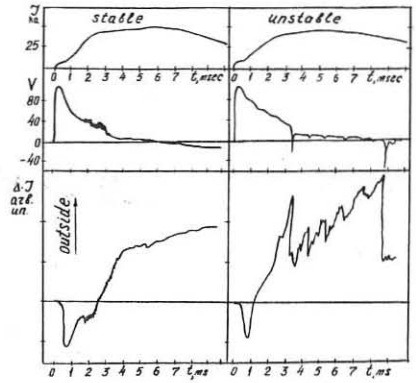

Fig.12.- Oscillograms of current, voltage and plasma column displacement under stable and unstable discharge conditions.

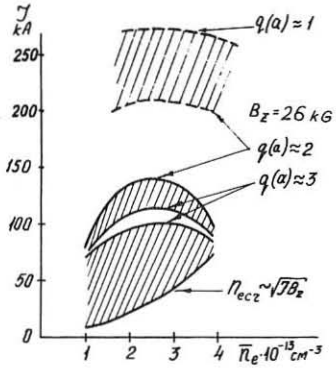

Fig. 13. Schematic drawing of stability for T-3a.

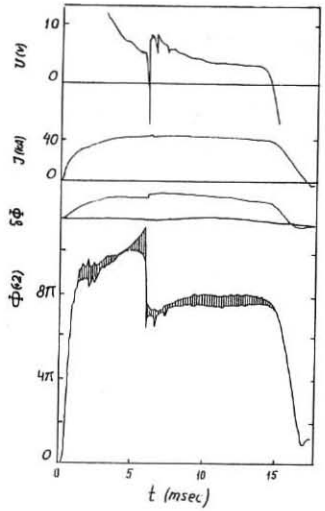

Fig. 14. Oscillograms of voltage, current, diamagnetic signal and microwave phase shift in T-6.

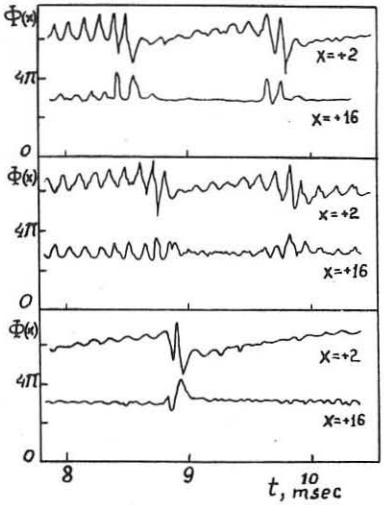

Fig. 15. Regions of the phase shift near the spikes.

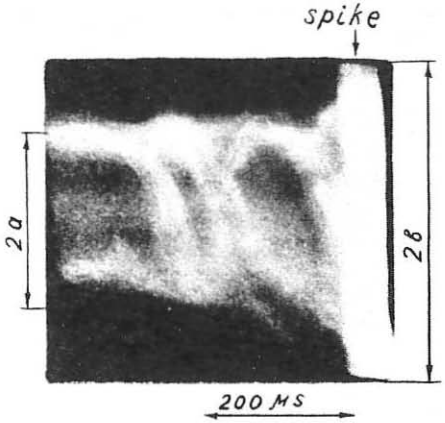

Fig. 16. Streak record of the plasma light emission near the spikes in T-6.

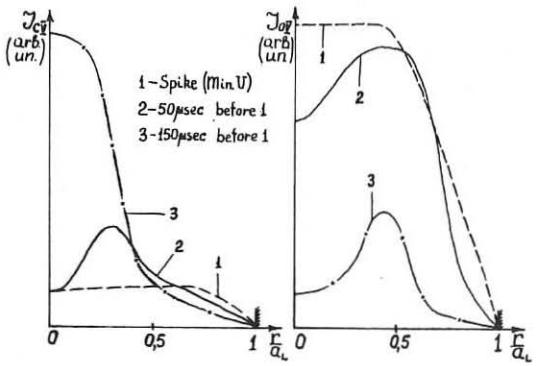

Fig. 17. - Distribution of the light emission intensity of CV and OV lines near the spike in T-6.

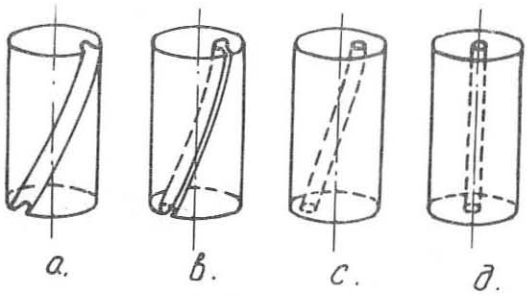

Fig. 18. - Formation of helical "bubbles".

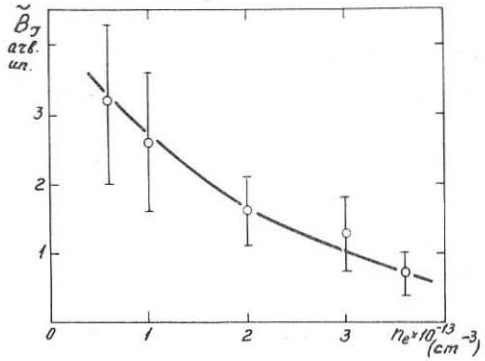

Fig. 19. - Amplitude of the kink perturbations as a function of the electron concentration.

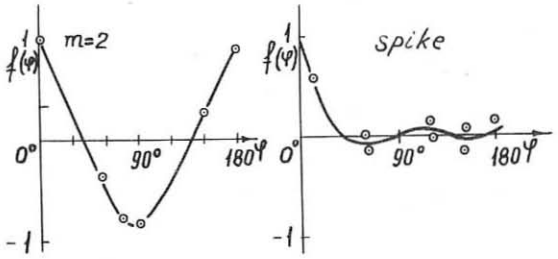

Fig. 20. - Structure of the kink perturbations with m=2 modes and disturbances during the spike in T-4.

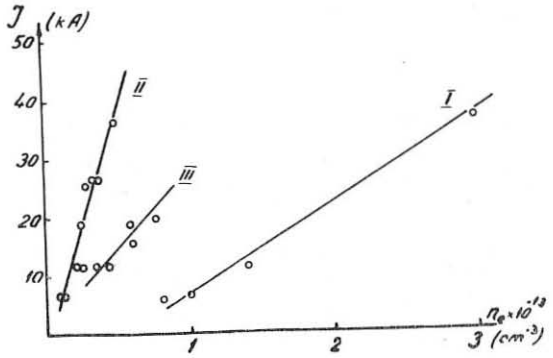

Fig. 21. - Schematic drawing of stability for TM-3. ($q > 3$).

FIRST RESULTS ON T.F.R.

*The T.F.R. Group**

ASSOCIATION EURATOM-CEA SUR LA FUSION
Département de Physique du Plasma et de la Fusion Contrôlée
Centre d'Etudes Nucléaires
Boite Postale n° 6. 92260 FONTENAY-AUX-ROSES (FRANCE)

I.- INTRODUCTION.-

The Tokamak program was started in Fontenay-aux-Roses in the beginning of 1970. The first T.F.R. (Tokamak de Fontenay-aux-Roses) experiment has been so designed as to explore the Tokamak scaling laws up to 400 kA currents and 60 kG toroidal magnetic fields. These parameters, extrapolating the results obtained in other laboratories [1], should bring about ion temperatures such that the diffusion regime be dominated by trapped particles. To get further into this regime, an additional heating using an injection of 10 A equivalent of 25 to 30 keV neutrals will be applied in a second step. Studying long discharges (up to 0.5 s) is also one of the purposes of this experiment. The impurity influx due to a long interaction between the plasma and the limiter can indeed considerably alter the energy balance in a Tokamak.

After a short description of the T.F.R. device, the first results obtained since the start of the experiment (March 1973) are presented. The maximum values of the current and the toroidal field were 200 kA and 40 kG.

II.- DESCRIPTION OF THE T.F.R. DEVICE.-

The main characteristics of the T.F.R. machine are shown on Fig.1 and listed below.

Table 1 : Basic parameters.

Major radius of the torus	0.98 m
Limiter radius	0.20 m
Maximum toroidal field	60 kG
Maximum expected plasma current	400 kA
Maximum discharge duration	0.5 sec

II.1. THE VACUUM SYSTEM AND THE LIMITERS.-

The vacuum vessel consists of 8 toroidal sections connected by 8 observation sections for diagnostics and pumping. All these elements are welded together. Each toroidal section is made of 0.5 mm thick inconel bellows bakable up to 450° C. The diagnostic sections are bakable up to 300° C. Two of them offer one horizontal and two vertical viewing ports through which a complete plasma diameter can be seen. Two others have been specially designed for a subsequent neutral injection heating.

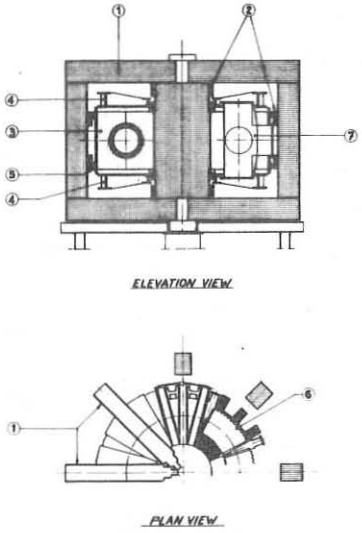

Fig.1 : Plan and elevation view of T.F.R.

1. *Magnetic circuit ;* 2. *Poloidal coils ;* 3. *Toroidal coils ;* 4. *Positioning plates ;* 5. *Precompression hoops ;* 6. *Vacuum vessel ;* 7. *Observation ports.*

The pumping circuit consists of a primary pump and two turbo-molecular pumps in series (600 l/s and 70 l/s). Two titanium pumps are also used in parallel with the turbo-molecular pumps in order to increase the pumping speed between two plasma discharges. The base pressure obtained after baking the chamber itself at 420° C and the observation sections at 200° C is 5.10^{-10} Torr. The outgassing rate of the walls is then 2.10^{-13} Torr.l.s.$^{-1}$ cm^{-2}.

The filling gas is let in through a fast valve with an indium joint, operated by a pneumatic system. A 100 mA electron gun helps to initiate the discharge breakdown at low filling pressures.

The walls of the vacuum chamber are protected by

- a removable limiter (radius 17 cm) which can be put on or out without opening the vacuum system,
- a main limiter (radius 20 cm) offering a curved surface to the plasma,
- several safety rings (radius 21.5 cm) for an extra shielding of the walls,
- two plates facing the neutral injection ports.

These four items are made of molybdenum.

The vacuum vessel is surrounded by the copper shell which will be described in another section. Between the liner and the shell a thermal insulation has been placed in order to reduce the heat losses when baking the liner. Magnetic pick-up coils for the measurement of plasma position modes of deformation and diamagnetism are imbedded in the thermal insulation.

II.2. THE TOROIDAL FIELD.-

II.2.1. The toroidal magnet [2].

It consist of 24 pyralene cooled Bitter type coils. Each coil consists of 35 turns of full hard copper plates containing 0.07 % silver. Each turn is insulated with polyimide sheets. Copper and insulators are stacked to form a helix, and clamped between two aluminum plates by bolts and spring washers.

Table II : Main electrical and thermal parameters.

Current for an on-axis field of 60 kG	35 000	A
Peak voltage	4 000	v
Peak power	120	MW
Energy dissipated per pulse	150	MJ
Mean power at full load and nominal repetition rate of 1 pulse every 4 minutes	600	kW
Adiabatic temperature rise	60°	C

The coils are cooled by "pyralene" circulating through slots in the body of the coil. The stresses resulting from the magnetic pressure are supported by the copper itself. They can reach 10 kg/mm^2. The toroidal centripetal force of 170 Tons is supported by the cylindrical core of the magnetic circuit, specially designed for that. The mechanical structure of the device is basically composed of two crown-like pieces between which the whole magnet structure is clamped with steel braces. This structure is reenforced by wedges bolted between the coils. This assembly will stand the torque resulting from the influence of the vertical field on the coils and additional forces that can arise in case of a short-circuit in one coil.

II.2.2. The power supply.

It consists of an alternator coupled to a flywheel storing 400 MJ at 6000 r.p.m., and driven through a gearbox by a 1.5 MW asynchronous motor running at 1500 r.p.m.. The alternator has been especially designed to deliver a power

of 120 MW in a pulsed regime. The overall pulse duration is 2 seconds and the repetition rate at full power is 1 pulse every 4 minutes.

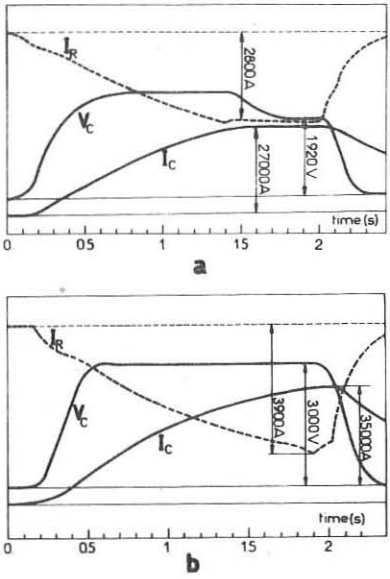

Fig.2 : Time evolution of current and voltage delivered by the rotating group to the load.

a/ *regime with overexcitation*
b/ *regime without overexcitation*

I_R : *rotor current*
V_c : *coil voltage*
I_c *coil current*

The excitation current is feedback controlled, which allows a preadjustment of the shape of the current delivered by the alternator. The rotor can thus be overexcited so as to reduce the current rise time (Fig. 2).

An optimisation of the alternator parameters for this pulsed operating mode has yielded a very high specific power : 10 MW/t compared to 3 MW/t for machines of a classical type.

The main characteristics of this alternator are the following :

. Rotor diameter	0.5 m
. Rotor length	2.2 m
. Overall mass of the alternator	15 t
. Flywheel mass	13.5 t

The system started in operation at the end of 1972 and the nominal power was reached in March 1973.

II.3. THE INDUCTION AND EQUILIBRIUM CIRCUIT.-

These circuits have two purposes

. to induce the current into the plasma
. to produce the vertical and horizontal fields needed for the plasma equilibrium.

This is achieved by means of two sets of coils and generators and by a copper shell.

II.3.1. The inductor circuit.

The coupling between the induction coils and the plasma current is provided by a laminated magnetic circuit. It consists of a central core and eight external branches. This circuit can be reverse biased in order to increase the flux variation during a pulse.

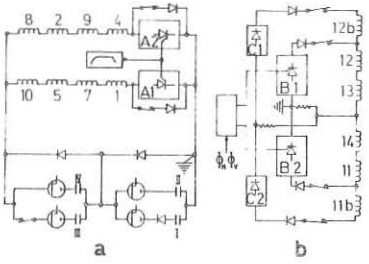

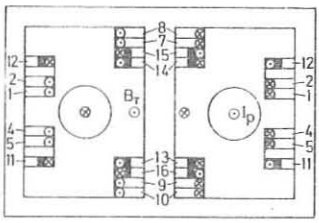

c

Fig. 3 -

a/*electrical diagram of the inducting circuit ;* b/*electrical diagram of the equilibrium circuit ;* c/*elevation view of the coils position. 15 and 16 are the premagnetisation coils in series with the toroidal coils.*

The induction coils generates the plasma current and produce a vertical stray field (roughly in phase with the plasma current) which is the main part of the equilibrium field.

The power source comprises a condenser bank to take care of current rise and a thyristor in series to maintain the current plateau (Fig.3). The condenser bank is crowbarred by diodes. The bank is divided into four sections : discharge breakdown, current rise (2 sections), additional pulse during the plateau. A safety device prevents the current rise section to fire whenever the breakdown of the gas fails. This prevents large electromechanical efforts along the cuts of the copper shell. The thyristor rectifiers are driven by a function generator that sets the current pulse shape.

Table IV : Parameters of the induction circuit.

Flux jump in the central core (with reverse biasing)	2 V.s
Energy stored in the condenser bank	800 kJ
Current rise time with various coupling	20-40 ms
Maximum plasma current	400 kA
Power available for the current plateau	3 MW
Maximum length of current pulse	0.5 s
Equilibrium field produced by the circuit	1600 G

II.3.2. The equilibrium circuit.

This circuit compensates the stray fields before the discharge breakdown and provides an adjustment of the vertical field, taking into account the variation of the internal energy of the plasma, the saturation of the iron etc ... It provides also a horizontal field. The energy is provided by diode rectifiers (C_1 and C_2) for stray field compensation and by thyristor rectifiers (B_1 and B_2) fig.3,whose current can be preprogrammed before the discharge and feedback controlled so that the copper shell be a magnetic surface. The horizontal field is created by an unbalance between the power supplies B_1 and B_2.

Table V : Parameters of the equilibrium circuit.

Power available for the equilibrium field	3 MW
Maximum vertical field produced by the circuit	400 G
Maximum rate of change of the vertical field	25 kG/s

A part of the equilibrium field can be provided by the copper shell, 1.5 cm thick with 8 meridian cuts (6 of theses cuts are short-circuited by removable straps). The penetration time for transverse field is about 80 ms (with straps). In normal operation the shell takes care of the equilibrium for small, fast displacement of the plasma.

II.4. DATA ACQUISITION SYSTEM.-

The experiment is connected to a computer (Télémécanique) through an optical-electronic link. This system collects different type of data:"industrial" measurements at 7 kHz, fast signals up to 1 MHz with digital oscilloscopes and signals from special diagnostics equipped with interfaces. All these data are recorded on a magnetic tape and are available for a subsequent processing. The computer also works on line giving, for each discharge, the control panel readings and a preliminary processing of the signals.

III.- EXPERIMENTAL RESULTS.-

The first plasma behaving as a Tokamak type discharge was obtained on March 28, 1973 after a very limited number of shots (about a hundred).

The data presented below result from a three month experimentation and are, therefore, of a preliminary character. During these three months, we have fired a total of 1100 discharges, most of which were aimed only at progressively

testing and tuning up all the components of the poloidal field system. In spite of this short experimentation time, we are getting to an already satisfactory description of the discharges and to significant achievements (200 kA maintained for 0.25 s). This can probably be attributed to the quality of the vacuum system. A small air leak has indeed shown the practical impossibility of getting good discharges in a polluted vacuum vessel with a base pressure of 10^{-7} Torr.

Several types of discharge have been observed. At high density ($n_e \simeq 10^{14}$ cm^{-3}), the discharge is of the disruptive type with negative voltage peaks ; the plasma resistance is high. At lower densities ($n_e \simeq 2$ to 6.10^{13} cm^{-3}) the voltage per turn drops to 2.5 Volts for a 200 kA current, and does not show peaks any more for the whole discharge duration, i.e. 0.25 s. Most of the data have been gathered without feedback control of the plasma position, for this type of discharge . A third type of discharge was obtained when the feedback centering of the plasma in the radial and vertical directions was in operation. It was then possible to make some of the discharges last more than 0.4 s with a negligible bulk motion of the plasma. Unfortunately, these tests were carried out on about ten shots only. They were interrupted by a puncture in the vacuum vessel due to the melting of a molybdenum part of the electron gun used for initiating the discharge.

A/ *Discharges with feedback.*-

In these experiments it was sought to make the shell a magnetic surface, i.e. to cancel the vertical and radial fluxes. The vertical field created by the equilibrium circuit is opposed to the strong vertical field of the primary winding. Thanks to this feedback, the discharge duration is between 430 and 460 ms, for a 100 to 120 kA current and a 25 to 30 kG toroidal field ; the plasma remains well centered ($\pm$ 1 cm in both directions) for most of the plateau duration (Fig. 4b).

In the first 50 milliseconds when the feedback cannot be felt, due to the shell time constant, the plasma centering has not been optimized. Such an optimisation will be made possible either by applying a correcting field produced by the diode rectifiers before the discharge breaks down, or by superimposing on the feedback a programming of the thyristors rectifiers. The large inward horizontal displacement observed during the last 50 milliseconds (Fig. 4b) is due to the magnetic circuit saturation and to the strong increase of the stray vertical field of the primary winding resulting from it

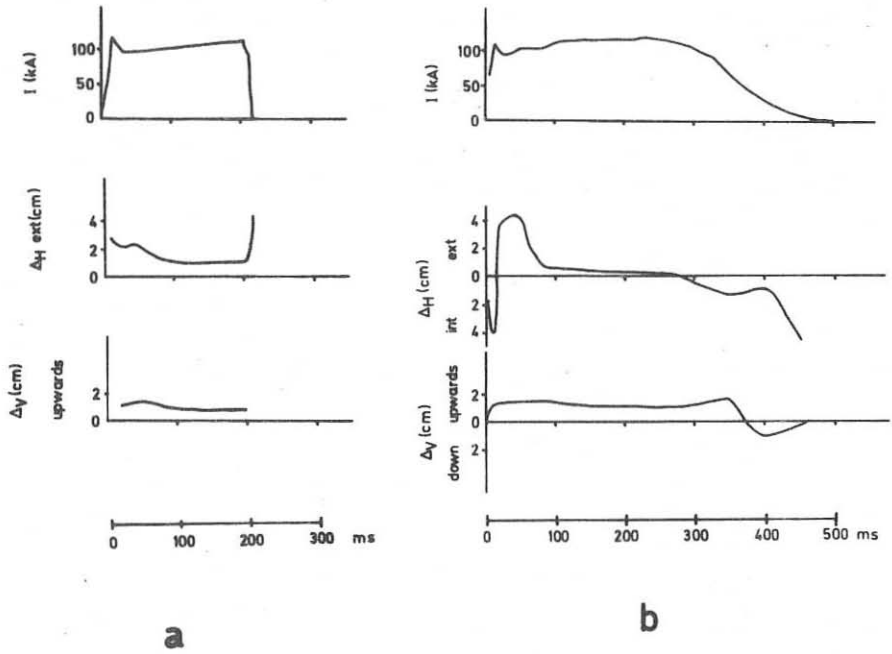

Fig. 4 - The plasma ring is piloted. Toroidal field B_T = 30 kgauss.

a/ *the current abruptly vanishes ; there is a fast drift of the ring outwards.*

b/ *the current slowly vanishes ; the magnetic circuit is satured and there is a fast drift of the ring inwards.*

In the course of these preliminary feedback tests, the discharge exhibited two different behaviours without any change in the parameter settings : the current would either end abruptly or slowly decay. The discharges with an abrupt end (Fig. 4a) stay well centered for 200-230 ms, then move quickly outwards in the last 5 to 10 ms. This fast displacement coincides with a positive voltage jump, and an explosive destruction of the plasma against the limiter with an intense emission of hard X rays and a shower of sparks. These sparks are molybdenum particles torn away from the limiter. These explosive discharges are characterised by weak oscillations on the $\frac{dI}{dt}$ signal.

The discharges with a slow decay (Fig.4b) have their duration limited by the magnetic circuit saturation, which causes a slow drift of the plasma towards the inside of the torus. These discharges are characterised by much larger oscillations on the $\frac{dI}{dt}$ signal.

B/ *A typical discharge without feedback : I_p = 200 kA ; B_T = 40 kG.*

This discharge is representative of most of the discharges created during this three months experimenting period. The current was maintained by thyristor rectifiers and the equilibrium was roughly established by the shell an a programmed vertical field. No compensation was applied to the radial field and the plasma had a slow vertical motion. An abrupt end of the current was always observed. The macroscopic properties of the discharge where very reproductible.

The filling gas for these discharges was deuterium injected in one section of the torus. The deuterium filling pressure just before breakdown was 4.10^{-5} Torr of D_2. The limiter used has a radius of 20 cm.

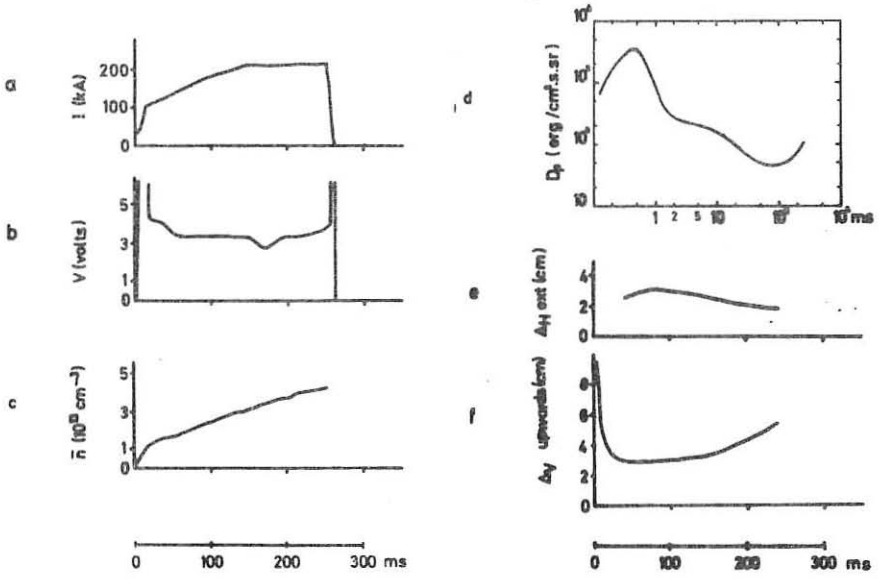

Fig. 5 - Typical discharge : $I_p \simeq 200$ kA $B_T = 40$ kgauss - filling pressure : $4\ 10^{-5}$ torr D_2

a/*plasma current ;* b/*measured loop voltage ;* c/*electron mean density ;* d/D_β *line measured at an angle position of 45° from the diaphragm and along a vertical diameter ;* e/*horizontal displacement ;* f/*vertical displacement.*

Fig. 5 shows the main characteristics of the discharge. The current fast rise is obtained by firing successively two capacitor banks. 8 ms apart. The abrupt ending at 250 ms was always observed in these discharges, it is a characteristic of the plasma, not of the external circuits. The voltage per turn exhibits a minimum of 2.8 volts at about 170 ms and increases again afterwards ; this increase is an essential fact that strongly influence the interpretations given in paragraph IV. After 100 ms the plasma is off-center by 3 cm outwards and 3 cm upwards, then it slowly drifts upwards. The hard X-ray is always very large in these discharges and appears very early.
The average electron density always increases with time during the discharge.

III.1. ELECTRON DENSITY PROFILE.-

The electron density profile is obtained thanks to a multichannel interferometer : 5 channels were used, whose locations are indicated on figure 6. The measurements are made along vertical chords at a frequency of 135 GHz ; the microwave source is a 3 Watts carcinotron.

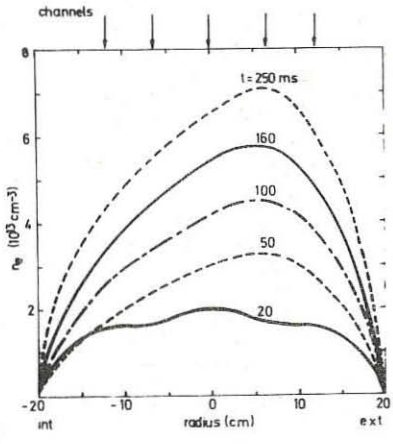

Fig. 6 - Time evolution of the electron density profile for the typical discharge.

The time evolution of the electron density profile is obtained by inversion of the Abel integral assuming zero density at the limiter radius. At 100 ms, the maximum density reaches nearly 5 x 10^{13} cm^{-3}. An outward displacement of the density maximum is noticeable ; this displacement is of larger amplitude than the displacement given by magnetic probe measurements (Fig.5e). With time, the density profile becomes more peaked and, towards the end of the discharge, the refraction is so large that the two extreme channels are unusable.

III.2. THOMSON SCATTERING MEASUREMENTS.-

The experimental set-up involves a 3 Joules, 20 ns ruby laser and a grating monochromator with ten fiber optics light guides and ten 56 TVP photomultipliers. The spatial resolution of the detection system is 3.3 cm vertically and 0.2 cm horizontally. The photomultipliers are pulsed for 10 μs. Channel 1 (centered on the laser line) is not usable because of the intense stray light and channels 4 and 5 can be used with great difficulty because of the D_α line. One is left, therefore, with a total of 7 usual channels.

The first measurements suggest an electron temperature of 2 to 3 keV, 100 ms after the onset of the discharge, for a volume element located in the mid-plane, 2 cm away (outwards) from the geometrical axis of the shell.

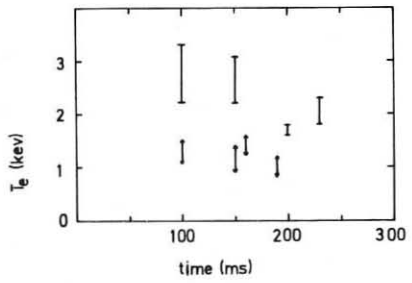

Fig. 7 - Central evolution temperature measured with Thomson scattering.

B_T = 40 kgauss I_p ~ 200 kA

B_T = 30 kgauss I_p ~ 140 kA

Each point is the mean value for 3 discharges.

Figure 7 shows the time evolution of the temperature for two sets of values of the plasma current and the toroidal field (200 kA, 40 kG and 140 kA, 30 kG). These results were got from a small number of shots (an average of three discharges for each experimental point), which explains the large error bars. They show that T_e increases with the current and decreases after 100 ms. This last statement should, however, be qualified ; it should be kept in mind that the plasma moves during the discharge. The measurements therefore could correspond to different regions of the plasma at each time.

III.3. BREMSSTRAHLUNG MEASUREMENTS.-

The flux of soft X-rays emitted by the plasma is monitored by 4 detectors, each comprising a 1 mm thick NaI scintillator and a photomultiplier. The whole system is placed in a horizontal viewing port whose vertical plane of symmetry makes an angle of 135° with the plane of the limiter. In front of each scintillator are placed two known absorbers ; the measurement reported here are relative to the two following absorbers : 75 μBe and 50 μBe + 20 μAl. The ratio of the X photon fluxes through these two absorbers goes through a maximum for

an electron temperature of 600 eV. This maximum is used to normalize the measured data, so that a relative calibration of the two channels is not necessary. Corrections due to impurity lines may be neglected in this case, although the X-ray flux is about 10 times that which a pure hydrogen plasma would emit.

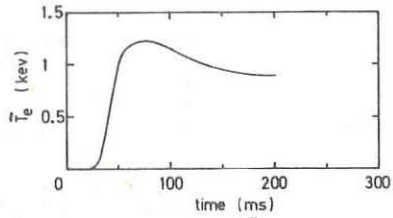

Fig. 8 - Time evolution of the mean electron temperature deduced from soft X-rays measurements.

The evolution of the electron temperature averaged over a horizontal chord 3 cm from the equatorial plane is shown on figure 8. This temperature goes through a maximum of 1.2 keV at the time 80 ms. From 200 ms on, the measurements are perturbed by the hard X radiation.

III.4. MEASUREMENT OF THE PLASMA NEUTRON EMISSION.-

The flux of neutrons emitted during the discharge has been measured with a BF_3 proportional counter surrounded with paraffin. The counter was placed above a vertical viewing port 1 m away from the magnetic axis. To decrease the X-ray flux, a 5 cm thick lead shield was placed between the port and the counter. Under these conditions it was possible to count single pulses due to neutron for the greatest part of the discharge (Fig. 9). A the end of the discharge, the pulse pile-up was too large for counting. In order to determine the source of the pulses delivered by the counter, a neutron absorbing shield made of a 30 cm thick paraffin layer and cadmium sheets was placed before the counter; under these conditions, the counting rate in the useful part of the discharge was reduced by a factor of 10. The counter has been calibrated in situ by moving a PuBe source along the geometry axis of the toroidal chamber.

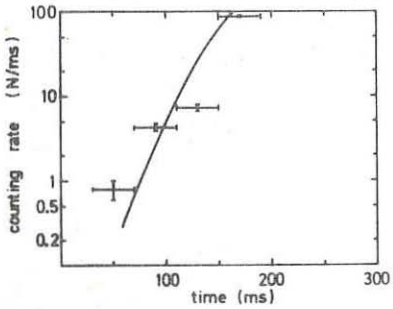

Fig. 9 - Time evolution of the counting rate of neutrons measured by a BF^3 counter. ⊢I⊣ experimental points. The curve is deduced from the numerical simulation described in § IV.

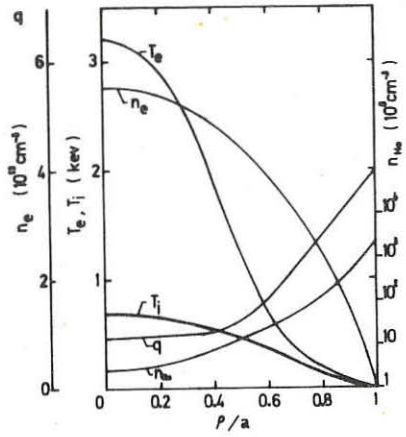

Fig. 10 -

Radial profiles at t = 150 ms obtained by the simulation model : T_e electronic temperature, n_e density of electrons, T_i ionic temperature, q safety factor and n_{H_o} density of neutrals.

the presently available measurements : voltage, radial profiles of electronic density, electronic temperatures on the axis by THOMSON scattering, the average electronic temperature which can be derived from the bremstrahlung measurements and finally the neutronic emission from the plasma if we assume $n_e \simeq n_D$.

We have represented on the Fig. 10 the results of the simulation for t = 150 ms. The values of some interesting parameters are derived from this simulation :

Energy confinement time	τ_E = 20 ms
Internal inductance	l_i = 1.6
Poloidal β	β = 0.3

we define the energy confinement time τ_E by the energy balance equation

$$\frac{dW}{dt} = Q - \frac{W}{\tau_E}$$

where W is the internal energy of the plasma (including electrons and ions) and Q the ohmic power. We do some comments on the radial profiles of the Fig. 10 :

- The electronic temperature has a "peaked" type profile like on S.T. [4].
- The ionic temperature on the axis (~ 700 eV) is in good agreement with the ARTSIMOVICH scaling law in plateau regime.
- The security factor q reaches the value 1 on the axis.
- The neutrals present in the plasma leads an important energy loss by charge exchange (40 to 50 %) in the ion energy balance.

The computed particle confinement time τ_p (4 milliseconds) is less than the energy confinement time · this is due to the fact that the renewal of the particles takes place preferentially on the external layers of the plasma which are cold. We have compared the computed and the measured flux of photons (D_β line), the computed flux is seven times bigger than the measured one.

This could be partly due to the position of the measurement section relatively to the diaphragm.

2/. For $t > 150$ ms, the continuation of the simulation gives divergent results with the measurements. The computed voltage continues to decrease while the measurements point out a significant increase. Moreover the measurements of the electronic temperature on the axis seem to indicate a cooling of the plasma while the computations given a heating.

We have tried an explanation of these facts by assuming an increase of heavy impurities concentration in the discharge (molybdenum for example). With a Z_{eff} continuously increasing with time from 2 to 10 (which corresponds to a final value of 1 or 2 % of molybdenum) and with an approximate expression of energy loss due to the radiations of these impurities we can explain very well the increase of the voltage. But, for this typical discharge, we cannot explain both the voltage increase and the temperature evolution on the axis.

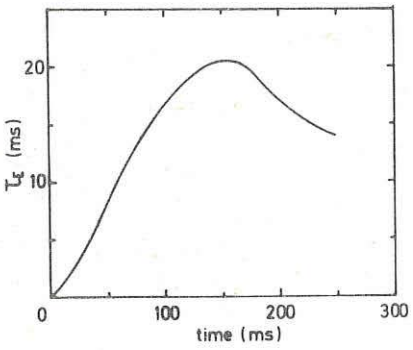

Fig. 11 - Time evolution of the energy confinement time τ_E obtained by the simulation.

It seems then quite normal to assume an increase of transport coefficients in the region of the plasma where $q < 1$. The radial profile of the electronic temperature stops then to be peaked and becomes more flattened (the same phenomena has been observed on S.T. where $q < 1$ [4]). The time evolution of the energy confinement time τ_E in this case is given in Fig. 11. The superposition of these two assumptions, increase of heavy impurities and turbulence in the region $q < 1$, leads to a consistent explanation of the first measurements on T.F.R. (Fig. 12).

3/. In the typical discharge, the discharge current is suddenly switched off. In view of finding a possible explanation of this fact, we carried on the computations with our model after 230 ms by maintaining constant the ratio of the entering flux of particles to the diffused flux (~ 1.07). This assumption is justified because in the previous phases of the discharge it has given a

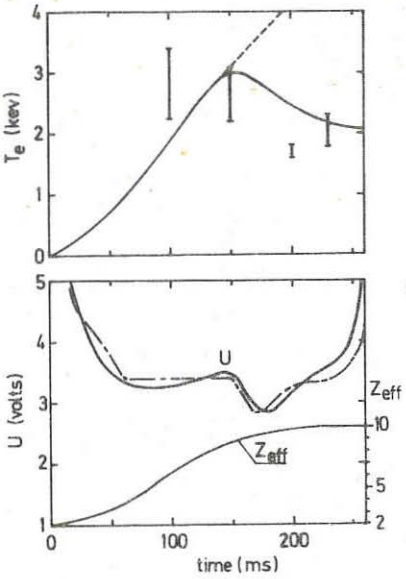

Fig. 12 - *Fig. 12 -*

Electron temperature on the axis $T_e(o)$ and voltage U vs time t, computed by the simulation with two assumptions (increase of heavy impurities and turbulence in the region q<1). On the upper figure $T_e(o)$ vs t , the dotted curve corresponds to computations without the assumption of turbulence in the region q<1. On the lower figure we have also represented the assumed Z_{eff}.

good fitting of the computed average density of electrons with the measured densities. By 250 ms the density profile becomes rapidly unstable, because the entering particles get ionized and stay in the external layers of the plasma : in few milliseconds there is a sensible increase of the particle density, particularly in the external layers of the plasma and the voltage increases very rapidly (Fig.12). These facts might explain the disruption of the discharge.

REFERENCES.-

[1] L.A.ARTSIMOVITCH, Nucl.Fusion 12 (1972).

D.L.DIMOCK et al., Nucl.Fusion 13 (1973).

G.G.KELLEY et al., 3nd Symposium on toroidal plasma confinement Garching, March 1973 - B3.

S.ITOH et al., 3nd Symposium on toroidal plasma confinement Garching, March 1973 - B4.

[2] P.H.REBUT et al., 4th Int.Conf.on Magnet Technology, Brookhaven (1973), p.60.

[3] C.MERCIER, SOUBBARAMAYER, Fifth European Conference on Controlled Fusion and Plasma Physics, Grenoble 1972 , Vol. II.

[4] W.STODIEK Fifth European Conference on Controlled Fusion and Plasma Physics, Grenoble 1972, Vol. II.

* THE T.F.R GROUP : P.H.REBUT A.BARIAUD C.BRETON, J.P.BUSSAC, J.P.CRENN R.DEI-CAS, C.DE MICHELIS, M.DELMAS, P.GINOT, J.P.GIRARD, C.GOURDON, F.HENNION, M.HUGUET, D.LAUNOIS, P.LECOUSTEY, D.MARTY, M.MATTIOLI, C.MERCIER, P.MORIETTE, P.PLATZ, P.PLINATE, Z.SLED, P.SMEULDERS, SOUBBARAMAYER, J.TACHON, A.TOROSSIAN, B.YA'AKOBI.

DIFFUSION IN TOROIDS - A REVIEW

R J Bickerton

UKAEA, Culham Laboratory, Abingdon, Berkshire, England

INTRODUCTION

If we assume that hydromagnetic stability and adequate magnetic surfaces can be achieved in toroidal systems then the key question is, what will be the residual (diffusive) rate at which particles and energy can cross the magnetic field to the wall? This question can be further subdivided; what will be the rates if the plasma is assumed completely stable with only Coulomb collisions and the thermal level of plasma waves as the contributing mechanisms? What will be the rates when instabilities are included, particularly the various trapped particle modes to which toroidal plasmas are prone? When it is recalled that ultimately the answers to these questions are required for a toroidal plasma with long mean-free path, $\beta \sim 10\%$ and with a significant fast (alpha) particle production rate through fusion reactions then the task appears daunting. Clearly definitive answers will only be obtained by experimental tests on an adequate scale. Such tests will be expensive and time-consuming; in the meanwhile we must increase our understanding of the containment in existing machines and of the underlying theory.

In the face of such complexity it is natural to look for general answers from thermodynamics. This has been done, particularly by Fowler[1], who assumed that the free energy of a confined plasma went into fluctuations; these fluctuations then leading to enhanced plasma transport. The upper bound on the particle diffusion coefficient found in this way is,

$$D_{\perp} \leqslant \alpha \frac{ckT}{eB} \qquad (1)$$

where $\alpha < 1$, its value depending on additional postulates to do with the nature and correlation of the fluctuations. Unfortunately we are interested

in the precise value of α, requiring $\alpha < \sim 2 \times 10^{-4}$ for an economic toroidal system[2].

Having failed to get much comfort from thermodynamics, one is then forced to return to the study of the problem in two parts - the classical loss rates and those produced by fluctuations.

The classical diffusion of plasma across a system of straight magnetic field lines was first discussed about sixty years ago[3]. Note that the cross field diffusion of a fully-ionized plasma has a special character. In a noraml diffusive process the diffusing particles move through a fixed background of scattering centres, but in the case of cross-field plasma diffusion the electrons, for example, scatter off the ions which are themselves diffusing at the same rate as the electrons. Each charge species crosses the magnetic field at the same rate due to the equal and opposite frictional forces between them, thus considering the electrons in a plane case with a density gradient in the x-direction and a magnetic field in the y-direction, plasma resistivity η , one has

$$V_x = \frac{F_y}{eB_z} \quad , \quad F_y = -e\eta j_y$$

$$j_y B_z = \frac{dn}{dx}(T_e + T_i) \rightarrow V_x = -\eta \frac{dn}{dx} \frac{(Te + Ti)}{B_z^2}$$

$$D_\perp = \eta \frac{(Te + Ti)}{B_z^2} \qquad ..(2)$$

The diffusion rate can also be derived from energy conservation, since in the absence of external driving fields the work done by the expanding plasma must equal that dissipated by the confining current, i.e.

$$-V_x(Te + Ti)\frac{dn}{dx} = j_y^2 \eta = \left\{\frac{(Te + Ti)}{B_z} \frac{dn}{dx}\right\}^2 \eta$$

$$V_x = -\frac{dn}{dx} \frac{(Te + Ti)}{B_z^2} \qquad ..(3)$$

These simple calculations illustrate two basic principles which apply not only to classical diffusion, but also to fluctuation driven diffusion. The first

is that particle flux across the field can only be the result of equal and opposite (frictional) forces on the two charge species; the second is that the work done by the expanding plasma must be dissipated in the plasma. These two principles are of course automatically satisfied by any rigorous calculation of classical diffusion but in the case of fluctuation-driven losses usually only "informed guesses" are possible and the principles have some value.

TOROIDAL GEOMETRY

A symmetric toroidal system has only one ignorable coordinate (φ) compared with two in plane and cylindrical geometry. The first consequence is that it is a non-trivial matter to find a self-consistent plasma equilibrium in a torus. Table I shows the assumed equilibria in various existing theories.[4,5] Evidently there is as yet no model which treats a self-consistent, long mean-free-path, collisional equilibrium even at low-β, let alone the values of ultimate interest. Thus present numerical calculations[6] are restricted to the use of toroidal transport coefficients in self-consistent calculations assuming cylindrical geometry.

The second and related consequence of toroidal geometry concerns the restrictions on particle motion. The conservation of canonical angular momentum of a particle about the symmetry axis may be written as

$$R\left(p_{\varphi} + \frac{e}{c} A_{\varphi}\right) = \text{constant}$$

where $R = R_o\ (1 + {}^{r}/_{R} \cos\theta)$, p_{φ} is the particle momentum in the φ direction and A_{φ} the vector potential of the magnetic field in the φ direction. Combining this with the conservation of particle energy leads to the so-called Tamm[7] theorem that the maximum radial departure of a particle orbit from the magnetic surface is

$$\delta_{MAX} = \frac{m\bar{v}c}{eB_{\theta}} = a_{\theta}$$

i.e. the gyro radius in the poloidal field component only.

If to these constraints is added the additional adiabatic invariant μ = constant, then the maximum excursion is reduced to[8]

$$\delta_{MAX} = \varepsilon^{\frac{1}{2}} a_\theta$$

this excursion being that for a particle just trapped in the toroidal magnetic field.

The full neo-classical theory of diffusion in a plasma toroid[5] takes these orbits into account and in particular the collisional interaction between trapped and untrapped particles. In the short mean free path case these effects are negligible and the loss rate is dominated by the resistive dissipation of the currents necessary to give plasma equilibrium in a torus. The results may be summarised as follows:- (see Fig. 1)

Short mean free path[9]

$$\lambda_{ei} \ll R/\varepsilon \qquad D_\perp = D_o\left(1 + \frac{1}{\varepsilon^2}\right) \qquad j_\theta = -\frac{dn}{dr}\frac{kT}{B_\varphi}$$

$$j_\varphi = -\frac{du}{dr}\frac{kT}{\varepsilon B_\varphi}\cos\theta$$

Intermediate mean free path

$$\frac{R}{\varepsilon} < \lambda_{ei} < R/\varepsilon^{\frac{3}{2}}\varepsilon \qquad D_\perp = (kTe)\frac{mc^2}{e^2 B_\varphi^2}\left(\frac{kT}{m}\right)^{\frac{1}{2}}\left(\frac{1}{\varepsilon R}\right) \qquad j_\theta = -\frac{dn}{dr}\frac{kT}{B_\varphi}$$

$$0 < j_{II} < -\frac{dn}{dr}\frac{\varepsilon^{\frac{1}{2}}kT}{B_\theta}$$

Long mean free path

$$\lambda_{ei} > \frac{R}{\varepsilon\varepsilon^{\frac{3}{2}}} \qquad D_\perp = D_o\left(1 + \frac{1}{\varepsilon^2\varepsilon^{\frac{3}{2}}}\right) \qquad j_\theta = -\frac{dn}{dr}\frac{kT}{B_\varphi}$$

$$j_{II} = -\varepsilon^{\frac{1}{2}}\frac{dn}{dr}\frac{kT}{B_\theta}$$

where D_o is the cross-field particle diffusion coefficient in a straight system (having $B = B_\varphi$). For thermal conductivity similar results hold with $\chi_i \sim (M/m)^{\frac{1}{2}}\chi_e$ due to the larger gyro radii of the ions.

It is of interest to write down the momentum equation for the gas of one charge species; Stringer[10] finds this to be,

$$\left\langle \frac{m_j}{2\pi q_j}\oint d\theta\, n\frac{dv_\varphi}{dt}(1 + \varepsilon\cos\theta)^2 \right\rangle$$

$$= B_\theta \Gamma_s + \left\langle n(E_\varphi - \eta j_\varphi)(1 + \varepsilon\cos\theta)^2 \right\rangle$$

where Γ_s is the particle flux across a magnetic surface and the averages are taken over a magnetic surface. In steady state diffusion the term on the left-hand side is zero since $\frac{dv_\varphi}{dt} = 0$ and the balance is between the two terms on the right-hand side.

In the short mean free-path (Pfirsch and Schlüter) regime the dissipation is entirely ohmic due to the containing current, and the momentum balance in the φ direction is maintained by the

$$\langle \eta j_\varphi \ (1 + \varepsilon \cos\theta)^2 \rangle$$

term despite the fact that $\oint d\theta \, j_\varphi = 0$ - i.e. there is no net toroidal current[11].

In the long mean free path case the dissipation is mainly due to magnetic pumping of the electrons[12] as they encounter a modulated magnetic field in carrying the diffusion driven current $j_{\parallel}$. The momentum balance is satisfied by the frictional force due to this net current density $j_\varphi \approx j_{\parallel}$ round the torus. This diffusion-driven current is a consequence of interaction between trapped and circulating particles. A full treatment including all cross-terms, heat fluxes etc. has been given by Rosenbluth et al[13]. For spatially uniform and equal temperatures they find,

$$j_{\parallel} = - 2.44 \ (r/R)^{\frac{1}{2}} \ \frac{(dp/dr)}{B_\theta}$$

With practical values of $r/R \sim 6$, this leads to $\beta_\theta \simeq 1$, a value too low for an economic Tokamak system[14] unless q = 1. If the pressure gradient is the result of a temperature gradient rather than a density gradient then the result is much less restrictive.

NON-SYMMETRIC SYSTEMS

In non-symmetric systems such as the stellarator there is no ignorable coordinate and angular momentum arguments cannot be applied. Indeed it has been shown[15] that there are particle orbits (super-bananas) which can depart from a magnetic surface by a distance totally unrelated to the gyro radius in either the poloidal or toroidal field. However, at high enough collision rates

these orbits are unimportant and then the diffusion takes place as though the system was symmetric with a mean poloidal field[16,17]

$$\bar{B}_\theta = \varepsilon \, B_\varphi$$

According to this work the diffusion driven current is also unaffected, although this point has been disputed[17].

FLUCTUATION INDUCED DIFFUSION

From the momentum equation we can say that if fluctuations are to increase the rate of particle diffusion then they must result in an equal and opposite toroidal force on the two charged species. This is an application to toroidal geometry of a principle first emphasized by Kadomtsev[18]. However it is interesting that a high frequency instability which only increases the electron-electron collision rate can change the particle diffusion by changing the diffusion driven current. Thus consider a long mean free path case in neo-classical theory and artificially increase the ratio ν_{ee}/ν_{ei} then one finds

$$j_\parallel \to \frac{p'}{B_\theta} \quad , \quad D_\perp \to \frac{nkT}{B_\theta^2}\,\eta$$

i.e. the toroidal current goes to the Bennett value required to contain the plasma in a pinch without B_φ, while the diffusion coefficient goes to the pseudo-classical value[20]. This effect ceases when the electron-electron collision rate is such that they are not trapped, the diffusion rate saturating at the intermediate value. (See Fig. 1). Thus in this model enhancing the electron-electron collision rate through high frequency fluctuations can increase the electron thermal conduction rate without limit but only serves to increase the particle flux to the intermediate value. However, most attention has been given to low frequency instabilities which could increase the effective ion-electron interaction[20,21]. This subject is too complex to review here.

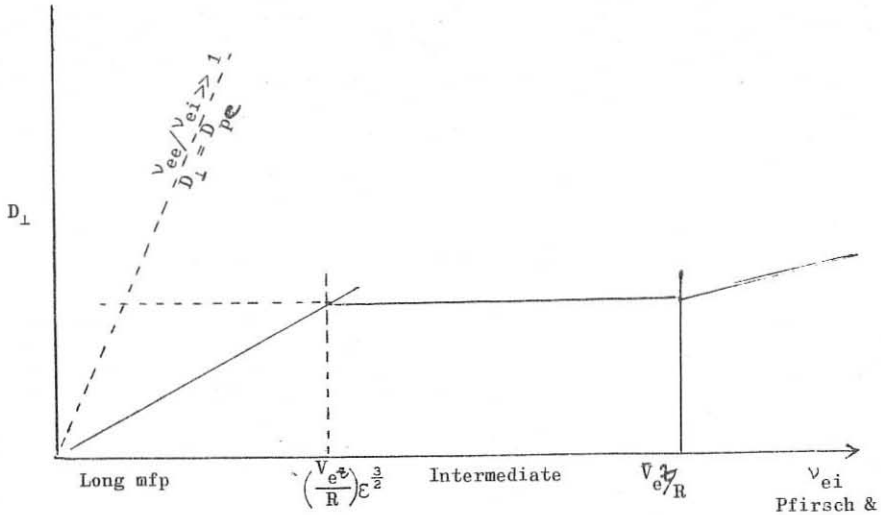

FIG. 1

EXPERIMENTAL EVIDENCE

What is the experimental evidence that classical or neo-classical diffusion ever occurs in practice? Table II lists the main parameters of those experiments in which detailed confirmation of classical theory has been claimed. Two are stellarators and two buried-ring devices. In the case of the stellarators it should be emphasized that many other machines not distinguished from these in any obvious way have not shown classical containment.

In the Wendelstein II experiments[22] the barium plasma was maintained in steady state by thermal ionisation on a hot ball in the centre of the plasma. Containment at rational transforms was poor but between these resonances containment in agreement within a factor 2 with that expected from the Pfirsch and Schlüter theory was obtained. The density was varied over a decade but the magnetic field by only ~ 50% and the plasma radius not at all. The transform was varied over about one order with the containment following the theoretical curve. The system had effectively zero shear.

In the Proto-Cleo experiment the shear is relatively high ($\theta \sim 0.1$) and the containment of pulsed plasmas has been studied over a wide range of

mean free paths[23]. It proved difficult to vary single parameters independently but on a universal plot of τ/τ_{ps} versus $R/2\lambda_{ei}$ the results showed remarkable agreement with the predictions of a theory modified to take account of the large ion-gyro radius ($\rho_{i\theta} > r$). (τ_{ps}= containment time predicted by Pfirsch and Schlüter). However, the diffusion driven current which should accompany the neo-classical diffusion was not found, throwing doubt on our understanding.

In the two buried ring devices $B\theta > B\varphi$ and so they can never test critically the neo-classical theory which shows the strongest effects when $B\theta \ll B\varphi$.

In the FM-1 Levitron[24] the confinement time is observed to follow classical scaling but absolutely 5-10 times below the predicted level until a critical number of Bohm times is reached, after which the confinement scales like Bohm. The maximum confinement observed corresponded to 300 x Bohm when $B\varphi/B\theta \sim \frac{1}{2}$. Higher values give poorer containment as do lower ones, although in the latter case flute modes are expected and seen.

In the San Diego octopole experiments full confirmation of the transport theory from the Pfirsch and Schlüter to the banana regime is claimed[25]. However, because of the small ratio between $B\varphi$ and $B\theta$ the difference in loss rates in the various regimes is only ~3.

Thus we must conclude that we do not have a convincing experimental demonstration of neo-classical containment theory. In the only case where this might have been obtained (Proto-Cleo) an essential prediction of the theory was not confirmed. The results on FM-1 indicate that in a levitron with $B\varphi \gg B\theta$ instabilities would make such a confirmation impossible.

Much work has been done in applying the neo-classical theory to Tokamaks Duchs[26] has listed the various respects in which the resulting predictions differ from the observations:-

(i) skin effect predicted but not observed

(ii) temperature profile - again skin effects predicted but not seen

(iii) density profile too peaked in model

(iv) E_z field predicted 20-30 times lower than measured

(v) particle and energy containment times predicted $\sim 10^2$ longer than observed.

In this situation a variety of recipes have been used to modify the coefficients to take account of instabilities. These recipes are of course not unique, and in the absence of stronger theoretical backing they can only be evaluated by their success in predicting the performance of the larger machines T-10 and PLT which will extend the parameter range.

SUMMARY.

(i) The theory of classical containment in toroids has undergone a dramatic revision in the last few years to take account of trapped particles. The consequence is a substantial reduction in the expected containment times.

(ii) There is some evidence to support this theory from experiments on systems with vacuum fields such as multipoles and stellarators. However the evidence is not conclusive and is in any case limited to low temperature plasmas.

(iii) In driven systems such as tokomaks the observed containment properties bear little relation to the neo-classical theory. Particular discrepancies are that the theory gives the wrong value for the radial particle flux while the observed thermal transport due to the electrons is ~ 2 orders larger than the theory predicts. Among possible explanations for these discrepancies are :-

(a) lack of adequate self-consistency in the theory when applied to driven systems.

(b) hydromagnetic instabilities

(c) high frequency instabilities giving enhanced

thermal transport.

(d) low frequency instabilities increasing particle fluxes.

(e) failure to form magnetic surfaces.

Experimentally these questions will be answered by extending the range of parameters, in particular by increasing the discharge current, and by more searching diagnosis of existing experiments, e.g. detailed measurements of fluctuating quantities inside the plasma.

TABLE I

EQUILIBRIA

CALCULATION	FIELDS	RESULTS	REMARKS
MHD EQUILIBRIUM $\sigma = \infty$	SELF-CONSISTENT	$\beta_\theta \leqslant R/a$	NO RESULT ON DIFFUSION
RESISITIVE MHD PLASMA TOROID (4) $\sigma \neq \infty$	$(B_r, B_\theta, B_z) =$ $(0, B_\theta(1-\varepsilon \Lambda \cos\theta), \frac{B_o}{h})$ $B_\theta \ll B_o$	VALID FOR $\beta_\theta \lesssim 1$	EQUILIB. $\beta_\theta = \frac{1}{q^2}$ $\beta_\theta > \frac{1}{q^2} \rightarrow$ Pfirsch & Schlüter LOSS RATE
PARTICLE MODEL NEO-CLASSICAL DIFFUSION (5) $\sigma \neq \infty$	$(B_r, B_\theta, B_z) =$ $\left(0, \frac{b(r)}{h}, B_o/h\right)$ $h = R_o(1 + \varepsilon \cos\theta)$ $b \ll B_o$	VALID FOR $\beta_\theta \lesssim 1$ TRANSPORT	$\bar{j} \wedge \bar{B} = \nabla p$ but $\bar{j} \neq$ curl $\bar{B}$ ONLY SELF-CONSISTENT IN SEPARATE CYL. CALC. USING "TOROIDAL" COEFFICIENTS

TABLE II

EXPERIMENTS

	R (cms)	r (cms)	q	n (cms^{-3})	T_e (eV)	τ_p (secs)	τ/τ_B
W II ba. STELLARATOR	50	4	5	10^9	0.18	~ 1	~ 10^2
PROTO-CLEO STELLARATOR	40	4	3	10^9-10^{11}	~ 2.0	~5×10^{-3}	~ 10
FM-1 LEVITRON	150	~ 50	0-0.3	10^{10}-10^{12}	0.1-1.0	~ 1	< 300
SAN DIEGO OCTOPOLE	300	~ 100	0-0.3	10^{10}	0.05-1.5	0.1	~ 10^2

REFERENCES

1. Fowler T.K., "Advances in Plasma Physics" I, 201, 1968 (John Wiley).
2. Carruthers R.C et al. Reactor Study. Culham Report R89 (1969).
3. Townsend, J. Electricity in Gases (1915).
4. Kadomtsev, B.B., and Shafranov, V.D., Dok.Acad.Nauk. SSSR 167, 6, 1273 1966)
5. Galeev, A.A. and Sagdeev, R.Z., Sov.Phys. JETP 26, 233 (1968).
6. Mercier, C. Vth European Conference on Controlled Fusion & Plasma Physics II, 157, Grenoble (1972).
7. Tamm, I.E., "Plasma Physics and Problems of Controlled Thermonuclear Reactions, I, Acad Nauk SSSR (1958) 3
8. Furth, H.P., and Rosenbluth, M.N. Paper CN-24/F-1, IAEA Conference Novosibirsk (1968)
9. Pfirsch, D., Schlüter, A. Max Planck Institute Report MPI/PA/7 (1962)
10. Stringer, T.E., Proc. IAEA Conference, Madison (1971), 2, 383
11. Bickerton, R.J., Nuclear Fusion, 13, 290 (1973)
12. Bickerton, R.J., Nuclear Fusion, 12, 609 (1972)
13. Rosenbluth, M.N. Hazeltine, R.D., and Hinton, F.L., Phys.Fluids, 15 116 (1972).
14. Gibson, A., Hancox, R., and Bickerton, R.J. Proc. IAEA Conference, Madison, III, 375 (1971).
15. Gibson, A., Taylor, J.B., Phys. Fluids 10 (1967) 2653
16. Stringer, T.E., Third Int. Symposium on Toroidal Confinement, F1-I Garching (1973)
17. Taylor, J.B. et al. Vth European Conference on Controlled Fusion & Plamsma Physics, I, Paper 15, Grenoble (1972).
18. Pfirsch, D., Nuc. Fusion 12, 728 (1972)
19. Kadomtsev, B.B., "P asma Turbulence", Academic Press, 28 (1965)
20. Yoshikawa, S. and Christofilos N.C., Proc. IAEA Conference, Madison, II, 357 (1971)
21. Kadomtsev, B.B., and Pogutse, O.P. Nuclear Fusion II, 67 (1971)
22. Berkl, E., Eckhardt, D., von Gierke, G., Grieger, G. Hinnov, E., von Hagenow, K.V., Ohlendorf, W., Proc. IAEA Conference, Novosibirsk 513 (1968)
23. Bolton, R.A.E., Hugill, J., Lees, D.J., Millar, W., Reynolds, P., Proc. IAEA Conference, Madison, III, 79 (1971).
    Adlam, J H., et al. Proc. IAEA Conference, Novosibirsk, I, 573 (1968)

24. Yoshikawa, S., Third International Symposium on Toroidal Confinement, C2-I, Garching (1973)
Chen, K., Meade, D., Okabayashi, M.,
Schmidt, J.A., and Yoshikawa, S. C8.

25. Ohkawa, T., Tamano, T., and Prater, R. Vth European Conference on Controlled Fusion (Grenoble) II, 25, (1972)

26. Duchs D., Third Int. Symposium on Toroidal Confinement, B10-I, Garching (1972)

TOKAMAK HEATING BY NEUTRAL BEAMS AND ADIABATIC COMPRESSION

H. P. FURTH
Plasma Physics Laboratory, Princeton University
Princeton, New Jersey 08540, USA

"Realistic" models of tokamak energy confinement strongly favor reactor operation at the maximum MHD-stable β-value, in order to maximize plasma density. Ohmic heating is unsuitable for this purpose. Neutral-beam heating plus compression is well suited; however, very large requirements on device size and injection power seem likely for a DT ignition experiment using a Maxwellian plasma. Results of the ATC experiment are reviewed, including Ohmic heating, neutral-beam heating, and production of two-energy-component plasmas (energetic deuteron population in deuterium "target plasma"). A modest extrapolation of present ATC parameters could give zero-power conditions in a DT experiment of the two-energy-component type.

I. Introduction

Classical or pseudoclassical energy confinement in tokamaks[1] would imply that $n\tau_E$ is independent of plasma density. The heating power required to meet an $n\tau_E$-criterion at given temperature can then be minimized conveniently by going to low density — and correspondingly long energy confinement time.[2,3] On the other hand, scaling laws based on trapped-particle instabilities[1] imply $n\tau_E \propto n^2$, and therefore strongly favor operation at the maximum density consistent with MHD limitations[4] on β.

Some familiar theoretical (or semi-theoretical) models[1] have been used in Fig. 1 to indicate a possible scaling of confinement with rising temperature.[5] The solid line represents the expected value of central $n\tau_E$ as a function of space-averaged T_e, for a tokamak current $I = 1$ MA, toroidal field parameter $b_t \equiv B_t/50$ kG $= 1$, aspect ratio parameter $A \equiv R/3a = 1$, poloidal electron beta $\beta_{pe} \equiv 8\pi n T_e/B_p^2 = 1$, and effective ionic charge $Z_{eff} = 1$. For different values of I, b_t, A, β_{pe} and Z_{eff}, each line segment should be displaced as shown by the respective arrows; the length of each arrow represents a factor-of-10 increase in I or its coefficient. (Lowest practical aspect ratios $R/a \sim 3$ are favored, since they maximize I; for safety factor $q \sim 2.5$, and $T_i \sim T_e$ one then has $\beta \sim 0.036\beta_{pe}$.) The diagram of Fig. 1 should not be taken

too seriously as a source of quantitative predictions about confinement, but it will serve to orient the present discussion of the tokamak heating problem. For simplicity, the discussion is specialized to tokamaks of circular minor cross-section, though vertical elongation has important potential advantages.

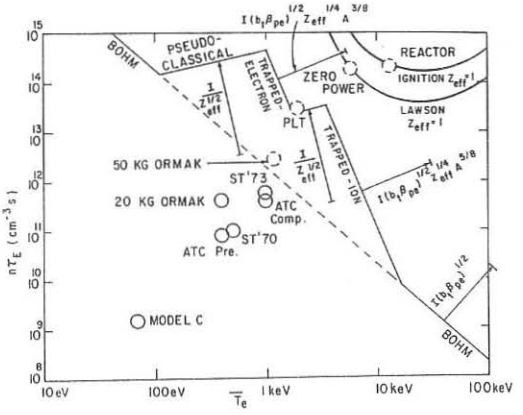

Fig. 1. Illustration of hypothetical scaling laws in relation to Lawson diagram.

Ohmic heating in the presence of Bremsstrahlung cooling and K times pseudo-classical energy transport would imply

$$\beta_{pe} \sim \frac{1}{2}\,[K + (I/1.6)^2]^{-1/2} \qquad (1)$$

where I is in MA. (The result is independent of Z_{eff}.) For large tokamaks, the β_{pe}-values given by Eq. (1) would thus fall well below the permissible MHD limit $\beta_{pe} \lesssim R/2a \sim 1$ — even if K were not large and if there were no line or synchrotron radiation losses. In the context of Fig. 1, we see that for pseudoclassical $n\tau_E$-scaling, a low β_{pe}-value does not matter; however, for the probably more relevant trapped-ion-mode scaling, the β_{pe}-value matters greatly. To offset the reduction of β_{pe} from 1.0 to 0.1, would require an increase of I by a factor of 3.2 — corresponding to a probable increase of 15-20 in device cost. The following discussion is therefore oriented towards the realization of β_{pe}-values of order unity (β-values of ~4%), by non-Ohmic heating methods: specifically, high-powered neutral-beam injection and adiabatic compression.

II. Adiabatic Compression

Adiabatic compression[6-9] occupies a unique place in tokamak heating technology. Being reversible, it is not among the primary methods for energizing the plasma: Ohmic, high-frequency and beam heating. Rather, it is a method for transforming the parameters of

tokamak plasmas from an initial irreversible heating phase at low magnetic field, density and temperature, to a final phase at high field, density and temperature. This transformation is not always advantageous compared with the alternative of heating irreversibly in the high-field phase. However, in particular applications, for example as an adjunct to Ohmic heating against radiation cooling, it can have significant advantages.[10] Some scaling laws for adiabatic compression of well-conducting tokamak plasmas at, respectively, constant R or constant B_t are given in Table I.

TABLE I

	B_t-compression, Constant R	R-compression, Constant B_t
Minor radius a	C^{-1}	$C^{-1/2}$
Major radius R	constant	C^{-1}
Density n	C^{2}	C^{2}
Temperature T	$C^{4/3}$	$C^{4/3}$
Plasma Current I	constant	C
Plasma β_p	$C^{4/3}$	$C^{1/3}$
Plasma β_t	$C^{-2/3}$	$C^{4/3}$
Safety factor q	constant	constant
Aspect ratio R/a	C	$C^{-1/2}$

Experimentally, the compression of the tokamak discharge in either minor[6] or major[9] radius appears to function well. Present-day compression experiments are somewhat too small to give good adiabaticity (i.e., they do not obey $\tau_{comp} \ll \tau_E$); even so, the plasma parameters obtained have been quite satisfactory. In the ATC (Fig. 2), compression of an Ohmically-heated plasma gives peak values[9] $n \sim 10^{14}\,cm^{-3}$, $T_e \sim 2.5$ keV, $T_i \sim 600$ eV. Comparable temperatures have been obtained in the somewhat larger T-4 and ST tokamaks, but the 5-fold volume-compression in the ATC permits exceptionally high particle and energy densities to be reached.

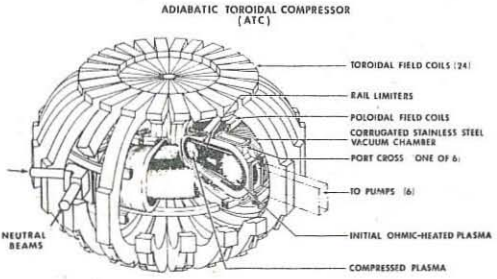

Fig. 2. Schematic of ATC. Neutral beams are tangential to torus magnetic axis.

The most useful type of adiabatic compression for practical thermonuclear purposes appears to be the compression in R at fixed B_t, rather than

the converse: both because it gives the most appropriate final plasma parameters (high current, high β, low aspect ratio), and because it avoids the necessity of pulsing the very large energy contained in the toroidal field. Considerably less optimism about energy confinement is required to envisage ignition in a larger device of the ATC type than with simple Ohmic heating.[10] Nonetheless, the technique of Ohmic heating plus compression over practical ranges of R does not exploit the maximum β-values permitted by MHD considerations.

The use of irreversible compression[11] in R by a rapidly modulated vertical field ($\tau_{comp} \lesssim \tau_{ii}$) would in principle permit continuous heating to high β-values. An extension of this technique to strongly R-dependent vertical fields[12] appears to enhance its engineering feasibility. Other high-frequency techniques — ion sound or cyclotron heating,[13] and heating at the lower hybrid frequency[14] — also appear promising, especially when used in conjunction with adiabatic compression, which lowers ω_p and ω_c in the precompression plasma, and multiplies the effective input power. The present discussion, however, will focus on the possibilities of neutral-beam injection, alone or in conjunction with adiabatic compression.

III. Neutral-Beam Heating

The injection of toroidal plasma with energetic neutral beams has long been a theoretically attractive possibility: in a closed system, the beam need not build up the plasma density, but need merely serve as a source of heat: a single injected particle can provide the thermal energy of 10-100 "hot" plasma particles. The advent of multi-ampere neutral-beam sources[15,16] with energies in the range 10-30 keV has now made neutral injection a practical experimental approach for tokamaks.[2,17,18]

Initial beam-injection experiments on the ATC device[19] (Fig. 3) have made use of a 30-45 kW, ~15 keV beam, from one of two sources of ~70 kW maximum capability each, which were developed and built at the Lawrence Berkeley Laboratory.[16] Several times larger powers can be injected with a peak energy component of 30 keV from the four guns of the ORMAK device.[17] Even allowing for imperfect energy transfer to the plasma ions, these injected powers are competitive with the 50-100 kW input from electrons to ions in present-day

Ohmic-heated tokamaks. Sources with individual ratings approaching 1 MW are now being developed; their capabilities should be well suited to the heating requirements of next-generation tokamaks.

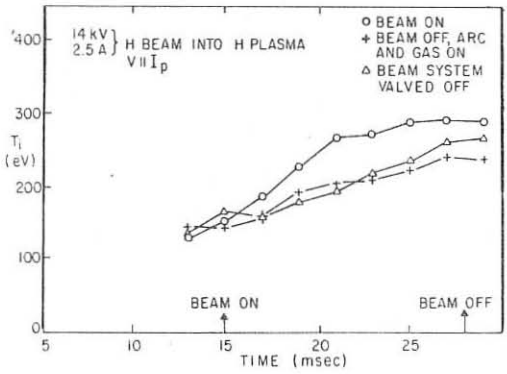

Fig. 3. Hydrogen beam injection into precompression ATC hydrogen plasma, with $\overline{T}_e$ ~ 700 eV, n = $1.5 \cdot 10^{13} cm^{-3}$, and I = 60-70 kA.

To obtain sufficient trapping of the injected beam in a tokamak discharge is not difficult, owing to the high ionizing power of the plasma target. (For tangential injection into ATC, for example, essentially all the beam is trapped — though not all into contained ion orbits.[2]) The real problem for tokamaks is excessively good trapping, which will force the use of inconveniently high beam energies (>200 keV) to reach the central plasma regions of large future devices.[3] The penetration problem can be solved, of course, by envisaging operation at low densities, but this approach requires almost the same degree of optimism about plasma energy confinement that is required for Ohmic heating to ignition (see above).

The confinement of injected ion orbits in present-day tokamaks with currents of ~100 kA (60-70 kA for precompression ATC) is rather poor even for ≲15-keV particles. Tangential injection is, in fact, a necessity, since most of the trapped-particle orbits would leave the plasma. (The associated anisotropy of the energetic ion population may possibly become a cause of velocity-space instabilities at higher heating powers.) The orbit-confinement problem will be eased greatly in future tokamaks at the 1-MA level and beyond. Another hypothetical source of trouble is the induction of local or global plasma rotations by the injected beam momentum.[20] At present power levels of the ATC[19] and CLEO[21] experiments, there has been no overt evidence of either velocity-space or rotational effects.

Following the trapping of a neutral-beam particle into a confined orbit, the resultant energetic ion slows down by collision

with the plasma particles, or is lost by charge-exchange (and possibly retrapped before leaving the plasma). For injected ion energy $W \sim 15\,T_e$, the rate of energy transfer to electrons and ions is equal; at higher energies, the heating of electrons predominates. In large tokamaks, this consideration is unimportant, since the $n\tau$-value for electron-ion equilibration is shorter than that for ignition; however, in present-day experiments, ion heating is favored significantly by low-energy injection. The slowing-down time of the injected ions, for example in ATC,[19] is of order 10 msec; since charge-exchange times in a typical neutral atom background of $\sim 10^9 cm^{-3}$ are of order 5 msec, the charge-exchange loss of injected ions is a dominant consideration in the energetics.[22] (H. P. Eubank points out that, in the present parameter range, raising the injection voltage could actually lower the power input into the plasma ions!) Since the slowing-down of injected ions in large tokamaks of the future will be in the 100-msec range, it is fortunate that neutral atom densities well below $10^8 cm^{-3}$ are expected on the interior of these plasmas.

The total plasma ion energy rise in the ATC experiment[19] is of order 30 J, and takes place in 5-10 msec, i.e., following injection of ~200 J of beam energy. This result is roughly as expected[2,22]: two-thirds of the beam energy is lost before thermalization, and about half of the remainder goes into the plasma ions.

In next-generation tokamak experiments, such as the PLT device (a = 45 cm, R = 135 cm, B = 50 kG), fairly large heating powers would be required to reach the $\beta_{pe} \sim 1$ regime. About half a megajoule of energy would then be stored in the plasma; the required power input into the plasma particles would be of order 5 MW. At an appropriate injection energy for beam penetration (~50 keV), the efficiency of neutralization for positive source ions would still be moderately good (50-60%). A total input power of 10 MW at the ion gun might thus suffice to give the desired plasma β-value, and this appears feasible from the point of view of neutral-beam technology. In order to carry out such a plan in practice, a solution must first be found to the problem of wall-atom-sputtering by charge-exchange neutrals, which threatens to become a source of intolerable plasma impurity levels for tokamaks with keV-range ion temperatures.[23]

In proceeding to still larger tokamaks, intended to approach ignition conditions, one technical problem will be the need to operate at much higher injection energies, where the neutralization efficiency for positive ions becomes small. A second problem has to do with the uncertainty regarding the minimum plasma size required to meet the $n\tau_E$-criterion. If confinement scales with temperature in the manner illustrated in Fig. 1, a tokamak current of ~10 MA would be sufficient, corresponding to a plasma energy content of ~300 MJ, and a heating power of ~100 MW deposited into the plasma particles.

IV. Compression of Injection-Heated Plasmas

In the ATC experiment,[19] the moderate ion temperature increments of 30-50 eV produced by neutral-beam injection at 30-45 kW can be amplified ~3-fold by compression. ATC data taken in the preheating phase are still insufficient to establish the functional dependence of T_i on injection power: If the dependence is roughly linear, then the total ATC ion-heating capability is equivalent to ~3 times the maximum preheat injection power, i.e., about 400 kW. If the dependence is weaker than linear, the equivalent power of injection plus compression would be increased substantially.

There are several other potential advantages of compression in the context of injection-heating larger tokamak plasmas. The problem of beam penetration is solved by injecting into the precompression plasma, where the product na is reduced by the factor $(R_1/R_o)^{3/2}$. Furthermore, since the compression amplifies the initial energy input by the factor $(R_o/R_1)^{4/3}$, the energetic efficiency of the source becomes a far less critical consideration in the over-all energetics. The impurity-evolution problem is not so severe in the precompression state, and one can hope to maintain good purity at least transiently in the compressed plasma by keeping it from making wall or limiter contact.[24] Finally, plasma decompression at the end of the cycle has the attraction of recovering the energy of the plasma (and charged reaction products) with an efficiency $1 - (R_1/R_o)^{4/3}$. This is of appreciable interest in regard to reactor economics, and also in regard to the nontrivial problem of terminating a larger tokamak discharge in a harmless fashion.

The principal draw-back of compression (of the ATC-type) is the added magnetic field volume required by the plasma motion: the total toroidal field energy, however, would be enhanced only by factors of 2-3 in an optimized coil system. If magnetic divertors must be incorporated into tokamaks to solve the impurity problem, as now seems likely, magnetic energy enhancement factors of order 2-3 may no longer appear excessive.

V. Two-Energy-Component Reactors

A conventional toroidal reactor can achieve arbitrarily large amplification factors for fusion power output relative to plasma heating power input, by operating sufficiently close to the "ignition condition" of Fig. 1. Alternatively, it is possible to envisage useful reactors with quite small power-amplification factors, as in the case of mirror machines. For this type of operation, a promising toroidal system is the so-called two-energy-component reactor, or "wet-wood burner." As shown in Ref. 25, an energetic deuteron beam (100-200 keV) decelerating in a toroidally confined tritium plasma with moderate electron temperature (T_e = 5-10 keV) and arbitrary ion temperature, can achieve somewhat better power amplification than a conventional-mirror machine, and about the same amplification as a two-component mirror reactor.[26]

A conventional toroidal reactor operated near ignition is obviously preferable to the wet-wood burner as a long-range goal for large-scale economic power production. The main drawback from the point of view of present-day reactor experiments is that the minimum size of a reactor plasma is not yet known. The linear size of the plasma must scale as $a \propto D^{1/2}$, where D is a measure of the energy transport coefficient; the cost scales roughly as $\$ \propto D^{5/4}$; unfortunately, authoritative present-day opinions concerning the magnitude of D in a reactor plasma range over considerably more than a factor of 10. An encouraging element in the situation is that an effective increase in confinement could apparently be obtained at reduced cost by improving the design of the torus minor cross-section,[27] instead of increasing its overall scale. In relation to the plasma heating problem, it is useful to note that the required power scales as $P \propto D^{3/2}$. On the other hand, once D is known for conventional reactors, the dependence of heating power on size is rather weak, scaling as $P \propto a$. The

experimental operation of next-generation tokamaks should serve to reduce the uncertainty in D substantially.

The wet-wood-burner approach has the significant short-range advantage that the required plasma target has parameters similar to those obtained in present-day experiments on small tokamaks. The required injection power and the output power are extremely steep functions of size ($P \propto a^3$) so that the plasma of a wet-wood burner both can be, and indeed has to be, rather small, even for injection powers as high as 100 MW. Accordingly, the size of the required tokamak plasma target can be estimated fairly accurately (something like the plasmas in PLT or T-10). Whether the approach of marginal power amplification in a tokamak is of genuine economic interest, of course, remains an open question. Addition of a fissionable blanket would eliminate all doubts about the power economics, but would reintroduce some other drawbacks that fusion power is intended to surmount. Attainment of a zero-power tokamak wet-wood burner thus seems more likely to stimulate interest in progressing to a conventional tokamak reactor, than to supplant it as a practical goal.

Initial experiments on the ATC[19] are testing some of the mechanisms of the wet-wood burner approach. A deuterium beam of ~15 keV, ~3 A, was injected into a precompression deuterium plasma of $\bar{T}_e \sim 600$ eV (Fig. 4). The slowing-down of the injected ions can be determined both from direct observation of tangentially emitted charge-exchange neutrals and from the decay of the neutron emission after beam shut-off. The observed decay rate of ~1 keV/msec is roughly consistent with expectation. The neutron production rate of $\sim 5 \cdot 10^8 \text{sec}^{-1}$ appears slightly too low (by a factor of ~2), but this remains to be verified. When the plasma is compressed immediately following injection, the neutron production rate increases to $\sim 5 \cdot 10^{10} \text{sec}^{-1}$,

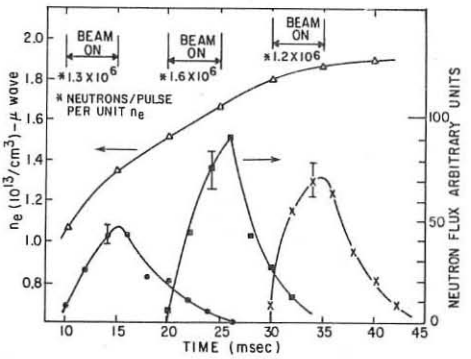

Fig. 4. Deuterium beam injection into ATC deuterium plasma. Ratio of neutron yield to electron density is roughly constant throughout discharge time.

again somewhat below expectation, perhaps because of noncontainment of the most energetic ion orbits.

As an introductory example of the two-energy-component idea, it is of interest to consider an uneconomical "mini-reactor" with about the same plasma parameters and dimensions as the compressed plasma in ATC: $n \sim 10^{14}\text{cm}^{-3}$, $\bar{T}_e \sim 2$ keV, a volume of $\sim 10^5\text{cm}^3$, and a current of ~200 kA. If this plasma is tritium, injected with 500 kW of 60 keV deuterons, the result is ~50 kW of fusion products. The required reaction time of the energetic deuterons is ~10 msec. Evidently, the charge-exchange and orbit-confinement problems in ATC would need to be improved somewhat — and, of course, velocity-space instabilities[28] are assumed to be absent. The present measured neutron-production density of $\sim 10^6\text{cm}^{-3}\text{sec}^{-1}$ in ATC, would rise to $\sim 10^9\text{cm}^{-3}\text{sec}^{-1}$, if one were to use a tritium target plasma and deuterons of 60 keV initial energy. The energetic deuteron density would rise from the present level of $\sim 10^{11}\text{cm}^{-3}$ to the β_p-limited density of $\sim 10^{13}\text{cm}^{-3}$, and the neutron production would reach the desired operating level of $\sim 10^{11}\text{cm}^{-3}\text{sec}^{-1}$. This is about the same reaction rate as that in a conventional DT plasma at $n = 10^{14}\text{cm}^{-3}$ and $T_i = 5$ keV.

A plasma somewhat smaller than PLT could be used to cross the zero-power reactor condition. If the tritium target plasma has parameters $n \sim 10^{14}\text{cm}^{-3}$, $\bar{T}_e \sim 4$ keV, volume $\sim 10^6\text{cm}^{-3}$, and is injected with a 10 MW deuteron beam at 150 keV, the fusion power output could also be 10 MW (Fig. 5). If one imagines the plasma thermal energy to be recovered with good efficiency (e.g., by decompression), this power amplification factor (F = 1) would be sufficient to "cross the zero-power condition." This example assumes an energetic-deuteron density of 10^{13}cm^{-3}. The required reaction time is 35 msec (Fig. 5); during this time, the energetic deuterons must not be lost, or degraded appreciably by means other than collision. Thus we have for the energetic particles, the criterion $n\tau_E >> 3 \cdot 10^{11}\text{cm}^{-3}\text{sec}$. "Zero-power operation" also implies that we do not require heating of the target electrons other than by the deuterons. This condition is met, provided that $\tau_{Ee} > 20$ msec, or $n\tau_E > 2 \cdot 10^{12}\text{cm}^{-3}\text{sec}$ for the target plasma.

To proceed from this point to the generation of useful power, the injection power should be raised and the amplification factor F should be doubled; this implies a plasma electron temperature of 10 keV. The plasma ion temperature, however can remain low. In view of the rather weak nτ-conditions,[25] this regime should still prove relatively straightforward to attain in a device with a PLT-size plasma.

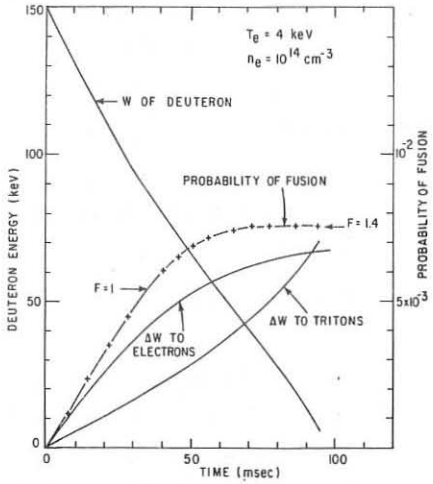

Fig. 5. Calculated slowing down of energetic deuteron in tritium plasma.[29] Mean fusion energy release becomes equal to initial deuteron energy, at point F = 1.

Acknowledgments

I should like to thank Drs. J. D. Callen, R. A. Ellis, Jr., H. P. Eubank, P. H. Rutherford, and T. H. Stix, for helpful discussions.

This work supported by U. S. Atomic Energy Commission Contract No. AT(11)-3073.

References

[1] B. B. Kadomtsev and O. P. Pogutse, Nuclear Fusion 11, 67 (1971).

[2] T. H. Stix, Plasma Physics 14, 367 (1972).

[3] D. R. Sweetman, Nuclear Fusion 13, 157 (1973).

[4] V. S. Mukhavatov and V. D. Shafranov, Nuclear Fusion 11, 605 (1973).

[5] This method of pictorial display was suggested by P. H. Rutherford.

[6] E. L. Beresovsky, et. al., Third International Symposium on Torodial Plasma Confinement, Garching, Munich (1973), Paper B19. A. I. Anisimov, et. al., Proceedings Conference on Plasma Physics and Controlled Nucelar Fusion Research, Madison 3, 543 (Vienna, 1971).

[7]H. P. Furth and S. Yoshikawa, Phys. Fluids 13, 2593 (1970).

[8]K. Bol, et. al., Phys. Rev. Lett. 29, 1495 (1972).

[9]K. Bol, et. al., Third International Symposium on Toroidal Plasma Confinement, Garching, Munich (1973), Paper B12.

[10]H. P. Furth, Third International Symposium on Toroidal Plasma Confinement, Garching, Munich (1973), Paper B9-I.

[11]L. A. Artsimovich, Nuclear Fusion 2, 215 (1972).

[12]H. P. Furth and R. A. Ellis, MATT-948, to be published in Plasma Physics.

[13]W. M. Hooke and J. C. Hosea, Fifth European Conference on Controlled Fusion and Plasma Physics, Grenoble (1971).

[14]V. M. Glagolev, et. al., Conference on Plasma Physics and Controlled Nuclear Fusion, Madison (1971), English Translation, p. 329.

[15]L. D. Stewart, et. al., Third International Symposium on Toroidal Plasma Confinement, Garching, Munich (1973), Paper E12.

[16]W. S. Cooper, et. al., Nuclear Fusion 12, 263 (1972).

[17]G. G. Kelley, Nuclear Fusion 12, 169 (1972).

[18]D. Aldcroft, et. al., Nuclear Fusion 13, 393 (1973).

[19]K. Bol, et. al., Sixth European Conference on Controlled Fusion and Plasma Physics, Moscow (1972), Supplementary Paper.

[20]J. D. Callen, J. F. Clarke and J. A. Rowe, Third International Symposium on Toroidal Plasma Confinement, Garching, Munich (1973), Paper E14.

[21]A. Gibson, et. al., Third International Symposium on Toroidal Plasma Confinement, Garching, Munich (1973), Paper B16-I.

[22]T. H. Stix, private communication.

[23]R. Behrish, Nuclear Fusion 12, 695 (1972).

[24]M. B. Gottlieb, private communication.

[25]J. M. Dawson, H. P. Furth and F. H. Tenney, Phys. Rev. Letters 26, 1156 (1971).

[26]R. F. Post, T. K. Fowler, J. Killeen and A. A. Mirin, UCRL-74790 (1973).

[27]L. S. Soloviev, V. D. Shafranov, and E. I. Yurchenko, Nuclear Fusion Supplement 1969, 25 (IAEA, Vienna).

[28]T. H. Stix, MATT-945 (1972), to be published in Phys. Fluids.

[29]Calculated by F. H. Tenney

TOKOMACS WITH NON-CIRCULAR CROSS-SECTION

G. LAVAL and R. PELLAT

Centre de Physique Théorique de l'Ecole Polytechnique
17, rue Descartes - 75230 Paris Cédex 05 - France
"Equipe de Recherche Associée au C. N. R. S."

INTRODUCTION

Whenever the quality of a plasma is measured by its ionic temperature, its density and energy confinement time, it is quite natural that the present trend in Tokomac research is towards larger installations with higher total current and higher magnetic fields. These improvements are more and more expensive and we are not far from the point where we need new methods to overcome the limits of ohmic heating in conventional Tokomacs. One of these new ideas is to use ohmic heating in discharge of the Tokomac type with a non-circular cross-section. The advantage of such a configuration can be seen on very intuitive grounds. Let us assume that the Kruskal-Shafranov stability condition yields upper limit for the current density and that this condition can be written $\frac{\iota}{2\pi} \leq 1$ where ι is the total rotational transform. If we elongate the plasma cross-section in the vertical direction, we shall need a larger value of the poloidal field and consequently of the current density in order to achieve the condition $\frac{\iota}{2\pi} = 1$. Thus ohmic heating will be more efficient. The density should be larger since it appears from A T C experiment that the maximum density increases with the heating rate. The final ion temperature should also be larger since it appears to be an increasing function of the total current. These optimistic considerations have motivated many theoretical and experimental studies[1]. In this paper we shall only deal with the theoretical results and try to put numbers where only qualitative estimates were up to now.

THE EQUILIBRIUM

We recall at first that the maximum value of β can be increased in a toroidal equilibrium by elongating the plasma cross-sections along the vertical axis. For an elliptic cross-section we found[2] :

$$\beta \leq \frac{1}{q^2} \frac{b}{R} \frac{1-\frac{E}{4}}{1-E} \qquad (1)$$

where b is the ellipse minor axis, a the vertical major axis, $E = 1 - \frac{b^2}{a^2}$ and R the magnetic axis radius.

Here we do not want to discuss the toroidal effects but only cylindrical equilibria pointing out the new features which arise when the cross-section is elliptical. In the low β case when the ratio of the poloidal field B_p to the toroidal one B_T is smaller than one, we can set :

$$\vec{B_p} = \vec{e_z} \wedge \vec{\nabla} \psi \quad .$$

The toroidal current $j(\psi)$ is much larger than the poloidal one and the equilibrium equation reduces to

$$\Delta \Psi = j(\psi) \quad .$$

If $j(\psi)$ = cte, the magnetic surface cross-sections are similar ellipses with the same ration $\frac{b}{a}$. If $j(\psi) = \lambda\psi$ with $\psi = 0$ at the edge of the plasma, the ellipticity increases as we go from the magnetic axis to the plasma-vacuum interface (fig. 1). When $j(\psi)$ is constant, the safety factor $q = \left(\frac{\iota(\psi)}{2\pi}\right)^{-1}$ is constant through the plasma so that the average magnetic shear is zero. On the other hand, when $j(\psi) = \lambda\psi$ with $\psi = 0$ at the edge of the plasma, q(axis)/q(boundary) is a decreasing function of the ellipticity (fig. 2). In this case, the ellipticity seems to increase the average shear. This last effect is understandable when we look at the vacuum magnetic field (fig. 3).

The main feature is the appearance of a separatrix which comes very close to the plasma in the second case when the ellipticity is increased. Thus the poloidal magnetic field becomes very small at the top of the ellipse. It is impossible to maintain a surrounding conducting shell on a closed magnetic surface. In the following the conducting shell cross-section and the plasma vacuum interface cross-section will be taken as confocal ellipses for this reason.

DIFFUSION

Since in present Tokomacs the ion energy losses seem to behave neoclassicaly we are going to estimate the ion temperature in a Tokomac with elliptic cross-sections by following the neoclassical theory[3]. We assume the magnetic surface cross-sections to be given by the equations :

$$R - R_o = \rho \cos\theta$$

$$z = k\rho \sin\theta$$

where R_o is the magnetic axis radius. The magnetic surfaces are given by ρ = cte and k can depend on ρ. The flat current case where $\frac{dk}{d\rho} = 0$ has been treated by Strauss[4]. The average trapped particle bounce frequency ω_a is still given by

$$\omega_a = \frac{V_{th}}{qR}\sqrt{\frac{\rho}{R_o}}$$

where V_{th} is the thermal speed. Then particles will follow the banana diffusion or the plateau diffusion law in the same range of temperature and density as in a Tokomac with a circular cross-section having the same aspect ratio. The total ion thermal flux can be estimated in the plateau regime by :

$$\Gamma \simeq \frac{V n m_i V_{thi}^5 q}{\Omega_{ci}^2 R_o k^2 \rho^2}$$

where V is the plasma volume, q is the safety factor defined by $q = \frac{B_T}{2\pi R} \oint \frac{d\ell}{B_p}$ where the integral is taken along the magnetic surface cross-section. Equating Γ with the energy influx from the electrons[5] we set :

$$\Gamma = \frac{4.2 \times 10^{-20} n^2 V}{A_i \sqrt{T_i}}$$

where A_i is the atomic weight of the ions. We obtain for the expected equilibrium ion temperature :

$$T_i^3 \propto \frac{n}{q} k^2 \rho^2 R_o B^2 . \qquad (2)$$

If we can achieve the same value of q as in circular cross-sections Tokomacs, we see that the ion temperature will increase like $k^{2/3}$ keeping the other parameters constant. The plasma volume will have increased only by a factor k. In order to achieve the same temperature increment in a Tokomac with circular cross-sections, we shou ld have been obliged to increase the plasma volume by a factor k^2.

Moreover, q is related to the current density j by :

$$j = \frac{B_T}{qR}\left(\frac{1}{k} + k\right) .$$

Thus for a given q, j is an increasing function of $k \geq 1$. Ohmic heating will be more efficient in the elliptical discharge and we can expect higher possible values of n. This advantage cannot be computed since we do not understand electron energy losses but we may expect a favorable effect.

We noticed that the transitión to the banana regime does not depend on k. Present Tokomacs are the verge of the banana regime for ions. The tem-

perature increment given by equation (2) can bring the ions in the banana regime where the flux Γ takes now the form :

$$\Gamma \simeq \frac{V n m_i V_{thi}^4}{\Omega_{ci}^2} \nu_{ii} q^2 \left(\frac{R}{r}\right)^{3/2} \frac{1}{k^2 \rho^2}$$

where ν_{ii} is the ion-ion collision frequency.

The equilibrium temperature is now given by :

$$T_i \propto \frac{B^2 k^2 \rho^2}{q^2} \left(\frac{\rho}{R}\right)^{3/2} .$$

The ion temperature is proportional to k^2. Thus we conclude that we can more easily cross the banana-plateau transition and reach higher ion temperatures in a Tokomac with an elliptic cross-section than in a Tokomac with a circular cross-section and the same plasma volume and magnetic field strength provided that we can achieve the same value of q in both cases.

The preceding evaluations have been done with the assumption that $\frac{dk}{d\rho} = 0$. If $\frac{dk}{d\rho} \neq 0$, it is an easy matter to include this term in the neoclassical theory and we find

$$\Gamma\left(\frac{dk}{d\rho} \neq 0\right) = \Gamma\left(\frac{dk}{d\rho} = 0\right) \times \left[1 + \frac{k'\rho}{2k}\right] .$$

In the case of figure 2, if k is 2 at the plasma-vacuum interface, $k'\rho \sim 0.4$ showing a negligible increase in the flux. Even for $k = 3$ at the plasma vacuum interface, the flux increment is about 15 %.

STABILITY

In estimating the advantage of a vertically elongated ellipse from the point of view of diffusion, we have assumed that the minimum value of q did not depend on the shape of the cross-section. The results showed the importance of this assumption. This minimum value of q is determined by stabili-

ty criterions against macrocospic modes. In the following we shall discuss the theoretical results in this area.

1. Ballooning-interchange modes

It is well known that the stability conditions against localized modes can be studied with the Mercier criterion. For circular cross-sections, it provides the usual conditions q(axis) > 1 which formally coincides with the Kruskal-Shafranov limit for kink modes. For a non-circular cross-section [1], the stability condition depends in a critical way on the coupling between elliptic and triangular terms by the formula :

$$q(\text{axis}) > \frac{\left(1-\frac{E}{4}\right)^{1/2}}{(1-E)^{1/2}} \quad \frac{1}{\left[1+\frac{3E}{8\left(1-\frac{E}{2}\right)}\,\frac{2c}{R}\,\frac{R}{b}\right]^{1/2}}$$

for magnetic surfaces given by :

$$1-\frac{x^2}{b^2}-\frac{z^2}{a^2}+\frac{2c}{R}\,\frac{x}{b}\,\frac{z^2}{a^2} = \text{cte} \ .$$

In order to improve the stability of a vertically elongated ellipse, the triangle must be pointed outwards. On the axis q can be smaller than one without violating the stability criterion. For instance if E = 0.6, i.e. k = 1,6 on the axis, a reasonable triangulation leads to 0,7 as the minimum value for q(axis). From figures 1 and 2 we conclude that the corresponding minimum value of q at the plasma vacuum interface will be 2.3.

A horizontal ellipse would allow a much more important gain. But we would loose on the diffusion ground and the kink instabilities would probably reduce the value of q(axis) to the same range as for a vertical ellipse as we shall see.

2. Kink modes

The analysis of kink-modes[6] has been performed in the usual range of parameters :

β < limiting equilibrium value $B_p/B_T \ll 1$

$b/R \ll 1$

$k_{//}\, b \ll 1$

where $k_{//}$ is the wave-number in the direction of the main toroidal magnetic field. We recall that in the case of an elliptic cross-section with flat current profile, the instability domains were considerably widened by the ellipticity so that the advantages of such a configuration was questionable (fig. 3). We have numerically solved the same problem for a current proportional to the flux function ψ :

$$j = \lambda\, \psi, \text{ and } \psi = 0 \text{ at the plasma boundary .}$$

The results of figure 4 show that the instability regions are now quite small for modes $m > 2$. The results of figures 3 and 4 have been obtained with a conducting shell which is a confocal ellipse such that $\frac{(a' - a)}{b} = 0.3$ where a' is the major axis of the conducting shell cross-section. With such a current distribution, it appears quite easy to find the same working regime as for Tokomacs with circular cross-sections namely $q \simeq 2$ at the plasma boundary. As we have seen before this can still be compatible with the stability with respect to localized modes on the axis.

In order to understand this strong stabilizing effect of the toroidal current density gradient, we have derived an asymptotic criterion for modes with large azimuthal wave-numbers or equivalently for large values of nq where n is the toroidal wave number.

The instability condition can be written :

$$0 < m - nq(S) < \frac{1}{2\pi} \oint \frac{d\ell}{B_p} j(S)$$

where q(S) and j(S) are the values of the safety factor and current density at the plasma boundary. If j(S) is zero, we obtain

$$\mathrm{Log}\left(\frac{nq(S)}{m} - 1 \right) < -m\,Q \qquad m \gg 1$$

with

$$Q = 4\pi \left[\frac{d}{d\psi_S} \mathrm{Log} \oint \frac{d}{B_p} \right] \left[\frac{dj}{d\psi_S} \oint \frac{d\ell}{B_p} \right]^{-1} .$$

For the case of an elliptic cross-section with parabolic current profile we find :

$$Q = 0.692 \left[1 + 3.6 \left(\frac{b-a}{b+a} \right)^2 + \ldots \right] \quad \text{for } \frac{b-a}{b+a} \ll 1$$

and

$$Q = \frac{4}{\pi^2} \frac{\frac{a^2}{b^2}}{1 + \frac{2b}{a}} \quad \text{for } \frac{a}{b} > 1$$

showing that the ellipticity in this case reduces the width of the unstable zone as found in the numerical results (fig. 4).

We have also studied finite conductivity tearing modes in the same asymptotic limit. We find as an instability condition :

$$\mathrm{Log}\left(1 - \frac{nq(S)}{m} \right) < -m\,Q \ .$$

Then the instability domain is symmetrical with respect to the kink mode instability domain. Nevertheless such modes differ from kink modes since resonant magnetic surfaces are inside the plasma so that they could lead to fast destruction of magnetic surfaces at the plasma boundary.

3. Axisymmetric modes

In a plasma with circular cross-sections, axisymmetric modes are found to be marginally stable. The cross-section ellipticity introduces a new unstable mode. Without stabilizing copper shell, the mode $m = 1$ is always unstable and corresponds to a translation parallel to the major axis of the ellipse. In the flat current case, and when the copper shell cross-section is a confocal ellipse, we find that the axisymmetric modes are stabilized when the stagnation point of the separatrix is out of the shell. For a parabolic current profile $j = \lambda\psi$, the results are plotted on fig. 5 showing a slightly more severe stability condition. If the copper shell coincides with a closed magnetic surface, the axisymmetric modes are found to be stable. It remains to be seen if a few passive rods will be able to stabilize these modes while making possible the use of the separatrix as a divertor and the penetration of the external winding magnetic fluxes.

CONCLUSION

We can now draw the following conclusions :

a) In a Tokomac with elliptical cross-section elongated along the symmetry axis it seems possible to reach the same values of q as in a Tokomac with circular cross-section. The main obstacle could come from the localized modes in the vicinity of the magnetic axis provided that one is convinced that these modes can really be dangerous.

b) In such conditions the ohmic heating power can easily be increased by a factor four providing higher electron temperature and helping to balance radiation losses at high temperatures.

c) Diffusion fluxes are reduced more rapidly than by increasing the volume of discharges with circular cross-section.

d) The ions will be sooner in the banana diffusion regime where the temperature increment is spectacular.

e) The separatrix can be used as a divertor.

f) The only serious drawback seems to be axisymmetric unstable modes though a copper shell or probably passive rods will be able to stabilize them.

REFERENCES

[1] L. S. Solovev, V. D. Shafranov, and E. I. Yurchenko in Plasma Physics and Controlled Nuclear Fusion Research (I A E A, Vienna, 1969), vol. I, 175 (Nucl. Fusion Supplement 1969, p. 25) ;

G. Laval, H. Luc, E. K. Maschke, C. Mercier and R. Pellat in Plasma Physics and Controlled Nuclear Fusion Research (I A E A, Vienna, 1971), vol. II, 507 ;

B. Coppi, R. Dagazian, and R. Gajewski, Phys. Fluids 15, 2405 (1972) ;

R. Gajewski, Phys. Fluids 15, 70 (1972) ;

L. A. Artsimovich and V. D. Shafranov, Zh ETF Pis. Red. 15, 72 (1972) [JETP Letters 15, 51 (1972)].

T. Ohkawa, and H. G. Voormies, Phys. Rev. Letters 22, 1275 (1969) ;

R. Wilhelm, and H. Zwicker, Proc. Fourth Conference Plasma Physics and Controlled Nuclear Fusion Research 1971, Madison, Wisconsin (I A E A, Vienna, 1971), vol. I, p. 259 ;

A. V. Bortnikov, Yu. T. Baiborodov, N. N. Brevnov, V. G. Zmukovskii, L. E. Zamarov, D. V. Orlinskii, V. I. Pergament, M. K. Romanovski, N. I. Sokolov, and A. M. Us, Proc. Third International Symposium on Toroidal Plasma Confinement, Garching 1973, paper B5.

[2] G. Laval, E. K. Maschke, R. Pellat, and M. N. Rosenbluth, I. C. T. P. Trieste, Internal Report IC/70/35, (1970).

[3] A. A. Galeev, and R. Z. Sagdeev, Zh. Exp. Teor. Fiz. 53, 348 (1967) ; P. H. Rutherford, Phys. Fluids 13, 482 (1970).

[4] H. R. Strauss, Phys. Rev. Letters 29, 8 (1972).

[5] L. A. Artsimovich, Nuclear Fusion 12, 215 (1972).

[6] G. Laval, R. Pellat, and J. L. Soulé, Fifth European Conference on Controlled Fusion and Plasma Physics, Grenoble, 21-25 August 1972 ;
G. Laval, R. Pellat, and J. L. Soulé, Submitted to The Physics of Fluids (1973).

Figure 1

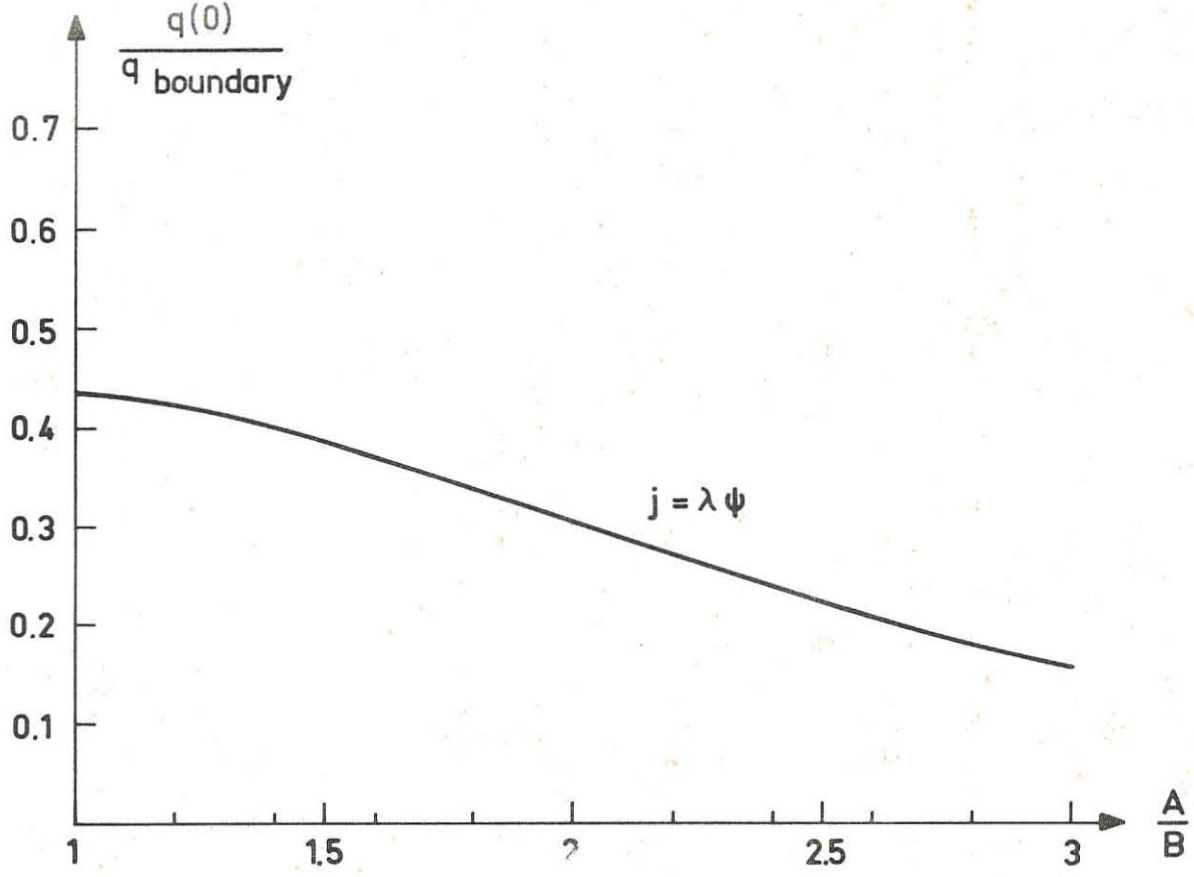

Figure 2

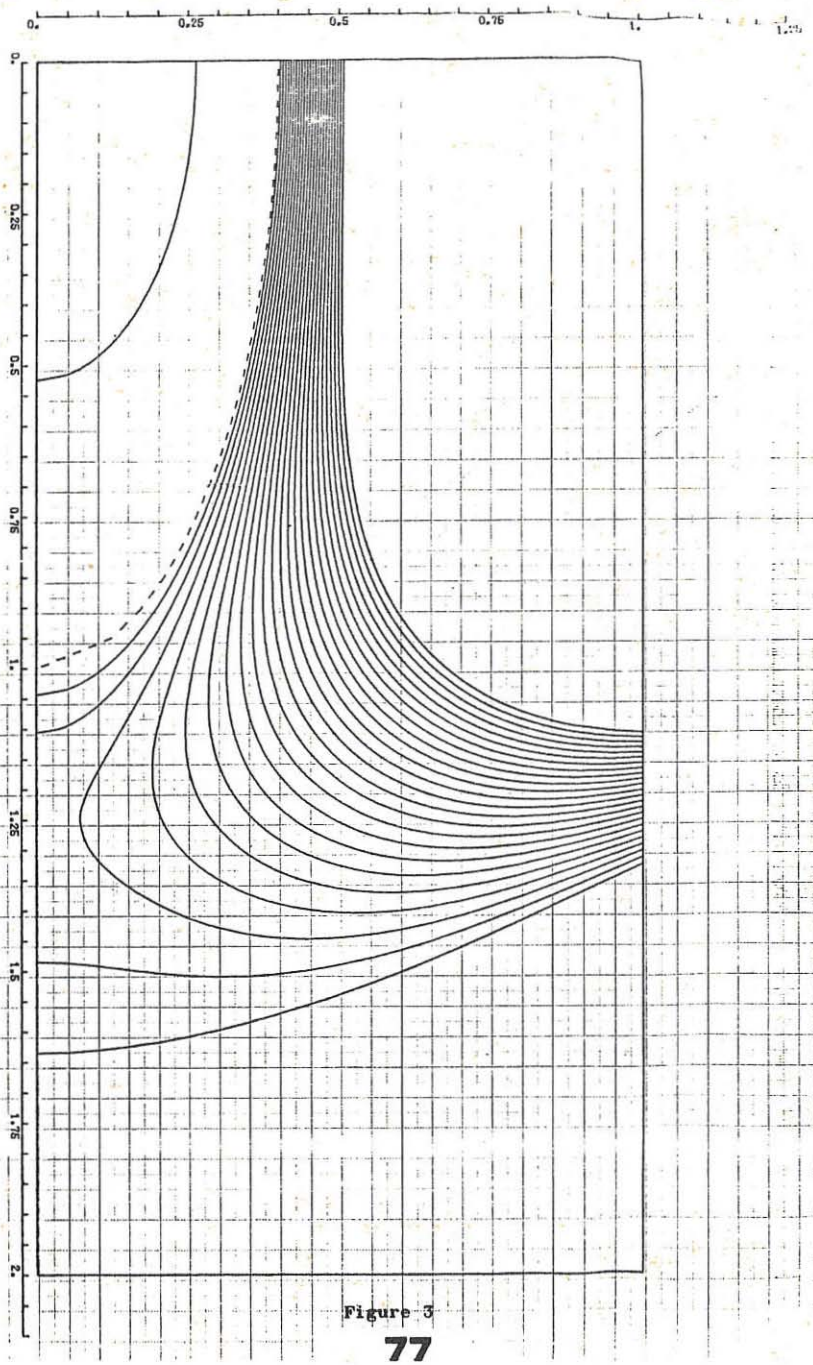

Figure 3

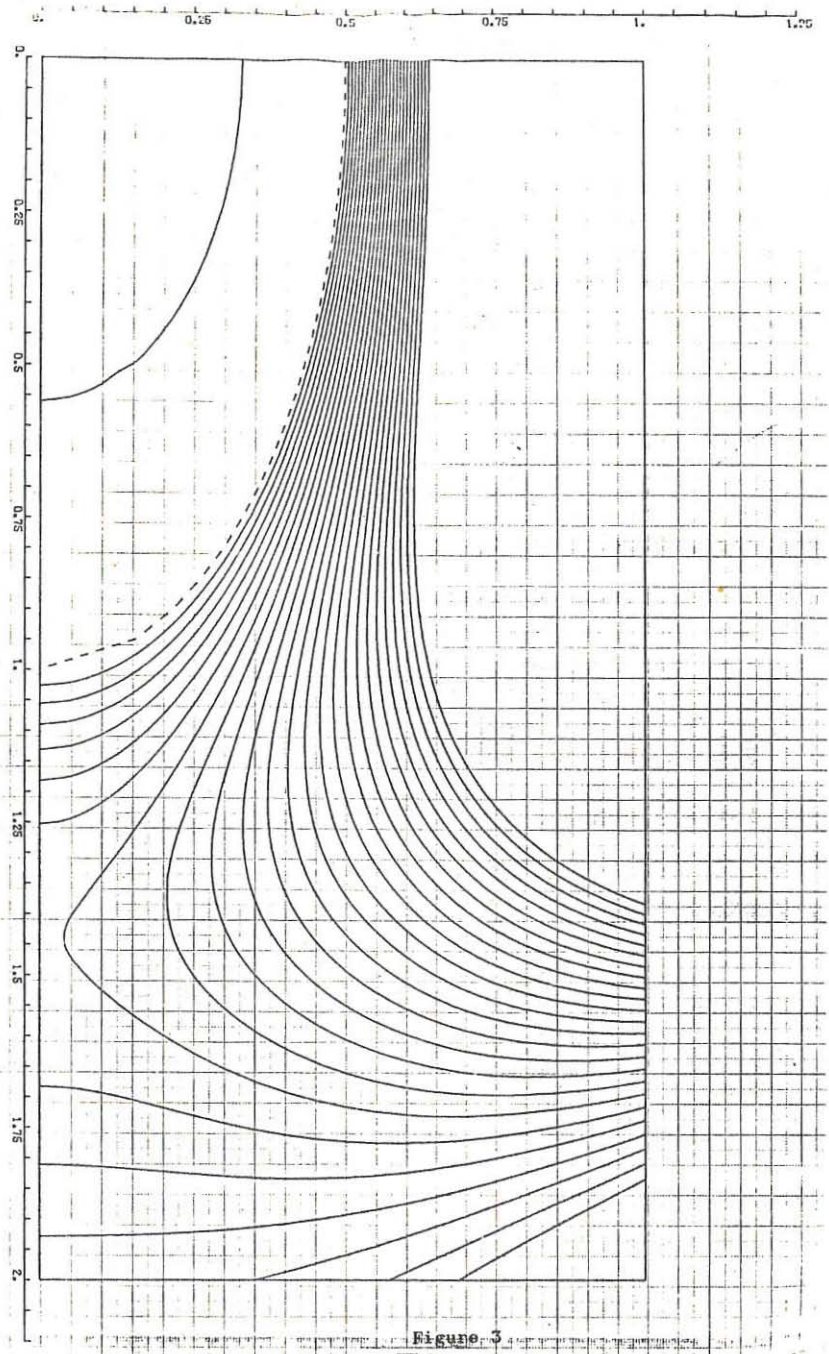

Figure 3

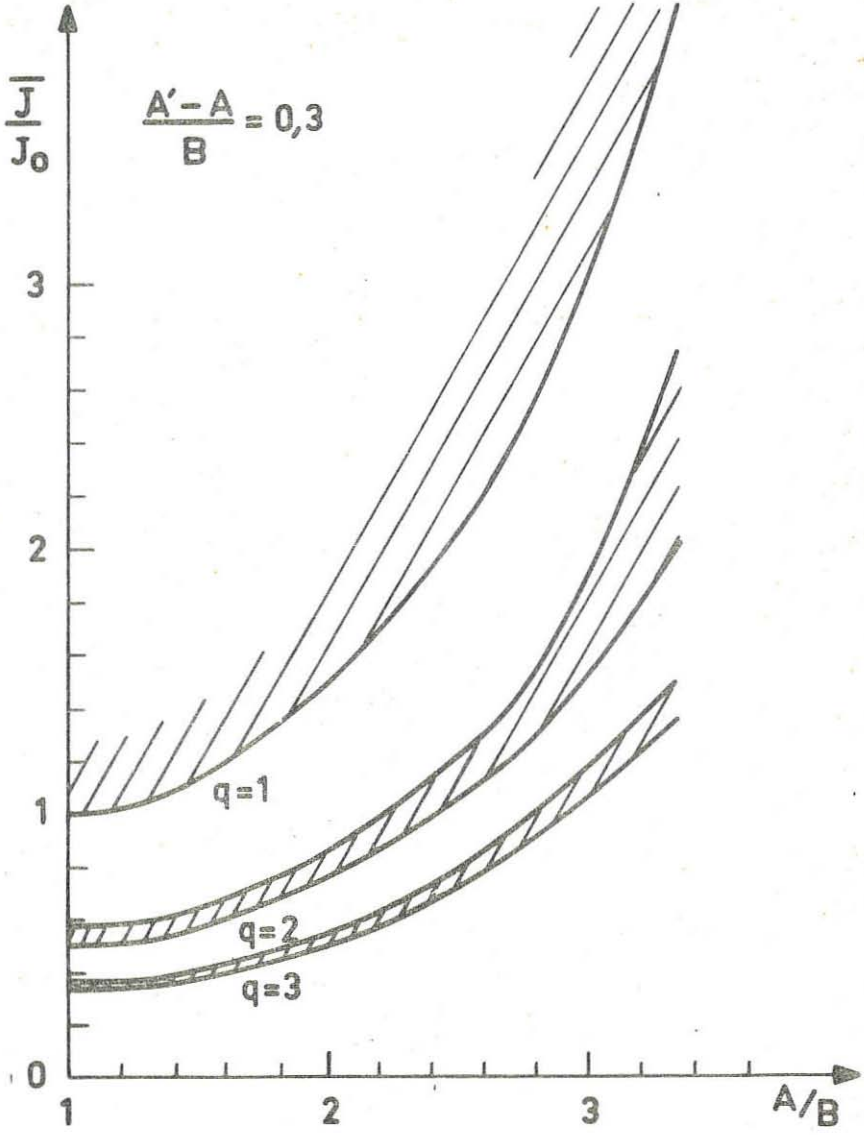

Figure 4

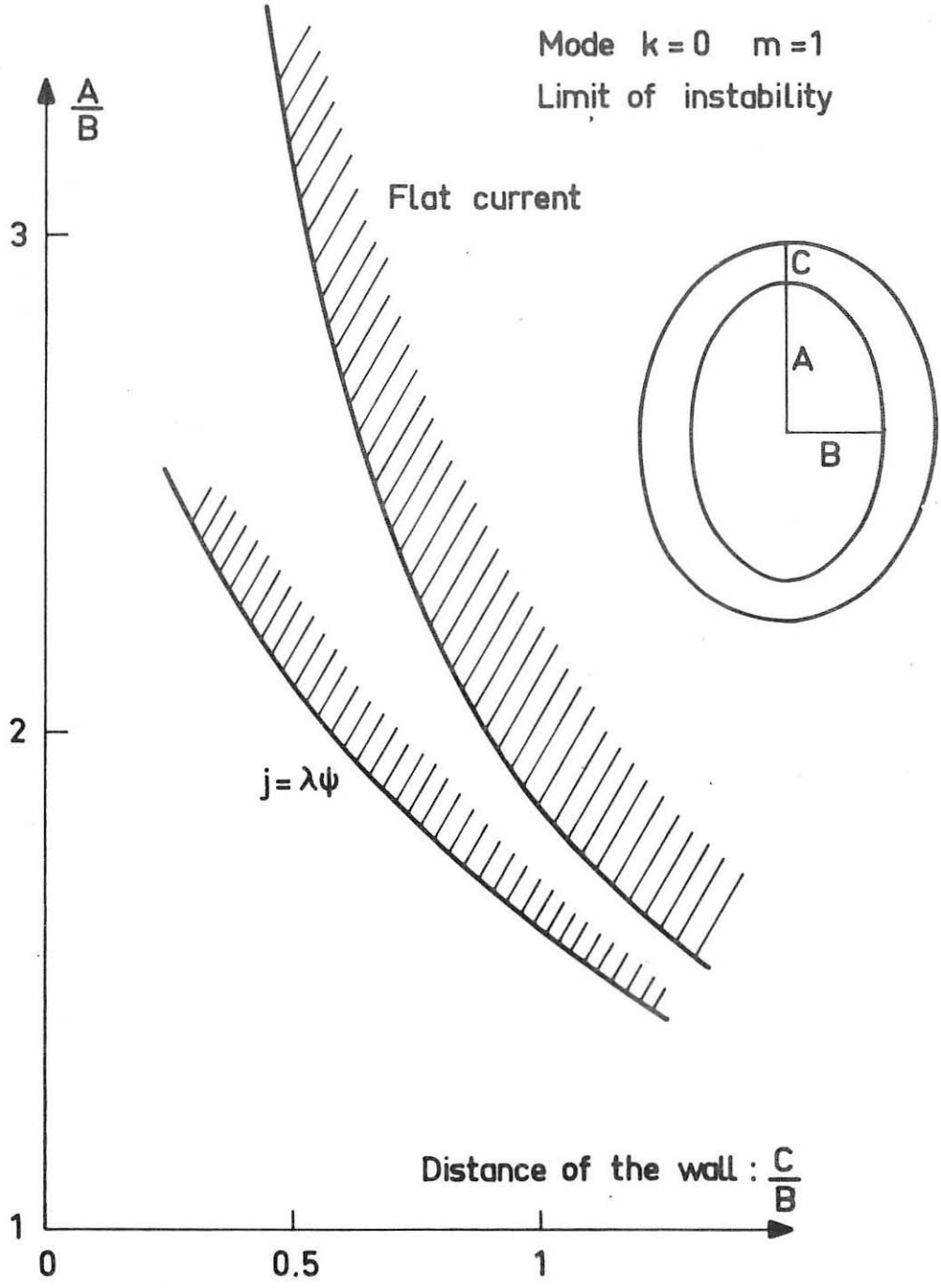
Mode k = 0 m = 1
Limit of instability
A/B
Flat current
C
A
B
3
2
j = λψ
Distance of the wall : C/B
1
0
0.5
1

Figure 5

THE RF-HEATING APPROACH TO THE IGNITION PROBLEM IN LOW-β TORI.

E. CANOBBIO

Association EURATOM-CEA
Département de Physique du Plasma et de la Fusion Contrôlée
Centre d'Etudes Nucléaires, B.P. 85
38041 - GRENOBLE - France.

ABSTRACT. Additional non-ohmic heating is necessary to get ignition in low-β tori. Besides neutral injection, a number of rf-heating methods are shown to have favourable thermonuclear prospects on the basis of the known theoretical scaling laws. The main areas for future work are indicated by stressing the need of a systematic experimental investigation of rf-heating under conditions which are relevant to the ignition problem.

I. Ignition and Heating Methods Other than RF

A feasibility test of the ignition process in Tokamak and Stellarator systems requires a substantial improvement of the plasma parameters compared to those of present day facilities. This is shown in the following Table, where T_i is the ion (deuteron) temperature, n_p the plasma density, and τ_E the energy confinement time. Unless stated differently in some cases, the following heterogeneous units will be used throughout the paper : cgs, T in keV, Electric Field in V/cm, Magnetic Field in Gauss (G), Electric Current in Amps (A), and Power in Watts (W).

	Present Devices	Ignition Experiment
T_i	several 100 eV	$\simeq$ 10 keV
$n_p \tau_E$	$\simeq 10^{12}$ cm^{-3}s	$\gtrsim 10^{14}$ cm^{-3}s

Such a progress apparently depends on :

a) increasing the toroidal current I_p from a few 100 kA to a few MA (in Tokamaks, I_p is the plasma current; in Stellarators, I_p is an equivalent external current).

b) increasing the plasma volume by a factor of $\gtrsim$ 30 by keeping constant the aspect ratio R/a $\simeq$ 4-3 (R > 500 cm is the major radius, a $\gtrsim$ 150 cm, the minor radius of the plasma). The toroidal magnetic field necessary to have plasma stability can be $\lesssim$ 50 kG in an Ignition Experiment, but it must be

$\gtrsim$ 100 kG in a full scale reactor.

c) applying auxiliary (non-ohmic) heating methods as the power released by ohmic heating ($\sim I_p^2/RT_e^{3/2}$) is limited to a few 100 kW both in present devices and in much larger ignition experiments. As shown by various authors /1-6/, a few 100 kW additional power can already introduce impressive changes in Tokamaks and Stellarators of high performances, while a much larger amount of power $\gtrsim$ 30 MW is necessary to make ignition possible at a density $\gtrsim 10^{14}$.

We consider too optimistic the possibility of 1) getting ignition by ohmic heating alone below $n_p \lesssim 3.10^{13}$ (which, by the way, would imply $\tau_E > 10^4\ \tau_{Bohm}$) and of 2) enhancing the electrical resistance of the plasma by no current-carrying microinstabilities etc.., and will focus our attention to point c) above.

Collisional heating by moderate currents ($\simeq$ 10 A) of fast neutral atoms with sufficiently high energy E_0 to ionize uniformly inside a plasma is usually considered to be the best candidate for additional heating. Since E_0 scales roughly as $\sim (n_p a)^2$, we must have $E_0 \lesssim$ 25 keV for present devices , which is almost available, $E_0 \sim$ 50-100 keV for an ignition device , which is still considered to be possible, but $E_0 \sim$ 1-5 MeV for a reactor, and this is impossible with the existing injector technology.

Both the physics of the interaction with the plasma (yet largely unexplored) and the engineering requirements of the structure surrounding a thermonuclear plasma may well impose additional constraints to this method. Thus it is highly desirable to have other possibilities which do not suffer from the same limitations.

In our opinion neither the methods implying very low frequencies like a) Adiabatic Compression and b) Gyrorelaxation, nor the very fast processes like c) Shocks, d) Turbulence, e) Intense V.H.F. Fields, f) Relativistic Electron Beams, etc..., which are at present probably the cheapest and most flexible ways to produce kilojoules of plasma energy, can really be considered as serious long term candidates for the thermonuclear goal in low-β tori /7/.

a) Adiabatic Compression, both in the single stage /8/ and in the cyclic versions /9, 10/ implies at the thermonuclear level exceedingly expensive devices allowing for large R excursions of the plasma ($\Delta R \gtrsim \overline{R}$) and involves dangerously large perturbations of the plasma equilibrium.

b) Collisional Heatings at a frequency up to about the i-i collision frequency also imply substantial perturbations of the MHD plasma equilibrium. In fact from Schlüter's heating rate /11/

$$\nu_H \lesssim \left(\frac{\Delta B}{B}\right)^2 \frac{\nu_{coll}}{18} \qquad (1)$$

it follows that in order to have $\nu_H \gtrsim 1\ s^{-1}$, in the thermonuclear case we must have $\Delta B/\vec{B} \gtrsim O(1/3)$, which, by the way, represents an enormous power amout.

c,d) when approaching ignition parameters, exceedingly expensive energy storage and enormous technical difficulties would be implied by the impulsive application both of several kV/cm electric fields for the purpose of Shock Heating ($c\,E/B_o > v_{Alfvén}$) and also of Turbulent Heating ($c\,E/B_o > c_s$ the sound speed) and of several 10 MA toroidal currents for longitudinal Turbulent Heating.

e) Electron Heating above $\nu \sim 30$ GHz is drastically limited by the fact that CW-power available from single hf-units falls below a few kW as steeply as $\nu^{-9/2}$ /12/.

f) REB's can deliver as much as 10^5 J to a target but are very hard to be introduced in a large low-β torus.

The concept of heating by a large population of toroidally runaway plasma electrons is at present not enough assessed.

2. RF-Heating Methods.

MW-CW power is already available from single rf-units below ≈ 3 GHz. In this frequency range there is a large variety both of waves which can exist in a magnetized plasma and of methods to excite them for the purpose of plasma heating up to thermonuclear temperatures. The useful frequency and wave length ranges, the corresponding heating process, and the available CW-power from a single unit are given in the following table, where v_{ti} is the ion (deuteron) thermal speed, the subscript // refers to the $\vec{B}_o$-lines of force, ν_{ci} is the ion gyrofrequency, ν_{pi} is the ion Langmuir frequency, and ν_{LH} is the lower hybrid frequency.

Frequency ν	Wave length λ	Heating process	CW-rf power
150 kHz	2 km	Transit Time Magnetic Pumping (TTMP) $\nu \approx v_{ti}/\lambda_{//} \ll \nu_{ci}$	5 MW
50-150 MHz	6-2 m	Ion Cyclotron and Harmonic Ion Cyclotron Heating (ICH) $\nu \approx n\nu_{ci}$ $n = 1,2$	1 MW
400-600 MHz	75-50 cm	Non-linear magnetoacoustic heating and Lower Hybrid Resonance Heating (LHR) when $n_p < 2.10^{13}$	1 MW
1-3 GHz	30-10 cm	LHR-Heating $\nu \approx \nu_{LH} \lesssim \nu_{pi}$ when $n_p \gtrsim 10^{14}$, $B_o > 50$ kG	0.5 MW

The wave-particle resonance condition is fulfilled in the entire plasma volume only in the TTMP case . In the ICH case there is a resonant shell of thickness Δx

$$\Delta x = \frac{R v_{ti}}{\lambda_{//} \nu} \qquad (2)$$

around the cylindrical surface $\nu = n\nu_c(R)$ ($n = 1,2, \ldots$). If $|n| > 2$, ICH is inefficient unless the EM-field be amplified near the LHR surface /13/. Since $(\nu_{pe}/\nu_{ce})^2 \simeq n_p/10^5\ B^2 \lesssim 1/3$, this surface is

$$\nu^2 = \nu_{pi}^2(r)/(1+(\nu_{pe}/\nu_{ce})^2) \simeq \nu_{pi}^2(r) \qquad (3)$$

If $2\ \nu_{ci} << \nu \lesssim \nu_{pi}(a) << \nu_{pi}(0)$, non-linear heating may occur in the regions where the $\nu = n\nu_{ci}$ Bernstein modes are excited parametrically by the magnetoacoustic wave /14/. These various processes will be discussed later in some detail.

In all cases the internal energy ε of the plasma, is governed by the transport equation /15/

$$d\varepsilon/dt = -\vec{\vec{P}}.\nabla\vec{v} + \vec{j}.(\vec{E} + \vec{v}\wedge\vec{B}/c) - \mathrm{div}\vec{q} \qquad (4)$$

where $\vec{\vec{P}}$ is the pressure tensor, $\vec{v}$ the fluid velocity and $\vec{q}$ the heat flow vector (viscosity has been neglected). The heating time $\tau_H \equiv \varepsilon/(d\varepsilon/dt)$ should obviously be shorter than the energy loss time τ_E due to $\mathrm{div}\vec{q}$ but longer than τ_{coll} in order to preserve a quasi-thermal equilibrium: $P_{ik} \simeq p\delta_{ik}$ In present day devices $\tau_H \lesssim$ $\lesssim$ 10 ms, while with reactor parameters $\tau_H \lesssim 1$ s.

Perhaps the main technical constraint upon the application of rf-heating in tori is imposed by the presence of a metallic vacuum vessel which does not allow for rf-field penetration and which gives also rise to significant rf-losses unless the rf-coupling structure be put inside the vacuum vessel.

The coupling structure has to consist of rf-coils if the vacuum wave length exceeds the radius of the liner ($\lambda_o > 20$ cm in present devices; $\lambda_o > 1$ m in the case of the reactor). In present devices the vacuum chamber can be made sufficiently rf-transparent by using either insulating sectors or some special all-metal sectors cut parallel to the oscillating $\vec{B}$-field /16/. Then the coils can be located around the liner. In a reactor the choice of material for the first wall is dominated by mechanical, thermal, and neutronic considerations and the coils which should be put inside the vacuum chamber, must be cooled, properly screened and insulated /17/, and must be located outside the diverted flux surface.

The use of rf-coils could be avoided if the vacuum vessel itself could act as a wave cavity. As discussed below this is an attractive possibility only for relatively small size devices but unfortunately not for larger ignition devices ! This conclusion concernes both the non-linear magnetoacoustic heating ($\lambda_o \sim 60$ cm) and the LHR heating ($\lambda_o < 30$ cm), the latter requiring the presence of a slow wave structure close to the plasma surface to make the plasma interior accessible to the wave.

3. Transit Time Magnetic Pumping

By imposing $\omega/k_{//} \simeq v_{ti} << v_A$ (the Alfvén speed) the radial wave number is imaginary ($k_\perp^2 + k_{//}^2 \simeq 0$). The radial attenuation is however irrelevant if $2\pi a/\lambda_{//} \lesssim$ $\lesssim 1/2$. Since, clearly, there is no propagation along $\vec{B}_0$, the pump field can pervade the entire torus only if N_c rf-coils are distributed around the torus ($N_c = 2\pi R/(\lambda_{//}/2)$). The plasma remains frozen to the oscillating lines of force and heating is produced only by the pressure term in Eq. (4) /18/, /19/. If $\nu_{coll} \gtrsim$ $\gtrsim \omega\, b^{3/2}$ ($b = \tilde{B}/B_0$) collisions are sufficient to prevent local distorsions of the distribution function of resonant particles /20/, /21/. Then a modulation rate $b \simeq 10^{-2}$ is necessary to double T_i in present devices /22/, while $b \simeq 10^{-3}$ is enough to achieve ignition in large dense plasma traps /5,23,24/ . In both cases the E_θ field at the coils (radius R_c) turns out to be 100-150 V/cm /25/

$$E_\theta \simeq T_D^{1/4}\, B_{o(kG)}\, R_{c(m)}/\sqrt{\tau_H} \qquad (5)$$

In moderate scale devices where we want to put into the plasma only 100-200 kW additional power, the power of the TTMP oscillator must nevertheless be as large as ~ 10 MW because of the large rf-dissipation into rf-coils and conducting walls. A much better efficiency can be achieved in large dense plasma devices where the ohmic loss per coil will be less than a few MW for < 100 MW deposited into the plasma.

Unfortunately, strong plasma losses were observed during the heating phase in the first TTMP experiment which was performed on the Proto-Cleo Stellarator /26/. More recent works /27/, /28/ indicate that the pump out can be reduced substantially by putting electrostatic screens around the rf-coils. The reason is the following. In the wave frame, the electromagnetic part of the $\vec{E}$ vector is transformed away, while its electrostatic part does remain. If the latter has a component normal to $\vec{B}_0$, the resonant particles would experience a $c\, E_\perp/B_0$ drift velocity, which is nearly constant within a bounce time of the particle in the wave. The resulting radial excursions may be large and may produce, by a random walk process, enhanced

neoclassical diffusion. Fortunately the selfconsistent electrostatic field ensuring plasma charge neutrality is essentially along $\vec{B}_0$. Usually, however, an external electrostatic field is produced by any many-turn rf-coil. Although evanescent in the plasma with a decay length of a few ion Larmor radii, this field can produce substantial pump-out indeed /28/ .

Apparently, other negative by-products should not be expected : both the EXB drift velocity and the relative e-i velocity are much smaller than v_{ti}; the TTMP modulation does not couple to low frequency drift - and trapped particle modes. Finally, although the frequency is close to electron bounce frequency ($k_{//} v_{ti} < \frac{v_{te}}{2qR} (\frac{2r}{R})^{1/2}$, q is the safety factor) the fraction of trapped particles affected by this resonance is small $\sim \sqrt{bR/r}$.

An ad hoc TTMP experiment (10 MW rf-power, 120 kHz, b ≃ 3%) which hopefully will settle the question of the pump-out observed on Proto-Cleo, is planned on the Petula Tokamak under construction at the Grenoble Laboratory /29/. Petula ($I_p \simeq$ ≃ 100 kA, R = 72 cm, a = 16 cm, $B_0 \simeq$ 15-25 kG) will use a liner with Al_2O_3 sections which allows to study a number of rf-heatings on an ohmic plasma with $n_p \simeq 2.10^{13}$, $T_i \simeq$ 100 eV, $\tau_E \geq$ 3 ms.

4. Ion Cyclotron Heating.

A cyclotron wave with $\nu \lesssim \nu_{ci}$ and $m \gtrsim 1$ (m is the poloidal angular wave number) can propagate around a torus and can, therefore, be excited by an rf-structure localized in one single section of the torus /30/. Plasma heating is produced by the $\vec{J}.\vec{E}$ term of Eq. (4) because $\vec{J} // \vec{v}$ and k.v = 0 for the cyclotron wave. Incouraging results have been obtained on moderately dense plasmas in Princeton /31/ and Kharkov /32/.

Unfortunately, ICH becomes inefficient in large dense plasmas because the component of the electric field which rotates in the same sense as the ions, E_i, is strongly screened by the plasma currents /24/:

$$E_i/E_{tot} \lesssim k_{//} v_{ti}/3\omega_{ci} \qquad (6)$$

if

$$\omega_{pi}^2 \gtrsim k_{//}^2 c^2 \quad \text{i.e.} \quad \lambda_{//} \gtrsim 2.10^8/\sqrt{n_p} \qquad (7)$$

On the other hand, $\lambda_{//}$ cannot be made arbitrarily small because d (the rf-coil-plasma distance) should be $\lesssim \lambda_{//}/2\pi$, otherwise the rf-field incident on the plasma would be reduced by a factor $\simeq \exp(-2\pi d/\lambda_{//})$. Hence condition (7) becomes $n_p d^2 \gtrsim 10^{15}$.

The efficiency of ICH in a dense plasma can be increased substantially in a two-ion species mixture if /24/, /25/

$$n_{1(Res)} < 10^{-2} (n_1 + n_2)$$

because then the E_i component can penetrate more easily into the plasma (in a reactor plasma 3 ion species would be required with H^+ resonant). The E_θ value at the coils is now comparable with the E_θ value required for TTMP, for the same τ_H value. This method has not yet been tested. What has already been tested is the completely different (collisional) heating at the $\nu^2 = \nu_{c_1} \nu_{c_2}$ Buchsbaum frequency in a dense (and cool) 50:50 HD mixture /33/.

5. Heating at the Harmonics of the Ion Gyrofrequency.

The nature of the rf-heating processes which are possible when $\nu_{ci}^2 < \nu^2 < \nu_{ci}\nu_{ce}$ is dominated by the properties of the fast magnetoacoustic wave propagating almost perpendicular to $\vec{B}_0$ /13/. If the frequency is such that $\nu \lesssim \nu_{pi}(a)$ ($n_p(a) < 10\% n_p(0)$) cut off and resonance occur both at the very edge of the plasma radial profile and the fast wave can then pervade the bulk of the plasma where the refractive index $N_\perp \simeq \nu_{pi}/\nu_{ci} \gg 1$. If $\nu = 2\,\nu_{ci}$ the ions experience in their own frame a wave with $\nu = \nu_{ci}$ rotating in the sense of their Larmor motion and such that $E_i \simeq \frac{k_\perp v_{ti}}{\omega} E_{tot}$ /24/, /25/. This E_i is much larger than that at $\nu = \nu_{ci}$ and $\omega_{pi}^2 > k_{//}^2 c^2$ (Eq. (6)). τ_H is comparable to that produced by TTMP, for the same field at the coils. Also in this case, the plasma being frozen to the lines of force, heating is produced by the pressure term in Eq. (4). Incouraging results at low rf-power level have been obtained in straight geometry /34/ and in the ST-Tokamak /31/. Unfortunately, the ions which are preferentially heated have now small parallel energy. They gain mainly perpendicular velocity and might escape from a toroidal configuration via banana orbits /7/, /35/. If $\nu > 2\,\nu_{ci}$ the linear cyclotron interaction becomes rapidly ineffective. This is a regrettable fact, for the vacuum wave length would now be reasonably consistent with the relevant dimension of the thermonuclear system. In fact the distance from the plasma edge to the liner is $d \simeq 30$ cm. So one could think to use some wave guide to inject the rf-power directly into the liner and to employ the plasma-filled vacuum vessel as a wave cavity. If $n_p(a) \simeq 5.10^{12}$ cm^3, λ_0 should somewhat exceed 50 cm. Inside the plasma the EM-field would be (very roughly) /13/:

$$E_\theta^P \simeq A \cdot \frac{1}{k_\perp d} \frac{J_1(k_\perp r)}{J_0(k_\perp a)} \quad ; E_r(r) \simeq i\nu E_\theta(r)/\nu_{ci} \tag{8}$$

where A = const and $J_{0,1}$ Bessel functions.
Close to the liner E_θ would be

$$E_\theta^L \simeq A\{1 + \frac{J_1(k_\perp a)}{k_\perp d\, J_0(k_\perp a)}\} \tag{9}$$

The number of radial eigen modes within the plasma would then be

$$n_r \simeq \frac{k_\perp a}{\pi} = \frac{2a}{\lambda_0} \frac{\nu_{pi}}{\nu_{ci}} \tag{10}$$

which can be of order 1 in present devices, but is very large ($O(10^2)$) in thermonuclear machines. Thus, only in the former case one can hope to amplify substantially the EM-field by making $J_0(k_\perp a) \simeq 0$ /36/, while in the latter case one will in practice have $E_\theta^P \sim E_\theta^L/k_\perp d$.

In both cases the amplitudes being too small for linear heating we must turn to non-linear effects.

The electron drift velocity cE_r/B_0 may easily exceed v_{ti} ($E_r > 0.3\ B_0\ T_D^{1/2}$) with reasonably small E_θ^L ($\lesssim 10^3$ V/cm) only in present devices /37/, /38/, where turbulent heating then occurs as a result of parametric microinstabilities (e.g.a transverse-current-plasma instability /39/).

For an ignition experiment one should find waves which can be driven unstable parametrically when $cE_r/B_0 \ll v_{ti}$. Following /14/ this is the case of the short wave-length ($k_\theta \to \infty$) ion Bernstein modes if

$$1 \lesssim \frac{cE_r}{\omega B_0} \cdot k_\theta \ll \frac{cE_r}{\omega B_0 \lambda_D} \tag{11}$$

(λ_D is the Debye length).

However, in the absence of eigenmode amplification, this would again imply $cE_\theta^L/B_0 > \omega_c \lambda_D k_\perp d \simeq O(v_{ti})$, which is likely to be realized in present day devices.

6. Lower-Hybrid Resonance Heating.

If $\nu \lesssim \nu_{pi}(0)$, the LHR occurs well inside the plasma. Then the field amplification and the concomitant wave conversion can be used to heat the plasma. However, as the rf-power can reach the resonant shell only through a zone of wave-evanescence (tunnel effect), a prohibitively large vacuum field should exist if substantial

heating has to be produced when $\nu_{pi} >> \nu_{ci}$ unless the field be amplified by the existence of eigenmodes in the core of the plasma. Large values of the Q factor (10^2-10^3) can be achieved in practice only if the n_r value ,Eq. (10), is reasonably small, i.e. if $\lambda_0 > a$ which is the case of moderate scale experiments /40/, /43/. In order that the wave power could reach the resonant shell from a region of propagation rather than evanescence, the wave number parallel to $\vec{B}_0$ must be such that /13/, /44/, /47/

$$(c\, k_{//}/\omega)^2 - 1 \gtrsim 2(\nu_{pe}/\nu_{ce})_{Res}. \qquad (12)$$

which means that the wave is radially evanescent in vacuum and in the outer layer of the plasma. If d is the distance between the slow wave structure and the plasma, the rf-field at the edge of the plasma will be attenuated by a factor $\sim$

$\sim e^{-\omega d\sqrt{2(\nu_{pe}/\nu_{ce})_{Res}}/c}$. On the other hand the E_r component is amplified in the plasma by a factor $N_\perp^{Max} \sim 10\ \sqrt{(c/v_{ti})} \sim 300\ T^{-1/4}$ /47/. In order to have a substantial benefit from this aplification we have to assume a vacuum attenuation factor larger than $\simeq 1/30$. This fixes an upper limit to the plasma density at the LHR zone

$$n_{Res} < 1.3\ (10^{12})(B/d^2)^{2/3} \qquad (13)$$

In order to have $n_{Res} \gtrsim 3.10^{13}$, $B_0 \sim 50$ kG, d must be smaller than 20 cm ! Fortunately, this slow wave structure could be only a few wavelenght long, thanks to the fact that the group velocity is nearly perpendicular to the phase velocity (which, by the way,is directed backward) so that the disturb propagates nearly parallel to $\vec{B}_0$ and may pervade a large portion of the torus.

Also from the point of view of the nature of the absorption meachanism there seems to be a substantial difference between present generation - and ignition LHR experiments. Non-linear heating should in fact be produced in the former case because cE_r/B_0 easily exceeds v_{ti} /48/, /51/,while linear harmonic cyclotron absorption seems to be the only realistic possibility in the latter case /47/. Whether this can produce enough heating or not, can only be decided on the basis of an evaluation which takes into account the relevant toroidal aspects of the problem and/or on the basis of an experimental determination of the scaling laws in tori.

A 100 kW-500 MHz-LHR experiment is planned on the WEGA device /52/ as a part of the joint effort between the Grenoble, Garching, and ERM-Brussels Laboratories on the problem of rf-heating. WEGA is a high current Stellarator ($I_p \simeq 80$ kA, $R = 72$ cm, $a = 15$ cm, $B_0 \gtrsim 15$ kG) which is designed to be flexible enough to study

1) the effects of various RF-heatings on toroidal confinement ($n_p \simeq 10^{13}$, $T_i \simeq$ $\simeq$ 100 eV, $\tau_E \geq 2$ ms), 2) to establish their scaling laws, and 3) to develop the necessary rf-heating technology. The LHR experiment will try to assess, in particular, the role of a slow wave-launching structure.

A large-power LHR-experiment is also planned on the Alcator Tokamak /46/.

Acknowledgements. It is a pleasure to acknowledge the valuable comments received from Drs. M. Brambilla, T. Consoli, and O. De Barbieri.

REFERENCES

/ 1/ D.R. SWEETMAN, Nucl. Fusion 13 (1973) 157.

/ 2/ L. ENRIQUES, Course on the Toroidal Reactors, Erice (1972), EUR 4999 e, p. 121 (1973).

/ 3/ T.H. STIX, Symposium on Plasma Heating, Varenna (1972), 1.

/ 4/ F. ENGELMANN, P. GIUPPONI, M. HAEGI, Ibid p. 222.

/ 5/ M. BERNARD, G. BRIFFOD, F. PARLANGE, Rapport EUR-CEA-FC-677 bis (1972).

/ 6/ J.P. GIRARD, M. KHELLADI, D. MARTY, V European Conference on Controlled Fusion and Plasma Physics, Grenoble (1972), Vol. 2, p. 241.

/ 7/ E. CANOBBIO (Conference Report) Nucl. Fusion, 13 (1973) 111.

/ 8/ H.P. FURTH, and S. YOSHIKAWA, Phys. Fluids 13 (1970) 2593.

/ 9/ H.P. FURTH, and R.A. ELLIS, Plasma Physics 15 (1973) 719.

/10/ L.A. ARTSIMOVICH, Nucl. Fusion 12 (1972) 215.

/11/ A. SCHLÜTER, Z. Naturforschg, 12 a (1957) 822.

/12/ L.S. NERGAARD, Microwave Journal, 13 (1970) 65.

/13/ T.H. STIX, The Theory of Plasma Waves, New York (1962).

/14/ N. MARTINOV and A. SAMAIN, Plasma Physics, 15 (1973) 783.

/15/ I.B. BERNSTEIN and S.K. TREHAN, Nucl. Fusion 1 (1960) 3.

/16/ T. CONSOLI et al., Nucl. Fusion, 13 (1973) 423.

/17/ J.E. CATO, M. KRISTIANSEN, M.O. HAGLER, Nucl. Fusion, 12 (1972) 345.

/18/ J.M. DAWSON, M.F. UMAN, Nucl. Fusion, 5 (1965) 242.

/19/ M. BRAMBILLA, to be published.

/20/ E. CANOBBIO, Nucl. Fusion 12 (1972) 561, see also Varenna Symposium on Plasma Heating (1972), p. 14.

/21/ E. CANOBBIO, R. NAKACH, III Int. Symp. on Toroidal Plasma Confinement Garching 1973, paper E-15.

/22/ M. BRAMBILLA and S. GIUFFRÉ, Nucl. Fusion, 12 (1972) 199.

/23/ D.J. WORTH, Proc. BNES Conf. Nuclear Fusion Reactors, Culham 1969, 517.

/24/ J. ADAM and A. SAMAIN, Report EUR-CEA-579 (1971).

/25/ E. CANOBBIO, Course on the Toroidal Reactors, Erice (1972), EUR 4999 e, p. 71 (1973).

/26/ W. MILLAR et al, V-ECCFPP , Grenoble (1972), Vol. II, p. 135.

/27/ W. MILLAR et al., III Int. Symp. on Toroidal Plasma Confinement, Garching (1973), paper E-6.

/28/ M. BRAMBILLA, Ibid. paper E-16.

/29/ M. BERNARD et al., Intern. Report CEA-DPh- 1096 (1972).

/30/ S.S. OVCHINNIKOV et al., Nucl. Fusion (Supplement 1972), p. 347.

/31/ W. HOOKE, Symposium on Plasma Heating, Varenna (1972), p.73.

/32/ A.G. DIKY et al., III Int. Symp. Garching (1973), paper E-17.

/33/ V.F. TARASENKO et al., V. ECCFPP, Grenoble (1972) Vol. I, p.112.

/34/ R. DOLLINGER et al., this Conference.

/35/ F.W. PERKINS, Symposium on Plasma Heating, Varenna (1972) 20.

/36/ A.M. MESSIAEN, P.E. VANDENPLAS, Nucl. Fusion 11 (1971) 556; see also this Conference.

/37/ L.I. GRIGOREVA et al., this Conference.

/38/ V.L. VOLOVIN et al., J.E.T.P. Letters 14 (1971) 149, and 17 (1973) 2.

/39/ L.I. GRIGOREVA et al., Nucl. Fusion (Supplement 1972) p. 335.

/40/ V. AGNELLO et al., IV-ECCFPP, Rome (1970) 131.

/41/ S.S. PESIC, Nucl. Fusion, 11 (1971) 461.

/42/ S. PURI, M. TUTTER, Nucl. Fusion, 13 (1973) 55.

/43/ Yu. N. DNESTROVSKII, D.P. KOSTOMAROV, and G.V. PEREVERZEV, Soviet. Phys., Tech. Phys. 17 (1973) 1637.

/44/ T.H. STIX, Phys. Rev. Lett. 15 (1965) 878.

/45/ V.M. GLAGOLEV, Plasma Phys. 14 (1972) 301, 315.

/46/ R. PARKER, MIT-QPR N° 102 (1971); see also MIT-QPR N° 105.

/47/ S.S. PESIC, Thesis, Univ. of Paris (1973).

/48/ V.M. GLAGOLEV, N.A. KRIVOV, Yu. V. SKOSYREV, Nucl. Fusion (Supplement 1972) p. 329.

/49/ W. HOOKE, Symposium on Plasma Heating, Varenna 1972, p.77.

/50/ V.F. TARASENKO et al., Soviet. Phys. Tech. Phys., 17 (1973) 1599.

/51/ V.V. ALIKAEV et al., this Conference.

/52/ The WEGA project, Intern. Report CEA- SIG (Grenoble 1972) and Internal Report IPP - Garching 1972.

REVIEW OF SCYLLAC THETA-PINCH EXPERIMENTS*

by

W. E. Quinn, W. R. Ellis, R. F. Gribble, C. R. Harder, R. Kristal, F. L. Ribe, G. A. Sawyer, R. E. Siemon and K. S. Thomas

Los Alamos Scientific Laboratory, University of California, Los Alamos, New Mexico U. S. A.

ABSTRACT:

Scyllac research on 5-m and 8-m toroidal sectors, and the 5-meter linear theta-pinch are discussed. In addition, we outline the plans for the full Scyllac torus, feedback stabilization, and a staged theta-pinch.

I. INTRODUCTION

Linear θ-pinch experiments during the past decade and a half have demonstrated the production of hot, dense, stable plasmas. The limitation on the time of confinement of these plasmas has been end loss and not escape across the magnetic field by means of macro- or micro-instabilities. In view of the end-loss containment limitation in linear systems the large aspect ratio toroidal θ-pinch Scyllac is being constructed at Los Alamos. During the past two years "Scyllac" research has been divided among four major experimental efforts: 1) 5-meter[1,2] and 8-meter, 120° toroidal sectors; 2) a 5-meter linear theta pinch with strong magnetic mirrors[2,3]; 3) studies of the $\ell = 1,0$ interference force and the MHD m = 1 instability with $\ell = 1$ and $\ell = 0$ fields on the 3-meter linear Scylla IV device[4]; and 4) the development of a feedback system for stabilizing the m = 1 instability[5]. The objective of these experiments, other than the linear Scyllac, has been to study various aspects of the equilibrium and stability of the high-β θ-pinch in toroidal geometry.

In the Scyllac sector, with a major radius R and plasma radius a, the toroidal drift force $F_R = \beta B_o^2 a^2/4R$ is compensated by a combination of $\ell = 1$ helical and $\ell = 0$ bumpy fields. The toroidal equilibrium [6,7,8] of this system and the stability [8,9,10,11] of a straight $\ell = 1$ or $\ell = 0$ plasma column have been treated in the MHD approximation. The $\ell = 1$ field is chosen because: 1) theory predicts a growth rate for the dominant $k \simeq 0$, m = 1 mode which vanishes in leading order; and 2) in high β, high temperature theta pinches [5] only long wavelength, m = 1 modes are observed experimentally. The $\ell = 0$ fields produce the asymmetry in the sum of the plasma excursions $\delta_1 \simeq B_{\ell=1}/B_o\, ha(1-\beta/2)$ and $\delta_o \simeq -B_{\ell=0}/2B_o(1-\beta)$ which is needed to produce the equilibrating force, $F_{1,0} = \beta(3-2\beta)\, B_o^2 h^2 a^3 \delta_1 \delta_o/8$, where $2\pi/h$ is the wavelength of the $\ell = 1,0$ fields. Equating the outward toroidal force to the $F_{1,0}$ force gives the equilibrium condition $\delta_1\delta_o \simeq 2/(3-2\beta)h^2 aR$. In the

initial toroidal-sector experiments [1,2,] with the $\ell = 1$ helical field provided by capacitor-driven windings and the $\ell = 0$ field formed by rectangular grooves in the inner surface of the compression coil, the plasma was observed to take up a helical toroidal equilibrium for 4 to 8 μsec in contrast to the case with no $\ell = 1$ field where the plasma accelerated immediately to the outer wall of the torus. Following the equilibrium period an $m = 1$, $k \approx 0$ sideward motion of the plasma column carried the plasma to the wall. Thus the plasma confinement is terminated in 6 to 10 μsec by $m = 1, k = 0$ transverse motion, whose characteristics were not differentiated between instability and loss of equilibrium. These experiments verified the theoretical MHD equilibrium of the toroidal Scyllac sector.

The experiments on both the 5-m toroidal sector ($R = 2.4$ m) and the 5-m linear Scyllac have been completed. The Scyllac system is now being converted to its full toroidal configuration. Results on the sector and on the Scylla IV-3 feedback experiment indicated the necessity of increasing the Scyllac major diameter from 4.8 to 8.0 m to decrease the growth rate of the $m = 1$, $k = 0$ instability to accommodate the technical characteristics of the feedback apparatus (cf. Sec. III below). The conversion of one-third of the torus to the larger radius has been completed and experiments resumed in this sector with an 8.4-m coil to study the plasma equilibrium and stability in the larger radius of curvature, prior to experiments on the full torus.

In present θ-pinches, the plasmas occupy only a small fraction of the coil radius. Because of this it is anticipated that the $m = 1$ MHD instability driven by the helical fields which produce toroidal equilibrium in Scyllac-type experiments must be feedback stabilized. Theoretical studies indicate that with larger plasma radii (more implosion heating, less compression heating) the feedback can be dispensed with in favor of stabilization by the conducting wall as in the staged θ pinch [12].

Experiments are beginning at LASL to study implosion heating and staging in theta pinches. Previous theta pinches have performed initial implosion heating of the ions and subsequent adiabatic compression with a single capacitor bank power supply. Projected theta-pinch feasibility experiments and fusion reactors will require separation of the two functions to achieve greater implosion heating and less adiabatic compression. One experiment will study the implosion-heating processes, and, a second will combine implosion heating with separate adiabatic compression (staging).

The objectives of the 5-m linear Scyllac were to study the effects of strong magnetic mirrors on the confinement and stability of a high β plasma and to provide scaling data on end loss and electron temperature with plasma length. Results

of experiments both with and without magnetic mirrors are reported.

II. EXPERIMENTS WITH ℓ = 1,0 HELICAL EQUILIBRIA IN THE 5-m AND 8-m TOROIDAL SECTORS

A. Experimental Arrangement.

For the past two years, Scyllac has been assembled in a preliminary configuration as a 5-meter long toroidal sector and a separate 5-meter linear theta pinch with strong mirrors as shown in the plan view of Fig. 1. The initial Scyllac toroidal sector [1,2] had a major radius of 237.5 cm, extended through an angle of 120° and had a coil arc length of 5 m. Each meter section of the compression coil was driven by a 700-kJ capacitor bank of 210 1.85-μF, 60 kV capacitors. The experiments were performed with one-half the bank charged to 45 and 50 kV to produce peak magnetic compression fields of 33 to 50 kG with risetimes of ~ 4 μsec, followed by crowbarred waveforms with L/R times of 250 μsec. The compression coil inner diameters were in the range of 14.4 to 20.5 cm and the inside diameter of the quartz discharge tube was 8.8 cm. A 50 kV, 0.9-kJ/m, θ-preionization bank, which produces a 400 kHz oscillating field, was used to preionize the initial deuterium gas fillings of 10 to 20 mTorr. In the initial experiments the ℓ = 1 fields were applied by means of capacitor driven, bifilar helical windings and the ℓ = 0 fields were generated by annular grooves in the inner surface of the compression coil.

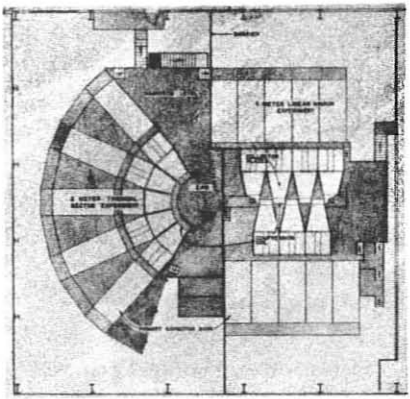

Fig. 1. Plan view showing arrangement of Scyllac 5-m toroidal sector and 5-m linear theta pinch.

A second set of experiments was performed in shaped compression coils in which the flux surfaces of the ℓ = 1 and ℓ = 0 fields were machined into the inner surface of the main coils. The advantages of this ℓ = 1,0 configuration are: (1) a constant ratio of both the ℓ = 1 and ℓ = 0 fields to the main field in time; (2) an improvement in the uniformity of the ℓ = 1 and ℓ = 0 fields; and (3) a technical simplification of the generation of the ℓ = 1 and ℓ = 0 fields. A disadvantage of this geometry is the fixed ratios of the ℓ = 1 and ℓ = 0 fields to the main toroidal field, B_o.

The new sector, which comprises one-third of the final Scyllac torus, has a larger major radius of 4.0 meters and a coil arc length of 8.4 meters; the ℓ = 1,0

equilibrium fields are generated by the shaped inner surface of the compression coil. The design product of these fields was determined through the sharp-boundary equilibrium relations [8] to give $B_{\ell=1}\ B_{\ell=0}/B_o^2 = f(\beta, ha)\ ha^2/R$. A graph of the equilibrium field-product ratio, $B_{\ell=1}\ B_{\ell=0}/B_o^2$, for β in the range of 0.6 to 0.9 is given in Fig. 2 for plasma radii in the range of 0.6 to 1.0 cm. Equal magnitudes of $B_{\ell=1}$ and $B_{\ell=0}$ were chosen; this produces a bumpiness δ_o of the plasma column which is small compared with the helical displacements δ_1. The experimental points on Fig. 2 show the agreement of the observed toroidal equilibrium with sharp boundary theory in the 5-m sector. (Measured radii = 0.7-0.8 cm).

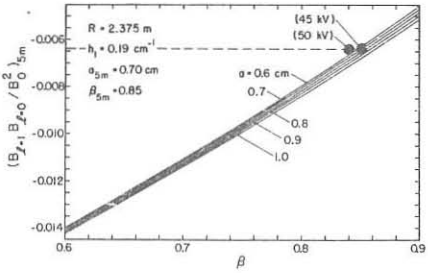

Fig. 2. Values of $B_{\ell=1}\ B_{\ell=0}/B_o^2$ predicted by sharp boundary theory for plasma equilibrium in the 5-m toroidal sector. Experimental points ($B_{\ell=1}\ B_{\ell=0}/B_o^2 = -0.0064$; $\beta = 0.85$, a = 0.7 cm; $\beta = 0.84$, a = 0.8 cm) are shown for 45 and 50 kV bank voltages.

The designs of the shaped coils were determined by calculating the shape of the magnetic flux surfaces for the required vacuum fields from

$$\bar{B}/B_o = \hat{e}_z\ (1 - \frac{r}{R}\cos\theta) + \nabla\phi\ , \qquad (1)$$

where

$$\phi = (B_{\ell=1}/B_o)\ [2\ I_1(hr)/h]\ \sin\ (\theta - hz)$$

$$+ (B_{\ell=0}/B_o)[I_o(hr)/h]\ \sin hz \qquad (2)$$

$$+ (B_v/B_o)\ r\ \sin\theta + (B_{1,2}/B_o)\ \sin\ (\theta - 2hz).$$

The small vertical field B_v and $B_{1,2}$ field are required for equilibrium according to the sharp boundary theory. The amplitudes of these fields are given by

$$\frac{B_v}{B_o} = \frac{B_{1,2}}{B_o} = \frac{B_{\ell=1}B_{\ell=0}}{4B_o^2}\ . \qquad (3)$$

The $B_{1,2}$ field varies in space as sin (θ-2hz), and produces a small ellipticity in the plasma cross section, in contrast to the $\ell = 1$ field with sin (θ-hz). Each wavelength, $\lambda_{1,0}$=41.9 cm, of the 8-m sector was divided into 330 steps with 1.25 mm/step and flux surfaces calculated for each step. A vertical field amplitude of $B_v/B_o = 0.00168$, 44% larger than the theoretical value, was used to give flux surfaces at the coil wall which have circular cross sections for

simplicity of machining. This larger value of vertical field shifts the inner flux surfaces inward in the horizontal plane and decreases their area. With this design the vacuum flux surfaces can be centered in the discharge tube by the addition of a vertical field from driven windings.

B. Results.

During the past year an extensive series of experiments on the Scyllac 5-m toroidal sector was completed. These included nine variations of $\ell = 0$ and $\ell = 1$ magnetic fields to provide toroidal equilibrium against the drift force F_R. The value of the $\ell = 1,0$ equilibrium fields in the 8-m sector experiment was scaled from the 5-m results. In both the 5-m and 8-m experiments with deuterium filling pressures of 10 to 20 mTorr, the average plasma β on axis is 0.7 to 0.9, the ion temperature 0.8 to 1.0 keV, and the plasma density 2 to 3 x 10^{16} cm^{-3}.

The following measurements were made of the plasma properties: (1) three high-speed streak cameras, viewing the plasma column side-on were used to record the transverse motions of the plasma column; (2) a coupled-cavity He-Ne laser interferometer was used to measure the time history of plasma electron density integrated along a chord of the plasma cross section; (3) a magnetic loop and probe arrangement was used to measure the magnetic flux excluded by the plasma. Combined with density profiles from the luminosity, the excluded flux can be expressed in terms of the plasma β; (4) a ten-channel, side-on luminosity experiment was used to obtain the intensity profiles of the plasma column. These luminosity profiles, in conjunction with the coupled-cavity interferometer data, give absolute density profiles; and (5) scintillation and silver-foil activation counters were used to measure the neutron emission.

1. Plasma Equilibrium and Stability. The streak photographs of Fig. 3A show the horizontal plasma motions in the 5-meter toroidal sector in the absence of $\ell = 1$ fields. The motion is a simple toroidal "drift" to the walls with no observable effect induced by the presence of bumpy $\ell = 0$ fields. In Fig. 3B the $\ell = 1$ coils were excited to 56 kA. After remaining in equilibrium for 6 μsec, the plasma begins to drift outward in both the land and groove regions and strikes the wall in the land region. The experiments show the following: (1) the plasma column takes up an initial helical shift and comes into an equilibrium position which lasts 4 to 8 μsec, in contrast to a complete absence of equilibrium without the $\ell = 1,0$ fields; (2) as the plasma moves away from the equilibrium position, the motion in the land and groove regions is usually similar, i.e., the column either moves radially outward or inward; (3) the motion of the plasma column develops largely in the horizontal plane of the torus rather than in random directions; and

(4) a few percent increase (or decrease) in the $\ell = 1$ equilibrium field causes the plasma column to move radially inward (or outward) away from its equilibrium position in both land and groove regions.

In experiments on both the 5-m and 8-m sectors with fixed $\ell = 1$ and $\ell = 0$ fields generated by the $\ell = 1,0$ shaped inner surface of the toroidal coils, the plasma equilibrium was achieved by adjusting the initial deuterium filling pressure to give a balance between the $F_{1,0}$ and toroidal F_R forces through their β dependence. The equilibrium and stability of the high-β plasma produced in the shaped $\ell = 1,0$ coils have been studied in the toroidal sector both with and without additional applied vertical fields (B_v = 100 to 600 G). The plasma confinement is slightly improved when the vertical field windings are excited to produce the theoretical vertical field amplitude of Eq. (3), but is not critically dependent on the magnitude of the vertical field. This result indicates that flux surfaces are not important in the sector experiments since larger values of the vertical field shift the vacuum flux surfaces at least partially out of the discharge tube cross section. However, flux surfaces are likely to be important on the longer time scale of the full torus.

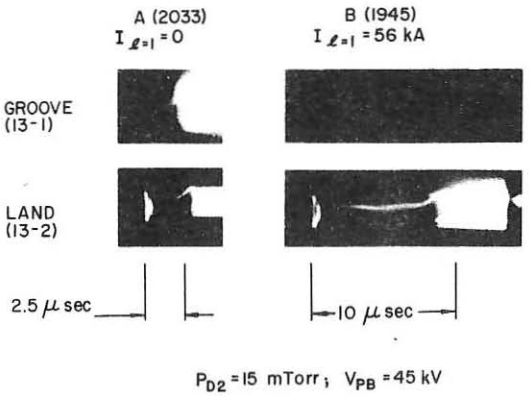

Fig. 3. Streak photographs of the 5-m toroidal sector plasma showing horizontal motion with and without $\ell = 1$ fields.

The streak photographs of Fig. 4 compare the plasma transverse motions in the 5-m and 8-m sectors with shaped compression coils. The general characteristics of the plasma motions are similar to those observed with the $\ell = 1$ driven windings, except that the long wavelength m = 1 motion tends to be somewhat more random in direction. As in the experiments with driven $\ell = 1$ windings, where a small change in the magnitude of the $\ell = 1$ fields moved the plasma from its equilibrium position, in the shaped coils with fixed $\ell = 1,0$ field ratios a few percent change in the deuterium filling pressure, with a corresponding change in plasma β, produces the same results.

The examination of many streak photographs shows that the plasma column remains in stable equilibrium for 7 to 10 μsec in the 8-m sector, compared with 4 to 7 μsec in the 5-m experiment, at which times the onset of the terminating m = 1 sideward motion occurs. The ratio of the onset times, $\tau_{os}(8m)/\tau_{os}(5m) \simeq 1.5$, can be compared with the Alfvén times, $\tau_A(8m)/\tau_A(5m) \simeq 1.6$, from the ends of the sectors to the center, and with the plasma end-loss times, $\tau_p(8m)/\tau_p(5m) \simeq 1.7$. Thus, the onset-time scaling is in good agreement with the assumption that it is produced by end-effects. The plasma is apparently stable until end effects propagate to the center of the sector. Assuming that the motion which terminates the stable period is the instability predicted by the theory, its measured growth rates are $\gamma_1(5m) \simeq 1.1$ MHz and $\gamma_1(8m) \simeq 0.6$ MHz. Theory [8] gives the following dispersion relation for the m = 1 mode:

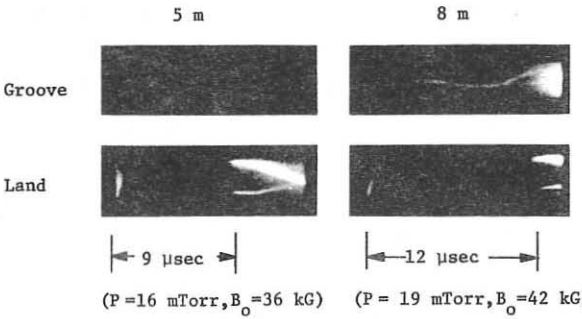

Fig. 4. Streak photographs comparing plasma behavior in the 5-m and 8-m toroidal sector experiments.

$$\gamma_1^2 = h^2 v_A^2 \delta_1^2 \left[-\beta^2 \left(\frac{a}{b}\right)^4 + \frac{\beta(4-3\beta)(2-\beta)}{8(1-\beta)} h^2 a^2\right] \simeq \frac{\beta(4-3\beta)}{2(1-\beta)(2-\beta)} v_A^2 h^2 \left(\frac{B_{\ell=1}}{B_o}\right)^2, \quad (4)$$

where the a/b term arises from wall stabilization and is small in the present experiments. The calculated growth rates are 1.0 MHz and 0.6 MHz for the 5-m and 8-m experiments, respectively. Thus the terminating γ_1's scale between the 5-m and 8-m experiments in good agreement with the theory. The scaling of the equilibrium-field product ($B_{\ell=1}\, B_{\ell=0}/B_o^2 = f(\beta, ha)\, ha^2/R$) from the 5-m to the 8-m experiment, given by sharp-boundary theory, has also been confirmed by experiment. This is shown in Fig. 5 where the curves represent the 8-m equilibrium field ratio scaled theoretically from its value at 5 meters (Fig. 2). The measured 8-meter ratio is shown by the horizontal dashed line, and the two points give the limits of the measured values of β.

2. Measurements of Plasma Parameters. Measurements have been made of the plasma radius as a function of time, determined by side-on luminosity profiles, and plasma excluded flux, determined by the balanced probe method. These data

have been combined to yield the plasma beta as a function of time. These variables have been measured in positions of minimum and maximum plasma radius [land (L) and groove (G), respectively] in order to study the approach of the plasma column to theoretically predicted transverse (or toroidal) and axial equilibrium.

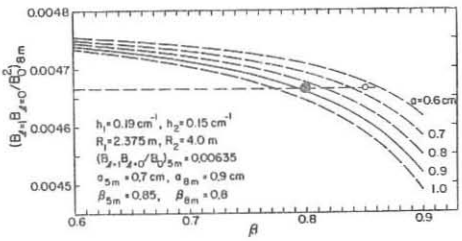

Fig. 5. Values of $B_{\ell=1}\ B_{\ell=0}/B_o^2$ predicted for plasma equilibrium in the toroidal sector, scaled from the 5-m-sector equilibrium. Experimental points are shown

According to sharp boundary (SB) theory, there exists for each plasma radius a unique value of beta for which toroidal equilibrium is possible. Figure 6 compares this predicted value of beta in a land for experiments J(5m) and K(8m) (using the observed plasma radius) with the measured plasma beta on axis. Theory and experiment show excellent agreement at later times, confirming the streak photograph behavior (cf. Fig. 4), but not at earlier times when axial pressure equilibrium between lands and grooves has not yet been achieved.

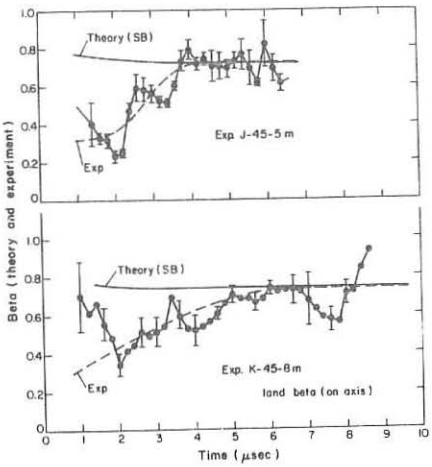

Fig. 6. Comparison of predicted and measured beta on axis vs. time in a land region from the 5-m (top) and 8-m (bottom) toroidal sector experiments.

A basic assumption of the SB theory is axial pressure equilibrium, i.e. nkT = constant independent of length, which requires $\beta_L/\beta_G = (B_G/B_L)^2$. This test has been applied to these data to study the approach to axial equilibrium, as shown in Fig. 7. The measured magnetic field ratio is compared to the design ratio $(B_G/B_L)^2 = (1 - B_{\ell=0}/B_o)^2/(1 + B_{\ell=0}/B_o)^2$, and also to the measured value of β_L/β_G as a function of time. The plasma is seen to reach axial equilibrium in $\sim$ 4 μsec in Exp. J (wavelength =

33 cm) and ~ 6 μsec in Exp. K (wavelength = 42 cm), and the β variation with time is consistent with a transfer of energy density from grooves to lands during this period.

Measurements of the plasma radius, beta, and magnetic field in the various experiments thus confirms in detail the stable toroidal equilibrium seen in the streak photographs during the first 4-10 μsec of the discharge. The initial absence of axial pressure equilibrium does not appear to affect the experimental toroidal force balance.

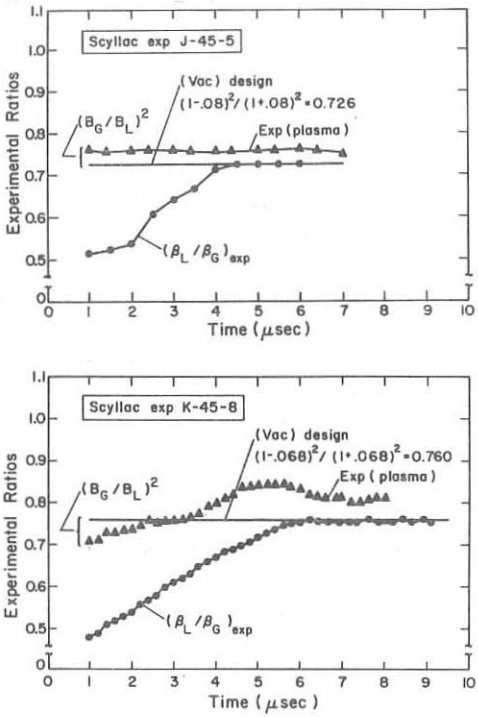

Fig. 7. Comparison of the measured ratio of beta's in the land and groove regions with experimental and design ratios of the magnetic field corresponding to axial pressure equilibrium. The upper curves are for the 5-m and the lower curves for the 8-m experiment.

III. FEEDBACK STABILIZATION SYSTEM FOR THE SCYLLAC TORUS

A. Feedback Considerations.

An $\ell = 0$ MHD feedback stabilization system has been developed for Scyllac to control the long wavelength m = 1 motion. The feedback control is implemented through the generation of small controllable $\ell = 0$ fields which interfere with the $\ell = 1$ equilibrium field to produce a perturbation $F_{1,0}$ feedback force. This is the same type of transverse body force that provides the toroidal equilibrium in the curved geometry and has been previously shown to exert the predicted force on a deliberately induced m = 1 instability in the linear Scylla IV-3 experiment [4]. Its magnitude per unit length is given by sharp-boundary theory as $F_{1,0} = [\beta(3-2\beta)/8]\, B_o^2\, h^2 a^3 \delta_1 \delta_o$ where δ_o is the plasma bumpiness produced by the $\ell = 0$ feedback fields. The destabilizing force per unit length due to the $\ell = 1$ fields is $F_1 = \pi a^2 \rho \gamma_1^2 \xi$, where ρ is the plasma mass density on axis, and ξ is the displacement from equilibrium. Equating these two forces and utilizing the approximate relations for δ_o and δ_1 gives the required feedback current to each $\ell = 0$ coil:

$$I_{FB} = \frac{80\pi(1-\beta)(1-\beta/2)}{\beta(3-2\beta)} \frac{f\rho\gamma_1^2\xi}{B_o B_{\ell=1}/B_o} = 5\,\frac{(4-3\beta)}{(3-2\beta)}\, fB_o\xi\, \frac{B_{\ell=1}}{B_o} \propto (hR)^{-1/2}, \qquad (5)$$

where $\delta_o = hI_{FB}/10(1-\beta)\, B_o f$ and f is a geometrical parameter of the $\ell = 0$ feedback coil. Computer modeling [14] indicates the additional constraint that the electrical system delay τ be less than $1/\gamma_1$.

B. Experimental Arrangement of the Feedback Stabilization System.

In Scyllac both the $\ell = 1$ and $\ell = 0$ equilibrium fields are generated by the shaped inner surface of the main compression coil, while the $\ell = 0$ feedback fields are generated by single-turn slotted coils inside the main coil as illustrated in Fig. 8. The feedback stabilization system consists of many components, starting with plasma-position optical detectors, and ending with power amplifier modules which drive the $\ell = 0$ coils.

Experience with the feedback equipment has been gained on the 3-m Scylla IV device, with 10 modules installed to provide a feedback force in one coordinate. These modules were used in a test of their ability to handle an instability that was deliberately induced with $\ell = 1$ fields. With $B_{\ell=1}/B_o = 0.04$, an m = 1 instability growth rate of 0.9 MHz was observed. The feedback system produced a 160 G field in the $\ell = 0$ coils, and with delayed turn-on times as great as 0.5 μsec following the initiation of the discharge, the module output was successful in overcoming the plasma motion to the wall. In Scyllac the feedback system will have a capability of 4.0 kA ($B_{\ell=0}$ = 235 G) with a risetime of 0.9 μsec. With the theoretically predicted growth rate in Scyllac of 0.6 MHz, the feedback should be able to control a plasma displacement of 6 mm.

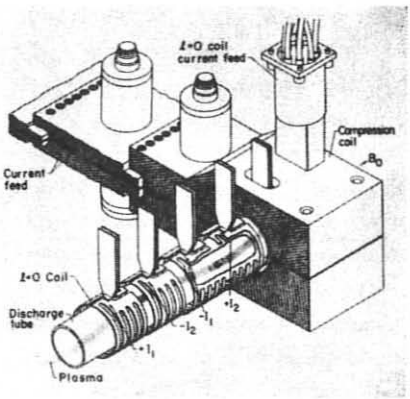

Fig. 8. Arrangement of the $\ell = 0$ feedback coils in the main Scyllac coil.

IV. WALL STABILIZATION AND STAGED THETA PINCHES

Adopting the assumption that the m = 1 motion is indeed the MHD instability predicted on the Princeton-NYU ordering [9,10], as indicated by Scylla IV-3 experiments [4], sharp-boundary theory gives the following dispersion relation:

$$\gamma^2 = h^2 v_A^2 \left[- \beta^2 \left(\frac{a}{b}\right)^4 \delta_1^2 + \frac{\beta(4-3\beta)(2-\beta)}{8(1-\beta)} h^2 a^2 \delta_1^2 + \frac{\beta(3-2\beta)(1-\beta)}{(2-\beta)} \delta_o^2 \right], \quad (6)$$

where a/b is the ratio of plasma and coil wall radii. The first term is a wall stabilization term arising from the $\ell = 1$ dipole currents in the plasma, as illustrated in Fig. 9. This term appears in all the theories, including those with diffuse plasma profiles, regardless of which expansion is used. Freidberg has also derived the first term using a simple magnetostatic model [15] with line dipole currents. The second and third terms are the destabilizing terms arising from the $\ell = 1$ and $\ell = 0$ fields.

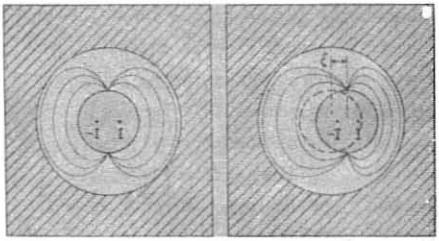

Fig. 9. Illustrating wall stabilization by $\ell = 1$ fields in θ-pinches.

From Eq. (6) it follows that the m = 1 mode can be stabilized by making the wall term dominate, that is by making ha and δ_o small. However, the requirement for toroidal equilibrium,

$$\delta_1 = - \frac{2}{3-2\beta} \frac{a}{R} \frac{1}{h^2 a^2 \delta_o}, \quad (7)$$

must also be satisfied. It is not possible with present Scyllac values of a/b to make both ha and δ_o small, keeping $\delta_1 \sim 1$, without requiring unacceptably large aspect ratios R/a.

A second approach to make the wall term dominate is to make the ratio a/b larger. Conventional θ-pinches produce highly compressed plasmas with a/b ~ 0.1. Because of this the dominant m = 1 motion in Scyllac-type experiments must be feedback stabilized. Despite the fact that the m = 1 mode is predicted to be only weakly unstable for an $\ell = 1,0$ system, the technological requirements on the feedback system are quite demanding. As a result, it is important to make wall stabilization effective. By creating a plasma with $\beta \simeq 0.8$, $\delta_1 \simeq 1$, $\delta_o \simeq 0.1$ and a/b ~ 0.3 to 0.5 it should be possible to wall stabilize the m = 1 mode. This will first be accomplished in linear-staged θ-pinch experiments and later in toroidal experiments. The staging principle is illustrated in Fig. 10.

The staged θ-pinch uses fast-implosion heating and subsequent slow compression from separate energy sources. In this arrangement the implosion heating can

be increased with less subsequent compression heating to produce increased a/b ratios to satisfy the wall stabilization requirements. The staged experiments at LASL will involve conventional filling densities and implosion-heating electric fields $\gtrsim$ 2 kV/cm at the inside of the tube, substantially larger than in the past. In the staged experiments the implosion-heated plasma will be further compressed using an 800-kJ, 50-kV capacitor bank, to demonstrate the staging process. The implosion-heating compression coil will have a length of 4.5-m, a coil bore of 22.4-cm, and a discharge tube bore of 20 cm. The compression field will be variable between 10 to 20 kG with a crowbarred e-folding time of approximately 50 μsec. The plasmas which will be produced in the staged θ-pinch will be collisionless with ion temperatures in the range 1.3 to 2.5 keV and compressed plasma densities in the range 0.2 to 0.8 x 10^{16} cm^{-3}. From Eq. (6), wall stabilization of the ℓ = 1 driven, m = 1 mode should occur provided the ratio of the plasma radius to coil radius has a value given by:

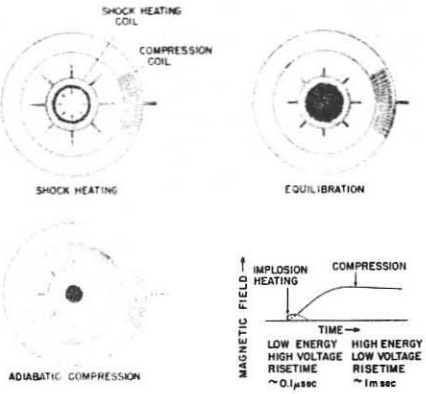

Fig. 10. Principles of the staged θ-pinch.

$$\left(\frac{a}{b}\right)^4 \geq \frac{(4-3\beta)(2-\beta)}{(1-\beta)} (ha)^2 \quad . \tag{8}$$

For plasma parameters: a = 3 cm, δ_1 = 1.0, β = 0.8, and ha = 0.13, Eq. (8) gives a/b = 0.4. In the wall stabilization experiments on the linear 4.5-m θ pinch, an ℓ = 1 helical field will be superimposed on the axial field to drive an m = 1 instability. With the larger a/b ratios, wall stabilization of the mode can be studied in detail. The staged θ pinch is particularly suited for these experiments since the implosion and compression phases of the heating can be varied independently to produce various a/b ratios.

VI. EXPERIMENTS WITH THE 5-METER LINEAR SCYLLAC THETA PINCH

A. Experimental Arrangement.

The linear Scyllac experiment was a five-meter-long, straight theta pinch

which used 5 of the 15 Scyllac capacitor racks to supply energy to the main compression coil. Two additional capacitor racks with a separate trigger system energized the 16-cm-long mirror coils. The inside diameter of both the main and mirror coils was 11 cm, and the quartz discharge tube had an inside diameter of 8.8 cm. The main bank was operated at 45 kV and the mirror bank at 40 and 45 kV. The magnetic field waveforms are shown in Fig. 11.

B. Results Without Magnetic Mirrors.

With an initial filling pressure of 10-mTorr D_2, the plasma had a measured density profile which was approximately Gaussian with an inflection-point radius of 0.8-1.0 cm, a peak density of 1.5-2.0 x $10^{16}/cm^3$, and an ion temperature (as indicated by neutron yields) of 2.5-3 keV. The plasma column exhibited the previously observed [13,16] "wobble" which usually began 4 to 5 μsec after the initiation of the main discharge. The top frame of Fig. 12 shows streak camera photographs which illustrate the plasma wobble.

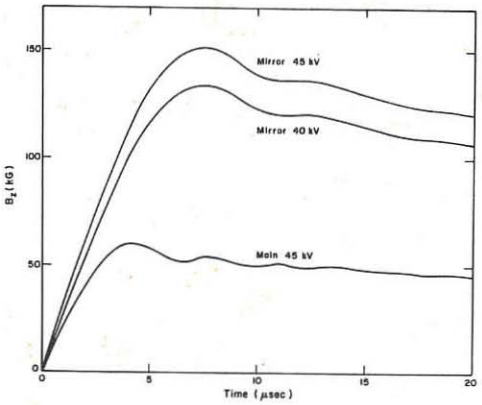

Fig. 11. B_z waveforms for main and mirror fields of the 5-m linear theta-pinch experiment.

The time for propagation of an Alfvén wave from the ends of the coil, using the peak magnetic field and the plasma density on axis, is about 4 μsec. The wobble is probably related to the shorting out of the electric fields in the plasma and the transfer of the diamagnetic current from the electrons to the ions [13,17]. The maximum amplitude of the wobble was about 1.5 cm from the discharge tube axis and the average value 0.5 to 1.0 cm. Stereoscopic views of the plasma column showed that the wobble was an m = 1 rotation with a frequency of about 300 kHz and an amplitude and phase which sometime varied along the coil axis.

C. Stability With Applied Mirror Fields.

The experiment was operated with mirror fields applied 0, 0.2, 0.5, and 1.0 μsec after the main compression field. The addition of the mirror field produced an m = 1, k ≃ 0 instability. (See the center frame of Fig. 12). For the zero delay and 0.2 μsec-delay cases this instability caused the plasma column to

strike the discharge tube wall 5 to 8 μsec after initiation of the plasma discharge. For the larger delays (0.5 and 1.0 μsec) the movement of the plasma column was less the plasma column never striking the discharge tube wall before 15 μsec and sometimes (particularly, with the mirror bank operated at 40 kV) the plasma column never struck the wall (bottom frame of Fig. 12). A change in the discharge tube geometry which shortened the distance between the plasma column and the discharge tube (measured along magnetic field lines) increased the stability of the plasma column. This indicates that the difference in plasma behavior with different mirror field delays is due to line-tying effects. With delayed application of the mirror fields, line-tying has a chance to become effective before the mirror ratio becomes large.

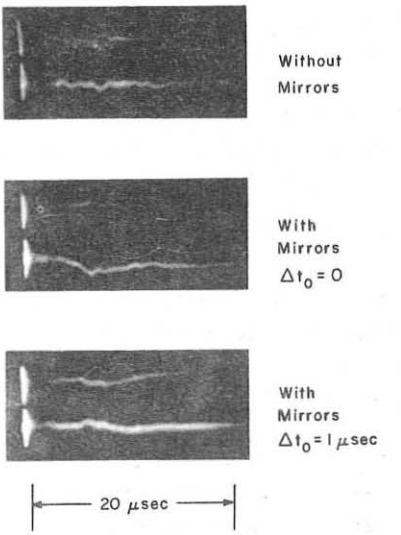

Fig. 12. Streak photographs from the 5-m linear theta pinch showing a no-mirror case and two mirror cases.

D. Plasma Confinement.

Plasma loss out the ends of the theta-pinch was measured using end-on holographic interferograms [13] for the case of no applied mirror field and for the case of delayed application (1.0 μsec) of the mirror field and mirror bank operation at 40 kV. Results are shown in Fig. 13. The end-loss time with applied mirror fields is 18.9 μsec, while that without mirrors is 11.5 μsec. These loss rates were compared with two theoretical models, a computer simulation by W. P. Gula [18] and an analytical model by J. P. Freidberg which extended the model of Morse [19] to diffuse plasma profiles. The two theoretical models are in agreement and predict a loss rate of 16-18 μsec without mirror fields and an increase of plasma confinement by about the mirror ratio (2.5) when mirror fields are added. The predicted loss rates, as well as their ratio, are in considerable disagreement with the experimental results. The experimental end loss times, however, scale from previous experimental results on Scylla IV-1 [20] and Scylla IV-3 [13] if it is assumed that the loss time varies as $L/T_i^{1/2}$ where L is the length of the coil and T_i is the ion temperature. Table I compares observed end loss times

TABLE I

END LOSS SCALING IN THETA PINCHES

	Length (m)	T_i (keV)	n (10^{16} cm^{-3})	τ observed (μsec)	τ scaled (μsec)
Scylla IV-1	1	3.2	2.1	2.4	2.13
Scylla IV-3	3	1.4	3.2	10.1	9.67
Scyllac Linear	5	2.7	2.0	11.5	11.50

in the three experiments without mirrors to the predicted values, normalized to the linear Scyllac data point.

E. Plasma Electron Temperature.

The electron temperature was measured by 90° Thomson scattering at 6943Å. The electron temperature at peak field was 610 ± 110 eV. The experimental value at peak field agrees well with the value (∿600 eV) predicted by the theoretical model of Morse [19] in which the electron temperature is determined by the relative rates at which energy is supplied to the electrons by collisions with the ions and is in turn lost out the ends of the main coil by electron thermal conduction. The theory correctly predicted the observed electron temperature for Scylla IV-1 [20], Scylla IV-3 [21], and the Scyllac linear experiment as shown in Table II.

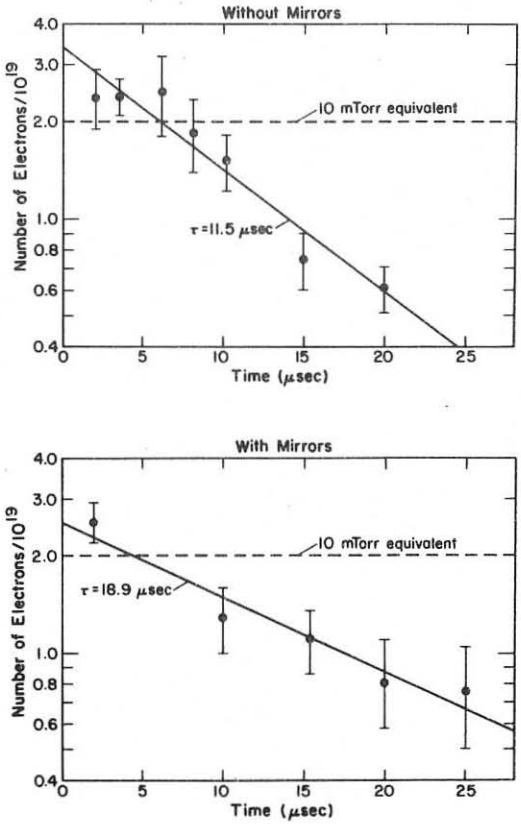

Fig. 13. End loss in the 5-m linear experiment with and without magnetic mirrors.

TABLE II

ELECTRON TEMPERATURE SCALING WITH PLASMA LENGTH

	Length (m)	T_e observed (keV)	T_e predicted (keV)
Scylla IV-1	1	.33	.29
Scylla IV-3	3	.39	.43
Scyllac Linear	5	.61	.53

REFERENCES

1. W. R. Ellis, et. al., Proc. 2nd Topical Conf. Pulsed High-Beta Plasmas, Max-Planck-Institut fur Plasmaphysik Report IPP 1/127, July 1972.
2. F. C. Jahoda, et. al., Proc. Fifth European Conference on Controlled Fusion & Plasma Physics, Grenoble, Aug. 1972.
3. K. S. Thomas, et. al., Proc. 2nd Topical Conference Pulsed High-Beta Plasmas, Max-Planck-Institut fur Plasmaphysik, Report IPP 1/127, July 1972.
4. K. S. Thomas, et. al., Phys. Fluids 15, 1658 (1972).
5. R. F. Gribble, et. al., Proc. 2nd Topical Conference Pulsed High-Beta Plasmas, Max-Planck-Institut fur Plasmaphysik, Report IPP 1/127, July 1972.
6. F. L. Ribe & M. N. Rosenbluth, Phys. Fluids 13, 2572 (1970).
7. H. Weitzner, Phys. Fluids 14, 658 (1971).
8. J. P. Freidberg, Plasma Phys. Contr. Nucl. Fusion Res. 3, 215 (1971).
9. M. N. Rosenbluth, et. al., Phys. Fluids 12, 726 (1969).
10. H. Grad & H. Weitzner, Phys. Fluids 12, 1725 (1969).
11. J. P. Freidberg & B. M. Marder, Phys. Fluids 14, 174 (1971).
12. F. L. Ribe, et. al., "Proposed Experiments on Heating, Staging, and Stabilization of Theta Pinches", Los Alamos Scientific Laboratory Report LA-5026-P.
13. R. F. Gribble, W. E. Quinn, & R. E. Siemon, Phys. Fluids 14, 2042 (1971).
14. K. I. Thomassen, Los Alamos Scientific Laboratory Report LA-4598-MS, 1971.
15. J. P. Freidberg, Phys. Fluids, to be published.
16. H. A. B. Bodin, et. al., Plasma Phys. Contr. Nucl. Fusion Res. 1, 193 (1971).
17. K. S. Thomas, Phys. Rev. Letters 23, 746 (1969).
18. W. P. Gula, to be published.
19. R. L. Morse, Phys. Fluids, 11, 1558 (1968).
20. E. Little, W. Quinn, & G. Sawyer, Phys. Fluids 8, 1168 (1965).
21. K. S. Thomas, et. al., Phys. Fluids 15, 1658 (1972).

*Work performed under the auspices of the United States Atomic Energy Commission.

VI Eur.Conf.Contr.Fusion and Plasma Physics, Moscow 1973

HIGH-BETA PLASMAS - PRESENT STATE AND PROSPECTS

Wolfgang Lotz

Max-Planck-Institut für Plasmaphysik, Euratom Association,

Garching bei München, Fed.Rep.of Germany.

Abstract: As a future fusion reactor will require beta-values around 0.1 or higher, it is necessary to investigate the properties of high-beta plasmas. At present beta-values between 0.1 and 1 and ion temperatures around 10 keV have been achieved with high-beta experiments, but confinement times are still much too low. In order to increase confinement times, a number of toroidal field configurations are being investigated: Screw-Pinch, Belt-Pinch, Reversed Pinch, and High-Beta Stellarator. Progress has been made in recent years and more is hoped for in the future. High-beta experiments as well as low-beta experiments have still a long way to go for the fusion reactor.

Introduction

In this paper I shall give a short history of high-beta plasmas which will essentially take the form of a review of shock-heated pinch experiments. Then I shall deal with the question whether there is a chance of high-beta plasma experiments leading eventually to a fusion reactor. At the end of my talk I shall try to give a survey of the present state of high-beta plasma experiments, compare these with present low-beta experiments, and give some idea of planned experiments or experiments already under way in different laboratories. It should be noted that it has not been possible to take into account all the results reported in papers to be presented at this conference. Thus the state of high-beta plasma physics as described in this paper may not be quite correct and complete and the results cited may not reflect the exact merits of the respective laboratories or scientists.

In this paper the quantity beta is the ratio of plasma pressure to overall pressure, while the term "high beta" is used for beta in the range between 0.1 and 1.

Short History of High-Beta Experiments

As you all well know, the precursor of present-day high-beta experiments has been the z-pinch, the theta-pinch, and combinations thereof, for example the screw-pinch. The z-pinch was the first to be examined both linearly and toroidally but it had to be discarded because of the poor stability characteristics even in the so called stabilized versions with superposed longitudinal magnetic field. Recently the Los Alamos group has revived the fast z-pinch with encouraging results as we have heard from Dr.Quinn the day before yesterday. And there is the Plasma Focus, of course, with quite few contributions to this Conference.

The next to follow were linear theta-pinches of the Thetatron, Scylla, and Isar family as well as low-density shock-heating experiments performed, for example, at Maryland, Jülich, and Garching. These experiments showed that it is possible to reach the necessary fusion temperatures of between 10 and 20 keV with at least marginally stable plasmas. The remaining problem seemed to be the confinement time, because these linear experiments are subject to end losses. In principle, it should be possible to use a linear theta-pinch to build a pulsed fusion reactor, but the necessary length of several kilometers does not make it very attractive /1/. Proposed remedies such as mirrors or "rough ends" do not seem to increase the confinement time by more than a factor of three or at most an order of magnitude.

End problems could be avoided by bending the linear theta-pinch into a torus, but then the well-known toroidal drift occurs, thus limiting the confinement time to even smaller values. To overcome toroidal drift, several proposals have been made over the years. One of the first had been the M&S-configuration by F. Meyer and H.U.Schmidt in 1958 /2/, characterized by a corrugated surface on the side towards the major axis. Theory and experiments showed that the toroidal drift could be overcome, but at the same time a fast-growing m=1 mode was found with little chance of wall stabilization.

More recently Blank, Grad, and Weitzner showed in 1968 /3/ that high-beta equilibria should be possible with magnetic fields of the Stellarator type. The similarity of the field structure to the well-known Stellarator of low beta led to the somewhat misleading name "high-beta Stellarator". Equilibria of the high-beta Stellarator type might be characterized as an extended class of M&S equilibria with, in general, no plane of symmetry and with a non-coplanar magnetic axis. The rotational transform does not play the dominating role as in the real Stellarator concept and Pfirsch-Schlüter diffusion is less important.

The equilibrium and stability of this class of configurations were investigated later on by theoreticians of the New York University group, and at Princeton, Los Alamos and Garching. It was found that the high-beta Stellarator with an $\ell=1$ distortion in leading order and admixtures of $\ell=2$ and/or $\ell=0$ should be favourable with respect to both equilibrium and stability.

The high-beta Stellarator concept is being intensively studied at Los Alamos and Garching. There are several contributions to this conference which show that progress has been made in recent years towards a better understanding of the behaviour of plasma in different field configurations, both linear and toroidal. The confinement time has been increased relative to the toroidal drift time.

There are other configurations that have been investigated in recent years which can be characterized as being combinations of the z-pinch and theta-pinch, for example the screw-pinch, the belt-pinch, the reversed pinch with field programming. The screw-pinch turned out to be in equilibrium as theoretically predicted, but in order to achieve equilibrium not too far from the outer wall, the toroidal current had to be above the Kruskal-Shafranov limit and the pinch thus tended to be unstable.

The belt-pinch is a screw-pinch with non-circular cross-section, namely an elliptical cross-section where the major axis is parallel to the major axis of the torus. In the belt-pinch configuration, equilibrium can be achieved with toroidal currents below the Kruskal-Shafranov limit even for high beta-values. Accordingly the belt-pinch

turned out to be unusually stable and could be observed for approx. 100μs at temperatures around 10eV. On the other hand Krause, Wilhelm, and Zwicker /4/ have presented a paper the day before yesterday, showing that the belt-pinch becomes unstable, as expected, when the Kruskal-Shafranov limit is exceeded. In a paper discussing the reactor aspects of the belt-pinch, Herold, Wilhelm, and Zwicker /5/ pointed out yesterday that the belt-pinch might be a configuration suitable for a pulsed reactor with a magnetic field produced by normal conducting coils. The favourable power balance of the belt-pinch with respect to nuclear power production and ohmic losses in the conductors is ultimately caused by the combination of high beta and toroidal fatness (small aspect ratio).

It may happen eventually that a high-beta plasma cannot be fully stabilized with stationary fields or that it is not possible to reach a fully stable equilibrium. In this case dynamic stabilization or feedback stabilization might be necessary. Experiments using both methods are under way in several laboratories. These show that stabilization is possible in principle, but that both methods at present still seem to be costly and might render a fusion reactor uneconomic.

High Beta and the Fusion Reactor

Before we go any further, let me first say something about the relation between high beta and shock heating. The fact that present-day high-beta experiments nearly without exception use shock heating as an effective heating method does not necessarily mean that the fusion reactor will also need shock heating.

In aiming at a fusion reactor with as high a beta as possible, it is mandatory to investigate configurations with high-beta plasmas even if the means used to produce them should not be feasible in a fusion reactor. It might well turn out that other heating methods (for example ohmic heating, magnetic pumping, neutral injection, laser produced or heated plasmas) will have to be used in a fusion reactor, but these other heating methods are not yet sufficiently well developed to heat a high-beta plasma to near fusion temperatures.

Current toroidal experiments may be assigned to one of the following four configurations:

	axisymmetric (Toroidal current necessary)	non-axisymmetric (Toroidal current not necessary)
Low Beta	Tokamak	Low-Beta Stellarator
High Beta	Screw-Pinch Belt Pinch Programmed Pinch	High-Beta Stellarator

As a toroidal current is necessary for the axisymmetric configurations, a fusion reactor based on one of these configurations will inevitably be a pulsed one, while the Stellarator configurations could be stationary, at least in principle. The term "low beta" in the above table is used in the sense that the configurations Tokamak and low-beta Stellarator have a theoretical upper limit $\beta_{critical}$ of a few per cent. This is true at least of a Tokamak with circular cross section, and it is true of the low-beta Stellarator as long as Pfirsch-Schlüter currents are essential. The limits between low beta and high beta might vanish for Tokamaks with non-circular cross-sections and for classical Stellarators with admixtures of helical fields of adjacent ℓ-numbers.

While a fusion reactor of the Tokamak, Screw-Pinch (Belt-Pinch, programmed pinch) or low-beta Stellarator type would most probably have a small aspect ratio (major radius divided by minor radius), the high-beta Stellarator would most probably have a large aspect ratio of 100 or higher for theoretical reasons (equilibrium, stability).

In the last decade, there have been many discussions on the probability of present-day high-beta plasma experiments eventually leading to a fusion reactor. The prevailing opinion about fusion reactors assumed that only machines with small aspect ratio would be favourable with respect to investment costs. This would include the screw-pinch and its derivatives.

Mainly economic reasons have led to the general conclusion that stationary fusion reactors with aspect ratios of as high as one hundred or more, seemingly necessary for the high-beta Stellarator, have little chance if the total output is to be below 20 GW, a limiting value which is prescribed by network and environmental restrictions. At this conference, Kaufmann and Köppendörfer /6/ have shown yesterday that reactors are not limited to low aspect ratios, because cost optimization does not necessarily require that the plasma radius be approximately equal to the blanket thickness if plasma physical requirements put certain restrictions on the aspect ratio and beta.

As long as superconductor costs are a considerable fraction of the total boiler costs, stationary high-beta reactors with aspect ratios of one hundred can readily compete with fat low-beta Stellarators and Tokamaks. This is mainly due to the fact that the magnetic field necessary for a high-beta Stellarator is much lower than that for a low-beta Stellarator or even a Tokamak.

Another point worth mentioning is that a high-beta Stellarator fusion reactor is not necessarily a pulsed device. For the time being, shock heating is the only proven way of instantly providing a high-beta plasma. To reach the ignition point directly by shock heating, however, is a serious technical problem because the electric field has to be about 10 kV/cm. A more realistic start-up procedure could be: shock heating up to 1 keV and an additional slow heating method, e.g. neutral injection. The start-up problems may be further eased by starting with reduced densities. After start-up, the reactor could be stationary.

Comparison of Low-Beta and High-Beta Experiments

Let us now have a look at the gap that separates low-beta and high-beta devices from the fusion reactor. Some quantities necessary for a fusion reactor will be approximately as follows:

Temperature:	10 to 20 keV
Density times confinement time:	10^{14} to 10^{15} s/cm^3
Beta:	0.05 to 1

Recent results with Tokamaks indicate that electron temperatures of more than 1 keV can be reached, that the product density times confinement time is higher than in any other configuration at confinement times of 10 ms, but that beta-values of only 10^{-2} were attained. Experiments are under way to show that all three values can be improved by, for example, using higher toroidal currents.

Low-beta Stellarator experiments have reached the largest confinement times at relatively low densities and temperatures, and thus beta-values of only around 10^{-3} were attained. Experiments are under way to increase temperatures and densities at even longer confinement times.

Screw-Pinch experiments with circular cross sections suffer from seemingly unavoidable instabilities, while the Belt-Pinch keeping within the Kruskal-Shafranov limit seems to be limited in confinement time by classical diffusion only, the temperature not being higher than 10 eV at the moment. Experiments to attain higher temperatures are under way. The programmed pinch, too, seems to be limited at present by classical diffusion at relatively low temperatures.

As to the high-beta Stellarator, there is agreement that fusion temperatures can be reached in the same way as in the linear theta pinch, but this is not an urgent problem at the moment. The problem here is to show that at least one stable equilibrium configuration exists or that the growth rate of instabilities is so low that feedback stabilization can be applied.

By way of summary, it can be stated that all configurations considered, low beta as well as high beta, are still far from a fusion reactor. It is not possible to say which configuration is closest to the fusion reactor because no simple common criterion is available. It might well be that the difficulties now encountered by high-beta experiments will hit low-beta experiments as well, only at a later stage - and vice versa.

Present State and Prospects of High-Beta Experiments

Let us now have a look at the present state and at the future of toroidal high-beta experiments in a selection of laboratories.

The compact torus experiment TEE at Jülich /7/, a high-beta Tokamak or a low-beta screw-pinch at beta-values between 0.02 and 0.4, has shown instability at "q"-values below unity, as expected, but enhanced stability for q-values between 1 and 2. Operating at lower densities than most high-beta devices, this experiment should provide information on low compression ratio toroidal plasmas and wall stabilization effects. Equilibrium is achieved by a variable transverse magnetic field and thus the broad plasma column can be well separated from the wall. The plasma lifetime is 100 to 200 μs at temperatures around 100 eV. The lifetime appears to be limited by a gradual drift of the equilibrium position towards the wall, which will hopefully be avoided by further improvements in the programming of the field components.

Two compact screw-pinch experiments are being built in Jutphaas /8/, of which the larger, SPICA, should be completed by now. Experiments in previous devices support the prospects for good stability when the security factor q is larger than 1. However, the beta-values were small, the temperature only around 1 eV and the plasma lifetime rather limited.

The high-beta reversed field experiment at Culham /9/ has shown that apparently stable configurations with field programming can be attained at temperatures of about 20 eV, the confinement time being limited to 40 μs by field diffusion only. Recent experiments at higher toroidal plasma currents near 100 kA have yielded higher electron temperatures of up to 50 eV, but then instabilities developed and the confinement time was not enhanced, being no

longer limited by diffusion alone. It has thus still to be shown that the seemingly profitable characteristics of the reversed field configuration at relatively low temperatures can be reproduced at appreciably higher temperatures. Tomorrow there will be an invited paper by R. Bickerton on the topic of diffusion.

The heating of a z-pinch to high temperatures has been resumed at Los Alamos /10/ and incorporated in a fast toroidal z-pinch. Kilovolt temperatures have been obtained and the question then arises whether or not the stability problem can be solved by field programming into a reversed field pinch similar to the configuration used at Culham. Current experiments seem to be concerned with this question.

Screw-pinch-like configurations with elliptically stretched plasma cross-sections have recently been tested at Jülich in the TESI experiment /11/ and at Garching in Belt-Pinch I./12/. The beta-values were 0.1 and 0.5 respectively and the temperatures were around 10 eV, and thus the observation times of 40 and 100 μs respectively appear to be limited by classical field diffusion without evidence of strong macroscopic instability. In order to reach higher temperatures and longer confinement times, two larger experiments, TENQ in Jülich and Belt-Pinch II in Garching, are being constructed and should deliver results in 1974. In TENQ, plasmas with moderately stretched cross-sections will be studied, with particular emphasis on the effect of the detailed geometry of the cross-section on the plasma confinement behaviour. In Belt-Pinch II, on the other hand, strong ellipticity is aimed at with ratios of 10 to 20. It should be possible to reach temperatures of around 1 keV, and confinement times of up to 1 ms are hoped for.

The high-beta Stellarator concept has been pursued at Los Alamos by the Scyllac group and at Garching in the Isar T 1 experiment. Both groups have carried out experiments with $\ell=1$ fields together with admixtures of $\ell=2$ and/or $\ell=0$ both in linear and toroidal geometry. There has been an invited paper by W.E. Quinn yesterday /13/ concerned especially with the Scyllac concept, and so I shall make only a few remarks on the results and plans of the Los Alamos group.

In the 120 degree sector experiment with a length of 5 m and 8 m respectively at Los Alamos, the $\ell=1/\ell=0$ fields were produced with shaped coils.
It has been shown that an equilibrium is well established, and that the confinement time is up to 6 times the toroidal drift time at temperatures around 1 keV. Containment is terminated by an m=1 motion of long wavelength (k=0) to the wall. This is in agreement with MHD theory, but may just as well be caused by end effects. Feedback stabilization has not been tried on the sector experiment, but has been successfully used in a linear Scylla experiment.

The 5m sector experiment had not been completed into a torus of the same radius; instead the 8m sector experiment was built and now a torus 4 m in radius is being constructed and should be completed in 1974. The Los Alamos group expects to have the 8 m sector in operation with feedback by September 1973. As wall stabilization cannot be investigated with Scyllac a staged linear experiment is under construction and should be completed in 1974. A staged toroidal experiment is under discussion, its completion time is not known yet.

The Isar T high-beta Stellarator at Garching is the first fully toroidal device of its kind to be completed. Recent results will be given tomorrow afternoon under the subject heading"stellarators" in a paper by Fünfer, Kaufmann, Lotz, Neuhauser and Schramm /14/. It is shown that there exists at least an M&S-like equilibrium with an l=1/l=2 field. Confinement times and instabilities are similar to those reported by the Los Alamos group, no higher m-modes have been found, in contrast to MHD theory.

As mentioned earlier, it should be possible by means of wall-stabilization to avoid the m=1, k=0 MHD instability observed. It is, therefore, in discussion, to build at Garching a larger torus with a major radius of approximately 8 m, containing a shock-heated plasma without adiabatic compression at a compression ratio near 2. The rise time of the magnetic field would be approximately 0.5 μs. In this larger experiment it should be possible to decide whether the dangerous m=1 modes can be suppressed by wall stabilization. The power-crowbar bank or the iron-transformer circuit will be designed in such a way that 10 times the growth time for the m=1 mode can be observed. In case wall stabilization works as it should, confinement

times of at least 50 μs at temperatures of about 1keV should be attainable in 1976.

References:

/1/ Köppendörfer, W., W.Schneider, and J.Sommer; Proc.5th Europ. Conf.Contr.Fusion, Grenoble, 1, 19 (1972).

/2/ Meyer, F., and H.U.Schmidt; Z.Naturforschg. 13a, 1005 (1958).

/3/ Blank, A.A., H.Grad, and H.Weitzner; Proc.3rd Conf.Plasma Physics, Novosibirsk, CN-24/K-6 (1958).

/4/ Krause,H., R.Wilhelm, H.Zwicker; This Conference, 1, 273 (1973).

/5/ Herold, H., R.Wilhelm, H.Zwicker; This Conference, 1,333 (1973).

/6/ Kaufmann, M., and W.Köppendörfer; This Conference, 1,341 (1973).

/7/ Noll, P., M.Korten, E.Kugler, F.Sand, F.Wadbroeck and G.Waidmann; This Conference 1, 14 (1973).

/8/ Waelbroeck F., Proc. 3rd Int.Symp. Tor.Plasma Confinement Garching, A 1 (1973).

/9/ Gowers, C.W., G.W.Long, A.A.Newton, D.C.Robinson, A.J.L.Verhage and H.A.B.Bodin. This Conference 1, 265 (1973).

/10/ Baker, D.A., L.C.Bürkhardt, J.N.DiMarco, P.R.Forman, A.Haberstich. R.B.Howell, H.J.Karr, L.W.Mann, and J.A.Phillips, This Conference 1, 293 (1973).

/11/ Plantikow, U., and J.Schlüter; Proc.3rd Int.Symp.Tor.Plasma Confinement, Garching, A.6 (1973).

/12/ Zwicker, H., and R.Wilhelm; Proc.5th Europ.Conf.Contr.Fusion, Grenoble, 2, 59 (1972).

/13/ Quinn W.E., et al. This Conference 2, ... (1973).

/14/ Fünfer E., M.Kaufmann, W.Lotz, J.Neuhauser. G.Schramm; This Conference 1, 109 (1973).

SOME FEATURES OF CURRENT AND FUTURE EXPERIMENTS:

Configuration	Device	T eV	n_e cm^{-3}	τ_E s	β –	Problems	Future
1	2	3	4	5	6	7	8
Tokamaks		10^3	10^{14}	10^{-2}	10^{-2}	Higher Temperatures Higher Densities Longer Confinement Times Higher Betas	Experiments under way in various countries
Low-Beta Stellarators		10^2	10^{13}	10^{-2}	10^{-3}	Higher Temperatures Higher Densities Longer Confinement Times; Higher Betas	e.g.Garching: Wendelstein VII (1976)
Compact Torus	Jülich: TEE	10^2	10^{14}	10^{-4}	0.02 to 0.4	Higher Temperatures Higher Densities Equilibrium	Jülich: TEE
Screw-Pinch	Jutphaas: Screw-Pinch Garching: Isar IV	10	10^{16}	10^{-5}	10^{-2}	Higher Betas Kruskal-Shafranow Limit	Jutphaas: SPICA (1973)
Programmed Pinch	Culham: HBTX	20	10^{16}	4×10^{-5}	0.6	Higher Temperatures Instabilities	Culham: HBTX Los Alamos: Fast z-Pinch

SOME FEATURES OF CURRENT AND FUTURE EXPERIMENTS (continued):

1	2	3	4	5	6	7	8
Belt-Pinch	Jülich: TESI Garching: Belt-Pinch I	20	10^{15}	10^{-4}	0.1 to 1	Higher Temperatures Longer Confinement Times	Jülich: TENG (1974) Garching: Belt-Pinch II (1974)
High-Beta Stellarator	Los Alamos: Scyllac Garching: Isar T 1	10^{3}	10^{16}	10^{-5}	~1	Longer Confinement Times m=1 MHD Instability Wall Stabilization Feedback Stabilization	Los Alamos: Larger Scyllac (1974) Staged Experiment Garching: Wall-Stabilized Stellarator (1976)

EXPERIMENTS ON THE CONFINEMENT OF COLLISIONAL PLASMAS IN MIRROR TRAPS

Yu.T.Baiborodov, Yu.V.Gott, M.S.Ioffe, B.I.Kanaev, E.E.Yushmanov

I.V.Kurchatov Institute of Atomic Energy, Moscow, USSR

Introduction. A few experiments have been carried out recently to investigate the stability and containment of hot-ion mirror plasma in the collisional regime. By the collisional regime is meant one in which the plasma losses are caused mainly by the ion Coulomb scattering, and not by other mechanisms such as charge exchange or instabilities.

What is interesting in such regimes? It is well known that a number of kinetic instabilities can develop in a mirror plasma. They are associated with the angular distribution anisotropy of the confined particles, in other words, due to the presence of loss cones in the velocity space. Conditions for such a particular instability to be excited depend on the particles distribution inside the allowed volume in the velocity space; a statisticaly smoothed distribution function provides more reliable stability. If plasma confinement is limited by the ion Coulomb scattering the smoothed distribution is established automatically due to the same Coulomb collisions, and takes the form of the so-called equilibrium-collisional distribution. It is just this form that it should take for a steady-state thermonuclear mirror plasma. That is why it is more preferable to study plasma stability in the collisional regimes. When there are no instabilities these regimes provide a proper model of a thermonuclear plasma with respect to such important characteristics as the equilibrium relationship between the ion and electron temperatures, ambipolar potential, Coulomb losses and others. Therefore, investigations of a collisional plasma, even if its density and temperature are relatively low, permit us to elucidate the principal physical problems of the behaviour of a hot and dense plasma.

In our paper, we shall consider the experimental results obtained with the PR-6 and PR-7 devices at the I.V.Kurchatov Institute /1,2/. They will be compared with the results obtained from two similar experiments with 2xII /3/ at Livermore and DECA II /4/ in

Fontenay-aux-Roses. The main data on these installations and plasma parameters are listed in the following table.

	PR-6	PR-7	2xII	DECA II
Central magnetic field (KG)	5.0	5.0	6.5	3.5
Longitudinal mirror ratio R_{II}	2.4	2.0	2.0	1.8
Distance between mirros (cm)	100	100	100	130
Multipole stabilizing field	6	4	4	4
Transversal mirror ratio $R_\perp$ (in the central plane)	1.75	1.25	2.21	1.05
Plasma diameter (cm)	10	7	12	9
Maximum plasma density (cm^{-3})	3.10^{12}	5.10^{12}	6.10^{13}	1.210^{12}
Mean ion energy $\bar{E}_i$(keV)	0.1-0.3	0.4	1-10	0.2
Electron temperature (eV)	5-15	15	80-250	
$\omega_{Pi}^2/\omega_{Bi}^2$ ($n=10^{12}cm^{-3}$)	800	800	900	1500

In all four cases, the pulsed injection technique was used therefore, all the results refer to decaying plasmas.

PR-6 and PR-7 Experiments. Reproducible regimes of stable plasma containment for $n \lesssim 10^{11} cm^{-3}$ and $E_i \simeq 1.0$keV have been achieved in the earlier PR-6 experiments /5/; the confinement time was 10-20msec. depending on the charge exchange losses. As the densities are an order of magnitude greater ($n=2-3.10^{12}$, $E_i \simeq 0.25$keV) new features in plasma behavior are revealed. The main features are as follows.

1. Three decay phases were observed from the density history in a decay cycle (Fig. 1a). During the first 150-200 μsec the density decreases with a characteristic time of 250 μsec. approaching $\approx 10^{12} cm^{-3}$. Then a more rapid decay with a characteristic time of 100 μsec. is observed. At the end of this phase the plasma density falls to $\approx 10^{11}$ cm^{-3}. Following that the plasma again decays slower, and smoothly passes into the charge exchange phase with the time $\sim 10^{-3}$sec.

2. Those three decay phases can be distinguished by the level of plasma HF noise (Fig.1b). During the first phase the intensity of oscillations is small, the amplitude being $\sim$ 0.1v at the plasma periphery. The second phase is accompanied by a burst of considerable stronger oscillations, their amplitude being 10v and even higher at a burst maximum. The third phase is characterized by a gradual damping ot the oscillations.

3. The plasma potential φ varies qualitatively in a similar fashion to the intensity of HF (Fig.1c). In the beginning of the first phase its typical value was 15 - 25v. After a slight increase in the potential during this stage it grows rapidly together with the oscillation burst. At a burst maximum φ can reach 150 - 200v - this magnitude is close to T_i/e. Then it decreases monotonically up to 15 - 20v.

4. The behaviour of the temperature T_e is similar to that of the plasma potential during the entire decay cycle. Numerically it remains approximately equal to $(1/3 - 1/4)e\varphi$.

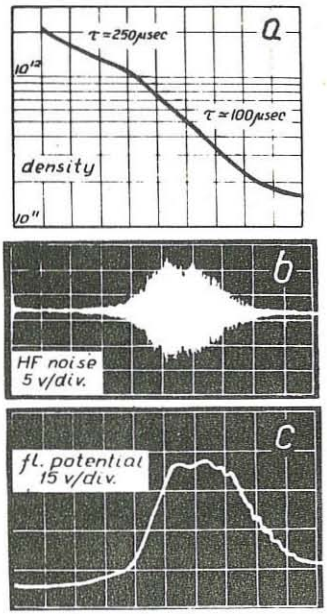

Fig. 1

5. Variations in the initial ion temperature T_i do not change qualitively the pattern of the decay described while they result in certain quantitative variations. As T_i increases: a) the characteristic density decay time at the beginning τ_o also increases; b) the duration of the first phase decreases; c) oscillations grow more rapidly and up to higher amplitudes; d) the plasma potential during a burst also increases to higher values (Fig.2).

It follows from the above results that a certain instability is very likely to appear in the plasma during the decay. Before proceeding to a more detailed analysis of these results it would be quite

reasonable to put a question: if these results do really reflect any general properties of mirror plasmas or they could depend mostly on individual "properties" of the experimental device as it often happens in plasma investigations. In this case we should primarily emphasize such properties as a possible specific character of the ion distribution function of the injected plasma, magnetic field configuration, vacuum conditions.

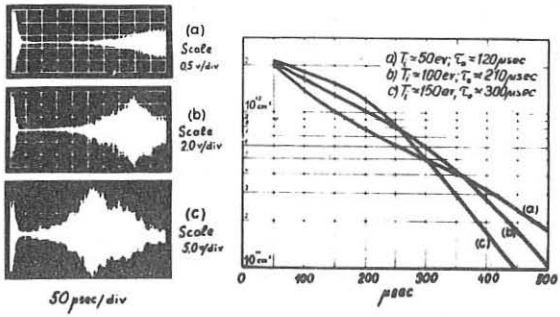

Fig. 2

In this connection let us draw our attention to the increasing delay of an instability burst as the ion temperature decreases. Thus, at T_i=50ev the instability appears in 350-400 sec. after injection. This time interval is five times greater than the time of ion scattering into the loss cone at a density of 10^{12}cm^{-3}. In this case the collisions have sufficient time to level all rough features in the initial distribution, and make it approach the equilibrium-collisional distribution. If, nevertheless, an instability appears so late it can in no way be attributed to the biography of the ion distribution function at the instant of injection.

To find out possible effects of the magnetic configuration, the experiments with PR-7 similar to those with PR-6 have been carried out. Both devices are identical in all respects with the exeption that the stabilizing field is hexapole in PR-6 while it is quadrupole in PR-7. This difference influences both the injection conditions and the spatial distribution of a confined plasma. In both devices, a hot-ion plasma was generated by ion-cyclotron heating of a cold plasma jet passed along the trap axis. Injection from an intense beam-plasma discharge has been also tried in the last runs on the PR-7. The results obtained with the PR-7 are shown in Fig.3. It is seen that the decay pattern is similar to that of PR-6. The micro-

wave interferogram indicates a sharp increase in the plasma loss rate after an initial phase of slow decay. Such an increase is accompanied by a rapidly growing plasma potential and HF intensity. The PR-7 frequency spectrum is also similar to that of the PR-6.

The only difference is that the decay anomalies in the PR-7 manifest themselves in a more pronounced form.

The vacuum conditions really exert strong influence on the entire decay process. As the pressure of neutral gas is increased the instability is gradually smoothed, and if the pressure is sufficiently high – of the order of 10^{-6} torr. – it disappears completely. Here, we do not mean the base pressure, but the pressure stated after injection. The latter depends on the amount of desorbed gas from the walls under plasma bombardment. Therefore, if the chamber walls are outgassed insufficiently the instability can be partly or even completely suppresed. As an illustration Fig. 4 presents the oscillograms of n(t) and HF in-

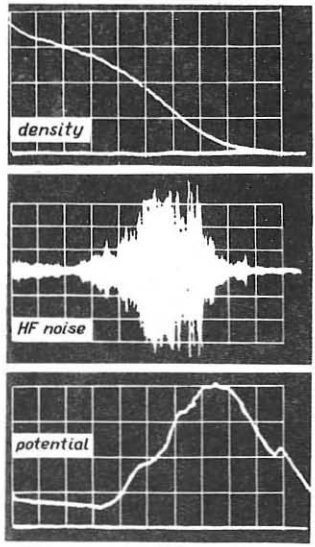

Time scale 25 μsec/div.

Fig. 3.

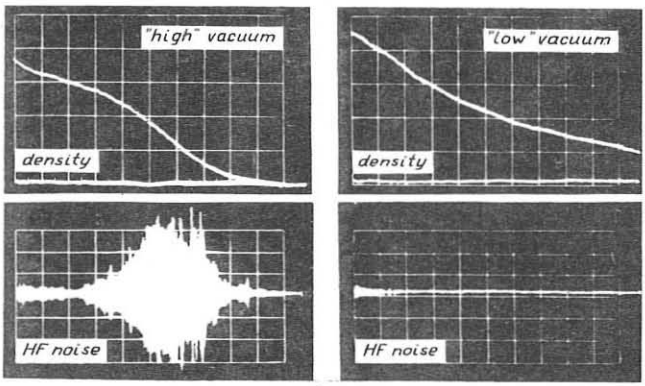

Time scale 25 μsec/div.

Fig. 4.

tensity for two cases which differ only by a degree of wall outgassing.

Thus, all the above data indicate that anomaluos plasma decay both in the PR-6 and PR-7 is attributed to the inherent plasma properties but not to any particular features of the experimental conditions.

Let us now consider the above results. As to the initial decay phase it seems to be quite explainable by the classical mechanism of Coulomb collisions. Really, within a factor of 1.5-2.0 the experimentally observed loss rate agrees with the calculated values, and what is still more illustrative, it decreases with the ion temperature as it should be due to Coulomb losses through the mirrors. The relation between the electron and ion temperatures in this phase also agrees with the collisional model.

The second phase is of the most interest. Spontaneous exitation of an intense oscillation burst accompanied by increased losses obviously shows that during a decay cycle the plasma passes from a relatively stable state into a strongly unstable. Two questions should be answered here. What kind of instability we are dealing with? and why does this instability excite only in a certain time interval after injection though it should apparently exist in a rather weak form in the very beginning of the decay?

Measurements of the frequency spectra and wave structure of the oscillations supply a partial answer to the first question. During the instability burst the dominating frequency ω is 0.7 ω_{Bi} (ω_{Bi} - the ion - cyclotron frequency at the trap centre). An appreciable amount of the second harmonics - 2ω - is also present, and by the end of the burst the fractural harmonics ($^1/_2\,\omega$, $^1/_3\,\omega$ and other) appear. The characteristic wave lengths in the trasverse direction ($\perp$ B) are comparable with the ion Larmor radius: $k_\perp \rho_i$ =4-5, while the waves are strongly elongated in the longitudinal direction: $k_\parallel \ll k_\perp$. These data even taken alone limit the possible choise among various kinds of instabilities known theoreticaly: the drift loss-cone mode near its excitation threshold could best correspond them /6/. Although the plasma density gradients in the initial decay phase are much higher then theoretical threshold gradients for this instability, in our case its weak excitation at that period may only imply that there should exist stabilizing factors

which were not taken into account in the initial theory. In particular, they include a stabilizing effect of a small amount of plasma (of the order of a few per cent) containing "warm" ions /7/. Such ions can be produced by charge exchange and ionization of cold neutrals entering the plasma. No matter what are the stabilizing factors in practice, their presence is not doubtful because the oscillation amplitude increases rather slowly during a major portion of the initial decay phase.

Therefore, it now remains to answer the question: what makes the plasma "leave" such a quasistable state? Supposing the ion distribution function to be responsible for the instability we should seek an answer in the fact that by the end of the first decay phase the distribution function is more nonequilibrium. Let us consider from this point of view the main experimental data and some resulting consequences, grouping them as follows.

1. It has been mentioned above that during the initial decay phase T_e rises slowly, and it grows rapidly when an instability burst occur. Without going into details concerning the initial increase in T_e, we may emphasize that the subsequent rapid growth is associated with electron heating in the electric fields of the growing oscillations.

2. Plasma potential φ varies in the same manner as T_e since $\varphi = \gamma T_e/e$ where γ - the numerical factor ($\gamma = 3-4$).

3. Any increase in the plasma potential is always followed by a deformation in the ion distribution function in its low energy range. This is due to the fact that an electric field $E_{\parallel} = -\partial\varphi/\partial z$ pushes out the ions, thus weakening the confining action of the mirrors. As a result, the collisional distribution is cut off in energy $E_{\perp min} = e\varphi/R-1$ as is shown in Fig. 5. Such a deformation increasing with time as φ grows makes the distribution be still more nonequilibrium. This, obviously, should lead to increasing instability growth rate, i.e. to more intense oscillations.

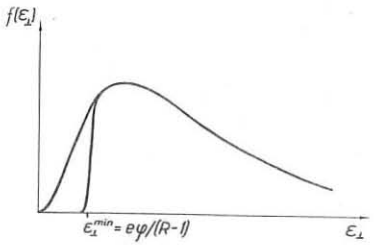

Fig. 5

4. The observations have really shown that in the entire course of the decay there is a complete correlation between the variations of the potential φ (the average time magnitude) and amplitu-

de of HF oscillations U. From inspection of the data on numerous measurments carried out in different modes of operation, U and φ are related by a sharp functional dependence of the form $U \sim e^{\alpha\sqrt{\varphi}}$

Taking into account the above facts we may picture the following sequence of the development of an instability burst. In the initial decay phase which is characterized by a low oscillations level the electrons are heated slowly (the plasma potential grows slowly too) mainly due to Coulomb collisions with the ions. As the oscillation amplitude gradually grows their contribution to the electron heating becomes more appreciable, finally being the main item in the electron energy balance. Since that moment all four above factors are closed in a regenerative circuit: the oscillations increase T_e, - this increase in T_e gives rise to an increase in φ , - the growth of φ enhances the nonequilibrium nature of the ion distribution function, - the more nonequilibrium is the distribution, the more intense oscillations are developed, - the latter give rise to a further increase in T_e, and so on. Thus, a process of nonlinear selfenhancement of instability is established. The instability growth can last until the oscillation amplitude is not limited by any new factors.

This qualitative scheme has been suggested by E.E.Yushmanov, - one of the authors of the present paper. Quantitative calculations to support it are difficult since they are concerned essentially with nonlinear instability phenomena. In this sense the scheme can be considered as a versimilar hypothesis. And as with all hypotheses it needs be experimentally proved.

The major assumption here is that the primary factor giving rise to an instability burst is an increase in T_e in the initial decay phase. To be convinced of the validity of this assumption an experiment has been carried out with additional electron heating by a short RF pulse at the instant before the burst appears. The idea of this experiment is quite evident. Such "artificial" heating should give rise to a more intense excitation of instability if it is really associated with an increase in the plasma potential, and as a consequence, with a displacement of the low energy boundary in the ion distribution. The results are shown in Fig.6. The left oscillogram is a natural oscillation burst; the right oscillogram - a burst with additional RF heating which is applied at the instant marked by an arrow. It is seen that the heating causes an enhanced instability as has been expected. This experiment will be considered

in more detail in paper 2.1.1. at this conference. Now I wish only

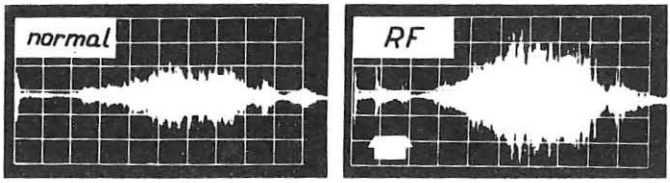

Fig. 6.

to point out that the result obtained is quite a strong argument in support to the suggested scheme.

In addition to other experimental data clarifying the nature of the instability let us consider the results of the preliminary PR-6 experiments on plasma stabilization by injecting a small amount of "warm" plasma. The experimental procedure is as follows. After injection and heating the plasma source is automatically operated so that a low-temperature plasma ($T_i \simeq$ 5-10ev) continued to be supplied to the trap volume. The warm plasma densities and injection duration could be varied in a wide range. The effect of such warm plasma on the instability has been clearly observed. The results are presented in Fig.7 where the oscillations in the hot-ion decaying plasma are shown for different intervals of injection of warm plasma. The duration is marked with a line below each oscillogram (the upper oscillogram is presented without injection). At the beginning of decay the density of the warm plasma in the central region of the trap did not exceed 10% of the hot plasma density. It is well seen that during the injection of the warm plasma the instability is not obser-

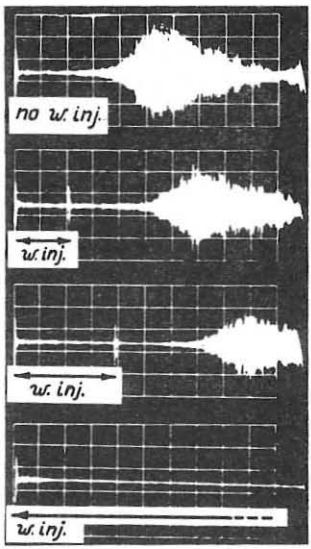

Fig.7

ved. However, as the injection is ceased the instability reappear again with the same time delay as before. In this case the oscillation bursts were absolutely simultaneous with an increase in the plasma potential too.

The experiments on injections of "warm" plasma are quite consistent with the above ideas about spontaneous transition of plasma from a stable state into unstable. On the other hand, they are very interesting and important since they have directly illustrated (so far only qualitatively) the validity of the Post's idea on stabilization of loss-cone modes by additional injections of small amounts of warm plasma /7/.

In summary, let us formulate the main conclusions from the PR-6 and PR-7 experiments.

1. At sufficiently high densities when plasma losses are caused mainly by the Coulomb scattering the plasma containment can be violated by a spontaneously excited instability. The wave characteristics of this instability suggest that it bears a most resemblance to the drift loss-cone mode.

2. It is an important feature of this instability that its intensity strongly depends on the plasma ambipolar potential.

3. The electrons are heated in the HF electric fields of the unstable oscillations. This may put into action a certain mechanism of a nonlinear instability self-enhancement based on a regenerative coupling between T_e and the oscillation intensity.

4. The instability is suppressed when a relative small amount of warm plasma is introduced into the hot plasma. As regards its possible application in future, this stabilization method needs more comprehensive quantitative studies.

5. It is worthy to emphasize the sensitivity of the instability to vacuum conditions. This seems to be related with the stabilizing action of plasma admixture produced in the trap itself due to charge exchange and ionization of neutral gas.

2xII and DECA II Experiments Plasma containment in 2xII was investigated, for plasma parameters: $n=5\ 10^{13}cm^{-3}$, $E_i=1-10$ kev. The plasma was formed by trapping and adiabatic compressing of a plasma blob injected along the magnetic fied lines.

The plasma decay depends on the injection regime. As a rule, it proceeds quietly without indications of instability defined clearly. In some cases, however, "Plasma dumps" are observed with considerable delay after injection as is shown in Fig.8a. These dumps are always

accompanied by: (a) an increased intensity of HF noise in the ion-cyclotron frequency range, (b) an increase in light emission, (c) an increase of the relative number of high energy atoms in the charge exchange particles flux. The plasma dumps are similar in appearence to those observed in PR-6 and PR-7. The authors associate them with "double-humped" instability. This conclusion is based on the fact that in these cases the ion energy spectrum has two or more maxima, being correlated with the instants of the dumps.

The energy distribution of quiescent plasma is single peaked (Fig.8b) and no strong turbulence is observed. The measured life times at the very beginning of the decay satisfactory agree with those calculated for Coulomb losses. In absolute values, they amount to a few hundred microseconds and differ from the calculated values not more than by a factor of two. Further decay, however, even in the best regimes, is in obvious disagreement with the collisional loss-rates. Instead of being constant, $n\tau$ decreases by about a factor of ten as the density diminishes from 2.10^{13} to 2.10^{12} cm^{-3}. To explain such a disagreement the authors have used the Baldwin-Callen calculations on the effect of "collective" scattering of ions by weak plasma oscillations related with the convective loss-cone mode instability /8/. Experimental results obtained with 2x and 2xII do not contradict these calculations. However, more definite conclusions seems to be premature.

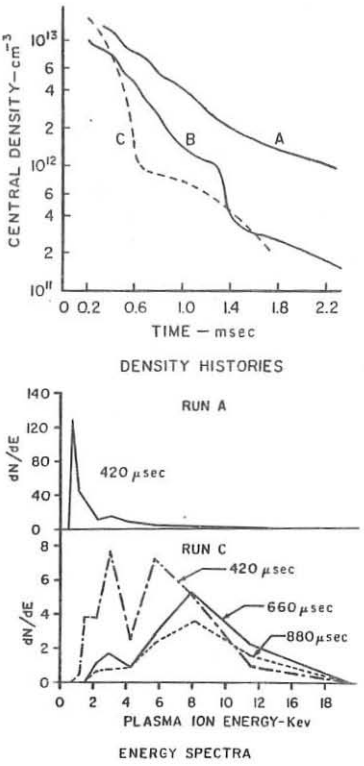

Fig.8.

In DECA II the plasma density and mean ion energy are practically the same as those in PR-6, e.g. $n=1.10^{12}$ cm^{-3}, $E_i=200ev$. The plasma was injected by a thetatron gun and trapped by a rapidly

growing field of the entrance mirror. Using this injection technique, the ion angular distribution is found to concentrate near the loss-cone angle θ_c . It undergoes transformation with time due to collisions and takes eventually a form typical of mirror traps with a maximum at θ =90°(θ - is the angle between the magnetic field direction and ion velocity vector).

The evolution of the angular and energy ion distributions, the density decay, variation of the ambipolar plasma potential and anisotropy, and some other problems have been studied. Experimental data are compared with numerical calculations made on the basis of the classical collisional model, taking into account cooling of ions by electrons, ambipolar potential and charge exchange. Without going into details a quite resonable agreement between the experiment and calculations may be ascertained. For illustration, Fig.9 shows both the measured and calculated curves of the plasma density and potential variations.

In contrast to 2xII, charge exchange in DECA II makes an appreciable contribution to plasma losses even at the initial phase of the decay, and at t=750μsec it is the primary source of losses. That is why the maximum life time does not exceed 450 μsec (for n=10^{11}cm^{-3}).

The authors point out that during the decay cycle some splashes of HF oscillations at the ion-cyclotron frequence and its harmonics are observed. However, no correlations between these splashes and density fluctuations or particle escape through the mirrors were found. As we have already mentioned the absence of a marked instability could be caused by an appreciable increase of the neutral gas pressure after injection.

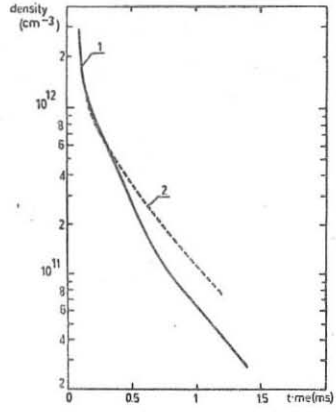

Density evolution.
1 - measurement 2 - calculation

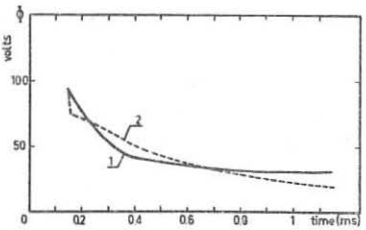

Time evolution of the ambipolar potential.
1 - measurement 2 - calculation

Fig. 9.

C O N C L U S I O N. In mirror confinement experiments, as well as those with other systems, one of the main difficulties lies in obtaining the subject of investigation itself, that is, in production of a hot ion plasma which could represent the physical properties of a future thermonuclear plasma. The most important property, as applied to a mirror plasma, is the form of the ion velocity distribution function, since it directly governs the stability conditions.

As has been mentioned in Introduction the collisional distribution due to ion-ion and ion-electron collisions in a thermonuclear plasma should be established. In this respect, the experimental studies considered in this paper are of interest just because they investigate the plasmas whose ion distribution functions are close to the collisional ones. In our opinion, the experiments are rather fruitful. They yeld new information about the plasma behaviour in most interesting regims. Let us list the main results.

1. Experiments carried out in all four installations indicate the existence of macroscopically stable states of a collisional plasma, which can last at least for several hundreds of microseconds. In those states, the plasma loss rate is defined by the classical mechanism of Coulomb ion scattering. The experiments include the initial densities ranged from 10^{13} to 10^{12} cm^{-3} and ion temperatures from a few tens of electronvolts to a few kiloelectronvolts.

These experiments are also of interest from the viewpoint that they did not support the initial pessimistic theoretical predictions on destructive actions of loss-cone instabilities, and on the plasma escape with a time of the order of the ion time of flight between the mirrors.

2. The PR-6, PR-7 and 2XII experiments revealed a phenomenon of spontaneous transition of the plasma from a stable state into an unstable state during free decay. This transition is accompanied by increased loss rates.

At the present time it is still not clear if the causes of that phenomenon are the same for these installations. The authors of PR-6 and PR-7 are inclined to attribute this phenomenon to nonlinear excitation of a drift loss-cone instability mode under the influence of the plasma ambipolar electric field, while the authors of 2XII believe that it results from double-humped instability.

Without predetermining how completely each of these explanations describe the transition of plasma into an unstable state we may

state that both cases involve a certain deformation in the collisional ion distribution function. Therefore, speaking more generally, the effect itself should be treated as a dramatic illustration how comparatively slight variations in the distribution function could influence the plasma stability.

3. Experimental confirmation of theoretical predictions on stabilizing loss-cone instabilities by injecting warm plasma is an important result of the research. This has been proved directly by the PR'6 experiments and indirectly the observations that the instability disappeared as the neutral gas pressure was increased.

4. Data on containement of quiescent plasmas in 2XII suggest collective scattering of ions by weak plasma oscillations and its contribution to the loss rates. These assumptions, however, need more thorough experimental verifications.

In conclusion we may add that systematic studies of collisional plasmas has been started only quite recently. However, the studies already performed make it necessary for us to revise or define more exactly some of the ideas formed previously. We may hope that further research in this direction should yield new useful information which will help us to achieve more profound understanding of the properties of high temperature and high density plasmas.

REFERENCES

1. Yu.T.Baiborodov et al., Madison conference, vol. II, 647(1971).
2. B.I.Kanaev, E.E.Yushmanov, Grenoble conference (1972).
3. F.H. Coensgen et al., Grenoble conference (1972).
4. D.Launous et al., Nuclear Fusion, 12, 673 (1972).
5. Yu.T.Baiborodov et al., Novosibirsk conference, IAEA, vol. II, 213 (1969).
6. R.F.Post, M.N.Rosenbluth, Phys.Fluids, 9, 730 (1966).
7. H.L.Berk et al., Novosibirsk conf. IAEA, vol. II, 151 (1969).
8. D.E.Baldwin, J.D.Callen, Phys.Rev.Lett., 28, 1686 (1972).

THERMONUCLEAR FUSION IN INSTALLATIONS WITH A DENSE PLASMA

G.I.Budker

Institute of Nuclear Physics, Novosibirsk, USSR

In my present talk I will speak about, so called, systems using a dense plasma. At various times different people put the quite different meanings into the words "dense plasma". We shall call the plasma "dense" if the mean free path of charged particles is comparable with the length of the device.

For the thermonuclear temperature range $T \approx 10^4$ Ev it means that the plasma density should satisfy the condition

$$n\ (cm^{-3}) > \frac{3 \cdot 10^{20}}{L\ (cm)}$$

and its length should satisfy the condition

$$p\ (atm) > \frac{10^7}{L\ (cm)}$$

(see Fig.1).

We shall be interested in traps with a dense plasma, that is in systems for which the magnetic fields are of great significance. Therefore I will not be concerned with ideas about thermonuclear reaction realization in microparticles of condensed matter about which there is much talk at present (despite the fact we are certainly dealing with a plasma which is dense in our sense of the word: $\lesssim 0.1$ mm, $P > 10$ atm).

The maximum pressure for which one can still speak of a plasma confinement in a trap is of the order of millions of atmospheres. This pressure is obtained by means of explosive

compression of a liner. The corresponding density of the plasma is of the order of 3.10^{19} cm^{-3} and the mean free path is about 10 cm. The final dimensions of a reactor after implosion are approximately 1 cm in the radial direction and several meters in length. The length I speak of here is determined from the condition that the time of the plasma longitudinal expansion should be on the order of a Lawson time:

$$\tau\,(sec) \sim 10^{14}/N(cm^{-3})$$

Work in this field has been carried out at the Institute of Nuclear Physics[1] and in the laboratory of Linhart in Italy [2]. At Novosibirsk the possibility of preliminary storage of the necessary energy as the kinetic energy of a liner was considered. The liner was accelerated by means of a magnetic field of about 100 kG. Magnetic compression of a liner has obvious advantages over the implosive compression both from an experimental standpoint and from the point of view of the final aim, since in the case of magnetic compression only the part of the D-T mixture which is actually put into the reaction of one experiment is used up (and all the rest is not wasted). In order to make it possible to carry out many cycles of a reaction with the same fraction of the mixture, we considered MHD-compression of a liquid metal liner located on top of a heavier insulating liquid and which is restored by centrifugal forces after each working cycle.

In fact, in our experiments of 1965-66 the liner compressed not the plasma but the magnetic field. In this way magnetic fields up to 2 MG and corresponding pressures of several hundred thousands atmospheres were obtained. In the purely thermo-

nuclear aspect this set of works was unsuccessful. It was unsuccessful not in the sense that negative results were obtained, but in the sense that the complexity and the cumbersome size of experiments as well as the defficiency in the staff, that were required to overcome the difficulties which we met, undermined the hope for obtaining conclusive results in a forseeable future. And we are very pleased that physicists of other laboratories have returned again in recent years to this question [3].

The next step along the descending curve shown in Fig.1 is the attempt to obtain in high pressure plasma within an unbreakable rigid vessel ($p < 10^4$ atm). Such systems were considered in particular by Morozov, Tuck and others[4,5]. Since in a dense plasma in the longitudinal direction neither thermal insulation ner confinement was assumed, the resulting length of the installation was getting to be on the order of several hundred meters. One can agree that a thermonuclear reactor length of several hundred meters is not hopelessly great. More than that, I would say that it is quite appropriate for a thermonuclear power station with power of commercial interest. However, in order to confine a plasma along this whole length, it is necessary to produce a magnetic field of the order of several hundred killogauss. And when the device has a length of about 1 km this task becomes really complicated and very expensive. In addition, it is very difficult to model this machine and an immediate start with the construction of a full-scale installation would require exeptional boldness on the part of experimentalists and their

financing institutions.

Therefore we considered another possibility which may seem unconventional at the first sight, namely: plasma confinement in the transverse direction not by a magnetic field but by the installation walls. The only role that is left for the magnetic field is to decrease the transverse heat conduction and this requires a considerably smaller magnetic field and the problem of stability is solved in a new way. In this way a system with $\beta \gg 1$ appeared. The technical feasibility of designing a cylinder capable of withstanding internal pressure iof tens of thousands of atomspheres as compared to that of designing a solenoid for a corresponding field is clear.

A bit later I wall dwell on the physics of the processes occuring in a thermonuclear plasma under the condition of plasma confinement by the walls.

Since a length of 1km is still cumbersome even in the case of confinement by the walls, we attempted to find a solution corresponding to an installation with more conventional dimensions. A few years ago we found such a method. The essence of the method is that at the ends of the installation a multiple mirror configuration of a magnetic field is produced [6,7] .

The work on dense plasma confinement by a multiple-mirror magnetic field is carried out in the laboratory headed by Ryutov and Kruglyakov. This work is a little more then half the whole CTR - program of the Institute. The other half involves investigations of the feasibility of a thermonuclear reactor based on a mirror machine with the plasma rotating in co

crossed fields. These investigations are carried out in the laboratory headed by Volosov and Zel'nik. In spite of the lack of success of the previous experiments on the "Ixion" and "Homopolar" [8,9], carried out at the Los-Alamos Lab, we maintained an interest in this field since we succeeded in getting a stable plasma due to special distribution of the potential. But I am not going to speak about this now, since the topic of my report today concerns a dense plasma.

The essence of the multiple mirror confinement of a dense plasma is that at the end of the machine the multiple mirror is installed which sharply decreases the plasma output at a given mirror ratio in comparison to a machine of the same length but having one mirror or no mirror at all.

If one chooses the length of every mirror so as to cause the particles passing through this mirror to be scattered at an angle $\Delta\theta \sim \sqrt{H_{min}/H_{max}}$, then the particles within the mirror length will be captured. Some subsequent scattering events will cause the particle to leave the trap but with equal probability that the exit will be in the forward or backward direction. Thus, a particle will move diffusively between the mirror and its lifetime will become proportional to the square of the system length and increased many times in comparison to that of a homogeneous field.

It is interesting to note that the positive effect disappears both at very low and at very high densities of a plasma. At lower density the particle passed through the first mirror will also pass freely through all the others mirrors. And at higher density due to the viscosity decrease the con-

ventional gasdynamic flowing through the corrugated tube will occur which differs only slightly from the flowing through the smooth tube. Thus, we have only specific parameter range where our effect is occured.

From the macrospocic viewpoint the picture looks as follows. At any given moment the plasma is a mixture of two gases: a gas of untrapped particles and a gas of trapped ones. The transport of matter along the axis of a system is naturally provided only by untrapped particles. Due to collisions the untrapped particles transmit their momenta to trapped particles and those in turn transmit them to the magnetic field of the mirror thus, the plasma behaves as if it experiences friction against the magnetic field and the character of the longitudinal motion of a plasma is qualitatively altered. Inertial expansion is transformed into a slow leakage of plasma through the system of mirrors similar to that through a porous medium. The leakage velosity in comparison to that of a homogeneous field is decreased by a factor of $k^2 \frac{L}{\lambda}$; where k is the mirror ratio. L/λ appears due to diffusive character of the motion. One power of k appears due to the fact that the number of untrapped particles is $\frac{1}{k}$ of the total number of particles; the second one due to decreasing in the scattering length with respect to capture into mirror. The general gain is so high that it is impossible to pay no serious attention to this effect.

From the exact mathematical equations the system of macroscopic equations was analytically obtained by Ryutov and

Mirnov (junior). This system of equations takes quantitatively into account all these effects mentioned above as well as the role of the polarization electric field [11,12] . The results of the investigation of the system confirm the simple estimates I mentioned above.

Despite the self-evident nature of these estimates they were not immediately accepted by the scientific community. We have even heard statements to the effect that our estimates contradict the momentum conservation law. I think that this was the effect of a certain psychological barrier connected with many years of experience in work with plasma, where $\lambda \gg L$. The situation is similar to that of about twenty years ago when great efforts were needed to overcome the opposite barrier for specialists in gasdynamics who joined thermonuclear investigations.

In order to overcome this barrier and to be assured that there were no major mistakes in the theory we have done a model experiment with an alkali plasma [13,14] . This work was presented at this Conference by Kruglyakov in his report.

The idea of the experiment is based on the fact that due to the large Coulomb cross-section in a low-temperature plasma one can manage to satisfy the condition $\lambda < L$ at low values of plasma density and at relatively small dimensions of the device. In the installation shown in Fig.3 of 3 m length the process of diffusive motion of a plasma with an average density of $\sim 10^{10} cm^{-3}$ through a system comprosed of 14 mirrors is investigated. The results given in Fig.4 are in full agreement with the

theoretical predictions: at the transition from a homogeneous magnetic field to a multiple mirror field the plasma density near the sources sharply increased, the increase being just required amount.

Simultaneously with our group and independently the idea of dense plasma in multiple mirror magnetic field was proposed by B.Logan, M.Lieberman, A.Lichtenberg and A.Makhijani [15]. They have done numerical calculations concerning the individual charge particle motion through the multiple mirror magnetic field in the presence of fixed scattering centres. By this the authors predetermined in advance the diffusive character of the motion and were able in essense to "fish out only the mirror ratio dependence of the confinement time. This same group has carried out a set of experiments on an installation with 3-5 mirrors and obtained results in agreement with ours [16].

At present in our Institute we are nearing the completion of an installation for studying multiple mirror confinement of a hydrogen plasma with a density of $n \sim 10^{15} cm^{-3}$ and a temperature of 100 eV. We have chosen 100 eV since at this temperature value the requirements for the inparted energy became comparatively moderate. Then imparted energy increases as a high power of a temperature and in the thermonuclear region is becoming of the order of tens megajould. The installation length is 6 m and the average intensity of the magnetic field is up to 20 kG. Plasma will be prepared with the aid of a high current relativistic electron beam.

Now I will return again to the problem of the transverse plasma confinement. As I have already said there are two substantially different possibilities: namely, the well known

magnetic confinement ($H^2 \ll 8\pi nT$) and plasma confinement by the chamber walls when the magnetic field serves only for suppressing the transverse heat conduction.

The first possibility has been fully studied and I will not dwell on this case. I will only note that in the case of an axially-symmetric multiple mirror field the plasma is unstable relative to flute perturbations and therefore it proves necessary to use a nonaxy-symmetric configurations which provide a magnetic well [17] . The well known disadvantage of such a configuration is the difficulty in getting a high mirror ratio. In spite of this, the strong magnetic field has advantages: since in this field plasma may be removed from the wall it turns out be reasonable to make movable mirrors (Fig.5) which provide the quasistationarity of the longitudinal confinement. The waves shown in the Figure on the left and right hand sides continuously "dash against" the region of homogeneous magnetic field and because of the frictional effect described above between the plasma and magnetic field they provide a constant force which opposes longitudinal expansion of the plasma. The velocity of these waves is not large. It is equal to the plasma flow velocity, i.e. much less than the ion velocities and the technical feasibility of such a moving field is of no difficulty. However, the previously mentioned difficulties in obtqining strong magnetic fields in large volumes justify our paying attention to systems with plasma confinement by the walls.

For simplicity let us consider first the problem of plasma confinement in a cylindrical tube (with no corrugation). Even in this case the physics of nonmagnetic confinement is some-

what more complicated than it seems at first sight. The reason for these complications is connected with bremmstrahlung. Really, the bremmstrahlung power, per unit volume of hot plasma is proportional to $n^2\sqrt{T}$. But under the condition $nT \gg H^2/8\pi$ the equalibrium condition has the form $nT = const$, i.e. the power of the radiation is altered in proportion to $T^{-3/2}$ and in the layer of cool plasma attached to the chamber walls the radiation power becomes very large. The radiation is so strong that even the weakened magnetic field does not provide the flux required for the compensation of radiation losses. This was predetermined our lack of success in searching for stationary sclutions in the work during 1967-69 [18, 19] . Recently quasistationary solutions were found by Chebotaev, Ryutov, Spector and Vekstein that were presented at the conference by Ryutov. The meaning of this is the following:

While they are cooling, the external layers of the plasma are pressed against the wall and are in some sense "eaten up" by the wall. As a result there develops a plasma flow toward the wall. The plasma flow velocity is determined by the velocity of the plasma "eating up" which in turn depends upon the heat conduction processes and the radiation in the layer near the wall. In particular, the presence of plasma flow causes the lifetime of plasma to increase not as R^2 as it does with ordinary heat conduction but only linearly with R.

At the same time the calculations showed that the lifetime oa a plasma turns out to be sufficient enough for obtaining positive energy output even in the case of very modest transverse domensions of the reactor and in the case of comparati-

vely low fields (R~5cm and H=2.10^4G in the case of classical heat conduction and H = 10^5 G in the case of Bohm heat conduction). I would also like to underline again that $\beta \gg 1$ and energy losses in the coils even when H = 100 kG can be neglected.

In the course of calculations the distributions of T and H were obtained along the installation radius at various moments in time. A typical example of the corresponding results is shown in Fig.6. One can easily see the layer near the wall where the density is two orders of magnitude higher than that in the centre.

It is necessary to take into account the corrugation because of two new problems. First is the problem of the deformation of force lines during the plasma expansion. In order that the desired magnetic field configuration be preserved in a plasma with $\beta > 1$, it is necessary to have the wall conductivity high enough (to prevent the penetration of the magnetic field through the wall during the processes of deformation and to maintain the shape of the field lines at least near the wall). Under these conditions the various alterations of the radial profile of plasma density during the processes of heating and cooling cannot lead to substantial change of the magnetic field profile in the main part of the trap volume. Here the field intensity may be altered by not more than an amount of order unity. Numerical calculations confirm this conclusion.

More substantial may be the field line deformations connected with the longitudinal pressure gradient. If the magnetic field is too weak, it may be smashed and carried away by the plasma flux. Obviously this will not occur if, roughly speaking, the following condition is satisfied:

$$\frac{H_{max}^2}{8\pi} > \delta p \sim p/N$$

where δp - is the pressure change along a single mirror and N is the number of mirrors. The meaning of this condition is that the high pressure of the plasma is distributed among many mirrors and each individual mirror withstands a small pressure drop. It is seen that for large values of N the last equation is quite consistent with the inequality $\beta \gg 1$.

The second problem is the stability of the plasma confinement by the rigid corrugated liner. This problem was investigated at our Institute by Spector[20]. In this case the plasma turned out to be, generally speaking, unstable (as in the case of $\beta < 1$) but due to the effect of longitudinal ion viscosity the growth rates are sufficiently small and in the case of $\beta > N^2/2A$ there is no time for the instability to develop during the time of plasma confinement (where A is logarithm of the ratio of the allowed fluctuation amplitude to the initial amplitude). In the task under consideration in addition to the problem of plasma confinement and plasma thermal isolation the problem of plasma heating is also of decisive significance. Of all the possible methods of plasma heating (with the configuration taken) we have chosen the

method of plasma heating by a powerful relativistic electron beam. For this choice there were the following grounds.

First. The absence of substantial distortions of the magnetic field in the case of plasma heating by relativistic beams (as opposed say, Joule plasma heating by a longitudinal current of shock heating).

Second. The availibility at the Institute of experience in producing powerful electron beams.

Third. The presence of a large group of physicists (theorists and experimentalists) at our Institute whose interests lay in the field of collective effects in plasmas and the processes of beam-plasma interactions.

In addition to that we proceeded from the general philosophical assumption that the high power requires high voltage. Although the transition to voltages of the order of a million volts seems to be a complicated task, in practice it will give significant simplifications.

Works on plasma heating are divided into two parts: the investigations of beam-plasma interactions and the production of the corresponding electron beam sources.

First experiments on the relativistic beam-plasma interactions have been carried out in 1970-71 at our Institute by the Kurtmullaev group [21]. These experiments showed that in the case of plasma density of $\sim 10^{12} cm^{-3}$ the beam can impart to plasma 10-15 per cent of its initial energy. The energy transfer from beam to plasma cannot be connected with Coulomb collisions since the Coulomb mean free paths of the beam particles and the plasma exceed the device length by several orders

of magnetude. The only reasonable explanation is the excitation of microscopic fluctuations in the plasma with the subsequent scattering of the beam on these fluctuations. A corresponding theory was made by Breizman and Ryutov[21-23]. This theory enables the qualitative understanding of many experimental results. Recent results were reported in the paper presented by Breizman at this Conference. In new experiments carried out at our Institute during the last two years[24] also reported here by Koydan we have obtained a significance advance to higher plasma densities: effective beam-plasma interaction was observed for densities $n \sim 3 \cdot 10^{14} cm^{-3}$.

Extrapolation of the data, taking into account the available experimental and theoretical findings, makes us believe that the problem of plasma heating up to thermonuclear temperatures will be overcome in case when we solve the problem of producing beams with voltages of $\sim 10^6$ V, total currents $\sim 10^6$ A and lifetimes of $\sim 10^{-4}$ sec.

The second part of our program is connected with the production of powerful beams. First beams with currents up to 30 kA with the particle energies up to 4 MeV were obtained at our Institute in 1969 with aid of a Tesla transformer in a compressed gas. Financial means do not allow us to construct installation as big as "Hermes" or "Aurora" and therefore we keep our attention on the design of relatively small low impedance lines with insulation provided by super pure water. This work was set up in 1969. Now we have at our disposal a water line of 2 m length at 40 cm in diameter with

the impedance 2,3 Ω . The current obtained is up to 110 kA with 800 keV particle energy.

The strengthnening of the water gap due to the production of conductive diffusive layers in the vicinity of the electrode surface was recently investigated by Ryutov[25]. The results obtained give us hope of success in raising the break-down intensity of electric field by a factor of 4. This will permit a substantial decrease in the resistance of the water line.

In conclusion I would like to draw your attention to what would be a thermonuclear reactor designed on the principles I have previously described. The reactor is a strong conductive shell (see Fig.7) of about 10 m length with an internal diameter of about 10 cm; the average intensity of the magnetic field is 10^5G; and the mirror ratio is 3. The number of mirrors is about ten on both sides of the shell. Plasma with a density of about $10^{18}cm^{-3}$ is prepared in the central part of the device with the aid of an electron beam which is injected from the one end of the shell. The thermal energy of the plasma is about 10^8J; and the lifetime of the plasma of about 10^{-4} sec is sufficient to obtain a positive energy putput.

I do not dwell on the problems of engineering since in general they are common to the other systems using dense plasmas (like θ-pinch with a liner) which are being discussed at this Conference.

Of course, the design of such a system under the conditions of the successful solutions of all the principal pro-

blems is still a very complicated task. Nevertheless these difficulties are on the order of the aim advanced and lie within the limits of modern technological potential.

I would like to return again to that viewpoint I have already expressed at the closing of the Conference which was held in Novosibirsk in 1968, namely that the data accumulated in plasma physics investigations are enough to start on the realistic design of thermonuclear systems.

We have undertaken a reorganization at our Institute, having left only the plasma physics investigations which are directly connected with the design of thermonuclear machines. I was very pleased to be concinced here at the Conference that this my point of view became to be well approved and now it is not regarded as indecent to talk about realistic thermonuclear systems.

REFERENCES

1. Alikhanov S.G., Budker G.I., Komin A.V., Polykov V.A., Estrin B.S. Proceedings 7th Intern. Conf. on Ioniz. Events in Gases, Belgrad, 1966.

2. Linhart J.G., Proc. Conf. MGauss Field - Gener., Euratom Publ EUR 2750e (1965), 387.

3. Boris J.P., Shanny R.A., Vth European Conf. on Contr. Nucl. Fus. and Plasma Phys., Grenoble, 1972, V.1, p.20.

4. Morozov A.I., Report CN-24/ on 3rd Intern.Conf. on Plasma Phys. and Controlled Thermomuclear Fusion, Novosibirsk, 1968.

5. Tuck J.L., Report CN-24/K-5 on 3rd Intern. Conf. on Plasma Phys. and Controlled Thermonuclear Fusion, Novosibirsk, 1968.

6. Budker G.I., Mirnov V.V., Ryutov D.D., JETP Letters 14, 320, 1971.

7. Budker G.I., Mirnov V.V., Ryutov D.D., Proc.Intern.Conf. on Plasma Theory, Kiev, 1971, p.145.

8. Baker D., Hammel J., Ribe F., Phys.Fl., 4, 1534 (1961).

9. Halbach K., Baker W., Layman R., Phys.Fl., 5, 1482 (1962).

10. Konstantinov S., Miskin O., Sorokin A., Zelnik F., JTP, 41, 2527 (1971).

11. Mirnov V.V., Ryutov D.D., Nucl.Fus., 12, 627, 1972.

12. Mirnov V.V., Ryutov D.D., Proc. 5th Europ.Conf.on Plasma Physics and Controlled Thermonuclear Fusion, Grenoble, 1972, p.100.

13. Budker G.I., Danilov V.V., Kruglyakov E.P., Ryutov D.D., Shun'ko E.V., JETP Letters, 14, 320, 1973.

14. Budker G.I., Danilov V.V., Kruglyakov E.P., Ryutov D.D. Shun'ko E.V., JETP, 65, 562, 1973.

15. Grant Logan B., Lichtenberg A.J., Lieberman M.A., Makhijani A., Phys. Rev. Lett., 28, 144 (1972).

16. Grant Logan B., Brown I.G., Lieberman M.A., Lichtenberg A.J., Phys. Rev. Lett., 29, 1435 (1972).

17. Furth H.P., Rosenbluth M.N., Phys.Fluids, 7, 764 (1964).

18. Alikhanov S.G., Kichigin G.N., Konkashbaev I.K., Preprint n 140, Novosibirsk, Inst. of Nuclear Phys., 1967.

19. Alikhanov S.G., Konkashbaev I.K., Chebotaev P.Z., Preprint N 309, Novosibirsk, Inst. of Nuclear Phys., 1969; Nuclear Fusion, 10, 13, 1970.

20. Spector M.D., PMTF (Journal of Applied Mathematics and Technical Physics), N 2, 1974.

21. Altinsev A.T., Breizman B.N., Es'kov A.G., Zolotovsky O.A., Koroteev V.I., Kurtmullaev P.Kh., Masalov V.L., Ryutov D.D., Semenov V.N., Proc. 1V Intern.Conf. on Plasma Phys. and Nucl. Fus., V.2, p.309, 1971.

22. Breizman B.N., Ryutov D.D., JETP, 60,409, 1971.

23. Breizman B.N., Ryutov D.D., Chebotaev P.Z., JETP, 62, 1409, 1972.

24. Koidan V.S., Lagunov V.M., Lukyanov V.N., Mekler K.I., Sobolev O.P., Proc. V Europ. Conf. on Plasma Phys., and Contr. Nucl. Fus., Grenoble, 1972, p. 161.

25. Ryutov D.D., PMTF (J. of Appl. Math. and Techn. Phys.), 1973, N 4, p.186.

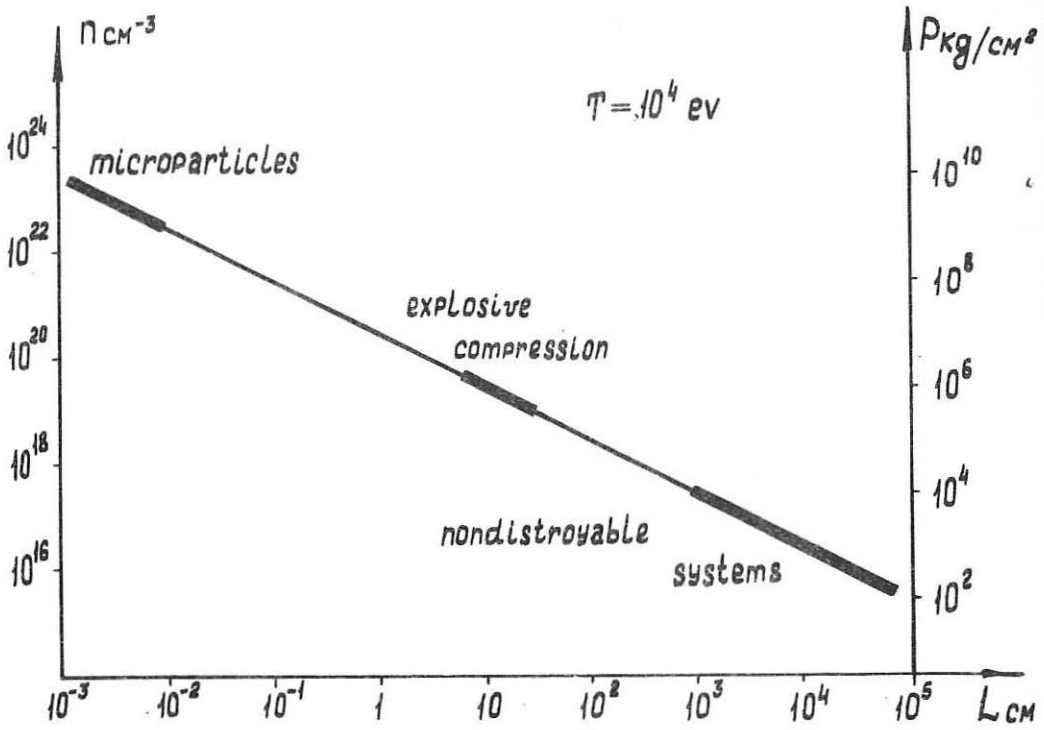

Fig. 1. Graphs of n and p versus L with double logarithmic scale.

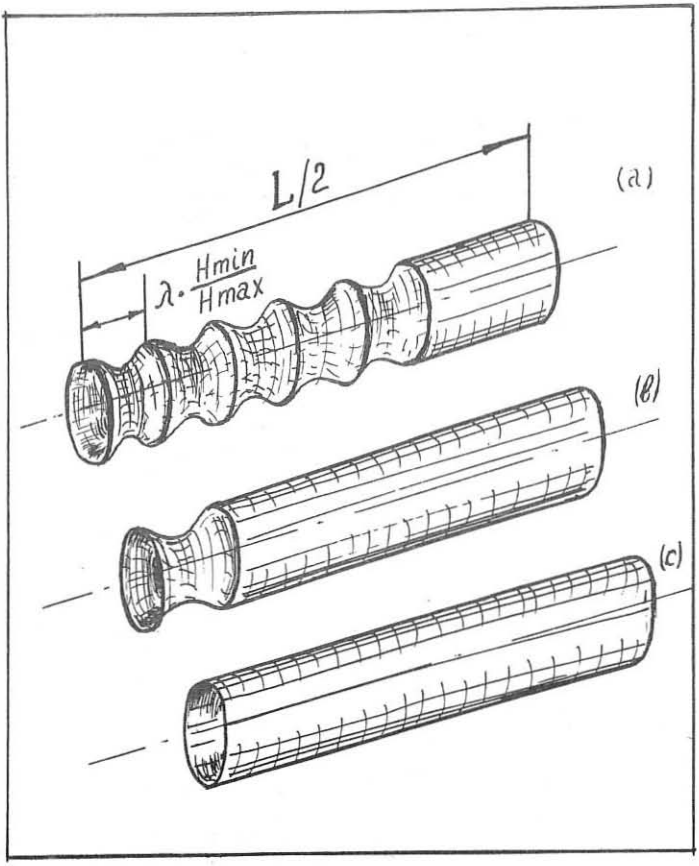

Fig. 2. Magnetic surface for:
a) corrugated system;
b) mirror machine;
c) straight system.

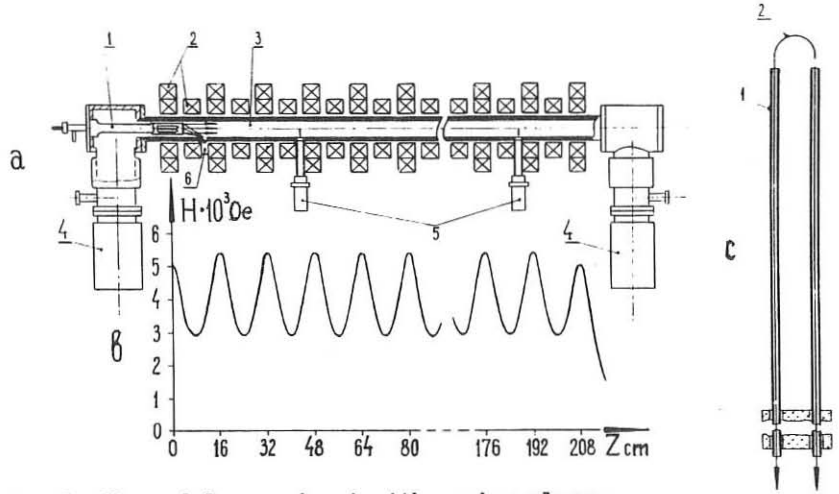

Fig. 3. The model experiment with cesium plasma.
a - diagram of a device: 1 - ionizer; 2 - coils of magnetic field; 3 - vacuum chamber; 4 - pumps; 5 - probes; 6 - cesium vapor inlet.
b - magnetic field profile at the axis of the system.
c - incandescent probe: 1 - quartz capillary; 2 - tungsten wire.

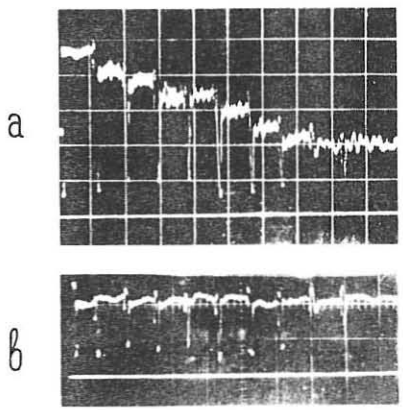

Fig. 4. Distribution of plasma density along the system axis;
a - in a corrugated magnetic field;
b - in a uniform magnetic field.
The sensitivity is $3{,}2 \cdot 10^{9} cm^{-3}$ per division.

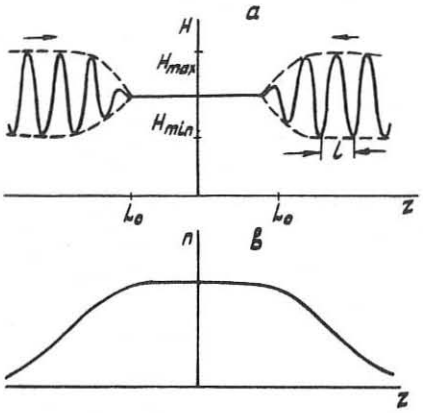

Fig. 5. Stationary confinement of the plasma.

a - profile of a magnetic field (waves shown in the figure on the left and right hand sides, continuosly "dash against" the region of homogeneous magnetic field; points - L_o and L_o are fixed;

b - the profile of concentration.

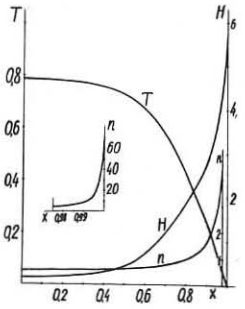

Fig. 6. Radial distributions of concentration n, temperature T and magnetic field H (dimensionless units) at the moment of time when the temperature in the centre is maximum.

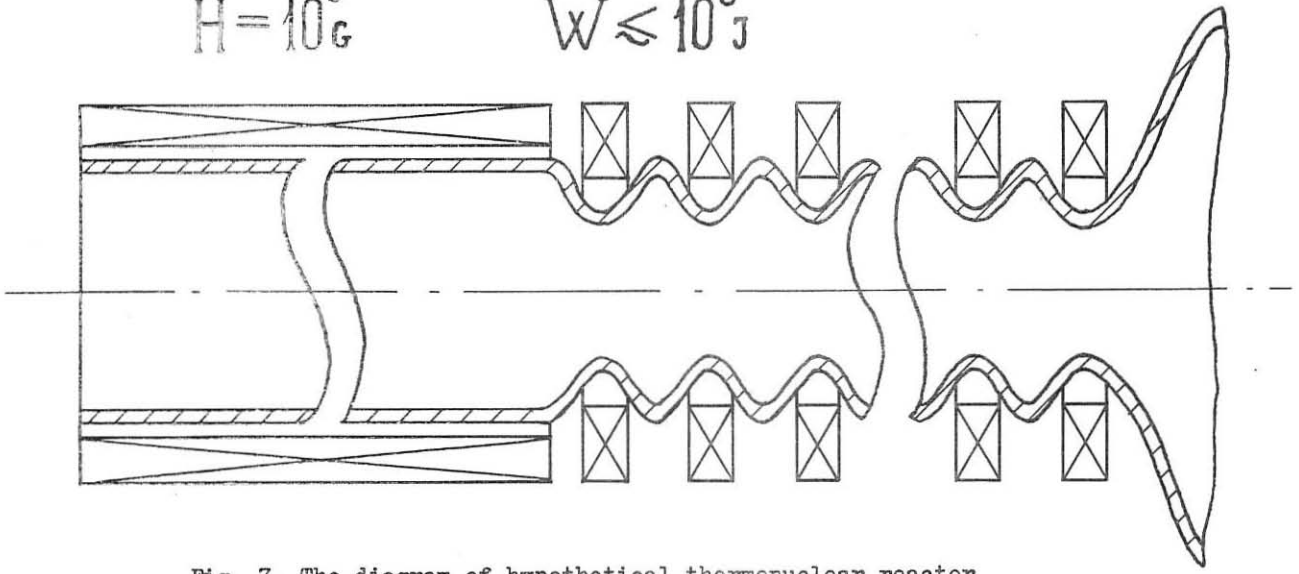

Fig. 7. The diagram of hypothetical thermonuclear reactor with the multiple-mirror magnetic field (Bohm diffusion).

COLLECTIVE INTERACTION OF RELATIVISTIC BEAMS WITH A PLASMA

Ya.B.FAINBERG, V.D.SHAPIRO
(USSR)

Review Report *

I. Theoretical and experimental investigations of collective interaction of relativistic and nonrelativistic beams with a plasma have convincingly demonstrated a high efficiency of this interaction. During a short time 10^{-8}-10^{-7} sec at a small length of some santimetres beam takes off a considerable part of its energy for the excitation of wave, for heating and accelerating of plasma particles. This part is 10-40% of the initial energy of the beam for the experiments, in which the conditions of a long resonance interaction of beam electrons with a wave are provided. It is important that this part of energy is not small for relativistic beams with a power of 10^8 - 10^{10} W. That is why the possibility on principle of using of high-

---

*Report is founded on the theoretical and experimental investigations, carried out by V.I. Kurilko, S.S.Moiseev, V.I.Shevchenko, A.K.Beresin, E.A.Kornilov, S.M.Krivoruchko, Yu.V.Tkach, L.J.Bolotin their collaborators and authors.

powered relativistic beams for effective heating of plasma with a density of 10^{13}-10^{18} cm^{-3} has not given rise to doubt. At the experiments carried out not long ago on the Linear Plasma Betatron (LPB) it is shown that there exsists the correlation between energy losses of the beam, plasma heating and intensive radiation from a plasma. For the beam power of 5.10^{8}W the radiation oscillations power is not less than 20% of beam power.

Together with a heating by a beam, the problem of excitation of the regular waves with a large amplitude (simple wave and solitary impulse) that is necessary for particle acceleration in a plasma is of a considerable interest. Until recently the possibility of excitation of the large amplitude wave with fixed phases and narrow frequency spectra has been called in question. For its solving it has been necessary to prevent the natural process of development of plasma-beam interaction, that has given an excitation of a wide wave-packet and then a turbulent station accompanied by plasma heating and anomalous diffusion. The methods, worked out in Physical-Technical Institute of Academy of the Sciences of UkSSR (P.T.I.), of a governing of beam instabilities gave possibility to advance in solving of the problem. At the same time the main processes are now clearly determinated that give reduction of plasma-beam interaction efficiency, increasing the time and length relaxation, and consequently make difficult to use such an interaction. These effects

are conditioned by disturbing of beam particle resonance interaction with excited waves owing to: a) nonlinear saturation of amplitude, increasing as a result of resonance trapping, b) nonhomogeneity of plasma density, that leads to phase velocity and wave frequency changing, [2a] c) spectral overpumping of waves as a result of induced scattering of plasmons on the thermal plasma particles [2b] and of decay processes, [2c] d) changing of plasma parameters caused by escitation of oscillations that leads to the disturbing of resonance interaction conditions. In the case of relativistic beams as it is known there is decreasing of the growth rate and increasing of relaxation length, caused both reduction of separate particle excitation intensity and automodulation percentage owing relativistic growth of electron mass. The other essential reason of not reaching the possible maximum of collective plasma-beam interaction efficiency for the beam power of 10^{11}--10^{13} W is that there are not solved the problems of focusing, modulation and improvement of beam monoenergeticality (making the beam more monoenergetic), though recently there have appeared the works on focusing of high-powered electron beam in vacuum and plasma diods.

As it is known, for the relativistic beam-plasma interaction low-frequency (LF) waves heating the ions are not directly excited beaause beam electron velocity exceeds considerably the velocity of LF-waves. The ions can be heated by means of transformation high-frequency (HF) waves into LF-waves or as a result of ion-sound and others LF-waves excitation by electrons of back current, whose velocities are near the sound velocity. The second mechanism is not sufficient, ~~especially~~ in the case of $n_b \ll n_p$ because the energy containing in the back current is $\left(\frac{n_b}{n_p}\right)^2$ times less than that in the forward current. At the experiments carried out in P.T.I. the anomalous efficiency of transformation of HF-oscillations into LF-ones for plasma-beam interaction have been found. About 70% of HF-oscillations energy was found to transform into LF-oscillations.

In this report the possible methods of eliminating of processes decreasing the plasma beam interaction efficiency are discussed, some possibilities of focusing and modulating of high-powered beams are considerated and possibilities of using of anomalous transformation of HF-wave into LF-ones for plasma heating by the beam are discussed too.

II. The possibility of effective transformation of relativistic beam energy into plasma oscillations energy has been firstly shown in the work of the authors and Shevchenko /1/. The main conclusions of the theory - the quasilinear relaxation of the beam has onedimentional character; the most effective relaxation takes place for so called "monochromatic" beams with a small angle spread $\Delta\theta \ll \left(\frac{n_b}{n_p}\right)^{1/3}$ (n_b, n_p - beam and plasma densities, correspondently). In this cose the beam loses the energy, compared wi with initial beam energy $W \sim n_b mc^2 \left(\frac{n_b}{n_p}\right)^{1/3} \gamma^2$ at the length

$$l_Q \sim 10 \left(\frac{n_p}{n_b}\right)^{1/3} \gamma \frac{c}{\omega_p} \left(\frac{T_e}{mc^2}\right)^{1/3}$$

(T_e - temperature of plasma electrons).

For the beams with a great angle spread the energy loss $W \sim n_b mc^2 \gamma$ is gained at the considerably greater length

$$l_K \sim 10 \frac{n_p}{n_b} \gamma \frac{c}{\omega_p} \frac{1}{(\Delta\theta)^2} \frac{T_e}{mc^2}$$

For the case of relaxation of the beam in plasma with a density $n_p \sim 10^{14} - 10^{15}$ cm^{-3} and beam current $J \sim 10^5$A relaxation length is of some centimetres. In this case $\frac{n_b}{n_p} \sim 10^{-1}$, 10^{-2} and for the real beams the criterion of monochromaticaliyy is fulfilled. For the beam power $10^{13} - 10^{14}$, achieved at present, it is possible to heat the highdensity ($n_p \sim 10^{18} - 10^{19}$) plasma in the magnetic trap (transition to such a density allows to reduce containement time considerably) and also to use the relativistic beams for the initiation of impulse thermonuclear reaction in the solid D-T target. In all t these cases $\left(\frac{n_b}{n_p} \sim 10^{-3} \div 10^{-6}\right)$ the monochromatical criter-

rion is not fulfilled and the beam relaxation becomes slower.

Nevertheless, for these cases relaxation length is small compared with system sizes and thus collective mechanism of relaxation provides oan efficient energy transformation from the beam to the plasma oscillations. At the same time as it has been noted in the introduction, the disturbing of the phase resonance between the beem and wave caused by the nonlinear interaction of waves, nonhomogeneity of plasma and others, prevents to realize the collective interaction of relativistic beam with a dense plasma and extends the relaxation length in such a plasma.

To reduce or to obviate the injurious influence of the nonhomogeneity of plasma and nonlinear wave interaction it is necessary to provide the conditions for which the length of collective relaxation were less than the length of spectral overpumping and less than the characteristic value of density gradient leading to the break-down of collective relaxation process /2/. The decreasing of the relaxation length and hence the increasing of the plasma-beam interaction efficiency can be achieved by pre-modulation of the beam and decreasing of its an angle divergence. Programmed changing of the density allows not only to avoid injurious influence of the nonhomogeneity of plasma density but to use it for the increasing plasma-beam interaction efficiency and in particular for the eeliminating of the effects of nonlinear saturation of the oscillations. In thes these directions there are being made the experimental and theoretical investigations in P.T.I.

As it has been shown in theoretical and experimental investigations, made in P.T.I. , when the electron beam to pre-modu-

late, the plasma-beam interaction efficiency is increasing considerably and the relaxation length can be decreased /3/. It is essential that owing exponential growth of the initial signal amplitude in the process of the beam interaction with plasma or decelerating structure the power needed for modulation is not high, because for a small depth of initial modulation the needed effect has already achieved. This circumstance is especially important for the case of relativistic beams because in this case, when γ to increase, the spatial beam bunching is essentially difficult Let us consider now the interaction with plasma of pre-modulated beam with a small angle divergence. In this case the instability is developing in one-mode regime and, as it is known /4/, the growth saturation of plasma wave amplitude is connected with the beam particle trapping in the potential wall created by the wave. The trapped beam particles perform phase oscillations with respect to zero phase of the wave and when to average over the period of these oscillations do not exchange any energy with the wave and the instability is stabilizing. The part of beam energy, transformed into oscillations, is relatively small $\sim \left(\frac{n_b}{n_p}\right)^{1/3} \ll 1$. The transition to the relativistic beam energy leads, on the one hand, to the decreasing of the growth rate $\left(\sim \frac{1}{\gamma}\right)$ and on the other hand owing to considerable growing of the longitudinal mass $(m_{\parallel} \simeq m_0\gamma^3)$ to the increasing of field amplitude corresponding to the trapping. In Fig. 1 there are shown the result of solving the problem of interaction of pre-modulated monochromatic relativistic beam with plasma by means of computer /5,6/. Fig. 1 shows how the ratio of the energy flow of the plasma oscillations to the beam energy flow depends of relati-

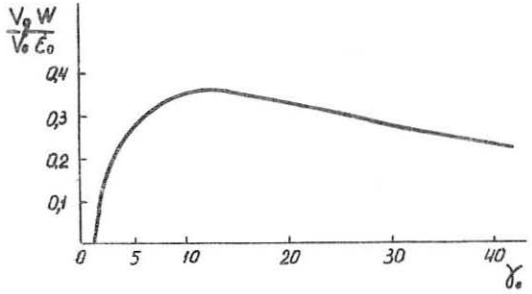
$\frac{V_0 W}{V_0 \mathcal{E}_0}$
0,4
0,3
0,2
0,1
0
5
10
20
30
40
γ_0

Fig.1

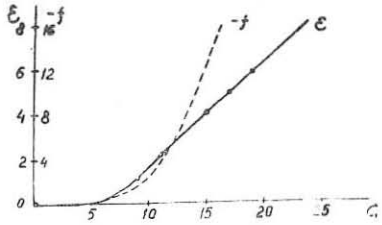
$\mathcal{E}_0$
$-f$
$\kappa\mathcal{E}$
6
12
4
8
2
4
0
5
10
15
20
γ_0

Fig.2

vistic parameter γ . It is evident, that at the maximum $\left(\left(\frac{n_b}{n_p}\right)^{1/3}\left(\frac{v_0}{v_g}\right)^{1/3}\gamma \sim 1\right)$ about 40% of the beam power transform into oscillations. Further increasing of the efficiency of such a transformation can be achieved by means of maintaining of the synchronism between beam and excited wave when phase velocity is decreasing in the direction of beam motion. Being trapping by the wave the beam particles are bunching in the decelerating phase, for which their velocity coincides with phase velocity of the wave, and continue to lose their energy. It is essential that as a result of bunching of the beam not only the particle with an equilibrium synchnistical phase $\varphi = \varphi_s$ but many particles for which $\varphi \neq \varphi_s$ are trapping into synchronistical motion, so that maximum power of the excited wave is comparable with the beam power. In Fig.2 and Fig.3 there are presented the results of the calculations of this problem by the computer /7,8/ for the case, when synchronism between the beam and the excited wave is maintained owing to the profiled changing of the plasma density

$$n_p(z) = n_0\left[1 + \left(\frac{n_b}{n_p}\frac{v_g^2}{v_0^2}\right)^{1/3}\gamma_0 f(\zeta)\right],$$

$$\zeta = \frac{\omega_p z}{v_0}\left(\frac{n_b v_0}{n_p v_g}\right)^{1/3}\gamma_0$$

v_g - group velocity of plasma waves, $f(\zeta)$ is shown on Fig 2. (the other possibility of the providing with the necessary law of phase velocity changing is the using deceleorating structure with a variable step)*.

*These theoretical conclusions are in a qualitative agreement with the experiment (see /7/).

For the synchronism conditions about 90% of the beam power are transformed into oscillations (see fig.2). From the analysis of the phase plane (fig.3). it is seen that 85-90% of the amount of beam particles are trapped into bunches, moving synchronistically with the wave and decelerate upto the velocity compared with thermal plasma velocity.The rest of particles does not trapped into synchronistical motion and practically does not exchange any energy with the wave. There are some others possibilities to maintain the synchronism between the monochromatic beam and the excited waves. In Fig.4 there is presented one of these possibilities - the using of the electric field $E_0 \sim \frac{m\delta^2}{eK}$ (δ - growth rate) allows to compensate the beam losses for the wave excitation and provide the continuous growth of wave amplitude. Thus the carried analysis indicates the possibility of the effective energy transformation of the relativistic monochromatic beam into plasma oscillations.

III. Above we have confined themselves to the investigation of the excitation of the periodic waves by the relativistic beam. To rise the plasma-beam interaction efficiency and for some applications it is necessary to investigate the possibility of the excitation of solitary waves (solutions) by the intense electron beam. Below we shall dwell on the preliminary theoretical and experimental results of the solving of the problem, obtained in /9/. In the plasma, placed in a magnetic field, the wave propogating under the angle to the field with a phase velocity $V_\phi > \frac{\omega_p}{K_\perp (1+\frac{\omega_p^2}{\omega_H^2})^{1/2}}$ represents solitary electron density impulse (solution) /9,10,11/.

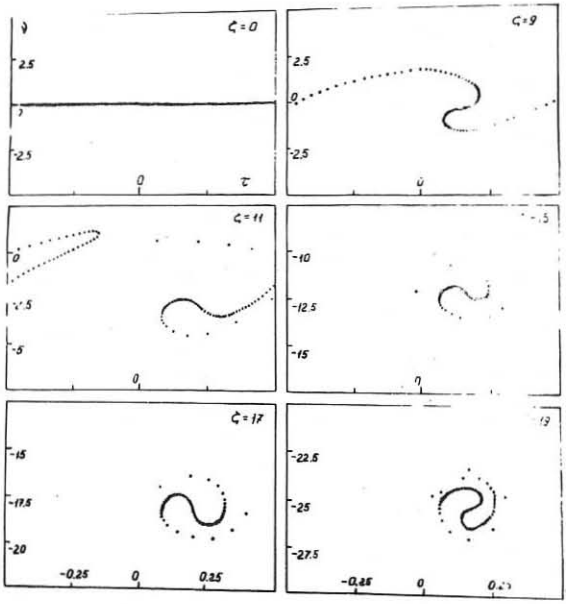
ζ = 0
2.5
0
-2.5
τ
ζ = 9
ζ = 11
-5
-10
-12.5
-15
ζ = 17
-15
-17.5
-20
-0.25
0.25
-22.5
-25
-27.5

Fig.3

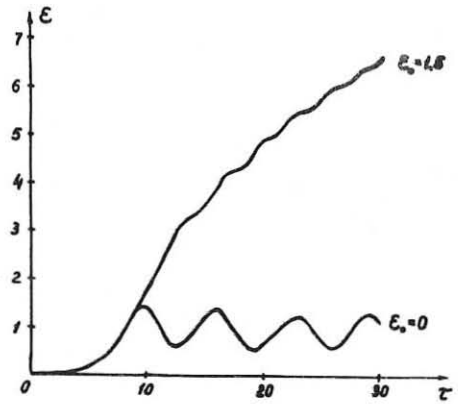
ε
7
6
5
4
3
2
1
0
10
20
30
τ
ε₀=4.8
ε₀=0

Fig.4

The mechanism of the origin of such a solution can be easily explained for the limit case of infinite strong magnetic field field. At the centre of the electron bunch, forming the soluton, the effective plasma dielectric x constant $\varepsilon = 1 - \frac{\omega_{p\,max}^2}{k_\perp^2 v_\parallel^2}$ is negative and the Coulomb repulsion of the charges of the same sign changes on their attraction, while on the periphery of the bunch $\varepsilon > 0$ and the repulsion of the electrons takes place. During the soliton motion through the plasma it occurs that the soliton is strongly damping owing to the soliton energy absorption by the resonant particles, reflected from the potential hump. Similarly to the electron beam moving through the plasma and allowing to reverse the Landau damping on the periodic waves, the soliton interaction with the electron beam moving faster than soliton, leads to the reversibility of the effect of soliton damping and to its amplification. For the beam with a diffuse distribution over the velocity $\frac{\Delta V}{V} \gg \left(\frac{n_b}{n_p}\right)^{1/3}$ the adiabatic amplification of the soliton takes place without dhanging soliton form. The amplitude of soliton potential is growing to the value the electric field energy density $\left(\frac{n_p}{n_b}\right)^{2/3}$ times of that for the excitation the monochromatic wave by electron beam. In Fig. 5 there is represent the series of the oscillograms for the case of damping of the soliton (oscillogram (a) - without the beam) and for the case of amplifying of the soliton (oscillograms (б -g) - withbeam).

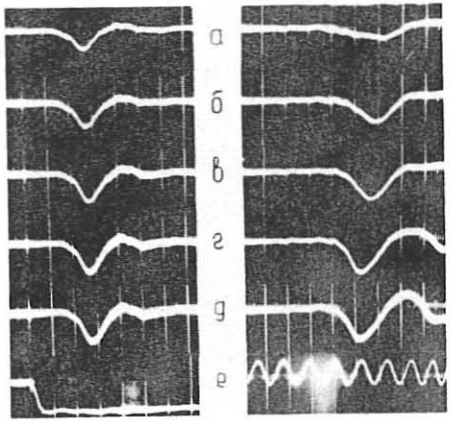

Fig.5

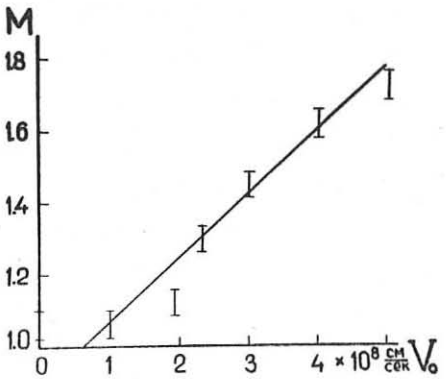

Fig.6

On the left series of oscillograms the soliton is shown to be registered by a probe which is situated at a distance 5 cm from a grid exciting the soliton; on the right series there are the oscillograme of soliton after passing the distance 20cm. For the oscillograms $\ell - d$ the beam velocity V_0 is a parameter. From these oscillograms the spatial distribution of the soliton is determined. The soliton is being amplified ultil its phase velocity does not exceed the beam velocity, therefore the experimentally measured maximum value of Mach number is proportional to the beam velocity (Fig.6).

IV. In some experiments with high-current relativistic beams $J \sim 10^4 \sim 10^5$ A the high beam-plasma interaction efficiency has been shown. The part of energy lost under such an interaction was 10-50%, it was also observed the beam heating and acceleration of the plasma electrons and ions /12/. However, the SHF - radiation from plasma was not investigated. The purpose of the experiments carried out at Linear plasma Betatron (L.P.B.) (in P.T.J.) is to show that for the interaction of high-current beam with plasma the SHF - radiation power is comparable with beam power. The beam current obtained at LPB-model was changed from 5 kA to 15 kA, the energy was changed from 100 kev to 150 kev. The main measurements were carried out for current 5-7 kA, energy 100 keV, current impulse duration 10^{-6} sec. It was shown that for the beam power $\sim 5.10^8$w the SHF-radiation power was 20% of the beam power. and the frequency of excited oscillations was changed within $(11\text{-}12).10^9$ cycles per second at the further growing of the beam power the radiation power was increasing so, that the break-down took

plase, that however can be removed if the more effective taking-off arramgements are used. In the experiments the next method of measurement of SHF - radiation was used. The plasma-beam interaction took place in the region which is limited by semispherical mirrors of the open resonator. One of the mirrors was connected with a waveguide. The measurement of the power was carried out with calorimeter and with help of calibrated detectors too. In the last case the signal was pre-attenuated by means of set of T-branchs and attenuators on 100-120 decibels. Thus caried experiments show a high efficiency of energy transformation from the high-current beam into SHF - oscillations. The further increase of the transformation efficiency can be achived by using the pre-modulated beams.

The experiments, carried out in P.T.I. with a high--current ($J \simeq 50$ kA) relativistic ($\gamma \simeq 3$) beam show the possibility of modulation of such a beam at the interaction with decelarating structure of kind of waveguide loaded by discs at the frequency $f = 10^{10}$ ($\lambda = 3$ cm) which is resonant for the plasma density $n_p = 10^{12}$ cm^{-3}. The problem of beam modulation at the frequencies which are resonant for dense plasma $n_p = 10^{18} \div 10^{19}$ cm^{-3} and $n_p = 10^{22}$ cm^{-3} is more difficult. It is the most perspective to modulate the high-current relativistic beams by means of the light with using the powerful lasers worked out at present.* The modulation of the electron

---

* - The possibility of using of standing waves for the partical containement is considered in the work [13].

beam by the light has been considered in [18-20]. One of the possibility of beam modulation by the light is the using the transformation of the transverse oscillations into longitudinal ones by means of cylindrical diffraction grating filled with a dielectric. The using of the dielectric gives the possibility to develerate the wave provides the synchronism between the wave and the beam. For these conditions the modulation of the beam density caused by the longitudinal field is determinated from the relation:

$$\frac{\delta n}{n} \sim \frac{e E_z k_z}{m_0 \gamma^3 (\omega - k_z v_0)^2}$$

where it is taken into account that in the taken system $k_\perp \ll k_z$. At resonance condition $\omega - k_z v_0 \sim k_z \Delta v$ ($\Delta v = \frac{c}{\gamma^2}\frac{\Delta \gamma}{\gamma} + \frac{c}{2}\theta^2$ - the longitudinal spread over the velocity in the beam). Assuming $\Delta v \sim 10^{-2} c$, $E_z \sim (0,1 \div 1) E_t$ $\gamma \sim 3$, $\omega = 2 \cdot 10^{15}$, We obtain that for appriciable modulation of the beam ($\delta n/n \sim 10^{-1}$) the necessary power of the electromagnetic wave is the value of order $3 \cdot 10^{11}$, $3 \cdot 10^{13}$ w.

The other possibility is the beam modulation with electromagnetic wave propagating under the angle ψ to the beam direction. In this case the force $\sim [\vec{v}_0 \vec{H}_\sim]$. Then

$$\frac{\delta n}{n} \sim \frac{e E_t k \sin\psi}{m_0 \gamma (\omega - k_z v_0 - k_\perp v_0 \Delta\theta)^2} \left(\frac{1}{\gamma^2} - \beta^2 \sin^2\psi\right)$$

where $\Delta\theta$ - angle spread over the velocity in the beam. The using of a dielectric, in particular gas, for the

deceleration of the wave can provide the synchronism between the beam and the wave, $\omega \simeq k_z v_o$. In this case assuming the angle spread in the beam $\Delta\theta \sim 10^{-1}$, the angle $\Psi \sim 1$, $\omega \simeq 2 \cdot 10^{15}$ we obtain that for the beam with $\gamma \sim 3$ and $\frac{\Delta n}{n} \sim 10^{-1}$ the electron wave power which is necessary for modulation is equal $\sim 10^{13}$ w.

In is necessary to note that the using of the beam with a modulation percentage $\frac{\delta n}{n} \sim 10^{-2} \div 10^{-1}$ gives the opportunity to decrease the relaxation length of the relativistic beam in the target to an order approximately. At the same time it is necessary to remark that the realy complete beam bunching can be provided at rather long distance from the modulating arrangment due to the using the klystron mechanism of bunching.

The question of the focusing is very important for the relativistic beam. This question is acquiring especial significance in connection with the problem of utilization the relativistic beams for the initiation of the impulse nuclear fusion in the solid D-T target and with the working out of combined beam-laser method of heating. At present considerable successes are achieved in the focusing of relativistic beam in the diod by using radial drift of beam particles in the crossing E and H field [14]. E_z is a longitudinal external electric field, created by the explosion of the wire, H - own magnetic field of the beam current. The drift $\vec{E} \times \vec{H}$ leads to the radial

focusing of the beam. This way at present the radial focusing of the relativistic beam with the current J = 100-250kA is provided up to the size of 2÷3 mm, the current density in the focused beam is the value of $\sim 5 \cdot 10^6$ A/cm^2. To provide the effective internation of relativistic beams with plasma there are important such methods of focusing which lead to decreasing of the angle divergence in the beam. In this connection we consider that the collective methods of focusing of relativistic beam connected with developing of instability are perspective. The angle divergence in relativistic beam is caused by betatron oscillations of beam particles in own magnetic field. These oscillations lead to the situation, when at the relativistic beam-plasma interaction together with usual instability of the longitudinal waves the electromagnetic instability is developing. The condition of the resonance interaction of beam particles with the wave is written in the form

$$\omega = k_z v_z + n\Omega, \quad n = 0, \pm 1, \pm 2 \ldots$$

Ω - the frequency of betatron oscillations. At $n > 0$ (normal Doppler effect) this condition is fulfilled for the fast electromagnetic wave $\omega > kc$ that leads to the development of electromagnetic instability of the beam in plasma. The growth rate of this instability is $\delta \sim \omega_b^{2/3} \omega^{1/3} \left(\frac{\Delta v_\perp}{c}\right)^{2/3}$ for monochromatic beams and $\delta \sim \frac{\omega_b^2}{\omega} \frac{\Delta v_\perp^2}{\Delta v_\parallel^2}$ for the beams with a large angle spread. The instability leads to the radiation of electromagnetic waves from the plasma and to the focusing of beam due to the recoil impulse.

Betatron oscillations of the particles are damping and angle divergence in the beam is decreasing. Characteristic length, on which the focusing occurs, $\ell \sim 2\pi Q \langle \Delta\theta \rangle \frac{\omega}{\delta} \frac{1}{1 - c^2/v_\varphi^2}$ is usually small so that the proposed mechanis of focusing is rather effective. We consider now the question about the mechanisms of dissipation of the plasma oscillations energy. The relativistic beam excitates directly the fast plasma wave which can dissipate due to the non-linear effects of transformation HF-oscillations into LF-ones. The dissipation of energy of the relativistic beam in plasma can be also achieved due to the excitation of LF - oscillations by the back current and due to the modulation at low frequencies. As theoretical and experimental investigations carried out in P.T.I. have shown the initial modulation of the beam at low hybrid frequency leads to the direct effective heating of electrons and ions. The lower frequency oscillations leading to the anomalous diffusion are not excited. It is shown experimentally that for modulation on low hybrid frequency about 30% of beam energy can be transfered into plasma heating. The transformation of HF - oscillation into LF - ones is connected with a decay of Langmuir oscillations into Langmuir and ion-sound ones. Such a transformation is especially effective for the interaction with plasma of the monochromatic relativistic beam. At the amplitude Langmuir oscillations excited by such a beam typical time of the non-linear transfirmation HF into LF-oscillations is $t \sim \frac{10}{\sqrt[4]{\omega_{pe}\omega_{Bi}^3}} \sqrt[4]{\frac{n_p T}{n_b m c^2 \gamma}}$

Because of the small value of the velocity of the LF - - oscillations typical length on which their excitation occurs is small too:

$$\ell_D \sim 10 \frac{v_T}{\omega_p} \sqrt{\frac{n_p T}{n_b m c^2 \gamma}}$$

This length can be compared with that on which the HF- - oscillation excitation occurs. At these conditions decay instability leads to the more effective taking-off the energy from the beam. Because the excitated HF - Langmuir waves have a negative energy (phase velocity is less than the velocity of the beam bunches) then at the decay the energy dissipation of these waves leads to the increasing of wave amplitude. In Fig. 7 the energy taken off from the beam is shown for the various value of parameter $\Lambda = \left(\frac{\ell_a}{\ell_D}\right)^2$. It is evident that including the decay instability leads to the considerable increasing of the total energy of the oscillations. The changing of the HF - oscillations amplitude along the beam is shown in Fig. 8. On this figure it is easy to observe the compli- tude beating with two typical periods - the period of the excitation of the HF - oscillations $\sim \ell_n$ (the period of phase oscillation of the trapped particles) and the period of the decay instability ℓ_n. At the Λ large enough ($\Lambda > \Lambda_{cr} = 4$) such a beating leads to the "phase mixing" in the beam (see Fig. 9 in which the dynamics of phase plane is shown) and at these conditions the total energy taken off from the beam due to the decay has not alrady increased. The amplitude of the ion-sound oscilla- tion excited at the decay is of order

$$E_{L.F.} \sim \left(\frac{n_b}{n_p} \frac{v_0}{v_g}\right)^{1/3} \gamma_0 E_{H.F.}$$

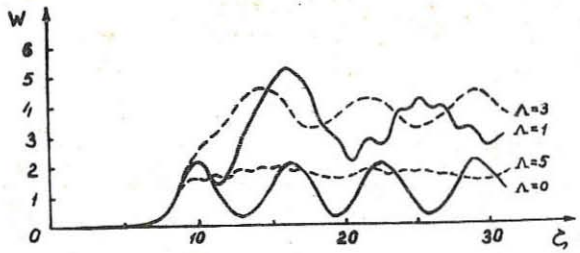

Fig.7

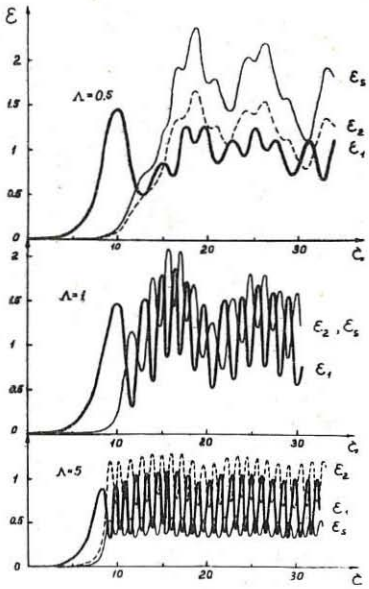

Fig.8

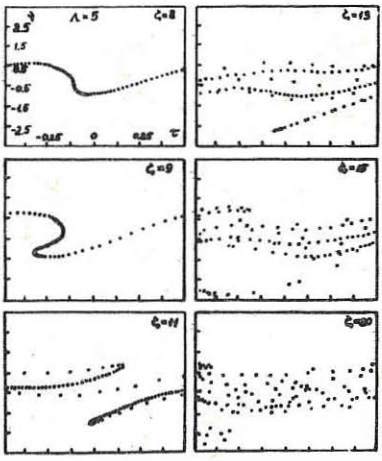

Fig.9

Thus the amplitude of the LF - oscillations and that of the HF - ones can be the same order at $n_p \sim 10^{14}$, $\gamma \simeq 5$ T ~ 1 kev: $E_{LF} \sim E_{HF}$, $l_D \sim 10$ cm.

Another possibility of the heating is the using of the back current, whose dissipation also leads to the excitation of LF - oscillation and to the heating of plasma [15, 16]. The advantage of this method is that the back current transform the energy directly to the ion-sound oscillations. The shortcoming is that the power of back current is a small part $(n_b/n_p)^2$ of the electron beam power. Therefore the heating time is essentially growing so that the working out of the sources with a great time duration is necessary. Let us compare the efficiency of heating to the transformation HF into LF oscillations with a heating by the back current. The ratio of the values obtained in these two cases is determined by the relation

$$\frac{(n_p T)_{decay}}{(n_p T)_{back\ current}} = \frac{n_p}{n_b}\gamma \frac{\delta_s}{\nu_{eff}} \left(\frac{n_p}{n_p}\frac{v_0}{v_g}\right)^{1/3}\gamma$$

(δ_s - decrement of ion sound ν_{eff} - effective frequency of the electrons for the turbulent plasma, $\nu_{eff} = \simeq 10^{-2}(\omega_{pe})$). For the beam and plasma parameters $n_p \sim 10^{14}$, $n_b \sim 10^{12}$, $\gamma \sim 3$, $\delta_s \sim 10^{-1}\nu_{eff}$,

The extimates, carried out above, the experimental investigations with a low-powered high-current beams show that in principle the collective mechanism of the heating of

plasma with a density $10^{14} \div 10^{18}$ cm^{-3} by the beam is realizable.

V. It is also advisable to dwell on the role of plasma non-homogeneity in the processes of the wave transformation. We consider first of all the question about the linear wave transformation in the non-homogeneous plasma - beam discharge ($\omega_H >> \omega_p$). The main pecularity is the strongly pronounced anisotrophy of the transformation processes. Remember first of all that when propagating in the direction of density growth excited plasma waves with a high reflection index are being transformed into radiated transvese oscillations and at the inverse propagation are strongly being transformed into Langmuir oscillation and are being damped [17]. It is essential how the beam modes transform into plasma ones. The exact analytical theory for the case of nonhomogeneity smoothly changed along the magnetic field shows that the slow beam mode, propagating into direction of large density begins to transform partly into transverse wave that does not amplify and then the amplification of the beam mode occurs. When beam moving into direction of the descent of density the amplified Langmuir wave is arising, i.e. the effective plasma heating is possible. Thus the plasma nonhomogeneity along the strong magnetic field promotes the heating of plasma but by itself the nonhomogeneity does not lead to increasing of radiation of transverse waves. On the other side taking into account the transverse nonhomogeneity the slow wave

of space charge (with a negative energy) flows out of the beam into plasma and excites the plasma oscillations which are being amplified in the beam direction. From the calculations it follows that the coefficients of transformation (Q) and amplification (K) in this case are connected by the next relation

$$K = \frac{v_{g\perp}}{4a\, v_{g\parallel}} \ln Q$$

Here 2a - the width of the beam, $v_{g\parallel}, v_{g\perp}$ - group velocities along and across the beam correspondently. It is also interesting to pay attention to some features of the transformation in the nonhomogeneitly plasma of the waves excited by a narrow beam. The influence of the nonlinear effects and the plasma temperature is growing with a growth of the beam energy. So the maximum coefficient of the transformation into the second harmonic of the transverse wave $Q_2 = \left(\frac{e\tilde{H}}{mc}\right)^2 \rho^{4/3}$ ($\tilde{H}$ is the value of the magnetic field of the fundamental wave, ρ is the parameter of the geometrical optics). Here it is supposed that $\beta^3 \rho \ll 1$ where $\beta^2 = \frac{v_{Te}^2}{c^2}$. Further, the carried calculations show the essential growing of the coefficient of amplification of the decay process in the singularity region of the pump wave field. We also remark that the taking into account of the nonlinear terms $\Delta\varepsilon_{NL}$ of dielectric constant of the fundamental wave can lead to the penetration of the wave over the returning point if $\Delta\varepsilon_{NL} \gg \frac{1}{\rho}$ is fulfilled.

REFERENCES

1. Ya.B.Fainberg, V.D. Shapiro, K.I. Shevshenko, JETP, 57, 966 (1969).
2a. B.N.Breisman, D.D.Ryutov, JETP, 60, 408 (1971).
2b. B.B.Kadomtsev, V.I.Petviashvili, JETP, 43, 2234 (1962).
2c. V.N.Oraevsky, R.Z.Sagdeev, JTP, 32, 291 (1962).
3. Ya.B.Fainberg "Atomic Energy", 13, 303 (1962).
   A.K.Berezin, Ya.B.Fainberg, A.M.Egorov, V.P.Kiselev, V.I.Kurilko, A.P.Tolstolushsky, JETP, 63 (1972).
4. I.N.Onishchenko, A.R.Linetsky, N.G.Matsiborko, V.D.Shapiro, V.I.Shevchenko, JETP Letters, 12, 407 (1970)
   Th.O'Neil, J.H.Malberg, J.H.Winfrey Phys.Fluids, 14, 1204 (1971).
5. N.G.Matsiborko, I.N.Onishchenko, V.D.Shapiro, V.I.Shevchenko, Plasma Physics, 14, 597 (1972).
6. L.E.Thode, R.N.Sudan, Phys.Rev.Lett., 30, 732, (1973).
7. A.K.Berezin, G.P.Berezina, N.G.Matsiborko, Ya.B.Fainberg, V.D.Shapiro, V.I.Shevchenko, Nuclear Fusion, 13, 6 (1973).
8. P.M.Lebedev, I.N.Onishchenko, Ya.B.Fainberg, J.T.P. 43, 12, (1973)
9. S.M.Krivoruchko, Ya.B.Fainberg, V.D.Shapiro, V.I.Shevchenko, JETP Letters, 17, 344 (1973).
10. B.N.Rutkevich, A.V.Paschenko, V.D.Fedorchenko, V.I.Muratov, JTP, 42, (1972).
11. H.T.Tkezi, P.J.Barrett, R.B.White, A.Y.Wong, Phys.Fluids, 14, 1997 (1971).
12. A.T.Altintsev, A.G.Eskov, O.A.Sovotovsky, B.I.Koroteev, P.X.Kurtmulaev, B.L.Masulov, B.H.Semenov, JETP Letters, 13, 197 (1971).
13. V.I.Veksler, A.M.Kovrishnich, JETP (1953).
14. J.Jonas, et al, Phys.Rev.Lett., 30, 164 (1973).
15. R.V.Lovelace, R.N.Sudan, Phys.Rev.Lett., 27, 1256 (1971).
16. A.A.Ivanov, L.I.Rudakov, JETP, 58, 1332 (1970)
17. A.K.Berezin, T.P.Berezina, N.S.Erochin, S.S.Moiseev, Ya.B. Fainberg, JETP Lett., 14, 149 (1970).
18. Ya.B.Fainberg "Plasma Physics and problem of nuclear fusion", Vol.3. Edited be Academy of Science of UkSSR, Kiev, 1963, p.300.
19. M.Djakov, D.Varshalovith. Phys.Lett., 35A, 277 (1971)
20. A.M.Dychne. Phys. Lett., 42A, 259 (1972).

APPLICATIONS OF INTENSE RELATIVISTIC ELECTRON BEAMS TO CONTROLLED THERMONUCLEAR FUSION*

R. N. Sudan

Laboratory of Plasma Studies, Cornell University, Ithaca, New York

INTRODUCTION. Technological advances have placed at our disposal intense electron beams with truly imposing characteristics; in electron energy up to 15 MeV, in currents above 10^6 A, in total energy per pulse up to 3 Mj, in power up to 10^{13} w, in beam current density up to 5×10^6 A/cm^2, for pulse durations of order 10^2 nsec. The availability of this powerful source of energy cannot but make a strong impact on our thinking with regard to Controlled Thermonuclear Fusion Research, electron and ion collective accelerators and related problems. In this talk because of limitations of time, I will address myself to nuclear fusion applications only. Broadly speaking, E-beams can be employed in currently popular magnetic confinement schemes or more dramatically, they can compete with lasers in inertial confinement schemes that involve zapping a suitable solid target with a high power source.[1,2]

The principal roles for E-beams in magnetic confinement schemes are (1) plasma heating[3-17] and (2) creating minimum-$|B|$ field geometry in toroidal systems,[18] e.g. the Astron. Success here depends critically on the ability to inject and trap beams in an appropriate magnetic field. Injection into a configuration with open lines of force is relatively straightforward. On the other hand, injection into a toroidal closed-line geometry requires greater ingenuity, and I will discuss later on some schemes for such injection. The major problems for inertial confinement schemes are concerned with pulse compression to create shorter pulses $\lesssim$ 10 nsec and beam focussing[19-22] to approximately $10^8 \sim 10^9$ A/cm^2. I will now treat a few of these problems in some detail.

HEATING OF MAGNETICALLY CONFINED PLASMA. Plasma heating by E-beams in the density range of interest is in large measure due to collective energy transfer mechanisms from the beam to the plasma. Of these there are basically only two viz., the two-stream instability generated by the beam electrons[4,6,10,11,23] and the turbulent heating caused by the plasma return current induced when a beam is injected into a plasma.[5,8] Both these processes can occur but in different regimes one or the other is dominant.

Two-Stream Instability Heating. It is well known that for a cold relativistic beam interacting with a collision-free plasma the fastest growing electrostatic modes are those propagating practically orthogonal to the beam.[24] However, as shown by

Fainberg, Shapiro and Shevchenko,[4] these modes self-stabilize by creating a spread in in the beam transverse momentum. In high current beams, there is always an initial spread in the transverse momentum $\Delta p_\perp \equiv m\gamma c \langle\theta^2\rangle^{\frac{1}{2}}$ created in the diode and also in traversing the anode foil. This spread can easily prevent the growth of transverse modes. More importantly, Rudakov[6] pointed out that since $\Delta p_\perp$ is accompanied by a spread in the parallel velocity of order $\Delta V_{||}/c \sim \gamma^{-1}(\gamma^2-1)^{\frac{1}{2}}(1 - \cos\langle\theta^2\rangle^{\frac{1}{2}})$ the strongly unstable 'hydrodynamic' phase of the longitudinal modes ($k_\perp \approx 0$) may be quenched. Thus it was predicted that for high current beams with sufficiently large $\langle\theta^2\rangle^{\frac{1}{2}}$ the two-stream instability is likely to be in the weakly unstable kinetic stage with the wave-spectrum dominantly in the beam direction. Several detailed analysis [4,6,23,25] of the quasilinear evolution of this instability have appeared in the Soviet literature. The estimated interaction lengths in these calculations are widely different because of different assumptions as to the nature of the dominant nonlinear process.

In order to resolve some of these difficulties, I will now describe the results of a one-dimensional computer simulation of a relativistic beam interacting with a uniform homogeneous plasma.[10] In most of the computations the initial spread in the beam velocity $\Delta V_{||}/c \ll (n_b/2n_e)^{1/3}/\gamma$ so that the instability begins in the hydrodynamic stage. As a check, in one of the simulation runs the beam electrons were given a distribution in energy which resulted in $\Delta V_{||}/c \approx (n_b/2n_e)^{1/3}/\gamma$. The final results were not significantly different from those given by an initially cold beam with a lower mean energy. Figure 1 shows the results of a typical run with $\gamma = 4$ and $n_b/n_p = 10^{-2}$ with the beam cold and plasma initially at 1.5 keV. The electrostatic energy increases exponentially at a rate predicted by linear theory for the mode with the maximum growth rate; 90% of the total energy is in this mode. This mode saturates abruptly. After saturation the wave energy fluctuates at approximately twice the trapping frequency of the beam electrons for perhaps an oscillation or two. At this point the large amplitude wave acts as a pump wave to drive the oscillating two-stream instability. Note the sudden rise of ion fluctuations in Fig. 1 that accompanies the decay of the primary spectrum. The observed growth rates and wave numbers of the unstable secondary spectrum are in fair agreement with the theoretically predicted growth rates for the oscillating two-stream instability[26-28] computed using the saturation amplitude of the primary spectrum. At high wave numbers where Landau damping becomes strong, the agreement is not so good (see Fig. 2). These secondary beat waves are close to the plasma frequency ω_e and their wavelength determined by the ion fluctuation is about $k\lambda_D \lesssim 0.2$. Their phase velocity is low and they resonate with the tail of the electron distribution function. During this stage the energy in the primary spectrum heats the tail of the electron distribution to high energy. The wave spectrum at $\omega_e t = 900$ is seen in Fig. 3 showing the emergence of the secondary waves. In Fig. 4(a) we see the spread in the beam momentum distribution at the instant of wave saturation $\omega_e t = 375$ and in Fig. 4(b) the plasma electron distribution with

its energetic tail is plotted at the end of the second stage $\omega_e t = 1000$. This stage is very similar to the calculations of anomalous electron heating by lasers with $\omega \approx \omega_e$.[29,30] In E-beam heating the large pump fields are self-generated by the beam.

A summary of a series of simulation runs is presented in Table I. The fraction K of the initial beam energy which is transferred to the plasma electron is of order 25% at the end of the second stage. Of this energy, the tail contains at least 60%. Following this stage the waves drop in amplitude and the heating rate is considerably reduced. The final electron energy appears to scale linearly with γ and n_b/n_p. In Fig. 5 the electric field energy at the time of wave saturation $W=\Sigma_k |E_k|^2/(8\pi n_b mc^2\gamma_o)$ is plotted as a function of the parameter $S=\beta^2\gamma_o(n_b/2n_p)^{1/3}$ from the simulation runs. A similar result has been reported by Matsiborko et. al.[31] Notice that W peaks at $S\sim 0.6$. The curve represents the theoretical prediction which I will discuss now.

A single unstable wave saturates by trapping the beam electrons.[32,33] The energy exchange between the wave maximizes approximately when the beam electrons have completed about 1/2 revolution in phase space. If f(x,p) is the beam momentum distribution in the waveframe at the time of wave saturation, the energy loss of the beam electrons as observed in the lab frame averaged over a wavelength λ is given by

$$\Delta\varepsilon = n_b mc^2 \gamma_w \int_{-\lambda/2}^{\lambda/2} \frac{dx}{\lambda} \int_{-\infty}^{\infty} dp\, f(x,p)\, \{\gamma_r - \gamma(x,p) + \beta_w(p_r - p(x,p))\} \equiv \Delta\varepsilon_1 + \Delta\varepsilon_2$$

where mcp_r and γ_r are the initial beam momentum and energy in the waveframe, $\beta_w = \omega_o/k_o c$, and $\gamma_w = (1-\beta_w^2)^{-1/2}$. Let $\Delta\varepsilon_1$ be the contribution from the $(\gamma_r-\gamma)$ term and $\Delta\varepsilon_2$ from the remainder; $\Delta\varepsilon_1$ represents the spread in energy and $\Delta\varepsilon_2$ is the change in the mean drift energy. As the wave grows in amplitude $|\Delta\varepsilon_1|$ and $|\Delta\varepsilon_2|$ both increase from their initial values; however $\Delta\varepsilon_1 < 0$ and $\Delta\varepsilon_2 > 0$. For $S \ll 1$ the energy spread is negligible $|\Delta\varepsilon_1| \ll |\Delta\varepsilon_2|$ and one can regard the bulk of the beam electrons to rotate rigidly in x-p space[32] so that the beam which was initially described by $f(x,p) = \delta(p-p_r)$ is now half a revolution later $\sim\delta(p+p_r)$. With this distribution $\Delta\varepsilon_1 \approx 0$ and $\Delta\varepsilon_2 \approx S/(1+S)$ which gives

$$W = \frac{|E_o|^2}{16\pi n_b mc^2 \gamma_o} = \frac{1}{2}\, S/(1+S)^{-3/2} \approx \frac{1}{2}\, S \text{ for } S \ll 1, \qquad (1)$$

noting that $\gamma_w/\gamma_o \approx (1+S)^{-1/2}$ and the factor ½ comes from equipartitioning the wave energy between the electrostatic and the oscillation energy of the plasma electrons. For $S \gtrsim 1$ the energy spread $|\Delta\varepsilon_1|$ becomes important. This is evident from Fig. 4(a) which shows the beam electron distribution at the time of saturation. If indeed we calculate $\Delta\varepsilon_1$ and $\Delta\varepsilon_2$ by assuming that the wave amplitude reaches its final value suddenly the energy loss $\Delta\varepsilon$ scales more like $S/(1+S)^{-2}$ and we obtain[10]

$$W = \frac{1}{2}\, S/(1+S)^{5/2}. \qquad (2)$$

An alternative viewpoint is to say that because of the increased energy spread in the beam the effective number of beam electrons that are trapped by the wave is given by[10]

$$n_{eff}/n_b = (\gamma_w/\gamma_o)^3 . \qquad (3)$$

As a corollary of Eq. 2 we conclude that for large S the beam transfers a small fraction of its energy to the wave. But from Fig. 4(a) we observe that the beam distribution is approximately constant up to some maximum momentum p_{max}. From conservation of beam energy we may conclude that the maximum energy to which the beam electrons are accelerated during this state is given by[10]

$$\gamma_{max} \simeq 2\gamma_o - \ell n(4\gamma_o)/2\gamma_o \quad , \tag{4}$$

which agrees well with the data shown in Fig. 6.

What conclusions can we draw from these simulation results? (1) A strong interaction takes place for a beam with a narrow spread in $V_{||}$. (2) A significant fraction of the energy transferred to the plasma ends up in a very energetic tail. (3) The ions are relatively unaffected. (4) The dominant nonlinear effects are wave saturation by beam trapping and the transfer of energy in the primary spectrum to low phase velocity beat waves taking place through a parametric instability or nonlinear Landau damping when the primary spectrum is broadened. We have observed nonlinear scattering to superluminous waves but this effect is not terribly significant for plasma heating.

A rough estimate for the interaction time τ_{TS} for rapid energy transfer to the plasma electrons is to take the sum of the time taken to reach wave saturation and the time for the primary spectrum to decay in the second stage. Since the two-stream saturates in a few growth times and the second stage is largely governed by the growth rate of the oscillating two-stream instability[27] we obtain,

$$\tau_{TS} \simeq (5\sim10)\left[\delta_{TS}^{-1} + \delta_{QS}^{-1}\right] , \tag{5}$$

where $\delta_{TS}/\omega_e = 0.87\ S/\gamma^2$ and $\delta_{QS}/\omega_e \simeq 0.707\ (m_e/m_i)^{1/3}(kV_E)(\omega_R^2 - \omega_o^2)^{-1/2}$ where $\omega_R = \omega_e(1+k^2\lambda_D^2)^{1/2}$, $\omega_o = \omega_e(1-S/2\gamma^2)$ is the typical frequency of the primary spectrum, $V_E = eE_o/m\omega_o$ and E_o is determined from (2); typically $k\lambda_D \lesssim 0.2$.

At the Naval Research Laboratory, Kapetanakos and Hammer[12] have found that the coupling efficiency of a 400kV, 40KA, $v/\gamma \simeq 1.5$ beam to mirror confined plasma is optimum ($\simeq$ 25% is claimed) when the beam and plasma densities are about equal and is independent of the magnetic field in the range 2.5 - 5 kg. This result may be interpreted as follows. The rms angular spread $\langle\theta^2\rangle^{1/2}$ for this beam is estimated at 30° which gives a spread $\Delta V_{||}/V_B \simeq 0.13$. As observed earlier, for strong interaction $0.5\gamma^{-1}(n_b/2n_p)^{1/3} \geq \Delta V_{||}/V_B$ which requires $n_b/n_p \sim 0.25$. Thus for high current E-beams which in general have a finite spread $\langle\theta^2\rangle^{1/2}$ the two-stream instability is strong only when n_b/n_p is above a critical limit. This is also a feature of the experiment reported by Goldenbaum et. al.[14] where a 1MV, 50kA beam was injected into a weakly ionized H_e plasma of initial density $5 \times 10^{12}\ cm^{-3}$. During the pulse the density rapidly builds up to 5×10^{14} and the electron temperature (as measured by observing the intensity of the H_e II 4686Å line) jumps to 500ev (initially ~1ev) in less than 25 nsec. Copious emission of X-rays, in the energy range 50 ~ 400kv with a maximum about ~200kv, is observed during the pulse. This supports the prediction that energetic tails in the plasma electron distribution are created (also a spread

of the beam electrons to lower energies). Furthermore, since burst of hard X-rays are observed about 10μsec after the beam pulse, energetic electrons must be confined by diamagnetic currents as the external magnetic field did not have any mirrors.

Return Current Heating. The magnetic energy per unit length W_M for a beam of radius 'a' propagating in a conducting tube of radius 'b' is given by

$$W_M/Nmc^2\gamma = \frac{1}{2}(\nu/\gamma)\,\beta^2 L \qquad (6)$$

where $Nmc^2\gamma$ is the beam energy $\nu = Ne^2/mc^2$ and $L = \frac{1}{2} + 2\,\ell n(b/a)$ is the inductance per unit length and $\beta = V_B/c$. As ν/γ approaches unity the Alfven-Lawson limit,[34] clearly propagation is not possible. When such a beam is injected into an ionized medium a return current I_p equal and opposite to the beam current is induced within the beam if 'a' exceeds the electromagnetic screening length c/ω_e,[35-38] thus neutralizing the magnetic field and allowing the beam to propagate. This is not a steady state however, because as a result of the finite conductivity σ of the medium, the induced currents will eventually decay with a characteristic time $T \simeq 4\pi\sigma a^2/c^2$, the magnetic field builds up and energy is dissipated in the plasma. The amount of energy dissipated per unit length, K, is given by[5]

$$K \equiv \int_o^t I_p^2 R\,dt = \int_o^t I_B \frac{d\Phi}{dt}\,dt - \int_o^t dt\,\frac{d}{dt}(\tfrac{1}{2}LI^2) = I_B\Phi - \tfrac{1}{2}LI^2 \qquad (7)$$

where $I = I_p + I_B$ the net current, $\Phi = LI_B$ is the flux linking the beam current and we have assumed that for a relativistic beam I_B remains reasonably constant even with a large drop in energy. If the net current at time t is the fraction $f \equiv I/I_B$ then

$$K = (2f - f^2)W_M \,. \qquad (8)$$

The maximum value of $f = I_A/I_B$ because by then the net current equals the Alfven-current and propagation ceases by virtue of Eq. (6). Thus

$$K_{max} = LI_BI_A \qquad (9)$$

for $I_B/I_A = \nu/\gamma >> 1$. In practice a guide magnetic field is necessary for stable operation whose magnitude should at least exceed the self-field generated by the net current I. Assuming I_B = 1 MA, γ = 3, L = 4.5 μhenries/m, we have K_{max} = 23 kj/m. The time τ_{RC} needed for this energy to be deposited is[5]

$$\tau_{RC} = (I_A/I_B)\,(4\pi\sigma a^2/c^2) \qquad (10)$$

which depends critically on the conductivity. If the drift velocity of the return current $V_p = c(n_b/n_p)$ is larger than the electron thermal velocity V_e or even the ion-acoustic velocity C_s then clearly we expect turbulent fluctuations to be excited and the conductivity should be governed by "turbulent" collision frequency ν* determined experimentally or theoretically by such expressions as Sagdeev's formula[39] $\nu^* = 10^{-2}(V_p/C_s)(T_e/T_i)\omega_i$. Taking $n_p \sim 2 \times 10^{14}\,cm^{-3}$, beam density ∿10kA/cm^2 and $\nu^* \sim 10^{10}$ for these conditions we obtain $\tau_{RC} \lesssim 10^2$ nsec which is about the pulse duration of currently available beams.

To understand the micro-turbulence created by the return current and its interaction with the waves generated by the two-stream instability we have executed a

series of one-dimensional computer simulation runs including both the beam and the return current. The net current is maintained at zero by the requirements of the problem and this generates an average electric field that is given by the quasi-linear equations,

$$\langle \underline{E} \rangle = -\frac{4\pi}{\omega_e^2} \sum_j e_j \int d^3v \, \underline{\underline{D}}_j \cdot \frac{\partial}{\partial \underline{v}} \langle f_j \rangle \equiv \frac{4\pi\nu^*}{\omega_e^2} \underline{j}_p \equiv \underline{j}_p/\sigma \qquad (11)$$

where $\underline{j}_p$ is plasma current density, j refers to the particle species $\underline{\underline{D}}_j = (e_j/m_j)^2 < \delta\underline{E}(\underline{x},t) \int_{-\infty}^{t} dt' \, \delta\underline{E}(\underline{x}(t'),t') >$ is the usual quasilinear diffusion coefficient given in terms of the fluctuating micro-fields $\delta\underline{E}$. $\langle E \rangle$ is the electric field that extracts energy from the beam and delivers it to the plasma. Since ν^* is proportional to $\langle \underline{E} \rangle$, in the simulation runs $\langle E \rangle$ gives a direct measure of ν^*.

Figure 7 and 8 show the rate of electron and ion heating respectively for $n_b/n_p = 1/9$ and a cold beam with $\gamma = 2$, 4 and 8. The results from an initially warm beam with $\langle\gamma\rangle = 3.07$ and $\Delta p_\perp/p_o \approx 0.25$ are also shown; no qualitative difference between the cold and warm cases can be observed. The peaks in the electron energy towards the beginning are caused by the rapid rise of the two-stream instability. A check run involving no beam but only a constant return current with the same drift as the other cases is also shown. Notice that the rate of electron heating is relatively unaffected by the presence of the return current while the rate of ion heating is not determined significantly by the two-stream instability since the case with no beam gives comparable heating. Up to about $\omega_e t = 500$ the Buneman-Budker instability of the drifting electrons and ions is operating ($V_p > V_e$ the electron thermal velocity) and after this time the instability develops into the ion-acoustic mode because at this point $V_e > V_p$ as shown by the electron distribution in Fig. 9 ($\omega_e t = 500$).

For the case $\gamma = 8$ the growth rate for the Buneman-Budker instability, δ_B, is higher than the two-stream instability δ_T. This results in a slightly higher ion energy at $\omega_e t = 500$ because the electrons take longer to heat and the transition to the more slowly growing ion-acoustic stage is delayed. The opposite is true for $\gamma = 2$ for which $\delta_B < \delta_T$. Figure 10 shows $\langle E \rangle$ as a function of time and $\nu^* \simeq 0.2\ \omega_i$ at $\omega_e t = 500$. The wave spectrum for $\gamma = 8$ case at $\omega_e t \approx 680$ is shown in Fig. 11; notice that spectrum is described approximately by $|E_k|^2 \alpha k^{-n}$ where n is approximately 2 over most of the range.

Figure 12 gives the ion distribution at $\omega_e t \approx 680$ for the case $\gamma = 8$. The mean ion energy has increased to 0.7 kev from an initial value of ~5 ev. The ions are continuing to heat at a rate given by $1.25 \text{ev}/\omega_e^{-1}$. The measurement of energetic ions in a beam-plasma experiment reported recently by Korn, Sandel and Wharton[16] gives an indication of return current heating. Beam currents up to 70kA at ≤ 500 kv were injected in a 5~8 x 10^{13}cm^{-3} fully ionized hydrogen plasma in a magnetic mirror 2.5 ~ 6kg. The perpendicular plasma energy as measured by the diamagnetic signal has a threshold around 8kA and thereafter increases linearly with beam current to ~100j at 60kA. Quantitative estimates as to the relative importance of two-stream instability

vs. return current heating are not possible because of lack of measurements of the individual electron and ion energies. Figure 13 shows the measured relative ion distribution for different beam currents.

Tokomak Heating. For this application we are required to heat a large volume of plasma in the density range 10^{13}-10^{15} cm^{-3} in magnetic fields ∿50kg. Based on pseudo-classical diffusion in an axisymmetric system Yoshikawa[40] computes the following parameters for a possible fusion device:

B_T (toroidal)	50 kg	Plasma volume	$2 \times 10^7 cm^3$
I (toroidal)	2 MA	Density	$2 \times 10^{14} cm^{-3}$
Major radius	256 cm	Ignition energy W_{ig}	19.2 MJ
Minor radius	64 cm		

For an energy confinement time τ of 1 sec the minimum power required is $P_{min} = W_{ig}/\tau$ = 19.2 MW. The total energy supplied by a constant power source is $W = P\tau \log_e(1-P_{min}/P)^{-1} \approx W_{ig}$ for $P >> P_{min}$. When P is just greater than P_{min}, W is correspondingly larger than W_{ig}. It is clear that high power sources like E-beams are competitive for this duty and will require the least amount of total energy. The plasma confinement time is also reduced since the time required to heat the plasma is negligible compared to the burn time. In this application one could tolerate pulse durations of order micro-seconds but this needs further development in technology. For this plasma density range high ν/γ beams of ≥1 MA rating will prove effective and the return current heating mechanism is likely to be important.

The main unknown is the ability to inject such beams into a toroidal magnetic system. An approach pursued by Brower, Kusse and Meixel[41] at Cornell is shown in schematic form in Fig. 14. The field lines at the port of entry are distorted by the magnetic field of the injected current. The toroidal path length is designed to exceed the beam pulse length so that when the head of the beam returns to the entry port the magnetic perturbation has disappeared. Currents of order 20kA at 400kv have been injected successfully into a field of 2kg in a quarter turn torus filled with neutral gas at 0.2 Torr[41]. The effect of a preionized plasma on the magnetic perturbation needs investigation.

High Density Plasma Heating. Recent progress[19-22,42] in focussing of E-beams has resulted in peak densities in excess of 2.5×10^6 A/cm^2, beam density ∿10^{15} cm^{-3}, energy density ∿10^{20}-10^{21} ev/cm^3, with total current in the focussed region well over 10^2kA. An attractive possibility is opened up by these well-focussed E-beams to heat directly a high density 10^{17}∿10^{19} cm^{-3} plasma to thermonuclear temperature. Dawson et. al.[43] have considered the use of high power CO_2-N_2 lasers to heat such a high density plasma. E-beams, however, have the advantage over CO_2-N_2 lasers of a much shorter absorption length and moreover their efficiency is higher and they are currently available in the required energy and power levels. Let us consider a D-T plasma with $n_D = n_T = n/2$. The confining magnetic field for $\beta = 1$ is given by

$$B = 8.9 \times 10^{-6} (nT)^{\frac{1}{2}} \text{ gauss} \qquad (12)$$

where T the temperature is in eV. The loss rate for $\beta = 1$ plasma confined in a magnetic cusp can be computed by (a) neglecting diffusion across the plasma surface and assuming uninhibited collisionless flow through a hole of an ion gyro-radius in size or (b) assuming diffusion across the plasma into a surface sheath and free flow along the magnetic lines of force in the sheath.[44,45] A rough estimate of the confinement times for these two models, without numerical coefficients, are:

$$\text{(a)} \quad \tau_a \approx (\ell/C_s)(R/r_i)(1+r_i/R)^{-1} \qquad (13a)$$

$$\text{(b)} \quad \tau_b \approx R(\ell/DC_s)^{\frac{1}{2}} \text{ ; sheath thickness } \Delta \equiv (D\ell/C_s)^{\frac{1}{2}} \qquad (13b)$$

where R and ℓ are the radius and length of the plasma spindle and C_s is the sound velocity. Introducing the Lawson condition which at $T \approx 10^4$ev is $n\tau \approx 10^{14}$ we obtain for the input energy

$$W_i^a = 10^{-2} RT^2/B \text{ MJ} \qquad (14a)$$

and $$W_{ig}^b = 5 \times 10^9 T^{3/2}(D/n) \text{ MJ , when } \Delta >> r_i. \qquad (14b)$$

The choice of D follows the fashion of the times. In the post-Bohm era we may pluck enough courage to use the pseudo-classical formula[40] which for $\beta = 1$ differs only in numerical coefficients from the classical. In this case $W_{ig}^b \approx 6.7\times10^9 T/B^2$ MJ. For $\Delta \lesssim r_i$, w_i^a provides the better estimate for the input energy. For B=1.5Mg, n=4.5×10^{18}cm^{-3}, $\pi R^2 L \approx 4.1\times10^3$cm^3, W_{ig}=60MJ at T=10^4ev. At these high plasma densities return current heating will not be particularly effective because τ_{RC} which scales as $n_p^{\frac{1}{2}}$ (assuming $\nu^* \propto \omega_i$) can exceed presently available pulse durations. The two-stream instability heating time that scales as ω_i (because of the parametric instability scaling) can be much shorter than the pulse duration. Assuming that the bulk of this energy is transferred to energetic electrons this energy equilibrates with the ions by Coulomb collisions in a time much less than the confinement time. The energy requirement is of course much reduced if uninhibited flow is disallowed in the plasma sheath postulated in model (b). Experiments on a reasonably large scale ($\gtrsim 10^5$g,$\sim$50kj beam energy) are needed to establish the scaling of the loss processes in this high density, high β regime.

FOCUSING OF E-BEAMS FOR SOLID-TARGET HEATING. There has been moderate success in radial compression of E-beams by guide magnetic fields and by injection into cone-shaped conductors. However strong focusing has been reported in those experiments in which the self-pinching forces of high ν/γ beams are utilized within the diode itself. By forming a dense plasma channel with an exploding-wire discharge within the diode, Vitkovitsky et. al.[22] have claimed current densities in excess of 10^7A/cm^2 at the anode. The current of electrons greater than 40 kev is about 2×10^5A and has a half width by order 0.1cm. The electron energy fluence at the target is $\sim$40kj/cm^2.

Current densities of 5×10^6A/cm^2 have also been achieved by Yonas et. al.[21] They have also numerically computed the electron trajectories in the diode. The electrons

emitted from the cathode $\underline{E} \times \underline{B}$ drift towards the diode axis for high ν/γ beams. The presence of a plasma in the gap (whether self-produced by exploding wires or externally introduced) appears to encourage the pinching of the beam by providing space-charge neutralization. Much needs to be done both experimentally (by way of diagnostics) and theoretically before a clear picture emerges of the physical processes occurring within the diode.

MAGNETIC FIELD SHAPING (ASTRON and RELATIVISTIC COILS). By injecting high current E-beams into a neutral gas at a pressure of a few hundred Torr, Andrews et. al.[18] demonstrated that fully reversed E-layers can be created by a single pulse in a magnetic mirror field $\sim$220g. Later experiments[46] have shown that such strong E-layers are focused by their self-fields into a doughnut configuration which is in line with the equilibrium of a relativistic electron coil[47]. These E-layers appear to be stable and their lifetime is in large measure determined by the scattering time of the high energy electrons with the background gas.[47a,48] An externally applied toroidal B_θ field stabilizes the "dump" of the layer that occurs when the $\zeta \equiv \Delta B_z/B_z$ on axis has dropped below a critical level. Recently Fleischmann and collaborators[49] at Cornell have been successful in creating E-layers with ζ(initial) = 0.8 which have a lifetime of $\sim$120μsec by injecting a 3.5MeV, 50 kA beam into magnetic field of 10^3g at $\sim$1 Torr pressure H_2.

At Livermore the Astron Group[50] has also tried injection into neutral H_2 at 0.1 Torr. E-layers with $\zeta \simeq 0.4$ and lifetimes of $\sim$1msec have been obtained by a single pulse of a 6MeV, 650A, 340nsec beam. A toroidal $B_\theta \lesssim B_z \sim 500$g is found to increase the beam trapping efficiency to 50% and circulating currents in excess of 13kA are recorded. Both at Cornell and Livermore the precessional instability of these layers is stabilized by the B_θ field.

These results are very encouraging for the concept of relativistic electron coils. Yoshikawa[51] has suggested the Astron-Spherator in which $B_\theta >> B_z$ and the beam is inforce-free equilibrium to minimize the synchrotron radiation losses that appear to doom the Astron concept using E-layers.

When the toroidal current of an axi-symmetric toroidal system is supplied by an injected E-beam (or runaway electrons)[51a] the equilibrium differs from the usual MHD calculation only by the effect of the centrifugal forces on the beam. The center of a beam propagating in a cold plasma is shifted outward by an amount δ_B which is[47]

$$\delta_B = \delta_{MHD} + \frac{r_c^2}{R} \frac{I_0(\xi)}{I_1(\xi)} \qquad (15)$$

where δ_{MHD} is the expression given by Shafranov,[52] R, r_c are the major and minor radii of the conducting vessel, r_p is the plasma radius, I_0 and I_1 are Bessel functions and $\xi = r_p \omega_b / \gamma^{\frac{1}{2}} c$. These calculations have been extended to a beam propagating in a plasma with finite pressure.[53]

The stability of the Kruskal-Shafranov mode for such a beam-plasma system has been computed by Lee[54] for a pressureless plasma and a cold beam. The maximum rotational transform consistent with stability is

$$\iota_{max}/2\pi = 1 + r_L/R$$

where $r_L = mc^2\gamma\beta_z/eB_z$, $\beta_z = V_B/c$. This indicates a slight improvement in stability when the E-beam carries the toroidal current.

ELECTROMAGNETIC AND MHD INSTABILITIES. Because of the short duration of the E-beam pulses many MHD instabilities e.g. the firehose, do not occur or they are easily suppressed by a guide magnetic field. Instabilities that do not involve significant motion of the ions however could occur. For a magnetically neutralized beam there is the possibility of Weibel-type instabilities.[3] A perturbation in density which is constant along the beam creates an uncompensated current since the change in plasma current is small. Electrostatic neutralization is maintained by the high density of the background plasma. This mode again is stabilized by a guide magnetic field. A quadratic form for the perturbation frequency ω is easily obtained in the limit of cold beam and plasma,[55]

$$\omega^2 = \frac{\Omega^2}{\gamma^2} - \frac{\omega_{bo}^2}{\gamma}\frac{\int_o^b drr(n_b(r)/n_{bo})(B_\theta^2+B_r^2)}{\int_o^b rdr(B_\theta^2+B_r^2(1+r^2/\ell^2\lambda_E^2))} \qquad (16)$$

where $\Omega = eB_o/mc$, ω_{bo} is the beam plasma frequency on axis, B_r and B_θ are field components of the perturbation $\lambda_E = c/\omega_e$ and ℓ is the aximuthal mode number. Since the typical size of the filamentation is of order λ_E a transverse spread in the beam momentum of order $\Delta p_\perp \gtrsim m(n_b/n_p)^{\frac{1}{2}}\gamma c$ will stabilize this mode.

Hollow annular beams of high current density, propagating in an ionized medium have been observed to break up into non-rotating flutes, but the scale lengths are much greater than λ_E.[56] A clear explanation for this destruction does not exist at present. There is obviously need for more theoretical work in this area.

Finally, I would like to add that it is timely now to take an interest in the generation of high intensity ion beams as these could have many uses both foreseen and unforeseen. By suitable modifications of E-beam technology viz, the suppression of the electron current by strong transverse magnetic fields and the creation of ion-emitting surface plasmas at the anode by powerful lasers,[57] it might prove feasible to create ion beams in the 10^5A range.

I would like to acknowledge many helpful discussions on the subject matter of this paper with L. Thode, R. Lovelace, P. Korn, C. Wharton, E. Ott, H. Fleischmann, B. Kusse, J. Nation, G. Goldenbaum, C. Kapetanakos, M. Lampe, D. Hammer, C. Striffler, R. Shanny, L. Levine, A. Robson, D. Mosher, I. Vitkovitsky, A. Toepfer, G. Yonas and C. Stallings.

*Work supported by the Office of Naval Research Contract No. N00014-67-A-0077-0025 and the U. S. Atomic Energy Commission Contract No. AT-11-1-3170MOD3.

REFERENCES.

1. F. Winterberg, Phys. Rev. 174, 212 (1968).
2. M. Babykin, E. K. Zavoiskii, A. A. Ivanov and L. I. Rudakov, Proceedings of the Fourth International Conference on Plasma Physics and Controlled Thermonuclear Fusion Research, Madison, Wisconsin, 1971 (International Atomic Energy Agency, Vienna (1972), Vol. 1, p. 635).
3. A. A. Ivanov and L. I. Rudakov, Zh. Eksp. Teor. Fiz. 58, 1332 (1970)[Sov. Phys.-JETP 31, 715 (1970)].
4. Ya. B. Fainberg, V. D. Shapiro and V. I. Shevchenko, Zh. Eksp. Teor. Fiz. 57, 966 (1969)[Sov. Phys.-JETP 30, 528 (1970)].
5. R. V. Lovelace and R. N. Sudan, Phys. Rev. Lett. 27, 1256 (1971).
6. L. I. Rudakov, Zh. Eksp. Teor. Fiz. 59, 2091 (1970)[Sov. Phys.-JETP 32, 1134 (1971)].
7. A. T. Altyntsev, B. N. Breizman, A. G. Eskov, O. A. Zolotovsky, V. I. Koroteev, R. K. Kurtmullaev, V. L. Masalov, D. D. Ryutov and V. N. Semenov, Pis'ma Zh. Eksp. Teor. Fiz. 13, 197 (1971); JETP Lett. 13, 139 (1971), and in Proceedings of the Fourth International Conference on Plasma Physics and Controlled Thermonuclear Fusion Research, Madison, Wisconsin, 1971 (International Atomic Energy Agency, Vienna (1972), Vol. 2, p. 309); V. S. Koydan et. al., Proc. Fifth European Conf. on Controlled Fusion and Plasma Phys., 1972 Vol. 1, p. 161.
8. J. Guillory and G. Benford, Plasma Phys. 14, 1131 (1972).
9. C. Stallings, S. Shope and J. Guillory, Phys. Rev. Lett. 28, 653 (1972).
10. L. E. Thode and R. N. Sudan, Phys. Rev. Lett. 30, 732 (1973).
11. A. Toepfer and J. Poukey, Phys. Lett. 42A, 383 (1973).
12. C. A. Kapetanakos and D. A. Hammer, Appl. Phys. Lett. 23, 17 (1973).
13. P. Miller and G. Kuswa, Phys. Rev. Lett. 30, 958 (1973).
14. G. C. Goldenbaum, J. Burton, R. Dixon, W. Dove, K. Gerber, W. Lupton, M. Young, Bull. Amer. Phys. Soc. 17, 1031 (1972); W. F. Dove, K. A. Gerber, G. C. Goldenbaum, D. A. Hammer, C. A. Kapetanakos and B. G. Logan, see these Proceedings.
15. C. Stallings, J. Benford and R. Schneider, Bull. Amer. Phys. Soc. 17, 1031 (1972).
16. P. Korn, F. Sandel and C. B. Wharton (to be published). See also these Proceedings.
17. S. D. Putnam and C. H. Stallings, Proceedings of Second Topical Conference on Pulsed High-Beta Plasmas, p. 245 (1972).
18. M. L. Andrews, H. Davitian, H. H. Fleischmann, R. E. Kribel, B. R. Kusse, J. A. Nation, R. Lee, R. V. Lovelace and R. N. Sudan, Proceedings of the Fourth Conference on Plasma Physics and Controlled Thermonuclear Fusion Research, Madison, Wisconsin, 1971 (International Atomic Energy Agency, Vienna, (1972), Vol. 1, p. 169).
19. W. C. Condit and D. Pellinnen, Phys. Rev. Lett. 29, 263 (1972).
20. L. P. Bradley and G. W. Kuswa, Phys. Rev. Lett. 29, 1441 (1972).
21. G. Yonas, K. R. Prestwich, J. W. Poukey and J. R. Freeman, Phys. Rev. Lett. 30, 164 (1973).
22. I. M. Vitkovitsky, L. S. Levine, D. Mosher and S. J. Stephanakis, Appl. Phys. Lett. 23, 9 (1973); D. Mosher, L. S. Levine, S. J. Stephanakis, I. M. Vitkovitsky and F. Young, see also these Proceedings.
23. B. Breizman and D. Ryutov, Zh. Eksp. Teor. Fiz. 60, 408 (1971)[Sov. Phys.-JETP 33, 220 (1971)].
24. S. A. Bludman, K. M. Watson and M. N. Rosenbluth, Phys. Fluids 5, 747 (1960).
25. V. N. Tsytovich, Nonlinear Effects in Plasma (Plenum Press, New York, 1970).
26. K. Nishikawa, J. Phys. Soc. Japan 24, 916, 1152 (1968).

27. P. Kaw and J. Dawson, Phys. Fluids 12, 2586 (1969).

28. J. Sanmartin, Phys. Fluids 13, 1533 (1970).

29. W. Kruer and J. Dawson, Phys. Rev. Lett. 25, 1174 (1970); Phys. Fluids 15, 446 (1972).

30. J. S. deGroot and J. I. Katz, Phys. Fluids 16, 401 (1973).

31. N. G. Matsiborko, I. N. Onishchenko, V. D. Shapiro and V. I. Shevchenko, Plasma Phys. 14, 591 (1972).

32. T. M. O'Neil, J. H. Winfrey and J. H. Malmberg, Phys. Fluids 14, 1204 (1971).

33. R. I. Kovtun and A. A. Rukhadze, Sov. Phys.-JETP 31, 915 (1970).

34. H. Alfven, Phys. Rev. 55, 425 (1939); J. D. Lawson, J. Electron. Control 3, 587 (1957), and 5, 146 (1958).

35. T. G. Roberts and W. H. Bennet, Plasma Phys. 10, 381 (1968).

36. D. A. Hammer and N. Rostoker, Phys. Fluids 13, 1831 (1970).

37. S. Putnam, Physics International Co. Report No. PIFR-105 (1970) (unpublished).

38. R. Lee and R. N. Sudan, Phys. Fluids 14, 1213 (1971).

39. R. Z. Sagdeev, Proceedings of Symposia in Applied Mathematics, edited by H. Grad (American Mathematical Society, Providence, R.I., 1967), Vol. 18, p. 18.

40. S. Yoshikawa, "Consideration of Power Requirement in Fusion Feasibility Experiment", Report No. MATT-803, Princeton Plasma Physics Laboratory, Princeton University, June, 1971.

41. G. Meixel, B. Kusse and D. Brower, Bull. Amer. Phys. Soc. 17, 1006 (1972).

42. Physics Today, Vol. 26, p. 17, April, 1973.

43. J. M. Dawson, A. Hertzberg, R. E. Kidder, G. C. Vlasses, H. G. Ahlstrom, and L. C. Steinhauer, Proceedings of the Fourth International Conference on Plasma Physics and Controlled Thermonuclear Fusion Research, Madison, Wisconsin, 1971 (International Atomic Energy Agency, Vienna (1972), Vol. 1, p. 673).

44. T. K. Allen, K. Doble, T. J. L. Jones, R. M. Payne and I. J. Spalding, Phys. Fluids 9, 1394 (1966).

45. I. J. Spalding, M. J. Eden, A. D. R.Phelps and T. K. Allen, Proceedings of the Third International Conference on Plasma Physics and Controlled Nuclear Fusion Research, 1968 (International Atomic Energy Agency, Vienna, 1969, Vol. II, p. 639).

46. J. J. Bzura, T. J. Fessenden, H. H. Fleischmann, D. A. Phelps, A. C. Smith, Jr., and D. M. Woodall, Phys. Rev. Lett. 29, 256 (1972).

47. E. Ott and R. N. Sudan, Phys. Fluids 14, 1226 (1971).

47a. D.Phelps,A.Smith and H.Fleischmann,Bull. Amer. Phys. Soc. 17, 999 (1972).

48. S. Humphries, "Diffusion Theory of Strong, Stable E-Layers", Laboratory of Plasma Studies, Cornell University, Ithaca, New York, Report NO. LPS 117.

49. H. H. Fleischmann, private communication.

50. R. J. Briggs, G. D. Porter, B. W. Stallard, J. Taska and P. B. Weiss, "Efficient Trapping of High-Level E-Layers in a Strong Toroidal Field", Lawrence Livermore Laboratory, Livermore, California, Report NO. UCRL-74673.

51. S. Yoshikawa and N. C. Christofilos, Paper CN-28/F-1, Proceedings of the Fourth International Conference on Plasma Physics and Controlled Thermonuclear Fusion Research, Madison, Wisconsin, 1971 (International Atomic Energy Agency, Vienna (1972), Vol. 2, p. 357).

51a. D. Spong,J. Clarke,J. Rowe,"Rel. Elect. Prod. in the Ormak". Oak Ridge Nat.Lab.ORNL-TM4120

52. V. D. Shfranov, in Reviews of Plasma Physics, edited by M. A. Leontovich (Consultants Bureau, New York, 1966), Vol. 2, p. 103.

53. A. Mandelli and E. Ott, "Straight and Toroidal Plasma Equilibria with an Intense Relativistic Electron Current Component", Laboratory of Plasma Studies, Cornell University, Ithaca, New York, Report NO. LPS 118.

RUN#	γ_o	n_b/n_e	S	W	K	T_e
R3	2	0.050	0.435	0.0685	0.25	1.5keV
R4	2	0.110	0.555	0.0615	0.26	0.1eV
R5	4	0.001	0.296	0.0460	-	0.1eV
R6A	4	0.001	0.296	0.0830	0.30	1.5keV
R6	4	0.001	0.296	0.0485	-	0.1eV
R7	4	0.010	0.617	0.0910	0.26	0.1eV
R8	4	0.010	0.617	0.0845	0.28	1.5keV
R9	4	0.050	1.150	0.0650	0.26	1.5keV
R10A	8	0.001	0.6	0.1250	0.35	1.5keV
R10	8	0.010	1.310	0.0720	0.30	1.5keV
R11	8	0.050	2.320	0.0515	0.27	1.5keV

TABLE I. Columns 2 and 3 give the basic parameters, column 4 the strength parameter $S \equiv \beta_o^2 \gamma_o (n_b/2n_e)^{1/3}$, $W \equiv |E_o|^2/16\pi n_b mc^2$ is given in column 5. The fraction of initial-beam kinetic energy gained by the plasma electrons after the second stage is denoted by K. The initial plasma electron temperature is T_e. In all runs, except R_5, which had a mass of 500, the ratio was 2000. There were a total of 40,000 particles: 20,000 ions, 18,000 electrons, and 2000 beam electrons.

FIGURE 1. Time evolution of the electrostatic wave energy and ion density fluctuation.

FIGURE 2. Measured and computed growth rates for the oscillating two stream instability for R_9.

FIGURE 3. Wave spectrum at $\omega_e t = 900$; L is the length of system.

54. E. P. Lee, "Hydromagnetic Kink Mode of a Relativistic Beam", Lawrence Livermore Laboratory, Livermore, California, Report NO. UCRL-74026.

55. R. N. Sudan, Bull. Amer. Phys. Soc. 18, 585 (1973).

56. C. A. Kapetanakos, D. A. Hammer, C. D. Striffler and R. C. Davidson, Phys. Rev. Lett. 30, 1303 (1973).

57. R. N. Sudan and R. V. Lovelace, "Generation of Intense Ion Beams by Pulsed Diodes", Laboratory of Plasma Studies, Cornell University, Ithaca, New York, Report NO. LPS 128.

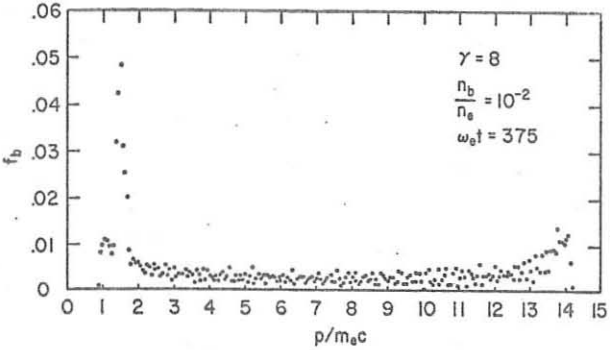

FIGURE 4a. Beam momentum distribution at wave saturation.

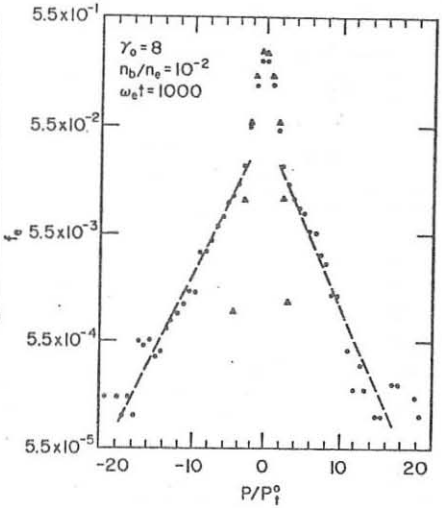

FIGURE 4b. Plasma electron distribution; ▲ shows initial distribution with spread $\equiv P_t^o$; • show distribution at $\omega_e t = 1000$ (end of 2nd stage).

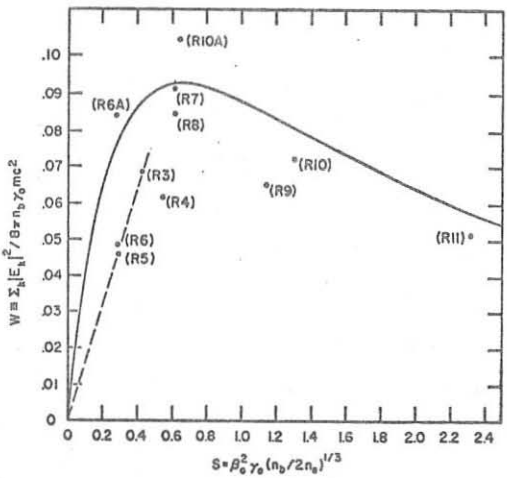

FIGURE 5. W as a function of S; dashed line quasilinear result; solid line is Eq. (2).

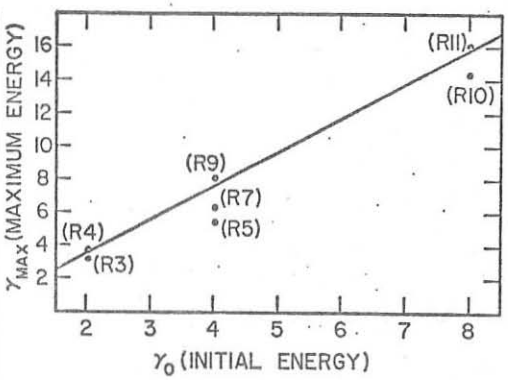

FIGURE 6. Maximum electron energy γ_{max} at wave saturation as a function of initial energy γ_o; solid line is Eq. (4).

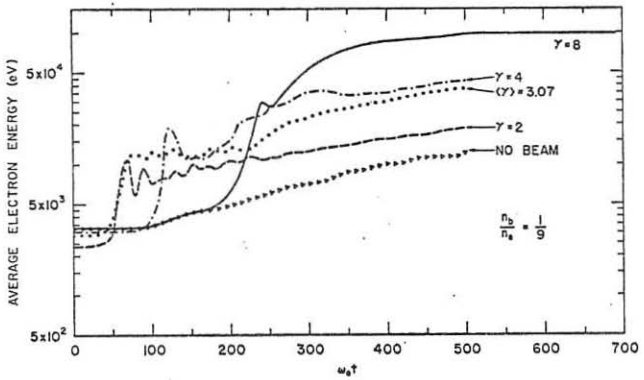

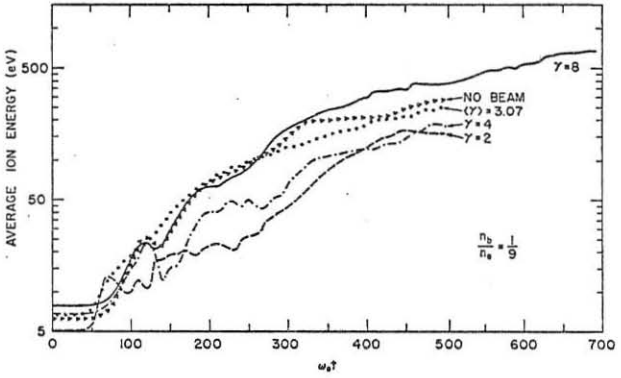

FIGURES 7 and 8. Electron and Ion heating as a function of time for different cases with return current.

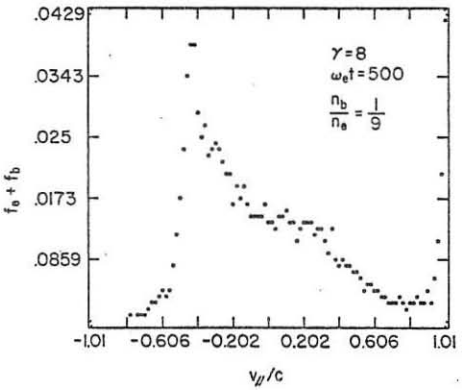

FIGURE 9. Plasma electron f_e and beam f_b distribution at $\omega_e t = 500$ with return current.

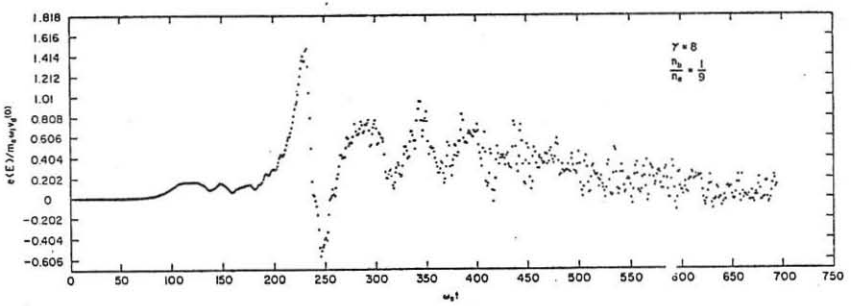

FIGURE 10. <E> as a function of time. The mean value of <E> at $\omega_e t = 650$ corresponds to $\nu^* \approx 0.2\ \omega_i$.

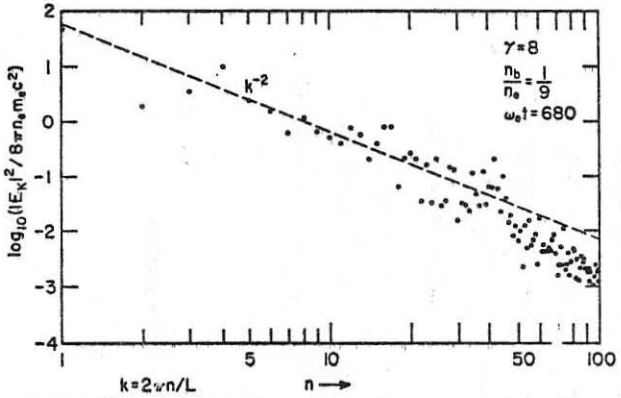

FIGURE 11. Wave spectrum for return current heating at $\omega_e t \approx 680$.

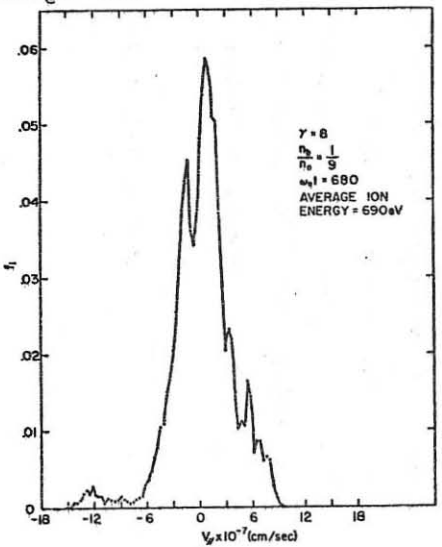

FIGURE 12. Ion distribution for return current heating at $\omega_e t = 680$.

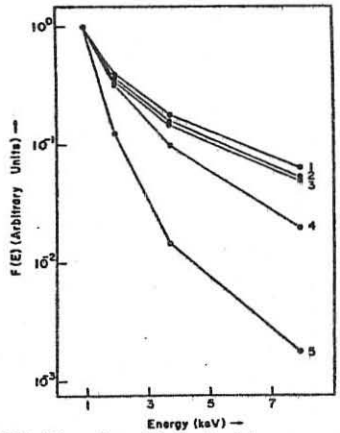

FIGURE 13. Ion distribution measured experimentally by P. Korn, F. Sandel and C. B. Wharton [16]. Curves 1-5 have total perpendicular plasma energy equal to 82,74,40,30 and 13 joules respectively as measured by a diamagnetic loop.

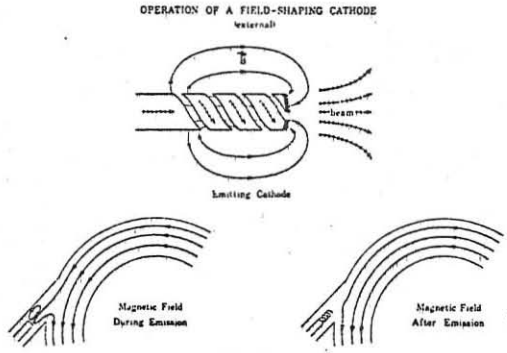

FIGURE 14. Schematic of E-beam injection system of Brower, Kusse and Meixel [41].

PULSED FUSION OF PELLETS USING ELECTRON BEAMS OR LASERS*

E. H. Beckner, J. R. Freeman, J. B. Gerardo,
E. D. Jones, A. J. Toepfer, and G. Yonas

Sandia Laboratories, Albuquerque, New Mexico 87115

Abstract

This paper is concerned with assessing the physical and technological concepts and barriers which are important for pulsed fusion of pellets using relativistic electron beams or lasers. We discuss recent numerical calculations of pellet dynamics for the two cases in order to illustrate the similarities that exist and to indicate the significant differences which can be utilized in the spatial and temporal scale of the implosions. These calculations specify the experimental parameter regime which must be achieved, with input energy ranging as low as a few hundred kilojoules in the case of electron beams and a few kilojoules in the case of lasers; power densities in the two cases tend to be comparable. An assessment of current technology, including some new results for electron beam pumped lasers, is then made for comparison. Finally, we present our assessment of the remaining physical problems and the solutions required for achievement of fusion break-even experiments.

*This work was supported by the U. S. Atomic Energy Commission.

I. Introduction

The concept of producing a thermonuclear plasma by imploding a solid pellet with either lasers or electron beams has by now been well documented.[1-8] It is the purpose of this paper to assess these approaches at this point in time, particularly from the view of the present level of understanding in theory, the existence of laboratory capabilities to test the concepts in the near or foreseeable future, and the existence of concepts which may be scaled to fusion reactors.

The essential laser fusion concept is best illustrated by the multibeam laser irradiation facility of Basov, et al[8], and by the predicted behavior of laser-imploded-spheres presented by Clarke, et al[2]. In the case of pulsed fusion with electron beams, the most recent ideas and results were presented by Babykin, et al[6], and by Yonas, et al[7]. It is now clear that the previous concerns regarding focusing of electron beams to dimensions appropriate for pellet fusion were overly pessimistic, and that the ready availability of large pulsed accelerators will motivate experimenters to attempt pellet fusion experiments with electron beams in the near future. We see then that, whereas the fundamental ideas are better developed in the case of laser fusion and the experiments -- though small -- can probably be better understood, the existence of laboratory facilities to do electron beam fusion at levels of 10's to 1000's of kilojoules makes it difficult to predict which approach may be most successful. This is particularly true since so very much of what we think we now know about laser fusion has been developed only

after an experimental result was obtained; we have to assume that the significant new focusing results for electron beams[7, 9-11] is a prelude of similar things to come as beam deposition and pellet experiments are attempted.

II. Energy Absorption Processes

The subject of absorption of high-intensity laser energy by plasmas has received an enormous amount of attention recently.[5, 12-23] This is not surprising since it is quite complicated for any laser-plasma heating scheme; furthermore, in the case of laser fusion, the pellet implosion dynamics are inextricably interconnected with the absorption processes, particularly those which give rise to substantial quantities of reflected laser light and/or production of nontrivial quantities of energetic electrons. We now know from theory[12-14] and experiment[15, 17-21] that laser intensities comparable to those required for efficient pellet compression give rise to anomalous reflected light intensities (probably Brillouin scattered), to copious quantities of anomalously hard X-rays (evidence of non-Maxwellian electron distributions), and quite possibly to neutron production via processes which have nothing to do with the thermal temperature of the ions.[24] Although these developments certainly make successful pellet implosions more difficult, the problem as a whole still appears to be surmountable. These developments do make it clear that intelligent pellet design and laser pulse shaping will be important; however, the rapidity with which theory (particularly computational physics) is being successfully applied to experimental findings makes the expectations quite bright for successful results.

Now, turning to implosion of pellets with electron beams, we simultaneously find much in common with laser fusion, as well as several new features. The details of the material presented here are contained in the papers presented at Erice, Sicily,[6] and at this conference by Yonas, et al[25]. They can be summarized as follows: (1) advances in beam focusing during the past year, as illustrated in Figs 1-3, now make these pellet fusion concepts a realistic fusion concept; (2) focusing of relativistic beams in plasma filled diodes is the most important new beam focusing development, as illustrated in Fig 3; (3) collective effects may be important in the energy absorption processes; (4) the unneutralized self-field of the beam may play a vital role in focusing, deposition, symmetric compression, and possibly confinement. There are two particular aspects to this last statement. For highly focused beams, magnetic effects dominate over elastic scattering of laser electrons even in solid targets. This may be demonstrated by considering the quantity:

$$\frac{\bar{y}}{r_L} = \left(\frac{1}{\gamma\beta^3}\right)(a\, I_A/IL)^{\frac{1}{2}}.$$

This relates the r.m.s. divergence of the beam envelope due to scattering, $\bar{y}$, to the Larmor radius, r_L. In this equation γ and β are the usual relativistic symbols, a is the beam radius, I/IA is the ratio of beam current to Alfven critical current, and L is the characteristic scattering length in the material. For $\bar{y}/r_L \ll 1$ scattering will be less important than magnetic effects, and when magnetic effects dominate,

we can expect, for hydrogenous materials, that beam electron ranges will be significantly shorter than classical coulomb ranges. For example, a 3MV, 3 MA, 1 mm beam into solid D_2 yields $\bar{y}/r_L \simeq 0.03$. Hence, these effects may allow for decreased pellet sizes and result in "break-even experiment" projections at levels of 100 kJ - 1 MJ utilizing 10-20 nsec beams, rather than the 1-10 MJ required otherwise.[4-5]

III. Computational Studies of Pellet Implosion Phenomena

There now exists substantial literature on laser-driven implosions of spherical targets, culminating with the calculations of Clarke, et al[2], which predict net fusion gain from solid shells and spheres irradiated with as little as 2.2 kJ of precisely tailored laser light. More conservative ideas tend to suggest that 10-1000 kJ will be required for laser break-even experiments.[3,5,26] In any case, it is clear at this point in time that, in order to reduce the required input energy as much as possible, computer experiments are tending to specify an increasingly high level of sophistication for the proposed pellet implosions. Fig 4 illustrates this quite vividly by showing the dramatic change in fusion yield that results from small changes in input energy rate, $\dot{E}_o$. If larger quantities of laser energy can be supplied, then much of this sensitivity disappears; unfortunately, the real experimental capabilities for the near future do not indicate laser energies much in excess of 10 kJ (even from arrays of lasers), so we are required to examine seriously these theoretical predictions and prepare the laser pulses accordingly.

In the case of electron-beam-driven implosions, the increased energy available makes it possible to use less sophisticated concepts and procedures, though by no means trivial ones; furthermore, the question of high-quality beam focusing is much more pertinent to this problem. We will have to look in detail at the experimental problems associated with uniform irradiation and compression of a sphere later in this talk, but will defer that problem until then so as to maintain continuity. For now, we want to present some theoretical results of implosions of solid DT spheres irradiated by a high ν/γ electron beam possessing a rather specialized pulse shape. These results are shown in Table I. Calculations (a) and (b) use waveforms of $\dot{E} = \dot{E}_o (1 - t/\tau)^{-2}$, whereas case (c) is for a square wave input of 0.5 nsec duration.

TABLE I

COMPUTATIONAL RESULTS FOR SOLID DT SPHERES IRRADIATED BY TAILORED ELECTRON BEAM PULSES

	Diameter (cm)	Mass (mg)	Total E-Beam Energy (MJ)	Total Pulse Length (ns)	Peak Power (watts)	Fusion Energy Produced (MJ)
(a)	0.1	0.11	0.1	36	5×10^{14}	2.0
(b)	0.24	1.5	1.0	36	1.44×10^{15}	46.6
(c)	0.1	0.11	0.1	0.5	2×10^{14}	0.003

The importance of pulse shaping for these simple geometries is easily illustrated by comparing the density profiles near the time of maximum compression for shaped and uniform pulses. Fig 5 presents this comparison for (a) and (c), the 0.11 mg cases shown in Table I. Case (c) is an

identical sphere to case (a), but is driven by a 2 x 10^{14} watt pulse deposited uniformly in time for 0.5 nsec. The lower central density for the uniform deposition reduces the rate of thermonuclear energy production and reduces the alpha particle trapping efficiency such that the fusion energy produced decreases to about 3 kJ, compared to 2 MJ produced by the shaped pulse case. Since pulsed electron accelerators inherently tend to produce output pulses with power increasing with time, the calculations for cases (a) and (b) are not too unreasonable. Our choice of this particular waveform was influenced by the published results of Clarke, et al[2]. It now remains for us to perform similar calculations for shaped pulses more representative of "achievable" machine waveforms. Preliminary results to date indicate that judicious adjustment of all the variables available to us will produce "break-even" calculations with input energies substantially below 1 MJ.

These results for solid DT spheres are based on electron ranges strongly influenced by magnetic effects so that the nominal electron range is $\sim r_L$, and they assume carefully tailored and repeatable beam current profiles.

From calculations like those shown in Fig 5, we conclude that power densities $\sim 10^{14}$ - 10^{16} watts/cm^2 will be required for break-even experiments. The uncertainty in this number comes from the fact that our pellet designs have not yet been optimized and from the fact that we do not know the importance or consequences that may accompany the self-field effects of the beam as it is stopped in the target. We feel that the electron ranges will be considerably shorter than "classical

ranges" -- more nearly the Larmor radius of a beam electron -- but will have to wait for experimental verification of this.

IV. Review of Experimental Results and Capabilities

Since this paper is primarily devoted to electron beam approaches to pulsed fusion, we will comment mainly on recent observations of focusing of beams and heating of solid materials with beams to produce neutrons. A number of workers have reported production of DD neutrons in excess of 10^7 n/burst by irradiating deuterated polyethylene with tightly focused intense electron beams.[27-30] Both Stephanakis, et al[30], and McCann, et al[27], assert that they observed thermonuclear neutrons, although other authors are uncertain. If computer codes are applied to these cylindrical or slab geometries, one quickly concludes that beam electrons of "classical range" could not drive the material to sufficient temperature to yield DD neutrons. However, at least two other observations on focused beams are important here: Yonas, et al[10], report observations best described as magnetic confinement of blowoff plasma which could affect the hydrodynamics of the problem; Vitkovitsky, et al[31], report that a tightly focused beam interacting with a high density exploded-wire plasma can result in more than an order of magnitude reduction in energy of a substantial number of beam electrons. An additional observation regarding intense beams -- that of collective ion acceleration -- must necessarily be discussed when the subject of neutron production is treated. It is well established that intense

electron beams can be responsible for acceleration of nontrivial quantities of ions to energies comparable to, and even greater than, the beam electrons.[32,33] The conditions under which this occurs are often somewhat special, however, so it is not possible to make conclusive statements regarding the importance or nonimportance of collectively accelerated ions in the experiments in which neutrons have been observed. The subject is, in fact, more controversial than we have implied with Bradley and Kuswa[28] showing that accelerated ions were important to their experiments and Vitkovitsky, et al[31], stating that such a mechanism was not required to explain their results.

We stated previously that power densities of $10^{14\text{-}16}$ watts/cm^2 will probably be required for fusion experiments. Several researchers have already reported $> 10^{12}$ watts/cm^2 from present machines.[10,11,31] Hence, it appears that we may already be close to the required power density levels. It is much more difficult to be confident that uniform irradiations of mm-sized spheres can be accomplished. The ideas presented by Yonas, et al[25], earlier at this conference represent our best thoughts at this time. They depend heavily on a symmetrizing effect accompanying the electron beam by virtue of the large spread in angles of the incident high ν/γ beam electrons. As a result, the beam behaves as if it were a high-temperature electron gas rather than a parallel flux of particles, and the required symmetric irradiation appears possible. It seems unlikely that an array of electron accelerators can be made to irradiate simultaneously sectors of spheres, in a manner similar to that considered for laser fusion, primarily because of the inevitable problems associated

with return current from the pellet required to prevent electrostatic charging of the target.

We will not dwell on conventional laser approaches for laser fusion since they have been treated in other sessions at this conference. Though the multibeam irradiation approach is conceptually simple, it is proving to be difficult to implement at energy input levels desired for meaningful experiments. We are all aware of the advanced facility of Basov and co-workers[6], of the development of a 10 kJ multibeam Nd:glass laser irradiation capability at Lawrence Livermore Laboratory[34], and of the LASL CO_2 laser development program intended for a multikilojoule facility[35]. Our approach at Sandia has been to develop a four-beam Nd: glass laser irradiation facility for physics studies[36], as depicted in Fig 6. This facility is capable of providing up to 500 joules of laser energy delivered to a freely-falling solid sphere of CD_2 or LiD. Previous work obtained with a single-beam configuration was reported by Olsen, et al.[23] Experimental results from the four-beam facility will be reported later. Another aspect of our program centers on utilization of intense electron beams for excitation of high-pressure gas lasers for future applications to laser fusion. These experiments are represented by the work on the nitrogen laser of Patterson[37] shown in Figs 7 and 8, by the work of Gerardo and Johnson[38] on the Xe_2^* laser shown in Figs 9 and 10, and by some recent work by Gerber and Patterson[39] on HF. Even though the HF laser system possesses extremely high gain and, as such, appears inappropriate for application as a laser amplifier, the promise of unusually high energy output may compensate for these shortcomings. As we noted earlier, so long as only "kilojoules or less" of

laser energy are available, then the fuel pellets must be very small, the irradiations done meticulously, and the laser pulses highly tailored. However, Zharov, et al[40], recently reported efficiency of conversion of electron beam energy to HF laser energy of 150-180%. That experiment provided only millijoules of output from an atmospheric mixture of H_2 and F_2. Now, Gerber and Patterson[39] have produced in excess of 200 joules of HF laser energy at a power level of 4 G watts from a mixture of $SF_6 + C_2H_6$. The efficiency of conversion from beam energy (2 MV, 50 kA, 70 nsec) to HF laser light was ~ 10%. These results are shown in Fig 11. The electron beam for excitation was obtained from the Reba accelerator as in the Xe_2^* experiments of Gerardo and Johnson.[38] There are obvious difficulties associated with high-gain laser media like these, but if 10's or 100's of kilojoules of laser energy can be obtained in the near future, it seems inevitable that we can find a good way to apply it to the pellet fusion problem.

V. Required Solutions to Physics and Technology Problems

We now attempt to present our opinion of the important physics and technology problems remaining to be solved in the next few years of pellet fusion research. These results are shown in Table II. The ratings displayed of 0, 1, 2 refer to the degree to which we feel the problem is near solution: 0 = no progress as yet, 1 = some progress reported, 2 = considerable progress reported.

TABLE II

TECHNOLOGY PROBLEMS

	Lasers	Electron Beams
Energy	1	2
Power	2	2
Pulse Shaping	2	1
Focusing	2	1
Concept for Spherical Irradiation	2	1

PHYSICS PROBLEMS

	Lasers	Electron Beams
Input Energy Absorption	2	1
Pellet Designs	2	2
Focusing of Energy	2	2
Fusion Reactor Concept	2	1

The conclusions to be drawn from this are obvious. Lasers must be developed capable of delivering at least 10 kJ in a single nsec pulse in order to have any hope of demonstrating fusion break-even. Meanwhile, several laboratories are pursuing experiments to examine the basic physical principles of the problem. For a fusion reactor to become a reality, it will be necessary for megajoules of laser energy to be supplied, and that almost without question requires the discovery

of a new laser system. In the case of electron beam fusion, it is easier to predict ways of supplying the necessary energy than to be confident of a means of assembling compressed pellets with it. In this case, the most crucial work to be done is that of demonstrating the validity of these preliminary ideas on focusing, energy deposition, and spherical irradiation.

REFERENCES

1. L. Wood and J. Nuckolls, "Prospects for Unconventional Approaches to Controlled Fusion," AAAS Philadelphia Meeting, 1971 (unpublished); E. Teller, "Modern Internal Combustion Engines," VII Int'l. Quantum Electronics Conf., Montreal, 1972 (unpublished); J. Nuckolls, L. Wood, H. Theissen, and G. Zimmerman, Nature 239, 139 (1972).

2. J. S. Clarke, H. N. Fisher, and R. J. Mason, Phys. Rev. Letters 30, 89 (1973).

3. N. G. Basov and O. N. Krokhin, Vestnik Akademii Nauk USSR 40, #6, 55 (1970).

4. F. Winterberg, Phys. Rev. 174, 212 (1968) and Nuclear Fusion 12, 353 (1972).

5. F. Floux, Nuclear Fusion 11, 635 (1971).

6. M. V. Babykin, Y. K. Zavoisky, A. A. Ivanov, and L. I. Rudakov, Nuclear Fusion Suppl. 1972, 75 (1972).

7. G. Yonas, "Applications of High Intensity Relativistic Electron Beams to Pulsed Fusion and Collective Ion Acceleration," Sandia Laboratories Report 73-5470.

8. N. G. Basov, Y. S. Ivanov, O. N. Krokhin, Y. A. Mikkailov, G. V. Sklizhov, JETP Letters 15, 417 (1972).

9. D. L. Morrow, J. D. Phillips, R. M. Stringfield, W. O. Doggett, and W. H. Bennett, Appl. Phys. Letters 19, 441 (1971).

10. G. Yonas, K. R. Prestwich, J. W. Poukey, and J. R. Freeman, Phys. Rev. Letters 30, 196 (1973).

11. W. C. Condit, D. O. Trimble, G. A. Metzger, P. G. Pellinen, S. Heurlin, and P. Creely, Phys. Rev. Letters 30, 123 (1973).

12. P. Kaw, J. Dawson, W. Kruer, C. Oberman, and E. Valeo, Sov. J. Quant. Electr. 1, 205 (1971).

13. D. W. Forsland, J. M. Kindell, and E. L. Lindman, Phys. Rev. Letters 30, 739 (1973).

14. J. S. DeGroot and J. I. Katz, Phys. Fluids 16, 401 (1973).

15. J. L. Bobin, M. Decroisette, B. Meyer, and Y. Vitel, Phys. Rev. Letters 30, 594 (1973).

16. D. W. Forsland, J. M. Kindel, and E. L. Lindman, Los Alamos Scientific Laboratory Report LADC-72-285.

17. J. W. Shearer, S. W. Mead, J. Petruzzi, F. Rainer, J. E. Swain, and C. E. Violet, Phys. Rev. A6, 764 (1971).

18. S. W. Mead, R. E. Kidder, J. E. Swain, F. Rainer, and J. Petruzzi, Appl. Optics 11, 345 (1972).

19. R. Sigal, H. Hora, H. Boumhacker, K. Buchl, K. Eidmann, S. Witkowski, H. Mennicke, P. Mulser, D. Pfirsch, and H. Salzmann, Sov. J. Quant. Electr. 2, 117 (1972).

20. P. Mulser, R. Sigel, and S. Witkowski, Phys. Letters 6C, 189 (1973).

21. C. Yamanaka, T. Yamanaka, T. Sasaki, K. Yoshida, and M. Waki, Phys. Rev. A6, 2335 (1972).

22. C. Yamanaka, T. Yamanaka, H. Kang, T. Sasaki, K. Yoshida, K. Ueda, M. Hongyo, and M. Waki, Sov. J. Quant. Electr. 2, 127 (1972).

23. J. N. Olsen, G. W. Kuswa, and E. D. Jones, J. Appl. Phys. 44, 2275 (1973).

24. G. H. McCall, F. Young, A. W. Ehler, J. F. Kephart, and R. P. Godwin, Phys. Rev. Letters 30, 1116 (1973).

25. G. Yonas, J. W. Poukey, J. R. Freeman, K. R. Prestwich, A. J. Toepfer, M. J. Clauser, and E. H. Beckner, "High Current Density Electron Beam Application to Fusion Studies," presented earlier at this conference.

26. M. S. Chu, Phys. Fluids 15, 413 (1972).

27. T. E. McCann, C. W. Rogers, D. N. Payton, Bull. Am. Phys. Soc. II, 17, 690 (1972).

28. L. P. Bradley and G. W. Kuswa, Phys. Rev. Letters 29, 1441 (1972).

29. H. Sahlin, B. Freeman, J. Luce, and D. Zucker, Bull. Am. Phys. Soc. II, 17, 1030 (1972).

30. S. J. Stephanakis, L. S. Levine, D. Mosher, I. M. Vitkovitsky, and F. Young, Phys. Rev. Letters 29, 568 (1972).

31. I. M. Vitkovitsky, L. S. Levine, D. Mosher, and S. J. Stephanakis, Appl. Phys. Letters 23, 9 (1973).

32. S. E. Graybill and J. R. Uglum, J. Appl. Phys. 41, 236 (1970).

33. J. Rander, B. Ecker, G. Yonas, and D. J. Drickey, Phys. Rev. Letters 24, 283 (1970).

34. J. L. Emmett, "Review of Laser Devices for Fusion," IEEE/OSA Conference on Laser Engineering and Applications, 1973 (unpublished).

35. E. E. Stark, W. H. Reichelt, G. T. Schuppert, and T. F. Stratton, "Nanosecond Pulse Amplification in Very High Gain CO_2 Amplifier Systems," IEEE/OSA Conference on Laser Engineering and Applications, 1973 (unpublished).

36. E. D. Jones, "The Sandia Four-Beam Laser System," IEEE/OSA Conference on Laser Engineering and Applications, 1973 (unpublished).

37. E. L. Patterson, J. B. Gerardo, and A. W. Johnson, Appl. Phys. Letters 21, 293 (1972).

38. J. B. Gerardo and A. W. Johnson, J. Quant. Electr., accepted for publication, 1973.

39. R. A. Gerber and E. L. Patterson, private communication.

40. V. F. Zharov, V. K. Malinovskii, Yu. S. Neganov, and G. M. Chumak, JETP Letters 16, 154 (1972).

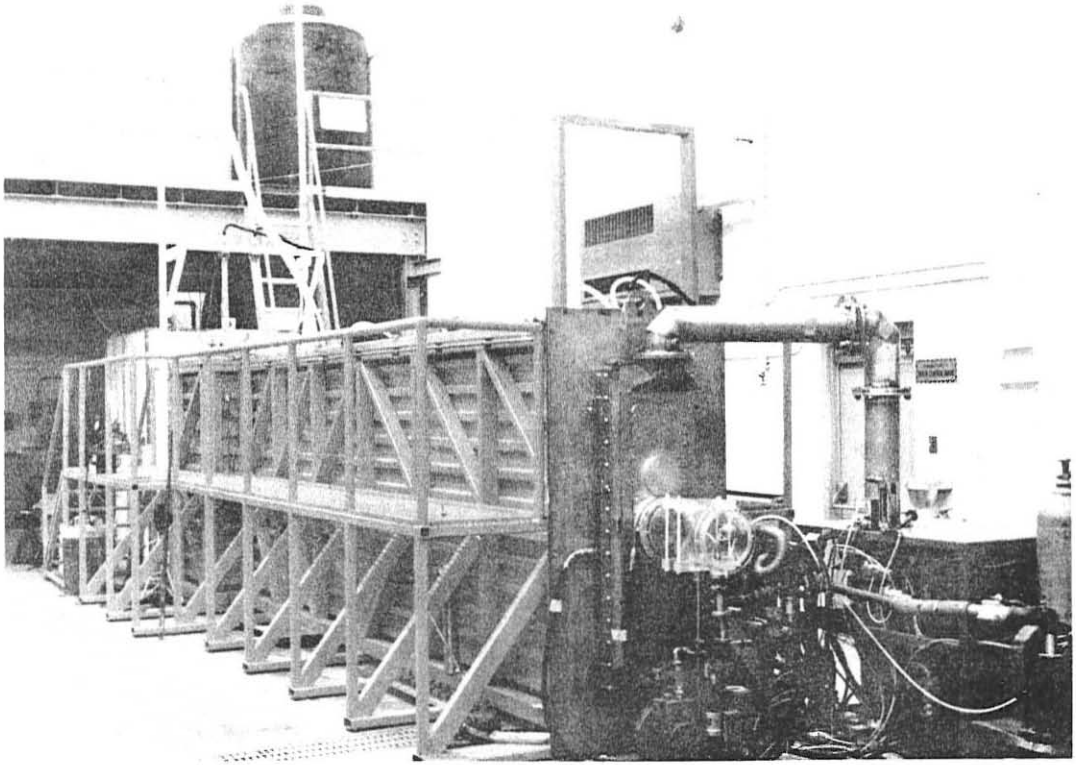

Fig 1 The Sandia SLIM accelerator used for numerous beam focusing studies. This accelerator consists of two sets of parallel-plate Blumlein lines, with mylar insulation, feeding a field emission diode. The nominal pulse output characteristics are: 300 kV, 250 kA, 100 nsec.

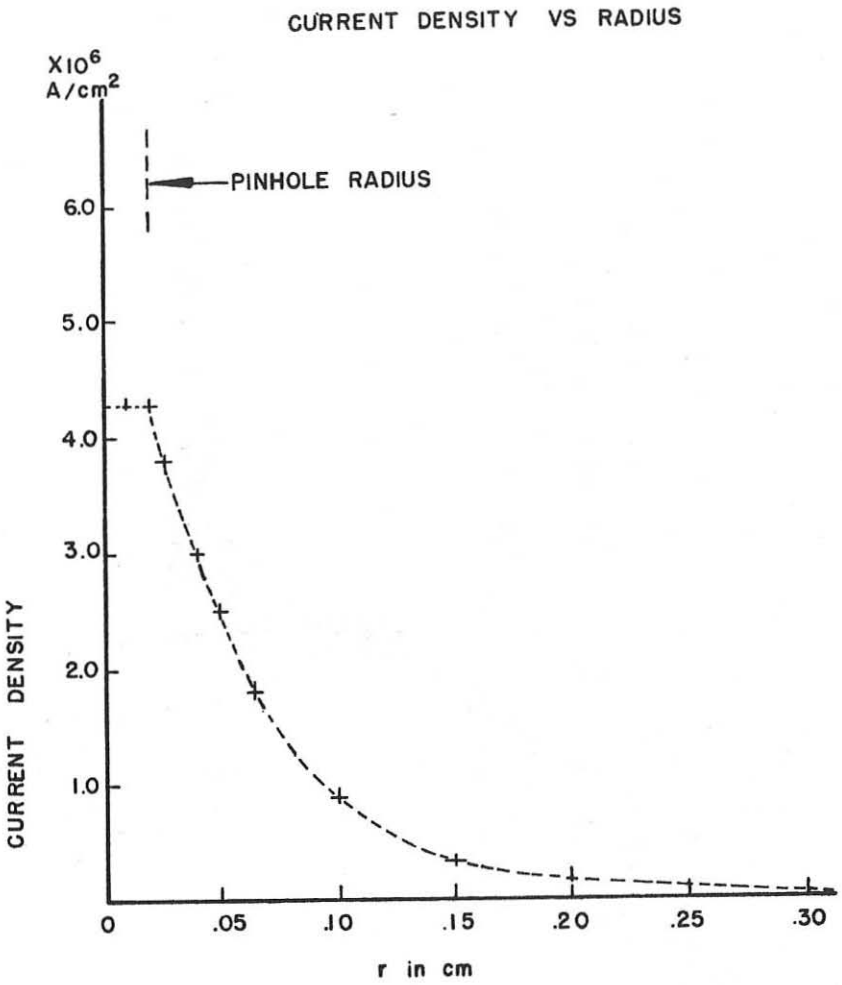

Fig 2 X-ray pinhole photograph showing the focused beam size obtained with a plasma filled diode (exploded wire plasma) on SLIM.

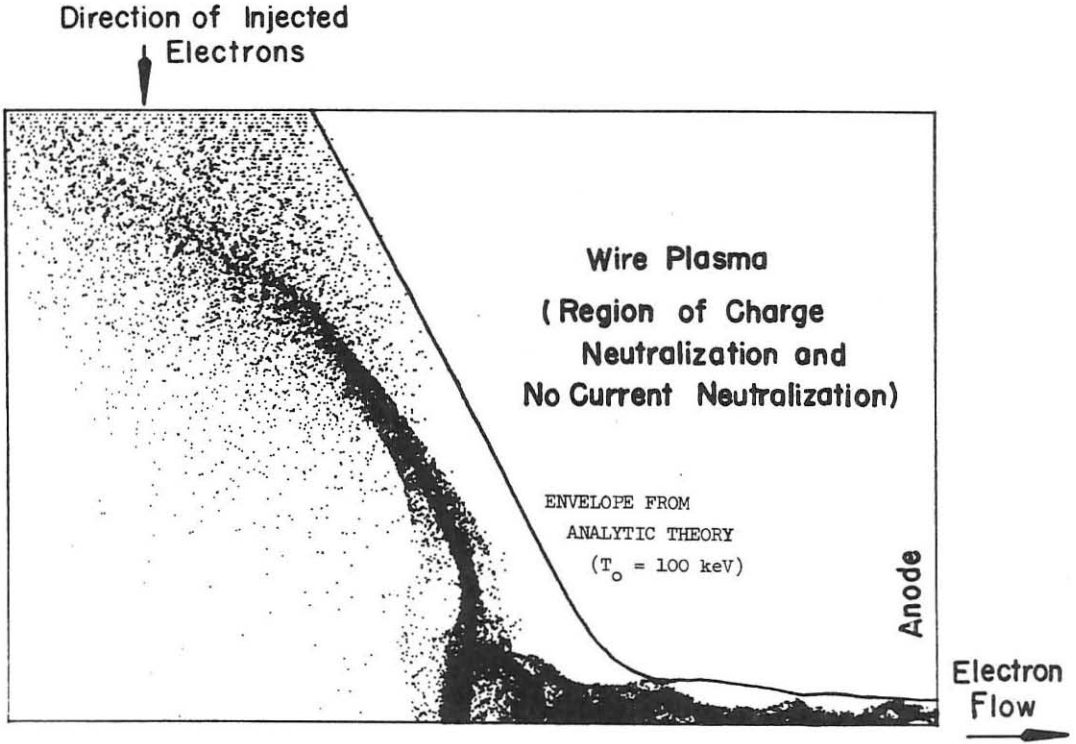

Fig 3 Theoretical results obtained in studies of beam focusing in plasma filled diodes. The figure shows only the central region of the diode (assumed in these calculations to be electrostatically neutral) with electrons entering from above, with large angular spread, and subsequently focused at the anode.

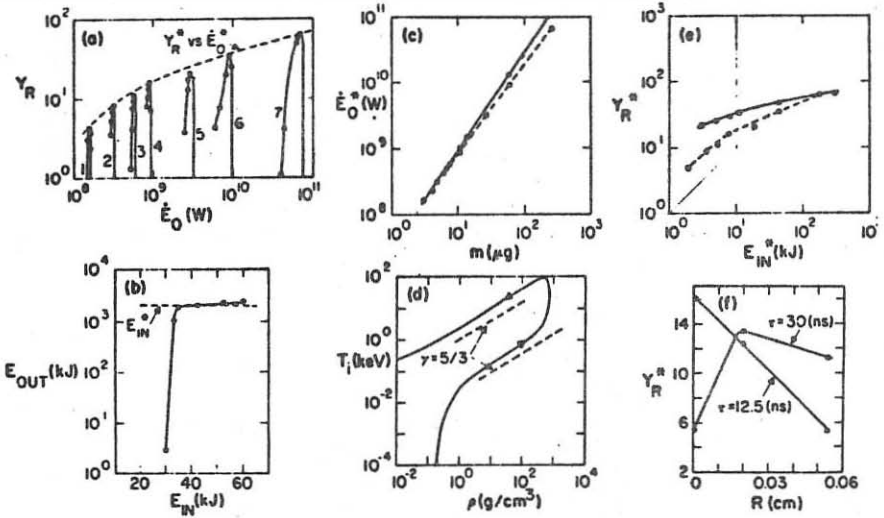

DT shell and sphere performance characteristics: (a) Y_R versus $\dot{E}_0$ for (1) 3-μg, 2.2-kJ, (2) 5-μg, 3.5-kJ, (3) 7.5-μg, 5.3-kJ, (4) 10.8-μg, 7.5-kJ, (5) 26-μg, 18.2-kJ, (6) 60-μg, 43-kJ, and (7) 250-μg, 178-kJ shells of initial inner radius $R = 3.4 \times 10^{-2}$ cm under profile (1) with $\tau_* = 30$ nsec and $p = 1.875$. (b) Input energy threshold, $\dot{E}_{in}^*$, determination. (c) Optimal $\dot{E}_0$ versus mass: solid line, for spheres ($\tau = 20$ nsec, $p = 2$); dashed curve, for the shells of (a). (d) 6-μg core trajectory, T_i versus ρ, for a 60-μg sphere during its implosion, thermonuclear burn, and expansion. (e) Optimal yield ratios versus input energy: solid curves, for the shells [in (a)]; dashed curves, for spheres. (f) Y_R^* versus inner radius for 7.5-μg shells imploded with the optimized (1) profile for $\tau = 30$ and 12.5 nsec.

Fig 4 Published results of Clarke, et al[2] showing the extreme sensitivity of these pellet compressions to input power $\dot{E}_0$.

DENSITY PROFILES NEAR PEAK COMPRESSION

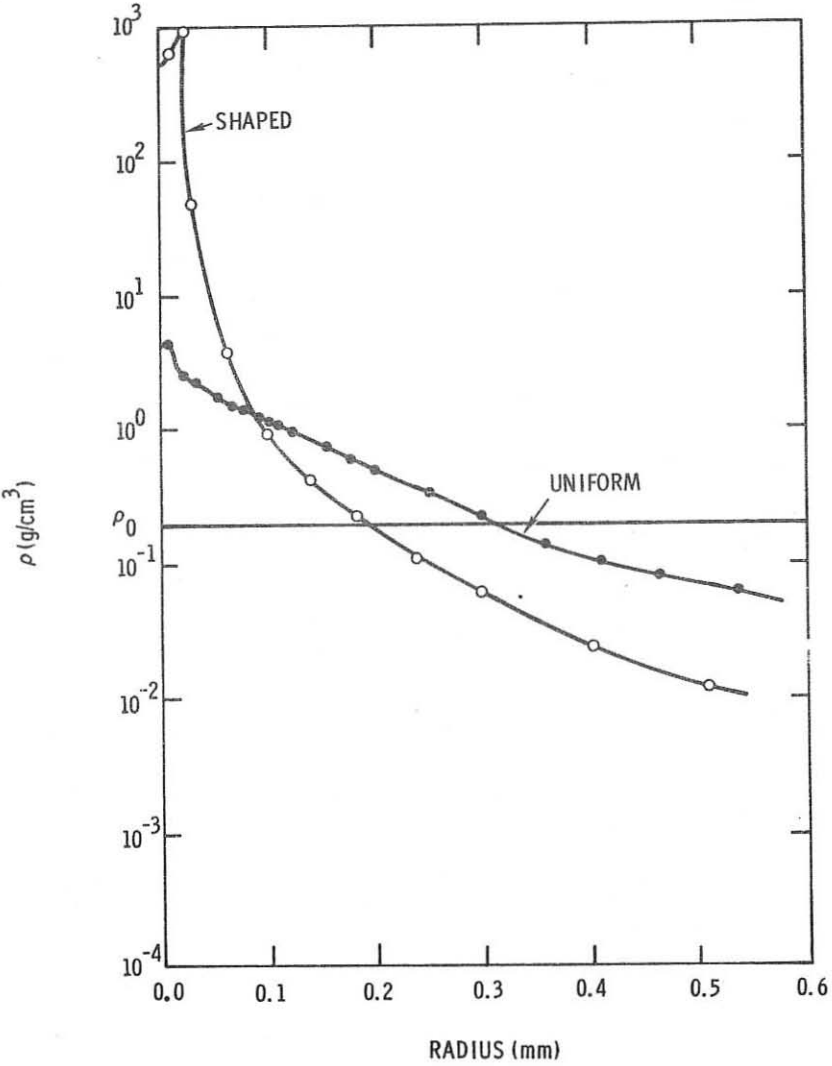

Fig 5 Plasma parameters of a solid DT pellet compressed by input electron beams of: (1) uniform square wave input of 1 megajoule input in 0.5 nsec; and (2) 1 megajoule input in 36 nsec with the waveform $\dot{E} = \dot{E}_o (1 - t/\tau)^{-2}$. These cases (a and c) are detailed in Table I. The fusion yield for (1) was $\sim$ 0.01 and for (2) was $\sim$ 50.

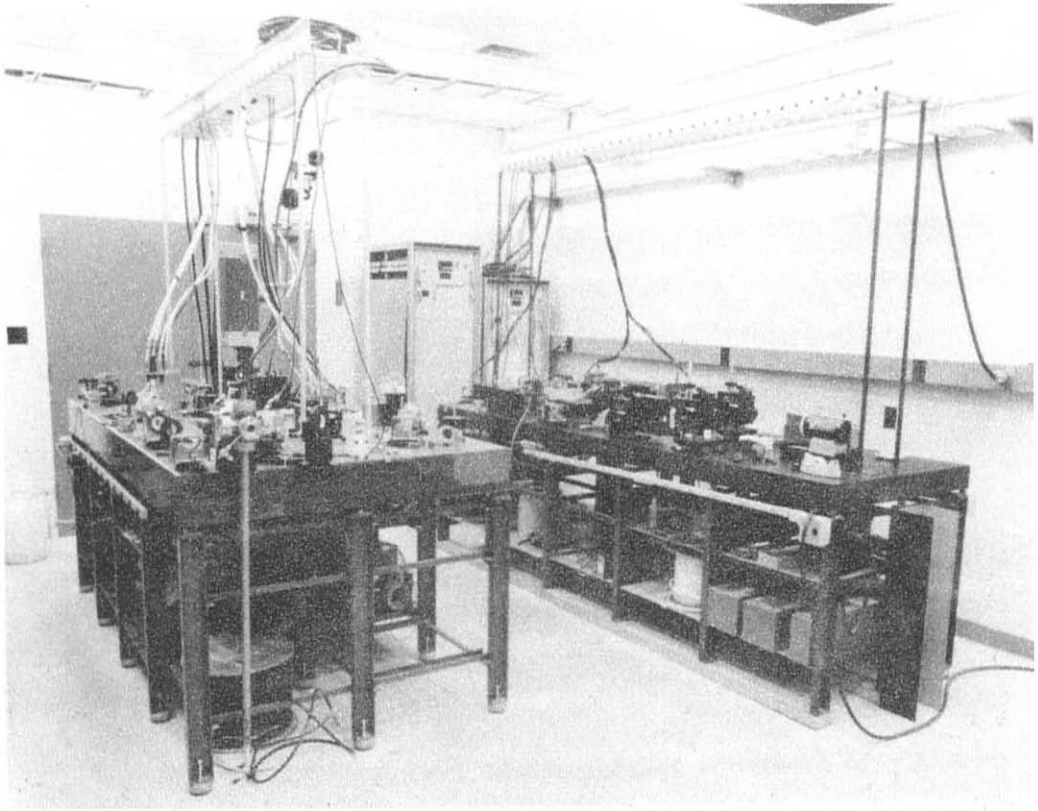

Fig 6 Photograph of the YAG mode-locked oscillator table and the first two glass amplifiers.

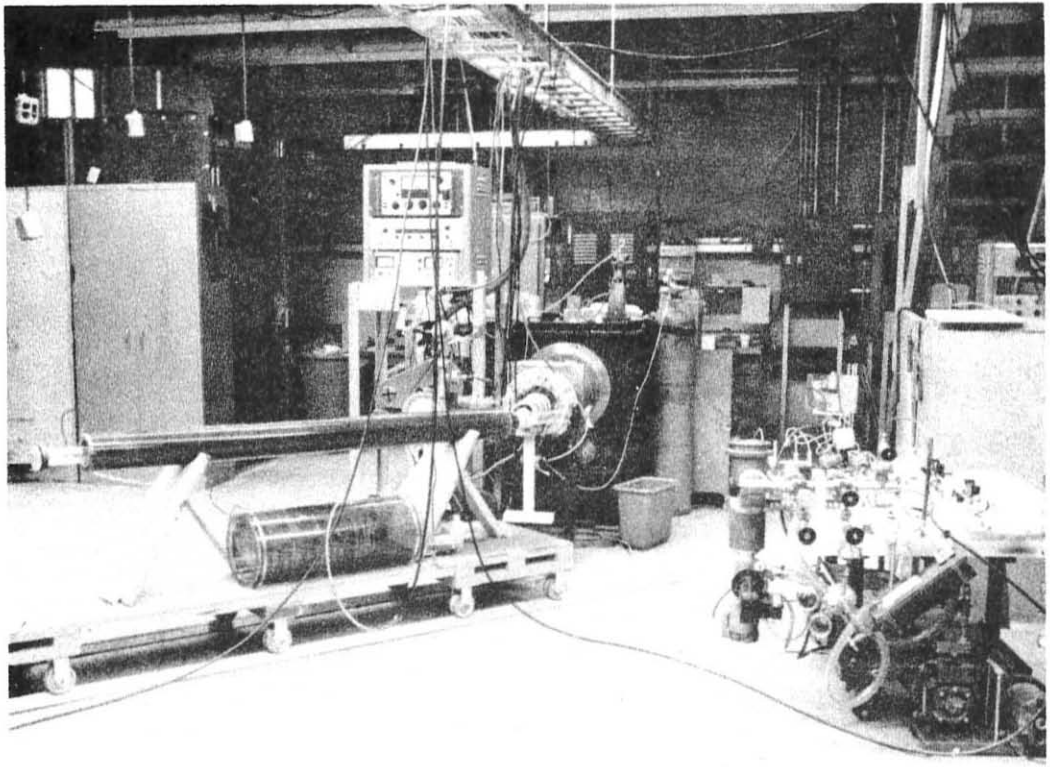

Fig 7 The Nereus electron accelerator and N_2 laser excitation apparatus. This water coax-line accelerator provides an output beam pulse of 350 kV, 50 kA, 50 nsec.

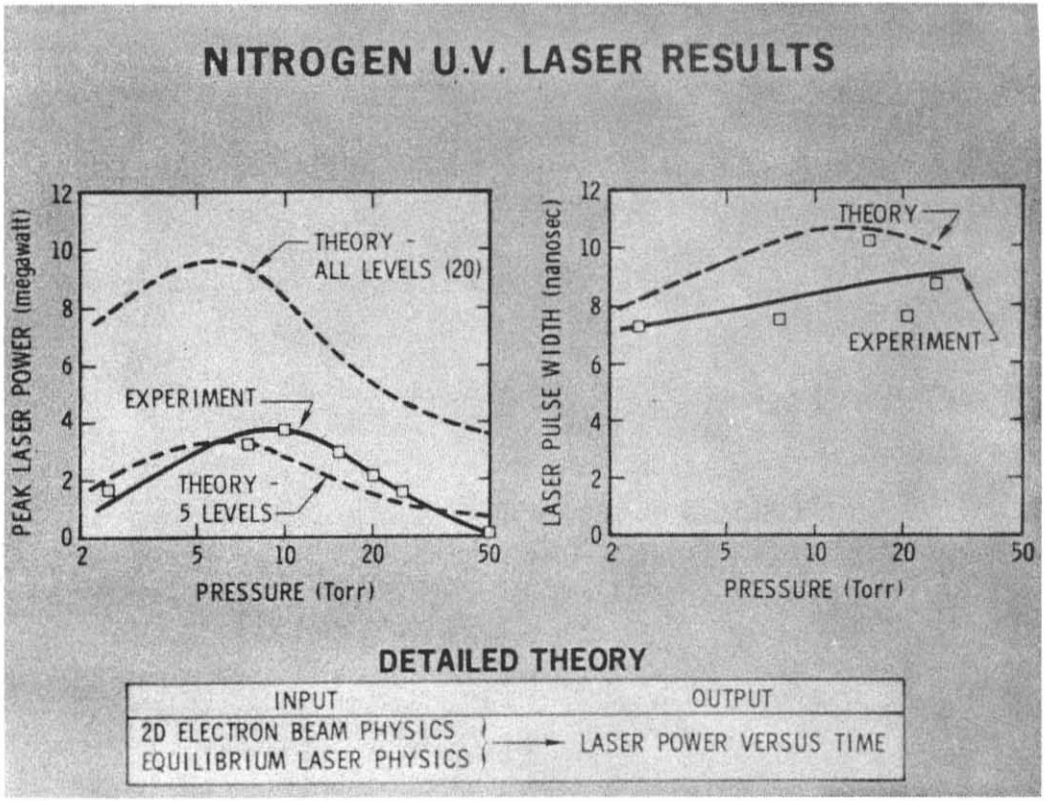

Fig 8 Experimental and theoretical results of the electron beam-excited N_2 laser.[37] These observations were for the molecular transitions $C^3\Pi \rightarrow B^3\Pi$ at 3371Å.

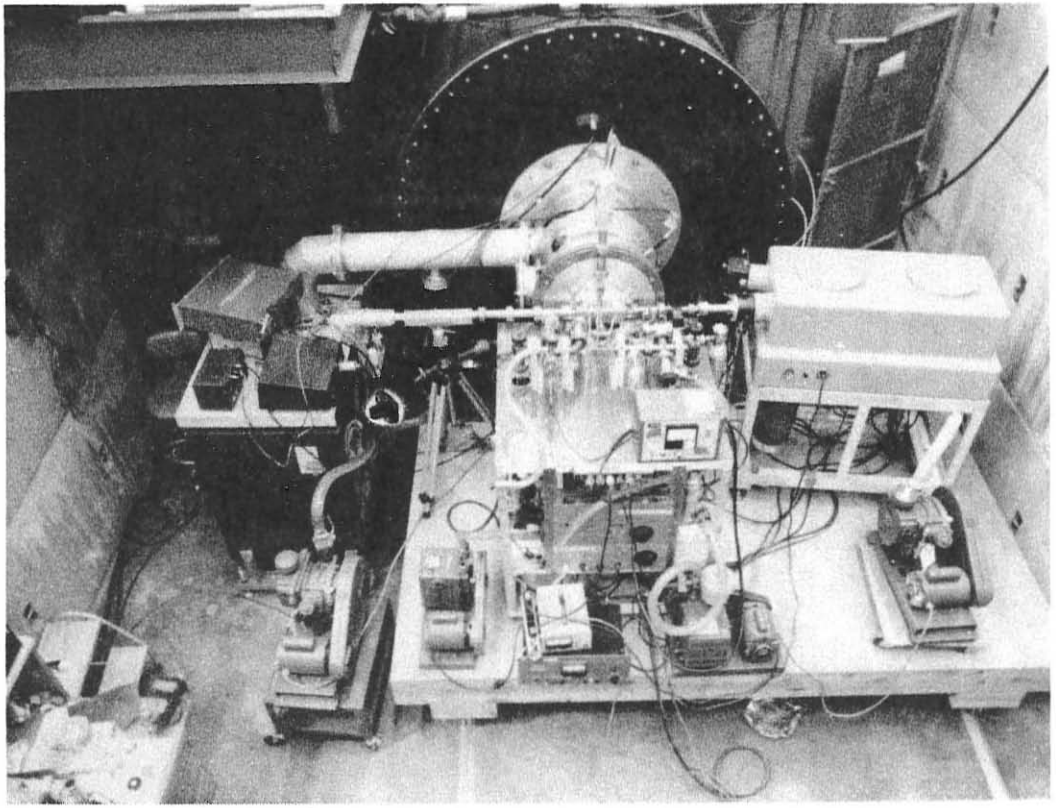

Fig 9 The Reba electron accelerator and Xe_2^* laser excitation apparatus. This oil Blumlein accelerator provides an output beam pulse of 1-3 MV, 50 kA, 70 nsec.

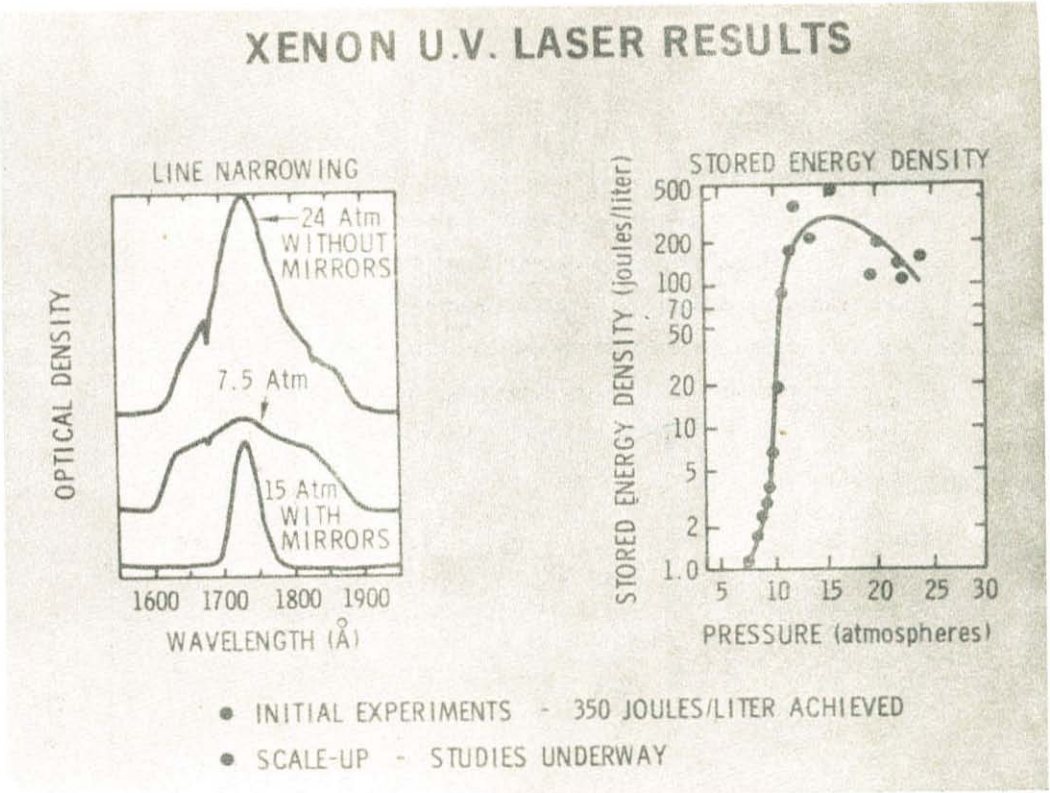

Fig 10 Experimental results obtained in the Xe_2^* experiment.[38] The left figure depicts the line narrowing observations, and the right figure shows the stored energy density data. Recent results have shown in excess of 1000 j/L of stored energy.

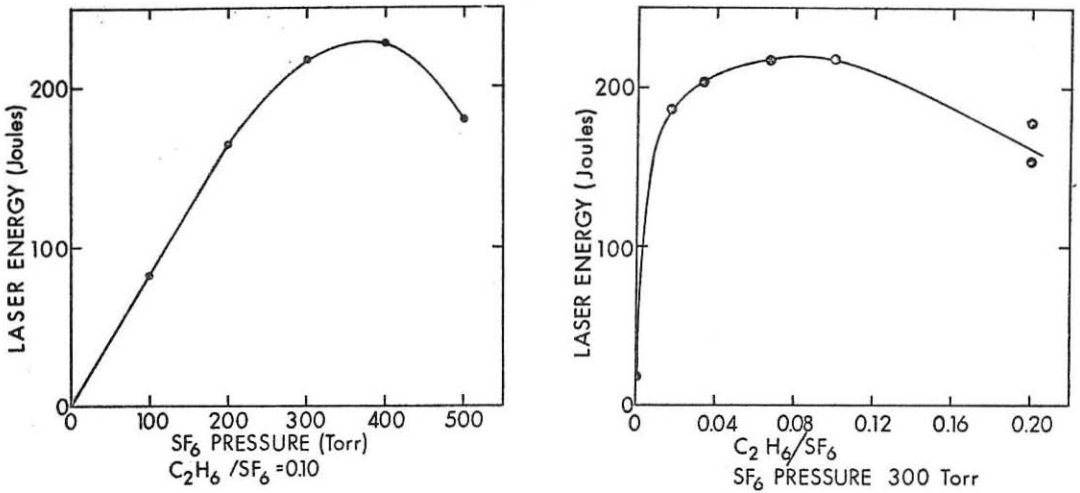

Fig 11 Experimental results obtained in the electron beam excited HF laser studies on the Reba accelerator.[39] The electron beam energy deposited in the excitation volume varied from 1000 to 4000 joules. The laser chamber was 15 cm in diameter and 1.3 meter long. These measurements are only of the energy emitted from one end of the chamber.

SUPER-HIGH DENSITY LASER FUSION CTR*

Albert Thiessen, George Zimmerman†, Thomas Weaver††, John Emmett,
John Nuckolls and Lowell Wood

University of California Lawrence Livermore Laboratory
Livermore, California
94550

Introduction and Summary

During the past three years the USAEC has accelerated the laser fusion program in the United States more than ten fold--to a total funding level comparable to that of magnetic confinement approaches to CTR [1,2]. This program may greatly improve the prospects for cheap, clean, inexhaustible fusion power in the foreseeable future. Laser fusion utilizes inertial confinement--which was experimentally demonstrated 28 years ago in the first nuclear explosion--and bypasses magnetic confinement, which has challenged controlled fusion researchers for 20 years. The key idea, recently declassified by the USAEC, is the laser implosion of small pellets of hydrogen to approximately 10,000 times their original density in order to initiate efficient thermonuclear burning [3]. Fusion energy releases 50-100 times larger than laser input energy for laser energies of 10^5-10^6 joules have been achieved in sophisticated computer simulation calculations. Ten thousand joule lasers are being planned by the USAEC Livermore and Los Alamos Laboratories, as well as by the Lebedev Institute in the USSR, to explore laser-induced implosion and fusion. If efficient thermonuclear burning is achieved experimentally, then commercial power production may be feasible, provided difficult technological-economic problems involving the laser efficiency and the power plant reliability can be solved.

The laser-fusion implosion system consists of a $\sim$ 1 mm diameter spherical pellet of deuterium-tritium surrounded by a low density, laser pre-pulse generated atmosphere extending to several pellet radii, located in a large vacuum chamber, and a laser capable of generating a precisely time-shaped, sharply peaked pulse of radiant energy. The laser pulse adiabatically compresses most of the pellet to a high density Fermi-degenerate state by the reaction forces generated by the subsonic ablation of its surface, at

---

*Research performed under the auspices of the U.S. Atomic Energy Commission.
†Also with the Dept. of Astronomy, UC Berkeley.
††Also Fannie & John Hertz Foundation Fellow, Physics Dept., UC Berkeley.

which point thermonuclear burn is initiated in its central region. See Figure 1. A thermonuclear detonation front then propagates radially outward from the central region, bringing the dense fuel sphere to $\sim 10^2$ keV temperatures, as shown in Figure 2.

With 10^7-10^8 joule fusion energy pulses initiated by 10^5-10^6 joule laser pulses, gigawatt electrical power levels may be generated by initiating $\sim 10^2$ microexplosions per second, perhaps in several thermonuclear combustion chambers. The combustion chambers would have a diameter of a few meters and might have walls wetted with Li to withstand the nuclear radiation and pellet debris. Sufficiently cheap pellets, which must cost less than a cent each, could be fabricated in a drop tower. Electricity would be generated via neutron-heated Li blankets as in conventional CTR approaches, or by any of a variety of direct conversion devices in more advanced power plant designs. The use of essentially radionuclide- and neutron-free, exotic fusion fuels—an especially attractive possibility in laser fusion systems—in quite advanced power systems offers the possibility of exceedingly clean, safe and inexpensive nuclear electricity sources.

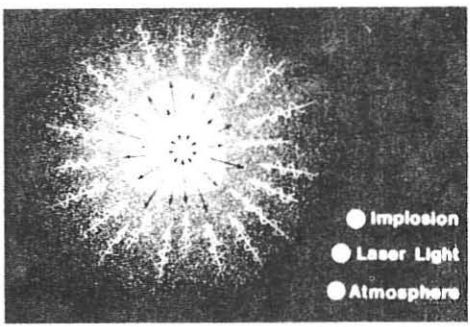

Figure 1A: Representation of a laser-energized pellet implosion, with the imploding pellet surrounded by its atmosphere of blow-off. Laser light penetrates the atmosphere up to the critical electron density.

Figure 1B: Typical laser fusion microexplosion for a 10^6 joule laser pulse and a 10^{-3} g DT pellet.

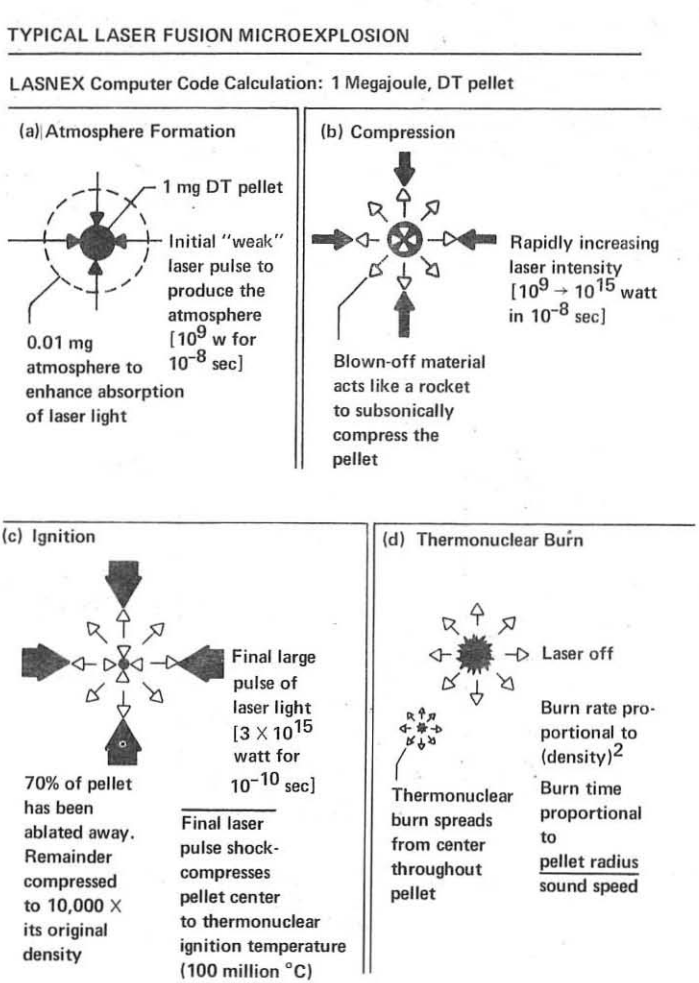

Figure 1B continued:

(e) Energy Conversion

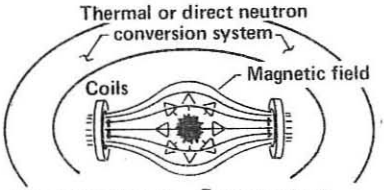

Expanding plasma compresses magnetic for direct conversion of plasma energy to electricity

Energy output
75% neutrons
20% expanding plasma
5% radiation

Cycle Specifications:

Total laser energy:
1 megajoule (1/4 kwh)
Total electrical energy input:
3-10 megajoule (1-3 kwh)
Total thermonuclear energy output:
100 megajoule (25 kwh)
Total electrical energy output:
35-70 megajoule (9-18 kwh)
Repeated 10-100 times/sec
for a 1-10 million kilowatt
(thermal) power plant

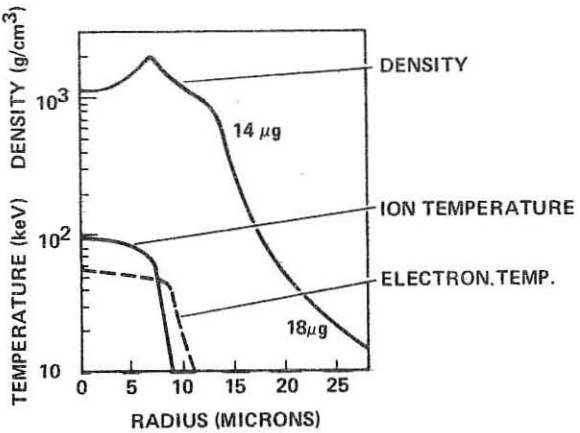

Figure 2: The initiation of thermonuclear detonation of a laser-imploded DT droplet.

Implosion Development and Application

The implosion of bubbles in water was considered by Besant in 1859 [4] and Rayleigh in 1917 [5]. A self-similar solution to the implosion of a shock wave was developed by Guderley in 1942 [6].

Early work on nuclear fission weapons at Los Alamos, beginning in 1943, by Neddemeyer, Von Neumann, Teller, Tuck, Christy, and others explored spherical implosion systems driven by high explosives [7]. Subsequently, moderately high compressions were experimentally demonstrated and utilized. However compressions approaching 10,000-fold (relative to liquid or solid densities)—which are required for practical laser fusion power reactors—have not been experimentally achieved.

In 1961, shortly after the invention of the pulsed laser, Nuckolls made implosion calculations of DT micro-spheres at our Laboratory, in which 10^4-fold compressions were achieved via pulse shaping, and proposed a laser fusion engine for CTR and propulsion applications. These calculations were based on laser pellet coupling physics developed by S. Colgate, R. Kidder and others. In the early-mid 60's calculations of laser-driven implosions were also made at our Laboratory by R. Kidder and R. Zabawski; by a group at Los Alamos; and at Cornell Aeronautical Laboratory by A. Hertzberg, W. Daiber and E. Wittliff [8,9]. In Kidder's 1964 calculations important advances were made in laser-pellet coupling physics. Subsequently, laser-energized implosion calculations were made by J. Dawson, M. Lubin, and others. In 1969, Nuckolls and Wood developed the super-high density, electron thermal conduction-driven adiabatic implosion approach to laser fusion described here that indicated for the first time the feasibility of breakeven at one kilojoule of laser energy and of CTR with practical lasers (10% efficiency, 10^5 joule laser pulses). This work and subsequent results were released by the AEC and published in 1972 [3]. Similar results have recently been published by Los Alamos scientists [10] and by Brueckner [11].

In 1963, J. S. Foster Jr., T. Merkle, and E. Teller started an experimental laser fusion program at our Laboratory. This program was directed by R. Kidder. In the mid-sixties Kidder and Mead constructed a 12 beam implosion-oriented laser [12].

In 1972, Basov and his colleagues at the USSR Lebedev Institute reported the implosion of a sub-millimeter diameter CD_2 micro-sphere with a few hundred joule, several ns, 9 beam laser pulse [13]. Approximately 3×10^6 neutrons were observed. More recent results from the Basov group indicate

that 30-fold central compressions and 300 e.v. central temperatures have been obtained with 100 μm radius CD_2 spheres, irradiated with 600 j, 6 ns, 9 beam pulses [14]. Calculations indicate that compressions to several hundred grams cm^{-3} and multi-kev central temperatures should be realized with the 400 j, 1 ns pulses which have very recently become available with this laser system; this will correspond to $n\tau$ products > 10^{14} cm^{-3} sec at DT ignition temperatures.

Thermonuclear Physics

The feasibility of explosive generation of thermonuclear energy was first demonstrated by a Los Alamos team led by Teller in the early 1950's [15].

In the laser-energized microexplosion approach to fusion, the density-radius product ρR of the imploded pellet core replaces the conventional Lawson criterion $n\tau$ in characterizing the fractional fuel burn-up and thus the ratio of fusion energy generation to input energy. In general, this comes about because the specific rates of fuel burn, energy deposition by charged reaction products, and electron-ion thermal coupling are proportional to the density; while the inertial confinement time (at optimal burn temperatures) is proportional to the fuel pellet radius. It also follows that the degree of self-heating and the feasibility of thermonuclear burn propagation are determined by ρR. In spherically convergent compression, ρR increases (because $\rho \propto R^{-3}$) and is proportional to $(M\rho^2)^{1/3}$, where M is the pellet core mass. Compression by 10^4 thus reduces the mass—and laser energy—required to initiate an efficient thermonuclear microexplosion by up to 10^8-fold, depending on the efficiency of the compression process.

More explicitly, we find that the fractional fuel burn-up, ϕ, is proportional to the product of the specific burn rate, $\rho\overline{\sigma v}$, and the inertial confinement time $\frac{R}{4c}$, where $\overline{\sigma v}$ is the Maxwell velocity-averaged reaction cross section and c is the sound speed. The factor of 1/4 in the inertial confinement time arises because in a uniform sphere half the mass is beyond 80% of the radius. Both $\overline{\sigma v}$ and c depend on temperature, but their ratio is approximately constant in the 20-50 keV ion temperature range characteristic of efficient deuterium-tritium burning in microexplosions. Evaluating $\frac{\overline{\sigma v}}{c}$ at 20 keV, and correcting for depletion, it follows that [16]

$$\phi \sim \frac{R\rho}{6 + R\rho}$$

Thus for $\rho R = 3$ g/cm^2, we find $\phi \approx \frac{1}{3}$ which corresponds to a fusion energy release of $\sim 10^{11}$ joules/g.

To achieve ρR's of ~ 3 g/cm^2 requires the compression of a 1 mg DT pellet to densities ~ 1000 g/cm^3. The electrons will have an internal energy, ε, given by:

$$\varepsilon = \varepsilon_F \left[\frac{3}{5} + \frac{\pi^2}{4} \left(\frac{\theta_e}{\varepsilon_F} \right)^2 + \ldots \right] \qquad \theta_e < \varepsilon_F$$

where $\varepsilon_F = \frac{h^2}{8m} \left(\frac{3}{\pi} n_e\right)^{2/3}$ is the Fermi energy, h is Planck's constant, m is the electron mass, θ_e is the electron temperature, and n_e is the electron density. For $\rho = 1000$ g/cm^3 ($n_e \gtrsim 2.5 \times 10^{26}$/cm^3), $\varepsilon_F \gtrsim 1$ keV. Thus, even if the compression takes place with $\theta_e \ll \varepsilon_F$, the implosion process must provide a minimum of 3×10^7 joules/g of internal degeneracy energy.

To achieve ignition, one must provide, in addition to the degeneracy energy, an average specific heat energy given by $C_v \theta_{ign} \beta$. Here C_v is the specific heat (measured from $\theta_e = 0$ at constant compression), θ_{ign} is the effective ignition temperature of DT ($\gtrsim 10$ keV), and β is a correction for self-heating by the 3.6 MeV DT alpha particles, and for thermonuclear burn front propagation. If $\rho R \gg 0.3$ g/cm^2, the alpha particle range in DT at 10 keV electron temperature, then only about 0.3 g/cm^2 in the central region need be heated to ~ 10 keV in order to initiate a radially propagating burn front which ignites the entire pellet. Note that a DT sphere having $\rho R = 0.3$ g/cm^2 will burn to a ϕ of 0.05, or 1.6×10^{10} joules/g. One fifth of this energy is in alpha particles, sufficient to heat 3 times more DT to 10 keV.

Due to the effects of shock convergence and pulse shaping during implosion, the DT temperature just prior to ignition may be made to vary approximately as $\theta_{ign} \frac{R_c^2}{r^2}$ where r is the distance from the pellet center and $R_c \gtrsim \frac{0.3 \text{ g/cm}^2}{\rho}$ is the mean free path of a DT fusion-born alpha particle. Comparing the specific heat energy of this configuration to that of a uniformly heated pellet at θ_{ign}, we find $\beta \sim 3 \left(\frac{0.3 \text{ g/cm}^2}{\rho R} \right)^2$. Because of practical limitations on implosion symmetry, a minimum of ~ 0.03 is imposed on β, which occurs for $\rho R \gtrsim 3$ g/cm^2. We then find the minimum mass-averaged ignition energy to be $\sim 3 \times 10^7$ joules/g.

The minimum total internal energy to effect thermonuclear ignition and propagation is then the sum of the ignition and degeneracy energies, or $\sim 6 \times 10^7$ joules/g. Note that since the ignition energy is the same magnitude as the degeneracy energy, further reduction in β, even if possible, could not reduce the required total internal energy by more than a factor of 2.

Since the fusion energy produced by the optimized $\rho R = 3$ pellet under consideration is 10^{11} joules/g, the raw energy gain is ~ 1500. Approximately 90-95% of the laser energy absorbed by the pellet during implosion, however,

is lost to kinetic and internal energy of the blowoff, depending on the degree of pellet compression. Consequently the energy gain relative to the laser light employed is 75-150-fold. This is sufficient for CTR applications with a 10% efficient laser, a 40% thermal-to-electric efficiency, and about 15-30% of the electrical energy circulated internally.

Figure 3 shows the variation of gain (relative to laser light energy) with compression and laser light energy [3,16]. The curves have been normalized to detailed computer calculations of the implosion and burn. Gains of the order of 100 are predicted for laser pulse energies of 10^6 joules.

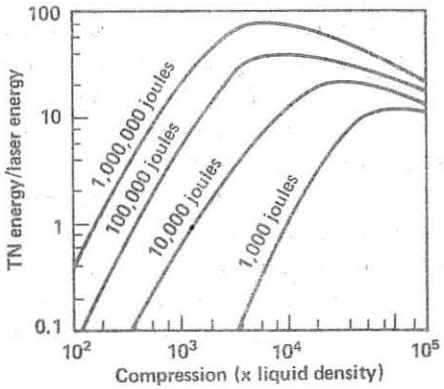

Figure 3: The ratio of fusion energy generated to laser pulse energy employed as a function of pellet compression factor, for several laser pulse energies from 10^3 to 10^6 joules, and DT fuel usage.

Our calculations indicate that less than 1 kJ of laser light may be sufficient for breakeven (gain $\gtrsim 1$), and 10^5 joules may be sufficient to generate net electrical energy with a 10% efficient laser. These predicted gains are probably upper limits to what can be achieved. Unforeseen difficulties may cause significant performance degradations when the predictions are experimentally tested.

Similar gain curves may be generated for D_2 and DHe^3 pellets with a small percentage of tritium included to facilitate ignition. Since these reactions have smaller $\overline{\sigma v}$'s than DT, higher ρR's are required for efficient burn. This may be achieved either by use of larger pellets and higher energy lasers, or by compressing the pellet to higher densities ($\sim 10^4$ g/cm^3).

Implosion Physics

Conditions involving pressure, symmetry, and stability must be satisfied in order to implode a DT sphere to a state at 10^4 times its liquid density, in which both Fermi-degeneracy and thermonuclear propagation can be exploited

to achieve the conditions for maximum gain outlined in the previous section [3].

A major free parameter available for insuring that the pressure and stability conditions are met is the shape of the laser pulse. By means of numerous computer calculations of laser-energized implosions, it has been found that the optimum pulse shape may be approximated by:

$$\dot{E} = \dot{E}_o \left(1 - \frac{t}{t'}\right)^{-s}$$

during most of the compressive phase of the implosion, where $\dot{E}$ is the laser power, t is time, t' is the collapse time, and $s \approx 2$ [16]. No satisfactory analytic derivation of the entire optimum laser pulse shape is known to us, due to the complexity of the physics involved. However, it has been found that this pulse shape may be approximated with sufficient accuracy by a histogram of 5-10 pulses. See Figure 4.

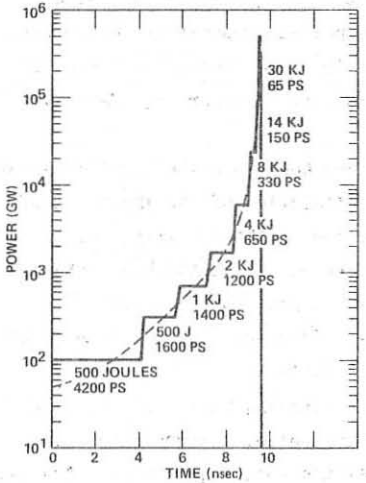

Figure 4: The ideal and a satisfactory histogram-approximation pulse shapes for implosion of a CTR-breakeven size DT droplet.

The optimum laser pulse shape generates an initial shock which is near-sonic ($\sim \frac{1}{2} \times 10^6$ cm/s) in the outer part of the pellet. This shock heats the pellet and thus increases its sound speed enough for most further compression to take place rapidly enough to be efficient and yet remain barely subsonic and thus adiabatic. At the same time the entropy generated by the shock is kept sufficiently small so that it is possible to attain a Fermi degenerate state in virtually all the imploded matter. These constraints generally require that the temperature behind the initial, weak shock be in the range 1/2-1 e.v., except in a small region near the center of the pellet where the shock converges

and strengthens sufficiently to produce significant heating.

The sharply rising mid-section of the pulse and the final peak rapidly increase the implosion velocity to a maximum of $\sim 3.5 \times 10^7$ cm/s, corresponding to the average energy density of 3×10^7 joules/g required for ignition. The rate of increase of the implosion velocity is such that the hydrodynamic characteristics in the compressing pellet coalese to form a strong shock near the time of maximum compression at about one DT alpha mean free path from the center, thus generating the sharply-peaked ignition-producing temperature profile specified earlier.

This procedure of compression along a cold, finally Fermi-degenerate adiabat followed by the centrally localized input of the heat energy for ignition, allows the compression to be effected by a maximum final pressure of $\sim 10^{12}$ atmospheres, which is the minimum possible pressure at 1000 g/cm^3. If instead the pellet had been placed on an initial adiabat with $\theta_e \sim 10$ eV so that a 10,000-fold compression would raise the average pellet temperature to ~ 5 keV, the maximum final pressures required would be $\sim 10^{13}$ atmospheres. This order of magnitude difference is crucial to the feasibility of super-high density laser CTR.

The compression and burn processes which have been described are illustrated in Figure 5 for a typical computer simulation calculation of the implosion of a fusion pellet to 10,000 times liquid density, and of the resulting thermonuclear microexplosion. This calculation was carried out at the Livermore Laboratory on the CDC 7600 computer with the LASNEX program [17]. LASNEX is a two dimensional (axially symmetric) finite difference code which includes detailed models of many physical processes. See Table 1.

The sequence of events described above is predicated on the efficient and roughly symmetric absorption of laser light in the pellet's atmosphere and on the transfer of this absorbed energy to the pellet's ablating surface. Analytic studies and elaborate 2-dimensional computer calculations of the type just illustrated have shown that adequate absorption, transfer, and symmetry can be achieved, at least in the case where the laser wavelength is shorter than a few microns. In this short wavelength case (including the 1.06 micron Nd:glass laser radiation), adequate laser energy absorption is possible via inverse bremsstrahlung; and this absorption takes place largely at the critical density, i.e. or the surface in the pellet's atmosphere where the laser optical frequency equals the electron plasma frequency. The absorbed energy is then transferred via electron heat conduction to the pellet's surface. Since the atmosphere has a radius large compared to the pellet radius, each point on the pellet surface

LASNEX CODE FEATURES

Hydrodynamics – Lagrangian; real and generalized Von Neumann artificial viscosities; pondermotive, electron, ion, photon, magnetic, and alpha particle pressures.

Laser light – refractive transport; absorption via inverse bremsstrahlung and plasma instabilities; reflection at critical density.

Coulomb coupling of charged particle species.

Suprathermal electrons – Multigroup flux-limited diffusive transport with self-consistent electric fields; non-Maxwellian electron spectra determined by results of plasma simulation calculations for laser light absorption by plasma instabilities; inverse bremsstrahlung electron spectrum for classical absorption.

Thermal electrons and ions – flux-limited diffusive transport.

Magnetic field – includes modification of all charged particle transport coefficients, as well as most of the equilibrium MHD effects described by Braginskii[30].

Photonics – Multigroup flux-limited diffusive transport; LTE average-atom opacities for free-free, bound-free, and bound-bound processes; Fokker-Planck treatment of Compton scattering.

Fusion – Maxwell velocity-averaged reaction rates; the DT alpha particle is transported via a one group flux-limited diffusion model with appropriate energy deposition into the electron and ion fields; one group transport of the 14 MeV neutron; super-dense pellet results checked against more sophisticated Monte Carlo-based thermonuclear physics codes.

Material properties – opacities, pressures, specific heats, and other properties of matter are used which take into account nuclear Coulomb, degeneracy, partial ionization, quantum, relativistic and other significant effects.

TABLE 1

is heated by—and averages over—almost 2π steradians of the hot laser absorbing region. This, combined with the fact that during most of the implosion the electron mean free path in the absorbing region is a significant fraction of the absorption radius, results in a large ($\sim$ 10-fold) reduction in the asymmetry with which the pellet surface is ablated.

In the compression of the spherical pellet by 10^4-fold, the radius decreases somewhat more than 20-fold. If, after compression, spherical symmetry is required to within 1/2 the compressed radius--or 1/40 the initial radius--then the implosion velocity (and time) must be spatially uniform (and synchronized) to about one part in 40, or a few percent. See Figure 6. The outer atmosphere may be heated uniformly to 10 to 20% by a many-sided irradiation system, consisting of beam splitters, mirrors, lenses, and other optical elements. This error is then reduced to less than 1% by the physical processes inside the atmosphere [3,25] just mentioned.

Figure 5a: A LASNEX simulation of the laser-energized implosion and ignition of a 60 microgram droplet of DT, surrounded by a prepulse-generated atmosphere. The Lagrangian hydrodynamic mesh of the simulation is depicted, with superimposed isotherms of the electron component of the plasma during the implosion (at 0.1, 0.3, 1.0, 3.0 and 10 keV), and of the ionic component during the thermonuclear detonation of the imploded pellet (at 10, 20 and 50 keV). The maximum electron and ion temperatures, TE and TI, (in keV) and matter density, D (in gm cm^{-3}), in the situation being simulated are indicated in the left-most column under the hydro mesh, while the total laser energy inputted to the imploding system, EL, and thermonuclear energy, EP, produced by it (in kilojoules) are shown in the middle column. The simulation time, TIME, (measured from an arbitrary zero after atmosphere formation) in nanoseconds and the scale size, SIZE, of the portion of the problem displayed, in micrometers, are indicated in the right-most column.

The laser energy is inputted in 10 beams with axial symmetry, with azimuthal angular intensity variation $I = I_0 (1 + 0.1 \sin 20\theta)$, θ the azimuthal angle; 5 periods of this intensity variation are shown in this quadrant of the situation simulated, which has four-fold symmetry. The first $\sim$ 1 kilojoule of laser light is inputted as 4 μm wavelength radiation, and the second as 2 μm wavelength laser light. The following $\sim$ 8 kilojoules are 1 μm radiation, and the final $\sim$ 44 kilojoules are of 0.5 μm wavelength.

Such a roughly spatially symmetric, crudely frequency-shaped and carefully time-tailored laser pulse is sufficient to simultaneously meet pressure, symmetry, stability, decoupling and preheat requirements of the implosion, if the pellet is doped with $\sim$ 0.1 atom-percent of high Z material to enhance the electron collisional frequency and inverse bremsstrahlung opacity in the atmosphere. This pellet-laser pulse combination is representative of those which operate completely within the "classical physics" regime, e.g. which may be adequately modeled within the Maxwellian electron velocity distribution approximation.

Implosion symmetry is seen to be quite satisfactory as late as 23.9141 nsec, when nearly 40% of the laser energy has been inputted, and the pellet has been compressed over 600-fold. Though not apparent in the configuration of the blow-off, pellet symmetry continues to deteriorate ever more sharply through 24.0347 nsec, when all of the laser pulse energy has been inputted and the pellet compression has exceeded 5000-fold.

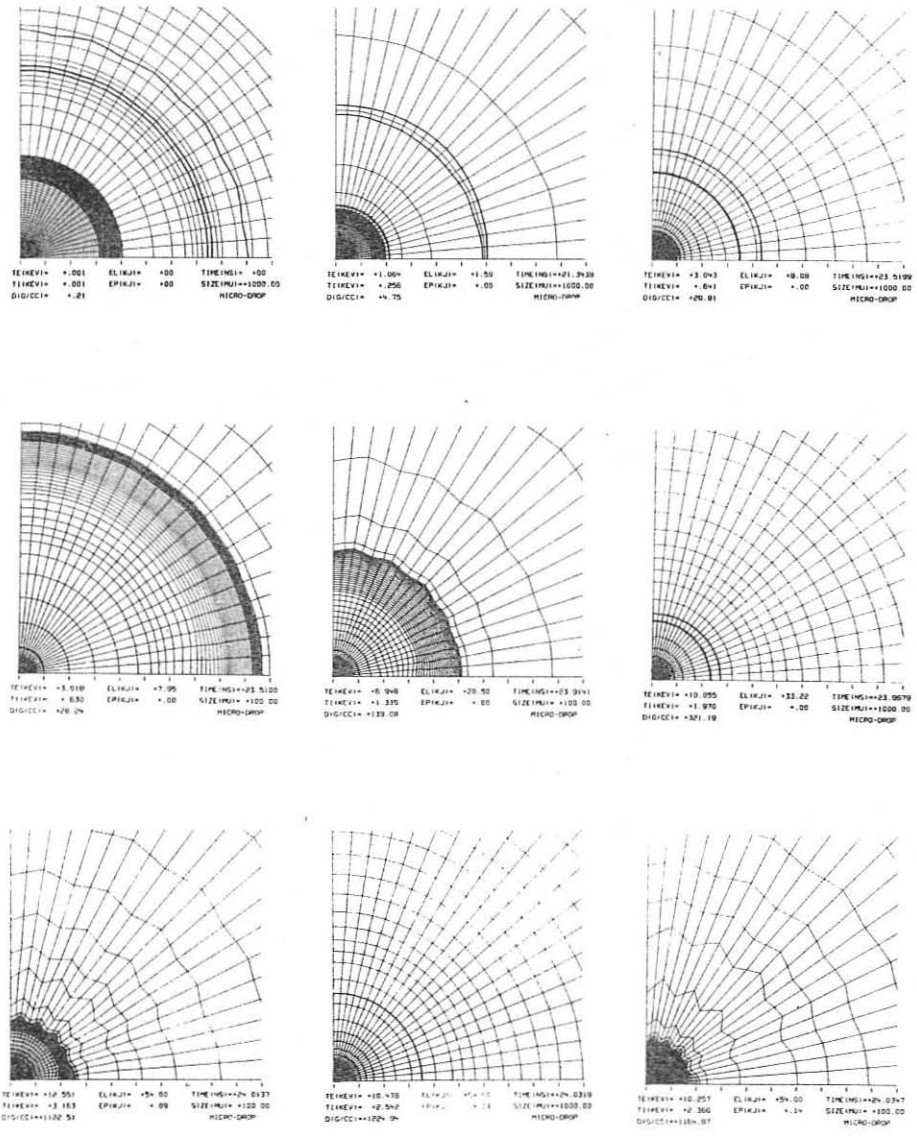

Figure 5a

Figure 5b: The hot atmosphere of the pellet continues to ablatively implode it to ever higher densities and, after one abortive ignition commencement, the pellet center thoroughly ignites at about 24.0472 nsec; the high velocity ($\sim 3.5 \times 10^7$ cm sec^{-1}), high density shell of DT imploding onto the pellet center was crucial to successful ignition. The supersonic nature of thermonuclear detonation is indicated by the sweeping of the 10 and then the 20 kilovolt ionic isotherms over the entire pellet mass, before the pellet has expanded significantly (at 24.0520 nsec). At this time, the 50 kilovolt isotherm has enveloped the matter inside half of the pellet radius, and a pronounced axial jet has become visible; about half the total thermonuclear energy has been produced, and the mass-averaged fuel temperature is at a maximum. From this time through 24.0639 nsec, the isotherms successively reconverge on the pellet center, due to hydrodynamic losses exceeding the thermonuclear energy generation rate of the ever less dense pellet.

Approximately 30% of the dense pellet nuclei undergo thermonuclear reaction during the microexplosion, producing about 32 times the energy from fusion as the laser pulse energy; this is within a few percent of the energy produced by an identical pellet imploded with completely symmetrically inputted laser light. This is approximately the performance level of a "CTR-breakeven" fuel pellet-laser pulse combination.

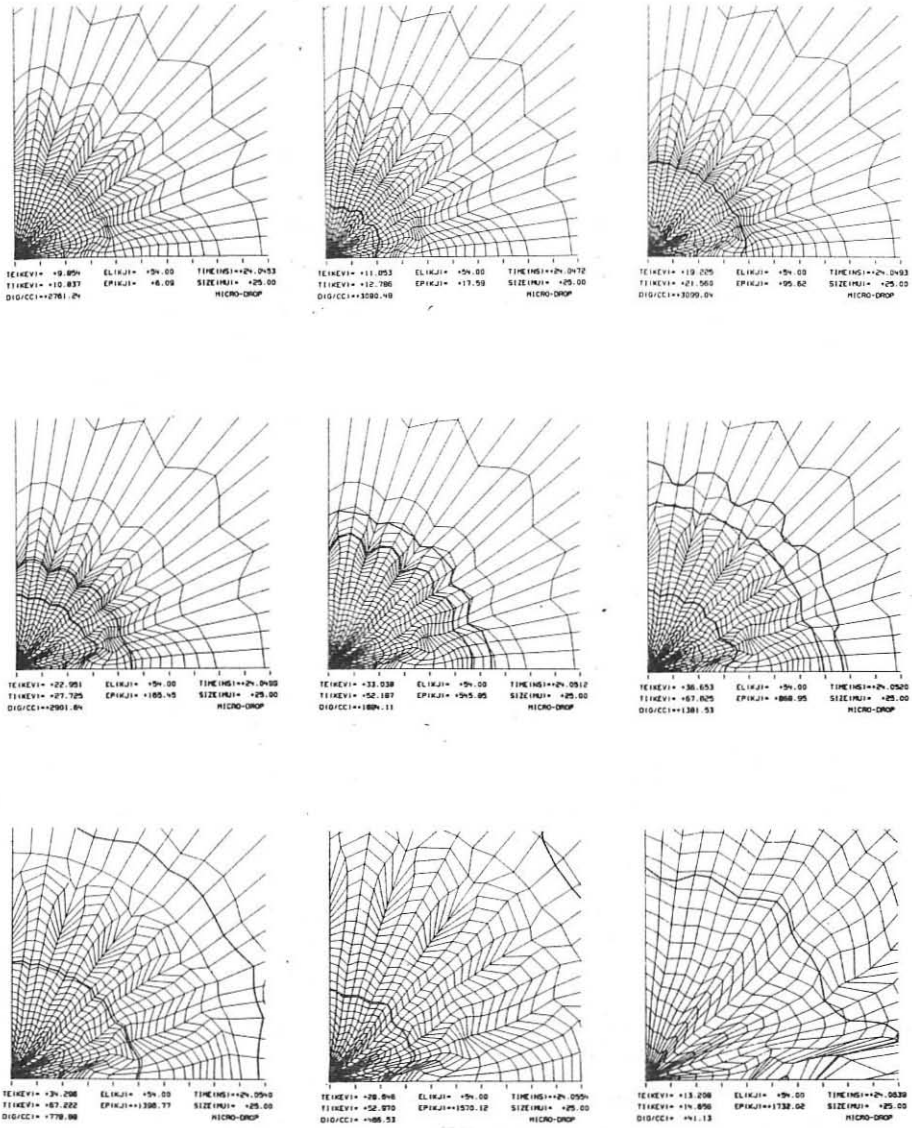
MICRO-DROP
MICRO-DROP
MICRO-DROP
MICRO-DROP
MICRO-DROP
MICRO-DROP
MICRO-DROP
MICRO-DROP
MICRO-DROP

Figure 5b

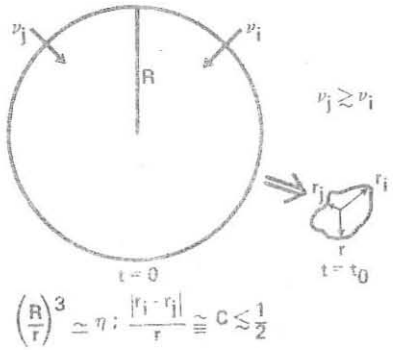

Figure 6: Symmetry considerations in the laser-energized implosion of a fusion fuel pellet. η is the pellet compression factor at the implosion culmination time t_0, at which time sphericity to within a factor of two is required of the pellet.

The implosion of the pellet by electron heat conduction-driven, ablation-generated pressures is hydrodynamically stable [3,25], except for relatively long-wavelength surface perturbations, which grow too slowly to be damaging, if the pellet is imploded in one sonic transit time. In part, ablative stabilization occurs because the peaks of surface perturbations are effectively closer to the heat source (than are the valleys) so that the ablation-driving temperature gradient is steeper. Consequently, the amplitude of any such perturbation is reduced, both because such a peak is more rapidly ablated, and because the ablation pressure is higher on the peak. See Figure 7.

For the long laser wavelength case, including the 10.6 micron CO_2 radiation, the pellet compression and energy gain may be strongly degraded by electron preheat [18,19] and decoupling [20]. Decoupling occurs when the electrons heated by the laser have a range in matter at the critical density comparable to the laser absorption radius. Then most of these electrons cross the atmosphere, re-enter the absorption region, and are heated to higher energies with longer mean free paths, etc., until the pellet is effectively decoupled from the laser-heated electrons over times comparable to the implosion time. (After a few hot electrons escape into the vacuum chamber, plasma potentials comparable to the

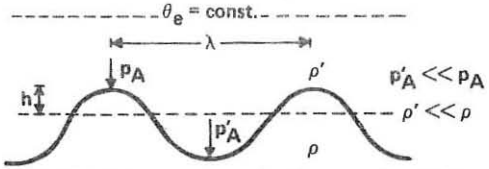

Figure 7: The effect of a spherically symmetric isotherm in the pellet atmosphere on the hydrodynamic stability of the ablating pellet surface. While nominally unstable to the Rayleigh-Taylor instability, the surface is actually stable for all but the longest perturbation wavelengths (of the order of the pellet radius, which grow too slowly to be damaging), due to the diffusively driven, subsonic nature of the ablative acceleration [25].

electron energy are developed. Subsequently, long range electrons are confined to the expanding plasma by electrostatic forces.) The maximum decoupling-limited implosion pressure which may be generated is, from flux-limited conduction and geometric considerations,

$$P_{max} \simeq 10^2 \frac{A_c}{A_p} A_c^{1/4} \rho_c^{3/2} \text{ megabars},$$

where A_c and ρ_c are the area and density of the critical layer of the pellet atmosphere and A_p is the area of the pellet surface, all in cgs units. Decoupling can be compensated for if the pellet volume is increased by making it hollow. Then the required implosion velocity may be achieved with smaller implosion pressures acting for longer times, with correspondingly smaller laser intensities and electron energies [19].

Preheat occurs when the laser-heated electron range is a significant fraction of the pellet radius—these electrons then heat the fuel internally, making it more difficult to compress. Such high energy electrons are generated by inverse bremsstrahlung absorption of long wavelength light. Moreover, efficient absorption of such light is not possible via inverse bremsstrahlung because the light absorption length is too long ($>>$ 1 cm at 10 keV) [21]. Absorption is possible via plasma instabilities [22,23]. However, if the thresholds for these instabilities are greatly exceeded, then sophisticated plasma simulation computer codes predict that non-Maxwellian electron velocity distributions may be generated, with high energy tails extending beyond 100 times the thermal electron energy [24]. See Figure 8. These tails are essentially due to "runaway" electrons produced by the strong electric fields generated by the plasma instabilities. Experiments are needed to determine the electron spectra in such situations. An estimate of the fraction of the absorbed laser energy which can be tolerated in these suprathermal electrons is the ratio of the rate of hydrodynamic work done on the pellet to the product of the laser-heated electron energy density and the electron thermal velocity just inside the critical surface; clearly, if the rate of suprathermal heating work on the pellet core is comparable to or greater than the rate of hydrodynamic work, the implosion will fail. At the early stages of the implosion, when preheat is most critical, this fraction may be as small as 10^{-2}. If excessive numbers of superthermal electrons are not generated, then long wavelength lasers may be suitable for CTR applications, provided that the hollow pellet can be constructed cheaply enough.

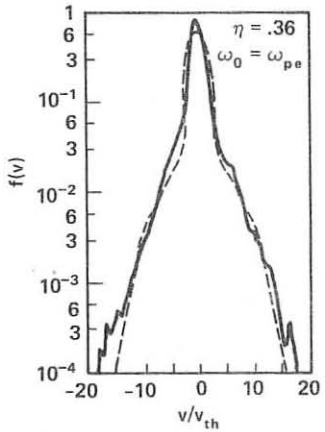

Figure 8: The theoretical (---) and plasma simulation code-computed (——) electron velocity spectrum f(v) as a function of the velocity in units of the thermal velocity v/v_{th}, for the situation

$$\eta \equiv E/\sqrt{4\pi NkT} = 0.36,$$

where E is the laser electric field, and NkT is the plasma electron thermal energy density; η^2 is the ratio of optical to thermal energy densities [24]. $\eta = 0.36$ corresponds to an intensity of about 10^{14} watts cm^{-2} and a 10 keV plasma temperature for CO_2 laser radiation; this intensity is comparable to the peak intensity required for implosion of hollow DT shells, and is about an order of magnitude below that required for DT droplet implosion. The broad wings of the distribution at high velocities, which branch out from the parabolic, Maxwellian center, are due to excitation of laser-driven plasma instabilities at/around the critical density in the pellet atmosphere. Such electron velocity spectra, if experimentally verified, preclude CO_2 laser usage in super-high density laser CTR, due to preheat limitations.

Laser	$\lambda(\mu)$	η(%)	S(J/ℓ)	τ_p(nsec)	E_o(J)	Pav	$\lambda_{conversion}$
Nd:Glass	1.06	0.2	500	$\geqslant 0.02$	350 (0.1 nsec)	Very Low	0.26-1.9 μ ($\geqslant$ 40% eff)
CO_2	10.6	5	15	$\geqslant 1.$	25 (1 nsec)	High (Flow)	—
I	1.32	0.5	30	2	12 (10 nsec)	High (Flow)	—
Xe_2	0.17	< 20	300	~ 10	0.1 (10 nsec)	High (Flow)	Not Required
New (Gas)	~0.4	> 5	100-1000	0.1-1.0	10^4-10^6 (0.1-1.0 nsec)	High (Flow)	Not Required

Table 2: Salient features of laser systems for pulsed fusion applications. λ is the laser output wavelength in micrometers, η is its pumping efficiency, S is its energy storage capability, in joules/liter, τ_p is the pulse length at which such systems have demonstrated high power gain, in nanoseconds, E_0 is the maximum energy pulses, in joules, which such systems have demonstrated at the pulse durations indicated, P_{av} is the average power generation ability of such systems under repeated pulse conditions, and $\lambda_{conversion}$ is an indication of the available spectral range and efficiency of demonstrated frequency conversion. The properties of the New (Gas) laser are those considered most appropriate for laser CTR power plant applications.

Laser Technology

The development of lasers for high density laser fusion applications poses a special set of problems that have not previously received much attention in the laser R&D community. In the optimum pellet-compressing pulse shape, about half the total energy is produced in the last 100 picoseconds. Thus, in terms of a simple, single pulse, a CTR laser system has to be capable of producing at least 50 kilojoules in 100 picoseconds. In addition, the optimum plasma heating process requires short wavelength lasers. Such lasers do not exist at present; however, development of short wavelength devices is receiving increased attention in the U.S. and several other countries.

Table 2 indicates many of the salient characteristics of four laser systems that are presently under consideration for scientific feasibility demonstration purposes and which are representative of the diversity that exists in the laser world. Neodymium glass is a laser medium developing gain at 1.06 μ wavelength using Nd^{3+} ions in a glass matrix pumped by xenon flashlamps. The CO_2 laser develops gain at 10.6 μ between vibrational energy levels of the ground electronic state of the CO_2 molecule. This system (actually a CO_2-N_2-He mixture) is pumped by relatively low power electrical discharges in the gas, which are often sustained by low current (5-500 mA/cm^2), high voltage (100-300 kV) electron beams. The iodine laser develops gain at 1.315 μ between electronic levels of the neutral iodine atom, which is produced in an excited state by photodissociation (near 2800 Å) of molecules such as CF_3I. Xenon flashlamps are typically used as the photodissociation pump source. The xenon laser specie is the Xe_2^* molecule formed in high pressure xenon gas pumped by high current density (100-5000 A/cm^2) relativistic (0.5-2 MeV) electron beams. The output wavelength of this system is 1722 Å.

What is interesting to note about these laser systems is the almost total lack of overlap in the technologies required for the development of each system. Thus, extensive development effort applied to one of these systems is not usually applicable to another. Also shown in Table 2 are the desired characteristics of a hypothetical laser system that matches the requirements of laser fusion as presently envisioned. The primary characteristics of this hypothetical laser system are high efficiency, high average power, short wavelength, and high energy. It is clear that none of the real lasers in Table 2 demonstrate all of these characteristics. To summarize Table 2, the following statements can be made: Nd:glass lasers have the best developed technology for operation in the subnanosecond region. In addition, the high second harmonic

conversion efficiency (60-80%) already demonstrated offers great potential for operation at 0.53 μ. Fourth harmonic generation (0.265 μ) and stimulated Stokes-Raman scattering (1.9 μ) offer potential for pellet compression at other wavelengths with efficiencies greater than 20%. Thus, the Nd:glass laser system apparently provides the best laboratory tool for near-term laser fusion experiments. However, the extremely low energy efficiency (0.1%) and the low average power capability (limited by the low thermal conductivity of glass) preclude any consideration of Nd:glass systems for eventual laser fusion power generation applications.

The CO_2 laser has demonstrated efficiencies of approximately 5% for one nanosecond duration pulses. Operation in the 0.1 nanosecond regime has yet to be demonstrated. With the addition of high speed gas flow, CO_2 lasers have the capability to generate high average powers. The major liability of the CO_2 system is the 10.6 μ emission wavelength. As noted above, it may well be that CO_2 lasers will never be useful for laser fusion, if current theoretical predictions of a significant high energy tail to the resultant electron energy distribution in the CO_2 laser-heated plasma are indeed correct. Efforts are currently underway to efficiently convert the 10.6 μ energy to shorter wavelengths, although success has yet to be achieved. Development of high energy, short pulse CO_2 lasers continues because of the high efficiency and high average power capability. The ultimate usefulness of this system remains to be determined.

The iodine laser has recently come under consideration as a possible lower cost replacement for Nd:glass. The emission wavelength and efficiencies are similar; however, the cost of CF_3I is much below that of Nd:glass. The stimulated emission cross section of I^*, even in the presence of a few atmospheres of a line-broadening buffer gas, is much larger than Nd:glass. This necessitates an entirely different approach to the laser design, in order to control parasitic oscillation within a single laser amplifier section. With the eventual solution to the parasitic oscillation problem and a more detailed understanding of the pumping requirements of the system, it is possible that iodine lasers suitable for laser fusion work may be built in the 1-10 kilojoule regime.

The xenon laser is the newest system to undergo consideration as an appropriate source for laser fusion experiments. The interest stems from the short wavelength (1722 Å) and predicted high (> 25%) pumping efficiency. Little detailed information is available on this system and the technology for the

generation of subnanosecond pulses has yet to be developed in this portion of the spectrum. Two comments are however appropriate at this time. First, the stimulated emission cross section is approximately 3×10^{-18} cm^2. Thus, a large high energy amplifier will be severely limited in performance by superfluorescence (amplified spontaneous emission) and parasitic oscillation. Second, lasers useful for fusion applications must operate at flux levels of 10^{10} watts/cm^2 (1 J/cm^2, 100 psec) or greater. At this flux level and 1722 Å, all transparent materials (window, lenses, coatings) from LiF to Al_2O_3 will exhibit two-photon absorption coefficients in the 1 to 25 cm^{-1} range. Thus, to use such a short wavelength, a new optical technology of gas lenses and aerodynamic windows will have to be developed. It is also interesting to note that at approximately 3×10^{10} W/cm^2 the estimated loss from two-photon ionization of ground state xenon atoms equals the gain achieved in the system.

From the foregoing discussion several conclusions are easily drawn. Clearly, Nd:glass laser systems provide the best technology base for the near-term laser fusion experiments. The wide range of pulse widths obtainable (20 psec - 20 nsec) and the range of wavelengths (0.265 - 1.9 μ) render it an almost ideal laboratory tool. For these reasons large multi-aperture Nd:glass laser systems with energies of 10 kilojoules are in design or construction stages in the U.S. and the U.S.S.R. At our Laboratory, a 10 kilojoule subnanosecond spherical irradiation facility is being designed. With this facility, it is hoped that the important milestone of significant thermonuclear burn and possibly breakeven energy production (light in = TN energy release) will be achieved.

It is quite clear, however, that the development of new lasers is required if laser fusion power production is to become a reality. The xenon laser represents a class of possible lasers based on the weakly bound or van der Waals molecules. Laser action has already been achieved from Xe_2^* and Kr_2^* and may be expected from some of the similar dimer systems of mercury, cadmium, and zinc. Other non-dimer systems such as LiXe or HgXe also look attractive. These systems are pumped by efficient, high current relativistic electron beam machines which have been extensively developed during the last decade. The availability of efficient pump source and the short wavelength of emission makes these systems of great interest for laser fusion. However, it is clear that stimulated emission cross sections smaller than in the xenon system will be necessary, as will extensive development of means of parasitic oscillation and superfluorescence control.

It seems quite clear, though, that the single most important characteristic

of any new laser system developed for laser fusion applications will be the ability to use energy efficiently.

Laser CTR Reactors

The fusion-fuel combustion chamber of a laser fusion power plant must not only serve to admit the fuel pellet and direct the laser beams upon it, but must also endure perhaps as many as 100 multimegajoule thermonuclear pulses per second for of the order of ten years, and be technically and economically feasible to construct and maintain. The fusion effects consist of an x-ray pulse, a neutron pulse, and blast and thermal effects from the plasma explosion debris. The x-ray pulse is fortunately heavily attenuated in the softest (10-1000 eV), most wall-threatening portion of the spectrum by inverse bremsstrahlung in the superdense fireball. See Figure 9. The neutron spectrum is dominated by a 14 MeV peak. See Figure 10. Calculations involving x-ray opacities, neutron cross sections, specific heats, thermal expansion coefficients, and compressibilities indicate that a chamber of about 3 meter radius with a wall of a few layers of properly chosen low-to-moderate Z materials (e.g. $\sim$ 0.01 cm of beryllium backed by titanium, niobium, or vanadium) will endure the x-ray and neutron pulses of a 10^7 joule microexplosion. If surfaced with a thin, low-Z liquid layer (e.g. Li a few hundred μm thick) by continuous exudation, the plasma pulse of a 10^7 joule explosion may also be repetitively endured by the combustion chamber [26,27].

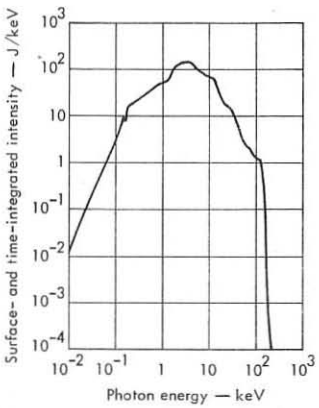

Figure 9: X-ray spectrum from 2 gm cm^{-2} DT microexplosion.

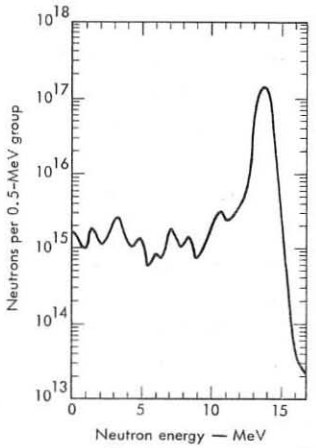

Figure 10: Neutron spectrum from 2 gm cm^{-2} DT microexplosion.

The impulse associated with an explosion determines the size and material strength of a chamber which must contain it. This impulse is proportional to the square root of the product of the explosion energy and the mass of the explosion debris. Relative to a chemical explosion of the same energy, a fusion pulse involves about six orders of magnitude less explosive debris mass and thus about three orders of magnitude less impulse—provided that the surface of the wall is not vaporized. Then a 10^7 joule fusion pulse produces no more impulse than a large firecracker.

If the combustion chamber is too small, the wall will be ablated by the thermonuclear debris. Then the peak pressures imposed on the wall may be multiplied as much as a thousandfold, and may be unacceptably high ($\gtrsim$ 1 kbar). A crucial advantage of not vaporizing the lithium on the wall is that the chamber pumpdown time does not severely limit the pellet burn repetition rate.

About 1 joule/cm^2 of thermonuclear plasma energy may be directed against a chamber wall "moistened" with a several-hundred-micron layer of liquid lithium before significant blowoff is produced. The suprathermal ion fluence (e.g. 3.5 MeV alpha particles, knock-on deuterons and tritons) associated with a 1 joule/cm^2 thermal plasma fluence poses no blowoff hazard, since it penetrates the moist layer relatively deeply and deposits its energy in a large amount of matter. Ten megajoule pulse rated, moistened-wall combustion chambers of $\sim$ 3 meter radius would thus be satisfactory from a plasma wall-loading standpoint. See Figure 11.

If the combustion chamber wall is shielded from the pellet debris by a minimum B magnetic field, the surface area requirement for the explosion chamber is determined by x-ray loading considerations. Then the chamber radius may be reduced by approximately a factor of two.

The chamber wall might also be satisfactorily shielded from the plasma pulse, as well as from a portion of the x-ray pulse, by pulsed injection of gas through the dry walls of the micro-explosion chamber. However, the required mass injection rates are uncomfortably large and the firing rate is limited by the chamber pumpdown time.

A very important problem for laser-fusion reactor design is how to input the laser light and target pellet while at the same time maintaining adequate neutron and x-ray shielding. Laser beams might be admitted through cheap, replaceable windows in the outer vacuum wall, passed through the neutron shield in neutronic-baffling dogleg tunnels on mirror trains, and focused onto the pellet atmosphere by aspheric mirrors facing into the explosion chamber through apertures in the inner wall. Continuous, low Z liquid-metal exudation-surfacing of the mirrors

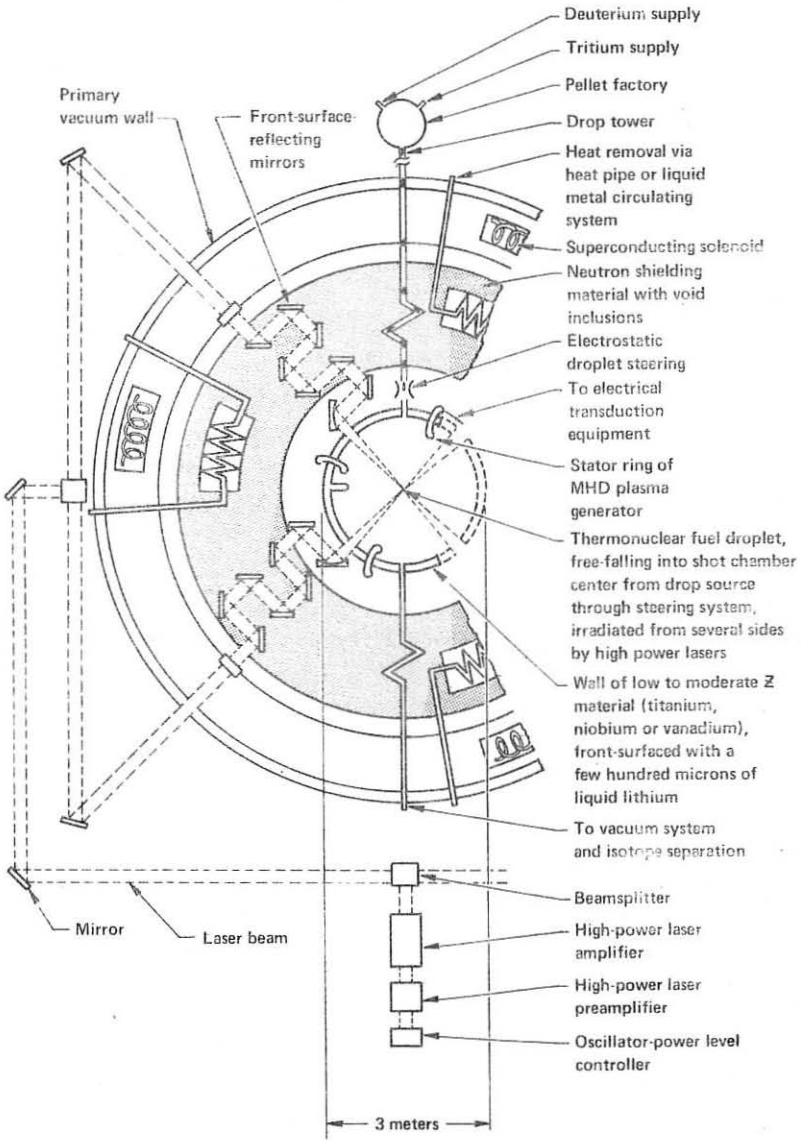

Figure 11: Conceptual design of laser pellet CTR power plant with direct conversion.

would prevent degradation of the reflectivity by the thermonuclear environment for laser wavelengths > 0.2 μm. The several mm-sized fuel pellet would free-fall or be electrostatically projected into the combustion chamber.

Tritium breeding and recovery, necessary for pure DT burning, would be conducted by use of a lithium-rich neutron blanket surrounding the combustion chamber wall similar to those being considered for magnetic confinement fusion power plant designs. A 1% void fraction in the lithium blanket is probably required to permit impulsive neutron heating of the lithium without mechanical damage to the wall.

Fusion Energy Conversion

Fusion energy pulses, as extremely high grade energy sources, apparently admit of several very different means of converting their energy into electricity, depending on pellet fuel composition, the ρR value at which the fuel is burned, and the combustion chamber system design and operation. Three types of systems have been identified so far: 1) ordinary thermal conversion, 2) MHD hot-gas-generator conversion, and 3) MHD plasma conversion.

For first-generation laser fusion power plants, which would burn DT pellets, ordinary steam-thermal conversion of fusion energy deposited by neutrons in the lithium blanket seems preferable. Such systems would have capital costs of several hundred dollars/KWe and energy conversion efficiencies of $\lesssim$ 40%—comparable to conventional and fission reactor systems. More advanced versions of such a system might employ neutron direct conversion means such as those indicated in Figure 12, in which high energy neutron-scattered protons do electrical work within an electrostatic converter. A sketch of such a reactor concept is shown in Figure 13 [32].

If the combustion chamber wall is shielded from the plasma pulse by injected gas, the heated gas might be exhausted from the chamber through a relatively inexpensive, pulsed MHD hot-gas generator. Several atmospheres stagnation pressure at a few thousand degrees temperature could be produced. Such a system might permit electricity generation with higher total efficiency ($\sim$ 60%) for moderate ρR ($\sim$ 10 g/cm^2) pellet DT or DD burn, or for a 5 g/cm^2, high-charged-particle-fraction (e.g. D-^{3}He) pellet burning. Such ρR's may be obtained with a few hundred kilojoule laser, if the pellet is compressed to 10^4 g/cm^3 densities. However, at these high ρR's, 10-30% of the fusion energy is radiated as x-rays. Hence the ultimate efficiency of this approach is limited by the efficiency with which the x-ray energy may be converted to electricity. Pulsed injection of higher Z gas around the microexplosion site just prior to detonation may prove to

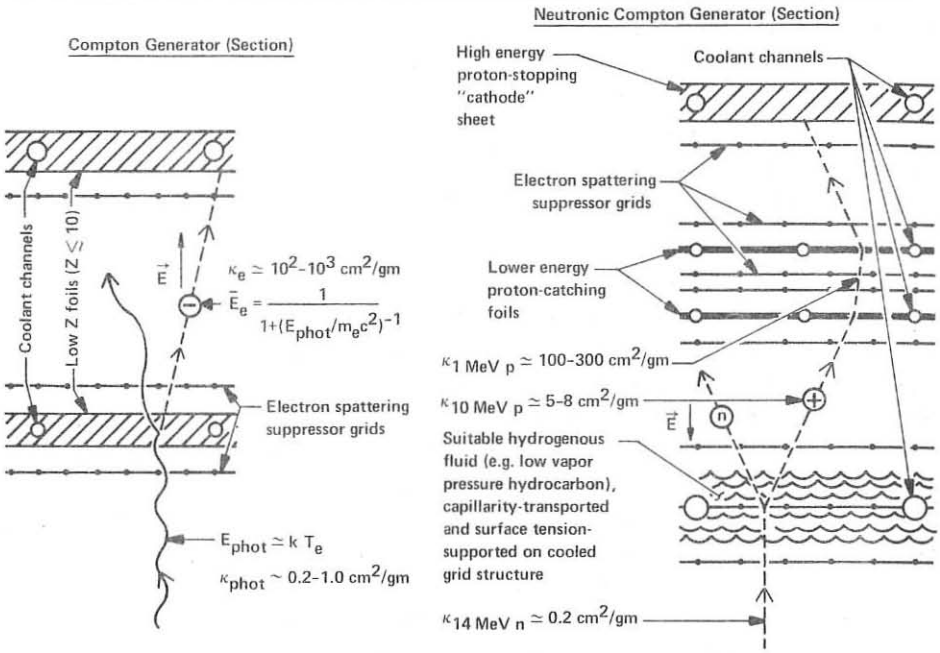

Figure 12

be a useful technique for converting such x-radiation to plasma which may then be processed in an MHD duct [26,32].

The rapidly expanding fusion fireball may be made to do magnetohydrodynamic work on a magnetic field imposed from outside the combustion chamber, transforming its energy into that of a compressed magnetic field. Induction coils suspended from the combustion chamber walls might be used to transform the compressed field energy directly into electricity, in a manner basically very similar to the way an ordinary power transformer works. The physical principles and typical operating parameters of such an approach are indicated in Figure 14. The basic feasibility of such fireball-to-electricity energy conversion has already been demonstrated [28]. Low capital cost, high efficiency ($\gtrsim$ 70%) electrical energy generation may thus be ultimately attainable, in advanced laser-fusion CTR systems.

Using conventional electricity generation methods, the heat from 100 10^8 joule (low-pellet-cost) fusion pulses per second could be used to generate about 4000 MW of electricity. Such a power plant would cost perhaps $800 million, of which

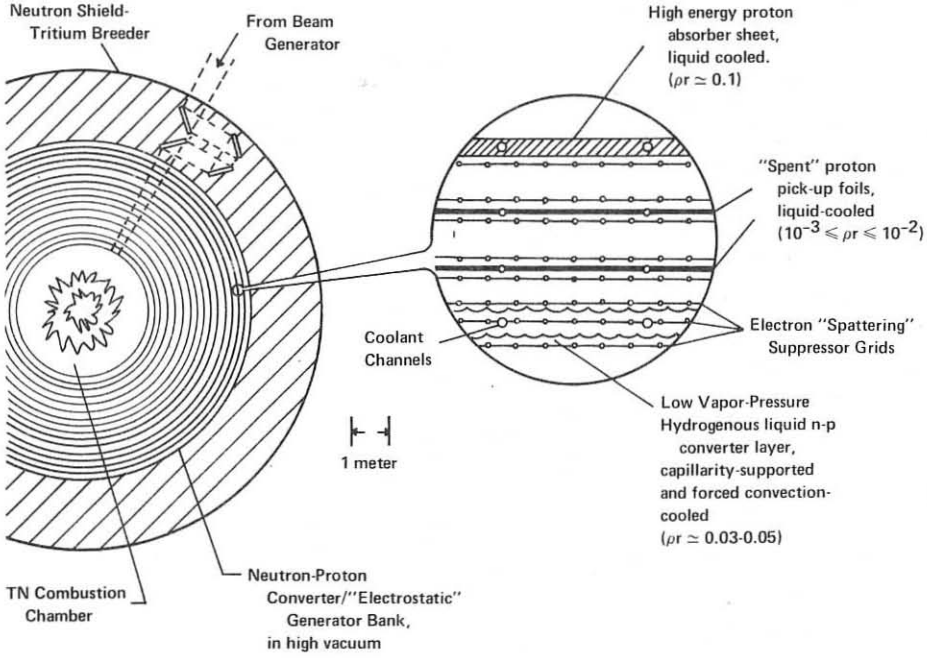

Figure 13

perhaps \$200 million could be devoted to the laser system. The laser and gas circulating equipment are expected to consume about half of this, leaving \$100 million to pay for a 10^7 joule, 100-pulse/sec power supply (assuming a 10^6 joule laser and a 10% laser pumping efficiency). Various estimates indicate that this amount (\$10/J) will suffice to purchase such a power supply with a 10 year lifetime [29].

An attractive alternative to such approaches is offered by the use of exotic fusion fuels in CTR combined with the associated direct conversion potentialities. The use of exotic fuels—neutron-and radionuclide-free proton burning of selected higher Z nuclei—is especially feasible in the super-high density approach to CTR, for electron-ion coupling and associated radiative losses are suppressed by small Coulomb logarithm values. Some of the more likely candidates for such fuels [31] and their salient properties are indicated in Figure 15. The $\langle\sigma v\rangle$ for the best of these exotic fuels, the p-B^{11} combination, is compared to these for DT, DD, and DHe^3 in Figure 16. A sketch of a pulsed fusion power plant concept which

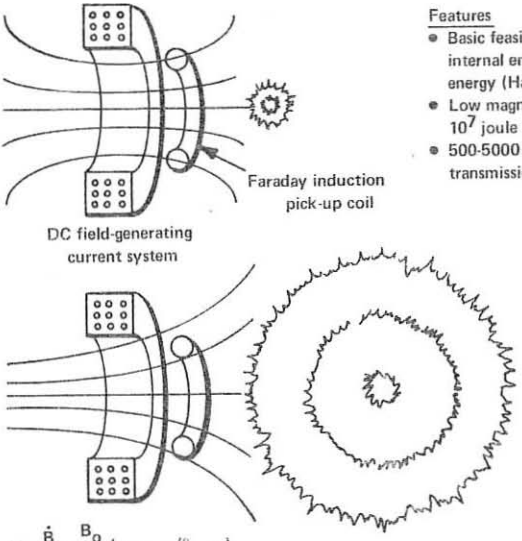

Features

- Basic feasibility demonstrated – $\gtrsim$ 70% of KeV fireball internal energy converted to compressed magnetic field energy (Haught, et al, 1970)
- Low magnetic field intensities suitable – 2-4 Tesla for 10^7 joule microexplosions
- 500-5000 kv, $\simeq$ 1 μsec rise time pulses available for direct transmission line excitation, or for transformation

$$V \propto \frac{\dot{B}}{C} \simeq \frac{B_o}{C} \left(v_{plasma}/\ell_{scale}\right)$$

$$p \propto \left(\frac{\dot{B}}{C}\right)^2 \frac{1}{Z} \lesssim 10^{13} \text{ watts}$$

$(p_{TN} \simeq 10^{18}$ watts)

Figure 14

DESIRED EXOTIC CTR FUEL CHARACTERISTICS

- 1) Reactions involving virtually no neutrons or radioactive elements.
- 2) Fuel reactants cheaply and inexhaustably available.
- 3) Principal energy output in charged particles to allow efficient direct conversion.
- 4) Non-prohibitive $n\tau$ requirements:

  i.e.: $E_{Thermonuclear} \times$ Conversion Efficiency $> E_{External\ Heating}$

  generally requiring:

  $$\dot{E}_{Thermonuclear} > \dot{E}_{Brems} + \dot{E}_{Other\ Losses} \quad \text{[Fuel Ignition Condition]}$$

- 5) Energy generation possible under technically accessible conditions.

Figure 15a

PROPOSED EXOTIC FUEL CANDIDATES

- $p + B^{11} \rightarrow 3He^4 + 8.7$ MeV (WZW): Essentially meets all above conditions.
- $p + Li^6 \rightarrow He^3 + He^4 + 4.0$ MeV (Post): Meets 1-3, but apparently not 4 and 5 (under quasi-thermal conditions).
- $p + Be^9 \rightarrow \alpha + Li^6 + 2.1$ MeV
  $\hookrightarrow D + Be^8 + 0.6$ MeV
  $\hookrightarrow D + D \rightarrow D + T$
  (McNally)
  Meets 2 and 3, but not 1
  Also not 4 and 5 under quasi-thermal conditions
- $D + Li^6 \rightarrow He^4 + He^4 + 22.3$ MeV
  $\hookrightarrow p + Li^7 + 5.0$ MeV
  $\hookrightarrow T + Li^5 + 0.6$ MeV
  $\hookrightarrow D + T$
  { Tritium Breeding Reaction
- Fusion Chains (Jetter, Post, McNally): Potentially meet 2, 3, 4; 1 and 5 in doubt.

Figure 15b

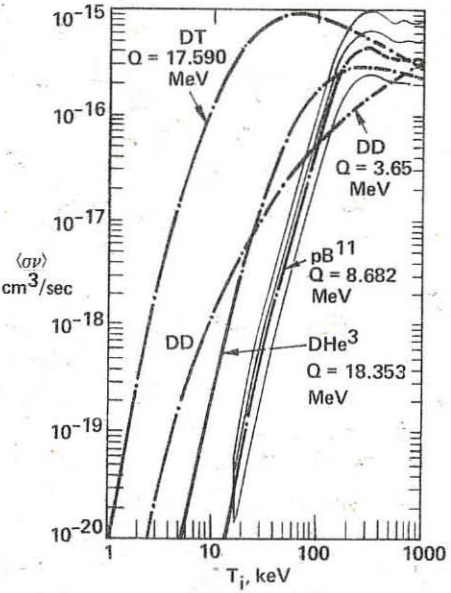

Figure 16: Thermonuclear Reaction Rates
The family of curves for p-B^{11} indicates the uncertainties with which its reaction cross-section and suprathermal burn rates are known.

directly converts both plasma and x-ray energy via exploitation of the neutron- and radionuclide-free nature of exotic fuel burn is shown in Figure 17 [32].

Our view of how the various forms of pulsed fusion energy might be most appropriately converted to electricity is indicated in Figure 18, for both early and advanced systems [32].

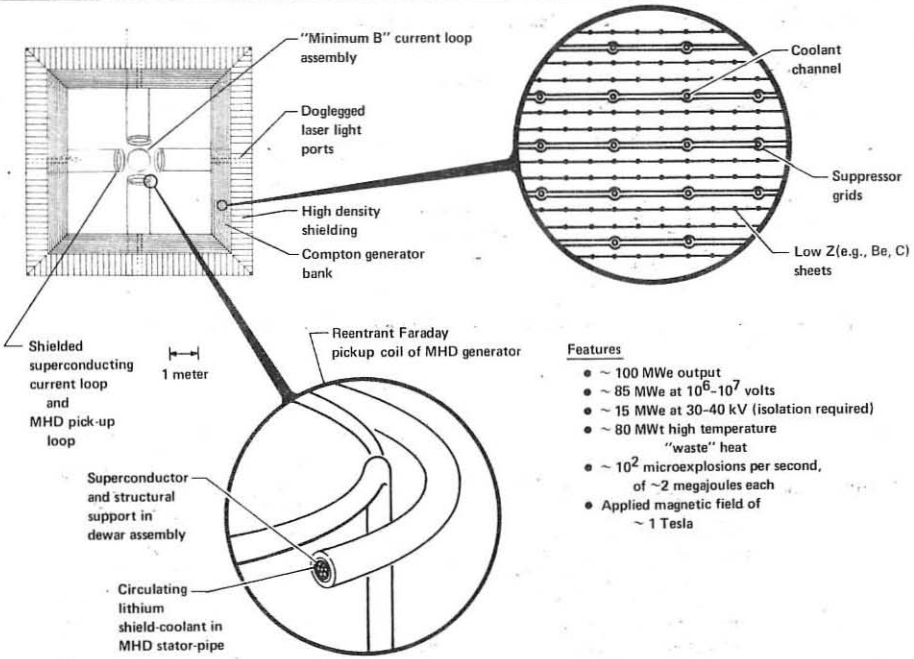

Figure 17

Prospects

In the mid-seventies crucial super-high density laser implosion experiments with be carried out with lasers now being designed. Edward Teller recently emphasized the importance of these experiments—"A third of a century ago, liquids were considered incompressible for all practical purposes. We are talking now about at least thousand-fold compression, if laser fusion is to be practical. This is a challenge which we cannot afford to ignore. I believe that we shall succeed, and that the effort will profoundly change our views of how man and matter can interact." Practical power production also depends on the success of programs now underway to develop pulsed lasers with sufficiently high power, energy, frequency, and efficiency, and on the engineering of economic reactors. We are excited by the challenge of these difficult and complex tasks, and by the prospect that the mastery of fusion may be more important to Man than the harnessing of fire.

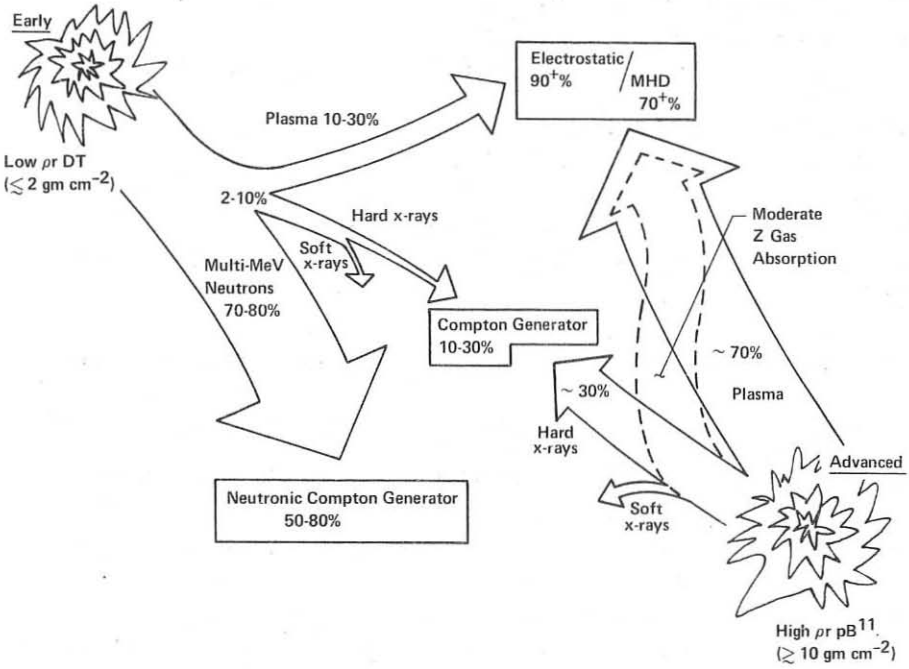

Figure 18: Direct conversion possibilities for early and advanced pulsed CTR power systems.

References

1. R. Hirsch, New Scientist 12, 86 (1973).
2. Physics Today, August 1972 (Search and Discovery).
3. J. Nuckolls, L. Wood, A. Thiessen, G. Zimmerman, Nature 239, 139 (1972).
4. W. Besant, "Hydrostatics and Hydrodynamics", Cambridge (1859).
5. Lord Rayleigh, Phil. Mag. 34, 94 (1917).
6. G. Guderley, Luftfahrtforschung 19, 302 (1942).
7. F. Hawkins, "Manhattan District History, Los Alamos Project", LAMS 2532 (1961).
8. K. Boyer, Astronautics and Aeronautics 11, 28 (1973).
9. W. Daiber, A. Hertzberg, C. E. Wittliff, Phys. Fluids 9, 617 (1966).
10. J. S. Clarke, H. N. Fischer, R. J. Mason, Phys. Rev. Letters 30, 89 (1973).
11. K. A. Brueckner, IEEE Transaction PS1, 13 (1973).
12. S. W. Mead, Phys. Fluids 13, 1510 (1970).
13. N. G. Basov, et al, JETP Letters 15, 417 (1972).

14. G. V. Sklizkov, private communication.

15. E. Teller, Science 121, 267 (1955).

16. J. Nuckolls, L. Wood, A. Thiessen, G. Zimmerman, Livermore Report UCRL 74116 (1972).

17. G. Zimmerman, Livermore Report UCRL 50021-72-1, 107 (1972).

18. S. Bodner, Livermore Report UCRL 74074 (1972).

19. J. Nuckolls, Livermore Report UCRL 74345 (1972).

20. R. Kidder, J. Zink, Nucl. Fusion 12, 325 (1972).

21. J. W. Shearer and J. J. Duderstadt, Livermore Report UCRL 73617 (1972).

22. P. Kaw and J. Dawson, Phys. Fluids 12, 2586 (1969).

23. W. Kruer and J. Dawson, Phys. Fluids 15, 446 (1972).

24. J. Katz, J. Weinstock, W. Kruer, J. Degroot, R. Faehl, Livermore Report UCRL 74334 (1972).

25. L. Wood, J. Nuckolls, G. Zimmerman, A. Thiessen, Livermore Report UCRL 74115 (1972).

26. B. Freeman, L. Wood, J. Nuckolls, Livermore Report UCRL 74486 (1971).

27. L. A. Booth, LASL Report LA 4858MS (1972).

28. A. Haught, D. Polk, W. Fader, Phys. Fluids 13, 2482 (1970).

29. R. Hancock, I. J. Spalding, Culham Report CLM-P310 (1972).

30. S. Braginskii, Reviews of Plasma Physics 1, 205, (1965).

31. T. Weaver, G. Zimmerman, L. Wood, Livermore Report UCRL 74191/74352 (1972); T. Weaver, L. Wood, Livermore Report UCID 16230 (1973).

32. L. Wood and T. Weaver, Livermore Report UCID 16229 (1973); T. Weaver, J. Nuckolls, L. Wood, Livermore Report UCID 16309 (1973).

THEORY AND EXPERIMENT IN LASER DRIVEN FUSION

Keith A. Brueckner

KMS FUSION, INC.

The production of fusion energy from a pellet of thermonuclear fuel can be achieved on a level useful for power production only if the pellet is highly compressed with efficient energy transfer from the external energy source into the pellet. The simple model of a uniformly compressed DT sphere can be used to determine the fusion energy production. Figure (1) gives the ratio of fusion energy output to initial thermal energy for a uniform initial temperature of 5 kev. The energy multiplication, for an initial thermal energy of one kilojoule, is 5 at a density of 300 gm/cm^3, 16 at 600, 40 at 1000, and 80 at 2000. For high energy input on high compression, the energy multiplication levels off at about 200 corresponding to about 35% burnup of the DT. The energy multiplication can be increased if the fuel is only centrally heated to the ignition point of 5 kev, with the rest of the fuel ignited by an expanding supersonic burning front propagating outward from the fuel center. Figure (2) shows a typical example of the propagation of a supersonic burning front. Figure (3) shows the energy multiplication with the fuel center heated to 5 kev over a few micron radius and the rest of the fuel at 500 ev. With an initial thermal energy of one kilojoule, the energy multiplication is 130 at $\rho = 600$ gm/cm^3, 400 at $\rho = 1000$ gm/cm^3, and 700 at $\rho = 2000$ gm/cm^3. The energy multiplication reaches a maximum of about 1200 for initial thermal energy of 5-10 kilojoules, independent of initial

density, corresponding to about 35% fuel burnup. The effect of the centrally-initiated burning wave increases the energy multiplication by about a factor of ten over the uniformly heated case.

Calculations of the implosion of a DT sphere in spherical symmetry show that high compression can be produced by a laser pulse with proper time variation. The pressure driving the implosion is produced by the penetration of energy from the underdense laser deposition region into the dense plasma which results in ablation of the dense pellet surface. The efficiency of this process depends on the efficiency of energy absorption from the laser beam into the underdense plasma and on the subsequent energy partition between the compression of the dense pellet core and the energy removed in the high temperature expanding plasma produced by the ablation process. The latter partition can be estimated from a hydrodynamic model or determined by computer simulation of the energy deposition, energy transfer, and hydrodynamic processes. The result is that 6 to 10% of the absorbed energy is transferred into compression and heating of the dense pellet core.

Detailed computer simulations of the full process of laser coupling for 1.06 micron wavelength, thermal energy flow, hydrodynamics, nuclear reactions, and of the energy transport in the nuclear reaction products and radiation, give results in approximate agreement with the numbers just given. Of particular interest for the experiments now being undertaken by several groups in the USA and other countries is the prediction that the "breakeven" condition, with fusion energy equal to laser energy, can be reached with laser energy of about one kilojoule. This prediction holds, however, only if several conditions are satisfied.

These are:

A. Configuration requirements
   1) laser pulse time variation properly matched to pellet configuration
   2) spherical symmetry of pellet illumination
   3) spherical symmetry of pellet configuration

B. Physics requirements
   1) stable hydrodynamic motion
   2) adequate laser-plasma coupling
   3) absence of appreciable pellet preheat.

If these requirements are not met, the breakeven energy can be very markedly affected. Particularly striking is the effect of a poorly matched laser pulse. The breakeven energy for a square laser pulse and a DT sphere is several hundred megajoules. A drop in compression of a factor of ten as a result of imperfect convergence can increase the breakeven energy by a factor of ten to one hundred.

The configuration requirements on the laser energy variation in space and time, although difficult to meet, can be satisfied with properly designed illumination systems and laser oscillators giving controllable sequences of stacked pulses. The pellet symmetry can also be provided by careful pellet fabrication and selection methods. We have studied the effect of variation in the laser and pellet parameters, using 2-dimensional computer simulation, and determined the allowable departures from complete symmetry. These conditions are imposed on our laser system and pellets.

The problems of the physics of the laser-driven process are too difficult to resolve without experimental results, although very important analyses and calculations have been made.

The stability of the pellet implosion has been studied analytically and by computer simulation, using a 2-dimensional code. The results show stable motion, with initial disturbances not being amplified during the implosion. The laser-plasma coupling presents difficult problems which are of a complexity very familiar for the past two decades in the controlled-fusion programs. Closely associated with the coupling problem is the effect of anomalous laser-coupling on the energy flow into the pellet. Present theories estimate that a wide range of anomalous phenomena can occur which may seriously alter the predictions of the laser-driven process. Experiments are intended to resolve these uncertainties.

We have carried out a number of experiments using a neodymium-glass laser brought to full operation during July of this year. The laser configuration is shown in Figure (4). The laser driving the main amplifier train is a VK800 laser built by CGE, with some modifications and with Owen-Illinois ED-2 glass replacing the original French laser glass. This laser operates reliably on a six minute cycle with an energy output from the 80 millimeter output amplifier of 250 to 350 joules. A considerably higher output is possible, but has not been used because of possible glass damage from self-focusing.

The output from the 80 mm amplifier is expanded to 100 mm diameter and further amplified in seven amplifier modules built by GE. Each module contains three disks of glass at Brewster's angle. The path length of the laser beam in each disk is 3 centimeters and the effective aperture is 122 cm^2. The glass stores 0.32 joules/cm^3 with 8 kev pumplamp voltage and 0.36 joules/cm^3 with 9 kev pumplamp voltage. With 200 joules input with 3 nsec pulse width (FWHM) to the GE system, the measured output from the first six modules is approximately 840 joules at 8 kev flashlamp voltage. The predicted output of seven modules at 8 kev is 990 joules and at 9 kev approximately 1400 joules. The measured gain is in good agreement with the design predictions.

The laser is protected against damage from reflected laser energy by Pockel cell isolators at the entrance to the 16 mm rod of the main amplifier chain, between the 23 and 32 mm rods, by a Faraday rotator between the 45 and 64 mm rods, and by a Faraday rotator at the exit of the GE amplifiers. The protection is adequate against the full output energy reentering the exit end of the GE rotator.

The laser pulse beam from the CGE oscillator is approximately Gaussian with a pulse width (FWHM) of 1.3 or 3 nanoseconds. The pulse is strongly distorted through the CGE and GE amplifiers due to partial saturation of the amplifiers. A pulse-stacking oscillator has been built to replace the CGE oscillator to give controllable pulse beams. The arrangement of the oscillator is shown schematically in Figure (5). This oscillator will be installed by mid-August.

The target area is shielded to allow breakeven experiments at the kilojoule level. The arrangement of the target area is shown in Figure (6). The chamber configuration allows the measurement of X-ray spectra by spectrometers, fast diodes, thermoluminescent diodes, and photographic plates. The neutron production is measured with several calibrated scintillators with large aperture and with time resolution of a few nanoseconds. In addition, the integrated neutron production is measured through silver foil activation. Provision has been made for time-of-flight measurement of the neutron energy spectrum. For measurement of the spectrum from a single neutron pulse, a DT neutron yield of about 10^8 is required.

The illumination system of the present laser configuration is shown in Figure (7). The illumination of spherical targets is uniform to 5-10%, the indicated correction plates perturbing the laser flux sufficiently to give uniform absorbed intensity on the target, after correction for the non-normal incidence. Other lens and mirror arrangements are being completed which will give further improvement in the illumination pattern.

Two-dimensional, cylindrical geometry computer simulations have been made of the response of CD_2 shells to non-uniform illumination by the KMS Fusion laser. Two configurations are shown here. The first is two-sided illumination with two f/2.6 lenses. The second is two-sided illumination with two f/1.0 lenses. The calculated energy absorptions versus angle from the axis of symmetry are plotted in Figure (8) for the two cases. The calculated

plasma distribution at the time of collapse of a spherical 2 μm thick shell of 200 μm diameter is plotted in Figures (9) and (10) for the f/2.6 and f/1.0 lenses, respectively. The grossly non-spherical convergence resulting from the f/2.6 lenses is in striking contrast to the much improved convergence resulting from using f/1.0 lenses.

The reflectivity of targets under intense laser illumination has been the subject of intensive theoretical and computational analysis and of more limited experimental study. The theory of laser deposition predicts two principal classes of instabilities resulting from coupling of ion density waves, electron plasma oscillation, and the incident and reflected laser waves. One class of instabilities resulting from the excitation of transverse ion and plasma waves with wavelength much less than the laser wavelength is expected to increase the laser energy absorption and to produce a marked increase in electron energy together with a strong departure of the energetic electron distribution from Maxwellian. Another class resulting from longitudinal ion or electron density fluctuation, i.e., stimulated Brillouin or Raman scattering, is predicted to lead to a marked increase in reflectivity, possibly saturating at high laser power with reflectivity coefficient approaching unity. The threshold for the instability is expected to depend on target material and the illuminated area and pulse length, the latter since they determine the density

gradients in the region of laser deposition. The thresholds are, however, expected to be reached for one-micron laser wavelength for power in the range of 10^{12} to 10^{13} watts/cm^2, for illuminated areas with characteristic dimensions of the order of 100 microns.

We have measured target reflectivity and electron temperature using an energy output up to 300 joules in a pulse with 3 nanosecond duration (full width at half maximum), delivered on plane CD_2 and CH_2 targets through a f/1.5 aspheric lens giving a measured vacuum focal spot of 60-80 microns diameter. The laser energy incident on the target chamber was measured calorimetrically; the energy on target was obtained by correction for window and focusing lens losses. The reflected energy was measured with fast photodiodes which directly compared a reference signal reflected from the incident laser pulse with the reflected energy from the target. An independent measurement was made calorimetrically of the energy from the target reflected from the 80 mm output face of the output amplifier of the laser. Relative measurements of the target reflections were also made calorimetrically at stations in the amplifier train of the laser.

The apparent electron temperature for photon energies in the 8-12 kev range was measured by a pair of fast diodes with aluminum foil attenuators. More complete measurements over a wide range of photo energies were also made on selected laser pulses using a film detector with graduated aluminum attenuators.

The reflectivity was found to vary rapidly with target position, with the maximum reflectivity associated with the vacuum focus 50 to 75 microns above the target surface. This position also corresponded with the point of maximum hard X-ray yield and with the maximum soft X-ray flux.

The measured reflected energy was that collected by the 8 cm diameter f1.5 illuminating lens. This target reflection was also monitored at 45° and appeared to be very low, in agreement with previous measurements of the angular distribution of the reflected energy. We cannot at the present, however, exclude the possibility that some diffuse scattering occurs, increasing the true target reflectivity over our measurements. Improved reflectivity measurements will be carried out in the near future.

The variation of CH_2 and CD_2 reflectivity with target position for laser energy on target in the range of 100 to 110 joules is given in Figure (11). Figure (12) gives the measured peak reflectivity in CH_2 and CD_2 as a function of laser power on target, for a 80 micron vacuum focal diameter. The reflectivity peaks in the range of 40 to 80 joules on target or 3 to 4×10^{14} watts/cm^2, and drops by a factor of two to three at the maximum energy of 160 joules on target or 10^{15} watts/cm^2. The high peak reflectivity at 3×10^{14} watts/cm^2 may be associated with the onset of stimulated Brillouin scattering and the subsequent drop to saturation of the stimulated Brillouin scattering and the onset of anomalous absorption.

The variation of reflectivity during the laser pulse also clearly shows the onset of markedly increased absorption at high laser power. For energy less than approximately 40 joules, the reflected signal has the same time variation as the laser pulse. As the power increases, however, the reflected signal shows increased absorption, the signal becoming markedly distorted and the reflected power appearing to saturate. The details of the reflected pulse show some pulse-to-pulse variation, probably associated with small displacements of the target position relative to the laser focus. A characteristic pulse form at high power shows a strong late reflected signal following a saturated reflectivity plateau. This is an indication of the rising reflectivity with decreasing laser power for the strongly heated plasma produced by the maximum laser power.

We have also observed neutron production associated with a laser pulse directed on a solid CD_2 target. The neutron production has been observed with laser energy delivered to the CD_2 target in the range of 65 to 175 joules, corresponding to a peak power at the target in the range of 4×10^{14} to 11×10^{14} watts/cm^2. The plane target was positioned at the point of maximum reflectivity which also corresponded with the point of maximum production of hard X-rays. The neutron yield was measured with two plastic scintillators heavily shielded against X-rays, placed at 25 to 30 centimeters from the target. The time resolution of the scintillators was calibrated against a plutonium-beryllium source of known strength and against a beta source giving calibration pulses.

The characteristic signals detected consisted of an initial pulse of hard X-rays (several hundred kev) followed by a neutron pulse at 12-15 nanoseconds after the hard X-ray pulse. Delayed neutrons were also observed following the X-ray pulse by 60 to 70 nanoseconds. In several cases the delayed neutron signal was much stronger than the prompt neutron signal and occurred with a time spread of tens of nanoseconds.

The prompt neutron signals were not observed with laser energy under approximately 50 joules on target and were not always seen at the maximum energies of 175 joules on target. The strongest prompt pulses observed corresponded to several neutrons on the detector. From the detector sensitivity and geometry we infer a total neutron production of 4000 to 8000 , with a weak dependence on laser energy. The time delay of 12-15 nanoseconds from the hard X-ray signal is in agreement with the transit time of the neutron from the target to the detector; we conclude that these neutrons are produced by DD reactions in the target.

The delayed neutron pulse, which is often much more intense than the prompt pulse, might arise from primary neutrons from the target scattered in the chamber walls or from other more localized scattering sources distributed around the chamber. This explanation can, however, be ruled out since 1) the secondary scattered signal can be estimated and is easily seen to be considerably weaker than the prompt signal, and 2) the scattered neutrons should show time delays continuously distributed

from the onset of the prompt neutron pulse to many tens of nanoseconds, in contradiction with the clearly defined delay of 50-70 nanoseconds observed. The delayed neutron pulse is consistent with fast deuterons from the target impacting on CD_2 target debris from previous laser pulses distributed as a contaminant on the exposed inner surfaces of the chamber and on the illuminating lens.

The response of thick deuterated polyethylene foils to the KMS Fusion CGE laser has been computed in two-dimensional cylindrical geometry. The single fluid, two-temperature plasma model is used. Thermal conduction and electron-ion energy exchange are included. Shocks are treated by introducing a von Neumann-Richtmyer artificial viscosity.

The computed peak electron temperatures, θ_e, and neutron production, N, for laser energy outputs, E_L, of 100j, 200j, and 300j are presented in Table I for various spot sizes, R_0. (The spatial distribution of the radiation is taken to be proportional to $\exp[-(r/R_0)^2]$.)

TABLE I - CD_2 FOIL RESPONSE

Pulse Width (ns)	E_L (j)	R_0 (μm)	θ_e (kev)	N
3	100	50	1.2	$8 \cdot 10^2$
3	200	40	1.55	$6.5 \cdot 10^3$
1.2	100	30	2.0	$4.5 \cdot 10^3$
1.2	200	30	2.4	$3 \cdot 10^4$
1.2	300	30	2.56	$9 \cdot 10^4$

Although the computed peak electron temperatures range from 1.2 to 2.56 kev, the peak ion temperatures range from 0.4 to 0.7 kev . Peak ion temperatures are typically obtained in a region, between the critical density surface and the thermal conduction front, where the plasma density is of order 0.02 gm/cm^3 .

The computed neutron outputs of several hundred to a few thousand neutrons for 3 nanosecond pulses containing 100 to 200 joules are in agreement with the prompt neutron measurements. The data does not indicate any need to invoke any anomalous ion heating effects.

The calculated plasma distribution at peak conditions for the 200 joule, 1.2 nanosecond, 30 μm case is plotted in Figure (13). The relatively planar shape of the calculated critical density surface over the spot size can be seen in Figure (13).

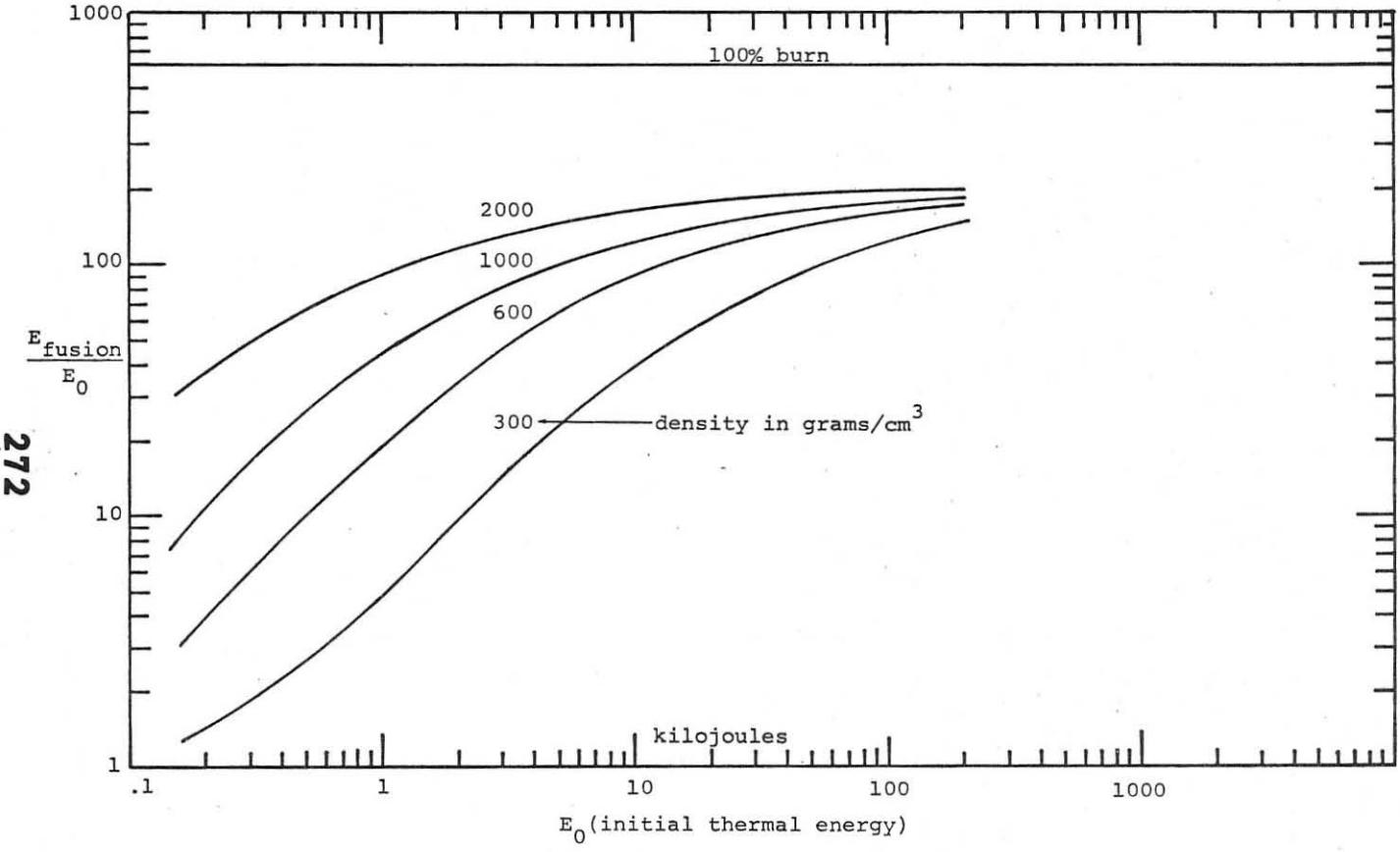

FIGURE 1 - Ratio of fusion energy to initial thermal energy for a uniformly compressed DT sphere initially heated to 5 kev.

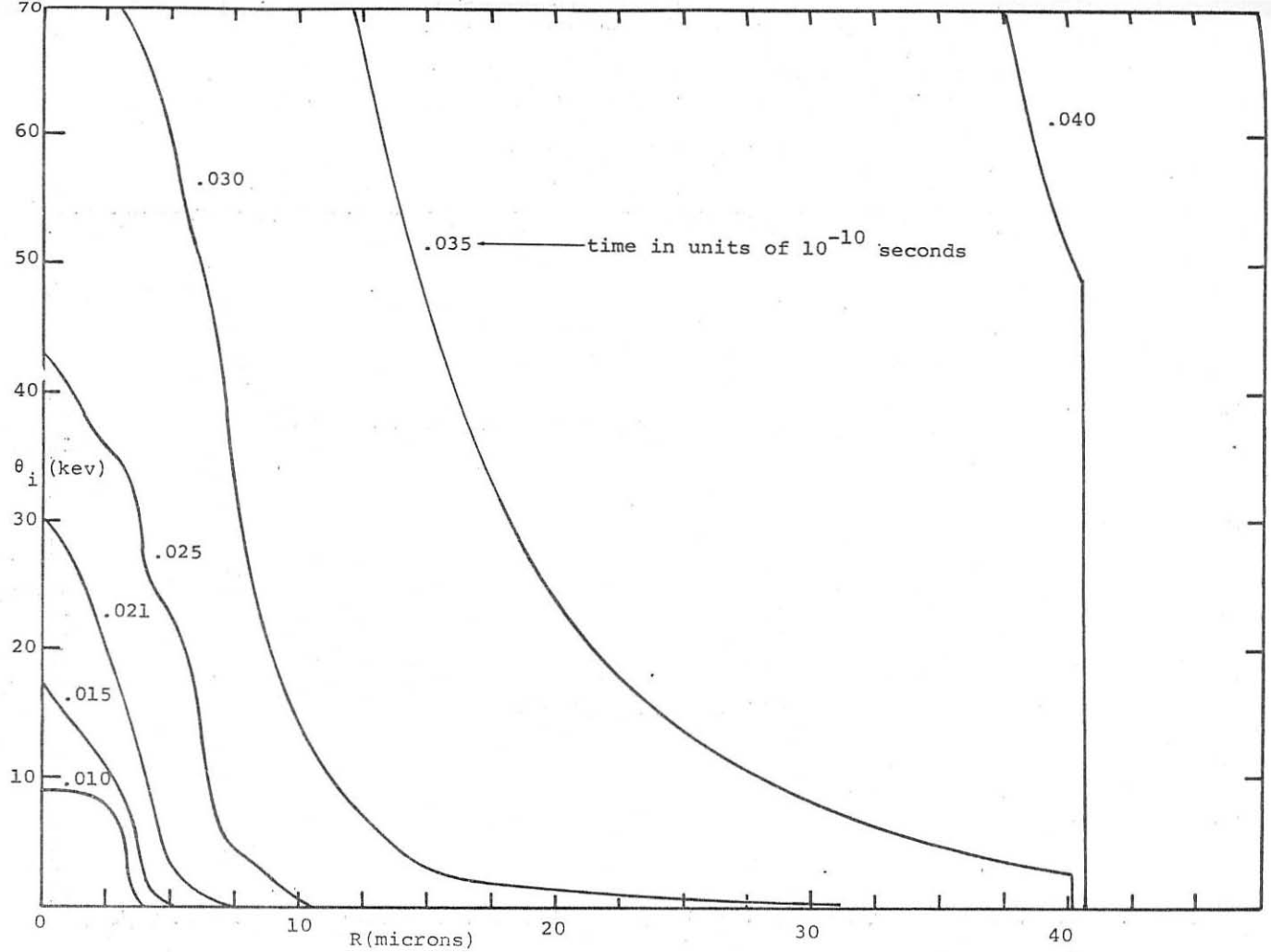

FIGURE 2 - Thermonuclear burning front in DT at an initial density of 2000 gm/cm^3 .

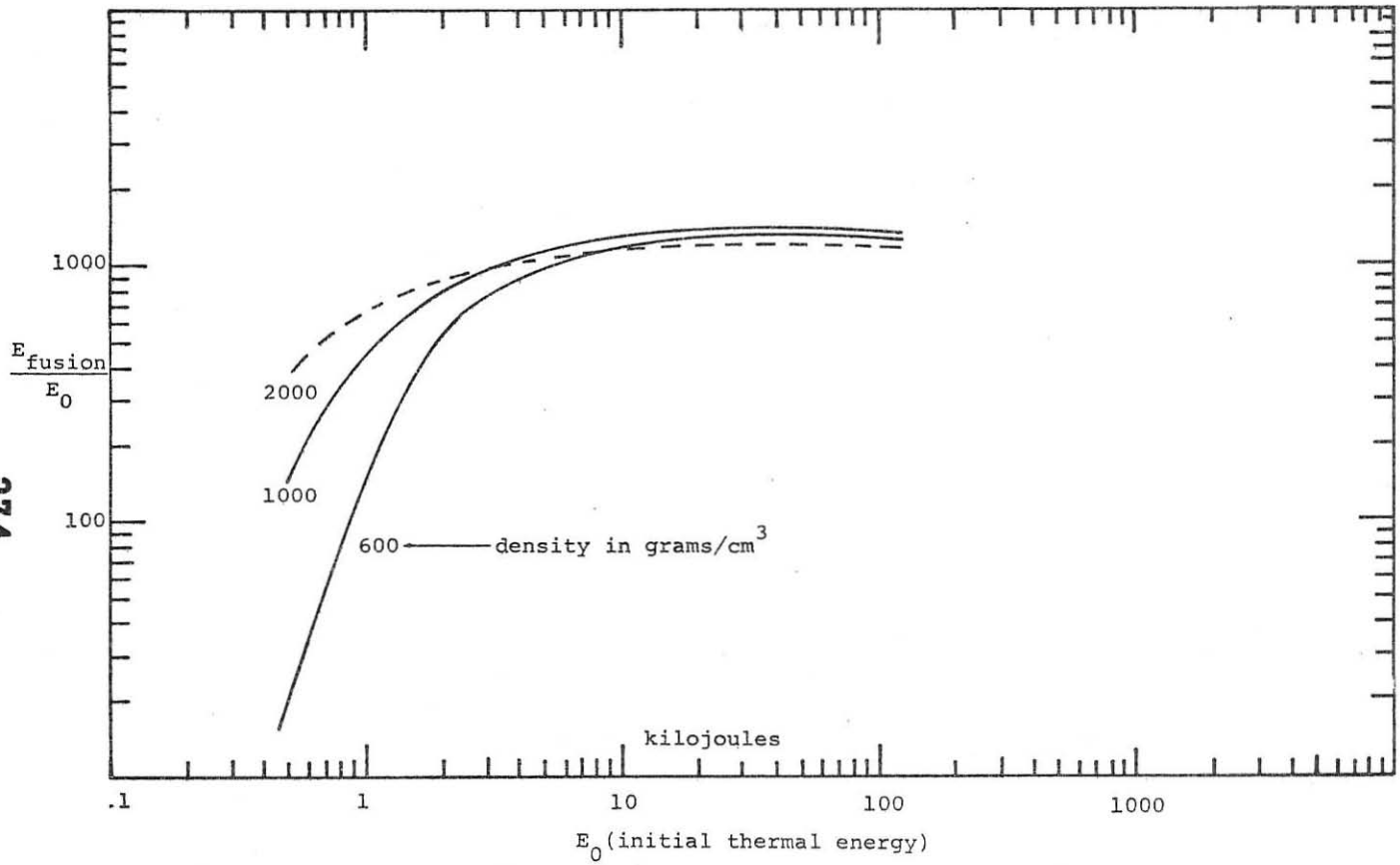

FIGURE 3 - Ratio of fusion energy to initial thermal energy for a uniformly compressed DT sphere initially heated to 5 kev over a few micron radius, with the rest of the DT at 500 ev temperature.

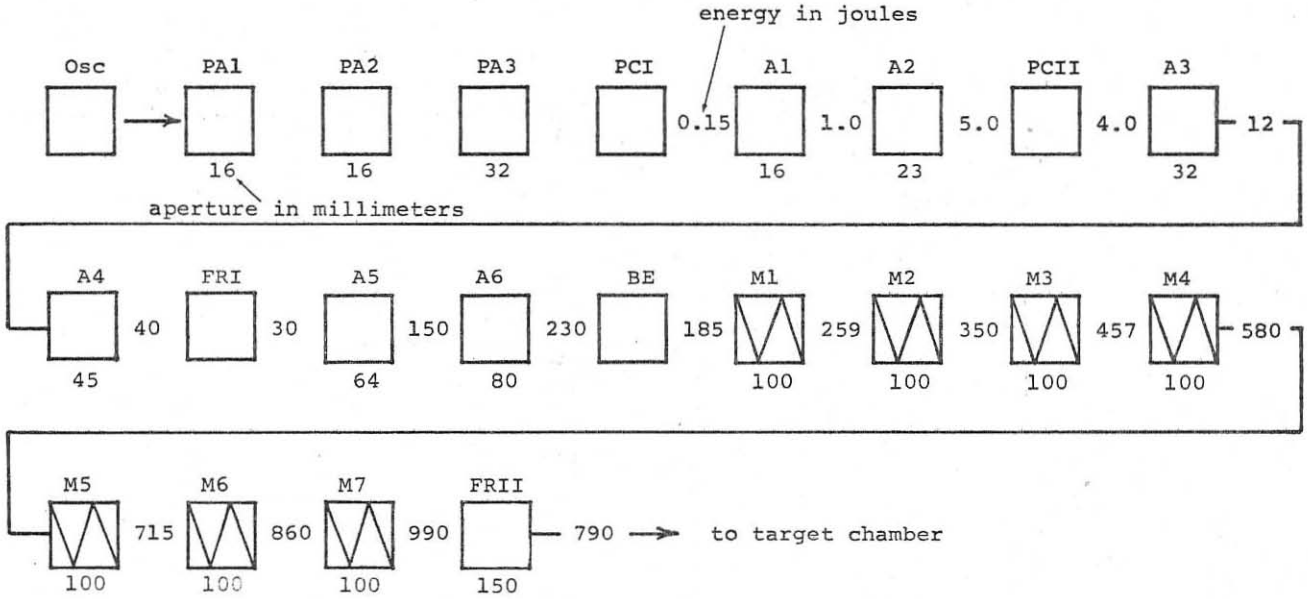

PA ≡ Preamplifier
PC ≡ Pockel Cell Isolator
A ≡ Amplifier
FR ≡ Faraday Isolator
M ≡ Disk Amplifier Module

PRESENT CONFIGURATION
AND GAIN AT 8 KEV
ON DISC AMPLIFIERS

FIGURE 4 - Configuration of KMSF laser.

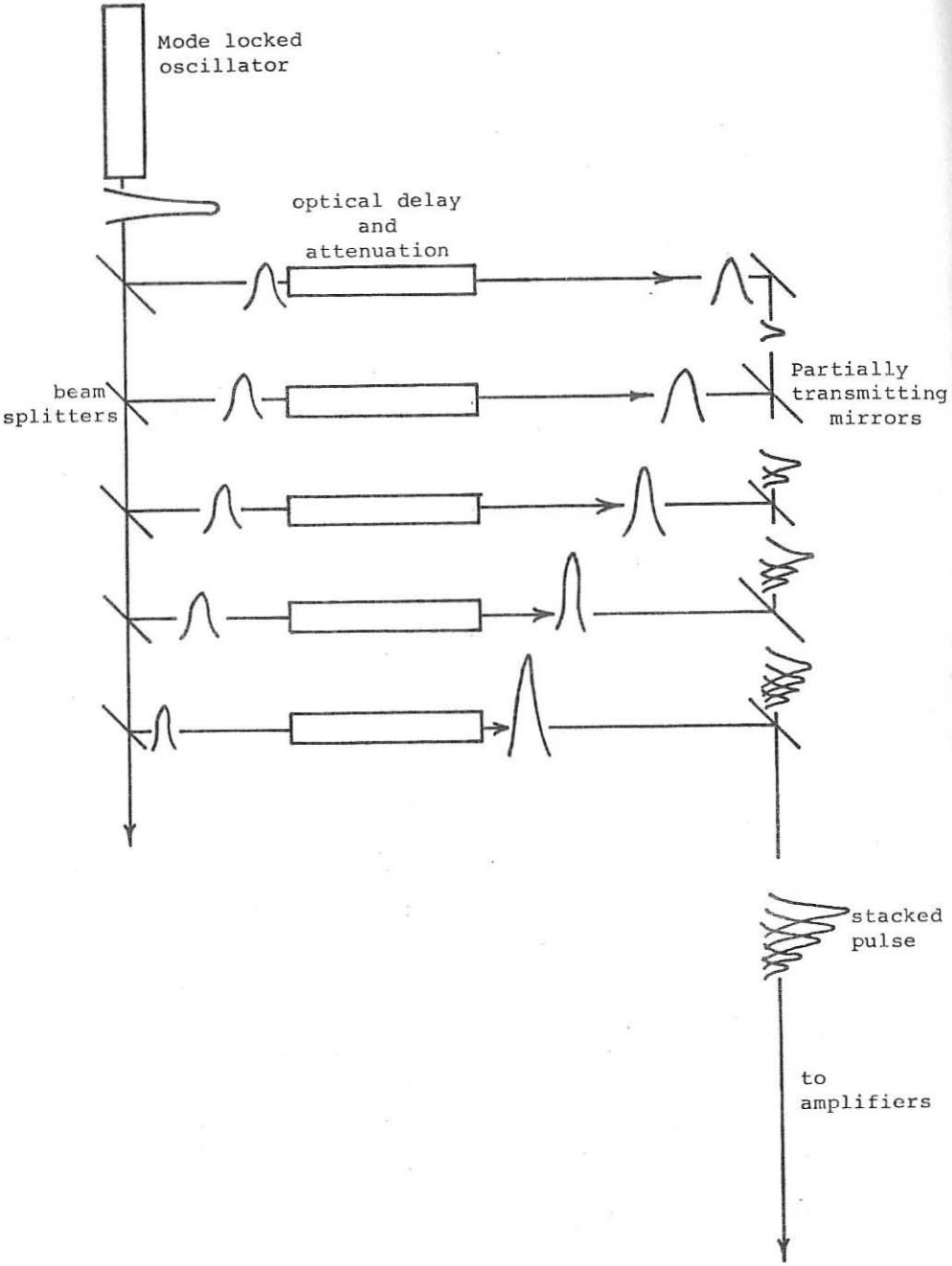

FIGURE 5 - Schematic layout of pulse stacker.

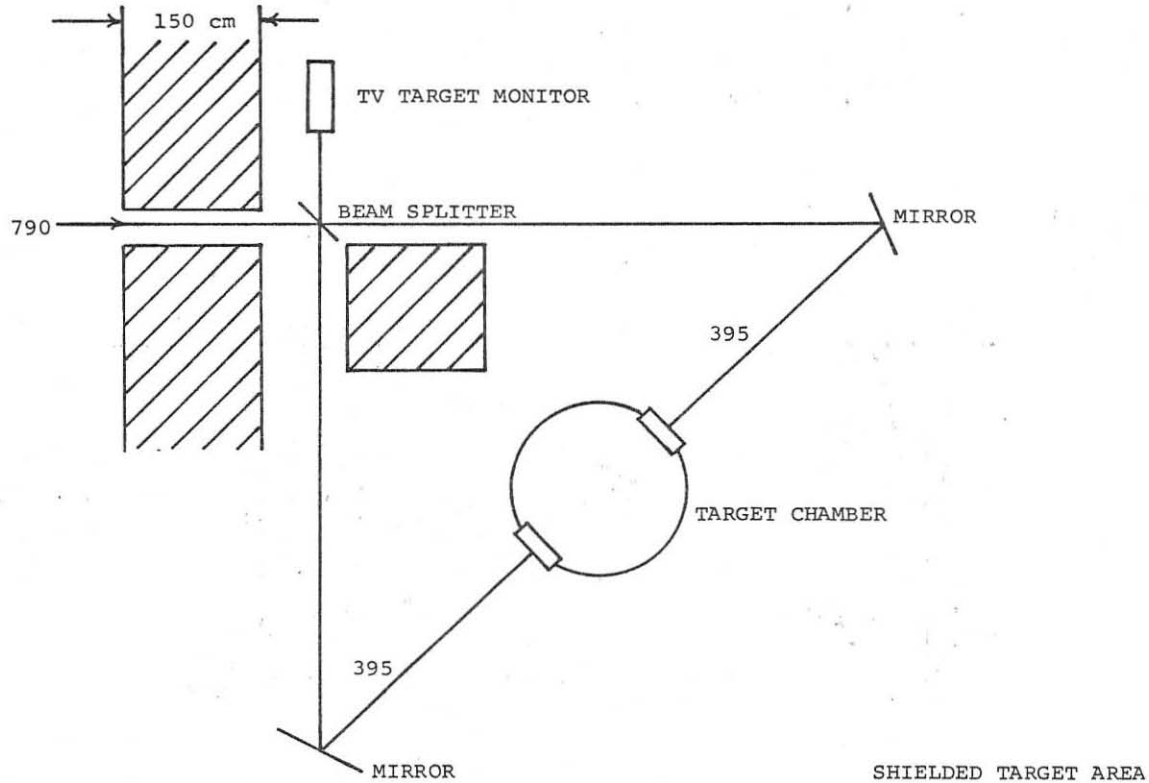

FIGURE 6 - Arrangement of target area.

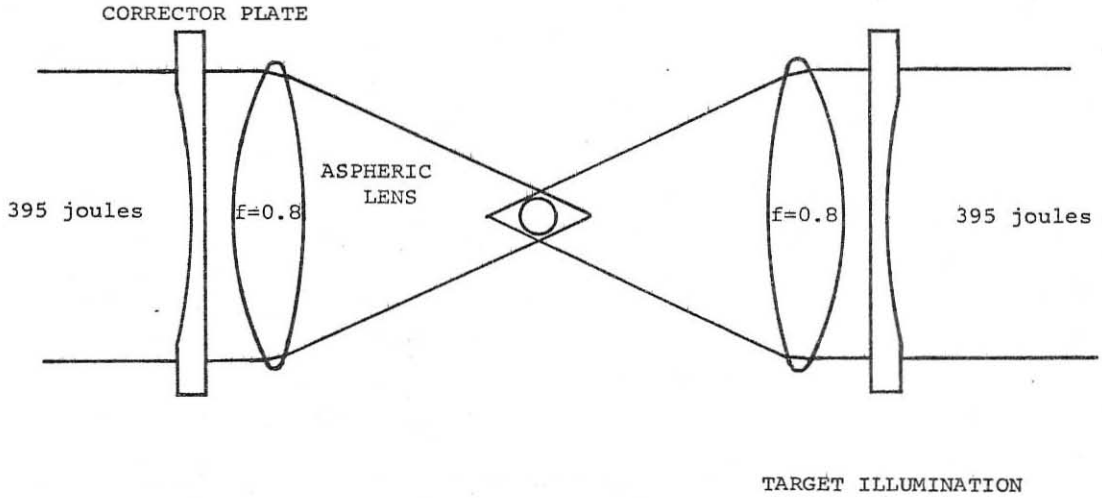

FIGURE 7 - Illumination system.

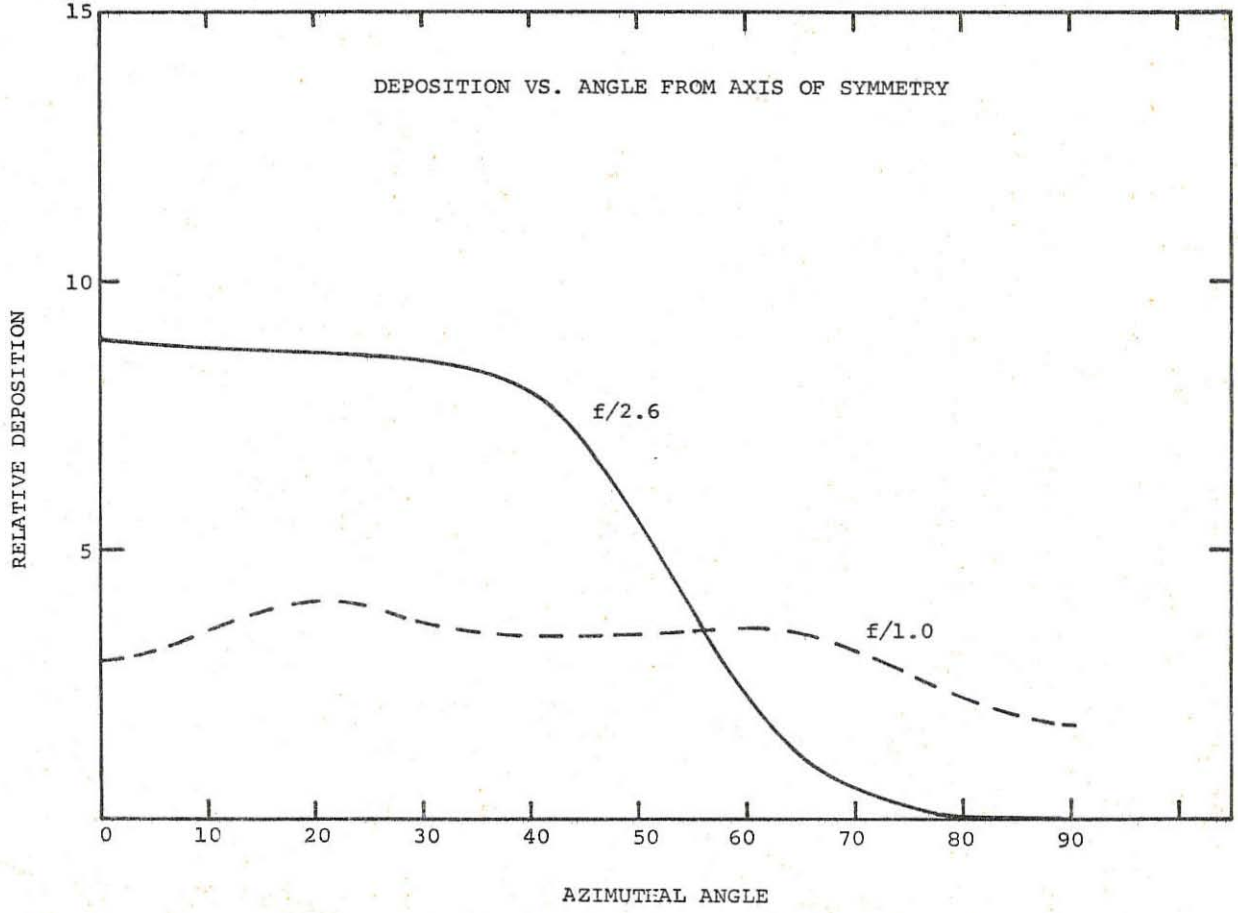

FIGURE 8 - Calculated energy absorption for two lens configurations.

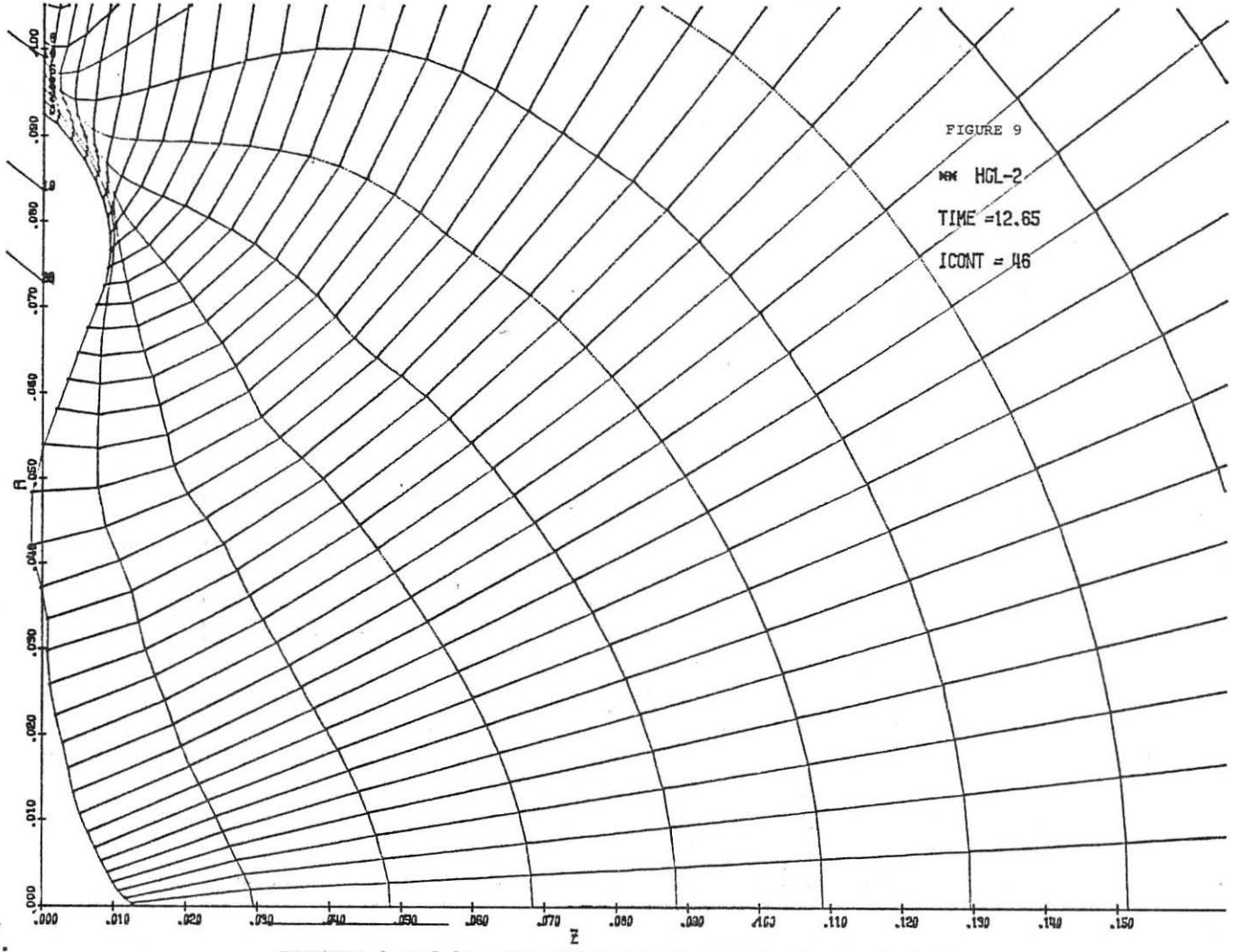

FIGURES 9 and 10 - Two-dimensional calculations of shell implosion. Dimensions are given in millimeters. The time unit is 10^{-10} seconds.

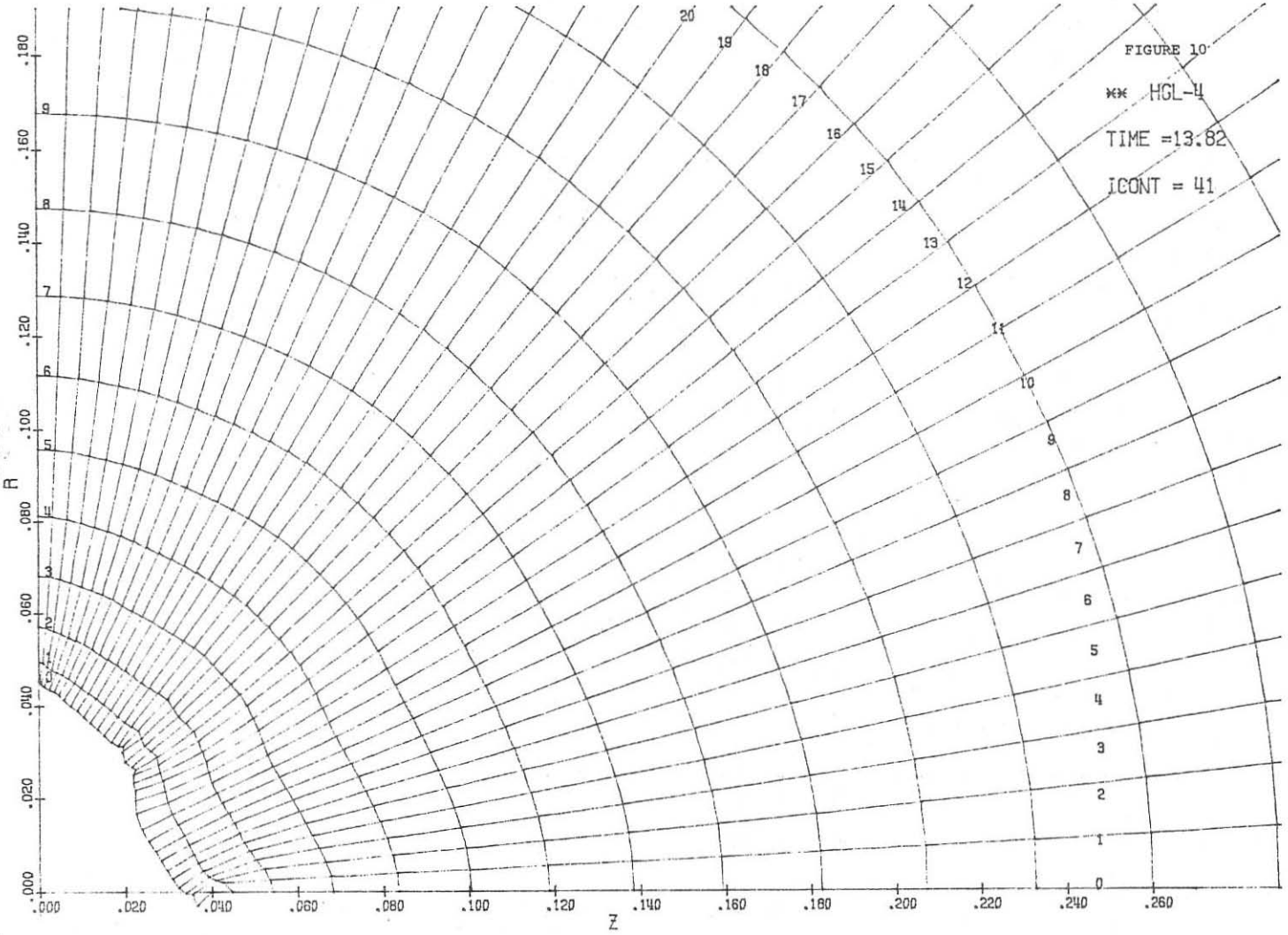
FIGURE 10
** HGL-4
TIME =13.82
ICONT = 41
R
Z
.000
.020
.040
.060
.080
.100
.120
.140
.160
.180
.200
.220
.240
.260

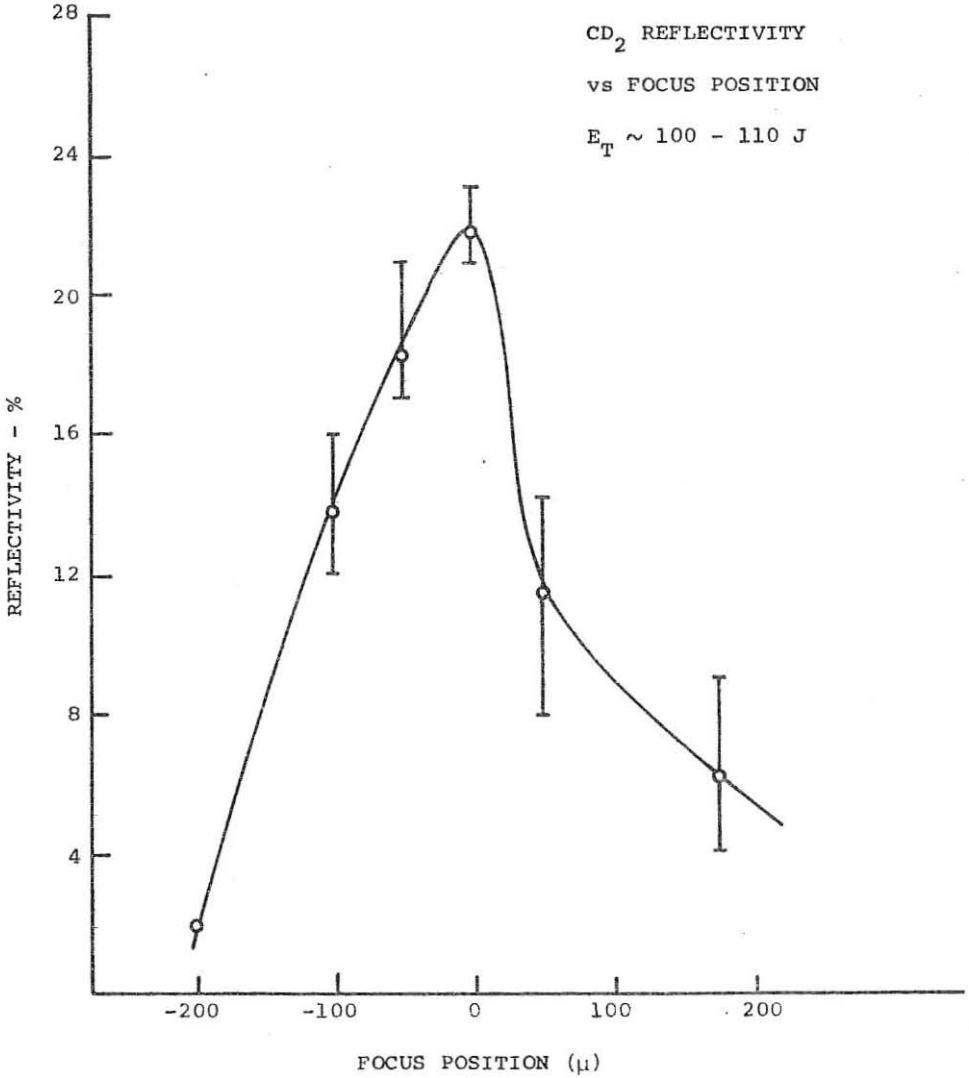

FIGURE 11 - Variation of target reflectivity with position.

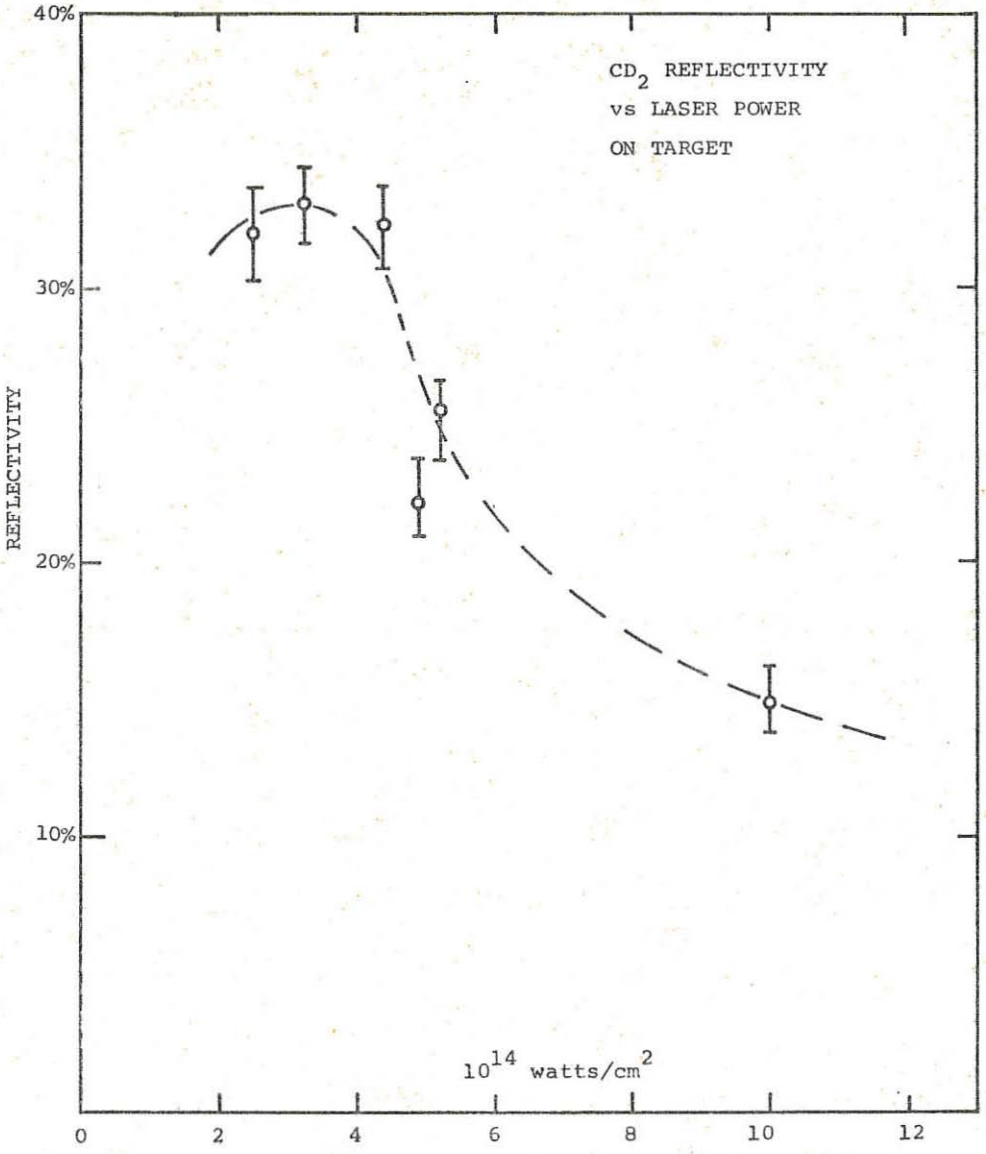

FIGURE 12 - Variation of target reflectivity with laser power.

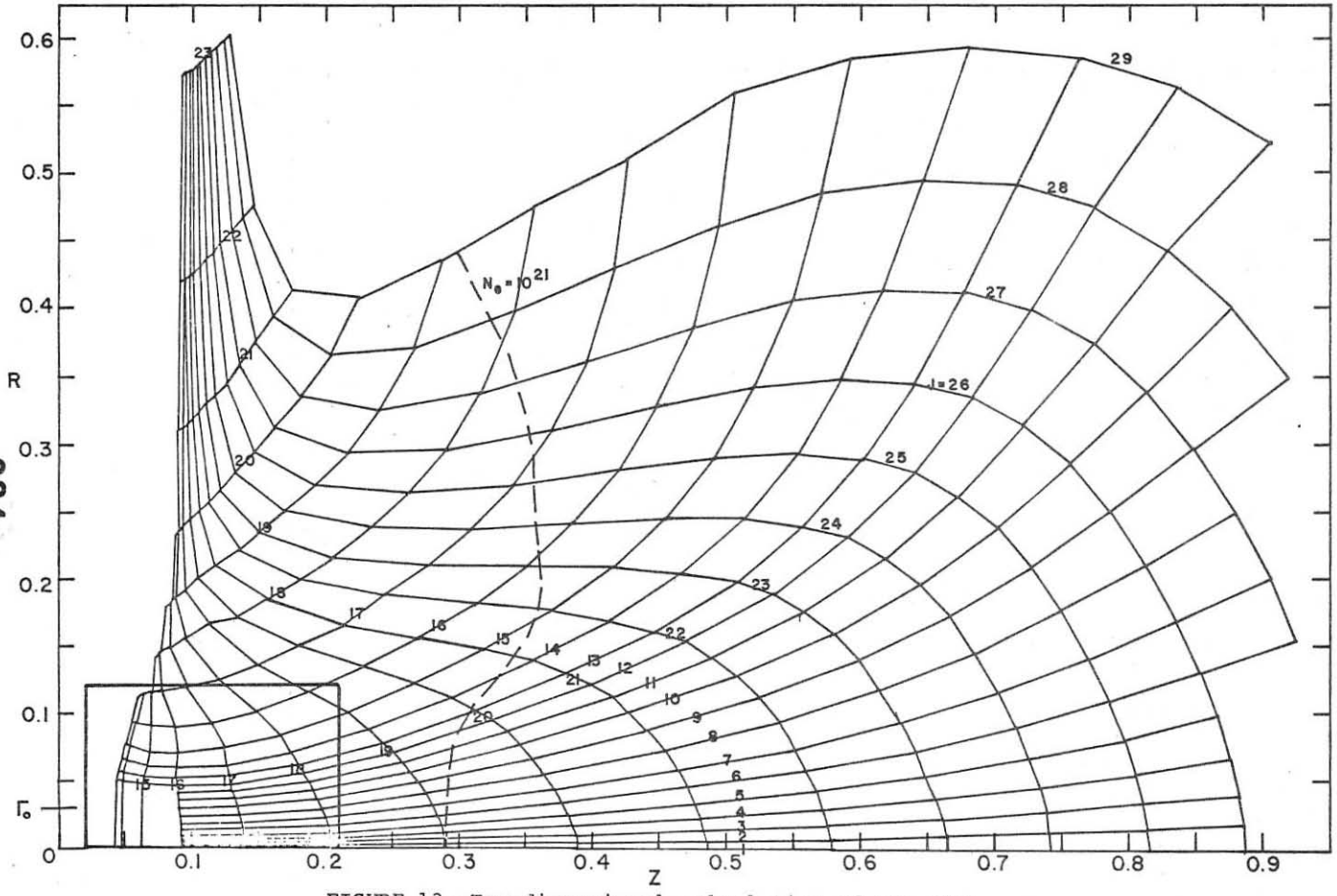

FIGURE 13 - Two-dimensional calculation of CD_2 slab illuminated by a Gaussian laser beam. The dimensions are given in millimeters. The time unit is 10^{-10} seconds.

PLASMA ACCELERATORS

A.I.Morozov

I.V.Kurchatov Institute of Atomic Energy
Moscow, USSR.

A machine that produces fast quasineutral flow of ions and electrons we call a plasma accelerator (PA). In a such flow an average directed velocities of ions and electrons are approximately equal. Hence an ions carry main part of the total Kinetic energy store. At a velocity range $V \lesssim 10^8$ cm/sec that is of interest for the fusion purposes an expenditure for the electron acceleration are small relatively as well as absolutely ($\lesssim$ I e.v).

So one can call plasma accelerator as a machine for the ion acceleration under quasineutrality conditions. A physics of the PA in distinction of the plasma throne physics is quite adjacent to the high temperature plasma physics. This is plasmadynamics of high velocities as soon as ionization and radiation processes are of minor importance.

The role of the PA in the development of physics and technics will grow.

One can see it in Fig.1 where typical regions of the gasdynamics, mechanical systems, charged particles accelerators and PA are indicated in the density-energy frame. The development of PA is of great importance not only by itself but also from the standpoint of general plasmadynamic progress.

Acceleration processes and electrostatic field in plasma

There are two approaches for analyzing the main problem of jusion - plasma confinement problem: a motion of an independent particles is investigated or an equilibrium MHD configurations are studied. Just the same can be made for the PA analysis.

At first some remarks concerning MHD approach to PA problems.

Basic equation of motion

$$\rho \frac{d\vec{v}}{dt} = -\nabla (P_i + P_e) + \frac{1}{c} \vec{j} \times \vec{H}$$

has intertial term, in distinction of the confinement problem equation.

In this survey I shall detally deal with the electromagnetic accelerators only for which a pressure gradient term. is relatively small. Another difference of the accelerator problem in comparison with the confinement problem is a Hall effect term in the Ohm law equation, i.e. essential difference in the electron and ion components behaviour.

The picture of processes inside an accelerator becomes more clear if one starts from eq. (1), but from analysis of the every component dynamics, i.e. uses two liquid plasmadynamic equation. Let us start from the equation of an ion motion

$$M \frac{d\vec{v}}{dt} = -\frac{\nabla P_i}{n} + e\left(\vec{E} + \frac{1}{c}[\vec{V_e}\vec{H}]\right) + \frac{e\vec{j}}{\sigma}$$

An ion can be accelerated either by the ion pressure gradient (∇p_i), by the electron friction ($\frac{e\vec{j}}{\sigma}$) or by the electrical field (E). A Lorentz force does not change an absolute value of velocity and if cannot be related to accelerating forces.

There are peculiar PA which operate due to the every of above mentioned forces.

But I shall concern only those PA for which p_i and terms are small and ions are accelerated by an electrical field. For this case let us write approximated equation:

$$M\frac{d\vec{v}}{dt} = e\left(\vec{E} + \frac{1}{c}[\vec{v}\vec{H}]\right)$$

It should be emphasized that our reduction does not put any limitations on the density of flow. Electrical acceleration is realised at any density and usual electromotor serves as good example. An electrical field in a plasma is weakened due to the high mobility of electrons. So, to clarify existence conditions of the electrical field in quasineutral plasma, let us write down equation of electron component motion ($n_i=n_e=n$)

$$m\frac{d\vec{v}}{dt} = -\frac{\nabla P_e}{n} - e\left(\vec{E} + \frac{1}{c}[\vec{v}\vec{H}]\right) + \frac{e\vec{j}}{\sigma}$$

If there is no renaway in the system, the electron inertia term can be discarded. Neglecting ohmic resistivity of plasma one gets simple equation for electrical field:

$$\vec{E} = -\frac{1}{c}[\vec{v}\vec{H}] - \frac{\nabla P_e}{n} \qquad (5)$$

From this basic equation one can see two extreme approximations

a) $\vec{E} \approx -\frac{\nabla P_e}{n}$

b) $\vec{E} \approx -\frac{1}{c}[\vec{V}_0\vec{H}]$

In the first case electrical field is formed by the electron pressure. Electron pressure acceleration is realised in so called nonisothermal accelerators of which some systems developed by Consoly (with UH electron heating), Semashko and Kuznetsov (with high-voltage injector) and Demirkhanov et al., Gabovich etc, are well known [1].

I shall not deal with these systems detally but I'll try to consider the second case which seems to me more general. In this approximation electrons are frozen and any motion along E is confined by the Lorentz force. Hence we can call such systems as Lorentz ones,

or systems with overequilibrium electrical field.

Everywhere below we shall consider stationary systems with electrostatic field. For such case $E = -\nabla\varphi$ and magnetic force lines are equipotential. ($dt \quad \nabla Pe \to 0, \quad \dot{\gamma}/\sigma \to 0$)

We can write down this fact as $\varphi = \varphi(\gamma)$ where γ is the magnetic force line index. As it is seen from (7) the drift of electrons is needed to maintain nonequilibrium electrical field obviously. The drift of electrons occurs aloud the surfaces $\varphi(\gamma) = \text{const}$. The condition of magnetic force lines equipotentiality determines the potential value along the line itself, but it says not about potential change while transition occurs from one line to another. Two different situations are possible:

a) magn. force lines are closed and do not cross the walls of the plasma chamber, where the flow passes. Such situations are realised for instance in coaxial guns, magnetoplasma compressors and so on (Fig.2a).

b) All magn. force lines (are) cross the chamber walls. Due to the limitations I shall confine myself with the second case (b). In these systems the dependence $\varphi(\gamma)$ is specified either by dissipation processes (which we neglected in (8) or by the boundary conditions. Having installed along the walls the mozaic of electrodes with proper potential distribution it would be possible therefore to obtain for the second case (b) any orbitrary dependence $\varphi(\gamma)$. Then, even weak interaction of flow with walls given the potential of the force line equals to the potential of corresponding electrode (with an accuracy order of KTe). It is obvious that at such supposition the equipotentiality condition (8) determines the electrical field in all volume of plasma, just as Laplace equation $\Delta\varphi = 0$ determines its distribution in a vacuum.

The most various electrical field structures can be formed in plasma by the change of the magnetic field geometry and potential distribution along the walls. One can therefore perform any transformation of the ion flow: acceleration, focusing, separation, deceleration (recuperation), confinement and so on. We shall consider a set of some peculiar systems based on above mentioned principles. Now let us make some general remarks.

First of all - about electron drift .

We have underlined that drift is principall necessary for maintenance of the nonequilibrium electrical field. The simplist way for supporting the drift is to use axially symmetrical magnetic field without asimuthal component ($H_\theta=0$).

For the steady state symmetrical conditions the electrical field has no asimuthal component, sequently the electron drift will be closed.

If magnetic field is descripted as function of the magnetic flux Ψ (where $H_r = -\frac{1}{r}\frac{\partial \Psi}{\partial z}$; $H_z = \frac{1}{r}\frac{\partial \Psi}{\partial r}$) , so one can write $\varphi = \varphi(\Psi)$ (10)

If a system has no axial symmetry (for instance, due to the asymmetrical fuel feed), it is possible to demonstrate the coincidence of surface of constant electrical potential, the drift surface and surface described by formula for the constant electrical potential surface, drift surface and surface

$$W = \int \frac{n\, d\ell}{H} = \text{const}$$

are the same ones. (We assumed $T_e \to 0$ and no electron losses to walls). Magnitude W is generalization of the well known in the theory of flat MHD flows parameter of frozen electrons $\varkappa = \frac{n}{H}$ and so called specifie volume of the magnetic pipe (tube) $U = \int \frac{d\ell}{H}$

The second remark concerns finite value of Pe . The matter is

that in the many cases the influence of the electron pressure is noticeable though not crucial.

If we assume the temperature to be constant along the magnetic force line (what is but natural for very wide range of parameters)

$$Te = Te(\gamma) \qquad (12)$$

so from (5) if follows that "thermalization" potential is constant along the line also

$$\varphi_*(\gamma) = \varphi - \frac{\kappa Te(\gamma)}{e} \ln \frac{n}{n_0}$$

Here n is relevant value of plasma density, n_0 is arbitrary constant.

Some general remarks will be made further.

Plasma lenses.

Above considerations were demonstrated most clearly by Zukov in his experiments with so called plasma lense. As it is known there are two simplest vacuum lenses: electrostatic and magnetic. The first one represents a ring with some voltage applied (Fig.3a). Its focusing distance is given by formula:

$$F_E = R \cdot \frac{128}{3\pi} \frac{Wi^2}{(eU_F)^2} \qquad (14)$$

Here R is ring radius W_i - ion energy.

For argon ion source at energy 10kV, R=5cm and U_F =1kV we get focusing distance F_E =68 metres. This is very big distance. Besides this lense is always converging with no respect to the sign of U_F, because F_E dependes on square of focusing voltage. Finally, this vacuum electrostatic lense has spherical aberration, that principally can not be excluded.

A magnetic lense in its simplest type also represents a current-

bearing ring (see Fig. 3b).

Focusing distance is given by formula

$$F_H = R\frac{16}{3\pi^3}\frac{MC^2}{e^2}\cdot\frac{C^2 W_i}{\mathcal{J}^2}$$

For the same parameters of ring at 1000 amper turns, focusing distance will be $F_H \simeq 350$ m. If the voltage will be applied to the ring under bias magnetic field for rarefied non compensated beam focusing distance is nevertheless very large $\sim F_E$. But the picture will change crucially if dense enough ion beam is treated and a quasineutrality is achieved.

Due to the above mentioned equipotentiality of the magnetic force lines the electrical field undergoes rearrangement and focusing power in changed. The focusing distance decreases to 25 cm and lense can be converging as well as diverging with respect to the sign of the voltage. By means some brush comb of electrodes (see Fig. 3c) the control of the potential distribution of the magnetic force lines is possible and one can get rid of spherical aberration.

The plasma lense focusing distance is given by formula [1]

$$F_{pe_1} = R\left(\frac{W_i}{eU_F}\right)\theta$$

where θ is some magnitude order of 1 depending on magnetic field geometry and potential distribution across magnetic force lines i.e. along the electrodes of comb.

The formula (16) was proved in experiments with the flow density and magnetic field high enough to have Debye radius and Larmor radius considerably less than lense hole. It is well seen in Fig.4a, 4b which reveal constant F_{pe} at $n > n_{er}$ $\cup$ $H > H_{er}$

It is obvious that lense with focusing distance calculated from (5') is electrostatic. Following conditions are featuring, for it

$$R_{el} \ll R$$

$$R_{il} \gg R$$

where R_{el}, R_{il} are Larmor radii of electrons and ions.

We promised to deal with PA of following conditions magneteforce lines of the external magnetic field cross the wall of chamber; the drift is closed, and ∇p_e, ∇p_i, $\nu/\sigma \to 0$.

Up to now only closed drift PA were investigated in which potential distribution was performed by the two electrodes. More complicated systems if made were not studided deeply enough.

We subdivide all published Kinds of closed drift PA on three classes.

a) accelerators with anode layer

b) one lense accelerators

c) many lense accelerators.

Accelerators of "a" and "b" Kinds are studied detally despite they did not work with hydrogen fuel.

a) Anode layer accelerator [1]. The idea of this accelerator was advanced by Zarinov and consists as follows. Let us consider some metallic box-ionizator with some "Foreward" emitting surface. This box is under high ($\sim$1-20kV) positive potential U_o and is placed between earthed magnetic poles producing magnetic field order of some kilogausses (Fig.5a). It was revealed that near ionizator (anode) a quasineutral layer with thickness "d" of order of electron cyclotron radius $R_{e\lambda}$ was created. $R_{e\lambda}$ is determined by magnetic field value and applied voltage. Inside the layer all the potential drop occurs and electrons are drifting perpendicularly to E and H. This layer proved to be very stable though a level of the small-scale noises is considerable. Nevertheless, the system keeps high voltage very well. A.V.Zarinov and collaborators succeded to obtain flows of heavy ions (thallium, bismuth) with densities up to $0.3^a/cm^2$ at interelectrode voltage $\sim 2 \div 10$kV.

The applied voltage governs an ion exit energy, the energy jitter is small.

The magnitude of an accelerated ions current equals to current generated by source. The current density of the accelerated ions is essentially more than predicted by "3/2" law of Lengmuire, that is due to the space charge compensation by electrons. This system can operate without special ionization, though with worse parameters. Accordning to theory and experiment for this case ionization occurs in anode layer with thickness growing to value

$$d = Re\lambda \sqrt{\frac{\nu_{ef}}{\nu_o}}$$

where ν_o - ionization frequency
ν_{ef} - effective collision frequency.

Operation of above accelerators was studied detally in "Ion magnetron" geometry (Fig.5b). Some drawbacks of the anode layer accelerators are large values of electrical and magnetic fields and necessity to arrange all sistem precisely. Nevertheless it seemed very useful to test anode layer accelerators on hydrogen.

b) One lense accelerators.

One lense accelerators were made as systems for which one tried to avoid large E and H fields and to eaneel precise arrangement. It was interesting also to check a possibility to make an accelerator with elongated electrical field ($L >> Re\lambda$). Stretched accelerating zone permit to use small values of el. and magnetic field and facilitates to control the field structure [1].

For two-electrode system the elongation of accelerators zone may be done by change the metallic chamber for dielectric one (Fig.2b)

But an elongation evidenty complicates the dynamics of electron component because here, in distinction of the anode layer accelerator collisions play essemtial role.

A long channel puts some demands on ion flow focusing because other way many particles will be lost on walls.

A focusing is achieved by special lense-like geometry of the magnetic field, as it shown in Fig.2b. Due to the equpotentiality of the magnetic force lines an electrostatic lense is formed that focuses the ion flow.

The first experiments with the one lense accelerator model proved its efficiency. The accelerator operates as follows: driven substance (gas, vapor) is feeded to the gas distributing anode and through a boles reaches accelerating channel. There it is ionized inside the electron cloud. Electrons are drifting in the crossed electric and magnetic fields. Typical values of T_e equal to 8 15eV.

The ions formed are extracted and accelerated by electrical field and then ions leave channel because channel bugth is much less than ion larmor radius. $R_{iL} >> L$

Of course, $R_{eL} << L$. Outgoing flow is compensated by electrons from the plasma cathode. Typical voltamper dependence for the discharge is shown in Fig.7. Typical accelerator diameter that produces ion flow of N, Ar, Xe at 10A current is order of 10cm. Magnetic field value - 200g.

In distinction of the anode layer accelerator this one lense P.A. is well operating at low voltage 1kV (At higher voltage a machine was not studied). Inside these accelerators the electrons have considerable movability mainly due to the electron fluctuations (noise). Electrons current amounts to (0,1 ÷ 0,5) x I discharge.

Just this movability is responsible for achievement the distribution $\varphi(\gamma)$. It turned out that usually inside the channel $E \sim H$ A study of the oscillations in 1mhz range revealed some peculiar features. Structure of oscillations depends on way by which the magnitude $W \equiv \int \frac{n d\ell}{H}$ changes along the channel.

A theory and experiment show that for W decreasing along the channel, the nondissipative potential oscillations are stable. (We call this regime a "positive field gradient" $\nabla H > 0$ regime). On the contrary, if W is increasing ($\nabla H \lesssim 0$), the plasma is unstable. A local investigations showed rotating with constant velocity "Equipotential shift" surface at $\nabla H < 0$. Typical frequencies of this zotations $\sim 20 \div 70$ KHZ .

In the analogous conditions but with positive magnetic field gradient usually small-scale irregular pulsations are observed. These pulsations have maximum of the spectrum at frequency time of flight

$$f \simeq \frac{v_{max}}{h}$$

It should be underlined that all above mentioned remarks relate to the "saturated" part of the voltamper dependence.

In the regimes with "noise" ion energy is $^2/_3$ of the discharge voltage and spectrum width is $^1/_3 U_0$.

The results of the experimental study of the time of flight oscillations showed these oscillations are not due to the instabilities of the whole plasma volume. They are activated by the "active" boundary conditions or by the right - wing parts of the perturbation equations. In the one-lense accelerator case "activity" of the boundary conditions is detemined initially at the entrance by the ionization and finally (at the exit) - magnetic field decreasing. ($\nabla H < 0$).

The right-wing parts in the small perturbations equation can arose due to the particles losses on walls and due to the ionization in channel.

As the recent investigations revealed the effective method for the operation improving is accurate choice of magnetic field with positive gradient. It allows to improve the electrical field structure (on terms of the ion flow focusing) and ionization zone structure. All it permits practically separate the beam from the walls, to supress the flight-time instabilities to correct field geometry and energetic spectrum of ions.

Let us notice recently shown possibility for the suppressing of the potential oscillations by virtue of the special fixers of potential which mounted on the walts [1].

Many lense accelerators

It was rather difficult to get hydrogen ion flows in the one-lense, two-electrode, accelerator because of poor ionizingability of the hydrogen. A simple calculations show that for H_2 and K_e the equal length of ionization zone will be at feeding ration (expressed in particles per second) ~ 100 at $T_e \sim 10$eV. As soon as power level needed for discharge firing at such conditions (i.e. without additional ionization systems) reaches hundreds of Kilowalts, we developed quasistationary two-lense accelerator. This accelerator was described widely, so I will not add anything I'll notice only that many-lense systems open new facilities in terms of flow focusing.

In the one-lense accelerator, we have only electrostatic focusing But in the many-lense P.A. strong magnetic focusing turns out to be effective. A transverse oscillations in this case are given by equations (for large lense number)

$$\ddot{y} + \Omega^2 y = 0 \qquad (20a)$$

where $y = r - R$ is shift from the equilibrium trajectory $r = R$

and $$\Omega^2 = \frac{1}{r}\frac{e^2 H_0^2}{m^2 c^2} + \frac{1}{16}\frac{e^2 E^0}{m^2 v^2} \qquad (20б)$$

we supposed the radial component of the magnetic field equal

$$H_r = H_0 \sin \alpha z, \quad dE_z \sim H^2$$

We succeded to obtain ion currents up to IkA with average energy 1.5keV in the two lense P.A. But the flow divergence was very high ($\sim 90°$).

Approximately two years ago we showed that in the four-lense P.A. it was possible to get double voltage with respect to the two-lense P.A. without losses of current. Particles energy was doubed also. The flow divergence was lowered to 60° because of the special magnetic field geometry (with zero near the anode).

The broad spectrum of the ion energy the ligh out put divergence of the ion flow, a considerable flow of neutrals in the channel-all these circumstances indicate on dominating role of the reacharging process in volume of channel. We have analyzed recently a possibility to use this accelerators as injector of neutrals for the T-6 Tokamak. A calculations show that at available holes in the Tokamak jacket only 1 2% of the total ion current can enter the Tokamak volume. Besides, a power of the trapped particles will be 10 -20kwt, what is of one order of magnitude less than many-slit ion sources provides. So we suppose unreasonable to use existing many lense systems.

It seemed tha in some details the investigations of many lense P.A. should be started from the very beginning. A good ionizators should be developed as well as systems of effective neutral expelling and systems of the potentio fixing along the channel. All it needs hard work. This work seems very necessary and reasonable because many lense P.A. facilitate to get ion flows in hundreds and thousands amps uncomparibly easier that ion devices.

I want to underline that plasma systems with over equilibrium electrostatic field are not limited by the plasma lenses and accelerators. As an illustrations I mention a magnetoelectric trap, developed by O.A.Lavrentyev or an idea of trap with nonfrozen ions bu frozen electrons that was advanced by V.V.Zuckov and me. This systems can be considered as analogue of the one lense accelerator

or, more better, as analogue of the plasma lense, mentioned above. It was called "Ecspt" , which means "electrostatic plasma trap". An "Ecspt" has a wonderful ability to recuperate the energy of the escaping particles. But its descriptions lays out of my survey.

It seemed to me that all mentioned above demonstrates unlimited facilities of the P.A. and plasma systems with over equlibrium electrical fields. Theirs efficiency is proved by experiments and with some practical devices. But it stays much more to do.

REFERENCES

1. Plasma Accelerators, supervised by L.A.Artsimovitch, Moscow, Mashizdat , 1973.
2. Zukov V.V., Morozov A.I., Schepkin G.Ya., Ion beams focusing by a plasma lense, JETP Letters, v.9, No.1, p.24, 1969.
3. Morozov A.I., Esipchouk Yu.V., Kapoulkin A.M., Nevrovsky V.A., Smirnov V.A., Influence of the magnetic field configuration on closed drif accelerator operation" JTP, v.42, w 3, p.612, 1972.
4. Morozov A.I., Kislov A.Ya., Zubkov I.P. "A High-current plasma accelerator with closed electron drift" JETP Letters, v.7, n 7, p. 224, 1968.
5. Zubkov I.P., Kislov A.Ya., Morozov A.I., "High-current accelerator optimization", JTP, v 42, N 4, p.898, 1972.

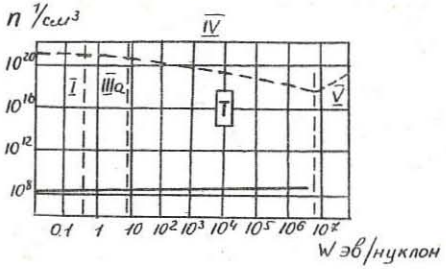

Fig 1

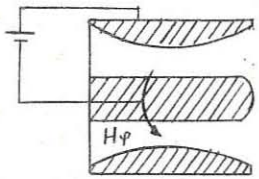

Fig 2a

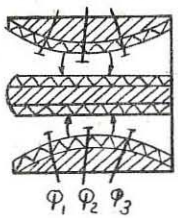

Fig 28

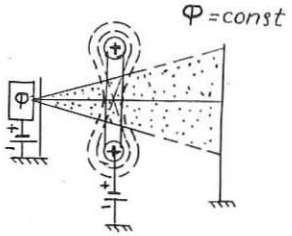

Fig 3a

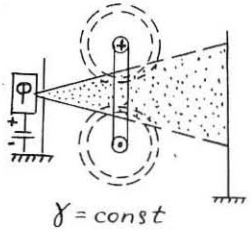

Fig 3b

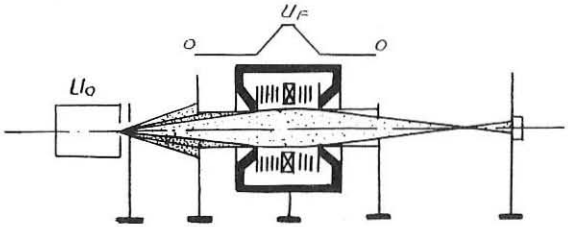

Fig 3c

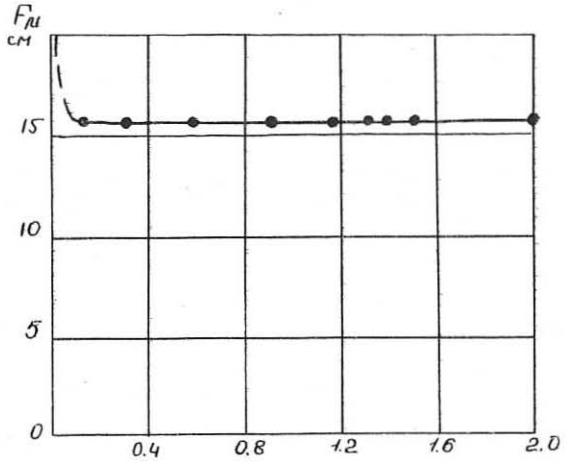

Fig 4a

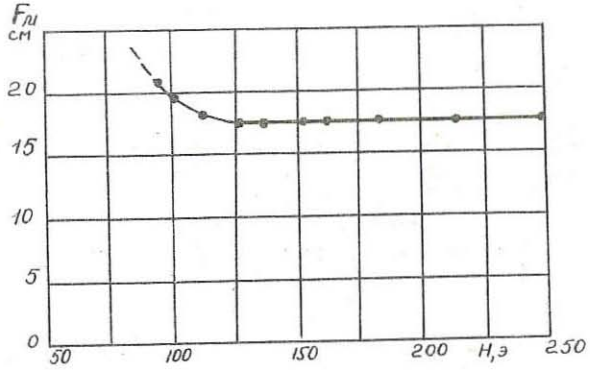

Fig 4B

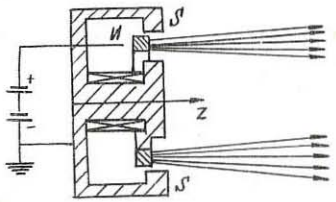

Fig 5a

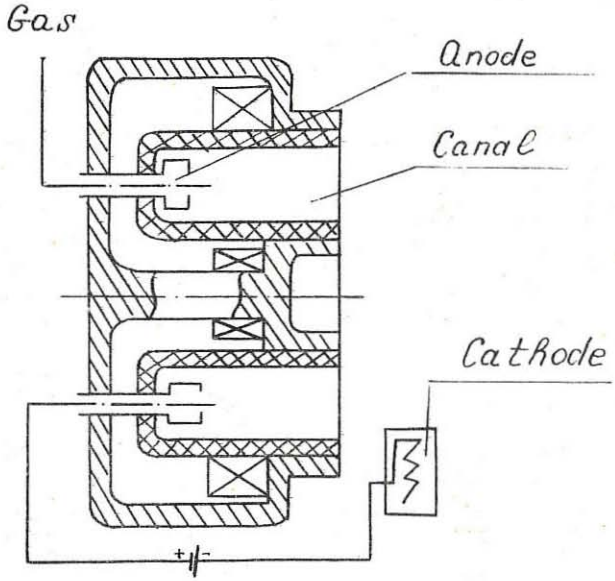

Fig. 6

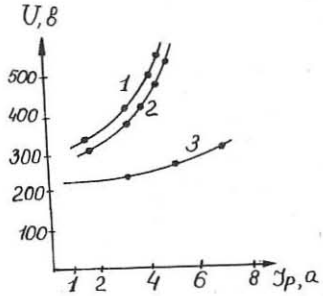

Fig 7

1. $\nabla H > 0$; 2. $\nabla H = 0$; 3. $\nabla H < 0$

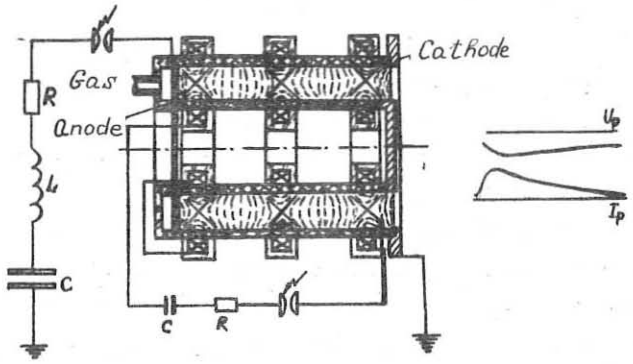

Fig 8

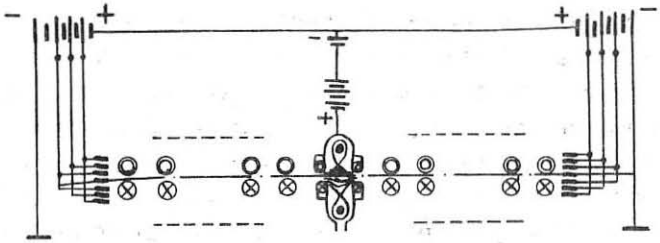

Fig 9

ENGINEERING PROBLEMS IN CTR

by R Carruthers

UKAEA Research Group, Culham Laboratory,
Abingdon, Berkshire, England

The title was suggested by the Committee, but this is not to be a catalogue of the engineering hazards lying on the road to a fusion reactor. There are enough papers which do this - unfortunately displaying a general lack of practical solutions.

In this talk I am going to try and give you an engineer's thoughts on the future programme to achieve useful power production from a fusion reactor.

I start with the premise that the plasma physics is in good shape. Progress to the point at which the key plasma parameters of temperature, density and containment time are within almost an order of magnitude of reactor requirements is a heartening position - even though experimental success and theoretical understanding are not necessarily in accord.

We must remember that fusion is just another possible resource in the highly competitive energy market. A programme of development leading to a practical fusion reactor must take account of this market, so I shall be examining the energy situation in which the future fusion research programme will be conducted. A place for fusion in this market will be dependent upon dealing satisfactorily with the questions "Why?" and "When?". That is, "Why should fusion power be adopted as a major energy resource?", and, "When must it achieve credibility to be available to meet the market demands?".

Fusion Power - Why and When?

Fusion power is advocated as a preferred way of filling the potential gap between the growing world demand for energy and the likely supply from fossil fuels. As compared with nuclear fission reactors, there is good reason to believe that fusion reactors could be designed to operate without producing such undesirable problems of radioactivity.

A further advantage is the cheapness and ready availability of the fuel supplies. The long term benefits claimed for fission power are dependent upon first establishing the economic claims of the fast breeder reactor, and then ensuring its widespread acceptability. In the absence of the breeder reactor, fission fuel reserves are limited, and the cost of energy will be closely linked to rising fuel prices as the readily worked reserves become depleted. Fusion power avoids this problem - it is difficult to envisage conditions arising which would lead to fuel prices having other than a minimal effect upon fusion energy costs.

Turning from this brief consideration of "Why fusion?", let us turn to "When?" and consider factors affecting the future time-table of research and development. Several attempts have been made to outline such a future programme, and they are all tending towards a number of common features[1](Fig.1). Firstly there is a consensus that "feasibility" will be demonstrated before 1980 and, secondly, that the practical demonstration of reliable power generation will occur around the turn of the century. The intervening years allowing a "reasonable" time for developing all the envisaged technologies and experiments which will demonstrate reactor conditions, non-economic prototypes etc, leading to a "commercial" design operating by about 2000. This is what I would describe as a "roll-forward" programme. It is the technique appropriate to scientific programmes which are essentially open-ended. Is this a justifiable approach? It proceeds with proper scientific caution and assumes that when the practical objective has been attained and proven, then the world will inevitably choose to obtain most of its energy requirements from fusion power plants.

A recent examination of forecasts[2] for energy supply and demand leads me to doubt this assumption and to propose that a future programme for fusion should be based much more on the alternative "roll-back" analysis, where completion target dates are set and used to establish critical dates in the programme and the resources required to meet them.

The problem of forecasting future energy demands and the expected level of resources can be a very emotive topic. I think the subject should be first approached as a technical problem in which estimates are made by established techniques and, usually,

justified by reference to previous trends. This gives a background of what could happen.

My next diagram (Fig.2) shows the likely pattern of energy demand and fossil fuel resources over the next 50 years. The limits on demand might be regarded as those of the reasonable pessimist who assumes that the rate of growth in demand on a world basis will settle down to the value at present prevailing in the more advanced countries, and the cautious optimist who assumes that there will be no further acceleration in the rate of growth of demand, although there has been a steady acceleration during at least three decades up to a rate which is now about 5% p.a. on a world basis.

The suggested upper limits for the rate of production of energy from fossil fuels are derived from King-Hubbert[3]. They envisage an increase in annual production of up to three times that prevailing at present. It must be remembered that an even greater increase would imply running down the limited reserves of oil and gas even more rapidly, and an earlier dependence upon coal from increasingly expensive reserves and with high transport costs to the point of usage.

From this diagram we see that the gap between fossil fuel supply and energy demand can be expected to appear somewhere between 1985 and 2005. This is the position we are likely to face if world development continues to follow present patterns, and is the only sound basis on which to plan a future energy programme. There are those who talk of an energy crisis and would like to see future growth drastically curtailed. Whether or not one agrees with this objective, it is difficult to envisage any action due to conservation or environmental pressures which would do more than defer the problem for a decade or two. The pattern established over many decades could only be changed significantly by decisions made now and acted upon universally.

Responsible energy plans can only be based on realistic forecasts - any downward trends as a result of international pressures can only be considered as they develop and accepted, thankfully, as relieving the relentless pressure on resources.

Let us now try and fit fusion into this energy supply and demand picture. As fossil fuel reserves are depleted and costs rise there will be pressures for the exploitation of other resources to fill the gap. It is a gap which will grow rapidly - between 200 and 400 MTCE per annum depending upon whether or not fossil fuel production has reached its plateau. If the gap is to be filled by electricity from nuclear reactors, this could represent a yearly installation rate of up to 600 GW of power plant working at 50% load factor. An investment programme of this magnitude is going to call for proven reliability and a demonstrated life for the equipment. This is an unfortunate fact which fusion must face - novelty alone, even with a modest cost advantage is never accepted as a reason for a change in technology. Only if the new development meets a requirement in a way which is uniquely advantageous can a new technology become established. This can be seen in the history of the electric power industry. Originally, the accepted advantages of electric lighting more than offset some of the eccentricities of its supply, but now we have a conservative industry which, understandably, demands that new methods of generation and transmission will give as little trouble as their present equipment.

The decision-making years are between 1980 and 2000 - a power programme must be planned many years in advance. If we look first at fission reactors, then we find that development plans slot nicely into this timetable. Thermal reactors of various types have been with us since the 1950s and will have sufficient integrated experience to justify a large expansion in their construction, should the energy gap materialise at the earliest date suggested. Fast breeder reactors are not in quite such good shape. Although there are more than 10 years of working experience with experimental reactors, plans for prototype reactors have slipped. Nevertheless there should be sufficient commercial operating experience for major decision making in 15 to 20 years' time.

The "roll-forward" programme for fusion, leading to pilot plants around 2000, appears to put fusion at a disadvantage since

performance demonstrated to the standards usually required of a displacing technology would not be possible before 2015 to 2020. By this time there could be several thousand GW of fission power plant in operation, and in the absence of any major disaster, the world would have come to terms with the hazards of fission waste. An argument to introduce fusion and prevent a further growth of waste would not necessarily meet a favourable response.

It appears to me that if fusion is to play a major role in meeting future energy needs, then consideration should be given to establishing its credibility at a much earlier date. Full development and adequate life experience is obviously not possible within this time scale, so it is important to identify those features of a fusion reactor which present problems requiring serious attention before an acceptable engineering proposal can be made.

Requirements of a Fusion Reactor

Although recent years have seen the publication of a number of conceptual design studies[4], I think it is opportune to reflect upon some basic requirements to be satisfied by any proposal for the design of a reactor:

1. It must be possible to build the reactor;
   - without invoking unexpectedly advanced developments in materials properties.
2. The reactor must be capable of reliable operation over a designed life;
   - routine maintenance and all possible repair work must be possible without requiring a technological tour de force.
3. The reactor must be acceptably safe.
4. The reactor must produce "economic" power.

These may be felt to be so obvious as to need no comment - but as evermore sophisticated solutions are proferred for a widening range of detailed problems it is clear that such simple requirements are easily forgotten.

Most attention has been devoted to the last two items, safety and economics. This is quite understandable - unless a generous assessment of the economic potential of a possible route to a fusion reactor showed it to be in the same ball park as competing energy sources, then preference should be given to a more favourable route. The concern with safety is to ensure that the potential advantages of fusion are properly quantified so that justifiable comparisons can be made with fission.

This first round of conceptual design studies has been valuable in encouraging a wider appreciation of the way in which reactor requirements can react back on the plasma physics requirements - as for example in establishing that toroidal reactors will require a relatively high β and be of large size - several GWs. To this extent is is a useful discipline in establishing a fusion reactor orientated plasma physics programme. The publication of such studies has however demonstrated to hard-headed fission reactor engineers how far we are from having credible solutions to many of the non-plasma physics problems of fusion - let alone solutions with a preliminary engineering assessment. In short, without more attention to the first two items - construction and operation - further estimates of economics and safety are unlikely to be taken seriously.

Towards a Fusion Reactor

I referred to the present programme predictions as being of the "roll-forward" type. In the simplest terms it has been considered to have three stages:

(a) Scientific feasibility;

(b) Technological feasibility;

(c) Economic feasibility.

This simple approach has grave weaknesses. The experimental arrangement selected for the demonstration of "scientific feasibility" may not be suitable for extrapolation to meet the technological requirements of a power producing reactor. A technological solution which, although workable, did not satisfy economic constraints, would not be acceptable. The three parts

cannot be separated in preparing the "critical path" towards a fusion reactor - it is clearly preferable if the scientific programme is based upon approaches which can be shown to have some real reactor potential.

Another lesson has to be accepted as the programme becomes more reactor orientated: Scientific certainty is expensive. It requires ever more ambitious experiments - but never a more than justifiable extrapolation of current data. All such experiments can be considered "successful" in that they add to the sum total of knowledge. However, progress towards a fusion reactor may be expedited by some bolder experiments which really tested possible reactor concepts. By the standards of research some of these would be failures, but to an engineer it is useful to know that a concept will not work even if, at the time, no one understands why. This is, after all, the pattern of technological progress - if the standards of plasma physics were applied to raising steam in coal or oil-fired boilers we should still be awaiting the Industrial Revolution!

The alternative is the "roll back" analysis. We start with a hypothetical reactor concept, worked out to the limits of present knowledge for a particular containment geometry and question why such a reactor could not be built now. The answers help to formulate a programme aimed to resolve specific problems as expeditiously as possible rather than await the answers from a broader, open-ended plasma physics programme.

The Turning Point

This envisages a turning point in the fusion power programme - a necessary decision point in any programme with clear, practical requirements as the ultimate objective. The emphasis must move from a research phase to a development and construction phase.

After a research phase which has lasted, so far, for about 25 years, it is not inappropriate to consider when the turning point for fusion might occur.

Let us examine the problem with the aid of my next diagram (Fig.3). I have drawn this in a way which emphasises the change of

philosophy which has to be faced at the turning point. The research phase is, quite rightly, a divergent one - although endeavours have obviously been made to limit the range of containment geometries for the study of the wide variety of plasma physics problems. When the development phase is entered the programme has to become convergent. Although the activity is shown as expanding to cover a wider range of problems, the motivation is now project-orientated, and there has to be a certain ruthlessness in the concentration of the research effort. For example - and I admit an oversimiplification - if a containment time of 10 sec were observed on an experiment when theory predicted 100 sec, the resolution of the discrepancy would be of interest, but not of vital importance to the design of a reactor which required no more than 1 sec of containment. In fact the reactor designer might be much more appreciative of research leading to a controlled reduction of the containment time!

My own view is that we are already at the stage where we must consider the implications of the change to a convergent programme. Many laboratories are now working on plans for experiments on a much larger scale than hitherto; T 10, PLT, JET. The associated time scale is inevitably longer than for earlier projects - 5 to 6 years from initial concept to the first experiments. This time scale and the level of investment in both money and manpower makes it important to ensure that the experiments are considered not only for the advances they are expected to make to plasma physics, but also for their relevance to the problems of fusion reactors, and the extent to which they can be used to develop reactor technologies. Wherever possible the problems of experiments should be solved with approaches which could be expected to extrapolate to reactor requirements, although there will of course be times when a compromise must be accepted to avoid undue delays.

Some Fusion Reactor Problems

At the beginning of my talk I expressed my optimism in the present state of plasma physics. In general, results are as good as the apparatus would allow - further progress being

dependent upon a scaling up in dimensions, magnetic field, or both. To minimise the time to establish the credibility of fusion power there should not be too many steps before reaching the "Technology Demonstration Model". I use this latter term because the scaling laws for fusion are such that it is a stage which is more appropriate than the power producing prototype which is usual in fission reactor development.

What are the problems which such a "Technology Demonstration Model" must show to have been satisfactorily solved?

They can be obtained from the consideration of a fusion reactor as having three main regions:

(a) The interior - the subject of plasma physics;

(b) The exterior - where neutrons are moderated, energy extracted and tritium is bred. A region having much in common with fission reactors.

(c) The interface region - where there are problems of magnetic fields, high vacuum, surface physics and chemistry, particle sources and plasma control.

This latter region has so far received only scant attention - the problems are wide ranging and appear to call for a new discipline - Fusion Reactor Science.

Because so little work has been undertaken, the problems of this region have been somewhat glossed over in conceptual design studies which have concentrated on problems of the confining magnetic field structure and neutronics.

It has been assumed that such problems as:

Reactor start-up and heating,

Refuelling,

Removal of the 'exhaust' fuel,
Control of particle and energy containment times,
Control of plasma profile,
Control of power level,
Radiation damage,
Plasma/wall interactions,

will all eventually be dealt with by solutions which would only have a marginal effect upon the initial concept.

Is such an assumption justified? One has only to look at the Princeton concept for the introduction of an axysymmetric divertor and see its effect upon the dimensions of the toroidal field winding to have some doubts - and this is for a concept which does not at present appear to satisfy either the anticipated vacuum requirements or the need to be readily demountable for 'hot' maintenance.

Unfortunately, it is all too common to minimise the significance of problems outside the main discipline, a fact which has been recognised as contributing to the delays in several fission reactor programmes. It is a practice which stems from the tendency to try and separate scientific feasibility from technical feasibility - particularly in a chronological sense - probably due to fears that first thoughts on the solution of a serious technical problem could cast doubts upon a scientifically attractive approach - doubts which subsequent research could remove. It is far preferable to have a parallel programme of research on the non-plasma physics problems. There can then be a progressive re-assessment of the practicability of the various approaches to a fusion reactor and, hopefully, an increasing realisation that there must be a close interaction between the physics and the technology if a convincing case is to be made for fusion power.

Conclusions

To conclude I should like to restate my optimism on the present state of the plasma physics. There are many possible pit-falls ahead; but the doubts are not, for the most part, concerning whether or not power from fusion is scientifically

feasible but whether it can be demonstrated to be achievable on an acceptable scale.

I have suggested that more attention should be given to the problems of Fusion Reactor Science. In mission-orientated research it is surely just as wrong to do too much physics on an impractical approach as it is to undertake too large a technological programme on an approach which could prove to be scientifically unsound.

Finally I suggest that the time scale is perhaps not as long as many have assumed. Important investment decisions are going to have to be made on future energy resources within the next 20-30 years. The credibility of the various alternatives ought to be established by then - it would be a pity if fusion became an advanced technology which just missed the market.

References

1. Marsham, T.N. and Pease, R.S. "Nuclear Power - the Future" British Association for the Advancement of Science, Leicester, 1972.

2. Brookes, L.G. "Energy and Economic Growth" Atom, p.7, January 1972.

3. Hubbert, M.K. "Energy Resources" published in "Resources and Man", U.S. National Academy of Sciences, 1969.

4. "Fusion Power: An Assessment of Ultimate Potential Division of Controlled Thermonuclear Research". U.S. AEC Report WASH-1239, February 1973.

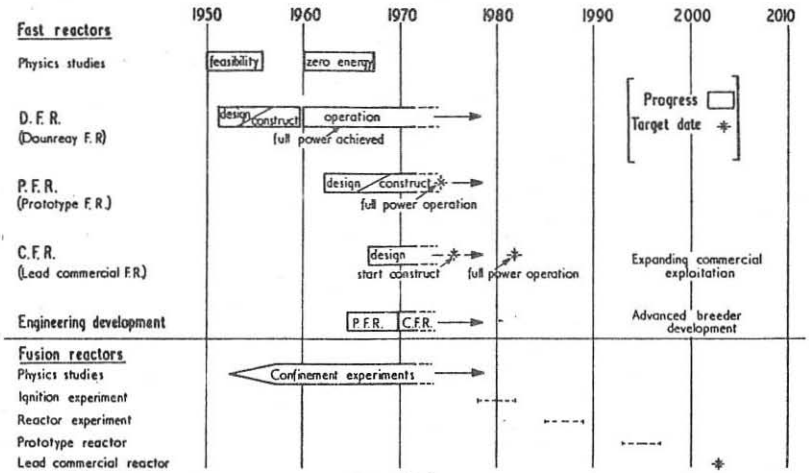

FIGURE 1

Development programmes – fast breeder and fusion reactors

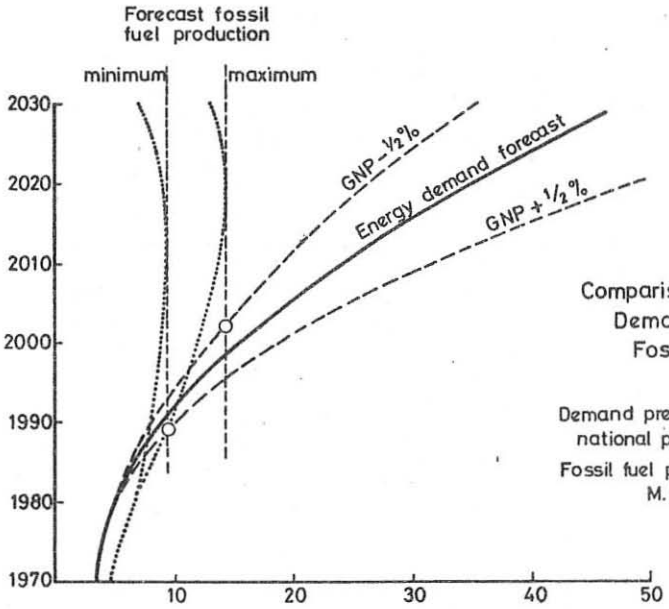

Comparison of World Energy Demand and Available Fossil Fuel Supply

Demand predictions based on forecast gross national product and population growths

Fossil fuel production from 'Energy Resources' M.K. Hubbard – US NAS.

FIGURE 2

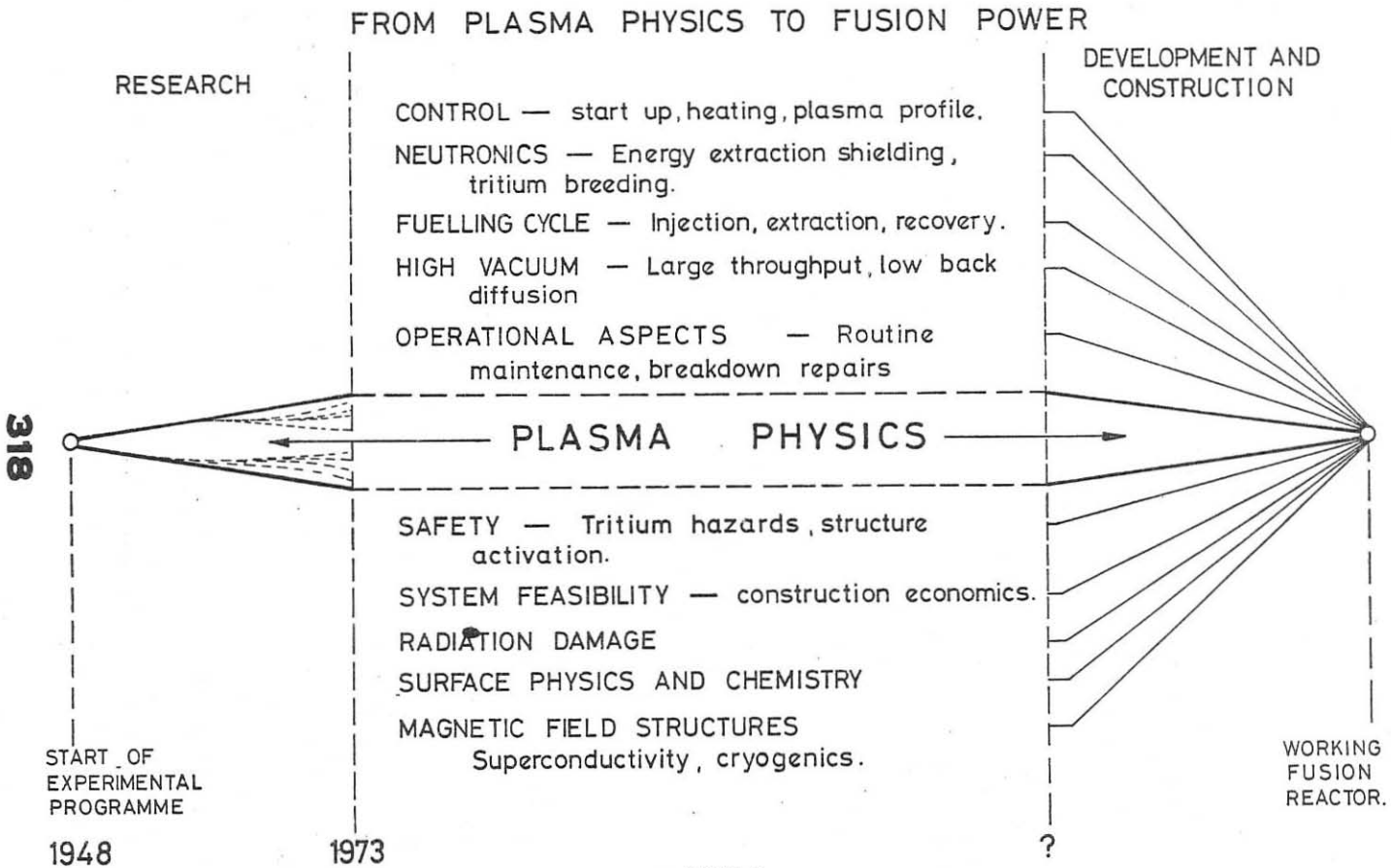
FROM PLASMA PHYSICS TO FUSION POWER
RESEARCH
DEVELOPMENT AND CONSTRUCTION
CONTROL — start up, heating, plasma profile.
NEUTRONICS — Energy extraction shielding, tritium breeding.
FUELLING CYCLE — Injection, extraction, recovery.
HIGH VACUUM — Large throughput, low back diffusion
OPERATIONAL ASPECTS — Routine maintenance, breakdown repairs
PLASMA PHYSICS
SAFETY — Tritium hazards, structure activation.
SYSTEM FEASIBILITY — construction economics.
RADIATION DAMAGE
SURFACE PHYSICS AND CHEMISTRY
MAGNETIC FIELD STRUCTURES
Superconductivity, cryogenics.
START OF EXPERIMENTAL PROGRAMME
1948
1973
?
WORKING FUSION REACTOR.

FIGURE 3

SUPPLEMENTARY PAPERS

ADDITIONAL MATERIAL

THE CLEO TOKAMAK EXPERIMENT: J W M Paul, A Gibson, J Hugill, J Lang*, P Reynolds P E Stott.

PLASMA EQUILIBRIUM IN CLEO TOKAMAK: J Hugill, J W M Paul, G W Reid and P E Stott

Additional co-authors: A Costley≠, M Forrest, M Haegi⁎, R Prentice, D D R Summers

U.K.A.E.A. Culham Laboratory, Abingdon, Berkshire, England

1. Equilibrium

The tokamak equilibrium has been extended to 180 ms for peak currents of 70kA as shown in Fig.1a. The plasma remains within ± 5mm of centre for 100 ms. This improvement results from using a feedback system on the radial magnetic field as well as on the vertical field (δB_R = ± 0.6 mT, δB_z = ± 1.9 mT). The radial field system is used to cancel asymmetric flux leakage from the transformer core.

From measurements we estimate the average value of the non-uniform vertical field $\bar{B}_z/I$ = 0.32 mT/kA. This agrees with the theoretical value for equilibrium with $\beta_\theta \sim 0.3$ (see below) provided the current profile is flat rather than parabolic.

Reducing the plasma radius (using a small probe limiter) from r_L = 0.18m has no gross effect on the plasma until $r_L < 0.16$m ($q \simeq 4$), for which it disrupts. This is consistent with the fact that the plasma column can move 20 to 30 mm without gross effects. For $r_L \geq 0.10$m, the maximum current without disruption is always given by $q \sim 4$ (B_ϕ = 2T).

2. Plasma Temperatures

Electron temperatures at the centre of the plasma have been measured by photon scattering at the two times used for neutral injection and corresponding values for $\beta_{\theta e}$ have been derived:

t = 20 ms T_{eo} = 230 ± 35 eV $\beta_{\theta e}$ = 0.31

t = 50 ms T_{eo} = 230 ± 70 eV $\beta_{\theta e}$ = 0.37

The latter measurement is at peak current and can be compared with the conductivity temperature (T_σ) so as to derive an effective Z. The value of T_σ depends on the assumed radial variation.

a) Flat $T_e(r)$ T_σ = 80 eV Z_{eff} = 4.8

b) Parabolic $T(r)$ $T_{\sigma o}$ = 150 eV Z_{eff} = 1.8

The flat profile gives a more reasonable Z_{eff} and such a profile was used to obtain $\beta_{\theta e}$ above.

Preliminary diamagnetic loop measurements yielded $\beta_{\perp\theta}$ = 0.2 at 20 ms and 0.4 at 50 ms. These are reasonably consistent with the above values.

Although the electron temperatures reported here are lower than in similar tokamaks, the β_θ is similar. We are operating at higher density with flatter profiles.

---

* Astrophysics Research Division, RSRD, Culham Laboratory
≠ National Physical Laboratory, Teddington, England
⁎ C.N.E.N., Frascati, Italy

Very recent experiments, with a symmetrical core bias winding, have produced discharges for 0.19s with equilibrium $\Delta z \sim \Delta R \leq 10$ mm for 0.17s. These plasmas have lower densities ($n_e \sim 1.6 \times 10^{19} m^{-3}$) with similar β_θ and consequently higher diamagnetic temperatures in the range 300 to 450 eV. Preliminary measurements of the ion temperature using a multichannel neutral particl detector give a value in the range 100 to 150 eV.

3. Neutral Injection

The injected power has been raised to 65 kW(~ 30% ohmic power) and the gas introduced to the tokamak made negligible small. There is no observable change of any gross characteristics of the plasma on injection. The measurements place a limit on the change of conductivity temperature $\Delta T_\sigma \leq 3\%$. This is consistent with recent estimates of the expected electron heating after taking account of charge exchange losses.

The steady Mirnov oscillations during the discharge provide a monitor of rotation round the major azimuth. The fact that we see no change of frequency of these oscillations on injection, limits the velocity acquired from the injected beam to less than 2% of the sound speed, assuming no change in minor azimuthal velocity. This corresponds to a momentum loss time of 1.3 ms.

A study of the development of the energy spectrum of the injected particles is reported in an accompanying paper by J. Sheffield et al. and these measurements are related to the plasma parameters quoted above.

4. Microwave Emission

We have made preliminary measurements of the microwave emission in the range λ = 0.1 to 5 mm which includes the electron cyclotron frequency and its harmonics. High levels of emission are strongly correlated with copious x-ray emission and hence runaway electrons but this may not be true for the much lower levels of emission discussed here.

The total emission in the range is unpolarized and above the classical expectation for electron cyclotron emission directly from the plasma (i.e. neglecting wall reflections). The emission is below that from a black body.

The observed radiation has been spectrally resolved by using a Fourier transform spectrometer with rapid scan. The resulting spectrum Fig.2a, appears to follow the black body emission within the experimental uncertainty of a factor two on absolute values. The peak of the emission is at $2\omega_{ce}$ (2.8 mm) and for higher frequencies the emission decreases. The width of the cyclotron emission lines and the resolution of the instrument are such that the observations are not inconsistent with the presence of broad cyclotron emission bands. The discrepancy in amplitude and polarization might be explained by reflections within the torus.

THE CLEO TOKAMAK EXPERIMENT

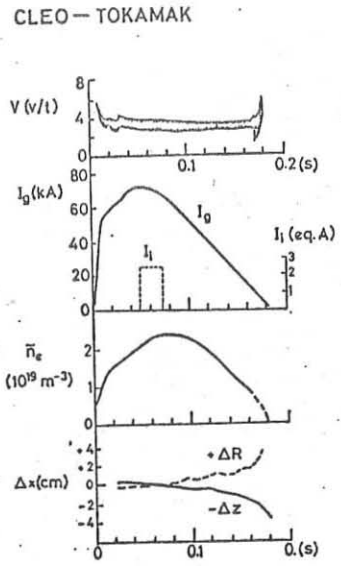

FIG 1a

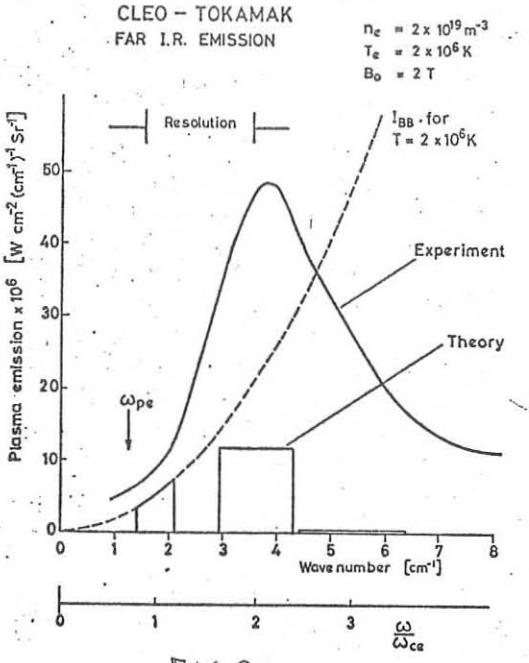

FIG 2a.

Acknowledgements

We wish to acknowledge assistance of the members of the CLEO group.

CONFINEMENT OF AN ANOMALOUSLY HEATED PLASMA IN A TOKAMAK (T.T.F.)

M. Martone
Laboratori Gas Ionizzati (Associazione EURATOM-CNEN), C.P.65,
00044 Frascati, Rome, Italy.

INTRODUCTION

In the T.T.F. experiment the pyrex torus has been replaced by a stainless steel torus with the same major radius R = 30 cm, made from 23 straight tube pieces (1 mm thick, 100 mm inner diameter), cut and than welded in such a way as to form a polygonal vacuum chamber. A glass break 5 cm wide allows the longitudinal electric field, applied directly at the break, to penetrate across the liner. A circular niobium limiter 80 mm inner diameter has been used. The copper shell has been eliminated and a vertical field up to 100 G d.c. has been provided with a curvature ensuring stability. The remanent components of the experiment are the same as in the case of the first part of the paper.

RESULTS

With the stainless steel vacuum chamber we have obtained discharges at less than 1 mTorr H_2 filling pressure. Fig. 1 shows the plasma current I_p, primary voltage V_s, and plasma radius a (from streak pictures with a slit parallel to the torus major radius) versus time, for B_T = 6 kG. The filling pressure was 8.5 10^{-4} Torr and the vertical field B_V was varied to position the discharge at R = 30 cm, the optimum vertical field resulting B_V = 30 G. The plasma position was controlled by streak photography. The plasma current stays approximately flat for 50 usec and then decays. At the change of the slope an increase in the primary voltage is observed and the streak picture shows a brighter plasma with a filamentary structure giving indication of plasma touching the wall. From the measured values of a, I_p, V_s ignoring the inductive effect due to the contraction of the plasma column, a value for the plasma resistivity can be obtained. After 20 μsec the plasma resistivity is

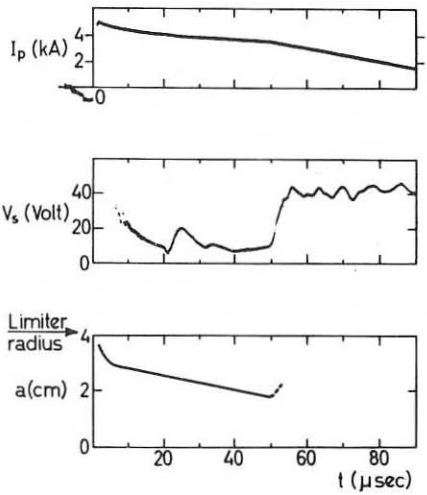

Fig. 1

$\eta = 5 \cdot 10^{-6}\ \Omega \cdot m$ corresponding to a temperature $T_e = 25$ eV ($Z = 1$) Before this time, just after the fast rise of the current the plasma, contraction is so pronounced that the inductive effect excludes the possibility of deducing a value for the temperature at this time, and so confirm the presence of a fast turbulent heating observed at higher filling pressure (reported in the first part of the paper). The q value at the plasma radius is of the order of one. This fact suggests that increasing the value of the toroidal field more stable discharges could be obtained. In our case, increasing the value of the toroidal field, the discharge was displaced more and more towards the inner side of the vacuum chamber. Reducing the value of the vertical field, it was possible to compensate this displacement but the discharge was no longer stable.

Moreover in the case of Fig. 1, reversing the direction of the toroidal field, the discharge was swept inwards. This fact suggests the presence of stray fields, mainly due to the toroidal field coils. In conclusion, a fast rising plasma current (risetime 1 μsec) has been produced in a Tokamak with conducting liner at less than 1 mTorr H_2 filling pressure. The corresponding voltage on the primary is 3.6 kV.

A resistivity temperature of 25 eV has been obtained ($Z = 1$) and the plasma is well confined for a limited time. In fact, the maximum plasma current possible in the experiment has an upper bound, since there appears an instability, when q tends to be small and at the sametime B_T cannot be increased above 6 kG due to the presence of a stray field of the B_T coils.

Radial Transport of Ions in Tokamaks Including Diffusing Oxygen and Carbon impurities.

D.F. Düchs

Max-Planck-Institut für Plasmaphysik, 8046 Garching, F.R.G.

H.P. Furth and P.H. Rutherford

Plasma Physics Laboratory, Princeton University, Princeton, U.S.A.

In previous calculations using the "pseudo-classical model" without diffusing impurities a constant Z_{eff} (≈ 6) seemed necessary to reproduce the measured data from the ST-Tokamak (a=14 cm, R= 109 cm, B_t= 30 kG, I_t= 40 kA). Such a Z_{eff} is reached in the calculations shown in the figures by a prescribed impurity flux $\Gamma_0(a) = -3 \times 10^{14}$ cm^{-2} s^{-1} at the boundary. In all runs made for different initial and boundary conditions, for oxygen or carbon impurities, Z_{eff} is found to decrease towards the wall as shown in Fig. 1. The parameter α indicates the ratio $O_{total}/n_{e,\,total}$. The profiles for O are quite similar because the lower stages of ionization are only present close to the boundary. A distribution of O among the stages of ionization is shown in Fig. 2 (for the densities and temperatures of Fig. 3b).

Such Z_{eff}- profiles have a marked effect on the current density through the resistivity: a skin current appears which causes an MHD-unstable -profile (Fig. 3b).

Fig. 3 presents a comparison

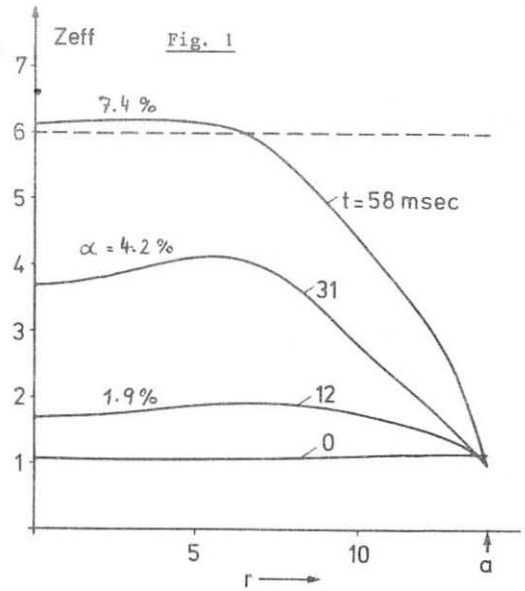

between a computation with (b) and without diffusing impurities.[(a)] The decrease in T_e is mainly due to lack of heating; a T_e-skin is prevented by the losses.

It might be concluded that the previously used "Z_{eff}" cannot be interpreted as average ion charge; it only expressed some kind of anomaly because the profiles of Fig.1 seem likely to occur[10] and Fig.3a, not 3b, agrees with the measurements.

[10] V.A. Vershkov, S.V. Mirnov, Proc. V.Europ.Conf. on CTR and Plasma Phys., Grenoble, Vol 1, (1972), p. 1

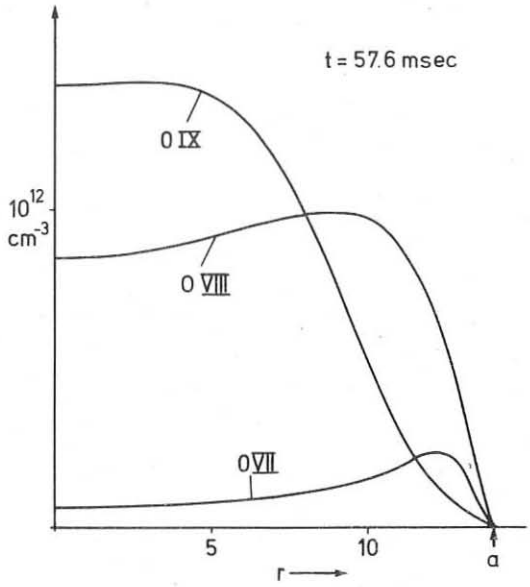

Fig. 2

a

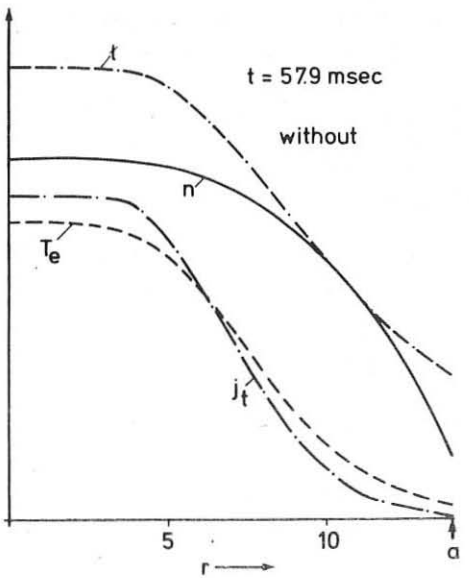

Fig. 3

b

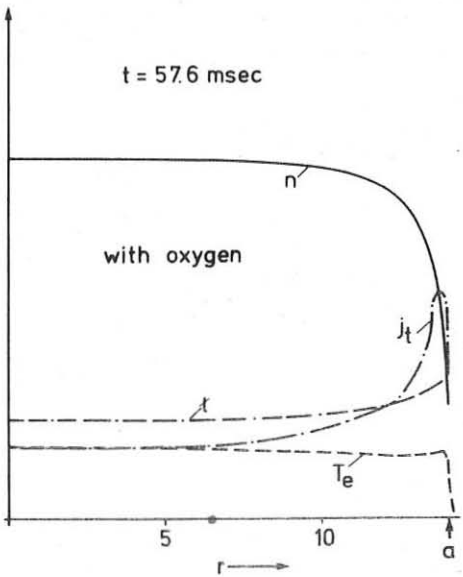

Supplement to, Neutral Injection on the Cleo Tokamak

J. Sheffield, D. Aldcroft, J. Burcham, H.C. Cole, J.G. Cordey, M. Cowlin, E. Speth, and P.E. Stott. Culham Laboratory, England.

A neutral beam, 1 amp each of H^0 at 22.5, 11.25 and 7.5 keV, has been injected in the direction of the ohmic heating current, parallel (gap voltage φ_G positive) mean angle to B_{TOR} $\theta_o \sim 35°$, and anti-parallel, (φ_G negative), $\theta_o \sim 15°$. The high energy ions contained have been studied with a high energy neutral particle detector, band width $\pm$ 3%, Figure 1. The energy spectra at peak signal level are in Figure 2. The normalization factor of $E^{-\frac{5}{2}}$ allows for detector bandwidth, scintillator response and neutralization and stripping cross sections. The detector signals for selected energies are shown in Figure 3 and 4. Following the peak at $\sim$ 6 msecs, these signals decay, even though the beam is maintained for 25 msec. This phenomenon, possibly caused by a charge imbalance generated by the beam, is under investigation. The theoretical spectra and signals, for the E_o = 22.5 keV component were obtained from a linearized version of the Fokker Planck equation [1], averaged over angle (θ).

$$\frac{\partial \bar{f}}{\partial t} = \underbrace{\frac{D_p \cdot T_e}{2E_o \tau_s} \cdot \frac{\partial^2 \bar{f}}{\partial x^2}}_{\text{Vel Diff.}} + \underbrace{\left[\frac{\left(1+\left(\frac{E_c}{E_o}\right)^{\frac{3}{2}}\right)}{\tau_s} - \frac{e\varphi_G^* \xi_o}{m_h v_o}\right]\frac{\partial \bar{f}}{\partial x}}_{\text{Friction. Elect.Accel}} + \underbrace{\left(\frac{3}{\tau_s} - \frac{1}{\tau_{cx}}\right)\bar{f}}_{\text{Charge Exchange.}} + \underbrace{\delta(x)(1-e^{-t/\tau_R})}_{\text{Source}}.$$

$$x = \frac{v-v_o}{v_o}, \quad E_o = \tfrac{1}{2} m_h v_o^2$$

$$\tau_s \simeq \frac{1.5 \times 10^{12}[T_e(\text{keV})]^{\frac{3}{2}}}{n_e(\text{cm}^{-3})}\text{sec.} \qquad \tau_{cx} = \frac{10^7 \text{sec}}{n_n}, \quad \xi_o = \cos\theta_o$$

$$E_c \simeq 15\, T_e, \quad \varphi_G^* = (1 - 1/Z_{eff})\varphi_G, \quad \bar{T}_e = (Zeff)^{\frac{2}{3}} T_{con}$$

The parameter (D_p) is used to adjust the velocity diffusion above the Spitzer value. We measure $n_e \simeq 1.5 \times 10^{13}\text{cm}^{-3}$, $\tau_R \simeq 2$ msec, , E_o, $\varphi_G \simeq \pm$ 3.5 V, and $I_{gas} \simeq$ 60 kA $\rightarrow \bar{T}_{con} \simeq$ 80 eV. The difference between the two high energy tails is due to the sign change in (φ_G). For Zeff = 1 the electric acceleration is balanced by a drag on the drifting electrons, the relative extent of the

tails in our case is consistent with Zeff ~ 6. This leads to $\overline{T}_e \sim$ 280 eV which is consistent with provisional results from Thomson scattering of 230 ± 35 eV[2]. To get the absolute extent of the parallel tail we need $D_p \sim 4$. We are investigating effects which may contribute to the apparent anomaly, these include collisions between the beam-ions, geometric effects and fluctuations.

The computed results are not sensitive to neutral density, but the slight initial increase towards lower energies suggests that $n_n < 1.5 \times 10^9$ cm^{-3}, the subsequent decrease in level around 18 keV is probably due to the neglected angular scattering terms, J.G.Cordey was responsible for the theoretical analysis.

We are grateful to Drs. R.J. Bickerton, J.W. Connor, A. Gibson, J. Hugill, J.W.M. Paul and other colleagues for stimulating discussions.

[1] Rosenbluth, M.N., et al. 1957. Phys. Rev. 107, 1

[2] Paul, J.W.M., 1973, supplement to this conference.

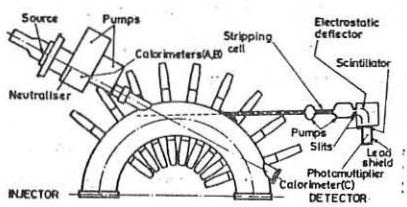

FIG 1.

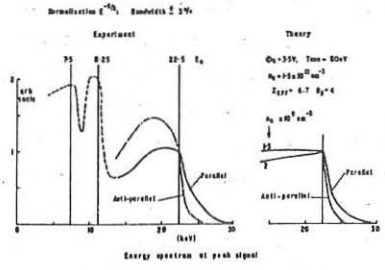

FIG 2.

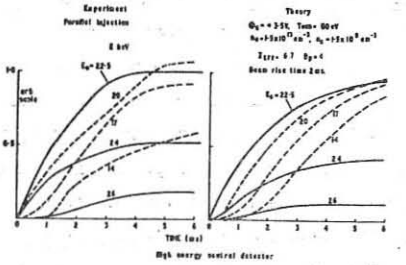

FIG 3.

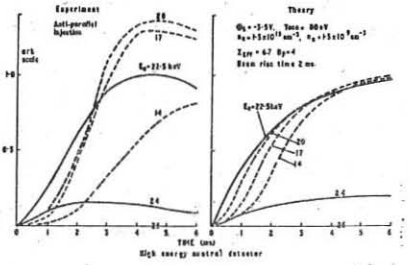

FIG 4.

ORMAK AND NEUTRAL INJECTION*

C. F. Barnett, L. A. Berry, J. D. Callen, J. F. Clarke, O. B. Morgan, R. J. Colchin, A. C. England, J. T. Hogan, G. G. Kelley, L. D. Stewart, J. R. McNally, Jr., M. Murakami, R. V. Neidigh, M. Roberts, J. A. Rome, T. C. Jernigan, W. R. Wing, and W. L. Stirling

Oak Ridge National Laboratory
Oak Ridge, Tennessee 37830 U.S.A.

Abstract. One of the four ORMAK neutral injection modules[1] has been installed and operated successfully at a power level of 70 kW. An ion temperature increase of about 25% has been observed, which is in agreement with predictions of theory.

ORMAK Plasma Conditions. The ORMAK plasma conditions during these injection experiments were characteristic of those usually encountered during initial operation of the device, namely, relatively high C and O impurity content and MHD activity. Typical parameters are given in Table I. The observations of m = 2 and 3 MHD oscillations at a limiter q = 6 is indicative of the shrunken current channel expected at high impurity levels. This impurity level is also reflected in the large ratio of electron temperature obtained from the plasma resistivity to that determined from the plasma bremsstrahlung radiation.

The level of neutral density indicated in Table I is about a factor of 2 lower than those previously quoted from ORMAK under similar conditions[2,3]. This results from a more realistic interpretation of the neutral spectrometer data using the ORMAK neutral transport code[4]. At the neutral density indicated the three ion energy loss mechanisms of conduction, convection and charge exchange are comparable in magnitude at the center of the plasma.

Injection Experiment. A 60 msec pulse of energetic neutral atoms composed of about 1.1 A @ 25 keV, 2.6 A @ 12.5 keV and 1.1 A @ 8.3 keV was injected into the plasma in a direction counter to the ohmic heating current. This 70 kW represents 70% of the injector capability. Because of the large drift orbits in the 80 kA discharge, we calculate that 59, 75, and 85% of the three energy species are retained in the plasma. The fraction of the beam power given to the plasma electrons is so small compared to the ohmic heating that we expect and observe no change in T_e. Taking charge exchange losses during the slowing down process into account, we calculate that about 10 kW are deposited in the plasma ions. This power is peaked[5,6] near the plasma axis and amounts to an energy input to the plasma ions of about .025 w/cm^3 compared to the usual 0.1 w/cm^3 from electron ion collisions. This increment in power produces a central ion temperature rise of about 25% as indicated in Table I.

Table I

Typical ORMAK Plasma Conditions With Injection

		Injection Off	Injection On
B_t (kG)		13.5	13.5
V (Volts)		3.5	3.5
I (k Amps)		80	80
$\bar{n}_e$ (mean electron density, $10^{13}cm^{-3}$)	t = 20-30 m sec	1.7	1.7
	t = 50-60 m sec	1.5	1.8
n_o (neutral density, $10^{8}cm^{-3}$)		4	4
T_e (Bremsstrahlung, eV)		700	700
T_e (resistivity, eV)		70	70
T_i (neutral spectrometer, eV)	t = 20-30 m sec	243 ± 20	287 ± 20
	t = 50-60 m sec	198 ± 15	256 ± 15
MHD azimuthal mode number		2 - 3	2 - 3
q limiter		6	6

This increase in T_i is also in agreement with that predicted by the ORMAK plasma simulation code using pseudoclassical particle diffusion and neoclassical ion heat conductivity.

Conclusion. The injection experiments described above show an ion temperature increase and no deleterious effects when neutral injection increases the energy input to the plasma by about 25%. This represents a promising beginning to the ORMAK injection program.

REFERENCES

[1] L. D. Stewart, et al., Third Int. Symp. on Toroidal Plasma Confinement, Garching, Germany (1973).

[2] C. F. Barnett, et al., 6th European Conference on Controlled Fusion and Plasma Physics, Moscow, USSR (1973).

[3] G. G. Kelley, et al., IBID.

[4] L. Berry, J. F. Clarke, J. T. Hogan, to be published.

[5] J. Rome, J. Callen, J. F. Clarke, to be published.

[6] J. D. Callen, J. F. Clarke, and J. A. Rome, Third, Int. Symp. on Toroidal Plasma Confinement, Garching, Germany (1973).

*Research sponsored by the U.S. Atomic Energy Commission under contract with the Union Carbide Corporation.

KINK INSTABILITIES IN ARBITRARY CROSS-SECTION PLASMAS

J. P. Freidberg, F. A. Haas†, B. M. Marder
Los Alamos Scientific Laboratory
University of California
Los Alamos, New Mexico 87544

A numerical method has been developed and tested to study the magneto-hydrodynamic stability to kink modes of plasmas with arbitrary cross section. By using a variation of Green's third formula the necessity of solving Laplace's equation in a region is eliminated.

Consider an arbitrary cross section parameterized by

$$r = a[1 + \eta(s)] \qquad \theta = \theta(s)$$

where s is arc-length along the curve. Let $\kappa(s)$ be the curvature. The plasma displacement is expressed as

$$\xi(s,z) = \exp(ikz) \sum c_m \exp(2\pi\, ims/L) .$$

L is the length of the curve. δW is a quadratic expression in ξ and is comprised of three parts, $\delta W = \delta W_s + \delta W_p + \delta W_v$ where

$$\delta W_s = \frac{-B_o^2}{2\mu_o} \oint |\xi|^2 \kappa(s)\, ds$$

$$\delta W_p = \frac{1}{2\mu_o} \oint \psi \frac{\partial \psi}{\partial n}\, ds$$

with a similar expression for δW_v.

On the surface

$$\frac{\partial \psi}{\partial n} = \underline{B}\cdot\nabla\xi - \xi\underline{n}\cdot(\underline{n}\cdot\nabla\underline{B}) \text{ and } \nabla^2\psi = 0 \text{ in the plasma.}$$

ψ is also expressed as $\exp(ikz) \sum \gamma_m \exp(2\pi ims/L)$. Since $\frac{\partial \psi}{\partial n}$ is known on the surface in terms of ξ from the boundary condition we need only find a relation between ψ and ξ on the surface. This is obtained from a modified form of Green's third formula:

$$\psi(s) = \frac{1}{\pi} \oint \left[\psi(t) \frac{\partial}{\partial n_t} \log R(s,t) - \log R(s,t) \frac{\partial \psi(t)}{\partial n_t} \right] dt$$

where $\frac{\partial}{\partial n_t}$ is the normal derivative at arc-length t. R(s,t) is the distanc between points s and t. Using this expression to eliminate the γ_n's we obtain δW as a quadratic expression in the c_n's and the growth rates are obtained from the eigenvalues of the resulting symmetric matrix.

Various cross sections were examined with the following results:

1) No cross section was found to be more stable than the circular one for straight systems.

2) For toroidal systems a "racetrack" cross section seems more favorable than an elliptical one.

3) The only importance which can be attached to the criterion $q \geq 1$ for stability is that $q = 1$ marks the stability transition for a circular cross-section at $\beta = 0$. Thus, in light of 1, no cross section achieves stability for $q < 1$.

---

†Permanent address: The Culham Laboratory, AERE, Abingdon, Berks. ENGLAND.

ENERGY CONTAINMENT IN THE WENDELSTEIN II B STELLARATOR WITH OHMIC HEATING

G. Grieger, H. Hacker, G. Pacher, St. Rehker, H. Renner, H. Ringler, E.Wuersching

Max-Planck-Institut für Plasmaphysik, Garching bei München, Federal Republic of Germany
EURATOM Association

Energy Confinement

Using an $Z_{eff} = 2$ we plot on slide 5 the energy content of the plasma against ohmic heating current. The external rotational transform is nearly $\iota_o = 0.1$ for the 3 different values of magnetic field. Similar results from URAGAN/6/ it would be possible to fit a straight line to the relation between n T and heating current over our parameter range. But within experimental scatter all the data points also fit on the line $\beta_\Theta = 0.65$, where the poloidal field from the helical windings is added to that of the plasma current. The line on the right give n T versus J for constant $\beta_\Theta = 0.65$ at 4.0 cm assuming all the poloidal field B_Θ is produced by a ring current as in a Tokamak. In comparison it follows that less power input is necessary for a given energy content in the Wendelstein W II b stellarator, as the heating current is reduced in relation to the B_Θ supplied by the helical windings. The reduction is 730 A at 4.5 kG and 2 kA at 11.9 kG.

We thus obtain Tokamak like behaviour in so far as a constant β_Θ results. However, a substantial difference appears in that identical energy densities result at appreciably lower heating currents. Unfortunately our OH current is limited to $\iota < 0.5$ caused by the beforementioned $l = 2$ stellarator effects, so the transition to the Tokamak line, where $\iota_o \ll \iota$ is not included.

For a given ratio of the total rotational transform to that of the helical winding the next slide /6/ shows energy containment versus temperature. One should mention that for ι/ι_o constant the plasma current is constant and that with increasing ι/ι_o the effect of external rotational transform is reduced. The laser dots are calculated by averaging over the temperature and density profiles. The other points are normalized on the basis of these laser

measurements. On this plot a family of parallel lines may be drawn, whose position depends on the ratio of τ/τ_o total transform. At two such lines drawn for $\tau/\tau_o = 2.4$ to 3 resp. can be seen that the energy confinement is decreased at higher τ/τ_o values.

Conclusions

1. In our parameter range, that is in the intermediate regime, the energy confinement does not scale like Bohm.

2. The achieved energy density within the plasma at $\tau_o = 0.1$ is always above those, which should be obtained in a Tokamak discharge at the same heating current.

Our future work will be on the particle confinement time. There are indications that τ_p should be higher than τ_E^1 /5/.

/6/ A.G. Diky et al., Nucl. Fusion Supp. 1972, p.295, Conf. Pl. phys. Madison 1971
IAEA - 28/4 - 11

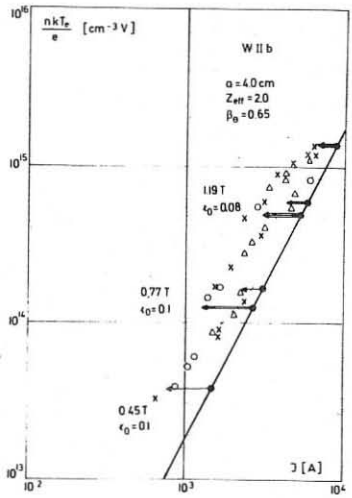

Fig. 5

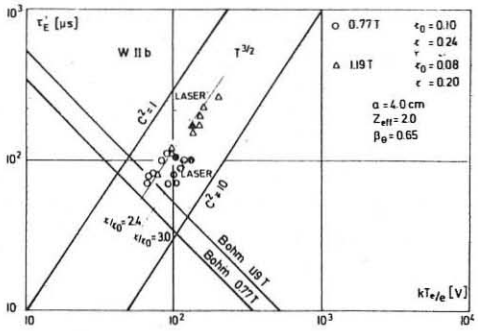

Fig. 6

RECENT RESULTS FROM THE GARCHING HIGH-BETA STELLARATOR TORUS ISAR T 1 (Part II).

E.Fünfer, M.Kaufmann, W.Lotz, J.Neuhauser, G.Schramm
Max-Planck-Institut für Plasmaphysik, Euratom Association,
Garching bei München, F.R.G.

A description of the ISAR T 1 experiment and a survey of the main results were given in Part I of our contribution. Some additional results are given in the following:

1) Equilibrium: The theoretical equilibrium condition is

$$\bar{r}_p\, \delta_1[\delta_2(2-\beta)+\delta_o(3-2\beta)] = \frac{2}{h^2 R}\cdot\alpha \quad \text{where } \alpha_{theory} \equiv 1.$$

a) $\ell=1/\ell=2$ - system: For $\beta \approx 0.7$ we needed for equilibrium about $\bar{r}_p\,\delta_1 \approx 2.0 \pm 0.2$ cm, $\delta_2 \approx 0.28 \pm 0.07$, yielding an experimental $\alpha_{12,exp} \approx 1.5 \pm 0.4$.

b) $\ell=1/\ell=2/\ell=0$ - system: In this case we found for $\beta \approx 0.7$: $\bar{r}_p\,\delta_1 \approx 1.8 \pm 0.2$ cm, $\delta_2 \approx 0.25 \pm 0.07$, $\delta_o \approx 0.07 \pm 0.02$ and consequently $\alpha_{120,exp} \approx 1.6 \pm 0.5$. As an illustration the motion of the centre of gravity of the plasma helix in the direction of toroidal drift x is shown in Fig.3 for different α-values. The inward or outward drift of the plasma for $\alpha > 1.6$ and $\alpha < 1.6$ respectively is readily seen. At early times ($t < 2.5$ µs) during the formation of the helical deformations the plasma is driven outward even with the right equilibrium fields.

In both cases a) and b) the experimental plasma distortion must be slightly higher for equilibrium than theoretically predicted, thus indicating a nonlinear effect.

2) Transverse drift: As stated in Part I (Section III,2) a drift parallel to the main torus axis was observed. This was eliminated by a 15^o-rotation of the $\ell=1$ helix. The corresponding motion of the centre of gravity of the plasma helix parallel to the main axis is shown in Fig.4.

A similar drift also occured for the pure $\ell=1/\ell=2$-system, where no z-modulation of the $\ell=1$ mirror currents is present (main coil not corrugated). Thus, bending of the $\ell=1$ and

ℓ=2-windings also yields a transverse force, which again can be compensated by readjusting the phase between them.

3) Stability:

a) Short wavelength m=0, m=1, and m=2 modes are triggered in the dynamic phase and are proved to be stable in agreement with theory.

b) No fast growing long wavelength instabilities with $m \geq 2$ are found, in contrast to ideal MHD theory assuming a sharp boundary.

c) The plasma seems to be lost owing to a long wavelength m=1 instability (wavelength at least 4 m) in qualitative agreement with theory. This instability is to be suppressed in future by wall stabilization working with a low compression ratio.

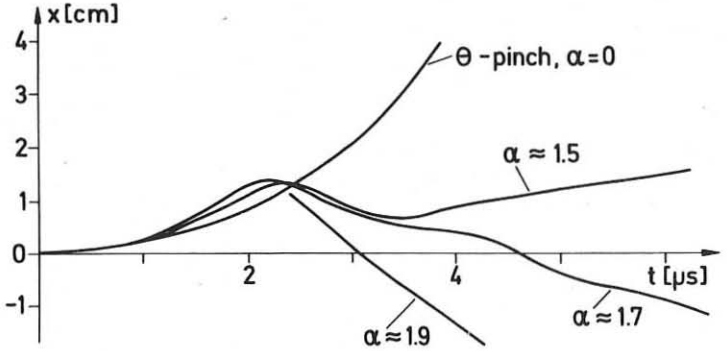

Fig. 3

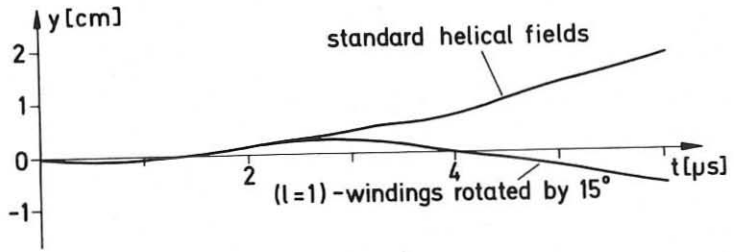

Fig. 4

FLUCTUATIONS AND CONTAINMENT OF PLASMA IN JIPP l=3 STELLARATOR

T. Dodo, M. Fujiwara, K. Miyamoto and A. Ogata

Institute of Plasma Physics, Nagoya University, Nagoya, JAPAN

In the main paper, the characteristic features of the experimental results and the outline of the interpretation are presented. In the following, a theoretical study is presented based on the fluid dynamical description and the slab model of the plasma cylinder.

Zero order quantities are the density gradient $\nabla n_0 = dn_0/dx = -\kappa n_0$, the static electric field E_0 directed to the density gradient, the electron drift velocity $V_e^{(0)} = (0, E_0/B_0 + \kappa T_e/eB_0, 0)$, and the ion drift velocity with the finite Larmor radius effect $V_i^{(0)} = (0, (1 - \delta)E_0/B_0 - \kappa T_i/eB_0, 0)$. The equation of motion of the ions includes the ion perpendicular viscosity, and that of electrons includes the electron-ion collision in the parallel motion. The dispersion relation thus obtained is

$$\{\omega_{0i}(1 + b) + it_\perp^{-1}\}(t_\parallel^{-1} - i\omega_*)/(t_\parallel^{-1} - i\omega_{0e}) - \omega_* + \lambda b\omega_{0i} + it_\perp^{-1} = 0 ,$$

where $\omega_{0i} = \omega - k_\perp(1 - \delta)E_0/B_0$, $\omega_{0e} = \omega - k_\perp E_0/B_0$,

$\omega_* = k_\perp \kappa T_e/eB_0$, $t^{-1} = b^2\nu_{ii}/4$, ν_{ii} is the ion-ion collision frequency, $b = k_\perp^2 \rho_i^2/2$, $t_\parallel^{-1} = k_\parallel^2 T_e/m_e\nu_{ei}$, $\lambda = T_e/T_i$, $k_\perp$ and $k_\parallel$ are the perpendicular and parallel wave number, respectively.

When $t_\parallel \ll t_\perp$ and (growth rate) $\ll (bt_\parallel)^{-1}$, the real part of the frequency ω_r and the growth rate γ are obtained from the above dispersion relation as:

$$\omega_r \simeq k_\perp (1 - \delta) E_0/B_0 + \omega_*/\{1 + b(1 + \lambda)\},$$

$$\gamma \simeq \omega_* t_{\shortparallel} \frac{b\omega_*}{\{1 + b(1 + \lambda)\}^2} \{\frac{(1 + \lambda)(1 + b)}{1 + b(1 + \lambda)} + (\frac{1}{b} + 1)\delta \frac{k_\perp (E_0/B_0)}{\omega_*}\}$$

$$- \frac{(1 + \lambda)}{1 + b(1 + \lambda)} t^{-1}$$

In the present experiment, $b \simeq 0.1$, $\lambda \simeq 10$, $\delta \simeq 1/2$, $k_\perp \simeq 2/3$ cm^{-1}, the rotation verocity E_0/B_0, the electron drift velocity $\kappa T_e/eB_0$, the parallel transit time of the electron $t_{\shortparallel}$, and the damping time by the ion viscosity $t_\perp$ are about 6×10^4 cm/sec, 6×10^4 cm/sec, 3×10^{-5} sec, and 10^{-2} sec respectively. The growth rate γ obtained from the above parameters has the same order of magnitude as the frequency $\omega_r (\gamma \simeq (\omega_r/4))$. This result is consistent with the large growth rate observed in the experiment (cf. Fig. 3 of the main paper). The frequency calculated from the above parameters is about 6 kHz and agrees well with the observed frequency.

In the present analysis, the relation between the fluctuation of the density $\tilde{n}$ and the fluctuation of the electric potential $\tilde{\psi}$ is

$$\frac{\tilde{n}}{n_0} = \frac{t_{\shortparallel}^{-1} - i\omega_*}{t_{\shortparallel}^{-1} - i(\omega - k_\perp E_0/B_0)} \frac{e\tilde{\psi}}{T_e} .$$

In the experiment, $t_{\shortparallel}^{-1} \simeq \omega_*$ and $\omega - k_\perp E_0/B_0 \simeq 0$, therefore, the phase difference between $\tilde{n}$ and $\tilde{\psi}$ is near to $\pi/4$. This large phase difference explains the observed rapid loss of the plasma during this instability.

PLASMA CONFINEMENT BY HYBRID STELLARATOR FIELD OF ℓ=2 AND ℓ=3

M. Fujiwara, K. Kawahata, A. Mohri and K. Miyamoto
Institute of Plasma Physics, Nagoya University, Nagoya, JAPAN

§1. Effect of Shear on The Resonant Losses.

When the plasma confined in the ℓ=2 stellarator field the confinement time during afterglow becomes small near the rational transform angle. The upper-left curve of Fig.5 shows the dependence of τ on the ratio of ℓ=2 helical coil current I_{h2} to the current I_t of toroidal coil while the toroidal field is 1.4 kG(3.8 GH_z). When the ℓ=3 stellarator field is supperposed, the shear is introduced. Increasing the shear, the structure of resonant losses of τ - I_{h2}/I_t curves becomes gradually weak. The other curves of Fig.5 show the dependence of τ on I_{h2}/I_t, while the ratio of the ℓ=3 helical coil current I_{h3} to I_{h2} is kept to be 0.5, 1.0 and 1.5. The rotational transform angle ι divided by 2π is approximately expressed by $\iota = 0.27(I_{h2}/I_t)^2 + 6 \times 10^{-3}\, r^2 (I_{h2}/I_t)^2$ with accuracy of about 4% in this device (r being the inner radius in cm). From these results, the resonant losses are reduced when the shear parameter $s = a(d\iota/dr)(a/R) \sim \Delta\iota(a/R)$ becomes larger than $0.06(a/R)$.

§2. Density distributions in The Rational and Non Rational Cases.

The density distributions of afterglow plasma are measured by a movable probe in a rational case near $\iota \sim 1/2$ and a non-rational case just above $\iota \sim 1/2$. As is expected, indication of convective motion is observed in the density distribution of the rational case and the convective cells persist to exist for long period.

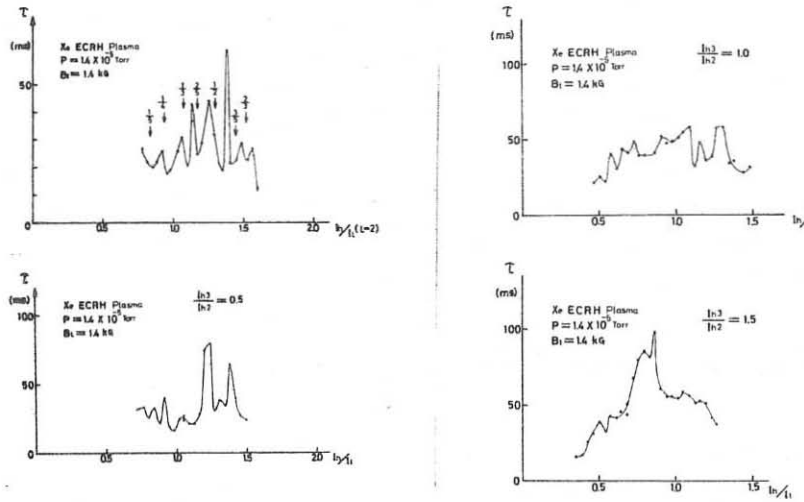

Fig.5 The dependence of confinement time τ on the ratio of I_{h2} to I_t, while the ratio of I_{h3} to I_{h2} is kept to be 0, 0.5, 1.0 and 1.5.

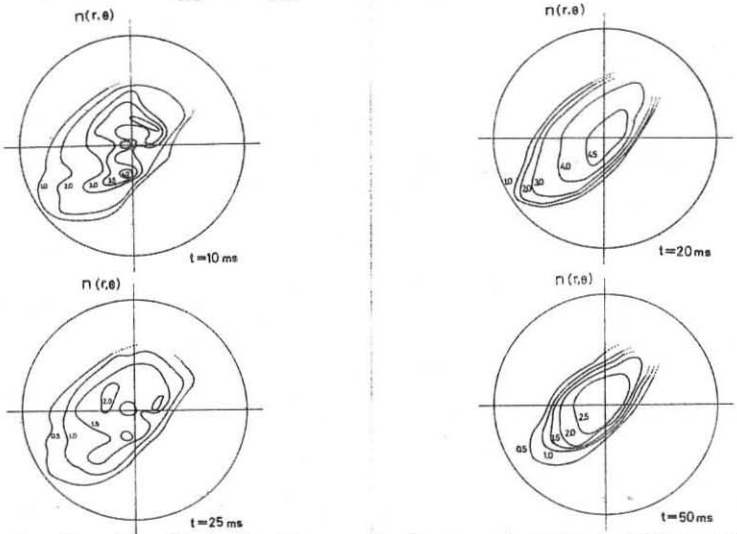

Fig.6 The density distributions of plasma at time t after switching off the ECRH power in the rational case (left-hand side I_{h2}/I_t = 1.37, $t \sim 1/2$) and non-rational case (right-hand side, I_{h2}/I_t = 1.43).

Heating Mechanism and Thermal Conductivity Coefficient in High Electron Temperature Plasma Produced by High Power Microwave Heating in the FM-1 Spherator

K. Chen, D. Meade, M. Okabayashi, M. Porkolab, and J. Schmidt

Plasma Physics Laboratory, Princeton University

Princeton, New Jersey 08540, U.S.A.

Abstract: In the previous paper[1] it was reported confinement properties of plasma produces high power microwave heating. Here we discuss the heating mechanism and the thermal transport from the localized heating region.

In order to investigate the heating mechanism, we measured ion temperature by Doppler broadening, etc. At the localized heating region (close to ECR surface), we observed a typical frequency decay spectrum.[2] Figure 1 shows the ion heating rate measured by the Doppler broadening technique. The heating rate ($\Delta Ti/\Delta t$) shows a threshold power level of 0.7 ~ 1K$\bar{W}$. The increase of ion temperature during the heating pulse is compared with numerical calculations (solid line). The classical electron-ion coupling is not sufficient to explain the observed ion temperature increase. An additional power input to ions of 25 ~ 30$\bar{W}$ is required. The most likely heating mechanism is the one through the parametric decay process, presumably the electrons are heated by upper hybrid waves and ions by lower hybrid waves.

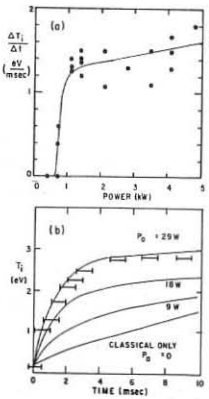

Fig. 1

---

1. K. Chen et al in this conference

2. M. Okabayashi et al MATT-992 Princeton University

Since the heating takes place close to the resonance region, the high electron temperatures are localized on the magnetic surface, which coinsides with the resonance surface. Figure 2 shows the behavior of initially localized electron heat source. By applying a 100μsec heating pulse, at the resonance region ($X=0_{cm}$), the ion saturation current (I_s) increased immediately. However, outside the resonance zone, X=0.5cm, X=1.0cm, the raise time of ion saturation current is gradually delayed. This indicates that heat localized initially at X=0cm is diffusing out.

In Fig. 3 the propagation of the front edge of electron temperature profile at different time points is plotted. The thermal conductivity is $K \sim 2X10^3 cm^2/sec$. This value is slightly higher than the particle diffusion coefficient D.

This work was supported by U. S. Atomic Energy Commission Contract AT(11-1)-3073.

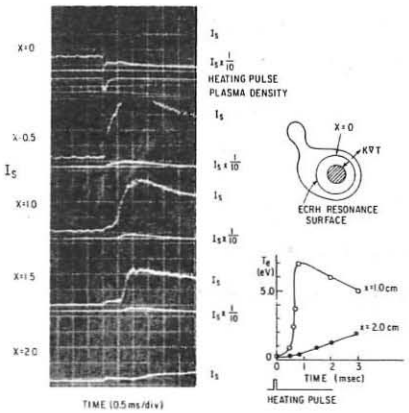

Fig. 2

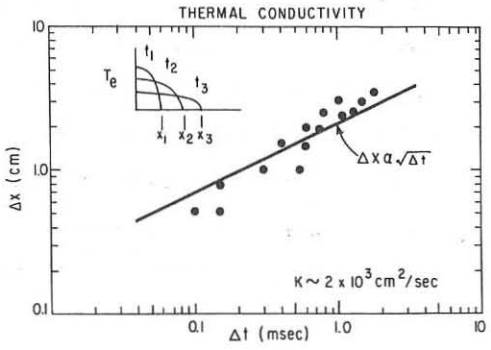

Fig. 3

Turbulent Diffusion Coefficients of Toroidal Plasmas

S. Yoshikawa

Department of Physics, University of Tokyo
Bunkyo-ku, Tokyo 113, Japan

In spite of progress in understanding the classical diffusion processes of toroidal plasmas,[1,2] there exist yet definite discrepancies between the observed plasma confinement times and theoretical values calculated from classical processes.[3,4] The phenomenological scaling laws for plasma confinement using both the Bohm law[5] and the pseudoclassical diffusion coefficients[6,7] appear to describe reasonably well the observed confinement times in the wide range of parameters (100 μsec to 3 seconds) in a variety of toroidal confinement devices such as stellarators, tokamaks, and multipoles.[8] Yet as the parameter $\gamma = nB^{-1} T_e^{-3/2}$ decreases, there appears

to be some discrepancy from the pseudoscaling law in Princeton spherator experiments.[9] Similar discrepancies were noted in octupoles[10] (although, in this case, the classical theory appears to apply in some range) and tokamaks[4] as the density, n, hence γ, decreases.

We shall try to present another version of the derivation of the pseudoclassical diffusion coefficients which makes the relation with the Bohm diffusion coefficient transparent and, because of the nature of the derivation, the range of the validity of the pseudoclassical diffusion becomes clear. We then try to compare these predictions with the experiments.

As is well known, the diffusion coefficient due to fluctuations can be expressed as

$$-D(\nabla n_0)_x = \frac{\langle \tilde{n}\, \tilde{E}_y \rangle_{av}}{B} \qquad (1)$$

where the tilda indicates the fluctuating quantity either in time or in space, or both. Assuming that the potential fluctuation and the density fluctuation have the phase difference α and assuming that the magnitude of density fluctuation and potential fluctuation have the drift-wave-like relation

$$\left|\frac{\tilde{n}}{n_0}\right| = \left|\frac{e\tilde{\phi}}{kT_e}\right| \qquad (2)$$

we get

$$D = |a k_y| \frac{kT_e}{eB} \left|\frac{\tilde{n}}{n_0}\right|^2 \sin\alpha \qquad (3)$$

Alternatively we can note that the diffusion coefficient should be a function of the dissipation due to current in the plasma.[11] The electric current due to the fluctuations can be expressed as

$$\tilde{J}^2 = \left(\frac{e}{m\nu_c} k_\parallel \tilde{n} k T_e \right)^2 |1 - \exp i\alpha|^2 \qquad (4)$$

if the fluctuation level is small compared with $|\alpha|$, where ν_c is the collision frequency.

Then the diffusion coefficient may be estimated as (ω_e is the electron cyclotron frequency)

$$D = \frac{kT_e}{eB} \frac{\omega_e}{\nu_c} (k_\parallel^2 a^2) \frac{1}{(1 + T_i/T_e)^2} \frac{\tilde{n}^2}{n_0^2} 4 \sin^2 \frac{\alpha}{2} \qquad (5)$$

Equating Eqs. (3) and (5), we arrive at

$$2 \tan \frac{\alpha}{2} = \frac{(1 + T_i/T_e)^2}{k_\parallel^2 a^2} |a k_y| \frac{\nu_c}{\omega_e} \qquad (6)$$

For α small,

$$D = \frac{kT_e}{eB} \left| \frac{\tilde{n}}{n_0} \right|^2 \frac{k_y^2}{k_\parallel^2} \left(1 + \frac{T_i}{T_e} \right)^2 \frac{\nu_c}{\omega_e} \approx \frac{\nu_c}{\omega_e} \frac{kT_e}{eB} \left| \frac{\tilde{n}}{n_0} \right|^2 \frac{k_\perp^2}{k_\parallel^2} \frac{1}{2} \left(1 + \frac{T_i}{T_e} \right)^2 \qquad (7)$$

This is identical to the expression for the pseudo-classical diffusion coefficient if $\frac{1}{2}(1 + \frac{T_i}{T_e})^2$ is replaced by unity.

If α becomes too small so that α is less than $|n/n_0|$, the above derivation is no longer valid. Thus, under that circumstance, we may expect that the diffusion coefficient exceeds the pseudo-classical diffusion.

REFERENCES

1 A. A. Galeev, and R. Z. Sagdeev, Zh. Eksp. Teor. Fiz. 53, 348 (1967); [Sov. Phys. - JETP 26, 233 (1968)].

2 M. N. Rosenbluth, P. H. Rutherford, J. B. Taylor, E. A. Frieman, and L. M. Kovrizhnykh, in Proceedings of the Fourth International Conference on Plasma Physics and Controlled Nuclear Fusion Research (International Atomic Energy Agency, Vienna, 1971) Vol. I, p. 495.

3 D. Dimock, D. Eckhartt, H. Eubank, E. Hinnov, L. C. Johnson, E. Meservey, E. Tolnas, and D. J. Grove, in Proceedings of the Fourth International Conference on Plasma Physics and Controlled Nuclear Fusion Research (International Atomic Energy Agency, Vienna, 1971) Vol. I, p. 451.

4 F. L. Hinton, J. C. Wiley, D. F. Duchs, H. P. Furth, and P. H. Rutherford, Phys. Rev. Lett. 29, 691 and 1050 (Errata) (1972).

5 D. Bohm in The Characteristics of Electrical Discharges in Magnetic Fields, edited by A. Guthrie and R. K. Wakerling (McGraw-Hill Book Co., Inc., New York, 1949) p. 12.

6 L. Artsimovich, ZHETF Piz. Red. 13, 101 (1971) [Sov. Phys. JETP Lett. 13, 70 (1971)].

7 S. Yoshikawa, Phys. Rev. Lett. 25, 353 (1970).

8 S. Yoshikawa and N. Christofilos, in Proceedings of the Fourth International Conference on Plasma Physics and Controlled Nuclear Fusion Research (International Atomic Energy Agency, Vienna, 1971) Vol. II, p. 357.

9 J. Sinnis, M. Okabayashi, J. Schmidt, and S. Yoshikawa, Phys. Rev. Lett. 29, 1214 (1972).

10 T. Ohkawa, M. Yoshikawa, J. R. Gilleland, and T. Tamano, in Proceedings of the Fourth International Conference on Plasma Physics and Controlled Nuclear Fusion Research (International Atomic Energy Agency, Vienna, 1971) Vol. I, p. 15.

11 M. D. Kruskal in Plasma Physics (International Atomic Energy Agency, Vienna, 1965) p. 115.

THE FIRST EXPERIMENTAL RESULTS IN FINGER RING TOKAMAK

(Supplement to paper 1.7.4)

A.V. Bortnikov, Yu.T. Baiborodov, N.N. Brevnov,
V.G. Zhukovskii, L.E. Zakharov, D.V. Orlinskii,
V.I. Pergament, M.K. Romanovskii, N.I. Sokolov,
A.M. Us.

I.V. Kurchatov Institute of Atomic Energy, Moscow, USSR

The experimental results presented below have been obtained after vacuum training of the machine. The initial pressure $p_o = 10^{-7}$ torr.

As judged from the discharge current oscillograms there are two modes of operation: a) small current regime $J < 12$ ka, and b) large current regime $J > 12$ ka.

The former regime oscillograms do not show any oscillations, the discharge current time is determined by the skin time of the copper shell (Fig.2 /1/). The current channel centre is located near the geometrical centre. The temperature T_e calculated from the conductivity is 20 – 40 ev.

The latter regime is characterized by spikes. The current spikes are accompanied by bursts of emission H and impurity lines, broadening of light region in the vertical derection (Fig.1). Magnetic probe oscillations ($\dot{B}_r$) in the symmetry plane are in

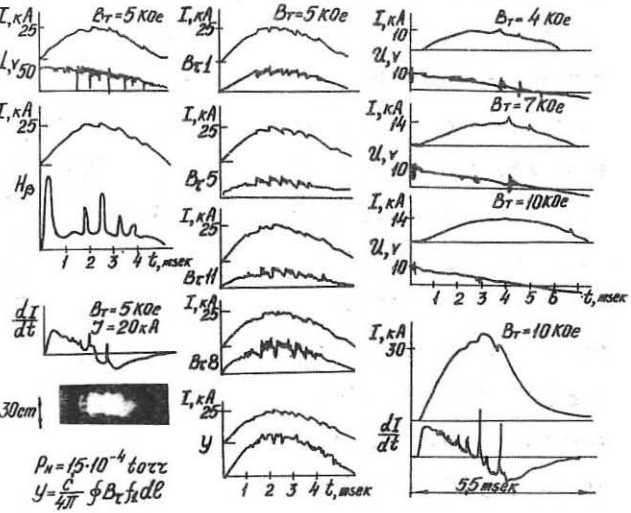

Fig. 1.

counterphase to the current fluctuations, while the probes in the upper and lower regions are in phase with current variations. Displacement of the current channel centre over R was monitored by an integral probe "Y" embracing the current. The displacement is proportional $\Delta \sim \frac{y}{J}$ /2/. From inspection of the oscillograms it is seen that before a spike the current channel centre is displaced towards R (to the outside from the geometrical centre of the device by the value ≤ 1 cm. If one compares the character of the displacement of the current channel centre and variation of B at the magnetic probes 1 it is possible to conclude that before a spike the plasma column displaces to the outside, increases l_r and decreases l_z, i.e. the column shape becomes more circular. At spike the plasma column enongates. Thus, at large currents the shape of the plasma cross section is observed to vary.

The averaged distribution B is in satisfactory agreement with theoretical calculations. (Fig.2) /2/.

The longitudinal field slightly influences the discharge at $J > 12$ ka. However, at $J \simeq 12$ ka as B_T increases the spikes are suppressed. (Fig.1). If the expression for q is taken from Ref. /3/ for $\frac{l_z}{l_r} = 2$, $B_T = 10$kOe and J=14 ka condition $q < 3,5$ is satisfied for the first regime, while $q > 3,5$ for the second regime.

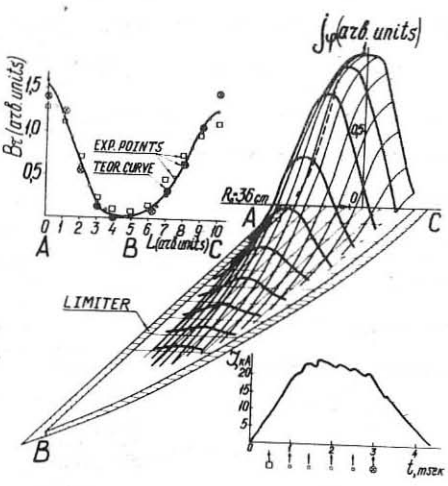

Fig.2.

References.

1. A.V. Bortnikov at all. The Ist volume of this conference, p. 165.

2. V.D. Shafranov, L.E. Zakharov, JTP, 43, N 2, 225 (1973).

3. L.A. Artsimovitch, V.D. Shafranov, JETP Pis'ma, 15, 72 (1972).

EQUILIBRIUM ROTATION OF A TOKAMAK DURING NEUTRAL INJECTION

E. Canobbio and O. De Barbieri

Association EURATOM-CEA
Département de Physique du Plasma et de la Fusion Contrôlée
Centre d'Etudes Nucléaires
B.P.85 - 38041 - GRENOBLE (France)

ERRATA

1) Section 1, line 6 : neglect "the slowing-down and".
2) The R.H.S. of Eq. (1) should read :

$$B_0\theta\langle j_r\rangle/c\ (1+O(r/R))$$

Addendum to:

The Simulation of Classical Toroidal Plasmas in the Plane.

D. E. Potter & G. H. Tuttle.

Preliminary Solutions in the Tokamak Regime

Solutions illustrating qualitatively the formation and structure of the pinch in the Tokamak configuration are included in Figures 1-5. The main feature briefly shown is the effect of varying $\beta_{pol} = \frac{2}{3}W_p/W_b$ where W_p is the total energy of the plasma and W_b is the total poloidal magnetic energy. The field structure for the three cases $\beta_{pol} = .02, 2.1, 15$ are shown in Figures 1, 2, and 3 respectively, for an aspect ratio of the torus of 3. It is clear that in the limit of $\beta_{pol} \to 0$, the assumption of shifted near-circular field surfaces is an accurate and appropriate approximation and suggests that one-dimensional models in this limit are applicable.

On the other hand, when β_{pol} is finite, the structure is essentially two-dimensional and expansions based on the aspect ratio would not appear to be appropriate.

The sequence illustrated in Figure 3 shows that the time evolution of the field surfaces for $\beta_{pol} = 15$. The fields are driven by the "E/B" flow structure illustrated in Figure 4 and the effect of image currents in the wall are reflected in the toroidal current distribution shown in Figure 5. Cutting of the lines (through the existence of only a small resistivity) on the central field surfaces changes the topology and produces a

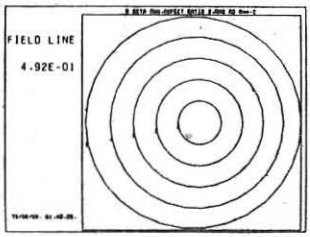

Fig.1. Equilibrium magnetia field surfaces for β_{pol}=0.02.

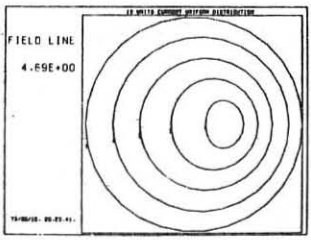

Fig.2. Equilibrium magnetic field surfaces for intermediate β_{pol}=2.1

double magnetic axis. Subsequent to Figure 3d, a neutral point is produced and a separatrix created within which there are two magnetic axes and outside of which the field surfaces have one imaginary axis. Our time-dependent solutions suggest that this phenomena will occur on ignition or if sufficient neutrals are used to heat the plasma. The mechanism illustrated in Figures 4,5,6 also suggests the manner by which the pinch is initially created. The flow occurs on a timescale $\kappa a/v_s$ where a is the minor radius, κ is the aspect ratio of the torus and v_s is the sound speed.

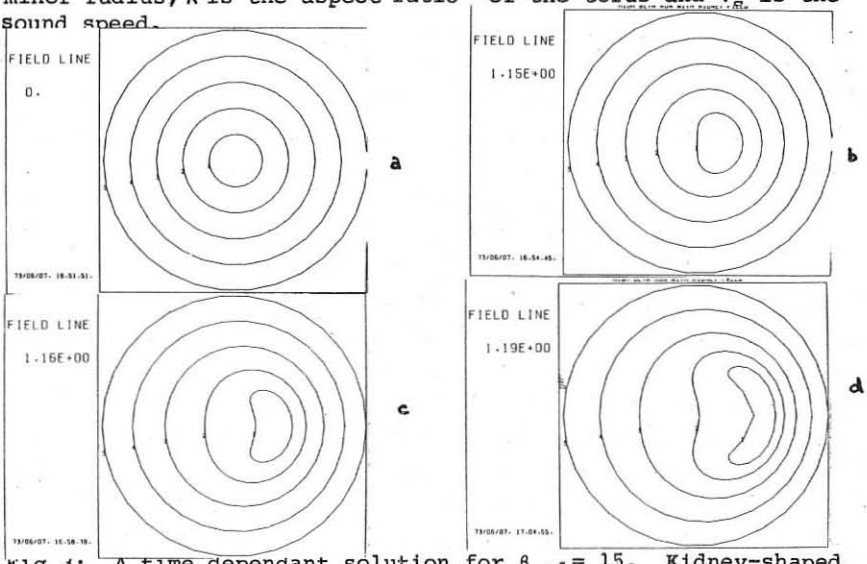

Fig 3: A time dependant solution for $\beta_{pol} = 15$. Kidney-shaped surfaces are produced (d). Resistive cutting of the inner lines produces a double magnetic axis at subsequent times.

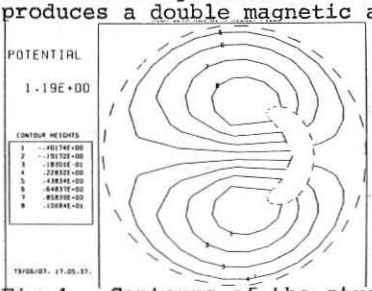

Fig.4. Contours of the stream function showing the dipole flow structure creating the fields of Fig.3d.

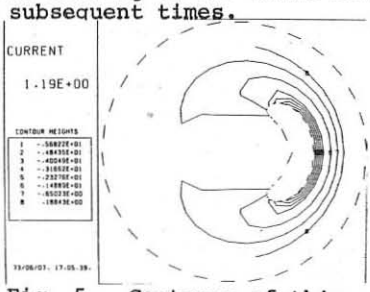

Fig. 5. Contours of this toroidal current density corresponding to Fig.3d.

Arbitrarily Shaped Resistive Tokamak Equilibria

B.J. Green, K.U. v. Hagenow, H.P. Zehrfeld

Max-Planck-Institut für Plasmaphysik, 8046 Garching, FRG

Supplement

We present here more results for the case of a torus with square cross-section and $\tau + q_p = 0$. Fig.4 shows the functional dependence of β_p on inverse aspect-ratio. The large variation of β_p in the case where p is assumed a linear function of poloidal magnetic flux, is to be contrasted with the small variation in the case where p is determined by ring voltage, mass sources and toroidicity.

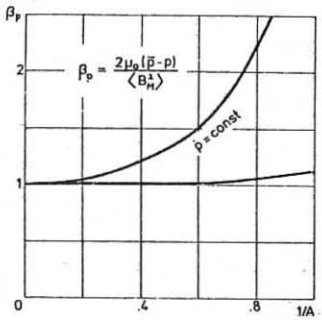

Fig. 4

The radial profiles, in the equatorial plane, of current density and rotational transform are shown in figs.5 and 6. In the case of current density (fig. 5) the curves have been normalised to their maximum values. In fact, the comparison is made for constant total current. Here one can clearly see the effect of toroidal curvature on the current distribution. Indeed, for smaller aspect ratios a skin effect is evident.

The curves of rotational transform (normalised to their maximum values) further illustrate the significant influence of toroidicity, in that the regions of shear and the value of the shear itself vary appreciably with aspect ratio. At present we are obtaining results for other plasma cross-sections and will proceed to treat other situations (dia or paramagnetic).

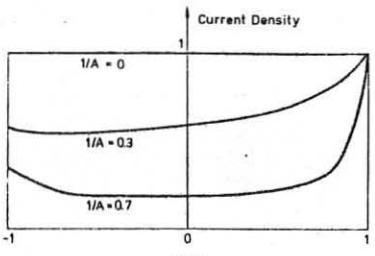

Fig.5

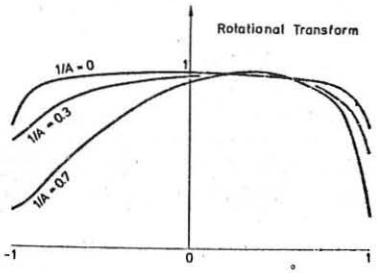

Fig 6

MHD TOKAMAK EQUILIBRIA IN PRESENCE OF WEAK DEVIATIONS FROM AXISYMMETRY

C. Lo Surdo and A. Sestero

Laboratori Gas Ionizzati (Associazione EURATOM-CNEN), C.P. 65
00044 Frascati, Rome, Italy.

With reference to the MHD equations of static equilibrium,

$$\nabla p = \underline{J} \times \underline{B}\,, \qquad \nabla \times \underline{B} = \underline{J}\,, \qquad \nabla \cdot \underline{B} = 0\,, \tag{1}$$

it is known that the only exact solutions which represent confined toroidal plasmas are either (a) symmetric with respect to an axis or (b) symmetric with respect to a plane (see, e.g., / 1 /). In practice, however, a high degree of symmetry is difficult to achieve in real containment devices; one is thus led to investigate possible approximate solutions of Eqs. (1). To this end, an asymptotic expansion scheme has been set up in / 2 /, which is appropriate to deal with weak deviations from axisymmetry in the Tokamak configuration, and solutions have been worked out to the lowest significant order in the expansion parameter.

Inasmuch the confinement times experimentally observed are much longer than typical MHD times, however, the existence of a solution to the lowest significant order is not enough. One ought to be able to show that the equilibrium equations can be satisfied to at least a few more orders, or possibly to all orders. Indeed, any "imbalance" in the equilibrium equations is presumably to be counterbalanced by non-equilibrium terms, containing time derivatives: hence the larger is the imbalance, the faster would be the decay of the configuration.

In this paper we therefore consider the problem of the existence of the solution in the higher orders, with reference to the expansion introduced in / 2 /. The latter is defined essentially by the following ordering assumptions in the small dimensionless parameter ϵ :

$$\begin{array}{ccccc} \bar{B}_T : \bar{B}_P : \tilde{B} & & \bar{J}_T : \bar{J}_P : \tilde{J} & & \bar{p} : \tilde{p} \\ \epsilon^{-1} : 1 : 1 & & 1 : \epsilon : \epsilon & & 1 : \epsilon \end{array} \tag{2}$$

Here the bar denotes the axisymmetric part, and the tilda the remaining part, of a given quantity, and the subscripts T and P denote the toroidal and poloidal components, respectively, of a given vector. The assumptions (2) are not all independent, because of Eqs. (1), but it can be easily seen that they are all consistent with each other, if one assumes, as we do, that the aspect ratio is finite. In this scheme the "β" of the plasma is of the order of ϵ^2, and the familiar quantity "q" is formally large, of the order of ϵ^{-1}, both this quantities being defined in terms of the axisymmetric part of the

equilibrium.

By taking into account the assumptions (2), from Eqs. (1) one obtains the equations to the various orders in ϵ. To the lowest significant order the equations have been solved in / 2 /. In the next order, for the existence of the solution we derive two compatibility conditions:

$$\oint d\eta\, r\left[\overline{\nabla(r^2 \frac{d\bar{P}^{(0)}}{d\psi^{(0)}}\nabla\psi^{(0)}\cdot\int_0^{\varphi} d\varphi'\,\tilde{\underline{B}}_P^{(0)})\cdot\tilde{\underline{B}}_P^{(0)}} + r\frac{d\bar{P}^{(0)}}{d\psi^{(0)}}\nabla\psi^{(0)}\cdot\overline{\tilde{\underline{B}}_P^{(0)}\,\tilde{B}_\varphi^{(0)}}\right] = 0, \quad (3)$$

$$\oint d\eta\, r^3\left[\overline{\nabla(r^2\frac{d\bar{P}^{(0)}}{d\psi^{(0)}}\nabla\psi^{(0)}\cdot\int_0^{\varphi} d\varphi'\,\tilde{\underline{B}}_P^{(0)})\cdot\tilde{\underline{B}}_P^{(0)}} + r\frac{d\bar{P}^{(0)}}{d\psi^{(0)}}\nabla\psi^{(0)}\cdot\overline{\tilde{\underline{B}}_P^{(0)}\,\tilde{B}_\varphi^{(0)}}\right. \quad (4)$$

$$\left. + \nabla\psi^{(0)}\cdot\overline{\tilde{\underline{B}}_P^{(0)}\int_0^{\varphi} d\varphi'\,\tilde{\underline{B}}_P^{(0)}}\cdot\nabla\mathcal{L}\,\psi^{(0)}\right] = 0.$$

Here and in the following, r is the distance from the axis of symmetry; φ is the angle coordinate in the toroidal direction; $\psi^{(0)}$ is the poloidal flux function associated with $\bar{\underline{B}}_P^{(0)}$ (the true flux being $2\pi\psi^{(0)}$); the superscripts (n) mean that the corresponding quantities are of the order of ϵ^n ($n = -1,0,1,2,\ldots$); the symbol $\mathcal{L}$ denotes the operator $\partial^2/\partial z^2 + \partial^2/\partial r^2 - r^{-1}\partial/\partial r$, where z is the height above the equatorial plane; finally, η is a cyclic coordinate, orthogonal to the coordinates φ and $\psi^{(0)}$, and defined essentially by the relation

$$\left(\frac{\partial}{\partial\eta}\right)_{\varphi=\text{cost};\,\psi^{(0)}=\text{cost}} \equiv \underline{e}_\varphi \times \nabla\psi^{(0)}\cdot\nabla, \quad (5)$$

where $\underline{e}_\varphi$ is the unit vector in the φ direction.

We recall that the axisymmetric theory of Eqs. (1) leaves room for two arbitrary functions, $p(\psi)$ and $I(\psi)$, where $I = r B_\varphi$. Similarly in our case $\bar{P}^{(0)}(\psi^{(0)})$ and $I^{(1)}(\psi^{(0)})$ are left arbitrary in the lowest order theory. One might ask whether Eqs. (3) and (4), plus the lowest-order equilibrium condition

$$\mathcal{L}\psi^{(0)} + r^2\frac{d\bar{P}^{(0)}}{d\psi^{(0)}} + I^{-1}\frac{dI^{(1)}}{d\psi^{(0)}} = 0, \quad (6)$$

interpreted as equations for $\psi^{(0)}$ $\bar{P}^{(0)}$ and $I^{(1)}$, could eventually lead to their determination. This poses an interesting but very difficult mathematical problem, beset by complicated nonlinearities. From the physical point of view, on the other hand, we cannot ignore that other independent equations for $p(\psi)$ and $I(\psi)$ can be obtained by suitably enlarging the set of Eqs. (1) (to include, for instance, a conductivity law, as well as other transport features). As a matter of fact, the experimental evidence is all in favor of $\bar{P}^{(0)}(\psi^{(0)})$ and $I^{(1)}(\psi^{(0)})$ being determined by the transport equations, and Eqs. (3), (4) do not seem in general to be satisfied. From what has been previously said, therefore, one is led to the conclusion that the Eqs. (1) of static, scalar-pressure MHD equilibrium are inadequate to account for long confinement times, if the deviations from axisym

metry are as large as prescribed by relations (2). A more flexible set of equations is presumably needed.

By contrast, if the deviations from axisymmetry are weakened by one order in ϵ (namely, if one takes $\tilde{B}$ of the order of ϵ, whence it follows that $\tilde{J}$ and $\tilde{p}$ are of the order of ϵ^2), preliminary results seem to indicate that a solution of Eqs. (1) can exist to all orders in the expansion scheme, essentially because in the higher orders there seems to be more freedom to satisfy the various compatibility conditions that are derived. In this case, it is probably fair to accept Eqs. (1) as an adequate model for the description of the equilibrium.

REFERENCES

/ 1 / H. GRAD: Phys. Fluids 10, 137 (1967).
/ 2 / A. SESTERO: Plasma Phys. (to appear).

HOT ELECTRON PLASMA ACCUMULATION IN AN OPEN ENDED MINIMUM B SYSTEM

BY

R. Bardet, P. Briand, L. Dupas, C. Gormezano, G. Melin.

ASSOCIATION EURATOM-CEA
Département de Physique du Plasma et de la Fusion Contrôlée
Service IGn - Centre d'Etudes Nucléaires
B.P.85 - Centre de Tri - 38041
GRENOBLE CEDEX (France)

In order to check the results of ion temperature measurements obtained by neutral analysis, an optical method has been used : ion temperature is evaluated by the Doppler broadening of the 4686 Å line of He^+ which is introduced into the plasma source. The light is analysed by means of a Fabry-Perot interferential disperser and a multichannel digital spectrometer.

Unfortunately, cold plasma creation and injection with a helium-hydrogen mixture are less efficient and less reproductible than with pure hydrogen. Consequently the accumulated densities are lower by a factor 2 to 4 and moreover the errors due to bad reproductibility are to be added to the intrinsic errors of the diagnostics.

The experimental parameters are the following : repetition rate = 2Hz - Injection time : 10 ms - Heating time : 10 ms -Basic pressure : 4.10^{-8} torr - Operating pressure $\simeq 10^{-7}$ torr - B = 2600 Gauss-$(B_\perp/B_{//})_{wall}$ = 2.6 - Gaz mixture = 50% H_2-50%He - The injected densities ranges between 4.10^{10} and 10^{11} e/cm^3.

We have tried to measure the diameter of the plasma by the angular analysis of the perpendicular emission of neutral by the plasma. We used a Faraday cage with a secondary emission target both of which are orientable with an angular displacement of 15 degrees. Although this measurement is limited by the parasites and by the geometry of the system, we could estimate the plasma diameter between 4 and 6 cm for the injected plasma, between 7 and 12 cm during the heating time and after this time, it increases rapidly but the precision is then insufficient for a quantitative evaluation.

The product nd of the electron density by the diameter of the plasma measured by Zebra-stripe interferometry is of the order of 2.10^{12} e/cm^{-2}. After the R.F. switch off, the first characteristic decay time of nd varies between 3 and 4 ms and the second one between 20 and 60 ms. Due to the bad reproductibility of injection, it is not possible to study the effect of the RF power on nd.

The variation of the diamagnetism B with the RF power is indicated on fig I. The corresponding β factor ranges between 4.10^{-2} and $1.02\ 10^{-1}$. The first decay time of diamagnetism is 5.5 ms and the second one varies between 35 and 50 ms.

The electron temperature evaluated by X rays analysis is plotted on fig 1.

The measure is done after the end of the heating pulse to avoid radiation from the walls. For the same reason, we measured only the second characteristic time of the X radiation which is 24 ms.

The potential well depth cannot be measured during the heating time because the important signal probably due to the axial hot electrons coming from source. After the RF switch off, the value of the well depth is deduced from the half amplitude of the cold electron current collected by the analyser. This value is slowly decreasing and varies from-35V to-10V in 40 ms. Ignoring the exact place where these electrons are created, it is quite difficult to deduce the absolute value of the well depth from this measurement.

We reported on fig 1 the variation of the H^+ ion temperature evaluated from neutral energy analysis. This temperature does not seem to vary during the plasma decay. The first characteristic time ranges between 3 and 3.5 ms and the second one between 12 and 20 ms. The optical measurement of He^+ ion temperature has shown the presence of parasite lines, which are not yet identified, on each side of the broadened He^+ line. In spite of that, we can conclude that the He^+ ion temperature is at least 40 eV and probably in the range of 100 eV.

In conclusion, electron and ion temperature increase with the R.F. power but the precision of the diagnostic system will be improved in order to find scaling laws.

fig.1

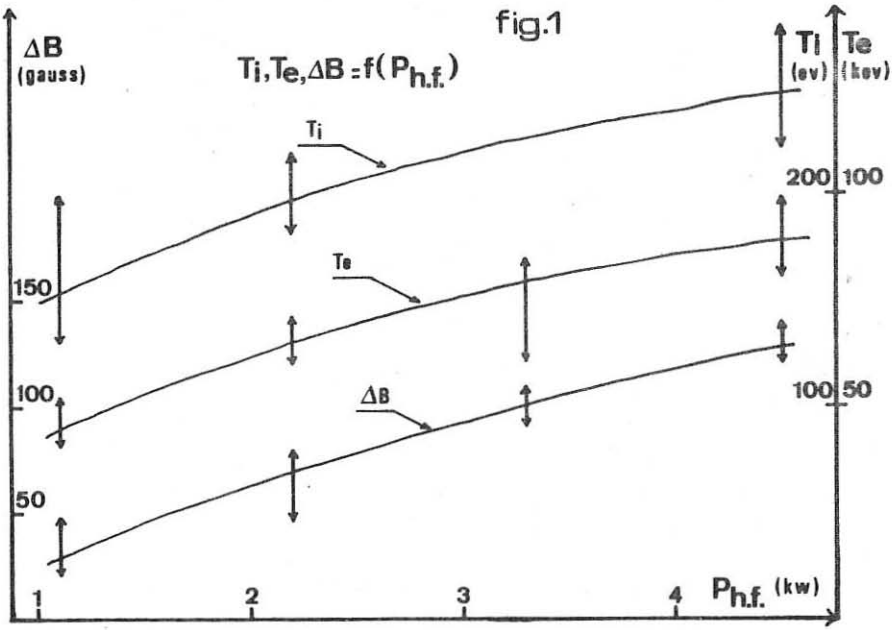

FURTHER STUDIES OF A HIGH-BETA REVERSED FIELD PINCH

(Supplementary Paper)

C.W. Gowers*, J.W. Long†, A.A. Newton, B.A. Norton+
D.C. Robinson, A.J.L. Verhage, H.A.B. Bodin

* AWRE, Aldermaston, Berkshire, † Oxford Polytechnic

\+ Royal Holloway College.

In this supplementary paper the observations on the emission of hard x-rays [1] from stable pinch discharges, which will be presented in the talk, are summarised.

X-rays with energies up to 1-2 MeV are observed to be emitted from stable reversed field discharges and from "stabilised" pinches provided stability is maintained. The energy was estimated from an absorption method and extended down to the limit of detection with the present arrangement of some tens of keV. This phenomenon differs from the more usual x-ray emission from runaway electrons in that the angular distribution of the x-rays indicates that the motion of the fast electrons as they escape from the plasma and hit the walls is primarily in the azimuthal (θ) plane. This is shown in Fig.1.

Fig.2 shows an oscillogram of the gas current and hard x-ray emission. In almost all conditions the emission begins at about 4.0-4.4 μsec from the start of the current pulse with half width typically 2 μsec. The onset time and pulse length are independent of the shape or amplitude of the current pulse, but the x-ray pulse shape does vary with conditions. Hard x-rays are only emitted in stable conditions and any instability before $\sim$ 4 μsec reduces the hard x-ray yield to less than 2% of its original value. The yield induced by inserting a probe into the plasma comes earlier and is of lower energy, indicating that fast electrons are born and accelerated at early times at radii comparable or less than that of the current sheath.

Fast electrons are accelerated by both E_z and E_θ, and the electric fields, deduced from magnetic probe measurements in similar conditions are $\gtrsim$ 10-30 V/cm, which can cause runaway and acceleration to MeV in a few μsec. The fast electrons are well confined, although it should be noted that the plasma column is pinching during the acceleration; electrons make between 25 and 100 revolutions of the major axis and some 2000 of the minor axis. The apparatus was calibrated using a radioactive Co^{60} source of known activity. The fast electron flux is about 2×10^8 cm^{-2} corresponding to a total fast electron energy of 1-2 joules as compared with plasma energy of some 100 joules. It is believed that the total accelerated electron energy may be an order of magnitude greater than that of the energetic (> 200 keV) component.

Correction: In the main paper the density scale in Fig.2 is incorrect; the scale should be multiplied by a factor of 0.75. It should also be pointed out that in Fig.4 the theoretical curves were obtained from model calculations based on experimental data at 3 μsec.

Reference

[1] Volkov, Ya.F., Tolok, V.T., Sinelnikov, K.D. Zh. Tekh. Fiz. vol.32, p.811, 1962.

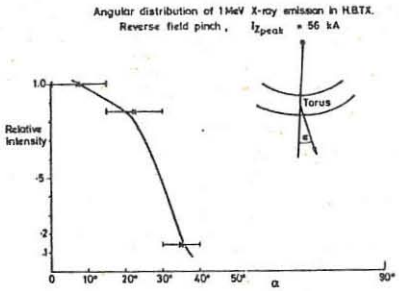

Fig.1 Angular distribution of hard x-rays

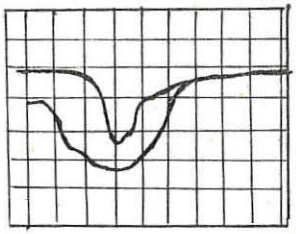

1. uncrowbarred

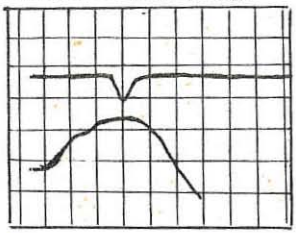

2. uncrowbarred

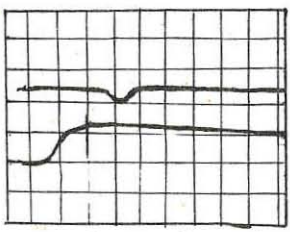

3. crowbarred

X-ray yields in reverse field pinches without pre-ionization. Deuterium filling pressure 40 mtorr.

Lower trace I_{Zpeak}	Upper trace X-ray pulse gain	Lead attenuator thickness inches	time base sec.	axial bias magnetic field
1) 60 kA	500 V/cm	0	2	1 KG
2) 60 kA	"	0.5	"	"
3) 50 kA	"	1.0	"	"

Fig. 2. Oscillograms of current and x-ray emission in different conditions.

ASPECTS OF DYNAMIC STABILIZATION OF HIGH-BETA PLASMAS
(Part II)

O.Gruber, G.Becker, H.Herold

Max-Planck-Institut für Plasmaphysik, Euratom Association,
Garching bei München, FRG.

Parametric excitation of m=0, k=0 oscillations by $\tilde{B}_z$ (Fig.1)

For the resonant case $\omega_s=\omega_k$ an example of the parametric excitation of m=0, k=0 oscillations by homogeneous oscillating $\tilde{B}_z$ is discussed (see Part I, 3). The enforced m=0 oscillation of the plasma is evident on the smear picture and on the diamagnetic signal. The signals show a 90° phase shift between driving field $\tilde{B}_z$ and plasma oscillation in agreement with the results for ϵ and δ obtained by solving the equation of motion (Part I,3). After some periods an α value of about 2 is found. The damping losses of the HF field, which heat the dense plasma, were determined by comparing the $\tilde{B}_z$ vacuum field (dotted curve) and the $\tilde{B}_z$-field for $\omega_s=\omega_k$.

Dynamic equilibrium of a toroidal Theta Pinch Sector

In a new series of experiments standing wave magnetic fields [3] have been applied to a toroidal theta-pinch sector in order to study dynamic toroidal equilibrium. Theoretical papers [5] predict a dynamic equilibrium if the following condition

$$\frac{1+\gamma^2}{4}\ h^2\ \delta^2 \geq \frac{\beta}{\Delta \cdot R_T} \qquad (7)$$

is fulfilled, where $h = \frac{2\pi}{\lambda_B}$ is the wave number of the standing wave, $\delta = \frac{\tilde{r}_p}{r_p}$ is the amplitude of the plasma oscillation in the bump of the wave, Y is nearly a constant equal to 2 and Δ is the toroidal shift of the plasma to equilibrium position. The experiments were carried out in two versions. In the 1st experiment the standing wave magnetic field (λ_B=29 cm) was superimposed to a 175 cm long torus sector with R_T = 400 cm, r_c = 5,5 cm and B_z = 18 kG. The plasma parameters are: $T_e=T_i \approx$ 60 eV; n_e(on axis) $\approx 2\times10^{16}\,cm^{-3}$; β = 0.3. In the bumps of the standing wave an amplitude of the plasma oscillation δ up to 0.1 is obtained

(δ=0.8 · ϵ; c.Part I). In the 2nd experiment the toroidal magnetic field was reduced to 12 kG without changing the coil geometry and the relative HF-field and plasma oscillation amplitudes were increased. In this case the plasma temperature is only 30 eV and δ amounts to 0.15. In both experiments the angular frequency ω_s of the standing wave was $5.5 \times 10^6 s^{-1}$, which is sufficiently large to satisfy the additional conditions: $\tau_D \gg \frac{2\pi}{\omega_s}$ and $\omega_s \gg h v_A$, where τ_D is the time the plasma needs to drift to the wall and v_A is the Alfven speed in the plasma.

According to eq.(7) an equilibrium at Λ=1 cm should be achieved for the above parameters and a plasma amplitude $\delta \approx 0.08$. In the 2nd experiment δ was twice as large as this theoretical value, but the plasma drift to the wall was not affected. A dynamic equilibrium could not be achieved, i.e. the dynamic force predicted by theory is not found. This result agrees with the experiments on dynamic stabilization by means of standing wave magnetic fields [3]. In our opinion the theoretical model is too much idealized because it is based on linearized MHD equations and therefore neglects direct coupling of the modes that is found experimentally with the $\tilde{B}_z$-stabilization method [1,2,4].

References:

[3] s.paper I.

[5] Wolf,G.H., G.Berge, Phys.Rev.Lett. 22,1096 (1969)

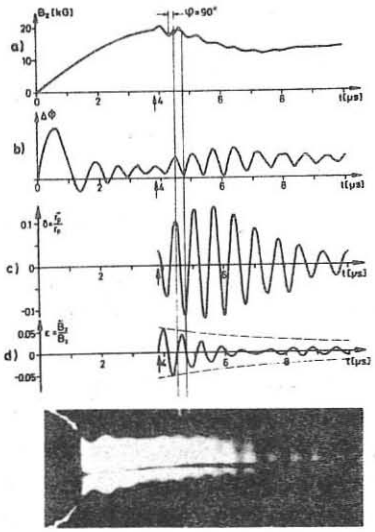

Fig.1:
$\Delta\phi$ measured diamagnetic signal
δ, ϵ calculated relative plasma oscillation and HF-field amplitudes.

THE TOROIDAL Z-PINCH PROGRAM AT LOS ALAMOS

D. A. Baker, L. C. Burkhardt, J. N. Di Marco, P. R. Forman, A. Haberstich
R. B. Howell, H. J. Karr, L. W. Mann, and J. A. Phillips
Los Alamos Scientific Laboratory, University of California
Los Alamos, New Mexico 87544 U.S.A.

The ZT-1 toroidal Z-pinch experiment has two modes of operation. A fast mode is achieved by establishing a current in an inductive storage system and then transferring this current to the discharge by means of four fuses and transfer switches. A slow mode is achieved by removing the fuses and shorting out the transfer switches. Thomson scattering measurements can be performed in both cases before the plasma strikes the wall due to instabilities.

Preliminary measurements have been done at 1 cm below the minor axis of the machine. A plasma volume, 8 mm long and 2 mm in diameter, was viewed at 90 degrees from the incident laser beam. The scattered light detector had four channels located at 65 Å intervals. The k-vector, important for the interpretation of the results, had both radial and poloidal components but no toroidal component. Figure 1 shows the data taken in the slow mode. The time indicated is in μsec and is measured from the initiation of the toroidal current. The temperature is obtained from a least square fit to a gaussian. The data is typical of many shots taken in the slow mode, and the electron temperature varies from 10 to 50 eV, depending on the time of the measurement. The density, typically 3×10^{15} cm^{-3}, obtained by comparison with Raleigh scattering in nitrogen, is as expected from compression of the filling gas. Figure 2 shows data obtained in the fast mode. The solid squares and the dashed data points have been measured on two separate shots. The solid curve is the computer's attempt to fit a gaussian to the solid squares. Clearly, the temperature obtained from this fit is not realistic. The dashed curve is a higher order fit to the two measurements as well as to other shots. It is seen to be symmetric about the laser line at 6943 Å. It should be noted that α is much smaller than one in this experiment.

The wave number and frequency of the double humped feature shown in Fig. 2 coincides with the dispersion relation of Bohm-Gross modes, assuming an electron temperature of 30 eV. That these modes might be responsible for the observation is under investigation. Whatever the phenomenon is, it appears

that it must be associated with electrons. Ion oscillations or waves are orders of magnitude lower in frequency. The distorted spectrum is observed for times ranging from 0.75 μsec to 5 μsec in the discharge. Since the Landau damping of these waves is large a strong driving mechanism would have to be present. There is experimental evidence for runaway electrons in the plasma.

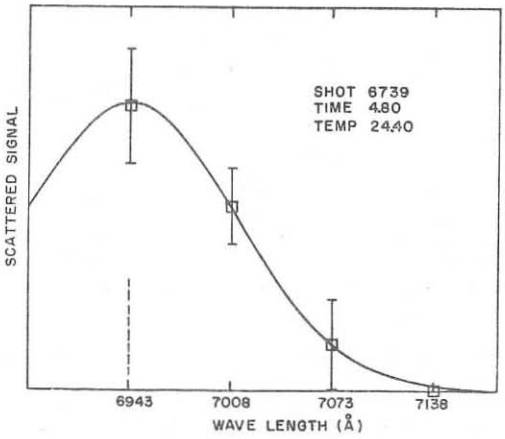

Fig. 1 Scattered spectrum at 4.8 μsec after initiation of the discharge. Electron temperature in eV. Slow mode.

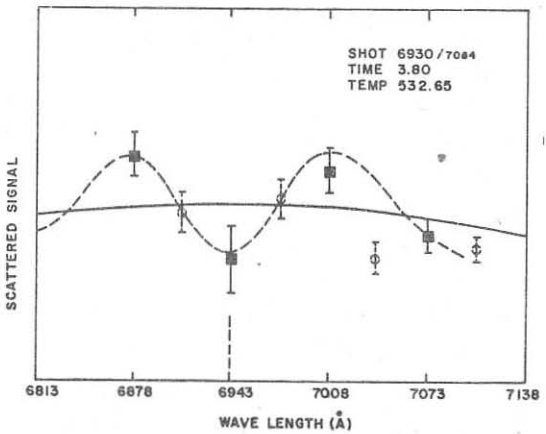

Fig. 2 Scattered spectra of two discharges at 3.8 μsec. Fast mode.

INJECTION OF PLASMA INTO A THETA-PINCH MAGNETIC FIELD

Yu.V.Skvortzov, V.G.Solovyeva, V.M.Strunnikov,
V.N.Lyashenko, S.S.Tserevitinov.

I.V.Kurchatov Institute of Atomic Energy
Moscow, USSR

Abstract. The motion of deuterium plasma ($\beta \sim 1$) in into longitudinal magnetic field is studied, Plasma transmission of the mirror field and nT increase due to plasma reflection are estimated.

Adiabatic compression of plasma by the moving metallic liner is a problem which attracts new attention as a way to achieve controlled fusion. In this case the final plasma characteristics should be deteremined by the initial temperature To and density n_o as well as by the degree of liner compression. The Lawson criterion is satisfied at $n \approx 5 \cdot 10^{15} cm^{-3}$ and To =50÷100 ev for an egual constituent deuterium - tritium mixture /1/. The total quantity of N is assumed to be $5 \cdot 10^{22}$ in a liner 10 m long and 80 cm in diameter.

The parameters of plasma flows produced by modern electrodinamic accelerators are rather close to those required with respect to N and T. Thus, $N \geq 3 \cdot 10^{21}$ for the particle velocities 10^7 cm.sec^{-1}were observed in /2/ and these could by further increased.

In spite of having carried out a lot of studies of interactions between the plasma and longitudinal fields the problem of plasma injection and its trapping by the θ-pinch magnetic field still has to be investigated in more detail.

We have continued our studies of the motion of nonmagnetized highly ionized plasma blobs in longitudinal magnetic fields and investigated the mirror-plasma nonisothermal interactions.

The experiments were conducted with a deuterium plasma flow ejected from a coaxial gun /3/ operated under the regime of plasma focus formation /4,5/. Under these conditions the plasma flow separates to several blobs during its flight. The velocity of the frontal blob is $4 \cdot 10^7$ cm.sec^{-1}. The plasma diameter can be controlled by chosing a proper value of the magnetic guide field B_o. At B_o=2 kG, the pressures $B_o^2/8\pi$ and nkT were equal for a blob 5 cm in diameter. In this case the blob was 100 cm long, the density being $2 \cdot 10^{15} cm^{-3}$, Te =25±5 ev.

The schematic drawing of the experimental device is shown in Fig.1.

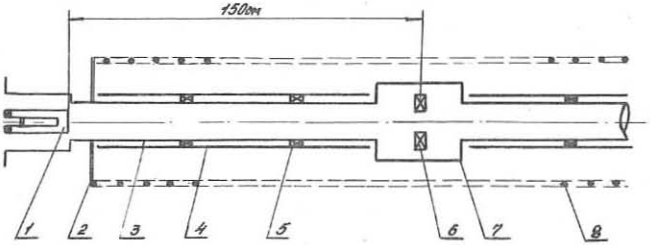

Fig.1. Schematic drawing of the device: 1-injector, 2-steel, 3-glass tube, 4-liner (the thickness-1mm), 5-diamagnetic coil, 6-($B_=$)-coil, 7-diagnostic cube, 8-guiding field B_0-coil.

The plasma pipe is 375 cm long. A short coil (the inner diameter 80 mm) generating quasi-stationary barrier field $B_=$ up to 20 kG was placed into the diagnostic cube. An array of 19 small magnetic probes, 5 diamagnetic loops, Mach-Zender interferometer with a streak camera and laser lighter, as well as two monochromators with photomultipliers calibrated for absolute measurements were used to determine the plasma parameters. These techniques used simultaneously enabled obtaining the information about the flow structure in every experiment. This is of particular importance in the case when the plasma is removed from the walls (the glass tube of the plasma pipe is 15 cm in diameter) while the blob symmetry axis does not always coinsides with the chamber axis.

Plasma injected into the theta-pinch should not be apreciably magnetized when passing through the guide field. The gun, however, could not be placed near the liner entrance because in this case the effects of impurities as well as the currents from the injector are very dangerous. Taking these facts into account, the length of the plasma pipe should be chosen so as to ensure time lagging of the impurities during the flight. We have estimated the maximum flight-length using the Bohm diffusion coefficient. For B_0=2 kG, the above plasma parameters and blob geometry the diffusion rate is 3.10^4cm. $.sec^{-1}$ while the field penetrates into the blob in about 10^{-4}sec. After this period of time the blob should be at a distance of 40 m from the gun ($v=4.10^7$ $cm.sec^{-1}$). To ensure the blob boundary constancy it is necessary that the flight-length should be one order of magnitude less. This requirement determined the distance between the gun and winding $B_=$ as 150cm. A contaminated plasma enters the region of the barrier field 8÷10μs after the main blob, and consequently,

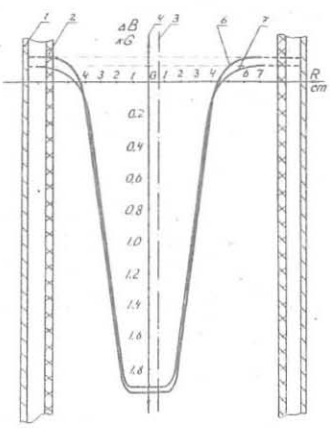

Fig.2. Field distribution inside the liner in presence of the frontal plasma blob: 1-liner, 2-chamber wall, 3-the axis of the chamber, 4-the axis of the blob, 5- ΔB-probe measured field, 6-distribution at 97 cm from the gun, 7-distribution at 200 cm from the gun.

can not influence the interaction between the magnetic field and the frontal blob. The interruption of the UHF (λ =4mm) signal penetration also indicated the efficiency of plasma separation. Fig.2 illustrates the radial magnetic field distribution inside the liner and plasma at a distance of 97 and 200 cm from the gun. The curves were plotted using the magnetic probe data. For each cross section they were averaged over a lot of experiments. The radial dimension of the blobs does not actually vary during the passage, it is consistent with the mean diameter determined from the interferogramms taken in the region of the diagnostic cube.

Numerous processes accompaning the interaction between the plasma flow and magnetic barrier field make it difficult to predict the confine ourselves only obtaining the most essential information in the initial stage. This involves determination of the mirror field transmittance for a $\beta \sim 1$ plasma and nT increases by the blobe reflection.

The measurements have shown that the barrier transmittance is 1,5% for B =20 kG. When the field strength was decreased up to 12 kG it increased by a factor of 3. These data have been obtained from the spatial distributions of nT plotted for the regions before and behind the barrier. Fig.3 shows one of such distributions (for B_{max}=20 kG). They were used to determine the blob dimensions. The flow density was estimated from the interferogramms.

It is seen, in Fig.3 that nT sharply increases in a region 10 cm from the coil plane B_o. Shock heating cannot occur in this case, because the ion free-path length calculated fron longitudinal velocity is many times greater than the blob dimension. It is likely that this region is a zone of the flow reflection from the barrier. Maximum density currents which heat the plasma are generated there. The reflection is detected both by magnetic probes (as second maximum

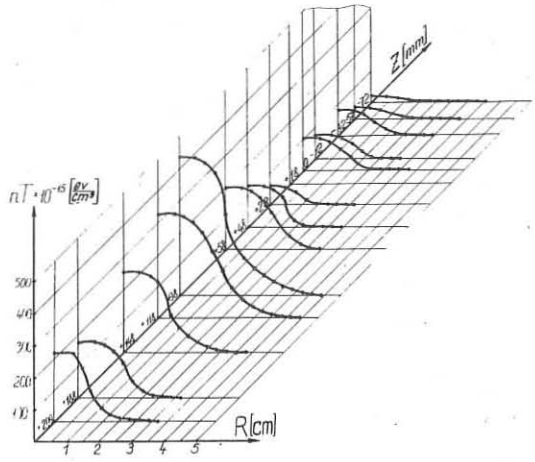

Fig.3. Spacial distribution of nT value for B_0 = =2 kG and $B_=$=20 kG. Coil $B_=$centre was disposed at the plane z=0.

appear in their signals and nT doubles) and by an interferometer (as the particle flow density doubles). An increase in nT solely due to the counter-streaming is observed in 70% of the events. In the other cases nT was observed to increase more appreciably in the reflected flow.

The mechanisms responsible for this phenomenon have not yet been found. It seems that these mechanisms could be used for thermalization of reflected flows of plasma. It is, however, possible that the thermolization could be easily provided by particle density increasing in the blobs when more powerful flows are injected into a theta-pinch.

References

1. J.P.Boris, R.A.Shaany. Proc.of the II Top.Conf.on Pulsed High Beta Plasmas, 1972, Munich.
2. G.N.Aretov et al. Proc.of the II Top.Conf.on Pulsed High Beta Plasmas. 1972, Munich.
3. V.I.Vasiliev et al. Proc.of the VII Int.Conf.on the Ioniz. Gases Phenom. Beograd, 1965.
4. G.N.Aretov et al. Proc.of the VII Int.Conf.on the Ioniz.Gases Phenomena. Beograd, 1965.
5. K.P.Vasilieva et al. Plasma Phys.and Control.Nucl.Fusion Res. Vol.II, p.39-50, Vienna, 1969.

LINEAR and NON-LINEAR PERTURBATIONS of a PINCH surrounded by a FORCE-FREE FIELD.

by

Dirk K. CALLEBAUT*, Jan G. KRUGER** and Hugo OTTOY

*Departement Fysica, Universiteit Antwerpen (U.I.A.), Universiteitsplein 1, B-2610 Wilrijk. Belgium.

**Seminarie voor Wiskundige Natuurkunde, Rijksuniversiteit Gent, Krijgslaan 271, B-9000 Gent. Belgium.

Abstract. The mhd theory for a simple plasma column pervaded by a homogeneous magnetic field and surrounded by a force-free field which in turn may be surrounded by a concentric metallic boundary is derived to second order in the perturbation amplitude.

1. INTRODUCTION. The method for studying perturbations of finite amplitude investigated extensively by one of us for liquid, plasma and gravitational cylinders [1]-[5] is exposed here for a fairly simple pinch. The aim is to investigate the non-linear behaviour, to look for the influence on the stability criteria, to set limits on the domain of validity of the linearized theory and to have a guiding model for the study of dynamic stabilization.

The present extension is an important one for several reasons.
(a) Experimental. There are indications at various laboratories (Jutphaas , Culham, Garching) that currents do flow in the pressureless region surrounding the pinched plasma.
(b) Theoretical
(i) Force-free fields are the most general equilibrium field possible in a pressureless region.
(ii) There are several arguments in favour of force-free fields with constant α (= current-to-field ratio) in view of properties of equilibrium, stability and evolution (due to resistive decay).
(iii) A more involved pinch case which can be solved analytically when surrounded by a vacuum field can also be solved analytically when surrounded by a force-free field, as well linearly as non-linearly. This is due to the fact that the perturbations of the force-free field in a pressureless region can be obtained for all orders; they do not involve non-linearity (of hydrodynamic origin); they are related to the plasma terms (having non-linearity) through the boundary conditions only.

2. MODEL. At equilibrium the plasma column is an infinitely long cylinder of circular cross-section (radius R_o). A concentric metallic cylinder of arbitrary radius qR_o may be present ($q>1$). The plasma is homogeneous, incompressible and has isotropic pressure and zero resistivity. The equilibrium magnetic field in the plasma is homogeneous and parallel to the axis (z-axis) of the cylinder: $H_o^{in} = H_o(o,o,1)$. If the surrounding region is pressureless, the most general field possible is a force-free one: div $H^{ex} = o$, curl $H^{ex} = \alpha H^{ex}$. We take α constant, several arguments favouring this case.

It can be shown, either directly or from the general solution, that if cylinder and rotational symmetry are required, then the only solution is the generalized Lundqvist field: $H^{ex} = H_o(o, Z_1(\alpha r), Z_o(\alpha r))$ with Z_1 $(=aJ_1+bY_1)$ and $Z_o(=aJ_o+bY_o)$ being the Bessel functions of first and zero order respectively (a and b are constants). Alternatively requiring that H_r^{ex} (r,φ,z) vanishes (and it has to vanish at least at R_o and at q R_o, and if pinching occurred even at a continuous range for r), we obtain again as only solution the generalized Lundqvist field.

3. METHOD.

(a) Hierarchy of higher order systems. At the surface the first order perturbation is taken as $R_o \varepsilon \cos kz$. Here $\varepsilon = \varepsilon_o \exp\sigma t$ is the relative (i.e. divided by R_o) amplitude at any time and ε_o is the relative amplitude at time t=o.σ is the growth rate or $\sqrt{-1}$ times the oscillation frequency and will be determined by the dispersion relation as a function of p (the density), R_o,q,k and m (the longitudinal, respectively azimuthal wave number), H_o,α, a and b. It has been argued [2],[3] that a series development in ε(instead of in ε_o only) is very plausible. Experiments have strongly confirmed this point of view. However this is not a trivial expansion and has to be used in connection with item (b) of the method. Through this development the time dependence is completely taken into account, but the system is replaced by a hierarchy of coupled systems. The indices o, 1, 2, ... are used systematically for quantities of zeroth, first, second, ... order.

(b) Family of non-linear terms belonging to a single linear term. Every term of the linear analysis generates sets of terms in the second, third, ... order E.g. with cos kz cos mφ as a first order term correspond terms proportional to cos 2kz cos 2mφ, to cos 2mφ, to cos 2kz and a constant; with cos 2(kz + mφ) correspond only two second order terms; the number of related terms increases with the order.

Just as a linear Fourieranalysis works with one term, now the non-linear analysis works with the family of terms generated by one (linear) Fourier term. However, besides some differences already indicated, a major difference consists in the fact that a Fourier analysis can study an arbitrary perturbation by just taking a linear combination of terms, while the non-linear analysis has to make a similar summation and add moreover interference terms.

(c) The perturbed fields are irrotational. It can be shown that the perturbed velocity and magnetic fields are irrotational at least to second order in the perturbation amplitude if one of the first order fields is a gradient. This is a great simplification. It has to be pointed out however that this third topic in the procedure of solving is not of as general a nature as topics (a) and (b). Including e.g. resistivity or taking the equilibrium field in the plasma as inhomogeneous destroys the irrotational character. However, here the importance of the argument presented under 1 (b) (iii) becomes appearent.

4. RESULTS. The part of the theory related to the plasma cylinder itself can be taken over integrally from ref. 3.

It can be shown that the perturbed field in the force-free region is again a force-free field with as current-to-field ratio the same constant α as the equilibrium field (exception: $k = m = o$).

(a) Linear theory. The dispersion relation reads

$$\frac{I_m}{\kappa I_m'}\left(\frac{\sigma^2}{\Omega_A^2}+1\right) = Z_1^2 + \frac{(mZ_1+\kappa Z_o)}{\mathcal{L}(x_o)}\left\{ Z_1\left[\left(\frac{mk}{\alpha x_o}I_m(x_o)+I_m'(x_o)\right)\mathbb{I}_m(qx_o)-\left(\frac{mk}{\alpha x_o}K_m(x_o)+K_m'(x_o)\right)\mathbb{K}_m(qx_o)\right]\right.$$
$$\left. -\frac{(k^2-\alpha^2)^{\frac{1}{2}}}{\alpha}Z_o\left[K_m(x_o)\mathbb{I}_m(qx_o)-\mathbb{K}_m(qx_o)I_m(x_o)\right]\right\}$$

where $\Omega_A^2 = \frac{\mu H_o^2 k^2}{\rho}$ (Alfvén frequency)

$$\kappa = kR_o$$
$$x_o = R_o(k^2-\alpha^2)^{\frac{1}{2}} \quad ; \quad x = r(k^2-\alpha^2)^{\frac{1}{2}}$$
$$\mathbb{I}_m(x) = \frac{m}{x}I_m(x)+\frac{k}{\alpha}I_m'(x)$$
$$\mathbb{K}_m(x) = \frac{m}{x}K_m(x)+\frac{k}{\alpha}K_m'(x)$$
$$\mathcal{L}(x) = \mathbb{I}_m(qx)\mathbb{K}_m(x)-\mathbb{K}_m(qx)\mathbb{I}_m(x)$$

with I_m and K_m the current notation for the modified Bessel functions; the argument is κ if not indicated; similarly the argument for Z_o and Z_1 is αR_o if not indicated.

A tremendous simplification occurs when $\kappa Z_o + mZ_1 = o$. This means physically that the "phase" of $\cos(m\varphi+kz)$ is zero (or constant) along the field lines on the interface between the plasma and the pressureless region. In this case the first order perturbed field in the pressureless region vanishes, making the dispersion relation, etc. independent of q, Z_1 and Z_o (except through the relation $\kappa Z_o + mZ_1 = o$)

(b) Second order theory. Corresponding to the first order displacement $\mathcal{R}_1 = R_o\varepsilon\cos(kz+m\varphi)$ we obtain

$$\mathcal{R}_2 = R_o\,\varepsilon^2\left(-\frac{1}{4}+A_2\cos 2(kz+m\varphi)\right)$$

with A_2 a very complicated function of $I_o(2\kappa)$, $I_1(2\kappa)$, $I_o(\kappa)$, $Z_1(\alpha R_o)$, $Z_o(\alpha R_o)$, etc. The coefficient A_2 has singularities. Obviously the linear theory is invalid there.

The "domain of validity" of the linear theory is obtained. Although the second order theory does not affect directly the stability criteria through σ, the singularities may change an oscillation into an instability.

Again the case $\kappa Z_o + mZ_1 = o$ yields a tremendous simplification and a strong disconnection between the plasma cylinder and the pressureless region; this can be further interpreted and exploited; however, the second order field in the pressureless region does not vanish in this case.

5. EXTENSIONS.

(a) Replacing the generalized Lundqvist field by a force-free field either of variable α or having constant α but both φ and z dependence and a H_r component is possible but cumbersome.

(b) The extension for finite plasma resistivity is easily obtained by combining the present results with those of ref.4.

(c) In a similar way viscosity can be taken into account.

(d) Again the extension for a magnetic field in the plasma having the form $H_o(o,o,1-ar^2)$, with a a constant is easily obtained by combining the present results with those of ref.5.

(e) Compressibility was considered in ref. 7 ($k = m = o$); a general way of taking compressibility into account is under development.

(f) Including higher orders and interference is possible but cumbersome.

References

[1] D.K. Callebaut, Plasma Phys. 10, 440 (1968)

[2] D.K. Callebaut, Proc. IV Eur. Conf. on Contr. Fus. and Plasma Phys., 44 (1970) Rome

[3] D.K. Callebaut, Simon Stevin, 45, 1 - 315 (1971)

[4] D.K. Callebaut and J.G. Krüger, Proc. V Eur. Conf. on Contr. Fus. and Plasma Phys. (Grenoble), p. 41 (1972)

[5] D.K. Callebaut and J.G. Krüger, Book of Abstracts "Internat. Conf. on Waves and Instabilities" (Innsbruck), p. C5 (1973)

[6] H. Ottoy and D.K. Callebaut, I.N.W. report Th 3/72. Rijksuniv. Gent (1972)

[7] W. Schuurman, Rijnhuizen report 68-48. (Ass. Euratom-Fom, the Netherlands)

Acknowledgement. Part of this work was performed while the authors were at the I.N.W. (Rijksuniversiteit Gent, B-9000, Gent, Belgium) and they like to acknowledge this.

Supplement to:

PLASMA DYNAMICS AND CURRENT SHEATH STRUCTURE IN COLLISIONFREE THETA-PINCHES

by

K. Höthker, K.J. Dietz, K.H. Dippel and E. Hintz

Institut für Plasmaphysik der Kernforschungsanlage Jülich GmbH
Association EURATOM-KFA
Jülich/FRG

Previously measurements of $n_e(t)$, $T_e(t)$ and B (t) at r=8cm (and r=6cm) have been reported and discussed. Meanwhile the same measurements have been performed further away from the axis at r=12cm. The imploding current sheath passes through this position without being intersected by the fast density pulse which is propagating ahead of the piston at 2 u_p and which is reflected at the axis; therefore a better investigation of the structure of the current sheath is possible.

The results are in agreement with the proposed interpretation for the previously observed density profiles (at r=8, r=6cm). The total number of particles in the first two density pulses (Fig. 1) is conserved and the pulses do not disperse. Between r=12cm and r=6cm the plasma encountered by the piston is trapped in the current sheath.

A comparison of the amount of energy absorbed in the piston due to the incoming and trapped plasma flow with the energy gain of the electron gas shows that the latter accounts only for about 10% of the total absorbed energy. One must expect therefore that the mean ion energy is larger than that of the electrons and this raises the question whether the conditions for the onset of ion sound instabilities are fulfilled throughout the sheath as it has been proposed previously.

The effective electron-ion collision-frequency, obtained from the energy balance equation on the assumptions that resistive dissipation is the only source for an energy gain of the electrons and that energy losses are negligible, is of the order of ω_{pi}. This is in agreement with the value of ν_{eff} derived from the observed magnetic field diffusion rates /2/.

The evolution of $v_d(t)$ and $v_d(t)/c_s(t)$ in the current sheath at r=12cm is shown in Fig. 5. There is qualitative agreement with the corresponding curves at r=8cm (Fig. 4). It is noteworthy that v_d/c_s tends asymptotically to a value $v_d/c_s \approx 2$, a limit which was also found by Biskamp and Chodura /4/ in computer ex-

periments on crossfield, current driven instabilities.
We can further report some preliminary measurements of microwave emission by the plasma at the wavelengths λ = 3, 0.8, 0.4 cm. Strong microwave radiation was observed at λ = 3cm at early times and at λ = 0.8cm at later times; at λ = 0.4cm there was no signal at all. As shown in Fig. 6 there is good indication that radiation is emitted only at a frequency equal to that value of the plasma frequency corresponding to the maximum electron density in the piston.
Microwave emission at λ = 3cm is observed when the sheath passes at about r=16cm. In Fig. 7 we show the 3cm-microwave signal and the B signal at r=16cm as function of time; the similarity is remarkable.

REFERENCE: /4/ D. Biskamp and R. Chodura, Proc. V. European Conf. on Contr. Fusion and Plasma Phys., Grenoble 21.-25. August 1972, Vol. I, p. 177

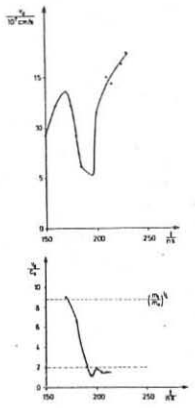

Fig. 5

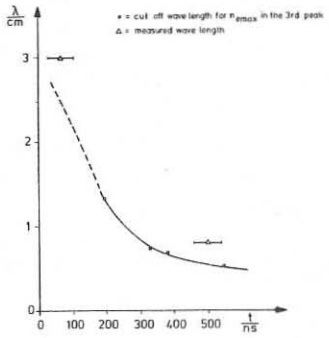

Fig. 6

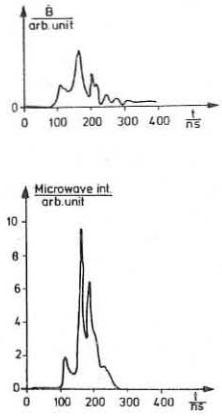

Fig. 7

Fig. 5: Drift velocity v_d and v_d/c_s as function of time (at r=12cm)

Fig. 6: Cut-off wavelength for $n_{e\ max}$ in the piston as function of time compared with the appearance of microwave emission at λ = 3cm and λ = 0.8 cm

Fig. 7: B at r=16cm and 3cm microwave intensity as function of time

THE PRODUCTION OF WEAKLY COMPRESSED HIGH-BETA PLASMAS BY SHOCK HEATING IN HIGH-VOLTAGE THETA PINCHES

M.Keilhacker, M.Kornherr, H.Niedermeyer, F.Söldner, K.-H.Steuer

Max-Planck-Institut für Plasmaphysik, Euratom Association
Garching bei München, F.R.G.

Since submission of paper No.2.3.2 published in Vol. I of these proceedings the laser scattering measurements of density and electron temperature on axis (r = 0) have been improved and then been repeated at about half the tube radius (r = 9.5 cm). From these and other measurements a picture of the plasma properties after shock compression can be drawn.

Fig. 1 shows the time development of the electron density n_e on axis together with the neutron flux and the external magnetic field B_e (initial density 2×10^{13} cm^{-3}). The density on axis starts to rise when the magnetic piston is at about half the tube radius (c. f. Fig. 2 of paper No.2.3.2 in Vol. I) thus indicating that ions are elastically reflected by the magnetic piston (free particle model).

Both density and neutron flux reach a first maximum at between 400 and 500 ns (a second maximum is clearly visible in the neutron flux only). For this time of first maximum compression Fig. 2 summarizes all the measured plasma quantities to give a rough idea of the kind of plasma that can be expected after shock compression. The density decreases from 4×10^{14} cm^{-3} on axis to 8×10^{13} cm^{-3} at r = 9.5 cm. The mean ion energy as calculated from the neutron yield is 1 - 2 keV. The electron temperature on axis is only 25 eV, which can be accounted for by adiabatic compression, while at the plasma boundary with its steep magnetic field gradients it is between 1 and 2 keV. These high electron temperatures seem to extend into the low density plasma region at r > 10 cm.

Thus one obviously has a dense $\beta \approx 1$ plasma core with radius $r \approx r_o/3$ consisting of hot ions and cold electrons surrounded by a low density high electron temperature (and possibly even high ion temperature) plasma halo in which the pressure slowly decreases towards the tube wall as indicated by the radial magnetic field profile. End-on framing camera pictures indicate that the low density plasma forming the halo is caused by Rayleigh-Taylor instabilities.

In view of the diffuse profiles and of the plasma halo in particular it is not quite clear how the compression ratio relevant for wall stabilization has to be defined. If one takes the radius at which $\beta = 0.5$ ($\beta = (B_e^2 - B(r)^2) / B_e^2$) then $\varkappa \approx 1.8$ results, while the position of the steep magnetic field gradient would yield $\varkappa \approx 3$.

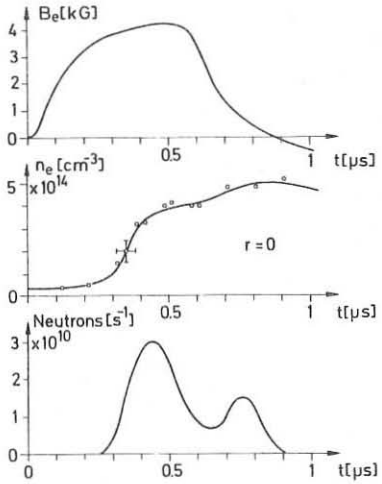

Fig. 1

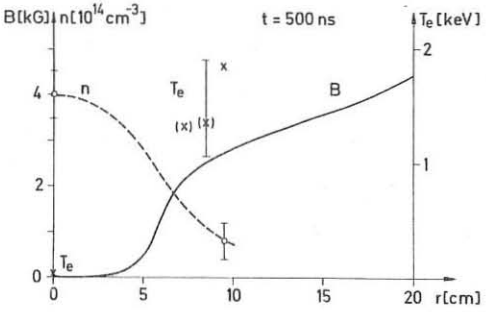

Fig. 2

ION HEATING IN A STRONG MAGNETIC COMPRESSION WAVE

R.Chodura, B.Röthlein

Max-Planck-Institut für Plasmaphysik, Euratom Association,

Garching bei München, F.R.G.

As a main result of our numerical simulation experiments we found a strong correlation between the efficiency of ion reflection in the implosion phase and the gain of thermal ion energy in the following relaxation phase.

The efficiency of ion reflection from the imploding wave front is essentially determined by the ratio of two time scales t_c and t_D, where t_c is the implosion time, i.e. the time it takes for the wave to run across the tube radius, and t_D is the diffusion time, i.e. the time it would take for the external magnetic field to penetrate into the resting plasma by finite conductivity up to the tube axis.

Omitting numerical factors, t_c and t_D are given by

$$t_c \sim \epsilon/\mu$$

$$t_D \sim \epsilon/\nu$$

respectively. So the ratio of these two times is given by

$$\tau = t_D/t_c \sim \sqrt{\epsilon\mu}/\nu$$

The dependence of ion heating on the relative diffusion time τ is shown in Fig.1. In this figure τ was varied by varying either ϵ, ν or μ independently. For small τ, i.e. fast diffusion rate, ion heating becomes inefficient.

In the special case when collision frequency ν_{eff} is coupled to the plasma frequency as is indicated by computer simulation of anomalous resistivity in a turbulent plasma and by experiments, τ becomes independent on initial density n_o. Thus also the

product $n_o T_i$ stays constant and the mean ion energy per particle varies as $1/n_o$ when varying n_o. This is shown in a special case using parameters of the shock wave experiment in our institute (Fig. 2).

In conclusion, we would like to point out that our hybrid model of fluid electrons and ion particles seems to describe the dynamics and dissipation in shock heating experiments quite well. Ion heating strongly depends on the effectiveness of ion reflection during implosion and this in turn is determined by the rate of field diffusion during the time of first compression.

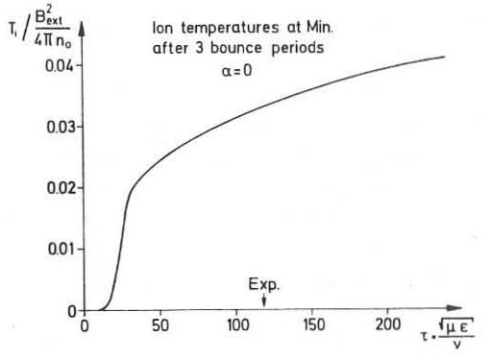

Fig. 1

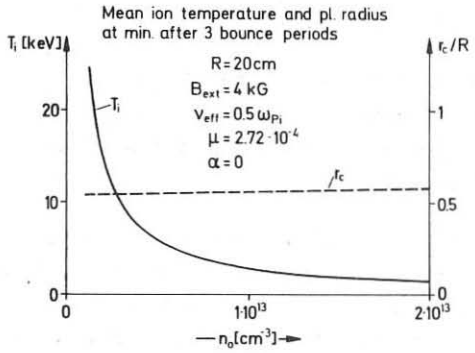

Fig. 2

ON THE EFFICIENCY OF VARIOUS DIVERTORS FOR SCREENING A FUSION PLASMA

D. Eckhartt, G. Haas, K. U. von Hagenow
Max-Planck-Institut für Plasmaphysik, EURATOM-Association
Garching b. München, F. R. G.

In the region outside the separatrix of a toroidal plasma the containment might be worse. The presence of a divertor or limiter interrupting currents and plasma flow along the magnetic field line might affect the plasma equilibrium. We have taken this into account by introducing an enhanced diffusion outside the separatrix. As expected, this enhanced radial diffusion makes the screening layer much thicker with a much lower density. In unfavourable cases, a considerable fraction of the flux of hot ions out of the plasma reaches the wall. If we do not assume an additional loss term on the wall in the case of Stellarator-divertor the transparency of the screening layer for neutrals coming from the wall is not changed. In the case of a Torsatron-like or a bundle-divertor there is a greater effect, but even with an enhancement of the radial diffusion by a factor of 100, which gives about Bohm-diffusion in the outer region, the screening layer is still opaque. In Fig. 5 we have used the same parameters as thosein Fig. 3 of our original paper except for the diffusion coefficient outside the separatrix. The most important feature is the thick dashed curve which, in arbitrary units, represents the hot plasma flux driven by diffusion. As seen from Fig. 5 there must be a very large distance between the separatrix and the wall in order to prevent an intolerable flux of hot plasma from hitting the wall.

In the case of the bundle-divertor the conditions are still worse, since the conductance to the divertor increases more slowly with x and therefore the pumping speed is lower in the outer region far away from the separatrix.

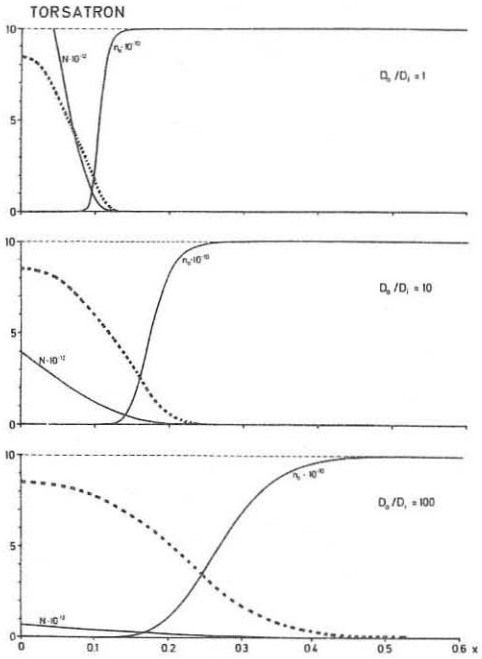

Fig. 5

NEOCLASSICAL DIFFUSION OF α-PARTICLES

A. Nocentini, M. Tessarotto
Istituto di Meccanica dell'Università, Trieste, Italy
and F. Engelmann
Laboratori Gas Ionizzati (Ass. EURATOM-CNEN), Frascati
Italy.

The formulae (3) and (4) of the paper for the radial α-particle flux and the supplementary electron flux due to the presence of α-particles in tori of large aspect ratio are in error. They should read

$$\Gamma_\alpha = -0{,}53\,\frac{q^2\,\nu_{\alpha e}^{(s)}}{\varepsilon^{1/2}\,\Omega_\alpha^2}\,\frac{d}{dr}\int d^3v\; v^2 f_\alpha^{(0)}(v) + 1{,}6\,\varepsilon^{3/2}\,\frac{E}{B_p}\int d^3v\, f_\alpha^{(0)}(v) \qquad (3')$$

and

$$\Delta\Gamma_e = \gamma\,\frac{q^2\,\nu_{\alpha e}^{(s)}}{\Omega_\alpha^2}\,\frac{d}{dr}\int d^3v\, v^2 f_\alpha^{(0)}(v) - 1{,}46\,Z_\alpha\,\varepsilon^{1/2}\,\frac{E}{B_p}\int d^3v\, f_\alpha^{(0)}(v) \qquad (4')$$

with γ a numerical factor of order 1. The supplementary ion flux due to the presence of α-particles is to lowest significant order in ε

$$\Delta\Gamma_i = 0{,}53\,Z_\alpha\,\frac{q^2\,\nu_{\alpha e}^{(s)}}{\varepsilon^{1/2}\,\Omega_\alpha^2}\,\frac{d}{dr}\int d^3v\; v^2 f_\alpha^{(0)}(v) - 1{,}46\,Z_\alpha\,\varepsilon^{1/2}\,\frac{E}{B_p}\int d^3v\, f_\alpha^{(0)}(v)\,. \qquad (A.1)$$

The ambipolarity of the particle fluxes, which holds, of course, exactly, can be verified explicitly from the preceding results to lowest significant order in ε. In fact, the diffusive flux of the α-particles is mainly balanced by a reduction of the ion diffusive flux (not by the modification of the electron diffusive flux), whereas the supplementary Ware terms of electrons and ions cancel each other, the Ware flux of the α-particles being of higher order in ε. This latter flux is outward in contrast to what appears for electrons and ions, due to the fact that the dominant effect of the toroidal electric field on the α-particles is via the drag connected with the electron current (opposite to E).

For reference, we give here also formulae for the α-particle energy flux Q_α and the supplementary electron energy flux ΔQ_e due to the presence of α-particles:

$$Q_\alpha = -0{,}53 \cdot \frac{q^2 \nu_{\alpha,e}^{(s)}}{\varepsilon^{1/2} \Omega_\alpha^2} \frac{d}{dr} \int d^3v \, \frac{3 m_\alpha v^2}{2} \, v^2 f_\alpha^{(0)}(v)$$

(A.2)

$$+ 1{,}6 \cdot \varepsilon^{3/2} \frac{E}{B_P} \int d^3v \, \frac{5 m_\alpha v^2}{6} \, f_\alpha^{(0)}(v) + 0{,}53 \frac{q^2 \nu_{\alpha,e}^{(s)}}{\varepsilon^{1/2} \Omega_\alpha^2} z_\alpha e E_r \int d^3v \, 5 v^2 f_\alpha^{(0)}(v),$$

$$\Delta Q_e = k T_e \cdot \gamma \frac{q^2 \nu_{\alpha,e}^{(s)}}{\Omega_\alpha^2} \frac{d}{dr} \int d^3v \, v^2 f_\alpha^{(0)}(v) - \frac{5}{2} k T_e \cdot 1{,}46 \, z_\alpha \varepsilon^{1/2} \frac{E}{B_P} \int d^3v \, f_\alpha^{(0)}(v).$$

(A.3)

They show that energy and particle fluxes are connected with the same time scales. Note that the energy flux of the α-particles contains a term which is proportional to the radial self-consistent field E_r. The appearance of this contribution is again due to the fact that the dominant collisional effect here is a drag rather than pitch angle scattering. Quantitatively this effect is, however, unimportant as it is typically by a factor $\frac{e E_r a}{\mu_{\alpha,0}} \approx \frac{k T_e}{\mu_{\alpha,0}}$ smaller than the diffusive flux.

Corrigenda and Addendum: "Remarks Concerning Experimental Simulation of the Pellet-Refuelling"

by C. T. Chang, Risø, Denmark.

Corrigenda:

i) In eq. (1) of the paper, the drag coefficient should be $C_D = C_D\,(M, \lambda/r_p, A)$

where $A = u/\frac{B}{(4\pi\rho\mu)^{1/2}}$ is the Alfvén-Mach number.

ii) In table 1, for the 5 GW reactor, the number density should be $n = 2.8^{14}$

Addendum: Time scale, t_o for ending the impact phase.

For impact particles at an average energy around and exceeding 10 keV, most of its energy is lost through the pair-production process[1], let Δr be the corresponding average penetration depth, then $N = 4\pi r^2\,\Delta r\, n_s$ is the number of particles contained in a shell of thickness Δr, and

$$t_o = n/G \qquad \text{(A-1)}$$

where $G = \lambda F 4\pi r^2/w_o$ (A-2)

is the ablation rate. Our main problem is to estimate the penetration depth Δr and the absorption coeff. λ.

i) If the impact particles are ions $\Delta r = \bar{s}$, the average path length obtained by integrating directly the stopping-power formula, i.e.

$$\Delta r = \int_{E-W}^{E} dE/(-\frac{dE}{ds}) \simeq W/(-\frac{dE}{ds}) \quad \text{for } E \gg W \qquad \text{(A-3)}$$

When the impact particles are electrons due to multiple scattering and straggling effect, we take emperically[2]

$$\Delta r = \bar{s}/4 \qquad (A-4)$$

ii) To estimate the absorption coefficient λ, we proceed as the following:

For ion impact, we take λ as the ratio between the stopping-power for ionization and excitation against the total stopping-power[1]. For electron impact we take λ as the percentage of inelastic collisions in collisions between electron and atomic hydrogen[3].

Using these considerations, the calculated results for particle of 20 keV energy are summarized in the accompanying table.

	Ion	Electron
F, Watt/cm^2	7.0×10^7	4.2×10^9
- dE/ds, ev/cm	2×10^8	3×10^4
Δr, cm	1.8×10^{-7}	3×10^{-4}
λ	0.50	0.91
G, sec^{-1}	2×10^{25}	1.4×10^{27}
t_o, sec	3×10^{-10}	7×10^{-9}

Note: $(dE/ds)D^+$ are computed from data of H^+ in H[4] by using stopping number $B(H_2) = 2B(H)$ and for D^+ at the same impact energy of H^+, $(dE/ds)_{D^+} = 2(dE/ds)_{H^+}$.

Refences

1) A.Dalgarno and G.W.Griffing, (1955) Proc.Roy.Soc, A232, 423

2) R.D.Evans (1955) "The Atomic Nucleus" McGraw-Hill, New York and London.

3) H.S.W.Massey and E.H.S.Burhop (1956) "Electronic and Ionic Impact Phenomena", Clarendon Press, Oxford, p. 177.

4) W.Whaling (1958) in "Handbuch der Physik", S. Flügge, ed. vol. 34, Springer, Berlin.

UNIVERSITY OF WISCONSIN TOKAMAK POWER REACTOR DESIGN

C. W. Maynard, R. W. Conn, H. K. Forsen
Nuclear Engineering Department-University of Wisconsin
Madison, Wisconsin, U.S.A.

Abstract

The basis for design decisions and summary of the main system parameters for a 5,000 MW_{th}. Tokamak designed by the Fusion Feasibility Study Team at the University of Wisconsin is presented.

Introduction

There is no minimum or sharp break in the dependence of the cost per unit on the total power of a D-T fueled Tokamak reactor. This measure of performance decreases slowly with increasing power and thus the size of the plant is likely to be determined more by the needs of the constructing agency than by the plant characteristics. Since cost decreases with increasing plant size, the unit described here is 5,000 MW_{th} which is as large a plant as seems reasonable today. With the output fixed in this somewhat arbitrary manner, a design philosophy has been adopted which chooses existing technology to the maximum extent possible. This has dictated use of stainless steel as the structural material in spite of the appealing potential of the refractory metals. The choice of liquid lithium as coolant seems very satisfactory despite the problems of flow of a conducting fluid in the magnetic fields present here. The remaining first order feature of the system to be fixed is the choice of Nb-Ti as the superconductor which is in keeping with our actual field requirements and current technological capabilities.

Geometry

There are a number of constraints which could limit the choices of the major radius and the aspect ratio. These include the maximum attainable field, yield stresses, and radiation effects. In fact, the most restrictive limit can be stated as the neutron wall loading, which is the power associated with the fusion generated neutrons per unit area of the first wall. The wall loading constraint is a result of several radiation effects which limit the useful life of this wall. Bulk effects due directly to the neutron flux are usually dominated by swelling due to void formation and embrittlement caused by atom displacement and by helium production. As these effects are also temperature dependent, the operating temperature is also related to this constraint. In addition, the electromagnetic and charged particle flux produces surface damage which must be considered. These include the sputtering of wall atoms into the containment chamber and blistering and flaking of the wall. The limiting constraint is one of the above two bulk effects, depending on the operating temperature. Data currently available indicate the embrittlement is prohibitive at any acceptable wall loading unless the temperature remains below that at which helium forms bubbles. This will limit the operating temperature to approximately 500°C in the case of a stainless steel wall. The wall loading is then limited by radiation induced embrittlement due to displacements to around 0.5 MW/m^2 if it is assumed that the first wall is replaced every two years. Due to the extensive extrapolations and uncertainties of the data, a somewhat more optimistic limit of 1 MW/m^2 has been used in our feasibility design. With the total power and the wall loading fixed, the surface area of the wall is fixed leaving only the aspect ratio of the torus to be chosen in determining the general geometry. Optimization studies of

the cost, considered as proportional to the energy stored in the magnetic field, show a minimum at a very low aspect ratio. However, this ratio cannot be reached when the finite blanket, shield and magnet thickness plus the Tokamak transformer space requirements are considered. The optimum aspect ratio is then the smallest consistent with the above constraints and was set at 2.6.

The optimization just described includes the main plasma physics requirements for confinement. The stability factor "q" should be as small as possible to optimize the power density of the plasma, but for stability must exceed unity by a safe margin. At the same time, if steady state operation is to be possible, the bootstrap current must provide the shear necessary for stability. This fixes beta poloidal as the square root of the aspect ratio. The temperature can still be adjusted to an optimal value by introducing the proper percentage of a high atomic number impurity to enhance radiation losses allowing a higher fusion rate at a different temperature. The resulting confinement time would then become too long if scaled using neoclassical theory and it is necessary to assume one can spoil confinement relative to the extrapolated neoclassical value, possibly by intentional field errors, to adjust the confinement time and the fractional burnup. There are two steady state operating points, one stable at a relatively high ion temperature and the other unstable at a lower temperature. The unstable point requires a considerably smaller confining field and thus has a lower cost. A premium can be paid for an adequate control system to allow use of the unstable point. We have found that the cost of the magnets required for operation at the stable plasma point is 50% higher. The requirements for a control system is still under investigation.

Divertor

Sputtering and blistering of the first wall as well as contamination of the plasma result from charged particles striking the wall. To minimize these effects, a divertor capable of carrying away most of the particles diffusing from the plasma is employed. This operates by introducing additional windings with an appropriate current to produce a field configuration such that field lines outside a particular surface close outside the confinement chamber. The path of particles following these field lines is interrupted by a medium capable of absorbing the energy and impact of these exhaust particles. The divertor can be a single or double null system. The design chosen is a double null one which simplifies the task of obtaining greater curvature of the divertor slots, and this in turn reduces leakage and the associated shielding requirements at the outer edge of the slots. There is also some merit in reducing the exhaust load to be handled in a single slot. However, the main advantage of the double null system is the elongation of the plasma in the vertical direction which allows the toroidal windings to be smaller for a given plasma volume. The efficiency of a divertor in reducing the charged particle current to the wall is not yet known. However, it hardly seems worth while if it isn't at least 90% efficient, while on the other hand, there are other limitations which are at least as restrictive as the sputtering and blistering at this efficiency. Thus, it is felt that the wall and plasma radii must in practice be adjusted to achieve at least 90% efficiency even though no figures are yet available.

Blanket and Shield

The thickness of the first wall is determined by stress and erosion. The stresses due to the pressure of the flowing coolant and the thermal gradients combine to give a stress curve with a minimum when plotted against the wall

thickness. The stress at the minimum must lie below the maximum tolerable in the wall material. Thus, there is normally a range of thicknesses that are allowable from the stress considerations. However, wall erosion will necessitate a minimum thickness which is the stress limit plus the thickness eroded by the charged particle surface effects on the outside and liquid metal corrosion on the inside. This in turn must not exceed the maximum thickness set by stress alone. All of the conditions above can be met in the present design if it is based on replacement of the wall every two years instead of a twenty year plant life. The wall is thin compared to a mean free path for 14 MeV neutrons and has little influence on the neutron flux, but for cost and radioactivity reasons, the wall is chosen as the thinest of those allowed above, namely, 2.5 mm.

The region behind the first wall contains liquid lithium and the structure needed to channel the lithium flow. The thickness of the region is fixed by the need to breed tritium, to remove most of the energy being produced and to allow for proper flow of the electricity conducting coolant in the presence of the required magnetic field. All of these needs are met with a 50 centimeter blanket zone followed by a 10 centimeter steel reflector and a final 5 centimeter lithium zone. This blanket absorbs about 95% of the neutron energy and further attenuation in the coolant is achieved at too high a price. The energy will be recovered in the shield. but at a lower temperature. The breeding is still higher than is really necessary to allow for losses from divertor slots and fueling ports and for nuclear data errors. Adequate flow configurations are very important since pumping power may be greatly increased if fast flow transverse to the field is demanded.

Behind the blanket, the shield composition and thickness are to be fixed by the limit on the radiation to the magnets. This limit which is set by constraints to be discussed later fixes the attenuation that must be achieved at the least cost to the system. Iron, or in the non-magnetic case, stainless steel, attenuated the 14 MeV neutrons most rapidly and allows the smallest magnets. This should actually be a mixture of stainless steel and boron carbide to insure suitable attenuation of the lower energy neutrons. However, the high fabrication costs for steel indicates a shield consisting partly of lead may be optimal, because the low cost of the lead more than offsets the increased cost of the magnets due to slight increase in the shield thickness. The amount of lead is severely restricted since the shield in part consists of the steel necessary to support the magnet structure, which cannot be diverted to another use.

Magnets

The magnets are subjected to a number of radiation, stress, and superconducting limits. The most obvious constraint is that of not exceeding the critical current density as in all superconducting magnets. To insure reliable operation, it is also necessary to provide stabilization against thermal fluctuations by providing an alternative flow path for the current. This stabilizer is usually copper. The radiation limits must consider damage effects to the superconductor, insulation, stabilizer and the energy load to the cryogenic refrigeration system. The most serious damage problem is in the stabilizer but proper design can allow for the expected resistivity changes. The actual limit seems to be the refrigeration load and is thus basically an economic one. The normal thermal losses from the magnet cryogenic system from radiation and leakage is one of the order of 5 Kw. However, in order to cool the system down in an acceptable time (30 days seems a practical maximum) the refrigeration capacity must be about 15 Kw. Thus, without increasing the capital investment and for an acceptable operating cost, the radiation load to the magnets can be set at 10 Kw. For our

5,000 MW_{th} plant, this requires an energy attenuation of 5×10^5 in the combined blanket and shield.

The main feature of the magnets is the amount of structural steel necessary to support the induced stresses. These are so large that the principal cost of the reactor is the magnet structural costs. The superconductor costs are expected to be minor. Costs have been made as small as possible by elongating the plasma and using a constant tension configuration over as much of the toroidal windings as possible. In spite of this, the cost of the magnets is expected to be the largest contribution to total costs.

Summary

The system parameters for the reactor determined as described above are given in Table I. The considerations used as a basis are primarily technical. While costs have not been ignored, no attempt has been made to be systematic with regard to the economics.

Acknowledgement

The reactor designed is the work of our feasibility study team and the authors have simply summarized their efforts.

TABLE I

Dimensions
- Major radius - 13 meters
- Plasma minor radius - 5.0 meters
- First wall minor radius - 5.5 meters

Plasma
- $q = 1.75$
- $\beta_p = \sqrt{A}$, $A = 2.6$
- $\tau_i = 13.5$ seconds
- $T_i = 12.6$ Kev - unstable
- $n_i = 0.98 \times 10^{20}/m^3$
- Fractional burnup - 7.8%

Power
- 5,000 MW_{th}
- 0.779 MW/m^3 average

Wall Loading
- Neutron 1 MW/m^2
- Bremsstrahlung 0.211 MW/m^2
- Synchrotron .002 MW/m^2
- Fuel loss rate 2.1×10^{22} ions/sec

Blanket and Shield

First Wall Thickness (316 Stainless Steel)	2.5 mm
Primary cooling and breeding region	
95% lithium, 5% stainless steel	50 cm
Stainless steel reflector	10 cm
Secondary cooling and breeding region	5 cm
Shield stainless steel inner wall	5 cm
Successive 5 cm regions of alternating	
B_4C (90% theoretical density) and lead	
B_4C	25 cm
Lead	20 cm
Outer Shield wall and dewar support	
structure (stainless steel)	25 cm

Magnets

1.25 m thick by 2.65 m wide

Total Mass 31.2×10^6 lbs. of which 22.7×10^6 lbs. is stainless steel

7.66×10^6 lbs. is copper

EVIDENCE FOR A BROAD AND UNIFORM NEUTRON-PRODUCING PLASMA COLUMN IN THE PLASMA FOCUS

Joint European Programme on Plasma Focus

P.D. Morgan(*,+), N.J. Peacock
The Culham Laboratory, Abingdon, Berks., U.K.

P. Cloth, H. Conrads
IPP-IRE, Ass. EURATOM-KFA, Jülich, FRG.

Ch. Maisonnier, F. Pecorella, J.P. Rager, M. Samuelli
Laboratori Gas Ionizzati (Ass. EURATOM-CNEN), Frascati, Italy

In the main paper evidence was presented to support a broad and uniform plasma column in the Plasma Focus device at the time of maximum neutron emission. This supplementary paper reports further electron density and soft x-ray measurements.

DENSITY MEASUREMENTS

The experimental arrangement was as described in the main paper.

In Fig.1, a composite sequence of interferograms is shown, together with typical neutron and soft x-ray signals. The times during the discharge at which the interferograms were obtained are indicated on the neutron signal.

The first frame occurred late in the collapse phase, before the peak of the first neutron pulse. At this stage the collapsing current-sheet is cylindrical in nature and does not have the oblique profile characteristic of the collapse at earlier times. The plasma column is $\sim$ 1.6 cm in diameter and $\sim$ 2.6 cm in axial extent. Frame 2 corresponds to the time of occurrence of the dense pinch at approximately the peak of the first neutron pulse. The fringes in this frame cannot be resolved since the magnification of the camera was chosen primarily to study the low-density plasma resulting from the break-up of the pinch. However, it is clear that the pinch is a thin filament of diameter $\sim$ 0.3 cm and of length $\sim$ 2.5 cm. The third frame occurred during the diffuse-pinch phase at the peak of the second neutron pulse. The plasma has the approximate form of a cylinder of diameter $\sim$ 4 cm.

Fringe-shift profiles obtained from the interferograms were used to derive radial, electron-density distributions as described in the main paper. Fig.2 shows two such profiles obtained from frames 1 and 3 of Fig.1, respectively.

Profile 1, obtained during the collapse, shows a lower electron density on

---

(*) Royal Holloway College (London)

(+) Supported by USAF under contract F.44620-71-C-0098

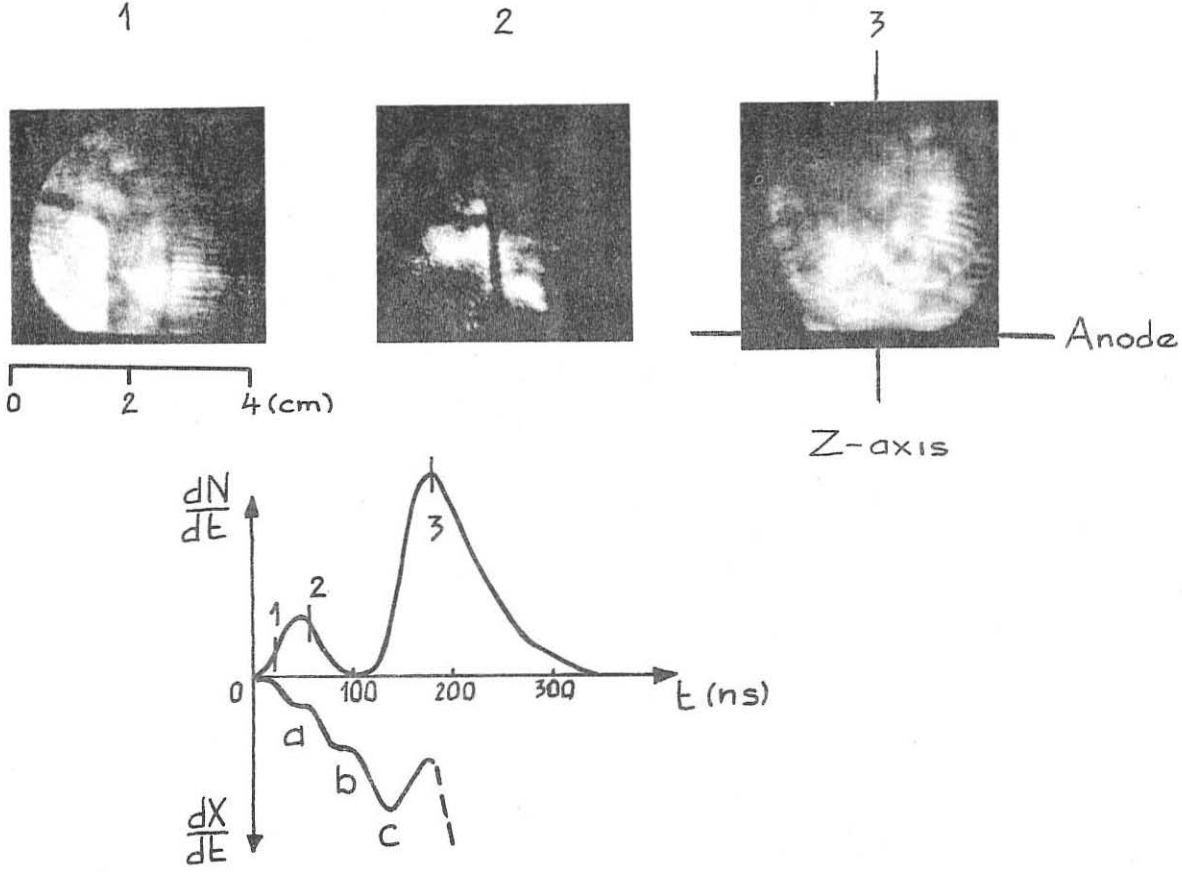

Figure 1.
392

axis than towards the edge of the plasma column due to the collapsing shock not yet having reached the axis. The peak electron density is $\sim 2 \times 10^{18}$ cm^{-3}. The second, radial profile, obtained at the maximum of the second neutron pulse, shows that the plasma column is, to a first approximation, of constant density with a sharp boundary. A peak electron density of $\sim 3.2 \times 10^{17}$ cm^{-3} is found.

The line density in the plasma column may be obtained by integrating the radial, electron-density profile, i.e.

$$N_e = 2\pi \int_0^R n_e(r) r \, dr \, .$$

The value of the line density evaluated from the data in Fig.2 and from interferograms taken at other times over a number of discharges was found to be remarkably constant, $\sim 2.6 \times 10^{18}$ cm^{-1}. Using the experimental observation of constant line density, the average density in the pinch (Fig.1 - frame 2) is $\bar{n}_e = 3.6 \times 10^{19}$ cm^{-3}.

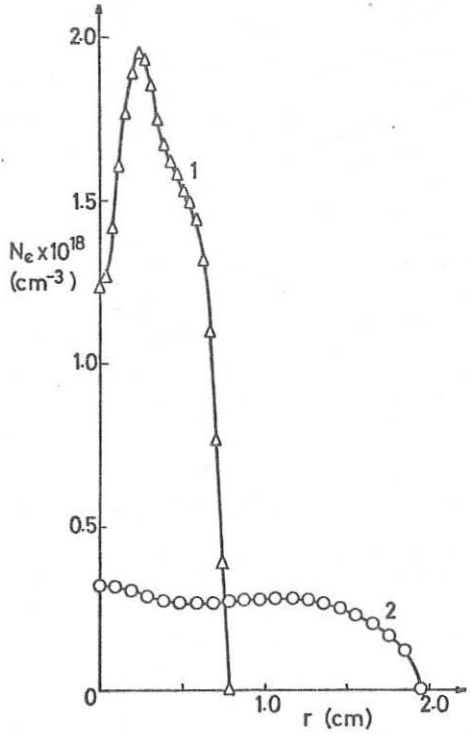

Figure 2.

X-RAY STUDIES

A space-resolved study of the soft x-ray emission from the plasma, as detected by Si surface barrier detectors through filters of different thickness [1], has shown the existence of a very soft component simultaneous in time with the first neutron pulse, a in Fig.1. The electron temperature using filter-absorption techniques is found to be below the 1 keV threshold of the detecting system, for the plasma lying between 0.5 and 1 cm from the anode. A second emission, b, can be accounted for by a plasma with an electron temperature ranging from 5-7 keV, shot to shot. This emission corresponds in time with features previously reported,[2].

An interesting feature is that, in agreement with soft x-ray, pinhole

photographs [2], the x-ray emitting region is of length 1-1.5 cm, while from interferometry the dense pinch is ∿ 2.5 cm in length, Fig.1. At a later time, a burst of harder x-rays, c, is observed, the integrated spectrum of which (with respect to absorber thickness) cannot be readily matched to a pure bremsstrahlung spectrum.

CONCLUSIONS

From holographic interferometry, a dense pinch of diameter ∿ 0.3 cm and of average density ∿ 3.6×10^{19} cm^{-3} has been shown to exist at the peak of the first of a series of neutron and soft x-ray pulses. Subsequently, the pinch is observed to expand as a body with the neutron emission decreasing to zero. However, at this time when the plasma is expanding, an electron temperature of 5-7 keV is estimated from x-ray studies. Finally, a second burst of neutrons is produced, at the peak of which the plasma is found to be a column of diameter ∿ 4 cm and average density ∿ 2.3×10^{17} cm^{-3}. These densities and plasma dimensions agree with the model previously proposed, [3].

REFERENCES

[1] ROBOUCH, B.V. and RAGER, J.P., J. Appl. Phys., 44, 4, pp.1527-1533, (1973).

[2] GRATREAU, P. et al., Proc. 4th IAEA Conf. on Plasma Physics and Controlled Nuclear Fusion Research (Madison 1971), 1, pp.511-521, IAEA, Vienna (1971).

[3] MAISONNIER, Ch. et al., Proc. 5th Europ. Conf. on Controlled Fusion and Plasma Physics (Grenoble 1972), 2, pp.183-194, Commissariat a l'Energie Atomique, Paris (1972).

DECAY OF THE MAGNETIC STRUCTURE OF DENSE PLASMA AND X-RAY AND MICROWAVE EMISSION

W. H. Bostick, V. Nardi, W. Prior
Stevens Institute of Technology, Hoboken, N. J., U.S.A.

Abstract. We present experimental data on the x-ray and microwave emission from dense D_2-plasma which is produced in a "plasma focus" type of discharge. The correlation of the radiation emission with the formation and the decay of magnetic-plasma cells is analyzed. A possible mechanism for the emission is outlined.

1. X-ray data have shown[1] that electron (and ion) beams are generated inside the dense plasma (plasma focus; electron density $\rho_e \sim 10^{20}$ cm^{-3}) produced by a coaxial accelerator which is operated under standard conditions: applied potential 15 kV, peak electrode current $i_E \sim 0.7$ MA, capacitor bank energy 5 kJ; neutron yield up to 5.10^8 per shot with 8 torr D_2 filling; hollow center electrode-anode-diameter 3.4 cm. The electron mean velocity u_e ($\sim 3\text{-}4\cdot10^9$ cm/s, along the discharge axis - or electrode axis - z) inside a beam was determined by the variations (with gas composition D_2, D_2+Ar and with photon energy ε) of the intensity anisotropy $I_{90}o/I_0o \sim 2\text{-}4$ (I_0o is along z)[2] in the bremsstrahlung emission from typical localized x-ray sources (X-LS, with linear dimensions $r \sim 0.05\text{-}0.1$mm by photons with $\varepsilon \gtrsim 2$ keV, as recorded on pinhole-camera photographs through a Be filter 0.05 mm thick) in the plasma and by using Sommerfeld's bremsstrahlung formulas[3]. The magnetic induction B reaches peak intensities $\sim 1\text{-}2 \cdot 10^2$ megagauss[1] within a X-LS by estimating $B \sim i$ (ampere)/5r(cm). Values of the local electric current $i = \pi r^2 e \rho_e u_e \sim 3\text{-}4$ MA $> i_E$ imply the formation of local circulating currents in the plasma (ρ_e was obtained from determinations of absolute x-ray intensity on X-LS photographs). Usually three-five X-LS's are formed in the axial region of each discharge. In previous work[4] we have related the production mechanism of the X-LS's to particle acceleration by the inductive fields which are generated during the decay of the current-sheath magnetic structure. In order to find a specific correlation among configurations changes in the current sheath (CS) and typical variations in the radiation emission from the plasma we have taken time-resolved data from x-ray and microwave detectors.

2. Oscilloscope (Tektronix 7704, rise time 2.5 ns) traces of x-ray scintillation detector (NE 102) signals show a time sequence of x-ray intensity peaks ($\varepsilon \gtrsim 2$ keV) which are distributed on a time interval $\sim 50\text{-}100$ ns starting at a time $t \sim 20\text{-}30$ ns after the first di_E/dt minimum.

show the same details (peak multiplicity and width for each pulse). (f) The microwave intensity is substantially the same in all directions [$\sim$ 10 watt at peak intensity on the interval $(1 \pm 0.5)\ \lambda$ on the solid angle; $\lambda \sim 3$ cm]. All these features of the microwave emission could be understood in terms of magnetic-dipole radiation associated with the rapid formation of current loops (with the magnetic dipole always orthogonal to the z axis) during the CS axial collapse.

4. The CS axial collapse can be followed on image converter (IC) photographs by visible light [we have compared IC photographs of a discharge with schlieren and shadowgraphs simultaneously obtained - by using a 10^8 watt ruby laser - and we have verified that all details on a IC photograph have corresponding elements on schlieren and shadowgraphs; specifically, peaks of luminosity on IC photographs corresponding to peaks of particle density]. Typical cusps appear on the CS even before the CS collapses on the discharge axis. At t=0 the CS reaches the axis near the end of the center electrode (the point of convergence of CS on the axis moves with a velocity $u \sim 3 \cdot 10^7$ cm/s - decreasing with time - along the z-axis), cusps are enhanced and the formation of the axial plasma column (diameter $\sim$ 4 mm) is completed at t $\sim$ 80-100 ns. The luminosity distribution in this column suggests that the column is hollow.[4] A "neck" with a diameter $\lesssim$ 0.5 mm and a variable length, may appear at any point of the column and at different times in different discharges (this is frequently called the second compression stage[5]). Our statistical analysis on many ($\sim 10^2$) IC photographs shows that two neighboring cusps are frequently connected by a luminous pattern which defines - together with the cusped border of the column - the boundary of a loop with a nearly circular cross-section (the luminous pattern connects neighboring cusps on the 4-mm-diameter column as well as neighboring cusps in a "neck").[4] These three-dimensional loops can span a large azimuthal angle $\Delta\theta \lesssim 2\pi$. Plasma outflow from the column cusps has been observed also by a high-speed-interferometry study at Lebedev Phys. I.[5]. The spacing between cusps ($d \lesssim 3$ mm) in some discharge can be remarkably constant along the column and in the off-axis part of CS ($d/u \sim 10$ ns can give an estimate of the time interval separating the formation of two consecutive loops along the column).

5. By assuming that the luminous pattern corresponds to mass and current flows (as it was verified for previous stages of the discharge), then the formation of the loops of circulating current will decrease the azimuthal B_θ-field on a broad region far ($\gtrsim 1$ cm) from the axis. The corresponding

The full width at half maximum (FWHM) of each peak is $\sim$ 10 ns. In $\sim$ 75% of the discharges a very hard x-ray peak (FWHM $\sim$ 5 ns) can be observed on the same time interval of the soft x-rays. This hard component is present in both D_2 and H_2 discharges and can cross a lead screen $\sim$ 5 cm thick so that for many photons $\varepsilon \gtrsim$ 1-5 MeV. The NE 102 crystal thickness ($\sim$ 0.1 mm) is smaller than the neutron mean-free-path in the crystal so that neutrons do not contribute to the x-ray signal [a second group of broader, frequently unresolved peaks ($\varepsilon \gtrsim$ 2 keV) is observed 200-300 ns after the first peak sequence]. All discharges ($\sim 10^2$) show that statistically the number of intensity peaks in this first sequence matches the number of X-LS's in the axial region of a discharge as it is recorded on a pinhole photograph (the same Be foil is covering film and NE 102 detector). By using a collimator pointing at different positions along z it was observed[4] that the times at which X-LS's are flashing increase with the distance of X-LS from the anode end. Our conclusion based on these data is that the image of each X-LS on a photograph is formed by a x-ray burst which lasts not longer than $\sim$ 10 ns and that as a consequence of the high space-resolution on our time-integrated photographs a time-resolution $\sim$ 10 ns is also achieved.

3. Different microwave detectors (for 3 cm and 10 cm wave-lengths) have been used at a distance$\sim$20 cm from the anode end and at different orientations $\phi = 70^\circ$, 80° and 180° with respect to the z axis. A sequence of microwave peaks with FWHM 3-10 ns is detected in each discharge during the axial collapse of CS. The number of peaks varies from 0 up to 15. The following properties of the microwave emission are observed: (a) All intensity peaks are sharp (for many peaks FWHM is determined by the scope rise-time). (b) Usually a first group of 2-10 peaks occurs on a time interval of 20-300 ns (more frequently 4-8 peaks on 100-150 ns); a second group of 1-3 peaks may follow 100-300 ns after the end of the first group. (c) The time-spacing between peaks is rather uniform (usually 5-30 ns); in some discharges this time-spacing can be remarkably constant for many peaks (see Fig.). (d) By using two identical detectors we have observed for each microwave peak the amplitude $E_{||}$ of the electric-field-component parallel to z and the amplitude $E_\perp$ of the orthogonal component. With the detectors at 70° and 80°, $E_{||} > E_\perp$ for all peaks and in all discharges (the two detectors were calibrated and were frequently interchanged for an alternative pick-up of $E_{||}$ or $E_\perp$). Usually $E_{||} \sim \alpha E_\perp$, $1 \leq \alpha \lesssim 14$ (the mean value $\bar{\alpha}$ on 35 discharges is $\bar{\alpha} = 2.4$). (e) Both $E_{||}$ and $E_\perp$ signals

Fig. 1. Oscilloscope trace from microwave detector for $E_{\parallel}$, $\lambda \sim 3$ cm. Notice uniform spacing $\Delta t \sim 16$ ns between pulses (sweep speed 50 ns/cm). Nine pulses are recorded. In this trace and in scope traces of Fig.2 time increases from left to right.

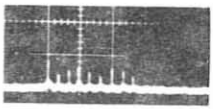

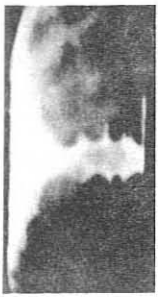

Fig.3. IC photograph by visible light (5 ns expos.) of the plasma column at $t \sim 80$ ns (with 4 cusps).

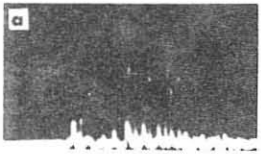

notice 4 short, 9 $\gtrsim$2cm peaks

Fig. 2. Microwave pulses with-$E_{\parallel}$, $\lambda \sim 3$ cm-(a) and x-ray pulses (b) start at the same time ($\pm$ 10 ns) in the same discharge. The microwave pulses which come at the same time of the first group of x-ray pulses have usually a smaller amplitude than subsequent pulses. The late (second) group of microwave peaks is not shown in (a). Sweep speed 100 ns/cm. The late (or second) group of microwave pulses is not detected in this discharge which shows only the first group of small and large amplitude peaks (spread $\sim$300 ns).

inductive field can accelerate particles in the axial region with a sharp increase in the local values of the electric current and consequently of B_{θ} near the axis. A loop spanning the infinitesimal (azimuthal) interval $\theta, \theta+d\theta$ will generate a magnetic dipole $\underline{m}(\theta,t)d\theta$ orthogonal to z. For magnetic-dipole radiation it is $E_{\parallel} > E_{\perp}$, in any direction close to the plane orthogonal to z and containing $\underline{m}$. The first group of x-ray signals is related in time with the rearrangement of the filamentary[4] structure in the (hollow) column. The concave-spool shape of the X-LS's suggests the formation of plasma cells (or toroidal vortices) with peak x-ray emission from the cell cores. It is likely that the loops observed by visible light[1,4] play a major role in the formation process of these cells where B-field buildup in the localized cell-cores can occur at the expenses of the field decay in broader regions. Because of the delay of the large-amplitude microwave peaks with respect to the x-ray emission from the column, it seems possible to relate these large peaks only with the loop formation in the off-axis region of CS or with the excitation of already existing loops by particle ejected in the loops during the propagation of disturbances in this region of CS. A more likely possibility is microwave emission during the final decay of long-lasting cells anywhere in the plasma.

Work supported in part by A.F.O.S.R., U.S. and by C.N.R., Italy
Stevens Institute of Technology, I.E.N. Galileo Ferraris Collaboration Program

1. Bostick et al. :Proc. II Topic.C.Pulsed High-β Plasmas, 1972, p.155
2. Bostick et al. :Proc. V Eur. Fusion C., Grenoble 1972, Vol.2, p.239
3. Kirkpatrick, Wiedman : Phys.Rev. 67, 321(1945)
4. Bostick, Nardi, Prior: J.Plasma Phys. 8, 7(1972)
5. Gribov, Korzhavin, Krokhin, Sklizkov, Filippov, Filippova: Zh.ETF 15, 329(1972)

COMPARISON OF LASER-HEATED FUSION PLASMA PROPOSALS*

J. W. Shearer
University of California, Lawrence Livermore Laboratory
Livermore, California

In recent years, high power lasers have become an important potential tool for manipulating fusion plasmas. Several fusion plasma proposals involving laser radiation are briefly reviewed here.

The classical collisional absorption mean free path L_a for laser light in a hydrogen plasma can be written:

$$L_a = \frac{10^{37}}{\ell n\, \Lambda} \frac{T_e^{3/2}}{\lambda_\mu^2 N_e^2} \left(1 - \frac{N_e}{N_c}\right)^{1/2} \qquad (1)$$

where T_e is the electron temperature (eV), λ_μ is the laser light wavelength in microns, N_e is the electron density, and N_c is the cutoff density; $N_c = \pi/r_o\lambda^2$ where r_o is the classical electron radius. The condition for propagation of light is $N_e < N_c$; therefore, the optimum value of density for strong absorption is near, but not greater than, N_c. For neodymium lasers, $\lambda = 1.06\mu$, and $N_c = 10^{21}$; for carbon dioxide lasers, $\lambda = 10.6\mu$, and $N_c = 10^{19}$. These plasmas are dense compared to most fusion plasma proposals; the corresponding pressures ($P = 2NkT$, assuming $T_e = T_i$), are $\sim 3 \times 10^7$ atm and $\sim 3 \times 10^5$ atm, respectively. Such pressures cannot be contained in stationary apparatus; this difficulty must be circumvented.

The laser-pellet proposal[1] uses the inertia of the reacting plasma itself as containment. The plasma is proposed to be formed at extremely high densities ($N_e \simeq 10^{27}$) by a symmetrical implosion driven by the absorption of laser energy at the surface of a tiny solid deuterium-tritium (DT) sphere suspended in a vacuum chamber. The outer layers of the sphere are ablated,[2] forming a high temperature plume which acts like a rocket to push the inner

*Work performed under the auspices of the U.S. Atomic Energy Commission.

layers together. It has been shown[3] that the Lawson criterion (for DT at a temperature of 10 keV), $N\tau \gtrsim 5 \times 10^{13}\alpha$ (where α is the desired energy multiplication) can be satisfied if the laser energy input E_L to the pellet is, approximately: $E_L \simeq 10^8\ \alpha^3/\varepsilon^4\eta^2$ joules where ε is the overall efficiency of conversion of laser light energy into the final compressed sphere, and where η is the ratio N_e/N_s, where N_s is the density of solid heavy hydrogen. The thermonuclear reactions occur before the sphere can come apart; the vacuum chamber is large enough to contain the resultant "microexplosion". The time scale for the nuclear reaction would be 10^{-12} - 10^{-11} sec; the laser pulse width would be 10^{-10} - 10^{-9} sec.

A nine-beam laser system is being used at the Lebedev Institute[4] for preliminary research into the unsolved problems of this pellet proposal; single beam lasers are in use at many other laboratories. There are, of course, no problems of magnetic field containment; however, several new effects such as parametric instabilities,[5] high energy electrons,[6] and self-focusing[7] are under study. At present these appear to be serious problems, but the research is just beginning, and the laser pellet proposal has the merit of being very different from other fusion research.

A more conventional proposal is to heat a plasma in a magnetic field with a long wavelength laser at low enough densities to permit plasma containment with stationary apparatus.[8] For example, at a density of $N_e \simeq 3 \times 10^{17}$ and a temperature of 10^4 eV, the collisional absorption mean free path (equa. 1) is 10^5 cm, which is about the length of a linear theta pinch that can satisfy the Lawson criterion, before the plasma streams out the ends. Such a 1 km long machine is large, but may not be unreasonable for a fusion power plant. The corresponding pressure is $\sim$ 5,000 atmospheres, which may be achievable in a stationary pulsed system. The high temperature and pressure would last about

1 millisecond. Detailed estimates of the required laser energy indicate that a few megajoules would be needed;[8] however, the laser pulse length can be $\simeq 10^{-4}$ - 10^{-3} sec instead of the much shorter pulses required in the pellet approach.

Megagauss magnetic fields have been proposed to contain laser-heated plasmas.[9][10] However, these proposals have the disadvantage that the magnetic field pressure is too great to be contained by stationary apparatus.

One possible laser-augmented pinch[8] is considered in detail -- laser heating to temperature of about 1 keV followed by pinch compression and confinement to reach the thermonuclear reaction temperature of 10 keV. In this example the absorption mean free path for laser light (equa. 1) at T = 1 keV and $N_e = 10^{18}$ is 300 cm, implying that much shorter machines are possible. Axial losses would be reduced by using end plugs[8] -- a procedure that is especially effective at high densities where thermal conduction losses are less serious. The laser-heated plasma bubble would be compressed to $N_e \simeq 10^{19}$ - 10^{20} by a cold, dense plasma sheath driven by a large magnetic pinch. This cold sheath would be thermally insulated from the hot plasma by the magnetic field. The major external energy source would be a conventional capacitor bank or large inductance to supply the pinch current; the energy of the laser should be rather modest in comparison.

The unique capability provided by the laser is its ability to provide localized heating at a prescribed position and time within a plasma. No other heating mechanism can presently provide the required temperature profile for this proposed reactor. Further evaluation is in progress.

REFERENCES

[1] John Nuckolls, Lowell Wood, Albert Thiessen, and George Zimmerman, Nature 239, 139-142 (1972).

[2] O.N. Krokhin, "High Temperature and Plasma Phenomena Induced by Laser Radiation" in Physics of High Energy Density, P. Caldirola and H. Knoepfel, Eds. (Academic Press, New York, 1971), pp. 278-305.

[3] R.E. Kidder, Some Aspects of Controlled Fusion by Use of Lasers, Lawrence Livermore Laboratory Report UCRL-73500 (1971), to be published in the Proceedings of the Esfahan Symposium on Fundamental and Applied Laser Physics, 1971 (J. Wiley & Sons, New York).

[4] N.G. Basov, O.N. Krokhin, G.V. Sklizkov, S.I. Fedotov, and A.S. Shikanov, ZhETF 62, 203 (1972) [English translation Sov. Phys. JETP 35, 109 (1972)].

[5] Marshall N. Rosenbluth, Phys. Rev. Lett. 29, 565 (1972).

[6] R.E. Kidder, J.W. Zink, Nuclear Fusion 12, 325 (1972).

[7] J.W. Shearer and J.L. Eddleman, Laser Light Forces and Self-Focusing in Fully Ionized Plasmas, Lawrence Livermore Laboratory Report UCRL-73969 (1972), submitted to Physics of Fluids.

[8] John M. Dawson, Abraham Hertzberg, George C. Vlases, Harlow G. Ahlstrom, Loren C. Steinhauer, Ray E. Kidder, and W.L. Kruer, "Controlled Fusion Using Long Wavelength Laser Heating with Magnetic Confinement", to be published in the Proceedings of the Esfahan Symposium on Fundamental and Applied Laser Physics, 1971 (J. Wiley & Sons, New York).

[9] P.P. Pashinin and A.M. Prokhorov, ZhETF 62, 189 (1972) [English translation Sov. Phys. JETP 35, 101 (1972)].

[10] J.L. Bobin, D. Colombant, G. Tonon, Nuclear Fusion 12, 445 (1972).

PROBLEMS OF THE LASER-AUGMENTED PINCH PROPOSAL*†

J. W. Shearer

Lawrence Livermore Laboratory
Livermore, California 94550 USA

Further evaluation of the laser-augmented pinch concept[1] has shown that this idea has some serious technical problems.

Assume a DT plasma of density $N_o \simeq 10^{18}$ which has been heated by a laser to a temperature $T_o \simeq 1$ keV. Now compress this plasma adiabatically to a density $N_1 \simeq 10^{20}$, which would heat it to a temperature $T_1 \gtrsim T_o(N_o/N_1)^{\gamma-1} \simeq 10$ keV, assuming that the radiation and conduction losses are not too severe. According to the Lawson criterion, $N\tau \geq 10^{14}$; consequently, this compressed plasma must be contained for $\tau \geq 10^{-6}$ sec. For plasma radii of $\sim$ 1-10 mm, the time τ corresponds to 10^2-10^3 sound transit times. The plasma pressure P is $\simeq$ 3 megabars.

Magnetic field containment of such a pressure requires a field of $\sim$ 9 megagauss, which cannot be contained by stationary apparatus. Possibly one might imagine a gigantic plasma focus machine, whose inner electrode is hollow so that no material electrodes are found near the large field regions. In such an experiment, the containment time should be limited by the stability conditions for a Z-pinch.[2] For a sheet current model of this pinch, the growth rate γ of the m=1 instability is given by:[2]

$$\gamma = 2\left[\left(\frac{B_\theta}{B_Z}\right)^2 \ell n \frac{1}{KR_p} - 1\right] \frac{(KR_p)^2}{R_p^2} \frac{1}{\rho} \frac{B_Z^2}{8\pi} \qquad (1)$$

for small KR_p where R_p is the total plasma radius (including the laser heated hot core), K is the wave number, ρ is the average density, and there is a stabilizing field B_Z, in addition to the pinch field B_θ. For a numerical estimate, choose $(KR_p) \simeq 0.1$, $B_Z^2 = 0.75\, B_\theta^2$, and pressure $P = B_\theta^2/8\pi$. Then, if we want the growth rate γ to be small compared to $1/\tau$, we must have a large average pinch density ρ:

$$\rho \gg \frac{10^5}{R_p^2} \text{ gm/cm}^3 \qquad (2)$$

This is a very large density criterion, and is a serious problem.

*Two-page supplement to UCRL-74628 (reference 1).
†Work performed under the auspices of the U.S. Atomic Energy Commission.

If one uses laser heated theta pinches, one cannot use the 3 MG magnetic field for containment because the coils would be wrecked in one pulse. One might, however, consider using much lower fields to accelerate a massive cold sheath to compress and contain the laser-heated plasma. However, this inertial containment scheme is found to require average plasma densities similar to those just estimated for the Z-pinch. For both pinches, the size of the electrical power supplies necessary to achieve the Lawson criterion with such dense sheaths corresponds to hundreds of megajoules per meter, which is very large. One is reminded of the explosive experiments with megagauss fields,[3][4] which have similar energies.

Nevertheless, despite these difficulties, an attempt to compress pinches with laser-heated cores would involve interesting plasma research. A longer wavelength pulsed laser, if available, would also be of interest for heating lower density plasmas.

REFERENCES

[1] J.W. Shearer, "Comparison of Laser-Heated Fusion Plasma Proposals", Lawrence Livermore Laboratory Report UCRL-74628, submitted to the 6th European Conference on Controlled Fusion and Plasma Physics, Moscow, July 30 - August 3, 1973.

[2] B.B. Kadomtsev, "Hydromagnetic Stability of a Plasma", pp. 153-199 of "Reviews of Plasma Physics", Vol. II, Ed. by M.A. Leontovich, (Consultants Bureau, New York, 1966).

[3] D.B. Thomson, et al, "Plasma Compression by Explosively Produced Magnetic Fields", pp. 491-514 of "Proceedings of the Conference on Megagauss Magnetic Field Generation by Explosives and Related Experiments", Euratom, Brussels, 1966.

[4] J.G. Linhart, ibid, pp. 387-396.

RATE-EQUATION TREATMENT OF X-RAY EMISSION FROM LASER-PRODUCED PLASMAS

J. Davis, G. A. Doschek, U. Feldman, B. M. Klein, D. J. Nagel, K. Whitney
Naval Research Laboratory, Washington, D. C. 20375, U. S. A.

ABSTRACT

Plasmas produced by ~ 1 ns laser pulses are not in ionization equilibrium. Hence, a rate equation treatment of the x-ray emission is being used.

INTRODUCTION

The coronal equilibrium model of emission from plasmas is based on the assumption of ionization equilibrium and equality of collisional excitation and radiative decay. It predicts useful relations between relative line intensities and plasma electron temperature T_e. These are used to extract T_e values from measured intensity ratios [1]. However, for short laser pulses ($\lesssim$ 1 ns), there is a question of whether or not conditions concordant with the assumptions of the coronal model have time to be established in the plasma.

EXPERIMENTAL

A 3 m grazing-incidence grating spectrograph [2] was used to obtain the F spectrum shown in figure 1. This spectrum is fully discussed elsewhere [3]. Here we focus attention on the longest-wavelength Li-like satellites of the He 2p-1s resonance lines; namely the $1s^2\ 2p\ ^2P - 1s\ 2p^2\ ^2D$ at 17.167 A and the $1s^2\ 2p\ ^2P - 1s\ 2p^2\ ^2P$ at 17.116 A. In ionization equilibrium, these lines should be in the ratio 7:1 [4], but the observed ratio is near 1:1. The departure from coronal equilibrium indicates a state of transient ionization and implies that the rate equations must be used to compute accurately the details of x-ray emission from plasmas produced by short laser pulses.

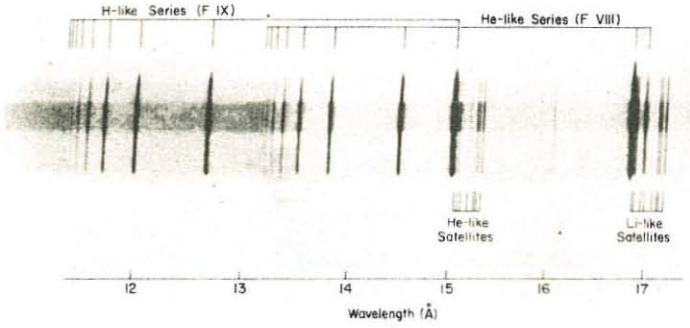

Figure 1. F spectrum from LiF target placed at focus of 100 GW Nd:glass laser. (Entire width: 2 shots, center: 4 shots.)

RATE EQUATION CALCULATIONS

A non-hydrodynamic rate equation model for K line emission has been constructed [5]. The absorbed laser energy heats the plasma within a small volume (5×10^{-8} cm^3). Conduction losses, plus heating and ionization of the ions, are included. The last factor, energy transfer between the electrons and the internal degrees of freedom of the ions is described by a set of rate equations based on the levels and transitions shown in figure 2 for the case of Al. The ion number densities N_μ for each state thus change in time according to the equations

$$\frac{dN_\mu}{dt} = \sum_\nu W_{\mu\nu} N_\nu, \quad \sum_\mu N_\mu = N_O .$$

The collisional rates all depend on the electron number density, which is determined from the ionic charges Z_μ via $N_e = \sum_\mu Z_\mu N_\mu$, and on the electron temperature.

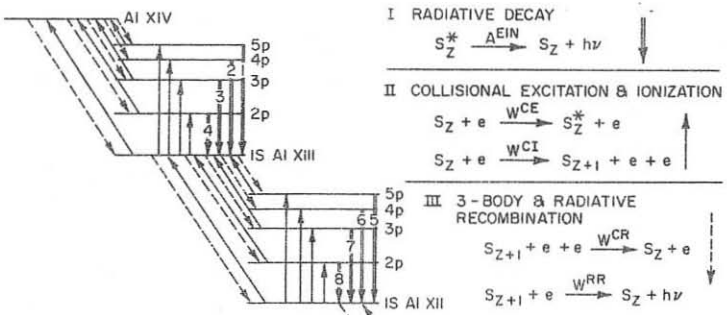

TRANSITION	λ[Å]	A^{EIN}[SEC^{-1}]	NAME
1. 5p→IS	5.6	1.18×10^{11}	H_δ
2. 4p→IS	5.8	3.65×10^{11}	H_γ
3. 3p→IS	6.1	1.59×10^{12}	H_β
4. 2p→IS	7.2	1.34×10^{13}	H_α
5. 5p→IS	6.2	1.9×10^{12}	He_δ
6. 4p→IS	6.3	3.2×10^{12}	He_γ
7. 3p→IS	6.6	7.7×10^{12}	He_β
8. 2p→IS	7.8	2.8×10^{13}	He_α

Figure 2. Levels, transitions and rates for Al.

Use of the rate equation model yields relative spectra and total line intensities in good agreement with experiment (figure 1, of reference 2). This approach is being extended to other atomic species, such as F shown in figure 1.

REFERENCES

1. B. M. Klein et al., this Conference.
2. W. E. Behring et al., Appl. Optics, 12, 528 (1973).
3. U. Fledman et al., Astro J. Ltrs., to be published.
4. A. H. Gabriel, M.N.R.A.S., 160, 99 (1973).
5. J. Davis and K. Whitney, to be published.

INVESTIGATION OF LASER-PRODUCED PLASMA ON "MISHEN" DEVICES

V.V.Alexandrov, E.P.Velikhov, A.G.Kaligin, N.G.Kiselev, N.G.Kovalsky, V.V.Korobkin, P.P.Pashinin, M.I.Pergament, A.M.Prokhorov, A.I.Yaroslavsky

I.V.Kurchatov Institute of Atomic Energy, Moscow, USSR
P.N.Lebedev Physical Institute, Moscow, USSR

Abstract: The results of the spectriscopic investigations in experiments with laser-produced plasmas are presented. Intense lines with frequencies $2\omega_0$ and $3/2\,\omega_0$ were observed when a Nd-glass laser (frequency ω_0) radiation was focused onto the solid targets. For LiD and $(CD_2)_n$ targets neutron yields were measured. Preliminary data on interaction of nsec laser pulses with a dense plasma in strong magnetic fields are reported.

I°. The aim of the experiments performed on "Mishen" devices is to investigate the interaction of powerful laser radiation with high temperature dense plasmas in a wide range of conditions including the irradiation of solid targets in strong magnetic fields up to I Moe. The experimental arrangement is scetched in Fig.I. The Nd-glass laser system "Mishen I" consists of a single-mode oscillator Q-switched by means of a Pockells cell, a fast optical shutter, which shapes laser pulses, and six amplifiers enhancing the energy level of the pulse up to $\sim$ 100 j. A fraction of the laser emission is used to trigger a spark-gap switch which controls the shutter.

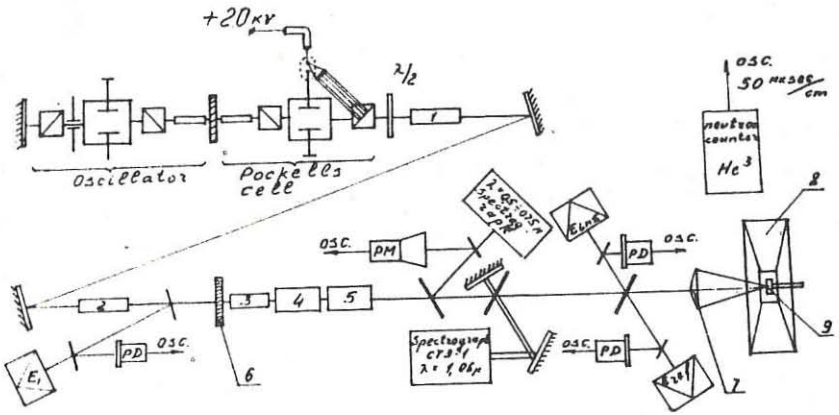

Fig.I. PM - Photomultiplier, PD - Photodiod, I,2,3,4,5 - amplifiers, 6 - passive shutter, 7 - focusing lens, 8 - magnetic coil, 9 - target.

Half-peak duration of the laser pulses is controllable between six and twenty five nsec and rise time is less than one nsec. The diameter of the output aperture is 45 mm, the beam divergence - less than 2.10^{-3}rad. and the dynamic contrast ratio is about 10^3. The further development of the laser system described above led to "Mishen II" device in which large rectangular cross-section active elements are used in the last amplifiers [I]. This device has been just arranged and tested.As a result, the predicted energy of the 6 nsec laser pulse has been achieved $\sim 10^3$j.

2°. The main results presented in this report were obtained on the "Mishen I" device when massive Al, LiD ans $(CD_2)_n$ targets were illuminated with the laser light in a vacuum. The experiments was carried out in the energy range from 10 j to 30 j for 6 nsec and 20 nsec laser pulses. The beam was focused onto the plane surface

of the targets with either f = 7.5cm or f = I5cm lenses. The pulse shape and total energy of the incident and reflected laser light were measured with fast photodiods and calorimeters. Spectral observations of the light, reflected from the plasma into the aperture of the focusing lens, were made using a grating- spectrometer with a mean dispersion of 20 Å/mm for recording in the infrared region. A grating spectrometer with an image amplifier for recording in the visible range and a monochromator with a fast photomultiplier (the time resolution $\sim$ 2 nsec) were used. The proportional He^3 filled counter with 5 cm thick paraffin shield was used for estimation of the total neutron yeild.

3°. The reflection coefficient was shown to vary strongly with the distance between target and focusing lens. Typically it drops by a factor of five when the target is moved from the optimum position to either side by 500 μk (f = I5 cm lens). The maximum values of the reflection coefficient achieved 5 ÷ 7%. The pulse shape of the reflected laser light nearly always follows that of the incident light.

The spectrum of the incident light in our experimental conditions consisted of a few-lines spaced $\sim$ 5Å apart. The envelope was nearly symmetrical with half-width about 40 Å. The spectrum of the reflected light in the experiments with massive targets (Al, LiD, $(CD_2)_n$) is shifted to the red by 3 Å and the line substructure disappeared. It should be mentioned that we saw the same lines in the reflected spectra as in the incident one when thin Al foils were illuminated. The distributions of the intensities among these components are however refersed relative to that in the incident

spectrum (see Fig. 2).

Spectral measurements in the visible showed the existence of the strong components with frequencies near $2\omega_0$ and $3/2\,\omega_0$ which confirms observations made in Limeil [2]. Our results are shown on Fig.2 and could be described as following:

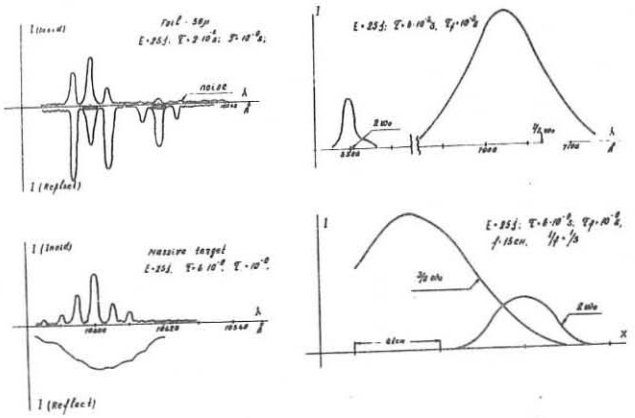

Fig.2. Results of spectral measurements.

a). Half-width of the second harmonic ($2\omega_0$) is about 10 Å, the line shape is asymmetrical with higher intensity on the red side.

b). The centre of the red line is shifted relative to the exact position of the $3/2\,\omega_0$ by 40 Å to the blue side. The half-width of this component is above 100 Å and its contour is symmetrical.

c). The intensity dependence of the $2\omega_0$ line on the focusing conditions is much sharper than that one for the $3/2\,\omega_0$ component. The maxima intensities of the lines corresponds to the different

positions of the target relative to the focusing lens. The results of the spectral measurements for different type of targets coincide within the experimental errors. The spectrogramms obtained with spatial resolution in the transverse to the incident beam direction showed that light emission at the frequencies $2\omega_0$ and $3/2\omega_0$ came from different plasma regions.

d). Time variation of the second harmonic intensity follows that one of the incident pulse.

When LiD and polyethylene targets were used the total neutron yields were also controlled along with spectral measurements. Neutron yield about $2 \div 3 \cdot 10^3$ neutrons per shot was detected simultaneously with the second harmonic signal.

The data obtained in our experiments definitely indicate the existence of the nonlinear effects in laser-plasma interaction at light flux densities above 10^{12} w/cm^2.

Acknowledgement. The authors are pleased to express their sincere gratitude to V.Zotov and V.Saveliev for assistence during these experiments.

REFERENCES

1. Ю.А.Ананьев, В.Н.Чернов, В.Е.Шерстобитов, Квантовая электроника, № 4,112 (1971).

2. J.L.Bobin, M.Decroisette, B.Meyer, Y.Vitel, Phys.Rev.Letters, 30,13,594 (1973).

HIGH-TEMPERATURE PLASMA PRODUCTION BY MEANS OF LASER PULSES OF SUBNANOSECOND WIDTH

V.D.Djatlov, A.D.Starikov, V.A.Serebrjakov,
V.I.Kryzhanovski, Ju.I.Dymashits, R.N.Medvedev,
A.N.Popytaev, V.N.Sizov
(USSR)

Interaction of short light pulses with LiD target has been investigated. The yield of fast neutrons $\sim 10^6$ per spark.

Experiments have been made on the interaction of short light pulses with LiD target. Light bursts with $(3\div4).10^{-10}$ sec duration were formed by a 3-line powerful neodimium glass laser /I/. The final stages had 60 mm aperture and could deliver 200÷300 joules with beams divergency (at half energy level) not more than 3.10^{-4} rad. The outputs were focused onto a solid target either by spherical single lenses (90 mm aperture, f = 233 mm) or by 3-lenses objectives (f = 60 mm; I:0,9) with subsidiary beam - preconverging lenses (fig.I).

LiD crystals of I÷3 mm were mounted inside the vacuum chamber on the revolving disc with 10 positions that allowed to expose one or another target without vacuum disturbance. Two-stage vacuum system pumped out the chamber to $(1\div2).10^{-4}$ mm Hg. To control the position of pellet with respect to focal spot we used a He-Ne laser provided an accouracy of no more than 5 μm. The intensity of incident light as well as scattered one was recorded by means of high speed electronic set with time resolution of 30 psec. Spectrography samples (fig.2) were taken by 30 Å/mm spectrograph for scattered light in vicinity of first and second harmonics.

For measuring neutron yield three methods were employed: activated blocks, plastic scintillator and thick photoemulsions. The

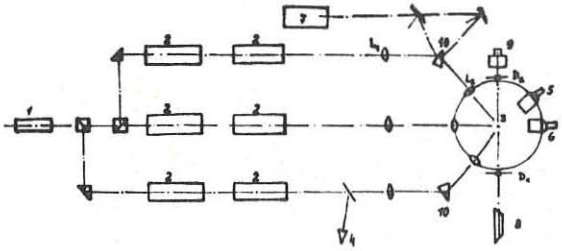

Fig.I. Schematic drawing of experimental apparatus:
I - laser oscillator; 2 - amplifier rods; 3 - target; 4 - calorimeter; 5 - neutron detector; 6 - X-ray detector; 7 - high speed electronic set; 8 - tracing laser; 9 - detector of tracing laser; I0 - prisms

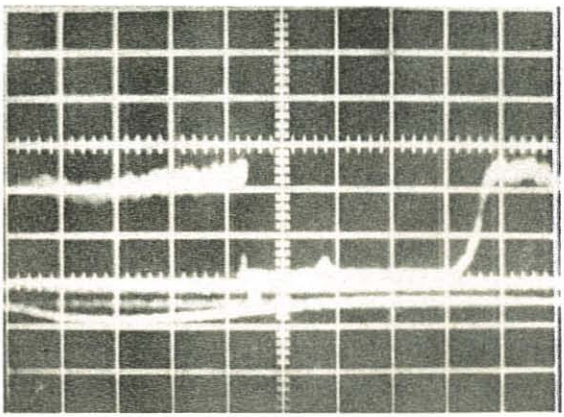

Fig.2. Tracing laser signal - upper beam, photodiode signal - lower beam

block being situated at the 35 cm distance from the target was able to count 10^5 $n^o/4\pi$. For calibration overall sensitivity of this detector we used Pu-α -Be source. Another method was performed by coupling plastic scintillator (p - terphenyl in polystyrene + POPOP ϕ 80 mm H = 80 mm) to photomultiplier with 10^2 $n^o/4\pi$ detection when arranged in vacuum chamber. Provision was made to protect the detector from hard X rays and electromagnetic fields. Nuclear emulsions calibrated by "cosmic stars" could trace 10^4 $n^o/4\pi$ quite near the target. Neutron yield measured by these methods was in good agreement in the range of accuracy methods used.

To evaluste electron temperature we employed techniques described elsewhere /2/. Aluminum absorbers 20.10^{-3} g/cm^2 and 40.10^{-3} g/cm^2 with plastic phospors setting in vacuum chamber were used. They were coupled to detectors by flexible light guides. Integrated on hotplasma-time-of-life electron temperature was foung to be I+3 kev.

The effect of background irradiation on the neutron yield was studied. It was found that maximum admitted background energy at which the neutron yield had a detectable counts amounted to 5.10^{-3} joules. Here no dense vapour cloud was observed near the target (fig.2).

The pulse to background energy ratio was not less than 10^4 and was provided by two Pokkels cells in oscillator and three dyed filters in each amplifier line. When only one line of amplifiers was used we registered the neutron yield 3.10^5 $n^o/4\pi$ while operation of all three lines gave us 10^6 $n^o/4\pi$.

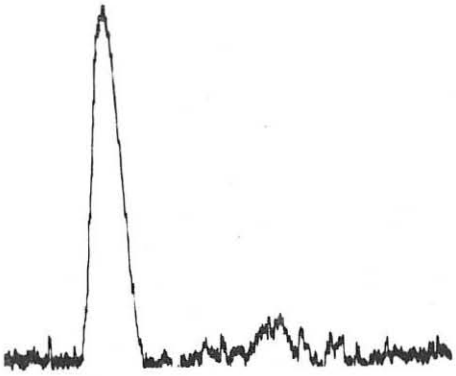

Fig.3. Incident and scatterd intensity.
I division 50 psec

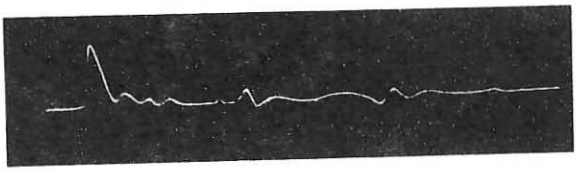

Fig.4. Neutron detector pulse

References

I. M.P.Vanyukov, V.I.Kryzhanovsky, V.A.Serebrjakov, V.N.Sizov, A.D.Starikov, Opt.-mech. Prom., No I2, 32, I972. /Sov. J. Opt Techn./.

2. F.C.Jahoda, E.M.Little, W.E.Quinn, G.A.Sawyer, T.F.Stratton. The Physical Review Second Series, v.II9, No.3, 843, I960.

SIMILARITY EQUATIONS OF CONCENTRIC LASER COMPRESSION AND FUSION OF PLASMA

S.Kaliski

WAT - Warsaw

Summary

The deriving of similarity equations of laser plasma compression, taking the thermal wave front and fusion energy recovery into account, was presented in this paper. Basing on the dynamics of bodies with variable mass the model of the Fermi liquid was assumed for the central part of D-T sphere, while for the external layer, determined by the thermal wave front, model of two-temperature ideal gas, was introduced. The numerical results give global evaluations, near the strict ones.

1. Introductions.

In the author's work [1] - [4] were presented the constructions an and solutions of averaged equations of the laser concentric plasma compression, taking the fusion energy recovery into account. These methods enable us to obtain some rough integral appraisals, considerably different from the numerical, strict approaches [5] , [6] . A certain evolution of averaged equations gives the integral similarity description [7] , [8] .

A further, more thorough study on similarity descriptions is given by the equations, basing on the average description, but separating the thermal wave front. The D-T sphere, subjected to a concentric laser pulse can be divided into two regions: the internal sphere, described by one-temperature model of the Fermi liquid and the external layer, comprised by the thermal wave front and undergoing the expansion. The external layer is described by the averaged model of two-temperature ideal gas. Both the sphere and layer are the system with variable reduced mass. The constructions of above mentioned equations is the aim of the present paper. In works [9] , [10] a further evolution of this model has been proposed allowing us, on the ground of averaged descriptions, to take into consideration the structures of both thermal and shock wave fronts.

The solution of equations and quantitative analyses are given, for the lack of place, in a separate elaboration.

2. The scheme of system

In fig.1 and 2 was indicated a scheme of system and assumed the distribution of velocities in the central sphere and external layer with variable region boundaries and various models of both media.

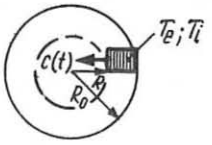

Fig.1

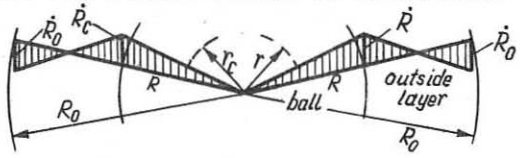

Fig.2

The value c(t) is determined by explicit approximate formulae on the ground of [11]. The simplified schemes of laser radiation absorption in external layer, discussion on the effects of brems-strahlung, linear and recombination radiation can be found in above mentioned papers.

Denotation for the sphere was assumed:

$$x = \frac{\dot{r}}{\dot{R}} = \frac{\dot{r}_c}{\dot{R}_c} \tag{2.1}$$

and for external layer:

$$x = \frac{\dot{r}_c - \dot{R}_c}{\dot{R}_0 - \dot{R}_c} = \frac{\dot{r} - R}{\dot{R}_0 - \dot{R}} \tag{2.2}$$

where: $\dot{R} = \dot{R}_c - c \; ; \; R = R_c - \int_0^t c(t_1)\, dt_1$

3. Equations of the problem

3.1. The central part equation of D-T sphere.

Assuming for the integral similarity model

$$\rho(x,t) = \rho_c(t) f(x); \; n(x,t) = n_c(t) f(x); \; p(x,t) = p_c(t) f(x); \; T = T(t) \tag{3.1}$$

and expression for energy and pressure for the degenerate Fermi's gas

$$E = \frac{3}{5} N E_r \left[\left(\frac{3N}{4\pi} \right)^{2/3} R^{-2} + \frac{5\pi^2}{12} \left(\frac{k}{E_r} \right)^2 \left(\frac{4\pi}{3N} \right)^{2/3} R^2 T^2 \right]$$

$$p(x,t) = p_c(t) f(x) = \frac{2}{5} E_r n^{5/3} \left[1 + \frac{5\pi^2}{12} \left(\frac{kT}{E_r} \right)^2 n^{-4/3} \right] \tag{3.2}$$

where

$$E_r = \frac{\hbar^2}{2m} (3\pi^2)^{2/3}$$

we can write the equations of momentum and energy conservation for a body with variable mass (the equation of energy conservation requires modification in relation to classical approaches) in the following form

$$\frac{2}{5}AE_r\left[C\left(\frac{N}{4\pi D}\right)^{5/3}R^{-3}+\frac{5\pi^2}{12}\left(\frac{k}{E_r}\right)^2\left(\frac{N}{4\pi D}\right)^{1/3}LRT^2\right]=$$

$$=2B\frac{d}{dt}\left[M(\dot{R}+c)\right]-2B\vartheta_s\frac{dM}{dt}+\bar{A}R^2\frac{k}{V_l}\left(N_eT_e+N_iT_i\right) \tag{3.3}$$

$$\frac{d}{dt}\left\{\frac{3}{5}NE_r\left[\left(\frac{N}{4\pi D}\right)^{2/3}CR^{-2}+\frac{5\pi^2}{12}\left(\frac{k}{E_r}\right)^2\left(\frac{4\pi D}{N}\right)^{2/3}LR^2T\right]\right\}-\bar{A}(\dot{R}+c)R^2\frac{k}{V_l}$$

$$\left(N_eT_e+N_iT_i\right)+B\frac{d}{dt}\left[M(\dot{R}+c)^2\right]-2B\left(\vartheta_s-\frac{\dot{R}+c}{2}\right)(\dot{R}+c)\frac{dM}{dt}+B_r=Q(T,R) \tag{3.4}$$

where $M=4\pi R^3\rho_c D$, $D=\int_0^1 f(x)x^2dx$; $C=\dfrac{\int_0^1 f(x)^{5/3}x^2dx}{D}$; $L=\dfrac{1}{D}\int_0^1 f(x)^{1/3}x^2dx$

$$\begin{cases}\vartheta_s=\dot{R}_c+(\dot{R}_0-\dot{R}_c)\dfrac{R_s-R}{R_0-R};\quad R_s=\dfrac{3}{4}\dfrac{R_0^4-R^4}{R_0^3-R^3};\quad V_l=\dfrac{4\pi}{3}\left(R_0^3-R^3\right);\quad \bar{A}=-4\pi\\ A=-4\pi\int_0^1\dfrac{df(x)}{dx}x^3dx;\quad B=\dfrac{1}{2D}\int_0^1 f(x)x^4dx\end{cases} \tag{3.5}$$

whereas we determine f(x) according to the known formulae.

In equations (3.3), (3.4) B_r - denotes Bremsstrahlung, Q(T,R)- characterizes the fusion energy recovery (see formulae in [1] - [4]) For C we have the approximate expression (we write it for shortening the formulae for q= const, where q = intensity of laser raration)

$$C=\frac{14\pi c_0 q T_e^{5/2}\dot{T}_e}{\left(14\pi c_0 T_e^{7/2}+\frac{q}{R_c}\right)} \tag{3.6}$$

In equations (3.3), (3.4), (3.5) the parameters of external layer T_e, T_i and R_o appear.

3.2. Equations of external layer

For the external layer, employing the equations for two-temperature ideal gas, with the distribution of velocities like in fig.2, and assuming f(x) = const, we obtain on the ground of dynamics equations of the body with variable mass:

$$4\pi\left(R_0^2\dot{R}_0 - R^2\dot{R}_c\right)k\left(n_{0e}T_e + n_{0i}T_i\right) + \dot{R}_c v_s \frac{dM_r}{dt} = v_s \frac{d(M_r v_s)}{dt}$$

$$\frac{3}{2}k\frac{d}{dt}(N_e T_e) + B_l = -k n_{0e} T_e \cdot 4\pi\left(R_0^2\dot{R}_0 - R^2\dot{R}_c\right) -$$

(3.7)

$$-\frac{3}{2}kN_e\frac{T_e - T_i}{\tau} - \eta_e\frac{dM_r}{dt}\left(\dot{R}_c - \frac{v_s}{2}\right)v_s + q(t)$$

$$\frac{3}{2}k\frac{d}{dt}(N_i T_i) = -k n_{0i} T_i\, 4\pi\left(R_0^2\dot{R}_0 - R^2\dot{R}_c\right) + \frac{3}{2}kN_e\frac{T_e - T_i}{\tau} - \eta_i\frac{dM_r}{dt}\left(\dot{R}_c - \frac{v_s}{2}\right)v_s$$

where M_r - reduced mass in relation to the point R_s

B_l - bremsstrahlung of the layer

$$\eta_e, \eta_i \sim \frac{T_e}{T_e + T_i};\ \frac{T_i}{T_e + T_i};\quad n = \frac{N}{V}$$

The system of equations (3.3), (3.4), (3.6) and (3.7) is a system of 6 equations of the problem in relation to the unknowns R_0, R, T, T_e, T_i, C. To the system are added the initial conditions that we do not write down.

4. The end remarks

The equations above formulated enable us, in average approximation for the similarity model, to describe the process of plasma compression and fusion energy recovery. The numerical results for initial R of order 0,04 cm and laser pulse energy of order 5 kJ give the compression $10^3 < K < 10^4$ and a positive energy recovery. The laser pulse energy may be reduced by applying explosive precompressing.

Literature:

[1] [4] [8] [9] S.Kaliski - Proc.Vibr.Probl. 4,13, 1972; 2,14, 1973; 3, 13, 1972, 3,14, 1972.

[2] [3][10][11] S.Kaliski - Bull.Ac.Polon.Sci.,Ser.Sci.Techn.- in print

[5] J.Nuckolls a.others - laser Conference in Montreal 1972.

[6] K.A.Bruckner UC San Diego 1972.

[7] A.F.Haught, D.H.Polk - Phys. of Fluids,ii, 13, 1970.

PLASMA HEATING WITH A RELATIVISTIC ELECTRON BEAM

P. Korn, F. Sandel and C. Wharton[+)]
Cornell University, Ithaca, N.Y., U. S. A.

ADDITIONAL RESULTS SINCE APRIL 25, 1973

Ion heating was measured with a 4-channel energy analyzer for fast neutral atoms arising from charge exchange. A background of krypton provided the target gas for charge exchange. Both momentum and energy analysis were obtained by magnetic and electrostatic deflection. The analyzer can observe fluxes at 4 angles, but data reported here were at 90 ° to the magnetic field. For turbulent heating we found that the ion heating was nearly isotropic.

The ion energy distributions for direct turbulent heating and for heating with the relativistic electron beam were nearly identical, except that the high energy tail is accentuated by beam heating. The curves shown in the figure were normalized to 925 eV; actually the REB curve lies well above the TH curve. Diamagnetic signals for the two cases looked qualitatively alike, but the REB signal was twice as large. The distribution is not Maxwellian, but more nearly follows an inverse power law, at levels up to 10^{17} eV/cm^3. At higher energy-densities the tail becomes accentuated.

Transfer efficiences from stored energy to nkT_i for direct turbulent heating were 3 to 6 %; for the REB we achieved up to 15 %. The efficiency was a strong function of the electron diode impedance, since maximum current density was obtained when the diode and energy storage line impedances were matched. For a foil-less diode the impedance was matched only when the proper plasma density was allowed in the anode cylinder; too high a density caused a short-circuit (closure) and too low a density gave a high impedance.

In further experiments we have found that injecting the beam into an already turbulent plasma greatly enhances the heating efficiency, presumably because the return-current is damped by the anomalous collisions.[1)]

References

1) P. Korn, F. Sandel and C. Wharton: "Interaction of a Relativistic Electron Beam with a Turbulent Plasma", Submitted to Phys. Rev. Letters, June, 1973.

+) Presently at Max-Planck-Institut für Plasmaphysik, 8046 Garching, Germany

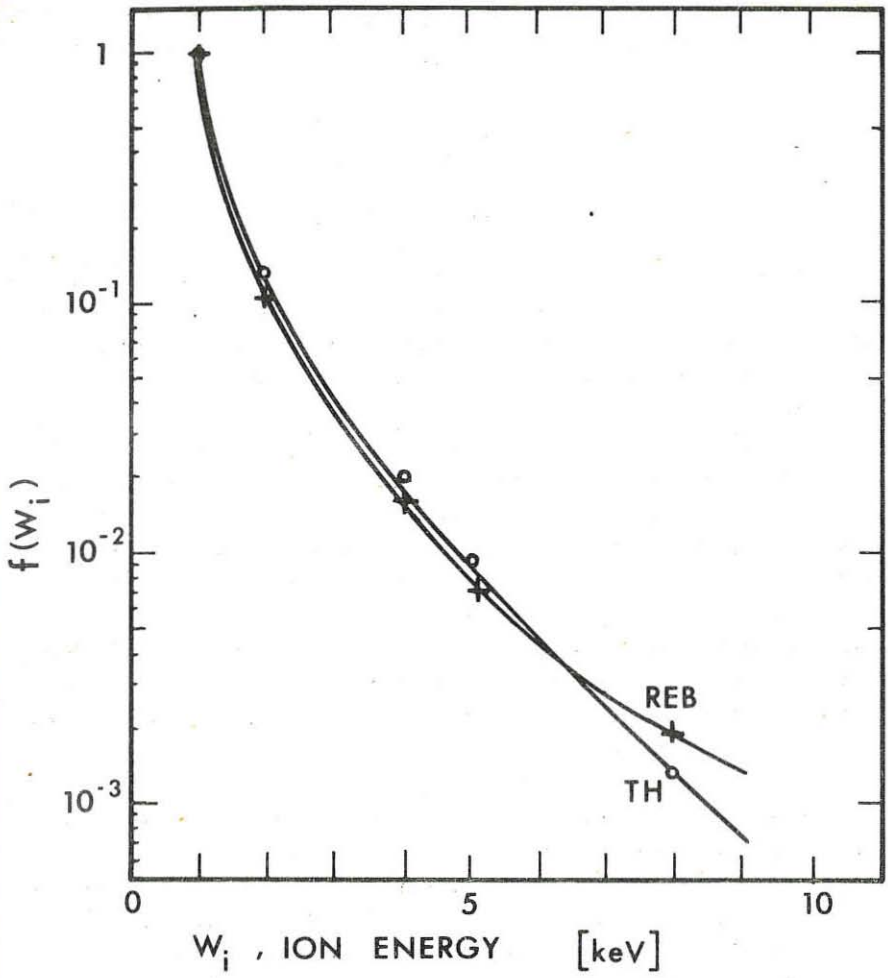

Ion energy distribution in 8 x $10^{13}cm^{-3}$ plasma from neutral atom analysis. TH: direct turbulent heating, $W_\perp$ = 6 joules. REB: E-beam heating, 5 cm diameter carbon cathode, 10 cm long foil-less anode cylinder with 6 mm gap, $W_\perp$ = 12 joules.

MEASUREMENTS OF THE LINEAR AND NONLINEAR STAGE OF THE BEAM-PLASMA INSTABILITY.

R. Aymar, H. Böhmer, F. Koechlin

ASSOCIATION EURATOM-CEA SUR LA FUSION
Département de Physique du Plasma et de la Fusion Contrôlée
Centre d'Etudes Nucléaires
Boite Postale n° 6. 92260 FONTENAY-AUX-ROSES (FRANCE)

An electron beam is injected into the afterglow plasma of a pulsed P.I.G. discharge, immersed in an uniform magnetic field of 2800 Gauss. The plasma diameter is 5 cm, the length is variable from 150 to 230 cm. At the time the electron beam is pulsed, the average plasma density, measured with a microwave interferometer, is in the range 10^{10} - 2×10^{11} cm^{-3}, the electron temperature, obtained with a Langmuir probe, is 0.75 ± 0.25 eV. Therefore, the ratio of electron collision to plasma frequency is 10^{-3}, so that collisions can be neglected in the dispersion relation for the hydrodynamic beam-plasma instability. The radial electron density profile, also measured by a Langmuir probe, is used to calculate the plasma branch of the dispersion relation, for $\omega_{ce}/\omega_{pe} > 2.5 >> 1$. The electron beam energy is 6.5 keV, with an initially narrow energy distribution ($\Delta E/E \sim 1\%$), its diameter is 0.8 cm, and the pulse duration is 15 μsec. The ratio of beam density to plasma electron density is $< 5 \times 10^{-3}$.

The unstable plasma waves excited by the beam are observed with capacitive probes followed by a narrow band amplifier and a gated integrator. Also, with an 8 mm microwave scattering system both frequency and wave vector spectra of the unstable waves can be measured [1]. Good agreement is found between both diagnostics when the plasma density is varied and the received frequency ω kept constant, at least for the first radial mode, as shown in fig.1. If the plasma density in the center of the column is assumed to be twice the average density, then there is good agreement between the value of density at resonance and the calculated dispersion relation.

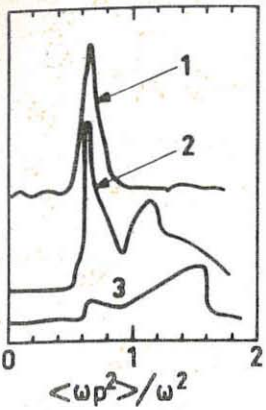

Fig.1: Measurements at 2.6 GHz and i_b=70mA.
1) Scattered power versus average electron density at d=100cm from the electron gun $k_{//}=3.4cm^{-1}$.
2) Capacitive probe signal, radial position r=16mm d=70cm.
3) Same as 2, except r=21mm.

In fig.1, the scattered spectrum is measured at $\vec{k}_o=\omega/v_b.\vec{B}/B$; the scattered power indeed is peaked at this value, as shown in fig.3(dashed curve ; the width is given by the resolution).

The spatial growth rate of the instability has been measured, using probes, between 20 cm and 70 cm from the electron gun. It was found to be $\sim$ 0.1 cm^{-1} for i_p=70mA. This value is in agreement with the theoretical growth rate for the hydrodynamic instability as given by O' Neil and Malmberg [2], taking into account the radial density profile of the plasma and the ratio of beam radius to plasma radius [3] . Unstable wave saturation and decay are observed with probes as well as with microwave scattering as shown in fig. 2.

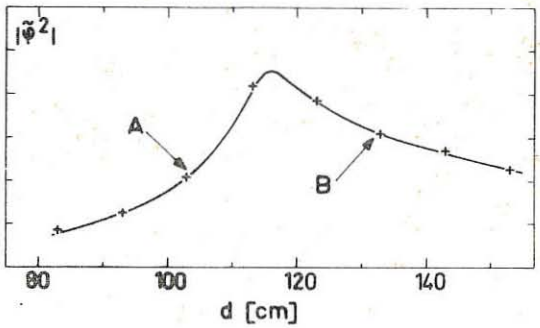

FIG. 2 -

Fig.2: Scattered power as a function of distance along the beam. i_b=70 mA.
$\tilde{\varphi}_{max} \sim$ 30 Volts.
f=2.6 GHz, $k_{//}=3.4cm^{-1}$

In fig. 3 the $k_{//}$ spectrum of the unstable waves is shown in two different regimes ; in the exponential growth (linear) region, the measured width is exactly the instrumental width ; in the nonlinear

decay region, the measured spectrum is considerably extended towards higher $k_{//}$ vectors, although the scattered frequency is maintained constant. This proves the existence of waves with phase velocities much smaller than the initial beam velocity : $0.4 < V_{ph}/V_b < 1$. A scattering measurement of the perpendicular wave vector shows that the unstable mode is axisymmetric with a diameter of ∿3cm, in agreement with radial probe measurements (fig.1). In the saturation and decay regime, the beam velocity distribution is found to spread considerably, primarily towards smaller velocities. For example, for i_b=70mA, E=6.5 keV and at a distance d = 150 cm, the energy spread ΔE is 2 keV and the average energy 5.7 keV. Therefore, one can assume that the enlarged $k_{//}$ spectrum interacts resonantly with the enlarged beam distribution function.

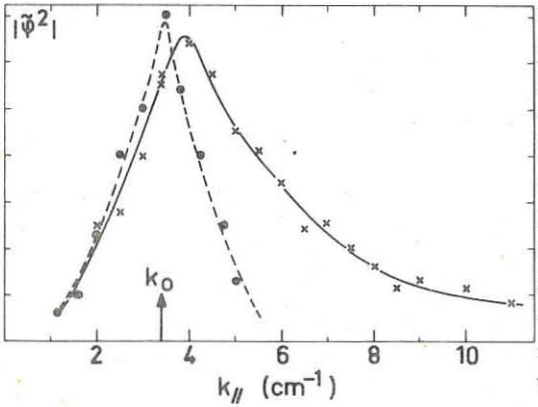

Fig.3 : Scattered power at f=2.6 GHz as a function of $k_{//}$.
--------• at point A in fig.2
———— x at point B in fig.2

The fluctuating density and potential of the plasma wave can be estimated by using the absolute calibration of the microwave scattering system. At the saturation level of fig.2, the fluctuating density is $2 \pm 0.5.10^8 cm^{-3}$ (integrated over the system resolution Δk and Δω) ; this corresponds to a fluctuating potential of 30 ± 10 V and an electric field of 110 ± 30 V/cm. This potential is of the order of the threshold for trapping of beam electrons in the hydrodynamicaly unstable wave [4]. It also is coherent with the measured width of the beam energy distribution as given by a trapped particles model : $\Delta E/E \sim 4(e\varphi/E)^{1/2}$. However, there is no evidence for particle trapping in this experiment.

One can also explain the observed spread in the beam velocity distribution function using a model by Tsytovich [5] ; it considers the velocity space diffusion of the beam electrons which are resonant with one wing of the finite width ($\sim\gamma_k$) wave spectrum in the linear regime. After a modification of Tsytovich's expression for finite beam and plasma, one obtains an energy spread of ~600 eV in the laboratory frame, using a potential of 20 Volts. This model obviously has to be modified when the linear hydrodynamic dispersion relation is no longer valid [2], and can only explain an initial widening of the beam distribution.

REFERENCES :

[1] H. Böhmer and M. Raether, Phys. Rev. Letters 16, 1145 (1966)

[2] T.M. O'Neil and H.G. Malmberg, Phys. Fluids 11, 1754 (1968).

[3] K.W. Gentle and C.W. Roberson, Phys. Fluids 14, 2642 (1971).

[4] W.E. Drummond, J.H. Malmberg, T.M. O'Neil and J.R. Thompson, Phys. Fluids 13, 2422 (1970).

[5] V.N. Tsytovich. Nonlinear effects in plasma, Plenum Press, N.Y. 1970, p. 186-193.

Electromagnetic Instabilities, Filamentation and Self-Focussing of a Relativistic Electron Beam, Martin Lampe and Roswell E. Lee,
Naval Research Laboratory, Washington, D. C., 20375, U. S. A.

Abstract: We report on theoretical and computer simulation studies of the Weibel or "pinch" instability of a relativistic electron beam propagating in a plasma. The instability produces beam filamentation, expulsion of the return current, and finally, recombination of filaments into a single beam, self-focussed to the background plasma density.

We study a system consisting of beam electrons, counterstreaming plasma electrons, and an immobile neutralizing ion background. Both beam and plasma are initially homogeneous and infinite in extent. The computer simulation code is relativistic, fully electromagnetic, has periodic boundary conditions, and is two-dimensional in the sense that spatial variations are permitted only in the plane perpendicular to initial streaming. Thus electrostatic two-stream instability is ruled out, but purely growing electromagnetic instability occurs, for wave vectors $\underline{k}$ perpendicular to streaming. The linear growth rate is given by $\delta^2 = \omega_b^2\gamma^{-1}(v/c)^2(1+\omega_p^2/k^2c^2)^{-1}-(\Omega_e/\gamma)^2$, for the case of a cold, weak beam. Stabilization thus occurs if B_z is so large that $\Omega_e \geq \gamma^{1/2}\omega_b v/c$. Also, δ falls off if the transverse beam thermal energy exceeds $<p_\perp^2>/p_z^2 \geq n_b/n_p\gamma$.

We have simulated and studied in detail a variety of cases: (1a) Weak beam ($n_p/n_b = 9$), $\gamma = 2.5$, $B_z = 0$, beam and plasma cold; (1b) $n_p/n_b = 9$, $B_z = 0$, beam warm ($<p_\perp^2>^{1/2}/p_z = 0.14$); (1c) $n_p/n_b = 9$, $B_z \neq 0$, $\Omega_e = 0.4\ \omega_p$, beam and plasma cold; (2) Strong beam ($n_p = n_b$), $B_z = 0$, beam and plasma cold. Although the linear behavior varies widely among these cases, we find that (provided that linear instability exists at all) the final non-linear state is very similar in all cases. The principal features of the development are as follows.

During the initial stage, many unstable modes grow, in good agreement with linear theory. The instability spatially modulates the density of each electron species, in such a way that the beam electrons separate from the plasma electrons, but the total electron density remains nearly uniform, so as to preserve electrostatic neutrality. If $n_b \ll n_p$ initially, the beam breaks into many distinct

narrow filaments. Each beam filament is compressed, by its self magnetic field, until its density reaches that of the background ions. At this point, the plasma electrons are totally excluded from each filament, further compression is prevented by the (approximate) requirement of electrostatic neutrality, and the linear stage ends. The magnetic energy at this point can be estimated, for each choice of parameters, from the filament separation, which is of the order of the dominant linear wavelength. However, the filaments are mutually attracting through (plasma-shielded) magnetic forces, so that during the nonlinear stage, they coalesce (over a period few X $10^2 \omega_p^{-1}$ typically) into fewer and fewer filaments. Finally, the beam recombines into a single current filament, at the density of the background plasma, and from which the plasma electrons have been expelled. The magnetic energy has grown to the point where $B_\varphi^2/8\pi\, n_b mc^2\gamma \sim \nu/\gamma$ and comparable plasma heating also occurs.

Our nonlinear study thus far is restricted to the case of an infinite homogeneous beam, with effective $\nu/\gamma \leq 1$ (corresponding to one box of the periodic system). However, we expect qualitatively similar behavior in a beam with finite radial profile. Recombination of filaments should be even faster, for the following reason. Since the beam electron longitudinal mass $m_e\gamma^3$ far exceeds the plasma electron mass m_e, and longitudinal momentum is conserved among the electrons, the plasma return current decreases much faster than the beam current. Thus at late times, the beam is no longer fully current neutralized, even globally. This gives rise to a global self-focussing force, in addition to the local forces discussed above. In some of our simulations, the beam current is less than 50% neutralized at the end (but in a <u>periodic</u> simulation system, this does not produce a focussing force).

Since the final result of the Weibel instability is to expel the return current from the beam, we may expect that this will prevent propagation of an (initially current neutralized) beam with $\nu/\gamma \gg 1$, in the absence of a sufficiently strong guide field. In fact, it may be possible to tune the propagation length by carefully choosing B_z.

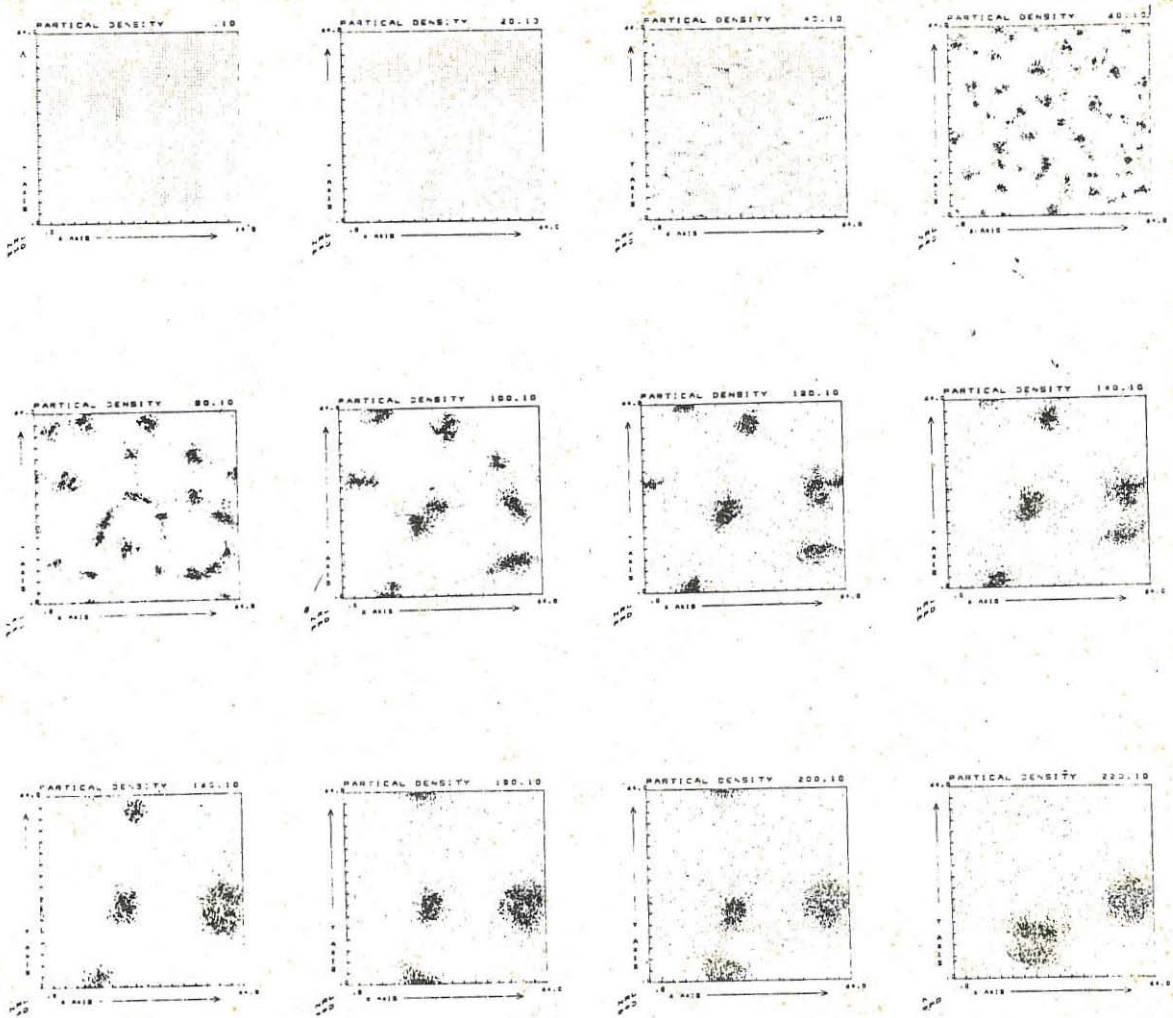

Spatial density of beam electrons, at times $\omega_p t = 0, 20, 40, \ldots$, for Case 1a, cold beam, $n_b = 9n_0$, $B_z = 0$, $\gamma = 2.5$

Beam (left) and plasma electron (right) spatial densities, at time $\omega_{pe}t = 160$, for Case 1a, cold beam, $n_p = 9n_b$ initially, $B_z = 0$, $\gamma = 2.5$.

EXPERIMENTAL INVESTIGATIONS ON HIGH-CURRENT BEAMS OF RELATIVISTIC ELECTRONS

L.I.Rudakov, V.P.Smirnov, E.Z.Tarumov, S.S.Kingsep, I.V.Koba, V.D.Korol'ev, G.P.Maksimov, I.L.Sidorov, A.M.Spector, A.D.Suhov.

I.V.Kurchatov Institute of Atomic Energy, Moscow, USSR

In the last years the technique of producing high-current electron beams has been intensively developed [1,2,3]. In Kurchatov Institute experimental investigations on plasma heating by high power electron beams have been carried out using four fast pulse generators. The parameters of these beam installations are presented in Table 1.

Table 1.

Main parameters of electron beam generators

Generator	Marx generator energy (kJ)	Electron energy (kev)	Beam current (kA)	Pulse duration nsec	Dielectric	Forming line	Match impedance Ω	Water switch
Neptune	2	800	30	40	water	Blumline strip	30	one channel
MS	3	400	40	40	water	Blumline coaxial	10	two channels
Triton	11,5	500	220	30	water	Blumline coaxial	2,25	six channels
Ural	12	600	250	50	water	coaxial	2,5	one channel

As follows from measurements of breakdown of deionised and deairated water, the strength of electric field in forming lines with a water insolation can reach up to 20 -25 kv/cm for the whole electrode surface equal to $10^4 cm^2$ and the effective time of the order of 10^{-7} sec. The charging time of the pulse forming lines was decreased by application of low inductance Marx generator with oil isolation ("Ural" generator) or the intermediate water capasity ("Triton" generator). The obtained charging time was equal to 0,15 μsec in the first case and less than 0,10 μsec in the second case.

The fast charging of forming lines ensured the possibility of

using the water selfbreakdown switches. As have been shown from model experiments with one channel 100 kv water switch the optimum current risetime was ≤ 10 nsec for the line impedance in the range of 5 - 15 Ω. These results were confirmed at "Neptune". The current risetime at "Ural" was about 15 nsec at 2,5 Ω impedance. The posibility of multichannel switching of a forming line with 1 Ω impedance was studied at "Triton" machine. Ussuly four channels from six were switched and the total spark current risetime ≤ 15nsec was obtained.

The influence of the plasma injected into a cathode - anode gap on the beam current density was investigated in special experiments. As a result the beam current density increased more than ten times [4].

The beam propagation in the neutral gas was studied in the 60cm long drift chamber. The measured value of return current in the plasma produced by beam was in accordance with the results of numerical calculations of Taunsend's ionisation by induced electric fields [5].

The maximum efficiency of the beam energy propagation reached approximately 60% with the air pressure being equal to 2 torr without the external magnetic field, and 75% if H_{II}=3,8 koe.

The possibility of the beam transportation across a magnetic field was studied at "MS" generator. The electron beam was injected along the cylinder filled with the air and inserted in the drift chamber at $H_{\perp} \leq 1$koe. The drift chamber was pumped out up to 10^{-4} torr. The gas pressure in the cylinder varied in the range of 0,5 - 1 torr. The cylinder was made of thin aluminium foil (the thickness was 1.2 10^{-2}mm) and according to our idea it had to imitate a plasma channel for the beam injection experiment in a closed trap. When the beam was deflected by the external magnetic field and went out of the cylinder the return current can be closed in such a way that the current along the cylinder would be equal to the current of electrons which leaved the channel. If the self magnetic field of the beam H_{φ} was more than $2H_{\perp}$, the beam could not leave the channel. The light emmited by the plasma produced by the beam in the magnetic field in the absence of the cylinder is shown in Fig. 1a. The radius of curvature of the beam tra-

jectory was roughly equal to the Larmour radius. When the drift chamber was pumped out the beam propagated along the cylinder and destroyed the collector as shown in Fig. 1b. In this experiment the length of the cylinder was approximately equal to the diameter of the beam trajectory in the drift chamber with a uniform gaseous filling. The efficiency of the beam transportation across the magnetic field reached 80-100% in these experiments.

Fig.1 a.

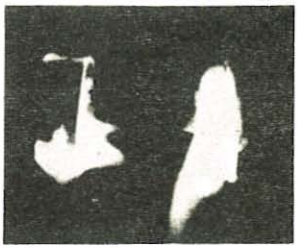

Fig. 1 b.

References

1. L.S.Levine, I.M.Vitkovitsky, IEEE Trans. on Nuclear Science NS-18, N 8, p.255-264 (1971).

2. О.П.Печерский, А.М.Сидорук, В.Д.Тарасов, В.А.Цукерман, ДАН, том. 192, № 6, стр. 1266, 1970г.

3. О.Г.Загороднов, А.И.Болотин, И.И.Магда, Н.П.Гадецкий, В.И.Беляев, Ю.В.Ткач, ПТЭ, № 5, стр.100-102,1970г.

4. С.Л.Недосеев, В.П.Смирнов, А.М.Спектор, Д.Г.Филькин, ЖТФ, том XIII вып.12, стр.2520-2525, 1972г.

5. И.В.Новобранцев, Л.И.Рудаков, В.П.Смирнов, С.С.Кингсеп, А.М.Спектор, ЖЭТФ, том 63, вып.6, 1972г.

INTERACTION OF MONOENERGETIC ELECTRON BEAM WITH DENSE PLASMAS.

A.A.Ivanov, V.V.Parail, T.K.Soboleva.

I.V.Kurchatov Institute of Atomic Energy, Moscow, USSR.

The interaction of a monoenergetic electron beam with dense collisional plasma is considered by means of partial numerical simulation method. Two cases are treated: when Langmuir frequency of plasma is greater then collisional freguency and when collisional frequency is greater then Langmuir frequency.

In the present paper the nonlinear regime of interaction of the electron beam with collisional plasma is treated when the beam density n_b is much less then that of plasma $n_b \ll n_o$. For investigation of relaxation process of the electron beam passing through the dense plasma the machinary simulation method was used. It is well known now a beam of charged particles when penetrating plasma gives rise to the exitation of instabilities. The amlpitude of electrostatic potential when $n_b \ll n_o$ is small enough and the condition of applicability of linear theory for the plasma particles is fulfilled. The basic assumption makes it possible to describe plasma as continuous medium and to use numerical simulation for the beam particles only. This method, which can be named as "partialy numerical simulation method" was already successfully used for the investigation of electron beam interaction with collisionless plasma[1].

The problem described here was made for two cases: $\gamma_1 < \nu < \omega_{pe}$ and $\gamma_2 < \omega_{pe} < \nu$. Here ν - is the frequency of collisions in plasma, ω_{pe} -Langmuir frequency of plasma. The linear grouth rates of instabilities are described by the folloing relations:

$$\omega=\omega_{pe},\ \gamma_1=\left(\frac{\omega_{pe}\omega_{be}^2}{2\nu}\right)^{1/2};\quad \omega=ku\ll\omega_{pe},\ \gamma_2=\left(\frac{n_б}{n_0}ku\nu\right)^{1/2} \qquad (1)$$

where $\omega_{be}=\left(\frac{4\pi e^2 n_б}{m}\right)^{1/2}$, u -the initial beam velocity.

I. The interaction of electron beam with plasma when $\gamma_1<\nu<\omega_{pe}$ /2/.

The frequency of the wave arising in plasma as a result of the development of a beam-plasma instability is close to ω_{pe} and the influence of higher modes with frequencies $n\omega_{pe}$ is expected to be negligible, because their amplitudes $E_n=\frac{\gamma_1}{\omega_{pe}}\frac{E_1}{n^2-1}$ are small compared to E_1. Hence for the amplitude of growing mode we have:

$$E(x,t)=E(t)\exp\left\{ik_0x-i\frac{\omega_{pe}}{\beta}t+i\alpha(t)\right\} \qquad (2)$$

where $E(t)$-the amplitude and $\alpha(t)$-the phase of the wave are slowly varying functions of time. The scale time of **their** change is of the order of $\tau\sim\gamma^{-1}\gg\omega_{pe}^{-1}$. Existance of two scales of time is essential in this case and makes it possible to find slowly varying values by averaging over fast varying coordinate $\xi=k_0x-\frac{\omega_{pe}}{\beta}t$. Making use of equations of motion and continuity and Poisson equation, substituting electric field in the **form** (2) we obtain after decomposing for **real** and imaginary parts the equations for the amplitude and the phase of growing wave:

$$\frac{\partial E}{\partial t}=-\frac{\nu}{2}E-2e\omega_{pe}\int_0^{2\pi}\frac{\partial^3 n_б}{\partial^3\xi}d\xi$$
$$\frac{\partial\alpha}{\partial t}=-\frac{2e\omega_{pe}}{E}\int_0^{2\pi}\frac{\partial^3 n_б}{\partial^3\xi}d\xi \qquad (3)$$

(here we put $\beta=1$ for simplicity).

Continuous electron beam we simulate by separate particles therefore density of the beam can be written in the form

$$n_б(\xi,t)=\frac{n_{0б}}{N}\sum_{p=1}^{N}\delta(\xi-\xi_p(t)) \qquad (4)$$

where summarisation is **expanded** over all particles, ξ_p -is the trajectory of the p-particle . Substituting (4) in equations (3) we

obtain after normalization:

$$\frac{d\mathcal{E}_{\beta\pm i}}{d\tau} = -\frac{\nu}{2\gamma_1}\left[\mathcal{E}_{\beta\pm i} - \frac{1}{N}\frac{(\beta\pm i)^2}{\beta}\sum_{p=1}^{N}\sin\left\{(\beta\pm i)\,\xi_p + \alpha_{\beta\pm i}\right\}\right]$$

$$\frac{d\alpha}{d\tau} = \frac{\omega_{pe}}{2\gamma_1}\frac{\left[(\beta\pm i)^2-\beta^2\right](\beta\pm i)}{\beta^3} + \frac{\nu}{2\gamma_1}\frac{1}{N\mathcal{E}_{\beta\pm i}}\sum_{p=1}^{N}\cos\left\{(\beta\pm i)\,\xi_p + \alpha_{\beta\pm i}\right\} \qquad (5)$$

Here $\mathcal{E} = E/E_{max}$, $E_{max} = \frac{8e\omega_{pe}N}{\nu p}$, $\tau = \gamma_1 t$.

Equations (5) with equations of motion for each particle of the beam:

$$\frac{d\eta_p}{d\tau} = -\mathcal{E}\sin(\xi_p + \alpha)$$

$$\frac{d\xi_p}{d\tau} = \eta_p \qquad \text{where} \quad \eta_p = \frac{\beta k u_p - \omega_{pe}}{\gamma_1} \qquad (6)$$

fully describe the system beam - plasma.

The system of equations (5), (6) was solved by computer. The number of particles was varied from 250 to 500. The results of machinery simulation shown on fig.1 and fig.2 indicate that nonlinear regime of beam-plasma instability leads to broadening of distribution function of the beam by the factor of γ_1/k within the time period of the order of some growth rates times, which results in decreasing of instability. The initially monoenergetic beam thermalized and now passes easily through plasma. To understand this fact we have to take into account that for monoenergetic beam ($\gamma > kV_{Tb}$) energy of waves is negative and collisional frequency (dissipation) causes the instability, meanwhile for the thermalized beam ($\gamma < kV_{Tb}$) energy of the waves is positive and $\nu > \gamma$ causes strong damping of the waves.

II. The interaction of electron beam with plasma when $\gamma_2 < \omega_{pe} < \nu$ /2/.

In a case of a dense plasma ($\nu > \omega_{pe}$) the linear growth rate of beam-plasma instability is proportional to $\sqrt{k}$ (2). Therefore it could be expected that in this case thermalization of beam does not

cause stabilization of instability. Using the same approach as in the part I, we have

$$\varepsilon_{\beta-i} = \frac{1}{N}\left\{\left(\sum_{p=1}^{N}\sin(\beta-i)\xi_p\right)^2 + \left(\sum_{p=1}^{N}\cos(\beta-i)\xi_p\right)^2\right\}^{1/2}$$

$$\frac{d^2\xi_p}{d\tau^2} = -\frac{4}{\beta}\sum_{i=0}^{m}\varepsilon_{\beta-i}\sin\left\{(\beta-i)\xi_p + \alpha_{\beta-i}\right\} \qquad (7)$$

where β -is the number of mode having the maximal growth rate, $i=1,2,3\ldots$. The results of machinery simulation shown on fig.3 and fig.4 indicate that as velocity spread in the beam increases the modes with shorter wave numbers become instable. Therefore instability takes place all the way and effective transfer of beam energy in plasma waves and then in plasma particles occurs.

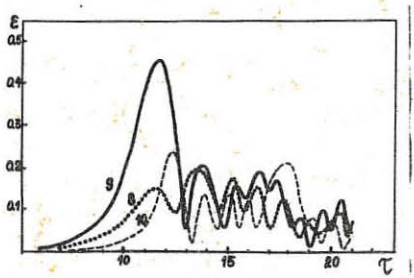

Fig. 1

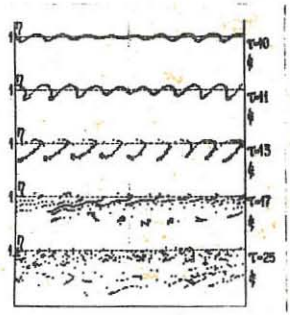

Fig. 2

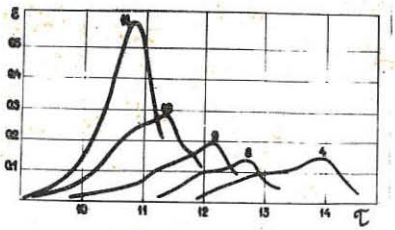

Fig. 3

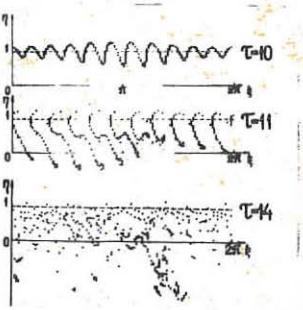

Fig. 4

References:

1. I.N.Onishchenko, A.P.Linetskii, N.Matsiborko, V.D.Shapiro, V.I.Shevchenko. JETP, Letters, 12, 407-411 (1970).

2. A.A.Ivanov, V.V.Parail, T.K.Soboleva. JETP, 63, 1678-1685 (1972).

ANOMALOUS RESISTIVITY AND RELATED MICROFIELDS OF A TURBULENT PLASMA COLUMN

by W.R. Rutgers, H. Schrijver, H.W. Piekaar, and H. de Kluiver

Association Euratom-FOM, FOM-Instituut voor Plasmafysica
Rijnhuizen, Jutphaas, The Netherlands

ABSTRACT

A turbulent plasma has been made by the discharge of a capacitor across the column of a hollow cathode arc in a magnetic field. The anomalous resistivity for different gases, its relation to microfields observed by microwave radiation emitted and the appearance of Stark satellites in hydrogen are reported.

The resistivity measurements

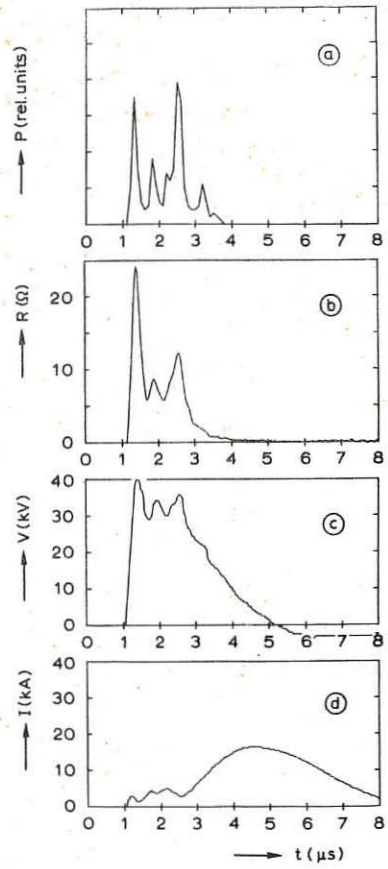

Fig.1. The recorded signals of an experiment in hydrogen as a function of time.

For the technical description and the experimental procedure we refer to earlier publications [1].

The anomalous resistivity (R) of the turbulent plasma has been measured simultaneously with the microwave radiation (P) emitted by the plasma around ω_{pe}. The plasma resistance is computed from the voltage along the plasma column (V) and the plasma current (I). A correction is made for the inductive part of the voltage. A strong correlation between R and P is found as a function of time (Fig. 1).

In the first few hundred nanoseconds the parameters which characterize the plasma state are the initial ones as has been argued in Ref. [2]. On a longer time scale the expansion of the plasma column and the ionization of neutral gas change the parameters. Therefore, the plasma conductivity σ and the corresponding effective collision time, τ_{eff}, have been computed only for the initial stage of turbulence as the dimensionless parameter: $\tau_{eff}\omega_{pe} = \sigma/\varepsilon_o\omega_{pe}$ (SI-units).

The effective collision time has been given in Fig. 2 as a function of the plasma density for experiments in H, He, Ne, Ar, and Xe. From the curves of Fig. 2 the average values at densities of 2, 5, and 10 × 10^{19} m^{-3} have been taken to plot $\tau_{eff}\omega_{pe}$ as a function of the ion mass in Fig. 3. At the density of 2 × 10^{19} m^{-3} the conductivity does not depend significantly on the ion mass. At higher densities the conductivity increases with a small power of the ion mass.

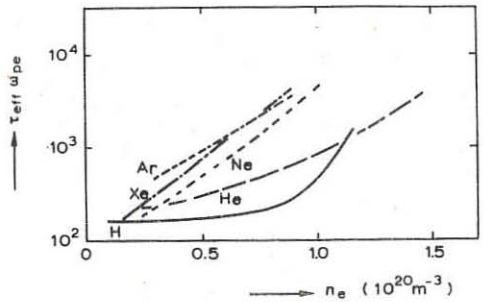

Fig.2. The effective collision frequency, expressed as a number of plasma oscillations, as a function of the plasma density for experiments in different gases. The electric field is 45 kV m^{-1} and the magnetic field is 0.4 T. Relatively few experiments have been performed in Ar.

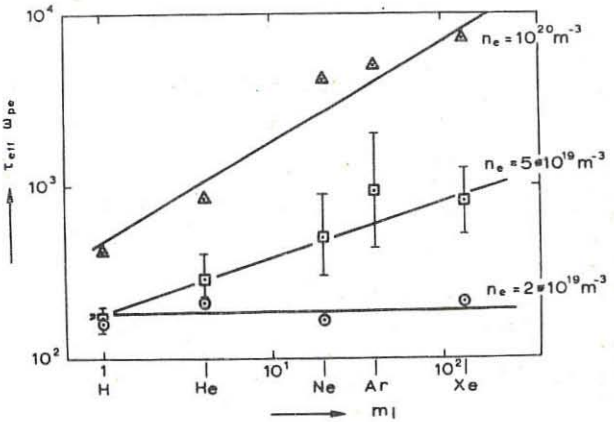

Fig. 3.
The effective collision frequency, expressed as a number of plasma oscillations, as a function of the ion mass at different plasma densities. The points are taken as average values from Fig.2.

Although the experiments cover the range ω_{ce} = 0.05 - 0.8 ω_{pe} a dependence upon the confining magnetic field is not found [2]. As a function of the applied electric field the plasma resistance increases almost linearly with the electric field.

The drift velocity in the initial stage of turbulence, at the time when the resistance is measured, is in the order of 5 - 20 c_s. Therefore, the turbulence must be due to the growth of ion-acoustic instabilities. The agreement of the effective collision frequency, $\nu_{eff} = \tau_{eff}^{-1}$, from the experiments with the values from the computer simulations of Biskamp and Chodura [3] is noted and we attribute the saturation of the ion-acoustic instabilities to the trapping of ions.

The H_β profile

The H_β profile is scanned in steps of 1/3 Å at relatively high plasma densities. The spectra are time averages over 0.5 μsec from three successive shots. Side on observations are carried out with a polarizer between plasma and monochromator. A specimen of a spectrum is given in Fig. 4. The H_β line is split up symmetrically by quasi-static fields from ion-acoustic waves ($f_{ac} \sim f_{pi}$) and by electron-plasma waves ($f_L \sim f_{pe}$) as indicated in this figure. This was also reported by Berezin et al. [6].

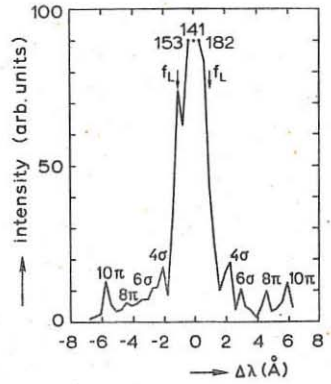

Fig. 4.
H_β profile for t = 1 - 1.5 μsec. The electric field applied to the plasma column is 45 kV m^{-1} and the density is 10^{20} m^{-3}. The orientation of the polarizer is parallel to the discharge axis.

To interpret the measured profiles a division into three components is suggested. Fig.5 a: At the position of the Balmer line a peak is present which is thought to be predominantly emitted by the cold plasma boundary. Fig.5 b: Components clearly symmetrically arranged around the central peak resulting from the quasi-static field. Fig.5 c: Satellites at ± 1 Å and less clear at ± 2 Å are due to electron-plasma oscillations. The satellites at ± 1 Å can be swallowed up by the central peak.

The time evolution of the side-bands is shown in Fig. 6. In the first 0.5 μsec streaming instabilities are excited resulting in satellites near f_L and 2 f_L, which can also be seen at later times when quasi-static Stark levels appear. These satellites may be caused by the interaction between Langmuir plasmons and the neutral hydrogen atoms.

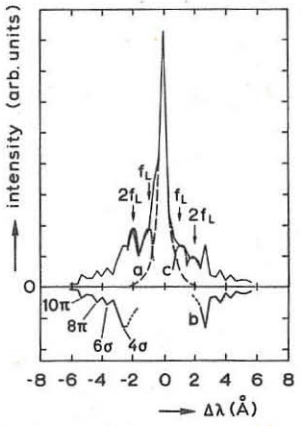

Fig. 5.
H_β profile for plasma conditions given in Fig. 6. a central peak b first-order quasi-static Stark components c satellites due to electron plasma oscillations.

The interaction can result in allowed transitions, symmetric with respect to the unshifted forbidden central component, due to the addition or absorption of one or more plasmons. f_L satisfies the dispersion relation $f_L^2 = f_{pe}^2(1 + 3k^2\lambda_D^2)$ with $k\lambda_D \sim 0.6$.

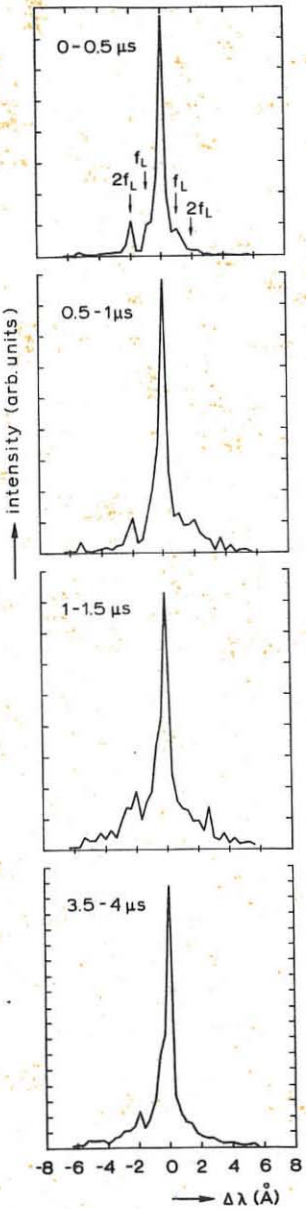

The discreteness of the static Stark components can be understood following the ideas of Blokhintsev [4] or Yakovlev [5]. In the present case the parameter $\Delta = \Delta\omega/\omega = 50 - 150$ where $\Delta\omega$ is the first-order Stark shift and ω the angular frequency of the oscillations ($\omega \sim \omega_{pi}$). For these parameter values separate peaks must be observable rather precisely near the position of the Stark components for time independent perturbations. The field strength calculated for ion-acoustic oscillations is $3\text{-}5 \times 10^6$ V/m, which corresponds to 0.5% of the thermal energy. With a polarizer the σ as well as the π components are observed simultaneously. Their intensities are rather insensitive for the orientation of the polarizer. This can be explained by a Cherenkov cone with a large top angle in which waves can grow unstable.

The authors are very much indebted to Mr. B. de Groot and Mr. R.A.A. Ambags for their technical assistance.

This work was performed under the Euratom-FOM association agreement with financial support from ZWO and Euratom.

References

[1] H.W. Piekaar, Plasma Physics, 15 (1973) 565.

[2] H. Schrijver, accepted for publication in Physica.

[3] D. Biskamp and R. Chodura, Max-Planck-Institut für Plasmaphysik Garching (1972) Report IPP 6/112.

[4] D. Blokhintsev, Phys.Z. Sowjetunion 4 (1933) 501.

[5] D.G. Yakovlev, Sov.Phys.-Tech.Phys. 17 (1973) 1248.

[6] A.B. Berezin, L.V. Dubovoi, B.V. Lyublin, and D.G. Yakovlev, Sov.Phys.-Tech.Phys. 17(1972) 750.

Fig.6.
H_β profile as a function of time. The electric field strength is 24 kV m^{-1} and the density is 10^{20} m^{-3}.

PLASMA HEATING AND DAMPING OF THE FAST WAVE NEAR THE SECOND HARMONIC OF THE ION CYCLOTRON FREQUENCY*

by

R. Dollinger, M. Kristiansen, M. O. Hagler
Department of Electrical Engineering, Texas Tech University
Lubbock, Texas 79409 USA

J. Bergström**
Royal Institute of Technology, Department of Plasma Physics
S-1044 Stockholm 70, Sweden

Figure 4 differs slightly from Fig. 2A (in the main paper) because of an improved technique for measuring B_0. Figure 5 is the unintegrated signal amplitude from a diamagnetic loop located at $z \simeq 10$ cm. Figures 4 and 5 (for $z \simeq 10$ cm) show the same good correlation between damping and heating as Fig's. 2B and 3 (for $z \simeq 15$ cm) in the main paper. The damping and heating correlation is thus independent of the location within the beach.

Figure 6 shows the radial profile of $\dot{b}_z$ at $z \simeq 15$ cm for three values of B_0. The B_0 values are representative of the range to the left of the dotted lines in Fig. 2B, between the dotted lines and to the right of the dotted lines. Thus, when the wave is damped, $\dot{b}_z$ is zero at all radii. The undamped wave has a profile somewhat indicative of a J_0 Bessel function for all B_0.

Preliminary integrated diamagnetic loop signals show that there is considerably more heating at $z \simeq 10$ cm than at $z \simeq 15$ cm (see relative values of $\dot{B}_d$ in Fig's. 3 and 5). Thus, the amount of heating apparently increases as the slope of the beach at the resonance point decreases (see Fig. 1).

*This work was supported in part by the National Science Foundation and the U.S. Atomic Energy Commission.

**Visiting Scientist.

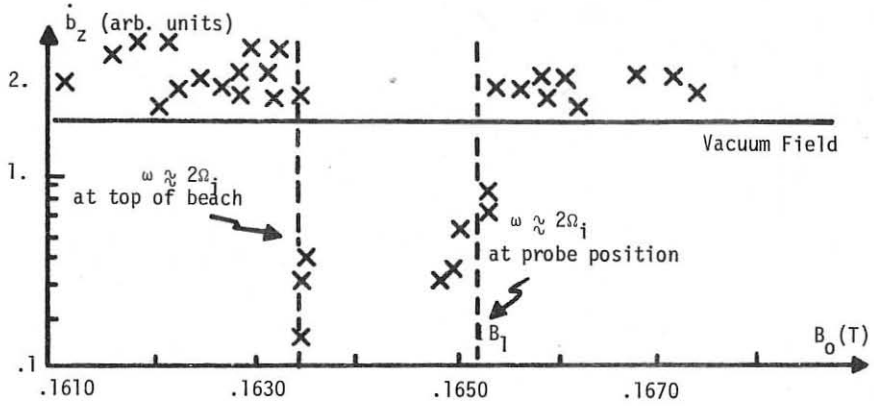

Fig. 4: Wave Signal vs B_0 at z = 10 cm (Replaces Fig. 2A)

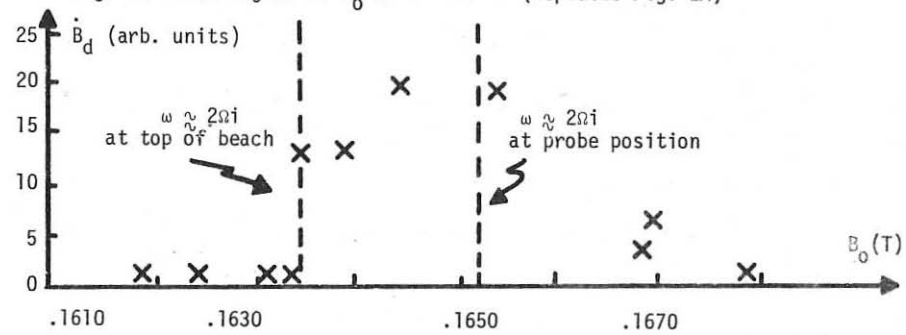

Fig. 5: Diamagnetic Loop Signal at z = 10 cm

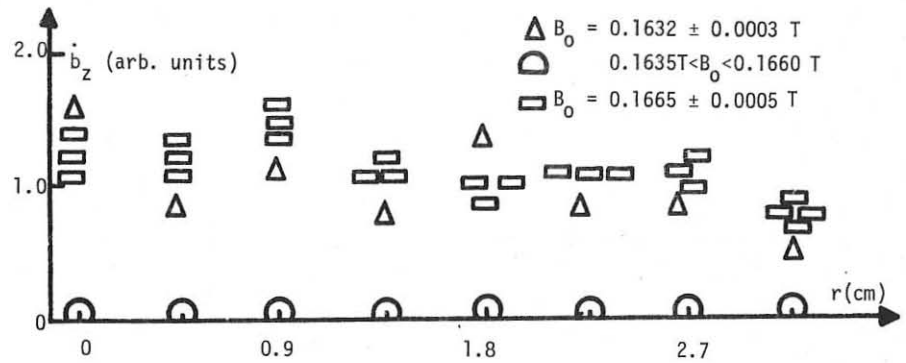

Fig. 6: Wave Signal vs Radius at z = 15 cm

INFLUENCE OF FINITE AMPLITUDE WAVES ON HEATING AND THERMAL INSULATION OF INHOMOGENEOUS PLASMA

A.A.Vodyanitsky, N.S.Yerokhin, S.S.Moiseyev, V.V.Mukhin, V.A.Rudakov.

Physico-Technical Institute Ukrainian Academy of the Science, Kharkov, 24, USSR

Taking account of the wave processes nonlinearity has more and more importance for understanding of the heating and containment of the plasma. Research of problems with interaction of the small number waves is often well corresponds to experimental situation and, from other point of view, it is more simple to understand a number important features of the plasma phenomena, as it can see from analysis described below.

1. Some decay instabilities in the inhomogeneous plasma.

The decay instabilities problem and its application to inhomogeneous plasma heating is investigated intensively in the recent years (see /1/ and references in it). In our work discussed decay instability in the resonance layer of the inhomogeneous plasma. Disturbance amplitude is described by a following model equation

$$\frac{d^2}{dz^2}E + \left[\left(\frac{\kappa_0 z}{L}\right)^2 - \frac{\varkappa^2 L^4}{(z^2+z_0^2)^2}\right]E = 0$$

For $z_0 \ll \varkappa L^2$ in the vicinity $|z| \lesssim z_0$ it take plase exponental grows of disturbance field. The amplification of disturbance field in region of the pumping wave field singularity is $\exp\left(\frac{\pi \varkappa L^2}{z_0}\right)$

Then the decay $\ell \to \ell + s$ in the inhomogeneous plasma is researched. Ion-sound oscillations are excited in a broad frequency spectrum and the amplification coefficient maximum is $\exp[\pi \kappa_0 L \frac{m_i}{m_e}(\frac{V_\sim}{2V_{Te}})^2 \kappa_0^2 r_D^2]$ where κ_0 is of the pumping wave vector, $V_\sim$ oscillation velocity of the electrons in the field of this wave, r_D Debye radius.

2. Overdence plasma clarification by self-focusing wave beams.

For laser and high frequency heating the overdense plasma clarification by wave beams is very important problem. In the case of the broad wave beam and small nonlinearity we can use equation

$$\frac{d^2E^2}{dz^2} + \frac{\omega^2}{c^2}[\varepsilon_0(z) + \alpha|E|^2]E = 0$$

If nonlinear part of a dielectric permittivity is positive ($\alpha > 0$), it is not difficult to show the wave penetrate to region $\varepsilon_0 < 0$ on distance of order L for origional wave amplitude E_0 to satisfy by condition $E_0^2 > \frac{c}{\omega L \alpha}$ where $L^{-1} = |d \ln \varepsilon_0 / dz|$. In this case for the wave equation is valid WKB-approximation. Analogous problem has been investigated in the resonance region also.

3. Second-harmonic generation in the inhomogeneous plasma.

In this part of the work on the basis results of a paper /2/ developed in strict succession the theory of second-harmonic generation of electromagnetic wave for arbitrary temperature of weakly inhomogeneous plasma. This effect is important for diagnostics and heating of the plasma. It is pointed out that the thresholds to be important for parametric instabilities taken place near resonance also, are absent

for second-harmonic generation. The second-harmonic amplitude don't depend from plasma temperature when the thermal electron velocity satisfy inequality $V_{Te} < c\,(3 K_\perp L)^{-1}$ where $K_\perp$ is component of the wave vector across density gradient, but for $V_{Te} > (c^2 K_\perp / \omega\sqrt{3})$ and a broad evanescent layer for the incident wave the second-harmonic amplitude is oscillatory function $\sim \cos\left[\frac{\pi}{4} + \frac{2\omega L}{3c}\left(3\frac{V_{Te}^2}{c^2} - \frac{c^2 K_\perp^2}{\omega^2}\right)^{3/2}\right]$. It has maximum at $V_{Te} = \sqrt{\frac{2}{3}}\,(c^2 K_\perp / \omega)$, and then monotonously decreased with temperature grows.

4. The particles and heat convective flow in plasma at the drift wave excitation.

It is well known that drift instabilities can lead to essential flows of particles and heat in the plasma (see /3/). For example, drift-dissipative instability in turbulent magnetoplasma leads to escape of plasma across magnetic field with Bohm diffusion coefficient. In the paper /5/ was studied diffusion of the plasma in the presence of regular drift waves. But the results /5/ can not believe finished because it was not take into account the temperature fluctuations to be important also in the case of the plasma without temperature gradient (but in presence of the density gradient, see /6/). In present report we have studied plasma transport across the magnetic field on the basis of magnetohydrodynamics fluid equations where we have taken into account the heat balance equation for electrons to be absent in the paper /5/. Transport coefficients are calculated with account of electron-ion friction, ion collision viscosity,

neutral-ion friction, longitudional collision heating conductivity of the electrons. For example, last dissipative factor leads to the loss of electron heat across the magnetic field. It was discussed in the case when the two drift harmonics are excited. Their amplitudes are functions of following parameters: $\gamma_1 = \frac{\nu_{ii}}{\omega_*}$, $\gamma_2 = \frac{\nu_{oi}}{\omega_*}$, $y = \omega_* / \lambda k_z^2$ where ω_* is drift frequency, ν_{ii} , ν_{oi} , ion-ion and neutral-ion collision frequences, λ coefficient of electron heat conductivity per one particle.

REFERENCES.

1. R.Z.Sagdeev, A.A.Galeev, V.N.Oraevsky. JETP Letters, 16, 194, (1972).
2. N.S.Yerokhin, V.E.Zakharov, S.S.Moiseyev. JETP, 56, 179, (1969).
3. B.B.Kadomtsev. Plasma turbulence, Academic press, (1965).
4. S.S.Moiseyev, R.Z.Sagdeev. JETP, 44, 763, (1963).
5. T.H.Stix. Physical Review Letters, 20, 1422, (1968).
6. S.S.Moiseyev. JETP Letters, 4, 81, (1966).

ION HEATING IN A MIRROR MACHINE NEAR HYBRID RESONANCE

Yu.V.Skosyrev, N.A.Krivov, V.M.Glagolev.

I.V.Kurchatov Institute of Atomic Energy
Moscow, USSR

This paper presents some results obtained from continuation of the studies described in Ref. [1] . When HF power of the frequency close to the hybrid resonance is applied to a mirror machine plasma the ions are observed to heat. A number of studies aimed at improving the methods of plasma heating have been recently carried out. As a result have been possible:

1. To modify the methods for producing a cold plasma.

2. To improve the vacuum conditions by separating the vacuum chamber walls from the plasma column.

3. To increase the strength of a static magnetic field up to 4.3 kOe.

4. To increase the power introduced in the plasma.

5. To obtain the ion energy spectrum.

6. To derive a relationship between the heated plasma parameters and heating conditions.

The HF power of a generator operating at the frequency of 140MHz was applied to the plasma by means of a two-conductors line equipped with a coupling loop. The coupling loop embraced the vacuum chamber - a quartz tube 100mm in diameter placed between two mirror coils. The cold plasma is produced by means of the titanium gun. A plasma blob produced in such a way spreads along the magnetic lines of force and enters the trap. It is heated by decelerated waves excited by the coupling loop in the plasma. Using magnetic and electric probes [2] , it was found that such high frequency

ge current as a function of energy. The ion temperature estimated by this plot was 300 eV. It is seen that as compared to the Maxwellian distribution the distribution was "enriched" by the high energy ions. An increased neutral gas pressure in the range of 10^{-6}-10^{-5} torr resulted by only in an increased absolute magnitude of the charge exchange current without any variations in the plot. This supported the assumption on a collosionless mechanism of acquiring the energy by the ions. The relation between the charge exchange current I and pressure can be expressed in the form $I=I_0[1+(P/Po)^{\alpha}]$ where $\alpha=2/3$. The plot of this relation did not pass the beginning of the coordinates. A possible cause of this phenomenon may be attributed to the wall gas release when the pressure is pulsed increased at an instant of heating. As the magnetic field was increased in the range of 2-4.3 Koe the charge exchange current was increased by a factor of 2-3. The magnetic field configuration in the region of heating appreciably affected the parameters of the heated plasma. In a mirror geometry magnetic field with the mirror ratio 1,5 the ion charge exchange current is an order of magnitude greater than that in the case of a uniform magnetic field. The longitudinal energies of the ions and electrons escaping the discharge along the magnetic lines of force were analyzed using a multigrid electrostatic probe. It was found that in the case of a uniform field the electron energy is 80 ev, and the ion energy is 300 ev while for a mirror geometry of the field, the longitudinal energy of the electron is 150 ev and that of the ions is 500 ev. The dependence of a plasma diamagnetic signal on the magnetic field was of the form of growing curve with some saturation when the magnetic field was 4.3kOe. The value nT was $\sim 3\cdot10^{14}$ ev$\cdot$cm^{-3}. The lifetime of ions having the energy I kev estimated by a decrease in the charge exchange current

input gave a rise both the nonordinary wave (of the H-type) and ordinary wave (of the E-type) in the plasma. It has been found that at the instant of heating no enhancement of the wave magnetic field typical of the magneto-acoustic resonance was observed. The ion heating was believed to be caused, due to generationg of the plasma waves during slowing down the ordinary electromagnetic wave. It was found out in [1] that the heating occurs only when the density varied in the range of $(1.2-4)\ 10^{12}\,cm^{-3}$. Studies of the source operation showed that after 100 μs flux of neutral gas appeared following the initial plasma blob. Since the period of the heating and decaying of plasma is less than 100 μs the instant when the plasma gun switched on with respect to the end of a heating pulse should be chosen so that the neutral gas could not interfere with the investigations of the heating process.

In addition to the diagnostic techniques discribed in [1] a method of double charge exchange [3] was used to study a heated plasma. Neutral hydrogen atoms produced as a result of charge exchange with fast ions in the volume of the chamber left the discharge near the mirror neck. The secondary charge exchange occured when the neutral flux passed a thin carbon foil. In analysis of the energy of ions appeared as a result of that charge exchange allowed us to estimate the ion distribution with respect to the transverse energies in the discharge

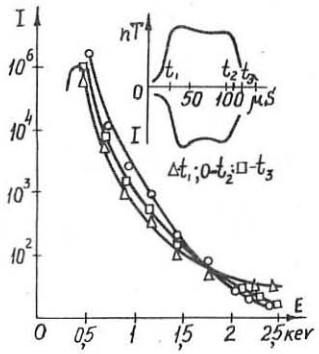

Fig.1. Charge exchange as a function of energy.

Fig.1 shows the charge exchan-

was 15 μs and decreased as the pressure was increased. This indicates that the plasma energy is concentrated in the main, in the ion component. Decrease in the plasma energy containment time compared to the particle confinement time seems to be associated with the presence of an additional amount of gas released from the walls of the quartz tube during its heating and subsequent cooling due to charge exchange. A more sharp increase in the charge exchange current as compared to the increase in the density during heating also pointed to this. To improve the vacuum conditions a work is being performed now to create a HF vacuum cavity, which could enable to reject from the quartz tube deviding the volume accupied by the plasma and that of the HF cavity. Furthermore, a new type of matching the HF generator and resonator has been desighed. It enables one to increase the power introduced into the plasma.

References:

1. Glagolev V.M., Krivov N.A., Skosyrev Yu.V., Report IAEA-CN-28/1-6. IV International Conference on plasma Physics and Controlled nuclear fusion research. Madison 1971. Vol. III p.559.
2. Skosyrev Yu.V., Krivov N.A., Glagolev V.M. Electromagnetic fields in plasma, heated at a frequency closed to the lower hybrid resonance. Atomnaja Energia 1973 (to be published).
3. Bayborodov Yu.I., Ioffe M.S., Sobolev R.I., Yushmanov E.E. Report on the IV Eurapean Conference on plasma Physics and Controlled nuclear fusion research Rome 1970, p.86.

EXCITATION OF ELECTROSTATIC MODES BY A MAGNETOACOUSTIC PUMP WAVE

K.D. Harms, G. Hasselberg, A. Rogister

Institut für Plasmaphysik der Kernforschungsanlage Jülich GmbH
ASSOCIATION EURATOM-KFA

Abstract: We have derived an integral equation which generalizes the dispersion relation describing electrostatic modes in the presence of a magnetoacoustic pump wave propagating orthogonal to $\underline{B}_o$. Parametric excitation of ion Bernstein modes is discussed as an example.

In recent years a great deal of theoretical effort has been devoted to the study of parametric effects in plasmas. The problem is directly related to that of auxiliary heating schemes, e.g. in Tokamaks. Pumping power in the magnetoacoustic mode could be conveniently achieved via a wave guide system for usual Tokamak conditions; further the wave could be made a resonant eigenmode of the plasma column. For simplicity we assume that the pump wave propagates in the plane orthogonal to $\underline{B}_o$ (Fig. 1). Its frequency satisfies the dispersion relation

$$\omega_o^2 = \frac{k_o^2 \, c_A^2}{1 + k_o^2 \, c_A^2 / \omega_{LH}^2} \qquad (1)$$

where $\omega_{LH}^2 = (1/\omega_{pi}^2 + 1/\Omega_i \Omega_e)^{-1}$ and c_A^2 is the square of the Alfvén velocity. The operating frequency must thus be smaller than the lower hybrid ω_{LH} at which the pump becomes evanescent.

The appropriate equations describing the electrostatic perturbations δf_J, $\delta\psi$ are

$$\left[\frac{\partial}{\partial t} + (\underline{v} + \underline{u}_J)\cdot\frac{\partial}{\partial \underline{r}} - (1 + \frac{b_z}{B_o})\frac{\partial}{\partial \varphi}\right] \delta f_J = \frac{q_J}{m_J} \frac{\partial}{\partial \underline{v}} (F_{oJ} + f_J)\cdot \frac{\partial}{\partial \underline{r}} \delta\psi \qquad (2)$$

In this equation, $\underline{u}_J(t)$ is the mean velocity of the particles of species J in the electromagnetic field of the pump wave; $f_J(t)$ is the corresponding distribution function in the frame moving with velocity $\underline{u}_J$; $b_z(t)$ is the magnetic field of the pump wave. Assuming the wavelengths of the electrostatic modes to be much smaller than the typical length scale of the pump, but much larger than the

electron Larmor radius ($kR_e \ll 1$), the terms proportional to f_J and b_z in Eq. (2) play a negligible role. Integration along the orbit yields after substitution in Poisson's equation

$$\delta\psi(t) + \sum_J \frac{\omega_{pJ}^2}{k^2 c_J^2}\left[\delta\psi(t) - \int_{-\infty}^{0} d\tau \exp\left[-\phi(\tau)\right] \frac{\partial}{\partial\tau}\left[\delta\psi(t+\tau)\exp\int_t^{t+\tau} dt'' i\underline{k}\cdot\underline{u}_J(t'')\right]\right] = 0 \qquad (3)$$

where $\phi(\tau) \equiv k_z^2 c_J^2 \tau^2/2 + k_\perp^2 c_J^2 (1-\cos\Omega_J\tau)/\Omega_J^2$.

In the absence of the pump, Eq. (3) where one sets $\delta\psi(t) \sim e^{-i\omega t}$ leads to the usual dispersion relation in a magnetic field:

$$\varepsilon(k,\omega) = 1 + \sum_J \frac{\omega_{pJ}^2}{k^2}\left[1 + \zeta_{oJ}\sum_{-\infty}^{\infty} e^{-\lambda_J} I_n(\lambda_J) Z(\zeta_{n,J})\right] \qquad (4)$$

where
$Z(\zeta)$ is the Fried and Conte dispersion function, $\zeta_{n,J} = (\omega - n\Omega_J)/\sqrt{2}k_z c_J$ and $\lambda_J \equiv k_\perp^2 c_J^2/\Omega_J^2$ [we recall that $k_\perp c_e/\Omega_e \ll 1$ and the summation for the electrons reduces to the term n=0]. In the limit $k_z = 0$ (more precisely $k_z c_e \ll \omega$), Eq. (3) reduces to the linear equation (4) if one assumes

$$\delta\psi(t) \sim \exp -i\int_o^t dt''\left[\underline{k}\cdot\underline{u}_i(t'') + \omega t''\right] ;$$

the same remark applies whenever $\underline{k}\cdot\underline{u}_i = \underline{k}\cdot\underline{u}_e$, k_z arbitrary.

We have particularly studied the nonlinear excitation of Bernstein modes. If $\int_o^t dt''\underline{k}\cdot\underline{u}_e(t'') \equiv \underline{k}\cdot\underline{r}_e(t) \ll 1$, the parametric growth rate, neglecting linear Landau damping, is given by

$$\gamma_{par} = \frac{k_\theta u_\theta}{\omega_o}\left|\varepsilon_e(\omega_1) - \varepsilon_e(\omega_2)\right|\left|(\partial\varepsilon/\partial\omega)_{\omega_1}^{-1}\ (\partial\varepsilon/\partial\omega)_{\omega_2}^{-1}\right|^{1/2} \qquad (5)$$

where $\varepsilon_e(\omega) \equiv (\omega_{pe}^2/k^2)\left[1 + \zeta_{oe} Z(\zeta_{oe})\right]$ and $|\omega_1| + |\omega_2| = \omega_o$.
Typically

$$\gamma_{par} = \alpha \frac{k_\theta u_\theta}{\omega_o}\ \frac{\omega}{k_\perp R_i} \quad \text{(note that } u_\theta \sim \frac{cE_r}{B}\text{)} \qquad (6)$$

where $\alpha \lesssim 1$, $\omega \lesssim \omega_o$, and it has been assumed that $k_\perp R_i \gg 1$.

The dependance of the parametric growth rate and threshold electric field [the azimuthal field E_θ is of order $(\Omega_i/\omega_o)E_r$] upon the angle of propagation of the Bernstein modes is given in Fig. 2.

If the resonance conditions are not (approximately) satisfied, destabilization of ion Bernstein modes can still occur through nonlinear electron Landau effect ($\omega_{B^-} + \omega_o \simeq k_z c_e$). In this case the groth rate is of order

$$\gamma_{nl} \sim \alpha' \frac{\omega}{k_\perp R_i} \left(\frac{k_\theta u_\theta}{\omega_o} \right)^2 \qquad (7)$$

where $\alpha' \lesssim 1$. The latter result agrees with the corresponding expression for the spatial groth rate given previously by Martinov and Samain /1/.

In inhomogeneous plasmas, the (approximate) matching condition for the parametric process to occur cannot be satisfied simultaneously at different points in space. The associated effects will be discussed. Furthermore, results on parametric excitation of ion sound waves will be presented.

It is a pleasure to acknowledge useful discussion with Dr. H. Kever.

/1/ N. Martinov and A. Samain, private communication.

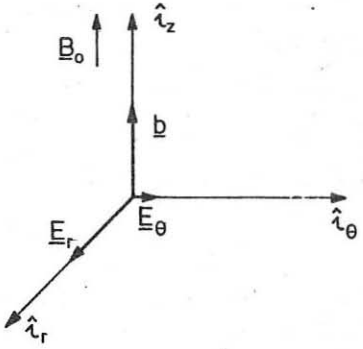

Fig. 1 Electromagnetic field of the pump wave. Propagation is in the radial direction.

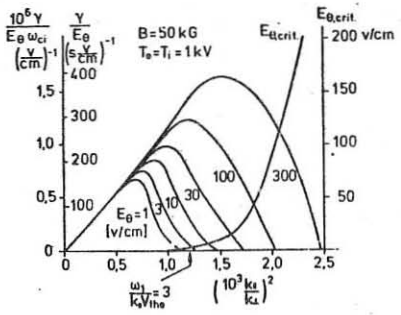

Fig. 2 Growth rate γ and threshold electric field $E_{\theta,crit}$ of the parametric instability for the decay $\omega_o = 7\omega_{ci} \rightarrow 3\omega_{ci} + 4\omega_{ci}$ in deuterium. $k_\perp R_i = 15$, $k_r = k_\theta = k_\perp/\sqrt{2}$, $k_o = 0$.

NEW OFF-ANGLE TEMPERATURE ANISOTROPY INSTABILITY

Ronald W. Landau

Dept. of Physics, Tel-Aviv University, Ramat-Aviv

Israel

A new instability, propagating almost perpendicularly to the magnetic field, is described, with growth rate magnitudes near the electron cyclotron frequency. It is unstable for $\beta_{\parallel} = 4\pi n \kappa T_{\parallel}/B^2 > .591$ when $T_{\perp} = 0$.

We have found a new temperature anisotropy instability propagating almost perpendicular to the external magnetic field. The mode is polarized quasi-longitudinally for $\beta_{\parallel} < 1$ and does not oscillate, i.e., it's purely growing. The mode is obtained by solving the linear Vlasov equation, assuming that $T_{\parallel}$ is maxwellian, $T_{\perp} = 0$ and neglecting the ions. Our motivation for examining such almost perpendicular modes arises from the occurence in the solar wind of enhanced electron density filaments[1] aligned along the magnetic field and from the demonstration by Taylor[2] that the diffusion of electron filaments across a uniform magnetic field has the same parameter dependence as Bohm diffusion.

The energy source for driving the instability is $T_{\parallel} > T_{\perp}$, which is the situation in the solar wind. Currents along the magnetic field also produce an effective $T_{\parallel} > T_{\perp}$. The equations are most easily derived from Landau and Cuperman[3] by assuming $T_{\perp} = 0$, neglect of ions and $\omega_{p,-}^2 >> \Omega_-^2$, Including the ions, we believe, will increase the growth rate, but finite $T_{\perp}$ or finite $\omega_{p,-}^2$ will decrease the growth rate. For the solar wind $\omega_{p,-}^2/\Omega_-^2 \gg 1$, but for Tokomaks this ratio is about 1/5.

The dispersion relation may be put into very compact form by assuming that the propagation is almost perpendicular so that $\theta = k_{\parallel}/k_{\perp} \ll 1$ while $k_{\perp} \gg 1$, which allows the neglect of terms $\propto \theta^2$ and $\propto 1/\ell_{\parallel}$ ($\ell_{\parallel}^{\frac{1}{2}} \equiv k_{\perp} \bar{v}_{\parallel}/\Omega_-$, $\bar{v}_{\parallel}^2 \equiv T_{\parallel}/m_-$)

but the retention of terms $\propto\theta^2\ell_{\parallel}$. This gives

$$F(g-\gamma G') + a^2 G'\bar{Z} = 0 \qquad (1)$$

where $F \equiv Z_r' a^2 - 1/\beta_{\parallel}$, $Z_r' \equiv \mathrm{Re}\ Z'$, $\bar{Z} = -\mathrm{Im}\ Z'$

$G' \equiv 2aZ_i$, $Z_i = \mathrm{Im}\ Z$, $a^2 = 1/(2\theta^2\ell_{\perp})$

$g = 2+Z_r'$, $\gamma = \omega_i/|\Omega_-|$

and Z is the usual plasma function[4], $Z<\zeta>$ where $\zeta=a(1+i\gamma)$, $a>0$ and for instability $\gamma>0$. Also $Z'<\zeta>=dZ/d\zeta$.

If we are interested only in obtaining stability criteria, then we set $\gamma=0$ in (1) and obtain

$$Z_r' + \bar{Z}^2/(2+Z_r') = 1/(\beta_{\parallel}a^2) \ , \qquad (2)$$

an equation which is rather easy to solve. A graphical solution is indicated in Fig. 1 by plotting the left side of this equation as a function of $1/a^2$ (called SUM) and drawing the straight line $1/(\beta_{\parallel}a^2)$. For $.591<\beta_{\parallel}<1$ there are two solutions, while for $\beta_{\parallel}>1$ there is but one. The surprising result, that instability exists only for $\beta \gtrsim .591$ is due, we believe, to the neglect of ion motion, which should give a complex solution for all β.

Growth rates are easily obtained from Eq. (1) using the various expansions of the plasma function in the $a\ll1$ and $a\gg1$ limits. Thus we find

$$\gamma = 1/\left[a\sqrt{\pi}\,(4-\pi)\right] \cdot (\pi-2-1/(a^2\beta_{\parallel})) \ , \qquad (a\ll1,\ \beta_{\parallel}\gg1)$$

and

$$\gamma^2 = \beta_{\parallel} - 1 + 3\beta_{\parallel}/(2a^2) \ , \qquad (a^2\gg1,\ \gamma^2\ll1, \beta_{\parallel}\simeq1)$$

$$\gamma^2 = \beta_{\parallel} - 1 \qquad (a^2\gg1,\ \beta_{\parallel}\gg1) \ .$$

These results may all be verified as being consistent with Fig. 2 whose solid lines are a computer solution of Eq. (1), while the broken lines give the solution for a more complete equation that includes $\theta\neq0$ (not

exactly 90° propagation) and finite values of ω_p^2/Ω_-^2. The large 'a', large β growth rate may be rewritten as $\gamma^2=\beta_{\parallel}$, or

$$\omega_i = \pm\omega_p \bar{v}_{\parallel}/c \qquad (3)$$

which is very similar to the Weibel[5] instability, except that here $T_{\parallel} > T_{\perp}$, i.e. the two equal temperatures of a temperature ellipsoid are less than the third.

This result is also consistent with the calculations of Kalman[6] et al. on temperature anisotropy instabilities without magnetic field for their 'coupled mode' instability. This mode is unstable for $T_{\perp} > T_{\parallel}$ with maximum growth at $\theta=0$, where the mode is quasi-transverse. However, they did not notice that their dielectric constants (their Eq. (42)), are unchanged under the substitution $T_{\perp} \to T_{\parallel}$, $T_{\parallel} \to T_{\perp}$, $\theta \to 90^o-\phi$ so that for each solution where $T_{\perp} >> T_{\parallel}$ near $\phi=0$, there is a corresponding solution $T_{\parallel} >> T_{\perp}$ near $\phi=90^o$. Thus Weibel's result goes over into Eq. (3) for perpendicular propagation. The polarization of their wave is quasi-transverse for large rates of growth, but becomes quasi-longitudinal for small growth rates, in agreement with our results.

We wish to thank Ilan Roth for his help in the computer programming.

References :

(1) Hewish, A. and Symonds, M.D., Planetary & Space Science 17, 313 (1969); Hewish, A., in 'Solar Wind', edited by C.P. Sonett, P.J. Coleman Jr. and J.M. Wilcox (NASA, Washington, D.C.,1972), p.483.

(2) Taylor, J.B., in 'Vth European Conf. on Controlled Fusion and Plasma Physics', Vol.II (Centre d'Etudes Nucleaires de Grenoble, Grenoble, France,1972), p.83.

(3) Landau, R.W., and Cuperman, S., J. of Plasma Phys. 6, 495 (1971).

(4) Fried, B.D. and Conte, S.D., 'The Plasma Dispersion Function' (Acad.

Press, N.Y.,1961).

(5) Weibel,E.S. Phys. Rev. Letters 2, 83 (1959);

Landau, R.W., and Cuperman, S., J. of Plasma Phys. (to be published) 1973.

(6) Kalman, G., Montes, C., and Quemada, D., Phys. Fluids 11, 1797 (1968)

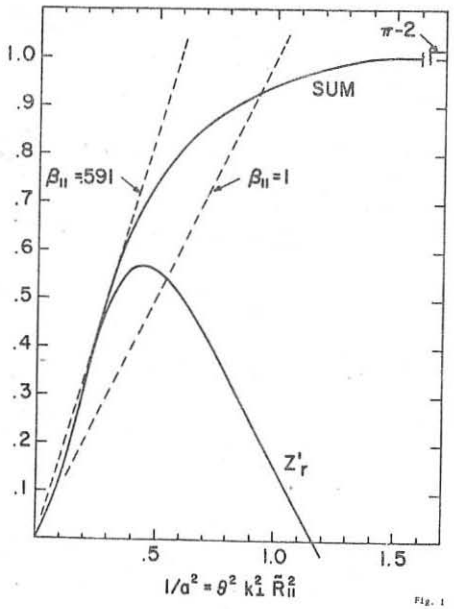

Fig. 1

Fig. 1 Graphical solution of Eq.(2) for the marginally stable case. Intersection of the straight (dashed) line with the 'SUM' curve gives a marginally stable solution.

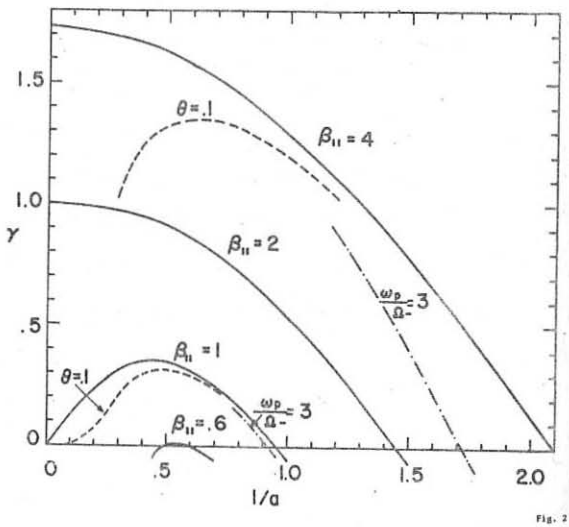

Fig. 2

Fig. 2 Growth rate, γ, for various parameters. The solid line is a solution of Eq. (1). Both dashed curves for θ=.1 have the same behavior near γ=0. The dash-dot curves are for θ=0, $\omega_{p,-}/\Omega_- = 3$.

AUTHOR INDEX

x/ Number in brackets refers to the page in the first volume.